



MONASH University

**Combinatorial Synthesis and Biological Activity of
Photoswitchable Carbohydrate Amphiphiles**

Yingxue Hu
BEng, MSc (Distinction)

A thesis submitted for the degree of Doctor of Philosophy at
Monash University in 2017
School of Chemistry
Faculty of Science

Dedicated to my family

献给我的家人

Copyright notice

© Yingxue Hu (2017). Except as provided in the Copyright Act 1968, this thesis may not be reproduced in any form without the written permission of the author.

I certify that I have made all reasonable efforts to secure copyright permissions for third-party content included in this thesis and have not knowingly added copyright content to my work without the owner's permission.

This page is intentionally blank

Table of Contents

Copyright notice	i
Table of Contents	iii
Abstract	vii
Declaration	ix
Publications during enrolment	xi
Thesis including published works declaration	xiii
Acknowledgements	xv
List of Figures	xvii
List of Schemes	xx
List of Tables	xxi
List of Abbreviations	xxii

Chapter 1 – Sweetness and light: design and applications of

photo-responsive glycoconjugates	1
Declaration for thesis chapter 1	3
Preface to chapter 1	5
1.1 Introduction	7
1.2 Applications of azobenzene glycoconjugates	8
1.2.1 Photoswitchable lectin inhibitors	8
1.2.2 Photocontrollable delivery vehicles	9
1.2.3 Photoswitchable cross-linkers	10
1.3 Conclusions	12
1.4 References	12

Chapter 2 – Carbohydrate-based surfactants and fluorosurfactants as photocontrollable inhibitors of ice recrystallization

inhibitors of ice recrystallization	15
Declaration for thesis chapter 2	17
2.1 Introduction	19
2.1.1 Cryopreservation	19
2.1.2 Biological antifreezes	21
2.1.3 Low molecular weight carbohydrate derivatives as IRI agents	22
2.2 Results and discussion	26

2.2.1 Library design and parallel synthesis of photocontrollable carbohydrate surfactants	26
2.2.2 Photoswitching studies	31
2.2.3 Photocontrollable surface activity	33
2.2.4 Photocontrollable IRI activity	39
2.2.5 Quantitative analysis of IRI activity	43
2.2.6 Antibacterial performance of fluorosurfactants	46
2.3 Conclusions	47
2.4 Experimental	48
2.4.1 General	48
2.4.2 Surface tension measurements	49
2.4.3 UV-vis spectroscopy	50
2.4.4 Measurement of 1-Octanol/water partition coefficient ($\log P$)	50
2.4.5 IRI assay	50
2.4.6 MTT assay with Hep G2 cells	51
2.4.7 Quantitative analysis of IRI activity	52
2.4.8 TH assay	53
2.4.9 Cryopreservation of Tf-1 α cells	54
2.4.10 Antibacterial assays	55
2.4.11 Synthesis of 2.36 and 2.37 : General procedure 1	56
2.4.12 Synthesis of 2.32 and 2.33 : General procedure 2	56
2.4.13 Synthesis of 2.30 and 2.48–2.50 : General procedure 3	56
2.4.14 Synthesis of 2.25 and 2.42–2.44 : General procedure 4	57
2.4.15 Synthesis of 2.39–2.41 : General procedure 5	57
2.4.16 Synthesis of 2.7–2.9 : General procedure 6	57
2.4.17 Synthesis of 2.10–2.21 : General procedure 7	58
2.4.18 Note on nomenclature	59
2.4.19 Analytical data	60
2.5 References	79

Chapter 3 – Photomodulation of bacterial growth and biofilm formation

using carbohydrate-based surfactants	89
Declaration for thesis chapter 3	91
3.1 Introduction	93

3.1.1 Antibacterial drug resistance and biofilms	93
3.1.2 Glycolipids	95
3.2 Results and discussion	98
3.2.1 Library design and synthesis	98
3.2.2 Photoswitching studies	102
3.2.3 Photocontrollable surface activity	106
3.2.4 Characterization of self-assemblies	108
3.2.5 Photocontrollable antibacterial studies	111
3.2.6 Photocontrollable biofilm studies	118
3.2.7 Bacterial motility studies	121
3.3 Conclusions	126
3.4 Experimental	127
3.4.1 General	127
3.4.2 UV-vis stability studies on <i>trans</i> and <i>cis</i> isomers	127
3.4.3 Surface tension measurements	127
3.4.4 Small angle neutron scattering (SANS)	128
3.4.5 Antibacterial assays	129
3.4.6 Minimum inhibitory concentration (MIC) test	129
3.4.7 Biofilm assays	130
3.4.8 Bacteria preparation for differential dynamic microscopy (DDM)	131
3.4.9 DDM measurements	131
3.4.10 Swarming motility assays	132
3.4.11 Synthesis of 3.15–3.18 : General procedure 1	132
3.4.12 Synthesis of 3.3–3.13 : General procedure 2	132
3.4.13 Analytical data	133
3.5 References	147
Chapter 4 – Photoswitchable Janus glycodendrimer micelles as multivalent inhibitors of LecA and LecB from <i>Pseudomonas aeruginosa</i>	155
Declaration for thesis chapter 4	157
Preface to chapter 4	159
Chapter 5 – Concluding comments and future directions	161

Appendix I – Thermal <i>cis</i>–<i>trans</i> relaxation UV-vis spectra	167
Appendix II – Air-water surface tension data	171
Appendix III – Raw data of log <i>P</i> measurements	175
Appendix IV – Published first and co-authored papers included in the main body of this thesis	183

Abstract

Carbohydrate amphiphiles are molecules of significant biological and industrial importance, and show a strong tendency to self-assemble in aqueous solution to give micellar structures. Recently, there has been considerable interest in the application of light as an external stimulus for controlling the molecular conformation and amphiphilicity of surfactants. By using carefully designed light-responsive compounds, the control of properties such as phase behaviour, solubility, aggregation and adsorption can be achieved.

In this thesis, we have synthesised a range of novel, photoswitchable carbohydrate-based amphiphiles incorporating an azobenzene moiety that undergoes clean and reversible *trans*–*cis* photoisomerisation upon UV light irradiation. The self-assembly / disassembly of aggregates formed from these molecules has been explored via small angle neutron scattering (SANS) and surface tension studies under the influence of UV and visible light. A diverse range of geometries and dimensions of self-assembled structures have been observed through variation of the carbohydrate head group, and subsequent photoisomerisation of the hydrophobic tail group.

By using these light-addressable carbohydrate amphiphiles, we reveal for the first time the photo-control of ice recrystallization inhibition (IRI) activity (Chapter 2), bacterial growth/biofilm formation (Chapter 3) and lectin binding properties (Chapter 4). In Chapter two, weak-to-moderate IRI activity is observed for carbohydrate (fluoro)amphiphiles that could be tuned through selection of carbohydrate head group, position of the trifluoroalkyl group on the azobenzene ring, and isomeric state of the azobenzene unit. In Chapter three, the bacteria- and photoisomer-specific inhibitory activity of these amphiphiles are observed against drug resistant *E. coli* and *S. aureus*. These compounds also showed inhibition of biofilm formation from Gram positive *S. aureus*, whereas they promote biofilm formation in Gram negative *P. aeruginosa*. In Chapter four, the first example of the self-assembly and lectin binding properties of photoswitchable glycodendrimer micelles is reported. Photoswitchable glycodendrimer micelles were assessed as self-assembled, light-responsive inhibitors of soluble lectins LecA and LecB from the opportunistic pathogen *P. aeruginosa*.

This page is intentionally blank

Declaration

This thesis contains no material which has been accepted for the award of any other degree or diploma at any university or equivalent institution and that, to the best of my knowledge and belief, this thesis contains no material previously published or written by another person, except where due reference is made in the text of the thesis.

Signature:



Print Name: ...Yingxue Hu...

Date:12 June 2017.....

This page is intentionally blank

Publications during enrolment

Yingxue Hu, Madeleine K. Adam, Jessica S. Poisson, Matthew J. Pottage, Robert N. Ben and Brendan L. Wilkinson, Photoswitchable carbohydrate-based fluorosurfactants as tuneable ice recrystallization inhibitors. *Carbohydr. Res.* **2017**, 439, 1–8. [DOI: 10.1016/j.carres.2016.12.004](https://doi.org/10.1016/j.carres.2016.12.004)

Yingxue Hu, Wenyue Zou, Villy Julita, Rajesh Ramanathan, Rico T. Tabor, Reece Nixon-Luke, Gary Bryant, Vipul Bansal and Brendan L. Wilkinson, Photomodulation of bacterial growth and biofilm formation using carbohydrate-based surfactants. *Chem. Sci.* **2016**, 7 (11), 6628–6634. DOI: [10.1039/c6sc03020c](https://doi.org/10.1039/c6sc03020c)

Yingxue Hu, Rico F. Tabor and Brendan L. Wilkinson, Sweetness and light: design and applications of photo-responsive glycoconjugates. *Org. Biomol. Chem.* **2015**, 13 (8), 2216–2225. DOI: [10.1039/c4ob02296c](https://doi.org/10.1039/c4ob02296c)

Yingxue Hu, Joshua B. Marlow, Rajesh Ramanathan, Wenyue Zou, Hui Geok Tiew, Matthew J. Pottage, Vipul Bansal, Rico F. Tabor and Brendan L. Wilkinson, Synthesis and properties of photoswitchable carbohydrate fluorosurfactants. *Aust. J. Chem.* **2015**, 68 (12), 1880–1884. [DOI: 10.1071/ch15434](https://doi.org/10.1071/ch15434)

Madeleine K. Adam, Jessica S. Poisson, Yingxue Hu, Geethika Prasannakumar, Matthew J. Pottage, Robert N. Ben and Brendan L. Wilkinson, Carbohydrate-based surfactants as photocontrollable inhibitors of ice recrystallization. *RSC Adv.* **2016**, 6 (45), 39240–39244. [DOI: 10.1039/c6ra07030b](https://doi.org/10.1039/c6ra07030b)

This page is intentionally blank

Thesis including published works declaration

I hereby declare that this thesis contains no material which has been accepted for the award of any other degree or diploma at any university or equivalent institution and that, to the best of my knowledge and belief, this thesis contains no material previously published or written by another person, except where due reference is made in the text of the thesis.

This thesis includes 5 original papers published in peer reviewed journals and 1 submitted publications. The core theme of the thesis is synthesis and characterisation of photoswitchable carbohydrate amphiphiles for biological applications. The ideas, development and writing up of all the papers in the thesis were the principal responsibility of myself, the student, working within the School of Chemistry, Monash University under the supervision of Dr. Rico F. Tabor and Dr. Brendan L. Wilkinson.

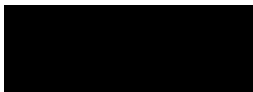
The inclusion of co-authors reflects the fact that the work came from active collaboration between researchers and acknowledges input into team-based research.

In the case of chapters 1, 2, 3, and 4 my contribution to the work involved the following:

Thesis Chapter	Publication Title	Status	Nature and % of student contribution	Co-author name(s) Nature and % of Co-author's contribution (Student Only)	Co-author(s) Monash student Y/N
1	Sweetness and light: design and applications of photo-responsive glycoconjugates	Published	70%. Literature search, wrote manuscript draft		
2	Synthesis and properties of photoswitchable carbohydrate fluorosurfactants	Published	47%. Synthesis and characterization of product, analysis of results	1) Joshua B. Marlow, physical characterization of product, analysis of results, 47% 2) Wenyue Zou, antibacterial assays, 4% 3) Hui Geok Tiew, Matthew J. Pottage, assisted in experimentation and physical characterization, 2%	Y N Y
2	Photoswitchable carbohydrate-based fluorosurfactants as tuneable ice recrystallization inhibitors	Published	47%. Synthesis and (physical) characterization of product, analysis of results	1) Madeleine K. Adam, antifreeze and cytotoxicity assays, 47% 2) Jessica S. Poisson, assisted in antifreeze and cytotoxicity assays, 5% 3) Matthew J. Pottage, assisted in physical characterization, 1%	N N Y
2	Carbohydrate-based surfactants as photocontrollable inhibitors of ice recrystallization	Published	30%. Synthesis and (physical) characterization of product, analysis of results	1) Madeleine K. Adam, antifreeze and cytotoxicity assays, 35% 2) Jessica S. Poisson, assisted in antifreeze and cytotoxicity assays, 33% 3) Geethika Prasannakumar, assisted in experimentation, 1% 4) Matthew J. Pottage, assisted in physical characterization, 1%	N N N Y

3	Photomodulation of bacterial growth and biofilm formation using carbohydrate-based surfactants	Published	47%. Synthesis and (physical) characterization of product, analysis of results	1) Wenyue Zou, bacterial and biofilm assays, analysis of results, 47% 2) Villy Julita, assisted in experimentation, 1% 3) Reece Nixon-Luke, DMM experimentation, 5%	N Y N
4	Photoswitchable Janus glycodendrimer micelles as multivalent inhibitors of LecA and LecB from <i>Pseudomonas aeruginosa</i>	Submitted	85%. Initiation, key ideas, experimental works, analysis of results, wrote manuscript draft	Ghamdan Beshr, lectin binding assays, analysis of results, 15%	N

I have not renumbered sections of submitted or published papers in order to generate a consistent presentation within the thesis.

Student signature: 

Date: 12 June 2017

The undersigned hereby certify that the above declaration correctly reflects the nature and extent of the student's and co-authors' contributions to this work. In instances where I am not the responsible author I have consulted with the responsible author to agree on the respective contributions of the authors.

Main Supervisor signature: 

Date: 13th June 2017

Acknowledgements

I would like to express my sincere gratitude and thanks to Monash University for providing me two awesome main supervisors: Dr. Brendan Wilkinson and Dr. Rico Tabor, both of whom are the most passionate supervisors I have ever worked with. Special thanks to my supervisor Dr. Brendan Wilkinson for his constant guidance, encouragement, support and patience throughout my PhD candidature, I will never have the chance to start this excellent and interesting PhD project without him. He trained me all the lab skills from the beginning, taught me to improve my writing skills for reports and publications and motivated me to do better than what I would expect from myself. Special thanks also give to my supervisor Dr. Rico Tabor, he trained me to think critically and independently, encouraged me to try innovative ideas and supported me when I was in stress. Both of my supervisors, Dr. Brendan Wilkinson and Dr. Rico Tabor, are always there to help me and guide me to enjoy both research and life, which will be treasured all my life. I really appreciate their supervision and enjoy working with them.

I gratefully acknowledge Faculty of Science Dean's International Postgraduate Research Scholarship and School of Chemistry Stipend Scholarship from Monash University for providing me the living allowance and tuition fee which made my PhD work possible.

A big thank you goes indeed to current and past members of the Wilkinson and Tabor groups, you have kept me smiling and made every day a pleasure for the last three years during my PhD. I would like to thank in no specific order: Jackson, Ragesh, Tom, Matt, Ali, Rajiv, Sumit, Shane, Joshua, Veena, Loki, Jamie, Patrick and Samantha. You have all filled the last three years, in the office and lab, with many laughs and good times.

I would like to thank Prof. Vipul Bansal and his group at RMIT, Prof. Robert Ben and his group at University of Ottawa, Dr. Alexander Titz and his group at Helmholtz Institute for Pharmaceutical Research Saarland (HIPS) and Dr. Christopher Garvey at Australian Nuclear Science and Technology Organisation (ANSTO), for their collaboration works. This PhD project would never be completed without their efforts. I also would like to acknowledge in no specific order: Dr. Kellie Tuck, Dr. Peter Nichols, A/Prof. Antony Patti, Dr. Boujemaa Moubaraki, A/Prof. David Lupton, and Ms. Anna Severin in the School of Chemistry at Monash University, for their kind help and suggestions during my PhD study.

I would like to express my thanks to all my dear friends outside of the lab, especially Jieting Chen, Mutong Li, Jin He and Zhifang Guo. Even though thousands of miles apart, they have shared with me my worries, frustrations and happiness. I will always appreciate their friendship in my life.

Last but most importantly, I would like to thank my beloved parents and every member in my family for their love and support through the past many years. To my Dad, thanks for passing me the gene of chemistry and encouraging me on my research by continuously asking “how many publications do you have?” “what is the impact factor of your journal?” and “when will you prepare the next manuscript?”. To my Mum, thanks for not asking my publication records and be the mentor of my life. I love you both.

List of Figures

Figure 1.1 Photocontrolled adhesion and release of <i>E. coli</i> from a) SLBs surface and b) HMEC-1 cell surface	9
Figure 1.2 Azobenzene glycoconjugates as delivery vehicles	10
Figure 1.3 Representative azobenzene glycoconjugate enable the cross-linking of (modified)peptides/proteins	11
Figure 2.1 Typical structure of native AFGPs 2.1	22
Figure 2.2 Structures of C-linked AF(G)P analogues 2.2 and 2.3	22
Figure 2.3 Structures of low molecular weight carbohydrate derivatives 2.4–2.6	23
Figure 2.4 Molecular structures of photoswitchable carbohydrate-based surfactants (2.7–2.9) and fluorosurfactants (2.10–2.21)	25
Figure 2.5 UV-vis spectra and thermal <i>cis–trans</i> relaxation of representative surfactants a) 2.7 GlcAzo, b) 2.10 Glc <i>p</i> -CF ₃ , c) 2.11 Glc <i>m</i> -CF ₃ and d) 2.12 Glc <i>o</i> -CF ₃	32
Figure 2.6 Expanded ¹ H NMR spectrum of surfactants 2.8 ManAzo (20 mM in CD ₃ OD) in the <i>trans</i> -dominated state (top) and <i>cis</i> -dominated state (bottom)	33
Figure 2.7 a) Customized experimental setup for surface tension measurements, b) determination of CMC values, c) a typical drop image captured by a digital camera	34
Figure 2.8 Air-water surface tension data for surfactants a) 2.7 GlcAzo and b) 2.8 ManAzo	35
Figure 2.9 Air-water surface tension data for representative surfactants a) 2.10 Glc <i>p</i> -CF ₃ , b) 2.11 Glc <i>m</i> -CF ₃ and c) 2.12 Glc <i>o</i> -CF ₃	36
Figure 2.10 CMC data plot for fluorosurfactants 2.10–2.21	37
Figure 2.11 a) IRI activity surfactant 2.7–2.9 represented as a % MGS of ice crystals relative to the PBS control. b) Images of the PBS control (top) and 2.8 ManAzo at 30 mM (bottom) after 5 minutes annealing	40
Figure 2.12 IRI activity of fluorosurfactants a) Glc-based 2.8–2.10 , b) Gal-based 2.11–2.13 , c) Man-based 2.14–2.16 and d) Cel-based 2.17–2.19 represented as a % MGS of ice crystals relative to the PBS control	42
Figure 2.13 Percent cell viability of Hep G2 cell treated with various concentrations of a) Glc <i>o</i> -CF ₃ 2.12 , b) Gal <i>o</i> -CF ₃ 2.15 and c) Cel <i>o</i> -CF ₃ 2.21	43

Figure 2.14 a) Dose-response curve for <i>trans</i> -dominated compound ManAzo 2.8 . A two-parameter sigmoidal curve was fitted to the data. V_{norm} is the normalized rate constant. b) Ice crystal habit image in the presence of 0.5 mg mL^{-1} <i>trans</i> -dominated form of 2.8	44
Figure 2.15 Percent post-thaw cell recoveries of TF-1 α cells cryopreserved with 30 mM ManAzo 2.8 in varying concentrations of DMSO	45
Figure 2.16 Percent post-thaw cell viability and apoptosis of Tf-1 α cells cryopreserved with 30 mM ManAzo 2.8 in varying concentrations of DMSO	45
Figure 2.17 TF-1 α cells incubated at 37°C for 30 minutes with or without 30 mM ManAzo 2.8 , a) percent cell viability and apoptosis; b) percent cell recovery	46
Figure 2.18 Dose-dependent antibacterial activity of a) Glc <i>o</i> -CF ₃ 2.12 , b) Glc <i>m</i> -CF ₃ 2.11 , c) Glc <i>p</i> -CF ₃ 2.10 , d) Cel <i>o</i> -CF ₃ 2.21 , e) Cel <i>m</i> -CF ₃ 2.20 and f) Cel <i>p</i> -CF ₃ 2.19 against Gram-positive bacteria <i>S. aureus</i> over a period of 24 hrs	47
Figure 3.1 Schematic diagram of biofilm development	94
Figure 3.2 Molecular structures of carbohydrate amphiphiles as reported by Grinstaff and co-workers (compound 3.1) (left) and by Chaveriat and co-workers (compound 3.2) (right)	97
Figure 3.3 Proposed photoswitchable carbohydrate-based surfactants 3.3–3.13	98
Figure 3.4 Time-dependent <i>cis–trans</i> thermal relaxation of representative surfactant GlcTz 3.3 at 20°C in water and the corresponding first-order plot for <i>cis–trans</i> conversion (inserted)	103
Figure 3.5 ¹ H NMR spectra of GalTz 3.9 in the <i>trans</i> -dominated PSS (top), the <i>cis</i> -dominated PSS (bottom) and expanded spectrum of triazole proton (inserted)	105
Figure 3.6 ¹ H NMR spectrum of GlcTz 3.3 before UV photoirradiation (top), after UV photoirradiation (middle), and after visible (blue) light photoirradiation (bottom). Spectra were recorded in CD ₃ OD at 20 mM concentration	106
Figure 3.7 Air–water surface tension data for representative surfactant GlcTz 3.3	107
Figure 3.8 CMC data plot of surfactants 3.3–3.13	108
Figure 3.9 SANS experimental data (symbols) and model fits (solid lines) of a) 3.3–3.13 (<i>trans</i> -dominated state) in D ₂ O at 4 mM; b) AraTz 3.8 at different concentrations; c) FucTz 3.11 at different concentrations and d) LacTz 3.12 at different concentrations. In (a) only, data have been offset vertically by multiplication for clarity of presentation. The SANS spectra for GlcTz 3.3 and GalTz 3.9 have been reported previously	111
Figure 3.10 Photoswitchable control compounds 2.25 and 3.31 in this study	112

Figure 3.11 Normalized bacterial cell viability with a) GlcTz 3.3, b) XylTz 3.4, c) RhaTz 3.5, d) ManTz 3.6, e) GlcNAcTz 3.7, f) AraTz 3.8, g) GalTz 3.9, h) RibTz 3.10, i) FucTz 3.11, j) LacTz 3.12 and k) CelTz 3.13 against <i>E. coli</i> DH5a after 24 h	115
Figure 3.12 Normalized bacterial cell viability with a) GlcTz 3.3, b) XylTz 3.4, c) RhaTz 3.5, d) ManTz 3.6, e) GlcNAcTz 3.7, f) AraTz 3.8, g) GalTz 3.9, h) RibTz 3.10, i) FucTz 3.11, j) LacTz 3.12 and k) CelTz 3.13 against <i>S. aureus</i> ATCC1698 after 24 h	116
Figure 3.13 Concentration-dependent antibacterial testing of <i>trans</i> - and <i>cis</i> -isomers of a) GlcTz 3.3, b) XylTz 3.4, c) RhaTz 3.5, d) ManTz 3.6, e) GlcNAcTz 3.7 and f) AraTz 3.8 against <i>P. aeruginosa</i> at 37°C in nutrient broth after 24 h incubation in dark conditions	118
Figure 3.14 Concentration-dependent influence of <i>trans</i> - and <i>cis</i> -isomers of a) GlcTz 3.3, b) XylTz 3.4, c) RhaTz 3.5, d) ManTz 3.6, e) GlcNAcTz 3.7 and f) AraTz 3.8 on biofilm forming of <i>S. aureus</i> at 37°C after 24 h	120
Figure 3.15 Concentration-dependent influence of <i>trans</i> and <i>cis</i> photoisomers of a) GlcTz 3.3, b) XylTz 3.4, c) RhaTz 3.5, d) ManTz 3.6, e) GlcNAcTz 3.7 and f) AraTz 3.8 on biofilm forming ability of <i>P. aeruginosa</i> at 37°C after 24 h of incubation	121
Figure 3.16 Influence of <i>trans</i> - and <i>cis</i> -isomer of a) RhaTz 3.5 and b) ManTz 3.6 on swimming motility of <i>P. aeruginosa</i> MDR283/1-6	122
Figure 3.17 Photograph of agar swarming motility assay demonstrating the influence of the increasing concentration of <i>trans</i> -isomer of a) GlcTz 3.3, b) XylTz 3.4, c) RhaTz 3.5, d) ManTz 3.6, e) GlcNAcTz 3.7, f) AraTz 3.8, g) 2.26 and h) 3.31 on swarming motility of <i>P. aeruginosa</i> MDR283/1-6 (swarming-positive strain)	124
Figure 3.18 Photograph of agar swarming motility assay demonstrating the influence of a) GlcTz 3.3, b) XylTz 3.4, c) RhaTz 3.5, d) ManTz 3.6, e) GlcNAcTz 3.7, f) AraTz 3.8, g) 2.26 and h) 3.31 at 100 µg mL ⁻¹ concentration in the <i>trans</i> and <i>cis</i> form on the swarming motility of <i>P. aeruginosa</i> MDR283/1-6 (swarming-positive stain)	124
Figure 3.19 Photograph of agar swarming motility assay demonstrating the influence of a) RhaTz 3.5, b) ManTz 3.6 and c) GlcNAcTz 3.7 at 25 µg mL ⁻¹ concentration in the <i>trans</i> and <i>cis</i> form on swarming motility of <i>P. aeruginosa</i> MDR283/1-23 (swarming-negative strain). An equal amount of deionized water without any compound was added to the agar media to serve as a control	125

List of Schemes

Scheme 2.1 Synthetic procedure for <i>O</i> -glycoside surfactants 2.7–2.9	27
Scheme 2.2 Synthetic procedure for mannose trichloroacetimidate 2.24	28
Scheme 2.3 Synthetic procedure for azobenzene-based building block 2.25	28
Scheme 2.4 Synthetic procedure for glycosyl azides 2.32–2.35	29
Scheme 2.5 Synthetic procedure for azobenzene-based building block 2.39–2.41	30
Scheme 2.6 Synthetic procedure for fluorosurfactants 2.10–2.21	31
Scheme 3.1 Synthetic procedure for glycosyl azides 3.14–3.20	100
Scheme 3.2 Synthesis of alkyne-functionalized fragment 3.30	101
Scheme 3.3 Synthetic procedure for surfactants 3.3–3.13	102

List of Tables

Table 2.1 Photocontrollable CMC, thermal half-life of the <i>cis</i> -isomer at 20°C and log <i>P</i> of carbohydrate-based surfactants 2.7–2.9	38
Table 2.2 Photocontrollable CMC, thermal half-life of the <i>cis</i> -isomer at 20°C and log <i>P</i> of carbohydrate-based fluorosurfactants 2.10–2.21	39
Table 3.1 Main glycolipids produced by several microorganisms and their minimum inhibitory concentrations (MIC) against different pathogens	95
Table 3.2 Thermal half-lives of 3.3–3.13 in water, Nutrient Broth (NB) and Brain Heart Infusion broth (BHI)	104
Table 3.3 Photocontrollable CMCs of surfactants 3.3–3.13	107
Table 3.4 Aggregation properties of carbohydrate based surfactants 3.3–3.13	110
Table 3.5 MIC results of <i>trans</i> and <i>cis</i> isomers of control compounds 2.25 and 3.31 against <i>E. coli</i> DH5α, <i>P. aeruginosa</i> and <i>S. aureus</i> at 37°C	112

List of Abbreviations

Ac	acetate
AcOH	acetic acid
Ara	arabinose
BF ₃ ·Et ₂ O	boron trifluoride diethyl etherate
Bu	butyl
Cel	cellobiose
CDCl ₃	deuterated chloroform
d	doublet
dd	doublet of doublets
dq	doublet of quartets
DBU	1,8-diazabicyclo[5.4.0]undec-7-ene
DCM	dichloromethane
DMAP	4-dimethylamino pyridine
DMF	dimethylformamide
DMSO	dimethylsulfoxide
equiv.	equivalents
EtOAc	ethyl acetate
EtOH	ethanol
Fuc	fucose
g	gram
Gal	galactose
Glc	glucose
GlcNAc	2-acetamido-2-deoxy-D-glucose or <i>N</i> -acetyl D-glucosamine
hr	hour
HPLC	high performance liquid chromatography
Hz	Hertz
L	litre
Lac	lactose
LC-MS	liquid chromatography-mass spectrometry
M	molarity
m	multiplet
Man	mannose

MHz	megahertz
mg	milligram
min	minute
mmol	millimole
mol	mole
NMR	Nuclear Magnetic Resonance
<i>p</i> -	para
ppm	parts per million
Rha	rhamnose
Rib	ribose
t	triplet
<i>tert</i> -	tertiary
THF	tetrahydrofuran
TLC	thin layer chromatography
δ	chemical shift
UV	ultraviolet
w/v	weight per volume
Xyl	xylose
μ L	microlitre
$^{\circ}$ C	degrees Celsius

This page is intentionally blank

Chapter 1

Sweetness and Light: Design and Applications of Photo-responsive Glycoconjugates

This page is intentionally blank

Declaration for Thesis Chapter 1

Declaration by candidate

For Chapter 1, the nature and extent of my contribution to this work was as following:

Nature of contribution	Extent of contribution (%)
Literature search, wrote manuscript draft	70

The following co-workers contributed to the work. If co-authors are students, the extent of their contribution in percentage terms was stated:

Name	Contribution	Extent of contribution (%) for student co-workers only
Brendan L. Wilkinson Rico F. Tabor	Manuscript preparation and editing	

The undersigned hereby certify that the above declaration correctly reflects the nature and extent of the candidate's and co-workers' contributions to this work.

Candidate's
Signature



Date

12 June 2017

Main
Supervisor's
Signature



Date

13th June 2017

This page is intentionally blank

Preface to Chapter 1

This chapter is a literature review of the research conducted on the design and synthesis of photoswitchable glycoconjugates, and is an extension of the review article published in *Organic and Biomolecular Chemistry* in 2015 (*Org. Biomol. Chem.*, **2015**, *13*, 2216–2225).

This page is intentionally blank

1.1 Introduction

Carbohydrates bound to proteins and lipids are of pivotal importance as signaling molecules that mediate cellular communication. These supramolecular recognition processes are dependent on the precise configurational and constitutional arrangement of the carbohydrate for presentation to the cognate receptor. Azobenzene-functionalized glycoconjugates have attracted considerable interest in various research fields, since these molecules are able to change molecular conformation and physicochemical properties upon UV-light irradiation in a temporally- and spatially-resolved manner.¹ Such responsive systems have emerged as promising tools for modulating multivalent presentation for interrogating carbohydrate-biomolecular interactions, host-guest inclusion complexation properties, as well as and supramolecular and macromolecular self-assembly (e.g. gel-sol transitions).^{2,3}

Azobenzene is a well-characterized chromophore that undergoes clean and reversible *trans-cis* photoisomerization in the presence of UV light (~350 nm). This venerable photoswitch offers numerous advantages over other environmental stimuli and molecular photoswitches, in that high recyclability and reproducibility of function can be achieved, along with the ability to tune the photochemical and physicochemical properties through modification of molecular structure (e.g. ‘push-pull’ azobenzenes and red-shifted systems with dual-visible light photoswitching properties for *in vivo* applications).^{4,5}

The following chapter will highlight recent advances (since 2015) in the design and applications of light-addressable glycoconjugates incorporating azobenzene photoswitches. Specific developments have focused on their use as light-controllable lectin inhibitors and delivery vehicles. A published review article is attached, which provides a more comprehensive literature review prior to 2015, describing the design and application of azobenzene glycoconjugates with applications in glycobiology, nanoscience and materials science.

1.2 Applications of azobenzene glycoconjugates

1.2.1 Photoswitchable lectin inhibitors

Azobenzene glycoconjugates have drawn considerable interest as investigational tools for controlling carbohydrate-protein binding and bacterial/cellular adhesion. Recently, the photo-triggered conformational change of glycoconjugates has been applied to investigate the influence of carbohydrate conformation on bacterial adhesion, in particular the mannoside-specific adhesion of *Escherichia coli*.^{6, 7} The Jonkheijm group have recently reported the photocontrolled immobilization of *E. coli* onto Cucurbit[8]uril modified surfaces (Figure 1.1a).⁸ Supramolecular supported lipid bilayers (SLBs) were functionalized with Cucurbit[8]uril that served as the cavity to accommodate an azobenzene mannoside through host-guest inclusion complexation. Photoisomerization of the SLBs provided a trigger for releasing the photoswitchable glycoside from the inclusion complex, thus releasing it from the surface, as determined by quartz crystal microbalance measurements with dissipation monitoring (QCM-D) and fluorescence techniques.

The surface immobilization strategy of bioactive ligands on smart surfaces is not limited to SLBs, but has also been used on self-assembled monolayers (SAMs).^{9, 10} Recent work from the Zhang and He groups has demonstrated the construction of SAMs based on (galactose/mannose)-decorated azobenzene derivatives for controlling cellular adhesion of Hep-G2 and M2 cells through lectin (PNA and ConA)-carbohydrate interactions.¹¹ By monitoring the electrochemical response following photoisomerisation, the binding and adhesion performance of the smart surfaces could be determined.¹¹

The first example of the photocontrollable adhesion of bacteria onto living cells has also been demonstrated by the Lindhorst group (Figure 1.1b).¹² In this study, metabolically engineered endothelial cells (variant 1, HMEC-1) underwent biorthogonal click chemistry to install photoswitchable glycoconjugates onto the cellular surface. The modified HMEC-1 cells were then incubated with GFP-fluorescent *E. coli* and the number of adherent bacteria were counted using high-resolution, live-cell fluorescence microscopy. The adhesion of *E. coli* cells was

reduced upon *trans-cis* photoisomerisation of the glycoconjugate, which could be quantified by measuring the reduced bacterial GFP-signal after irradiation with UV light at 365 nm. These studies demonstrate the effect of azobenzene *trans-cis* photoisomerization on modulating lectin binding avidity for controlling bacterial adhesion onto biotic and abiotic surfaces.^{4, 6, 12}

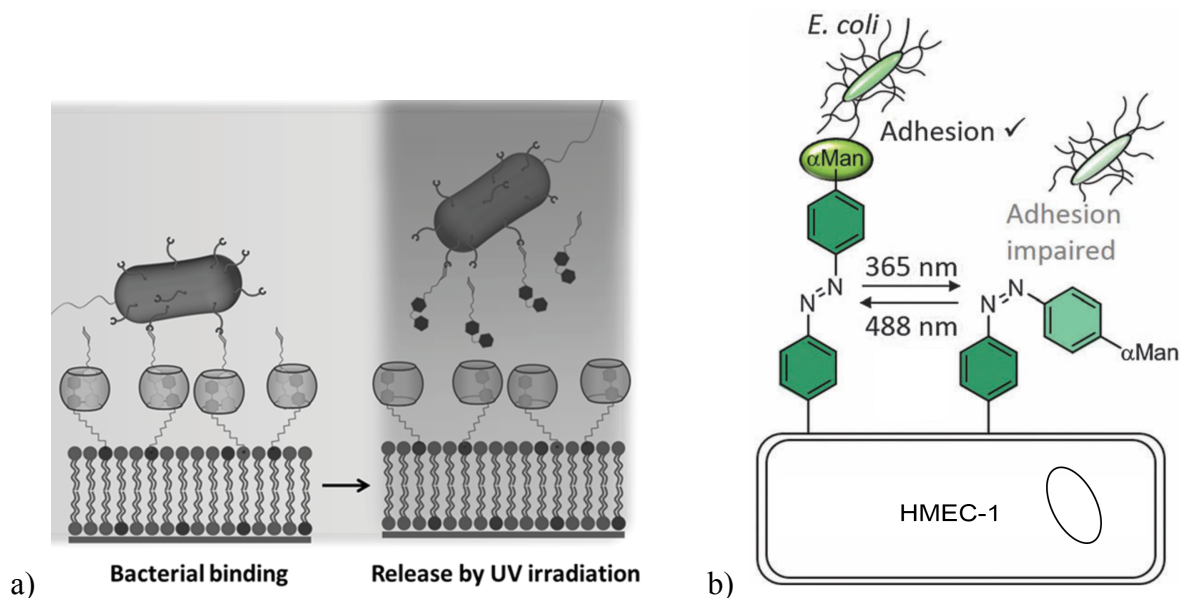


Figure 1.1. Photocontrolled adhesion and release of *E. coli* from a) SLB surface⁸ and b) HMEC-1 cell surface.¹² Reproduced with permission from references 8 and 12. Copyright 2015 Wiley-VCH and 2016 The Royal Society of Chemistry.

1.2.2 Photocontrollable delivery vehicles

Glycopolymers and synthetic sugar-containing macromolecules are of increasing interest in biomedical and biochemical fields including controlled drug/gene delivery and biomimetic chemistry.^{13, 14} Due to their biocompatibility, biodegradability and water solubility, amphiphilic glycopolymers are able to form well-defined aggregates in water that mimic the natural size/shape and surface recognition properties of cells.¹⁵ Recently, azobenzene glycopolymers were investigated as photocontrollable delivery vehicles by Das and co-workers (Figure 1.2).^{15, 16} This study described the partial release and re-encapsulation of Nile red by azobenzene glycopolymers. Exposure of the aggregates to alternating changes of UV and visible light resulted in geometrical changes from spherical aggregates to fiber-like

aggregates.¹⁵ The self-assembly of azobenzene block copolymers into spherical micelles was also reported by the Stenzel group, who demonstrated the successful loading and delivery of Nile red to melanoma cells.¹⁶ However, the disassembly of the micelles was not observed upon UV irradiation.¹⁶ Nonetheless, this work demonstrates the potential of azobenzene glycoconjugates and their incorporation into polymeric scaffolds for photo-triggered release applications.

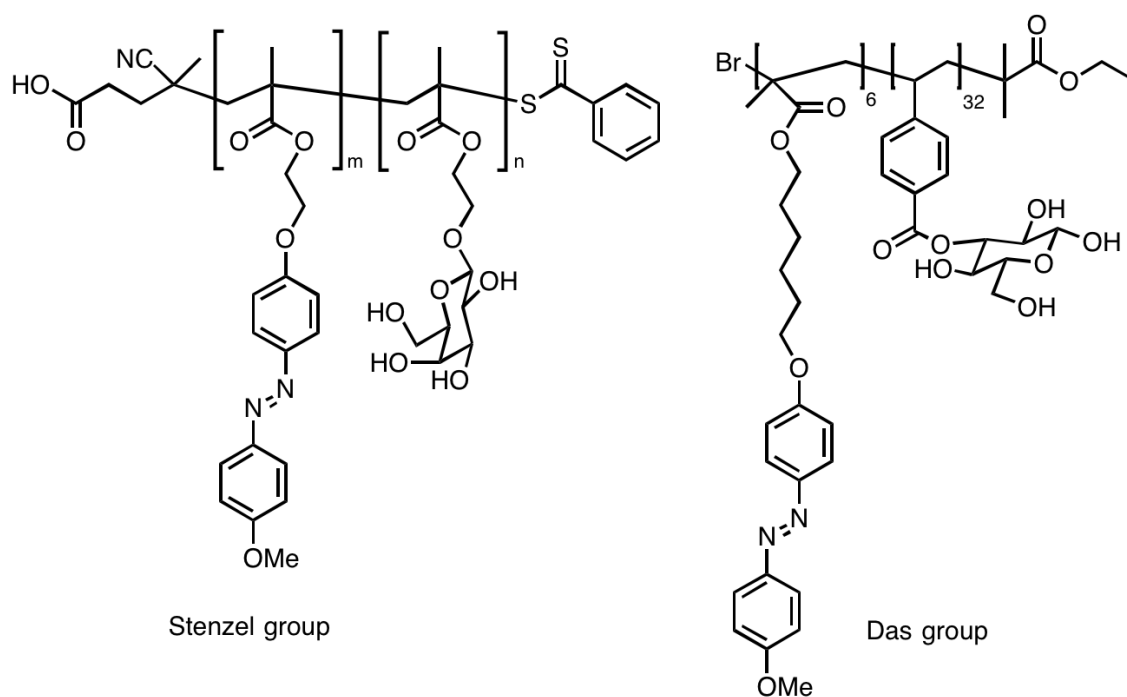
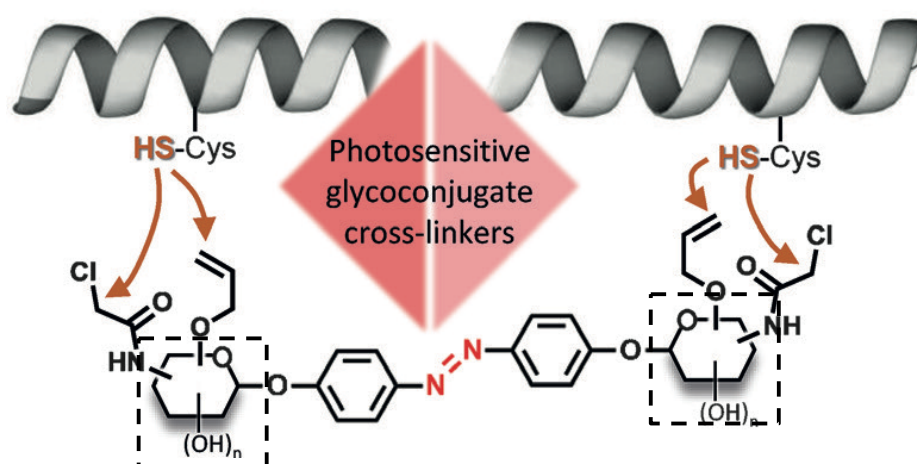


Figure 1.2. Azobenzene glycoconjugates as delivery vehicles.^{15,16} Reproduced with permission from references 15 and 16. Copyright 2014 Wiley-VCH and 2015 Elsevier Ltd.

1.2.3 Photoswitchable cross-linkers

The ability to remotely control the conformational dynamics of biomolecules, including proteins and nucleic acids, holds significant promise for studying biological signaling pathways and protein folding.^{2, 17-21} Photoswitchable biomolecules have recently attracted significant attention, especially azobenzene derivatives, as they provide a minimally invasive method for the precise, spatiotemporal control over the conformation of biomolecules.^{20, 22} The Lindhorst group have reported the synthesis of bifunctionalized azobenzene glycoconjugates as cross-linkers for reversibly controlling peptide and protein folding (Figure 1.3).^{23, 24} The ligation of

these novel azobenzene glycoconjugates with peptides/proteins could be achieved via chemoselective ligation involving nucleophilic substitution, thiol-ene reaction, click reaction or Staudinger-Bertozzi ligation. The photochromic properties of the glycoconjugated peptides and proteins were characterized using ^1H NMR spectroscopy and UV/vis spectroscopy. The photostationary states were found to be reached after 10–15 min irradiation at 365 nm and this photoisomerization process could be repeated without loss of function over many cycles to enable interconversion between the ‘contracted’ and ‘relaxed’ states (Figure 1.3). The changes in the end-to-end distances of cross-linked peptides/proteins upon photoisomerization were investigated through molecular dynamic simulations, whereby the most probable distances of the *trans*-isomers varied from 15 to 18 Å.²⁴ The bifunctionalized azobenzene glycoconjugates could be readily functionalized with different linking chemistries, thus enabling access to tailored chemical systems for studying a wide range of protein folding interactions.



*Variable structures in the dashed boxes, that can be glucose- or galactose-based derivatives with different functional groups.

Figure 1.3. Representative azobenzene glycoconjugate to enable the cross-linking of (modified)peptides/proteins.^{23, 24} Reproduced with permission from references 23 and 24. Copyright 2015 Wiley-VCH.

1.3 Conclusions

Within the last 10 years, photoswitchable glycoconjugates have emerged as promising molecular tools for probing biomolecular interactions and cellular adhesion, as well as controlling supramolecular self-assembly. Such materials have found wide-reaching applications in glycobiology, biochemistry, drug/gene delivery and materials science. Pertinent to this thesis, our group have highlighted the application of azobenzene *trans-cis* photoisomerisation for tuning the adsorption and self-assembly properties of amphiphilic carbohydrates. The following thesis describes the synthesis, physical characterization and applications of photoswitchable carbohydrate-based amphiphiles and their application as tunable antifreeze agents (Chapter 2), antibacterial agents (Chapter 3) and self-assembled lectin inhibitors (Chapter 4).

1.4 References

1. Hamon, F.; Djedaini-Pilard, F.; Barbot, F.; Len, C., Azobenzenes—synthesis and carbohydrate applications. *Tetrahedron*, **2009**, *65* (49), 10105–10123.
2. Beharry, A. A.; Woolley, G. A., Azobenzene photoswitches for biomolecules. *Chem. Soc. Rev.*, **2011**, *40* (8), 4422–4437.
3. Dugave, C.; Demange, L., *Cis-trans* isomerization of organic molecules and biomolecules: implications and applications. *Chem. Rev.*, **2003**, *103* (7), 2475–2532.
4. Dokic, J.; Gothe, M.; Wirth, J.; Peters, M. V.; Schwarz, J.; Hecht, S.; Saalfrank, P., Quantum chemical investigation of thermal *cis-to-trans* isomerization of azobenzene derivatives: substituent effects, solvent effects, and comparison to experimental data. *J. Phys. Chem. A*, **2009**, *113* (24), 6763–6773.
5. Dong, M.; Babalhavaeji, A.; Samanta, S.; Beharry, A. A.; Woolley, G. A., Red-shifting azobenzene photoswitches for *in vivo* use. *Acc. Chem. Res.*, **2015**, *48* (10), 2662–2670.

6. Bernardi, A.; Jiménez-Barbero, J.; Casnati, A.; De Castro, C.; Darbre, T.; Fieschi, F.; Finne, J.; Funken, H.; Jaeger, K.-E.; Lahmann, M., Multivalent glycoconjugates as anti-pathogenic agents. *Chem. Soc. Rev.*, **2013**, *42* (11), 4709–4727.
7. Hartmann, M.; Lindhorst, T. K., The bacterial lectin FimH, a target for drug discovery—carbohydrate inhibitors of type 1 fimbriae-mediated bacterial adhesion. *Eur. J. Org. Chem.*, **2011**, *2011* (20–21), 3583–3609.
8. Sankaran, S.; Van, W. J.; Voskuhl, J.; Karperien, M.; Jonkheijm, P., Photoresponsive Cucurbit[8]uril-mediated adhesion of bacteria on supported lipid bilayers. *Small*, **2015**, *11* (46), 6187–6196.
9. Weber, T.; Chandrasekaran, V.; Stamer, I.; Thygesen, M. B.; Terfort, A.; Lindhorst, T. K., Switching of bacterial adhesion to a glycosylated surface by reversible reorientation of the carbohydrate ligand. *Angew. Chem. Int. Ed.*, **2014**, *53* (52), 14583–14586.
10. Chandrasekaran, V.; Jacob, H.; Petersen, F.; Kathirvel, K.; Tucek, F.; Lindhorst, T. K., Synthesis and surface—spectroscopic characterization of photoisomerizable glyco-SAMs on Au (111). *Chem. Eur. J.*, **2014**, *20* (28), 8744–8752.
11. Zhang, J.; Ma, W.; He, X. P.; He, T., Taking orders from light: photo-switchable working/inactive smart surfaces for protein and cell adhesion. *ACS Appl. Mater. Interfaces*, **2017**, *9* (10), 8498–8507.
12. Möckl, L.; Müller, A.; Bräuchle, C.; Lindhorst, T. K., Switching first contact: photocontrol of *E. coli* adhesion to human cells. *Chem. Commun.*, **2016**, *52* (6), 1254–1257.
13. Ladmiral, V.; Melia, E.; Haddleton, D. M., Synthetic glycopolymers: an overview. *Eur. Polym. J.*, **2004**, *40* (3), 431–449.
14. Namazi, H.; Sharifzadeh, R., Regioselective synthesis of vinylic derivatives of common monosaccharides through their activated stannylene acetal intermediates. *Molecules*, **2005**, *10* (7), 772–782.

15. Menon, S.; Ongungal, R. M.; Das, S., Photoresponsive glycopolymer aggregates as controlled release systems. *Macromol. Chem. Phys.*, **2014**, *215* (23), 2365–2373.
16. Pearson, S.; Vitucci, D.; Khine, Y. Y.; Dag, A.; Lu, H.; Save, M.; Billon, L.; Stenzel, M. H., Light-responsive azobenzene-based glycopolymer micelles for target drug delivery to melanoma cells. *Eur. Polym. J.*, **2015**, *69*, 616–627.
17. Banghart, M.; Borges, K.; Isacoff, E.; Trauner, D.; Kramer, R. H., Light-activated ion channels for remote control of neuronal firing. *Nat. Neurosci.*, **2004**, *7* (12), 1381–1386.
18. Bonardi, F.; London, G.; Nouwen, N.; Feringa, B. L.; Driessen, A. J., Light-induced control of protein translocation by the SecYEG complex. *Angew. Chem. Int. Ed.*, **2010**, *49* (40), 7234–7238.
19. Stoll, R. S.; Hecht, S., Artificial light-gated catalyst systems. *Angew. Chem. Int. Ed.*, **2010**, *49* (30), 5054–5075.
20. Szymański, W.; Beierle, J. M.; Kistemaker, H. A.; Velema, W. A.; Feringa, B. L., Reversible photocontrol of biological systems by the incorporation of molecular photoswitches. *Chem. Rev.*, **2013**, *113* (8), 6114–6178.
21. Rappsilber, J., The beginning of a beautiful friendship: cross-linking/mass spectrometry and modelling of proteins and multi-protein complexes. *J. Struct. Biol.*, **2011**, *173* (3), 530–540.
22. Zhang, F.; Zarrine-Afsar, A.; Al-Abdul-Wahid, M. S.; Prosser, R. S.; Davidson, A. R.; Woolley, G. A., Structure-based approach to the photocontrol of protein folding. *J. Am. Chem. Soc.*, **2009**, *131* (6), 2283–2289.
23. Müller, A.; Kobarg, H.; Chandrasekaran, V.; Gronow, J.; Sönnichsen, F. D.; Lindhorst, T. K., Synthesis of bifunctional azobenzene glycoconjugates for cysteine-based photosensitive cross-linking with bioactive peptides. *Chem. Eur. J.*, **2015**, *21* (39), 13723–13731.
24. Müller, A.; Lindhorst, T. K., Synthesis of hetero-bifunctional azobenzene glycoconjugates for bioorthogonal cross-linking of proteins. *Eur. J. Org. Chem.*, **2016**, *2016* (9), 1669–1672.



Cite this: *Org. Biomol. Chem.*, 2015, **13**, 2216

Sweetness and light: design and applications of photo-responsive glycoconjugates

Yingxue Hu, Rico F. Tabor and Brendan L. Wilkinson*

Carbohydrate–protein binding is a supramolecular recognition process that underpins myriad biological events. However, the precise conformational and configurational requirements for biomolecular recognition are often poorly understood, since such phenomena often occur in a strongly spatiotemporal manner. Photoswitchable glycoconjugates have emerged as promising investigational tools for probing carbohydrate–protein recognition and for controlling bacterial adhesion. Reversible photoisomerisation, in particular that of azobenzene glycoconjugates, has also been exploited as a promising strategy for controlling supramolecular self-assembly and macroscopic properties, thereby facilitating the development of light responsive carbohydrate-based materials. The following review will highlight the recent advances in the design and applications of photoswitchable glycoconjugates, paying particular attention to the application of light as a stimulus for modulating protein and cellular adhesion, amphiphilicity and supramolecular assembly of carbohydrate-based materials.

Received 29th October 2014,
Accepted 23rd December 2014
DOI: 10.1039/c4ob02296c

www.rsc.org/obc

1. Introduction

The binding of a carbohydrate to its protein receptor is a supramolecular recognition process mediates crucial biological functions.^{1–3} The presentation of a carbohydrate ligand to its cognate receptor is dependent on the correct configurational and conformational arrangement of the ligand, which occurs in a strongly spatiotemporal manner.⁴ Such processes are often poorly understood and have prompted the develop-

ment of stimuli-responsive glycoconjugates for reversibly modulating glycan conformation. Of the stimuli that can be employed, including changes in pH and temperature, light is of particular advantage as it is a ‘clean’ stimulus that requires only photons of a specific wavelength to elicit a molecular response.^{5–7} To this end, various strategies have been reported for controlling the properties of biomolecules using light, such as the irreversible cleavage of light-sensitive protective groups or ‘cages’.^{8–10} The reversible photoisomerisation of photochromic small molecules (or ‘photoswitches’) between at least two photostationary states offers an attractive alternative, as it provides clean, spatiotemporal control over the molecular

*School of Chemistry, Monash University, Victoria 3800, Australia.
E-mail: brendan.wilkinson@monash.edu*



Yingxue Hu

Yingxue received her BEng Degree in Printing Engineering from Hangzhou Dianzi University (China) in 2008. She studied material science at University College London (United Kingdom) where she received her Master of Science with Distinction in 2013. In 2014 she joined the group of Dr Brendan Wilkinson at Monash University (Australia) to conduct her PhD studies. Her research is focused on the synthesis and characterisation of stimuli-responsive carbohydrate materials.



Rico F. Tabor

Rico completed his undergraduate and postgraduate degrees at the University of Bristol, UK, under the supervision of Professor Julian Eastoe. He moved to Australia for a post-doctoral position at the University of Melbourne, before taking up a lectureship at Monash University in 2012. At Monash, Rico started the Soft Materials and Colloids group, whose members research phenomena at the interface of self-assembly and responsive nanomaterials.

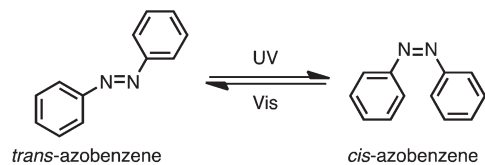


Fig. 1 Reversible *trans*–*cis* photoisomerisation of azobenzene.

structure and properties, and can be cycled many times without loss of function.^{8,11} To date, this strategy has been exploited as a tool for controlling supramolecular assembly processes, probing biomolecular interactions and controlling macroscopic properties of functional materials.¹² Such light-responsive materials have attracted considerable interest as self-healing polymers, optical devices, hydrogels, surfactants, and liquid crystals.

Of the photoswitches available, azobenzene has been the most widely studied.^{13,14} This is not coincidental, as its robust nature, simple synthesis and intense UV-visible absorption properties provide accessible photoswitching wavelengths, and has led to more than a century of study in these dye molecules.¹⁵ Azobenzene undergoes facile and reversible *trans*–*cis* photoisomerisation upon near-UV irradiation, which occurs in high quantum yields and is accompanied by a significant change in molecular geometry (Fig. 1).^{11,16} This results in a large variation in dipole moment: the thermodynamically less stable *cis* isomer exhibits a greater dipole moment ($\mu_{cis} = 3.1$ Debye) than the *trans* isomer ($\mu_{trans} = 0.5$ Debye) and accounts for the hydrophilic and hydrophobic nature of these isomers, respectively.⁸ In addition to the significant geometric changes affecting polarity and spatial orientation of attached groups, the readily accessible covalent modification of azobenzene ring(s) provides a means for fine-tuning electronic properties, and hence photochemistry, which can be tailored to provide a desired response.



Brendan L. Wilkinson

Brendan completed his undergraduate degree and PhD at Griffith University, Brisbane, Australia, under the supervision of Prof. Sally-Ann Poulsen (recently promoted). He moved to the UK to undertake a post-doctoral position at the University of Oxford under the supervision of Professor Antony Fairbanks, and later at The University of Sydney with Associate Professor Richard Payne. Brendan was awarded an ARC fellowship in 2012 and was

later appointed as a lecturer at Monash University. His main research areas are supramolecular assembly of stimuli-responsive carbohydrate and glycopeptide amphiphiles, and dynamic carbohydrate macrocycles with drug delivery applications.

Although receiving less attention than other classes of biomolecules, the covalent modification of carbohydrates with photoswitchable moieties has emerged as an extremely promising strategy for probing the topological requirements for carbohydrate–protein recognition, and as a mechanism for tuning the macroscopic properties of carbohydrate-based materials with precise spatiotemporal control. As such, these smart, sugar-substituted materials have attracted significant interest for their potential as responsive materials with diverse biomedical and technological applications.

This review will highlight the recent advances in this burgeoning area, paying particular attention to the design and application of azobenzene glycoconjugates as photoswitchable lectin inhibitors, amphiphiles and nanomaterials. This review does not aim to provide an exhaustive account of small molecule photoswitches, nor their application for the development of advanced materials, which are subjects of previous, excellent reviews.^{11–13,17}

2. Applications of azobenzene glycoconjugates

2.1 Photoswitchable lectin inhibitors

Carbohydrate–protein interactions are essential for myriad biological functions, yet individual binding interactions are typically weak in water ($K_a < 10^{-3} \text{ M}^{-1}$).¹⁸ In order to enhance binding avidity, multiple copies of carbohydrate ligands are often presented to the receptor for binding, a phenomenon known as the “multivalent effect” or “glycoside cluster effect”.¹⁹ Such interactions display fast binding kinetics and frequently occur at the fluid-membrane interface, suggesting a degree of flexibility and adaptability is required for binding.²⁰ The correct presentation of a carbohydrate ligand to a cognate receptor is a critical aspect of molecular recognition and is often complicated by the three-dimensional shape and orientation of highly branched carbohydrate ligands. In order to improve our understanding of these supramolecular processes, multivalent neoglycoconjugates have been actively pursued as biomolecular probes, antimicrobial drug candidates and biofilm inhibitors.^{21–25} In this respect, photoswitchable glycoconjugates have emerged as particularly promising tools for reversibly modulating the spatial orientation of glycan ligands using light irradiation.^{26–29} In their pioneering work, Jayaraman and co-workers reported the synthesis and photoisomerisation properties of a suite of azobenzene cluster lactosides and mannosides, and measured binding affinities for the high-affinity lectin peanut agglutinin (PNA) and concanavalin A (ConA), respectively.^{28,29} In addition to enhancing the binding avidity relative to monomeric analogues, UV irradiation resulted in a significant change in molecular geometry with a concomitant enhancement in binding affinity compared to the resting *trans* photostationary state.²⁸ Given the relatively short distances between each carbohydrate ligand, a glycoside cluster effect could not be detected. However, a much higher binding constant for the low affinity

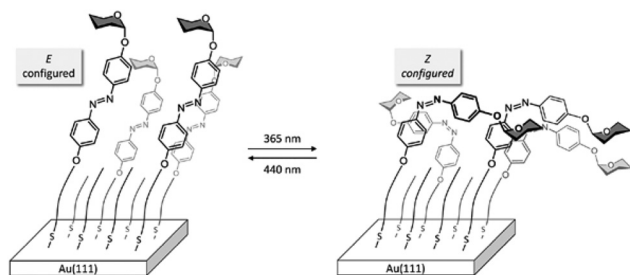


Fig. 2 Fabrication of glyco-SAMs with photoswitchable azobenzene mannosides.³¹ Reproduced with permission from ref. 31. Copyright 2013 Wiley-VCH.

part of the interaction was observed ($K_{b1} = 5.1 \times 10^4 \text{ M}^{-1}$) for the bivalent lactoside analogue compared with the monovalent analogues, suggesting a co-operative effect on ligand binding, which was more pronounced for the *cis*-azobenzene isomer.

The photo-triggered change in glycan conformation has recently been applied for probing the effect of carbohydrate conformation in relation to bacterial adhesion. Lindhorst and co-workers recently reported the synthesis and photo-isomerisation of an azobenzene mannoside and investigated the affinity of the *cis*- and *trans*-azobenzene isomers toward the high-affinity *E. coli* lectin, FimH.³⁰ In this example, FimH was shown to be insensitive to conformational changes in the glycan, with both *cis* and *trans* isomers displaying equal inhibitory potency, with similar IC_{50} values to the well-studied inhibitor, *p*-nitrophenyl α -D-mannoside.

In an effort to probe the spatial requirements for lectin binding at the fluid-surface interface, with a view of controlling cellular adhesion using light,^{12,32} the Lindhorst group have recently reported the fabrication and photoswitching properties of a self-assembled monolayer (SAM) comprising Au(111) nanoparticles immobilised with azobenzene glycosides (Fig. 2).³¹ The *trans*-*cis* photoisomerisation of solid-supported azobenzene glycosides was studied using infrared reflection absorption spectroscopy (IRRAS). Upon photoirradiation of SAMs at 365 nm, a characteristic reduction in intensity of the prominent band at *ca.* 1250 cm^{-1} was observed, which reflected the $C_{\text{aryl}}-O_{\text{Man}}$ stretching frequency. This spectral change was attributed to a change in molecular geometry following photoisomerisation. Conversely, irradiation of the glycoSAM at 440 cm^{-1} resulted in restoration of the absorption band at 1250 cm^{-1} , therefore indicating successful reversion to the *trans* photostationary state. This result demonstrates the feasibility of photoswitching azobenzene glycosides on solid surfaces, and paves the way for the future development of light-controlled glycan arrays for high-throughput diagnostic and screening applications.

Cyclodextrins (CDs) are naturally occurring carbohydrate macrocycles and supramolecular hosts that have found long-term industrial use as excipients and carriers, owing to their ability to form stable host-guest inclusion complexes with hydrophobic guests in water. Both α -CD and β -CD have long been known to form stable host-guest inclusion complexes

with azobenzene guests in aqueous systems, and interestingly, CDs show greater thermodynamic preference for *trans*-azobenzene over *cis*-azobenzene. Recently, CDs have been employed as supramolecular hosts for reversibly binding photoswitchable guests, thus providing a mechanism for attenuating lectin binding and microbial adhesion using light irradiation.

In their recent communication, Jonkheijm and co-workers reported the photocontrolled immobilisation of proteins and bacteria onto β -CD modified surfaces.³³ Supramolecular self-assembled monolayers (SAMs) were prepared by functionalising gold surfaces with amphiphilic β -CD, which served as supramolecular anchor points for a photoswitchable *trans*-azobenzene mannoside (*trans*-Azo-Man) through host-guest inclusion complexation (Fig. 3). Photoisomerisation of the supramolecular SAM provided a trigger for releasing the glyco-conjugate from the inclusion complex, thus releasing it from the surface. The photocontrolled functionalisation of SAMs with *trans*-AzoMan was next employed to attenuate binding affinity to the high affinity lectin ConA. Binding affinities to the functionalised surfaces were quantified using quartz crystal microbalance (QCM) measurements ($K_a = 5.8 \times 10^3 \text{ M}^{-1}$) and were shown to be in good agreement with values obtained in solution using isothermal calorimetry (ITC). The photo-induced assembly of whole *E. coli* cells onto β -CD functionalised SAMs was also performed and visualised using fluorescent microscopy.

The conformational prerequisites for lectin binding have also been investigated using photoswitchable systems employing multivalent scaffolds in bulk solution. Hartmann and co-workers have recently reported the synthesis of mono-disperse, photoswitchable di- and trivalent glycooligomers as multivalent tools for studying lectin binding in solution.³⁴ Glycooligomers were comprised of monosaccharide ligands appended to a polymer, with up to two azobenzene units

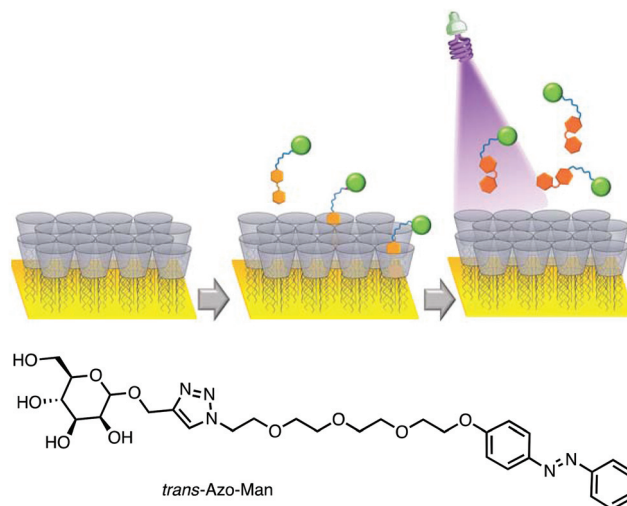


Fig. 3 Photo-controlled functionalisation of a β -CD fabricated SAM.³³ Reproduced with permission from ref. 33. Copyright 2014 Royal Chemical Society.

embedded within the backbone. Photoswitchable glycoligomers were capable of undergoing reversible photoisomerisation to control the intramolecular distance between carbohydrate ligands, and hence the binding affinity to lectins with multiple binding domains. The relative binding affinities of the *cis*- and *trans*-azobenzene configured oligomers varied considerably ($IC_{50}[\text{AZO-Gal}(1,3)\text{-}3\text{ E}] = 5.7\ \mu\text{M}$, $IC_{50}[\text{AZO-Gal}(1,3)\text{-}3\text{ PSS}] = 9.4\ \mu\text{M}$, $IC_{50}[\text{AZO-Gal}(1,3,5)\text{-}5\text{ E}] = 3.4\ \mu\text{M}$, $IC_{50}[\text{AZO-Gal}(1,3,5)\text{-}5\text{ PSS}] = 4.1\ \mu\text{M}$), demonstrating the capability of light for controlling the conformational dynamics of multivalent glycoconjugates in order to probe carbohydrate–protein recognition.

Protein immobilisation using azobenzene glycosides has also been reported using photoswitchable supramolecular ternary complexes. Recently, Jan Ravoo and colleagues reported the phototriggered release of lectins from self-assembled ternary complexes (Fig. 4).³⁵ These ternary complexes consisted of azobenzene lactosides non-covalently bound through host–guest inclusion complexation to multiple cyclodextrin (CD) hosts presented on a self-assembled bilayer vesicle. In this manner, the multivalent presentation of an azobenzene lactoside (G1) and maltoside (G2) facilitated immobilisation of the respective lectin protein, thus promoting self-assembly of the respective photoswitchable multilamellar complex. The binding affinity of supramolecular complexes to the lectin was quantified using isothermal titration calorimetry (ITC) ($K_{aG1} = 8.42 \times 10^3\ \text{M}^{-1}$, $K_{aG2} = 8.43 \times 10^3\ \text{M}^{-1}$). UV irradiation resulted in a *trans*–*cis* photoisomerisation of the azobenzene linker, thus triggering its release from

the CD host with concomitant disaggregation of the supramolecular complex, thus releasing the protein. Furthermore, the photochemical control of lectin binding was shown to be fully reversible, as demonstrated by UV/Vis spectroscopy, dynamic light scattering and transmission electron microscopy techniques.

2.2 Photoswitchable hydrogelators

Glycolipids are ubiquitous natural products comprising a polar carbohydrate head group and hydrophobic tail group. They mediate a number of key biological processes, including membrane formation, immune regulation and microbial infection.³⁶ Amphiphilic carbohydrates have found widespread industrial application, owing to their favourable biocompatibility and physicochemical properties. Carbohydrates are powerful polar head groups as they are abundant natural products endowed with rich stereochemical diversity and functionality, providing access to a virtually unlimited number of designer materials with tailored colloidal properties. The supramolecular assembly and self-organization of carbohydrate amphiphiles in water gives rise to diverse functional materials, such as hydrogels, surfactants and liquid crystals.³⁷ The coupling of carbohydrate head groups to hydrophobic azobenzene tail groups is a recent but exciting development in the field, since it gives rise to photoresponsive systems for reversibly modulating key colloidal properties such as aggregation, viscosity and phase stability. The azobenzene moiety delivers a strong driving force for aggregation in water through both hydrophobic attractions and π – π stacking interactions, providing also a mechanism for controlling amphiphilicity *via trans*–*cis* isomerisation.

Carbohydrate hydrogelators are low molecular weight amphiphiles that undergo hierarchical self-assembly through non-covalent interactions in water, such as hydrogen bonding, π – π stacking and van der Waals interactions. Their spontaneous self-assembly gives rise to complex, entangled networks of nanofibers, sheets, bundles, *etc.*, with the hydrophilic carbohydrate exposed at the surface. Since the early work of Reinhoudt and Shinkai, who described the first ‘super’ hydrogelator incorporating an azobenzene tail and sugar head groups, there has been considerable interest in the application of light for controlling gel–sol transitions of photoswitchable carbohydrate hydrogelators.³⁸ As the gelation ability of such materials is influenced by photoinduced *trans*–*cis* photoisomerisation, this allows for precise control over gelation, molecular aggregation and morphological properties.^{39,40}

Kitaoka and colleagues have recently reported the self-assembly of a panel of hydrogelators based on a variable disaccharide lactone head group appended to azobenzene and a glycine spacer.¹⁸ The carbohydrate hydrogelators were shown to spontaneously self-assemble in water to provide entangled helical nanofibres, which were subsequently utilised as a biomimetic scaffold for lectin binding and cell adhesion studies. Partial photoisomerisation resulted in a gel–sol transition, resulting in ‘chopping’ of long fibres to give short nanofibres. The photochemical control of gel–sol and sol–gel transitions

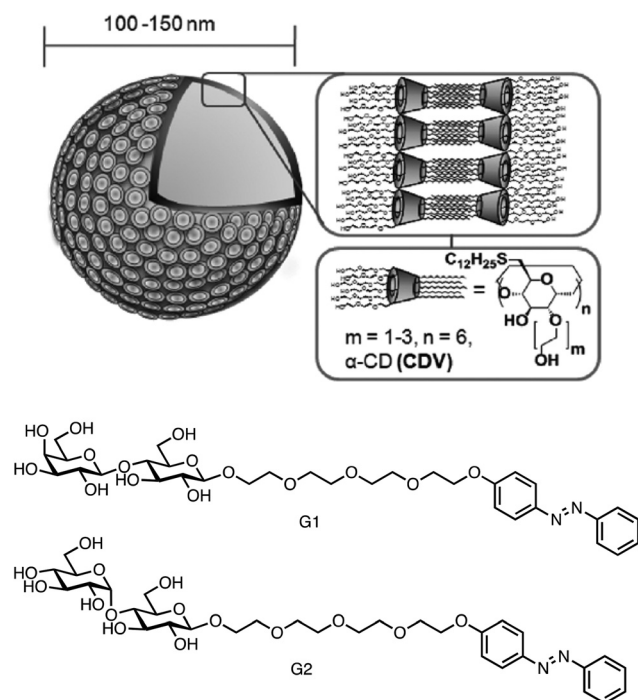


Fig. 4 Photocontrolled lectin binding of supramolecular ternary complex.³⁵ Reproduced with permission from ref. 35. Copyright 2012 American Chemical Society.

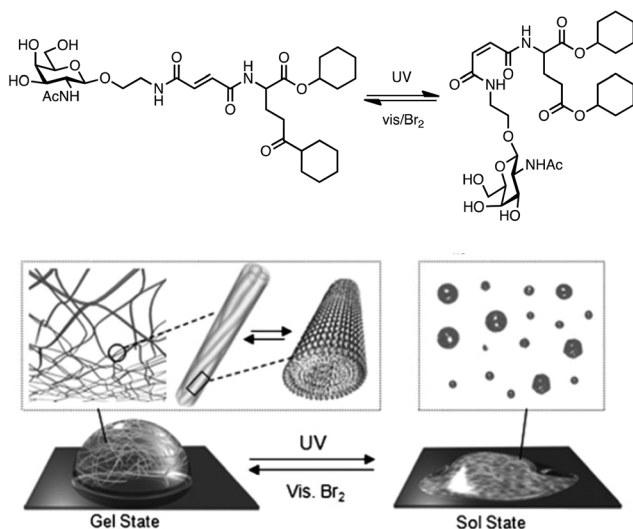


Fig. 5 Reversible gel–sol transition of hydrogel induced by UV/Vis irradiation.⁴¹ Reproduced with permission from ref. 41. Copyright 2008 Wiley-VCH.

has also recently been demonstrated to facilitate selective removal of aromatic solvents from aqueous emulsions, making these photo-addressable molecules attractive biomaterials for environmental remediation.³⁹

By adopting a similar strategy, Hamachi and colleagues reported the synthesis of a library of fumaric diamide glycosides as photoresponsive hydrogelators (Fig. 5).⁴¹ The glycosides were comprised of variable carbohydrate head groups linked to a hydrophobic alkyl tail, which incorporated a photo-switchable fumaric diamide unit. Hierarchical self-assembly of *trans* configured monomers gave rise to hydrogels consisting of extended fibrous networks, which was shown to be strongly dependent on the carbohydrate head group, linker and tail group.⁴¹ Irradiation of hydrogels with UV light resulted in partial isomerisation from the *trans* fumaric diamide to the *cis* maleic diamide form (>50%). The resulting bent molecular geometry caused significant disruption to the hydrogen-bonded network, thus triggering disassociation to result in a gel–sol transition. The gel–sol transition was reversed by irradiation with visible light in the presence of bromine. Subsequent studies focused on the use of an *N*-acetylglucosamine-based hydrogel (Fig. 5) possessing a bis-cyclohexyl tail, as it was shown to provide transparent and shear-stable hydrogels.

2.3 Photoswitchable surfactants

Carbohydrate-based surfactants of synthetic and natural origin are widely studied amphiphilic materials that combine a hydrophilic carbohydrate head group and a hydrophobic/lipid tail group. Such materials have been shown to give rise to diverse self-assemblies and colloidal structures in aqueous solvents, such as micelles, vesicles, foams and emulsions, *etc.*^{42,43} Carbohydrates of various size, hydrophilicity and stereochemical configuration provide virtually unlimited options for fine

tuning surface and aggregation properties to derive surfactants with tailored geometries, properties and applications.

Len and co-workers have recently reported a photoswitchable carbohydrate-based surfactant comprising a sodium glucuronate head group coupled to a butylazobenzene tail.⁴⁴ In this study, the authors demonstrated the phototriggered self-assembly of micelles to facilitate compartmentalisation and solubilisation of hydrophobic organic molecules in water. Surfactant micelles were shown to facilitate acylation of hydrophobic amines in water, with similar efficiency to the well-studied surfactant, sodium dodecyl sulfate.

Despite their promising potential, the development and application of photoswitchable, water-soluble carbohydrate-based surfactants has received less attention compared to other classes of carbohydrate amphiphile, with only one example appearing in the literature to date.⁴⁴ This may result from the challenges involved in their synthesis or deployment within colloidal systems, as attempting to couple the azobenzene chromophore to conventional tail-group chemistries can result in water-insoluble materials that find limited application.

In order to facilitate the first structure-function investigation of water-soluble, photoresponsive carbohydrate-based surfactants, we recently reported the parallel synthesis of a library of dual pH- and photoswitchable carbohydrate-based surfactants and examined their surface and aggregation properties (Fig. 6).^{45,46} Using a modular synthetic strategy, carbohydrates of variable size and hydrophilicity, including a pH-sensitive glucuronic acid head group, were introduced onto a butylazobenzene tail group, and the resulting surfactants characterized using small-angled neutron scattering (SANS), tensiometry and UV-visible spectroscopy. A profound effect of carbohydrate choice on surfactancy, aggregation number and morphology was revealed, with micellar structures ranging from near-spherical to extended cylindrical geometries.

In recent work, our group has studied the structural evolution of micelle size and composition by time resolved SANS (TR-SANS).⁴⁶ In this study, we identified three distinct micelle behaviours at, near and well above the CMC. Photo-

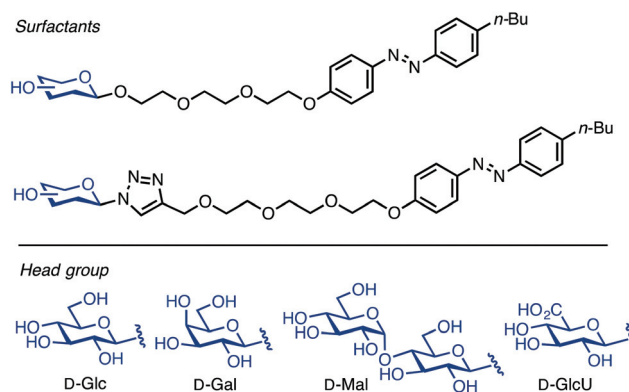


Fig. 6 Photo-switchable carbohydrate-based surfactants.⁴⁵ Adapted with permission from ref. 45. Copyright 2014 Wiley-VCH.

isomerisation to the *cis* form at surfactant concentrations just above the CMC resulted in complete disaggregation; however, when the concentration was increased slightly, a rod→sphere transition was observed. Finally, when the concentration was well above the CMC, photoisomerisation resulted in a pronounced thinning of cylindrical or ‘rod-like’ micelles. As rod-like micelles are well known for increasing solution viscosity and providing solution structure, these observations have clear implications for the design of photorheological fluids for drilling and energy applications.

2.4 Liquid crystals

A vast number of glycolipids in nature exhibit thermotropic and lyotropic liquid crystal (LC) phases, owing to their softness and self-organising properties.^{47,48} Such properties are believed to confer structural fluidity and adaptability to biological membranes and directly influence their biological properties. Carbohydrates are attractive mesogens for forming LC phases, owing to their high natural abundance, structural diversity, low toxicity and potential to form chiral nanostructures. Carbohydrate LCs have therefore emerged as promising tools for correlating mesophase behavior with biological activity, and for their wide-reaching technological applications.

Azobenzene has been widely used as a mesogen and a photoswitchable chromophore for controlling LC phase behaviour.^{49–51} The addition of the azobenzene chromophore serves to enrich LC phase behaviour, as the π -stacking characteristics have been shown to facilitate a range of smectic, nematic, lamellar and conic LC phases.⁵² A number of groups have reported the synthesis and properties of amphiphilic LCs consisting of carbohydrates conjugated to azobenzene (Fig. 7a–c).^{53–55} In their early work, Goodby and co-workers reported the synthesis and thermotropic LC properties of a panel of amphiphilic azobenzene glycosides (Fig. 7a),⁵³ prepared with various carbohydrates that acted as hydrophilic, microphase segregating and biocompatible head groups. The thermotropic LC properties of the amphiphilic glycosides were investigated using polarised light microscopy, differential scanning calorimetry (DSC) and X-ray diffraction. From this study, achiral smectic lamellar LC-phases were observed, with the only exception being the *D*-gluco configured analogue, which curiously exhibited an achiral lamellar LC phase.

Although carbohydrates possess an abundance of chiral centres, carbohydrate LCs incorporating azobenzene mesogens generally display achiral smectic and lamellar phases and do not normally exhibit chiral macroscopic phases. This is believed to arise from the strong hydrogen bonding between carbohydrate head groups, resulting in layered, head-to-head orientations. Although the disruption of such networks can be achieved by site-selective functionalisation of the head group, this can result in a pronounced loss of amphiphilicity and LC properties. Jayaraman and Das have reported the chiral LC phase of a series of azobenzene bolaamphiphile comprising unmodified *D*-glucose head groups linked to an azobenzene core *via* alkyl spacers of variable length (Fig. 7c).⁵⁵ The LC pro-

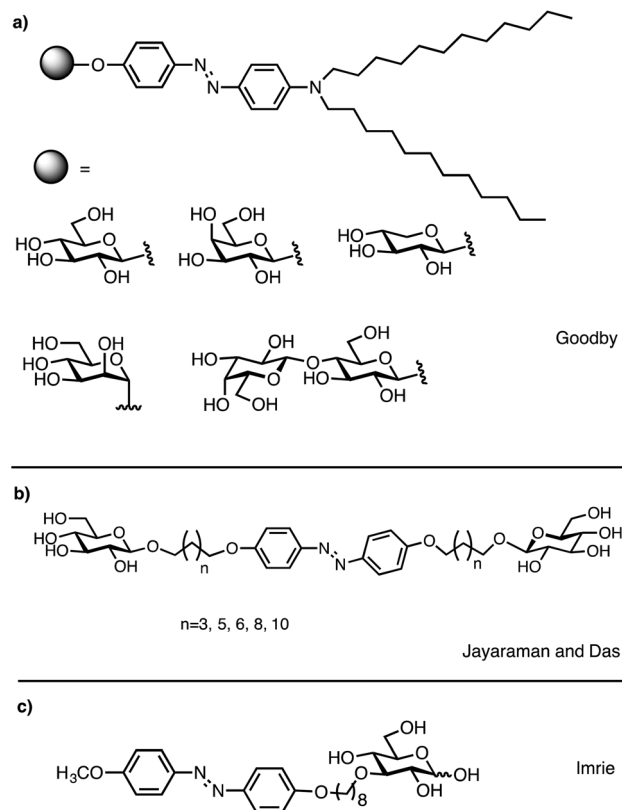


Fig. 7 Carbohydrate LCs containing azobenzene mesogens.^{53–55} Adapted with permission from ref. 53–55. Copyright 2003 American Chemical Society, 2012 Elsevier and 2005 Wiley-VCH.

erties of these amphiphiles were studied using polarised light microscopy, DSC and small-angle X-ray scattering. From this study, a number of bolaamphiphiles were discovered that displayed chiral smectic LC phases, a behaviour that was dependent on the positioning of the azobenzene and length of the spacer group.

Recently, Imrie and co-workers reported the synthesis and LC properties of an amphiphilic azobenzene glycoconjugate (Fig. 7c).⁵⁴ The amphiphile exhibited glassy behaviour and an interdigitated smectic A phase. The hydrogen bonding strength during both glass and smectic A-isotropic transitions was determined using variable temperature infrared spectroscopy and revealed no marked change from either the glass or smectic A-isotropic phase transition. This suggests that the smectic A-isotropic transition was dominated by van der Waals interactions, with hydrogen bonding persisting into the isotropic phase.

It is clear that the combination of azobenzene and carbohydrate mesogens allows for rich and varied LC properties. However, despite the demonstrated potential for controlling LC phase behaviour using light,⁴⁹ the application of this strategy for controlling LC phase behaviour of carbohydrate LCs is yet to be realised, thus presenting exciting opportunities for the future development of photoresponsive, biocompatible colloids.

2.5 Photoswitchable cyclodextrins

The application of an external stimulus for controlling the conformation and dynamics of supramolecular and molecular systems has also gained considerable interest in nanoscience and technology. Light has emerged as particularly useful stimulus for triggering and controlling conformation, which can be further coupled to changes in the physicochemical properties of the material. In the previous section, we described the recent applications of photoswitchable CD host-guest complexes for attenuating lectin binding and microbial adhesion. Reversible *trans-cis* photoisomerisation of intermolecular azobenzene-CD inclusion complexes has also been widely exploited for modulating binding affinity in order to control supramolecular assembly processes.^{56–59} Such intermolecular host-guest strategies have shown great potential for the development of functional nanodevices and materials, including amphiphilic, tuneable delivery vectors and molecular machines. Such approaches are the subjects of some recent reviews.^{60–62}

On the other hand, intramolecular host-guest complexes comprising photoswitchable guests covalently attached to the CD ring have emerged as promising materials for accessing light-controlled supramolecular assemblies, including threaded rotaxanes and pseudorotaxanes. Early applications of photoswitchable CDs focused on their use as photoswitchable sensors for low molecular weight organic molecules in water.^{63,64} However, the burgeoning fields of nanoscience and technology have stimulated renewed interest in the application of light for controlling supramolecular assembly through intramolecular host-guest inclusion complexation^{58,65} and this has paved the way for the development of light-responsive assemblies with promising applications as molecular scale machines,^{66,67} switches,⁶⁵ electronics⁶⁸ and gated ion channels.⁶⁹

Work from the Harada group has provided several noteworthy examples where supramolecular assembly is controlled using photoswitchable CDs, in particular azobenzene and stilbene-conjugated CDs using light.^{56,70,71} In an early example, a dual thermo- and light-responsive azobenzene CD complex was reported, which comprised a CD host covalently appended to a hydrocinnamoyl linker *via* a polyethylene glycol spacer that was terminated with an azobenzene host (Fig. 8).⁷⁰ The host-guest complexation of both *cis*- and *trans*-azobenzene isomers was measured using 2D ROESY NMR spectroscopy. The *trans*-configured complex was shown to form a threaded, self-inclusion complex at 60 °C, whereby the CD cavity alternately binds *trans*-azobenzene and the hydrocinnamoyl linker, respectively. This inclusion complexation behaviour of the *trans*-configured complex was also shown to be temperature and concentration dependent. Competing intermolecular host-guest inclusion complexation was observed at higher concentrations, giving rise to threaded rotaxane formation. Such behaviour was not mirrored for the corresponding *cis*-photo-stationary state, which provided only threaded self-inclusion complexes. More recently, the authors reported the application



Fig. 8 Proposed conformational changes of 6-Az-PEG600-HyCiO- β -CD in aqueous solution using temperature and light.⁷⁰ Reproduced with permission from ref. 70. Copyright 2007 American Chemical Society.

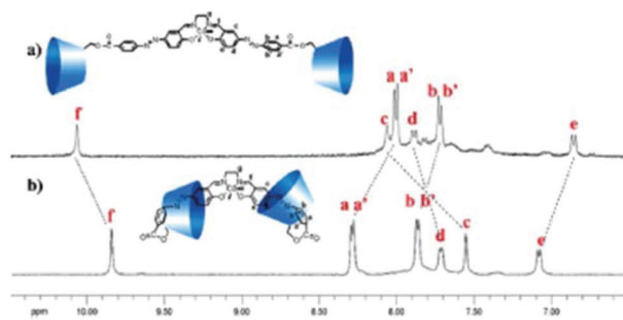


Fig. 9 A supramolecular 'stretch-contract' system based on photo-controlled [1]rotaxane formation.⁶⁷ Reproduced from ref. 67. Copyright 2011 Royal Society of Chemistry.

of *trans-cis* photoisomerisation of CD-stilbene complexes for controlling conformation and supramolecular assembly.⁷² Such molecules were shown to undergo broad changes in conformation and host-guest binding on photoisomerisation, leading to a diverse range of threaded and non-threaded supramolecular assemblies.

Recently, Tian and co-workers have reported the synthesis and light-driven supramolecular assembly of a symmetric [1]rotaxane (Fig. 9).⁶⁷ The switchable supramolecular system was comprised on an azobenzene-modified CD dimer bridged by a Co(III) Schiff-base complex. The conformation of the metal coordinated complex was determined before and after UV irradiation. ¹H NMR and induced circular dichroism (ICD) spectroscopy were employed to investigate the movement of the 'stretch-contraction' supramolecular system. This study demonstrated the potential for combining host-guest complexation and metal ion coordination for modulating the geometry of light-responsive supramolecular assemblies.

Gin and co-workers have reported a light-controlled gated ion channel employing intramolecular host-guest inclusion complexation (Fig. 10).⁶⁹ To this end, azobenzene was linked to the secondary β -CD face, while multiple hydrophobic alkyl

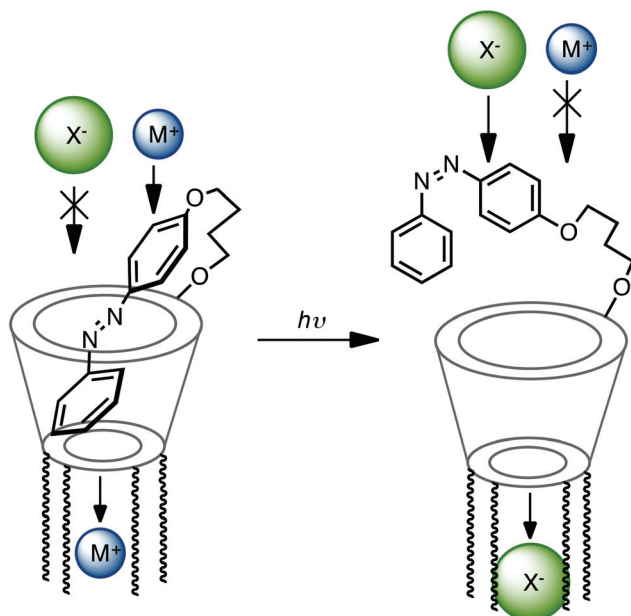


Fig. 10 A light-controlled gated ion channel as reported by Gin and co-workers.⁶⁹ Adapted with permission from ref. 69. Copyright 2008 American Chemical Society.

tail groups were attached to primary face to mimic the lipid membrane portion of the channel. UV irradiation of the tethered *trans*-azobenzene resulted in *trans*-*cis* isomerisation, thus triggering conversion of the threaded self-inclusion complex to give a dissociated structure. In this manner, the self-inclusion complex incorporating the *trans*-azobenzene guest represented the 'closed' gate and the dissociated *cis*-azobenzene complex represented the 'open' gate. Using UV irradiation to trigger this response resulted in an increase in transport of anions with a concomitant reduction in transport of cations, as determined by a pH-dependent fluorescent assay.

There is considerable interest in the development of molecular scale devices capable of performing information processing, owing to their potential applications as nano-computers and electronics. The development of sophisticated molecular scale devices capable of performing Boolean logic gates (AND, OR, NAND, *etc.*) has long been the primary goal in the field, with many such systems now being realised. To date, such supramolecular systems employ stimulus-responsive rotaxanes and pseudorotaxanes that respond to an external stimulus by changing molecular conformation, producing a recognisable output signal such as fluorescence, UV-visible absorption, circular dichroism, *etc.* Tian and co-workers have recently reported the INHIBIT logic operations of a photoswitchable β -CD pseudo[1]rotaxane using room temperature phosphorescence (RTP) and induced circular dichroism (ICD) output addresses.⁶⁸ To this end, the threaded pseudo[1]rotaxane was obtained by conjugating an azobenzene chromophore to β -CD in water, forming a threaded self-inclusion complex. UV irradiation of the threaded pseudo[1]rotaxane resulted in *trans*-*cis* isomerisation of the azobenzene guest to give rise to

a de-threaded complex. The reversible threading and de-threading process was addressed using ICD and RTP as outputs, which were coupled to various input stimuli including UV irradiation, temperature, oxygen purging and competing host-guest complexation with phosphor bromonaphthalene (α -BrNp), to derive a simple molecular device capable of INHIBIT molecular logic functions.

3. Conclusions and future directions

Carbohydrate-protein interactions mediate essential cellular communication events, yet the conformational and configurational basis of these supramolecular interactions is often poorly understood. Such challenges have prompted the development of photoswitchable glycoconjugates for controlling molecular conformation and configuration in a spatially and temporally resolved manner. Such light-controlled tools have enabled investigations into the structural dynamics of carbohydrate-protein binding with good spatiotemporal control. To date, this strategy has been applied for the photocontrolled immobilisation of lectins and whole cells in solution, or at the liquid-surface interface.

Looking to the future, it is anticipated that this strategy will find broad application in high-throughput screening of carbohydrate-protein interactions, particularly in microarray format, for diagnostic and drug development purposes. Reversible photoisomerisation has also emerged as an extremely promising strategy for controlling supramolecular assembly and triggering changes in the macroscopic properties of biocompatible materials, including responsive sugar surfactants and hydrogels. The photocontrolled host-guest inclusion complexation of azobenzene and stilbene guests covalently bound to CD hosts is a promising route to responsive supramolecular assemblies with exciting technological applications, for example as molecular scale machines, computers and electronics. The combination of typically hydrophobic photoisomerisable moieties with hydrophilic carbohydrates offers a vast range of potential amphiphiles with rich, complex and stimulus-responsive adsorption and aggregation properties. An underexplored avenue in this area is the application of photoisomerisation for controlling the phase behaviour of carbohydrate LCs, and this presents opportunities for the development of new, light-responsive, carbohydrate-based LCs and biocompatible colloids.

Acknowledgements

The authors would like to thank the Australian Research Council for funding (DE130101673 and DP140100677).

Notes and references

- 1 L. L. Kiessling and R. A. Splain, *Annu. Rev. Biochem.*, 2010, **79**, 619-653.

- 2 C. D. Rillahan and J. C. Paulson, *Annu. Rev. Biochem.*, 2011, **80**, 797.
- 3 J. E. Hudak, S. M. Canham and C. R. Bertozzi, *Nat. Chem. Biol.*, 2013, **10**, 69–75.
- 4 H.-J. Gabius, S. André, J. Jiménez-Barbero, A. Romero and D. Solís, *Trends Biochem. Sci.*, 2011, **36**, 298–313.
- 5 Y. Huang, R. Dong, X. Zhu and D. Yan, *Soft Matter*, 2014, **10**, 6121–6138.
- 6 X.-M. Liu, B. Yang, Y.-L. Wang and J.-Y. Wang, *Chem. Mater.*, 2005, **17**, 2792–2795.
- 7 V. Chandrasekaran, E. Johannes, H. Kobarg, F. D. Sönnichsen and T. K. Lindhorst, *ChemistryOpen*, 2014, **3**, 99–108.
- 8 F. Hamon, F. Djedaini-Pilard, F. Barbot and C. Len, *Tetrahedron*, 2009, **65**, 10105–10123.
- 9 G. C. Ellis-Davies, *Nat. Methods*, 2007, **4**, 619–628.
- 10 H.-M. Lee, D. R. Larson and D. S. Lawrence, *ACS Chem. Biol.*, 2009, **4**, 409–427.
- 11 A. A. Beharry and G. A. Woolley, *Chem. Soc. Rev.*, 2011, **40**, 4422–4437.
- 12 M. M. Russew and S. Hecht, *Adv. Mater.*, 2010, **22**, 3348–3360.
- 13 C. Brieke, F. Rohrbach, A. Gottschalk, G. Mayer and A. Heckel, *Angew. Chem., Int. Ed.*, 2012, **51**, 8446–8476.
- 14 H. Suginome, in *CRC Handbook of Organic Photochemistry and Photobiology*, ed. W. M. Horspool and P.-S. Song, CRC Press, Boca Raton, FL, 1995, pp. 824–840.
- 15 M. Christie, in *Colour chemistry*, Royal Society of Chemistry, Cambridge, 2001, vol. 1, ch. 3, pp. 45–68.
- 16 H. D. Bandara, T. R. Friss, M. M. Enriquez, W. Isley, C. Incarvito, H. A. Frank, J. Gascon and S. C. Burdette, *J. Org. Chem.*, 2010, **75**, 4817–4827.
- 17 C. Dugave and L. Demange, *Chem. Rev.*, 2003, **103**, 2475–2532.
- 18 Y. Ogawa, C. Yoshiyama and T. Kitaoka, *Langmuir*, 2012, **28**, 4404–4412.
- 19 R. T. Lee and Y. C. Lee, *Glycoconjugate J.*, 2000, **17**, 543–551.
- 20 J. M. Belitsky, A. Nelson, J. D. Hernandez, L. G. Baum and J. F. Stoddart, *Chem. Biol.*, 2007, **14**, 1140–1151.
- 21 J. L. J. Blanco, C. O. Mellet and J. M. G. Fernández, *Chem. Soc. Rev.*, 2013, **42**, 4518–4531.
- 22 K.-R. Wang, H.-W. An, Y.-Q. Wang, J.-C. Zhang and X.-L. Li, *Org. Biomol. Chem.*, 2013, **11**, 1007–1012.
- 23 B. Thomas, M. Fiore, G. C. Daskhan, N. Spinelli and O. Renaudet, *Chem. Commun.*, 2015, DOI: 10.1039/C4CC05451B.
- 24 J. Sebestik, P. Niederhafner and J. Ježek, *Amino Acids*, 2011, **40**, 301–370.
- 25 P. Niederhafner, J. Šebestik and J. Ježek, *J. Pept. Sci.*, 2008, **14**, 44–65.
- 26 V. Chandrasekaran and T. K. Lindhorst, *Chem. Commun.*, 2012, **48**, 7519–7521.
- 27 J. Robertus, W. R. Browne and B. L. Feringa, *Chem. Soc. Rev.*, 2010, **39**, 354–378.
- 28 N. M. Oruganti Srinivas, A. Surolia and N. Jayaraman, *J. Am. Chem. Soc.*, 2002, **124**, 2124–2125.
- 29 O. Srinivas, N. Mitra, A. Surolia and N. Jayaraman, *Glycobiology*, 2005, **15**, 861–873.
- 30 V. Chandrasekaran, K. Kolbe, F. Beiroth and T. K. Lindhorst, *Beilstein J. Org. Chem.*, 2013, **9**, 223–233.
- 31 V. Chandrasekaran, H. Jacob, F. Petersen, K. Kathirvel, F. Tuczek and T. K. Lindhorst, *Chem. – Eur. J.*, 2014, **20**, 8744–8752.
- 32 D. Liu, Y. Xie, H. Shao and X. Jiang, *Angew. Chem., Int. Ed.*, 2009, **48**, 4406–4408.
- 33 J. Voskuhl, S. Sankaran and P. Jonkheijm, *Chem. Commun.*, 2014, **50**, 15144–15147.
- 34 D. Ponader, S. Igde, M. Wehle, K. Märker, M. Santer, D. Bléger and L. Hartmann, *Beilstein J. Org. Chem.*, 2014, **10**, 1603–1612.
- 35 A. Samanta, M. C. Stuart and B. J. Ravoo, *J. Am. Chem. Soc.*, 2012, **134**, 19909–19914.
- 36 Y. Gu, R. LaBell, D. F. O'Brien and S. S. Saavedra, *Angew. Chem., Int. Ed.*, 2001, **40**, 2320–2322.
- 37 M. Sano, M. Amaike, A. Kamino and S. Shinkai, *Langmuir*, 2001, **17**, 4367–4371.
- 38 H. Kobayashi, A. Friggeri, K. Koumoto, M. Amaike, S. Shinkai and D. N. Reinhoudt, *Org. Lett.*, 2002, **4**, 1423–1426.
- 39 R. Rajaganesh, A. Gopal, T. Mohan Das and A. Ajayaghosh, *Org. Lett.*, 2012, **14**, 748–751.
- 40 S. S. Babu, V. K. Praveen and A. Ajayaghosh, *Chem. Rev.*, 2014, **114**, 1973–2129.
- 41 S. Matsumoto, S. Yamaguchi, S. Ueno, H. Komatsu, M. Ikeda, K. Ishizuka, Y. Iko, K. V. Tabata, H. Aoki, S. Ito, H. Noji and I. Hamachi, *Chem. – Eur. J.*, 2008, **14**, 3977–3986.
- 42 S. Savic, S. Tamburic and M. M. Savic, *Expert Opin. Drug Delivery*, 2010, **7**, 353–369.
- 43 (a) P. Andreozzi, G. Gente and C. La Mesa, in *Sugar based surfactants: fundamentals and applications*, ed. C. C. Ruiz, CRC Press, Boca Raton, FL, 2008, ch. 2, pp. 21–55; (b) J. Barker, in *Catalyst Deactivation*, ed. B. Delmon and C. Froment, Elsevier, Amsterdam, 2nd edn., 1987, vol. 1, ch. 4, pp. 253–255.
- 44 N. Drillaud, E. Banaszak-Léonard, I. Pezron and C. Len, *J. Org. Chem.*, 2012, **77**, 9553–9561.
- 45 R. F. Tabor, D. D. Tan, S. S. Han, S. A. Young, Z. L. Seeger, M. J. Pottage, C. J. Garvey and B. L. Wilkinson, *Chem. – Eur. J.*, 2014, **20**, 13881–13884.
- 46 R. F. Tabor, M. J. Pottage, C. J. Garvey and B. L. Wilkinson, *Chem. Commun.*, 2015, DOI: 10.1039/C4CC07657E.
- 47 W. Pfannemüller, E. Chin and J. Goodby, *Liq. Cryst.*, 1986, **1**, 357–370.
- 48 J. Goodby, V. Görtz, S. Cowling, G. Mackenzie, P. Martin, D. Plusquellec, T. Benvegno, P. Boullanger, D. Lafont and Y. Queneau, *Chem. Soc. Rev.*, 2007, **36**, 1971–2032.
- 49 T. Ikeda and O. Tsutsumi, *Science*, 1995, **268**, 1873–1875.
- 50 R. P. Lemieux, *Soft Matter*, 2005, **1**, 348–354.
- 51 M. L. Rahman, M. M. Yusoff and S. Kumar, *RSC Adv.*, 2014, **4**, 35089–35098.

- 52 Y. Zakrevskyy, M. Richter, S. Zakrevska, N. Lomadze, R. von Klitzing and S. Santer, *Adv. Funct. Mater.*, 2012, **22**, 5000–5009.
- 53 N. Laurent, D. Lafont, F. Dumoulin, P. Boullanger, G. Mackenzie, P. H. Kouwer and J. W. Goodby, *J. Am. Chem. Soc.*, 2003, **125**, 15499–15506.
- 54 A. G. Cook, J. L. Wardell, N. J. Brooks, J. M. Seddon, A. Martínez-Felipe and C. T. Imrie, *Carbohydr. Res.*, 2012, **360**, 78–83.
- 55 S. Abraham, S. Paul, G. Narayan, S. K. Prasad, D. S. Rao, N. Jayaraman and S. Das, *Adv. Funct. Mater.*, 2005, **15**, 1579–1584.
- 56 I. Tomatsu, A. Hashidzume and A. Harada, *Macromolecules*, 2005, **38**, 5223–5227.
- 57 X. Liao, G. Chen, X. Liu, W. Chen, F. Chen and M. Jiang, *Angew. Chem., Int. Ed.*, 2010, **122**, 4511–4515.
- 58 Y. Liu, Y.-L. Zhao, H.-Y. Zhang, Z. Fan, G.-D. Wen and F. Ding, *J. Phys. Chem. B*, 2004, **108**, 8836–8843.
- 59 G. Chen and M. Jiang, *Chem. Soc. Rev.*, 2011, **40**, 2254–2266.
- 60 D. P. Ferris, Y.-L. Zhao, N. M. Khashab, H. A. Khatib, J. F. Stoddart and J. I. Zink, *J. Am. Chem. Soc.*, 2009, **131**, 1686–1688.
- 61 A. Hashidzume, H. Yamaguchi and A. Harada, *Acc. Chem. Res.*, 2014, **47**, 2128–2140.
- 62 W. Shi, J. Deng, H. Qin, D. Wang and C. Zhao, *J. Membr. Sci.*, 2014, **455**, 357–367.
- 63 A. Ueno, H. Yoshimura, R. Saka and T. Osa, *J. Am. Chem. Soc.*, 1979, **101**, 2779–2780.
- 64 A. Ueno, T. Kuwabara, A. Nakamura and F. Toda, *Nature*, 1992, **356**, 136–137.
- 65 Y. Liu, S. Kang, Y. Chen, Y.-W. Yang and J. Huskens, *J. Inclusion Phenom. Macrocyclic Chem.*, 2006, **56**, 197–201.
- 66 Y. Liu, Z.-X. Yang and Y. Chen, *J. Org. Chem.*, 2008, **73**, 5298–5304.
- 67 C. Gao, X. Ma, Q. Zhang, Q. Wang, D. Qu and H. Tian, *Org. Biomol. Chem.*, 2011, **9**, 1126–1132.
- 68 J. Cao, X. Ma, M. Min, T. Cao, S. Wu and H. Tian, *Chem. Commun.*, 2014, **50**, 3224–3226.
- 69 P. V. Jog and M. S. Gin, *Org. Lett.*, 2008, **10**, 3693–3696.
- 70 Y. Inoue, P. Kuad, Y. Okumura, Y. Takashima, H. Yamaguchi and A. Harada, *J. Am. Chem. Soc.*, 2007, **129**, 6396–6397.
- 71 A. Harada and M. Kamachi, *Macromolecules*, 1990, **23**, 2821–2823.
- 72 K. Yamauchi, Y. Takashima, A. Hashidzume, H. Yamaguchi and A. Harada, *J. Am. Chem. Soc.*, 2008, **130**, 5024–5025.

Chapter 2

Carbohydrate-based Surfactants and Fluorosurfactants as Photocontrollable Inhibitors of Ice Recrystallization

This page is intentionally blank

Declaration for Thesis Chapter 2

Declaration by candidate

For Chapter 2, the nature and extent of my contribution to this work was as following:

Nature of contribution	Extent of contribution (%)
Conception and execution of experiments, synthesis and characterization of products, analysis of results, writing up	55

The following co-workers contributed to the work and the extent of their contribution in percentage terms was stated:

Name	Contribution	Extent of contribution (%) for student co-workers only
M. K. Adam J. S. Poisson	Anti-freeze and cytotoxicity assays	30
J. B. Marlow	Physical characterization	7
Wenyue Zou Rajesh Ramanathan	Antibacterial assays for fluorosurfactants section	5
Hui Geok Tiew Geethika Prasannakumar Mathew J. Pottage	Assisted in experimentation	3
Brendan L. Wilkinson Rico F. Tabor Robert N. Ben Vipul Bansal	Initiation and key ideas	

The undersigned hereby certify that the above declaration correctly reflects the nature and extent of the candidate's and co-workers' contributions to this work.

**Candidate's
Signature**



Date

12 June 2017

**Main
Supervisor's
Signature**



Date

13th June 2017

This page is intentionally blank

Carbohydrate-based surfactants and fluorosurfactants as photocontrollable inhibitors of ice recrystallization

This chapter is an expanded version of the following articles:

- **Hu, Y.**; Marlow, J. B.; Ramanathan, R.; Zou, W.; Tiew, H. G.; Pottage, M. J.; Bansal, V.; Tabor, R. F. and Wilkinson, B. L. Synthesis and properties of photoswitchable carbohydrate fluorosurfactants. *Aust. J. Chem.*, **2015**, 68 (12), 1880–1884.
- Adam, M. K.; Poisson, J. S.; **Hu, Y.**; Prasannakumar, G.; Pottage, M. J.; Ben, R. N. and Wilkinson, B. L. Carbohydrate-based surfactants as photocontrollable inhibitors of ice recrystallization. *RSC Adv.*, **2016**, 6 (45), 39240–39244.
- **Hu, Y.**; Adam, M. K.; Poisson, J. S.; Pottage, M. J.; Ben, R. N. and Wilkinson, B. L. Photoswitchable carbohydrate-based fluorosurfactants as tuneable ice recrystallization inhibitors. *Carbohydr. Res.*, **2017**, 439, 1–8.

2.1 Introduction

2.1.1 Cryopreservation

Cryopreservation is the process of using low temperatures (typically below -80°C) to freeze and store biological materials with applications in stem cell storage,¹ reproductive technologies,² blood transfusion³ and organ transplantation.⁴ An ideal cryopreservation protocol results from the recovery of cells from ultra-low temperatures with no changes in metabolism and cellular structure. Under normal cooling conditions, ice crystals first form outside the cell, where they cause an increase in solute concentration, leading to the cells losing intracellular water to compensate for this effective osmotic stress. Cells then become dehydrated which causes damage to cellular components.⁵ Eventually, when reaching a sufficiently low temperature – typically below -80°C , the solution within and outside the cells

turns into a glassy matrix (vitrification) that is necessary for long-term preservation. Another major source of cellular damage during cryopreservation involves the formation of intracellular ice crystals that predominantly occurs during faster cooling processes. Although the exact mechanism of damage from intracellular ice formation is still not clear, it can be lethal to cells as the ice crystals cause organelle disruption.⁵ To avoid tissue damage during the freezing process, exogenous antifreeze materials termed cryoprotectants are added during and prior to freezing in order to reduce intracellular ice formation and encourage vitrification.

Another challenge of cryopreservation is to prevent additional damage caused by ice recrystallization, which results in the growth of larger ice crystals at the expense of smaller crystals.⁶ Ice recrystallization occurs predominantly during thawing cycles of cryopreservation, and has been widely reported to reduce post-thaw cell viability and is a major cause of cell injury.⁷ Whilst conventional cryoprotectants can be employed successfully to inhibit ice growth, they are ineffective at inhibiting ice recrystallization.⁶ Current cryopreservation protocols often require complex mixtures of chemical additives and adaptation of freeze-thaw rates, which is highly cell- and tissue-dependent and provides only limited protection.⁵ Several studies have highlighted the potential of ice recrystallization inhibitors (IRIs) for enhancing post-thaw recovery and viability whilst mitigating the toxicity of conventionally used cryoprotectants.^{6, 8} Whilst the weak IRI activity of simple carbohydrates have been assessed, there are currently no standard protocols that combine IRIs with conventional cryoprotectants for biomedical applications, and there is a pressing need for new, non-toxic IRIs.

The first cryoprotectant was reported by Polge and co-workers in 1949, who demonstrated the revival of fowl spermatozoa after vitrification at -80°C using 10–20% glycerol.⁹ Since then, numerous efforts have been directed towards the discovery and application of cryoprotectants. Currently, the most widely used cryoprotectants are dimethyl sulfoxide (DMSO), glycerol, 1,2-propanediol, ethanediol, sucrose and trehalose.^{10–12} Such agents are believed to elicit antifreeze activity through correcting osmotic balance leading to freeze dehydration and/or promoting vitrification. However, many agents are toxic to cells, particularly at high concentrations, and

also present significant challenges with respect to the removal of the agent to acceptable levels following their use.¹³⁻¹⁴ Furthermore, these agents do not inhibit ice recrystallization. Thus, the key properties needed to make a ‘universal’ cryoprotectant include the ability to pass through lipid membranes, promote vitrification at relatively high sub-zero temperatures, and inhibit ice recrystallization during freezing and thawing cycles.

2.1.2 Biological antifreezes

Nature has evolved biological antifreezes (BAs) to protect organisms from cryoinjury and death.⁶ These biological antifreezes are mostly (glyco)peptides and proteins found in different plants, insects and fish that inhabit cold environments.⁶ In the late 1950s and early 1960s, Scholander and co-workers observed that Arctic fish did not freeze in water that was colder than the freezing point of their blood plasma.^{15, 16} Later on, DeVries and Wohlschlag discovered the presence of circulating glycoproteins in the fish blood plasma that were responsible for this activity.¹⁷⁻¹⁹ These naturally occurring materials were later termed antifreeze glycoproteins (AFGPs) **2.1** (Figure 2.1). The potent antifreeze activity of these BAs results from the irreversible binding of hydrophobic faces of the AF(G)Ps to embryonic ice crystals, thus reducing the localized freezing point and arresting further ice development. Owing to their unique biophysical properties, there has been significant interest in the use of AFGPs and structural mimics as a source of novel antifreeze agents.^{6, 20} Of those novel compounds, two C-linked AF(G)P analogues **2.2** and **2.3** previously reported by the Ben group^{21, 22} have been shown to possess potent IRI activity at very low concentration (5.5 μ M) (Figure 2.2). However, limited success has been achieved when using BAs in cryopreservation protocols due to their complex synthesis and isolation, as well as their undesirable thermal hysteresis (TH) activity that gives rise to dynamic ice shaping and damaging ice spicule formation.^{6, 23, 24} Therefore, the search for cryoprotectants with potent IRI activity and negligible TH activity, that are also low in cost and readily available has been actively pursued.²⁵

Since this discovery, various synthetic, low molecular weight carbohydrate analogues have been investigated as potential inhibitors of ice recrystallization. In 2012, Ben *et al.* reported the first example of low molecular weight, non-ionic carbohydrate surfactant **2.4** and hydrogelator **2.5** showing potent IRI activity at concentrations of 11 mM and 0.5 mM, respectively (Figure 2.3).²³ In addition to surfactants, *O*-aryl-glycosides **2.6** have been shown to possess potent IRI activity when used in combination with 15% glycerol for the cryopreservation of red blood cells.²⁸ Unlike AF(G)Ps, these small molecules do not bind to the ice surface and hence they did not exhibit TH activity. Low molecular weight carbohydrate-based derivatives are promising cryoprotectants that could be used in combination with DMSO to reduce its toxicity.^{7, 23} Although the IRI activity of small sugars can be attributed to the degree of hydration, the mechanism of the IRI activity for carbohydrate-based analogues and aryl glycosides is not well understood, but several studies have highlighted the importance of increasing hydrophobicity for invoking potent IRI activity.^{23, 29}

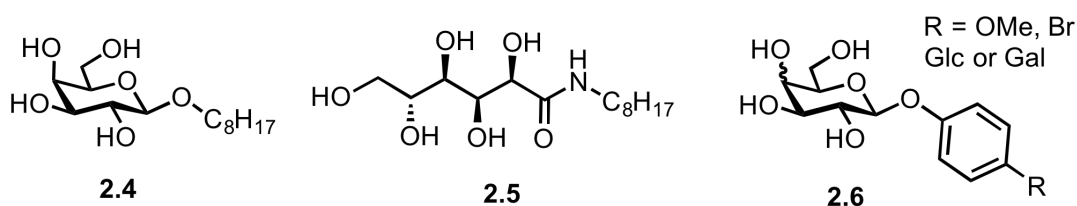


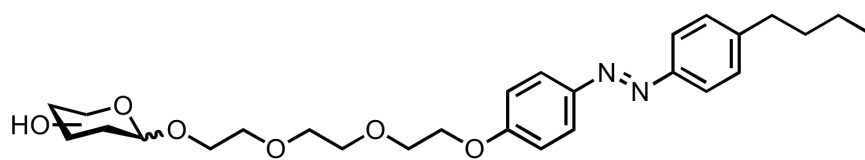
Figure 2.3. Structures of low molecular weight carbohydrate derivatives **2.4–2.6**.^{23, 28}

Adapted with permission from references 23 and 28. Copyright 2012 The Royal Society of Chemistry and 2016 American Chemistry Society.

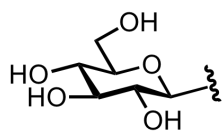
Fluorosurfactants are an important class of amphiphile consisting of a hydrophilic head group covalently linked to at least one hydrophobic, fluorinated or semi-fluorinated tail group. Compared with hydrocarbon surfactants, fluorosurfactants exhibit several desirable properties including enhanced surface activity, and excellent spreading and wetting characteristics, which is attributed in part to the enhanced hydrophobicity and oleophobicity of the fluoroalkyl tail group.³⁰ Many specialized fluorosurfactants have been reported in the literature as

biocompatible materials possessing low haemolytic activity, high fluidity and high gas dissolving capacities.³¹ Hence, they have attracted considerable interest in biotechnology and pharmaceutical applications as oxygen carriers³² and drug delivery systems.³³ However, the development of new fluorosurfactant systems is largely hampered by their high cost and issues of persistence in the environment. Carbohydrate-based fluorosurfactants are an attractive alternative because carbohydrates as polar head groups are abundant, readily biodegradable and are derived from natural resources. In particular, these biocompatible materials are of great interest for pharmaceutical applications, in particular as pulmonary drug delivery vehicles^{34–36} and blood substitutes.³⁷ Despite their promising biomedical applications, the effect of tail group fluorination/hydrophobicity on the IRI activity of this important class of amphiphile is yet to be verified.

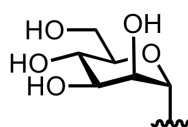
Through appropriate molecular design of carbohydrate-based surfactants, their molecular geometry and polarity can be altered, and ultimately, their ability to inhibit ice recrystallization can be tailored. To date, the IRI activity of fluorosurfactants has yet to be determined, and could provide a valuable new source of these materials. This could also facilitate much needed structure-function relationships for the rational design of improved IRI agents, as well as improve our fundamental understanding of the phenomenon of ice recrystallization. In this chapter, we describe the modular synthesis and IRI activity of a library of *O*-glycosidically linked, photoswitchable carbohydrate-based surfactants (Library 1, **2.7–2.9**), and regioisomeric fluorosurfactants (Library 2, **2.10–2.21**) (Figure 2.4). In addition to altering the molecular structure of the head and tail groups, we reasoned the incorporation of an azobenzene moiety within the hydrophobic tail group would provide an opportunity to tune hydrophobicity and molecular conformation, and thus a mechanism for probing their IRI activity in a spatial and temporally-resolved manner.



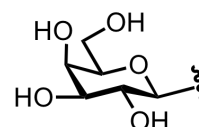
2.7–2.9



2.7 GlcAzo

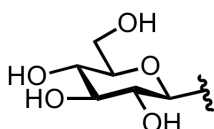
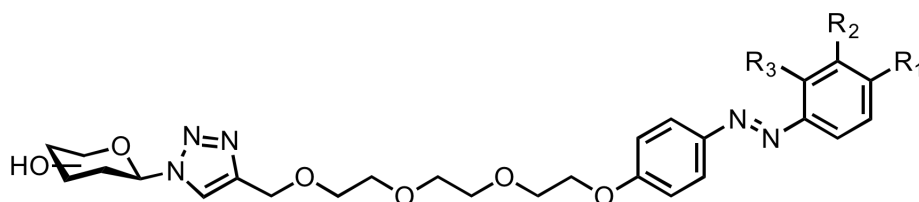


2.8 ManAzo

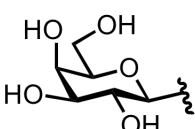


2.9 GalAzo

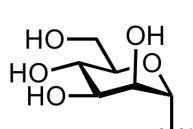
Library 1: Photoswitchable carbohydrate-based surfactants **2.7–2.9**.



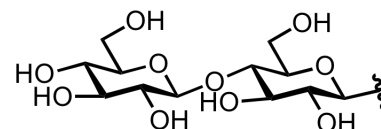
Glc **2.10–2.12**



Gal **2.13–2.15**



Man **2.16–2.18**



Cel **2.19–2.21**

2.10 Glc *p*-CF₃, R₁ = CF₃, R₂ = R₃ = H

2.11 Glc *m*-CF₃, R₁ = R₃ = H, R₂ = CF₃

2.12 Glc *o*-CF₃, R₁ = R₂ = H, R₃ = CF₃

2.13 Gal *p*-CF₃, R₁ = CF₃, R₂ = R₃ = H

2.14 Gal *m*-CF₃, R₁ = R₃ = H, R₂ = CF₃

2.15 Gal *o*-CF₃, R₁ = R₂ = H, R₃ = CF₃

2.16 Man *p*-CF₃, R₁ = CF₃, R₂ = R₃ = H

2.17 Man *m*-CF₃, R₁ = R₃ = H, R₂ = CF₃

2.18 Man *o*-CF₃, R₁ = R₂ = H, R₃ = CF₃

2.19 Cel *p*-CF₃, R₁ = CF₃, R₂ = R₃ = H

2.20 Cel *m*-CF₃, R₁ = R₃ = H, R₂ = CF₃

2.21 Cel *o*-CF₃, R₁ = R₂ = H, R₃ = CF₃

Library 2: Photoswitchable fluorosurfactant library **2.10–2.21**.

Figure 2.4. Molecular structures of photoswitchable, carbohydrate-based surfactants (**2.7–2.9**) and fluorosurfactants (**2.10–2.21**).

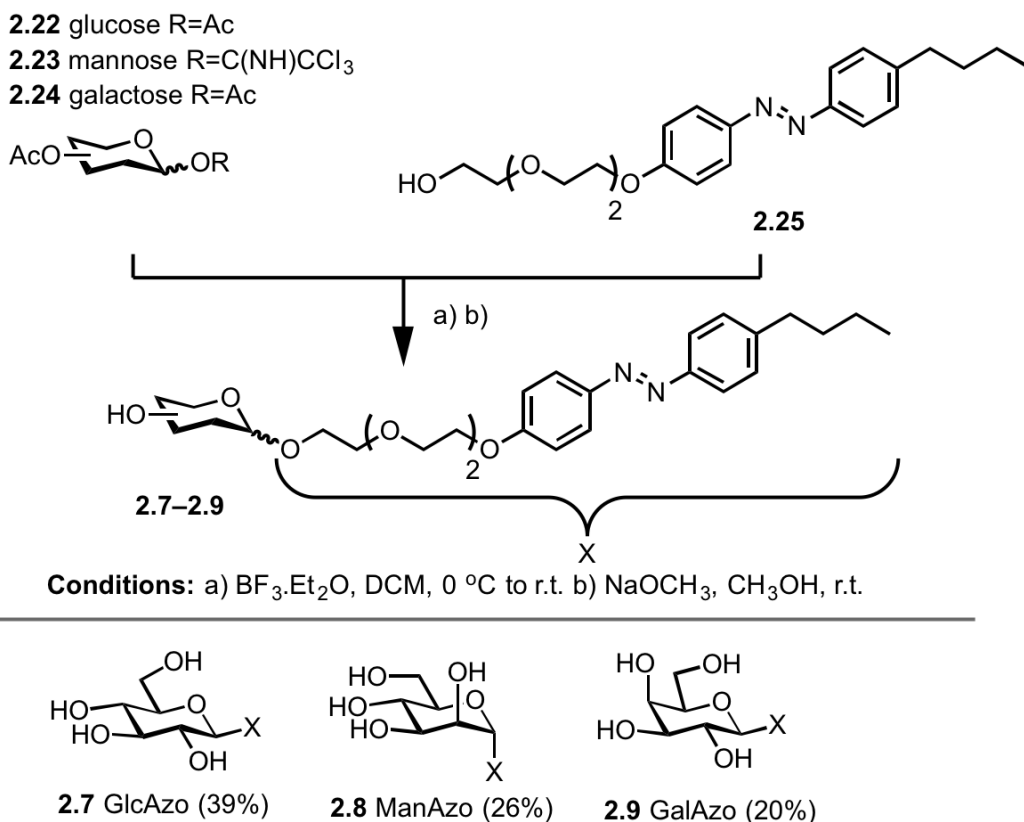
2.2 Results and Discussion

2.2.1 Library design and parallel synthesis of photocontrollable carbohydrate surfactants

Our investigation commenced with the synthesis and characterization of novel surfactants **2.7–2.9** and fluorosurfactants **2.10–2.21**. Variable mono- (D-glucose, D-galactose and D-mannose) and disaccharide (D-cellobiose) head groups were selected, which enabled products with diverse size, configuration and degrees of hydration.²⁷ The hydrophobic tail groups incorporated a photoswitchable azobenzene moiety incorporating a triethylene glycolate spacer to provide additional water solubility. Azobenzene *trans-cis* photoisomerization has been widely used as a strategy for modulating the adsorption and aggregation properties of surfactants.^{38, 39} The *trans* conformation of azobenzene is thermodynamically more stable than the *cis* isomer, and the molecular geometry of azobenzene can be altered from the less polar and planar *trans* isomer, to the more polar and bent conformation of the *cis* isomer upon UV irradiation (~340 nm).⁴⁰ However, the application of UV-visible light as an environmental trigger for tuning amphiphilicity of surfactant monomers for probing IRI activity of this class of molecules has not yet been investigated.

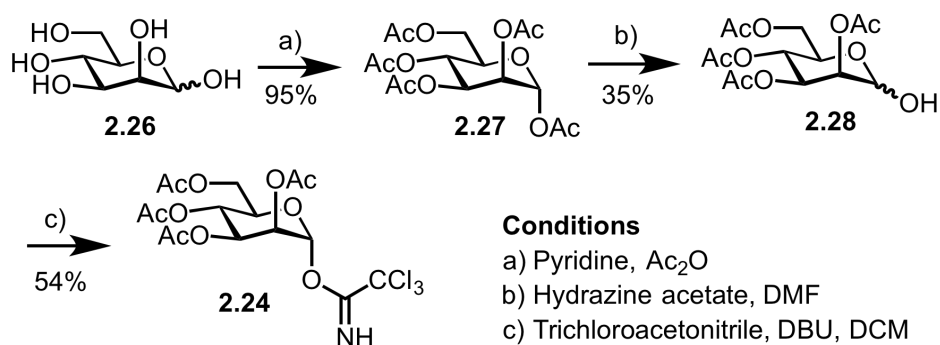
For fluorosurfactants **2.10–2.21**, their azobenzene units are substituted with an electron-withdrawing trifluoromethyl ($-\text{CF}_3$) group in the *ortho*, *meta* or *para* position relative to the N=N bond, which would give rise to regioisomeric fluorosurfactants with various photochemical and physicochemical properties. Hence, we could explore the effect of tuning polarity of the tail group through substituent effects, coupled with *trans-cis* photoisomerization to facilitate structure-activity relationships.

The *O*-glycosides **2.7–2.9** were synthesized through Lewis-acid promoted glycosylation of per-*O*-acetylated donors **2.22–2.24** with azobenzene-based acceptor **2.25** (Scheme 2.1).⁴¹ The crude intermediates were immediately deprotected under Zemplén conditions⁴² to provide the desired surfactants **2.7–2.9** in high purity following purification by reversed-phase, preparative HPLC, followed by lyophilization.



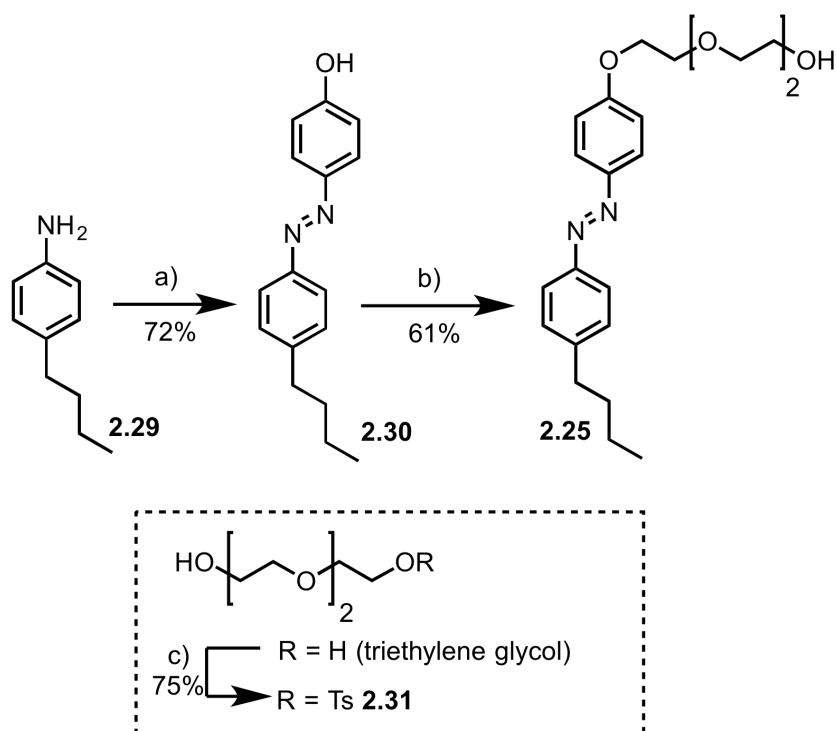
Scheme 2.1. Synthetic procedure for *O*-glycoside surfactants **2.7–2.9**.

Glucose pentaacetate **2.22** and galactose pentaacetate **2.23** were acquired from commercial sources. The mannose trichloroacetimidate donor **2.24** was used for the glycosylation reaction due to the low yield of the corresponding surfactant from the glycosylation of **2.25** with mannose pentaacetate as donor, as a result of intermolecular acyl migration. Trichloroacetimidate **2.24** was synthesized over three steps using a known literature procedure,⁴³ starting from commercially available D-mannose **2.26** (Scheme 2.2). Specifically, **2.26** was treated with acetic anhydride in pyridine to afford mannose pentaacetate **2.27** in 97% yield. Regioselective deprotection of the anomeric acetoxy group using hydrazine acetate in DMF then gave hemiacetal **2.28**.⁴³ Treatment of the hemiacetal **2.28** with trichloroacetonitrile and 1,8-Diazabicyclo[5.4.0]undec-7-ene (DBU) in DCM then furnished the trichloroacetimidate donor **2.24**.⁴³



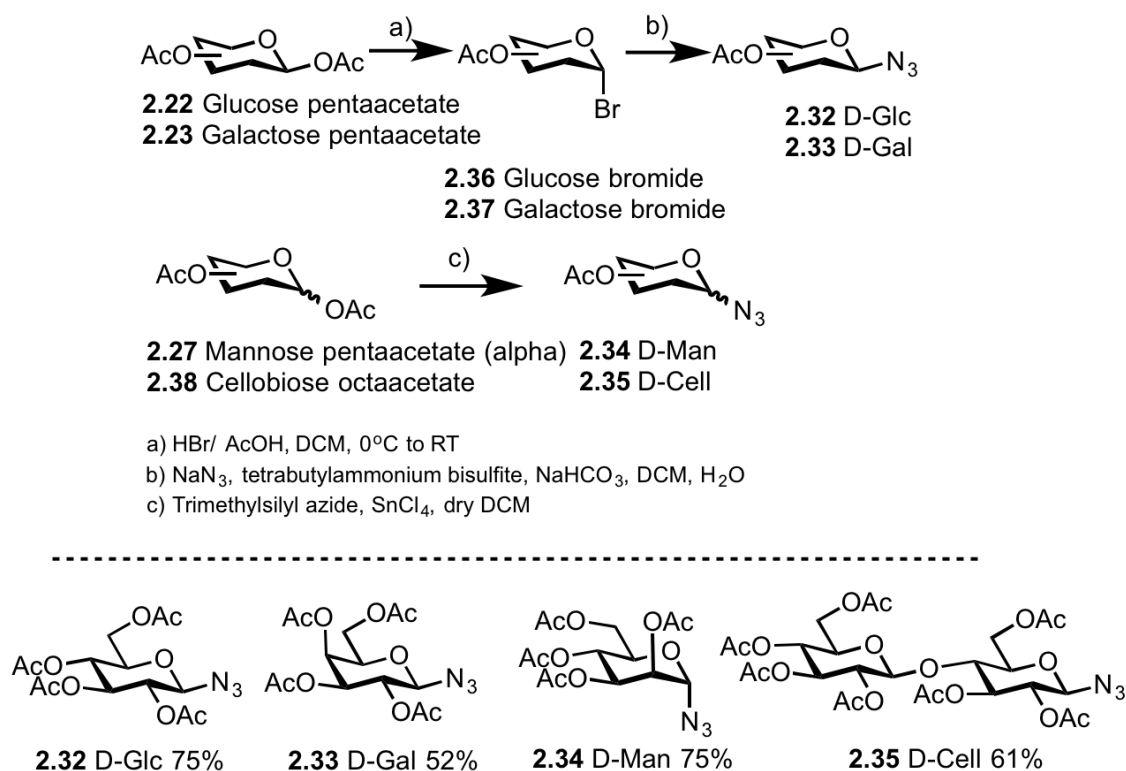
Scheme 2.2. Synthetic procedure for mannose trichloroacetimidate **2.24**.

The non-surface active and non-amphiphilic tail group **2.25** was synthesised over two steps (Scheme 2.3)⁴⁴ as follows: diazotization of *n*-butyl aniline **2.29** and subsequent coupling of the diazonium salt with phenol *in situ* to derive azobenzene **2.30**. Base promoted alkylation of the phenol **2.30** with the triethylene glycol monotosylate **2.31** then gave the azobenzene acceptor fragment **2.25** in 61% yield (Scheme 2.3).



Scheme 2.3. Synthetic procedure for azobenzene-based building block **2.25**.

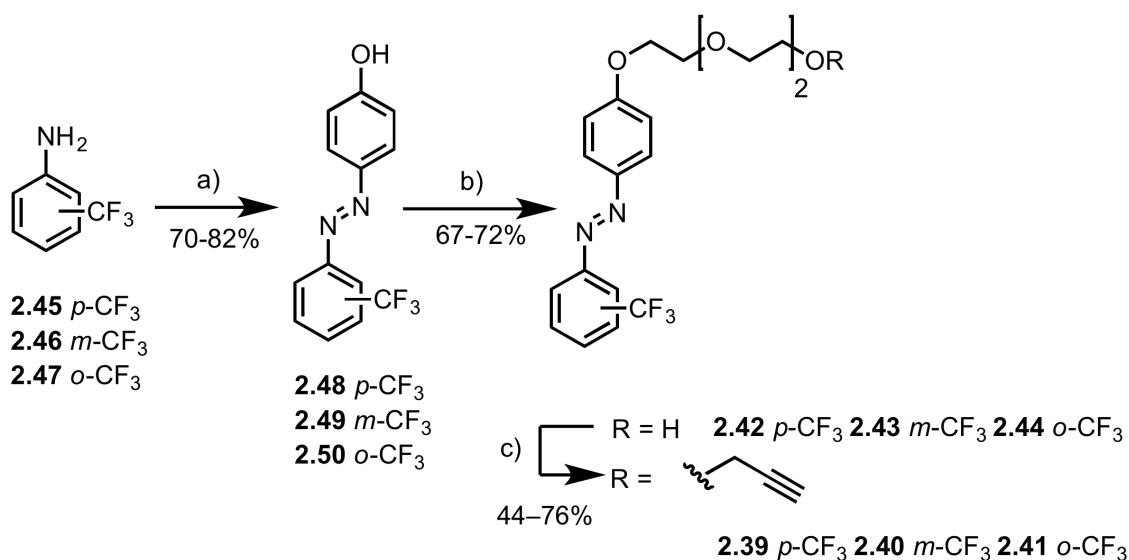
Prior to the synthesis of the fluorosurfactant library **2.10–2.21** (Figure 2.4), the requisite head and tail groups were synthesized. Glycosyl azides **2.32–2.35** were designed and synthesized as using well-established literature procedures, which was achieved by nucleophilic displacement of the corresponding α -D-glycosyl bromides **2.36** and **2.37** with sodium azide under phase transfer catalytic conditions to give optically pure building blocks in 52–75% yield (Scheme 2.4). The *D-manno* configured glycosyl azide **2.34** and the *D-cellobiosyl* azide building block **2.35** were synthesized by reacting the corresponding acetates **2.27** and **2.38**, respectively, with trimethylsilyl azide and stannic chloride in dry DCM. Compound **2.27** and **2.28** were then isolated in 75% and 61% yield respectively (Scheme 2.4).



Scheme 2.4. Synthetic procedure for glycosyl azides **2.32–2.35**.

With respect to the fluorosurfactants library (Library 2), three functionalized azobenzene compounds **2.39–2.41** were synthesized and served as tail groups for reaction with glycosyl azide building blocks (Scheme 2.5). The same synthetic method was used for preparing **2.42–2.44** as for the *n*-butylazobenzene derivative **2.25**. The appropriate substituted fluoroaniline

2.45–2.47 served as the starting material to derive compounds **2.48–2.50**, respectively, which were then alkylated with compound tosylate **2.31** to give azobenzene alcohol **2.42–2.44** in 67–72% yield. Alcohols **2.42–2.44** were then deprotonated with an excess of sodium hydride, followed by addition of an excess of propargyl bromide in the presence of tetrabutylammonium iodide (Bu_4NI) to obtain the substituted alkynes **2.39–2.41** in good yield (44–76%).⁴⁵

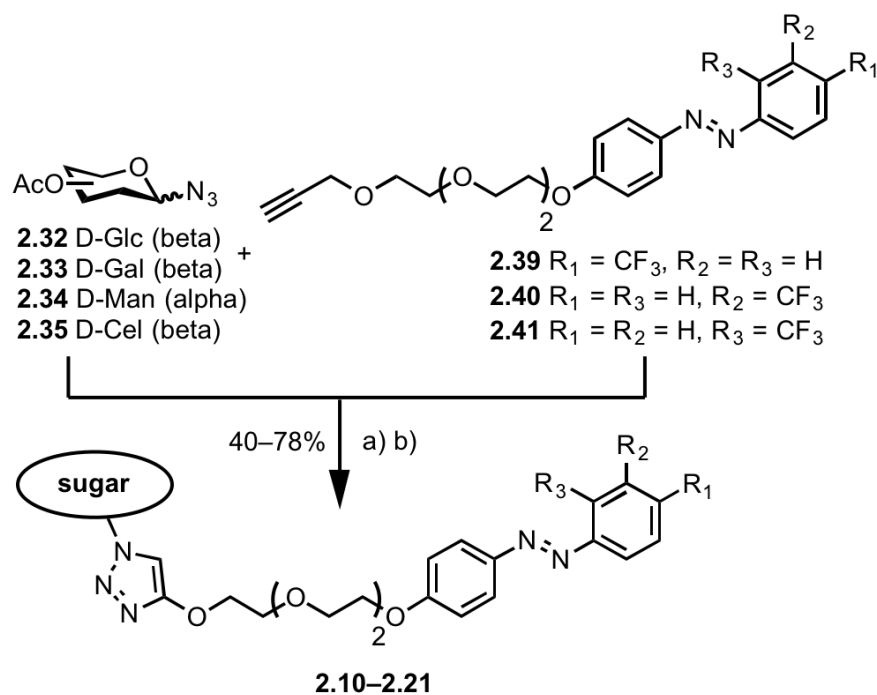


Conditions

a) NaNO_2 , HCl , H_2O , 0°C , then phenol, NaOH , H_2O , 0°C to r.t. b) **2.31**, K_2CO_3 , EtOH , reflux. c) NaH , propargyl bromide, Bu_4NI , THF

Scheme 2.5. Synthetic procedure for azobenzene-based building block **2.39–2.41**.

The carbohydrate-based fluorosurfactants **2.10–2.21** were synthesized by reacting glycosyl azides **2.32–2.35** with alkyne fragments **2.39–2.41** using the well-established Cu(I)-catalyzed azide-alkyne cycloaddition reaction (CuAAC) (Scheme 2.6).⁴⁶ Following CuAAC reaction, fluorosurfactants **2.10–2.21** were obtained by deprotection of the crude intermediates, followed by purification by reverse-phase preparative HPLC and isolated in 40–78% yield.



Conditions: a) $\text{CuSO}_4 \cdot 5\text{H}_2\text{O}$, sodium ascorbate; b) NaOCH_3 , CH_3OH , r.t.

2.10 Glc <i>p</i> - CF_3 , $R_1 = \text{CF}_3, R_2 = R_3 = \text{H}$	2.16 Man <i>p</i> - CF_3 , $R_1 = \text{CF}_3, R_2 = R_3 = \text{H}$
2.11 Glc <i>m</i> - CF_3 , $R_1 = R_3 = \text{H}, R_2 = \text{CF}_3$	2.17 Man <i>m</i> - CF_3 , $R_1 = R_3 = \text{H}, R_2 = \text{CF}_3$
2.12 Glc <i>o</i> - CF_3 , $R_1 = R_2 = \text{H}, R_3 = \text{CF}_3$	2.18 Man <i>o</i> - CF_3 , $R_1 = R_2 = \text{H}, R_3 = \text{CF}_3$
2.13 Gal <i>p</i> - CF_3 , $R_1 = \text{CF}_3, R_2 = R_3 = \text{H}$	2.19 Cel <i>p</i> - CF_3 , $R_1 = \text{CF}_3, R_2 = R_3 = \text{H}$
2.14 Gal <i>m</i> - CF_3 , $R_1 = R_3 = \text{H}, R_2 = \text{CF}_3$	2.20 Cel <i>m</i> - CF_3 , $R_1 = R_3 = \text{H}, R_2 = \text{CF}_3$
2.15 Gal <i>o</i> - CF_3 , $R_1 = R_2 = \text{H}, R_3 = \text{CF}_3$	2.21 Cel <i>o</i> - CF_3 , $R_1 = R_2 = \text{H}, R_3 = \text{CF}_3$

Scheme 2.6. Synthetic procedure for fluorosurfactants **2.10–2.21**.

2.2.2 Photoswitching studies

Having synthesized photoswitchable surfactants **2.7–2.9** and fluorosurfactants **2.10–2.21**, an investigation into their optical properties was conducted. Surfactants **2.7–2.21** share an azobenzene core that enables *trans-cis* photoisomerization in response to irradiation with UV light (361 nm). To explore the photoswitching activities of surfactants **2.7–2.21**, their optical properties and rate of thermal relaxation were evaluated using UV-vis spectroscopy. A UV-light source at 361 nm was used to trigger photoisomerization, the progress of which was monitored by UV-vis spectroscopy by observing a decrease in the intensity of the peak at 350 nm

corresponding to the π - π^* transition of the *trans* isomer, and an increase of the peak at 440 nm corresponding to the n - π^* transition of the *cis* isomer (Figure 2.5). For fluorosurfactants **2.10**–**2.12**, the wavelength for the absorption bands remained unchanged regardless of the changes in the position of the $-\text{CF}_3$ group on the ring. However, the molar extinction coefficients at 350 nm wavelength were significantly increased for surfactant **2.11** Glc *m*- CF_3 ($15,000 \text{ M}^{-1} \text{ cm}^{-1}$) compared with surfactant **2.10** Glc *p*- CF_3 ($8,000 \text{ M}^{-1} \text{ cm}^{-1}$) and **2.12** Glc *o*- CF_3 ($3,500 \text{ M}^{-1} \text{ cm}^{-1}$) (see Section 2.4.3 for details). The rate of thermal relaxation to the *trans*-isomer was investigated and revealed only minor thermal *cis-trans* relaxation at 20°C within 24 h under dark-adapted conditions (Figure 2.5, Table 2.1 and Table 2.2).

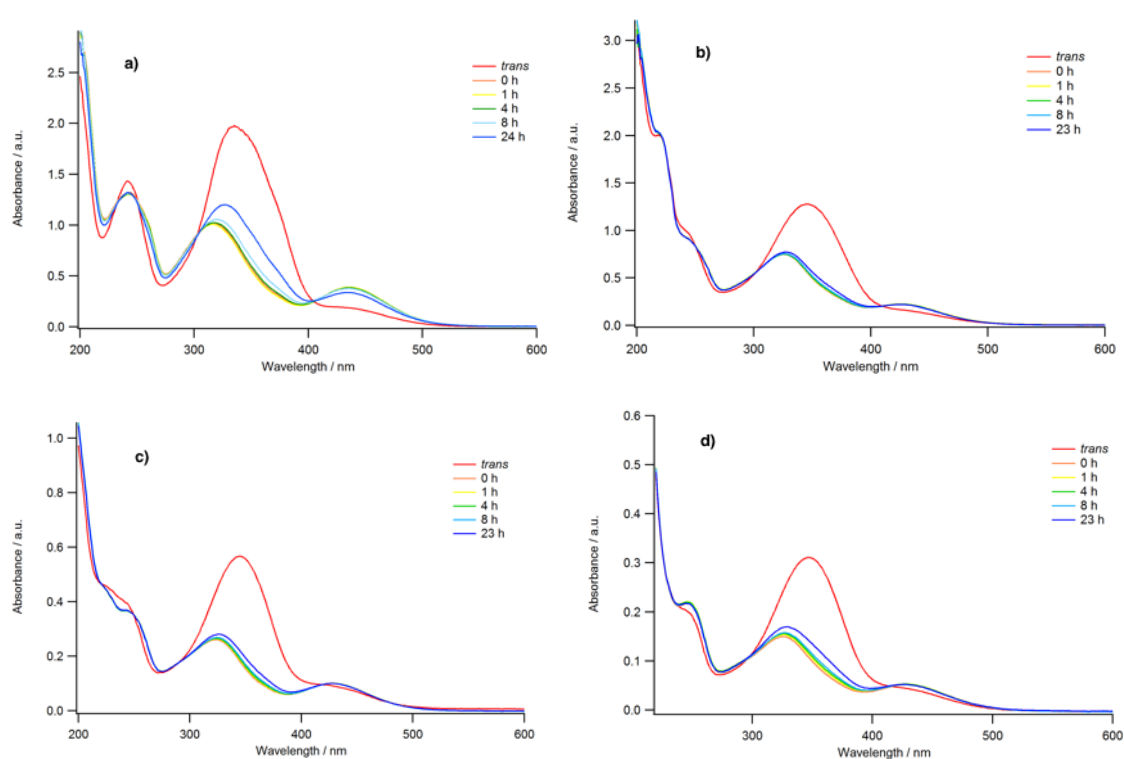


Figure 2.5. UV-vis spectra and thermal *cis-trans* relaxation of representative surfactants a) **2.7** GlcAzo, b) **2.10** Glc *p*- CF_3 , c) **2.11** Glc *m*- CF_3 and d) **2.12** Glc *o*- CF_3 . (See **Appendix I** for complete data).

The ratio of *cis*- and *trans*-isomers at either photostationary state (PSS) was determined by integrating resolved methylene signals of the *n*-butyl group in the ^1H NMR spectrum of

ManAzo **2.8**. Surfactant **2.8** was dissolved in deuterated methanol and irradiated at 361 nm for 10 min before acquiring the ^1H NMR spectra of the *cis*-PSS. Using this method, 96% of *trans*-isomer was obtained in the *trans*-dominated state while 65% of *cis*-isomer was observed in the *cis*-dominated state (Figure 2.6).

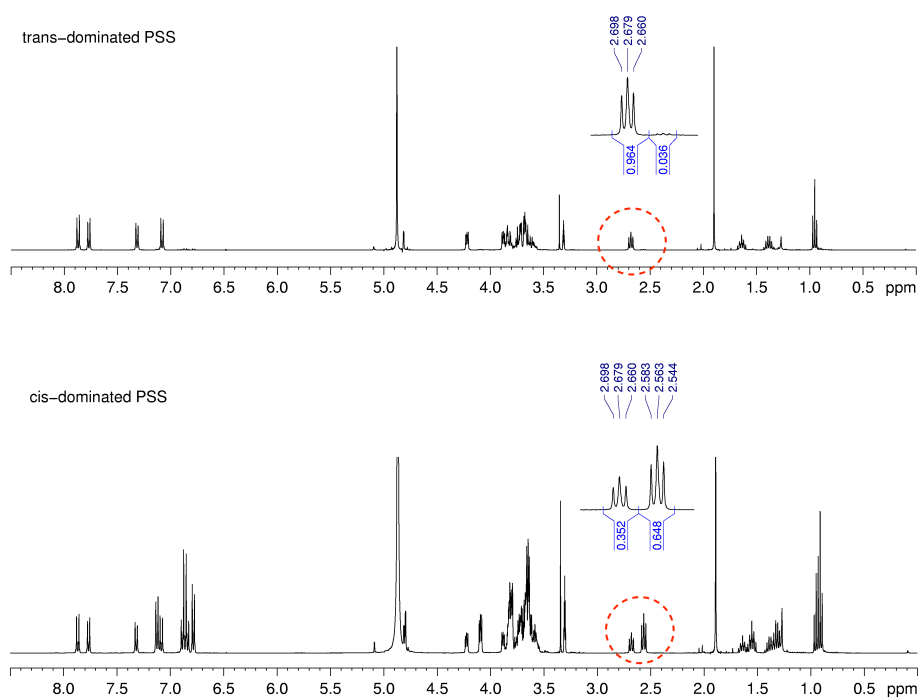


Figure 2.6. Expanded ^1H NMR spectrum of surfactants **2.8** ManAzo (20 mM in CD_3OD) in the *trans*-dominated state (top) and *cis*-dominated state (bottom).

2.2.3 Photocontrollable surface activity

With the photosurfactants in hand and their optical properties examined, the photocontrollable surface activity was then investigated and the critical micelle concentration (CMC) determined. To this end, pendant drop tensiometry was carried out using a customized pendant drop apparatus (Figure 2.7 a, see Section 2.4.2 for experimental details).^{47, 48} The surface tension at the air-water interface was determined by fitting the shape of a droplet (captured by a digital camera) to the Young-Laplace equation, which was achieved automatically by OpenDrop pendant drop tensiometry software.⁴⁷ The CMC can be extrapolated at the intersection of two

near-linear regions when surface tension is plotted as a function of surfactant concentration (Figure 2.7 b).

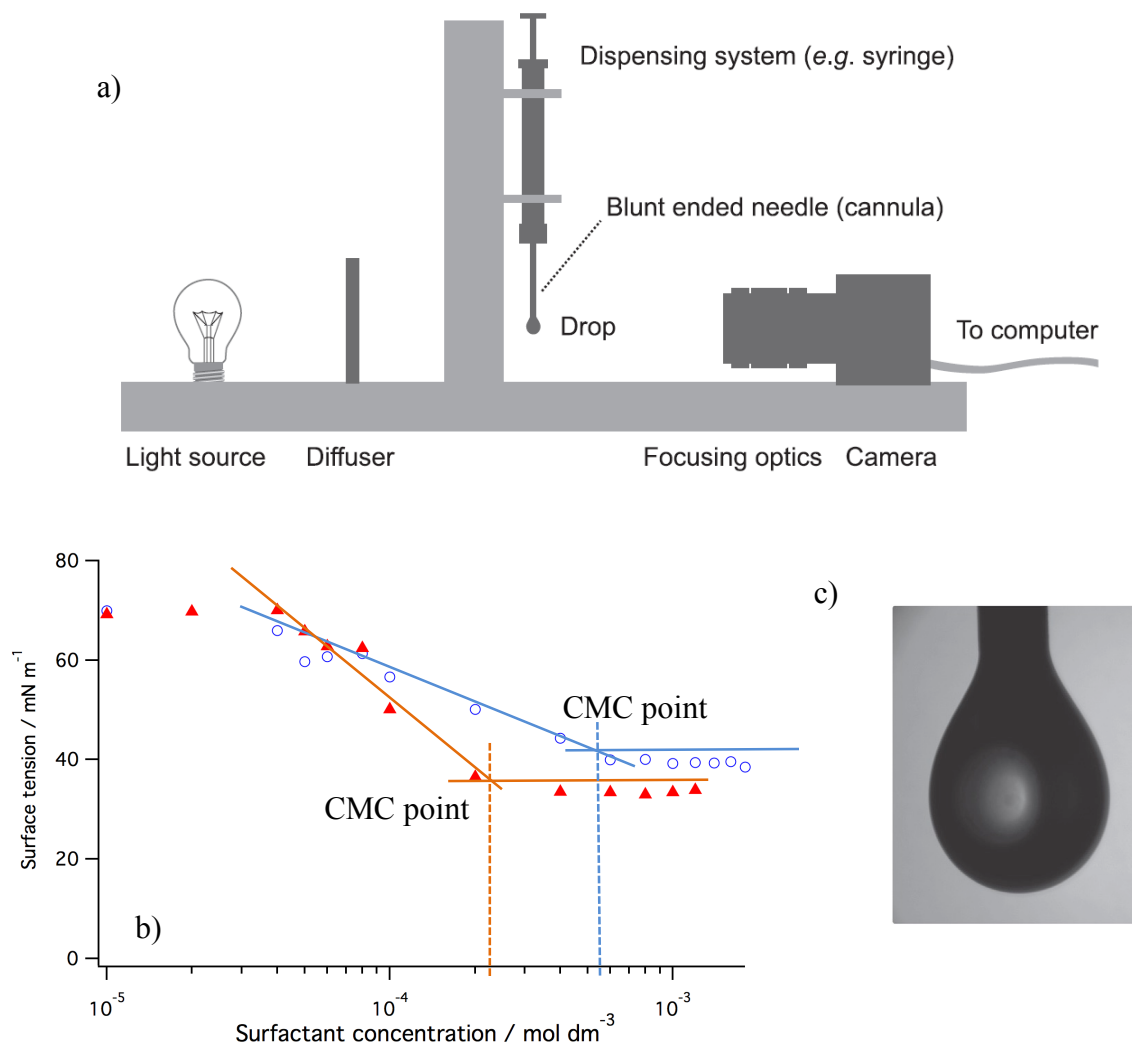


Figure 2.7. a) Customized experimental setup for surface tension measurement, b) determination of CMC values, c) a typical drop image captured by a digital camera.⁴⁷

The CMC values of surfactants **2.7–2.21** were calculated using the method described above, in the *trans*- and *cis*-PSS. The native *trans* isomers of surfactants **2.7–2.21** were converted into *cis* isomers by irradiation of the respective sample solutions at 361 nm for 10 min. The surface tension measurement of the *cis* isomers was carried out in the dark, using the lowest backlight setting to obtain the interfacial profile of the drop. The air-water surface tension data for *O*-

glycoside surfactants, GlcAzo **2.7** and ManAzo **2.8**, are shown in Figure 2.8 and the corresponding CMC values listed in Table 2.1. The CMC values of GalAzo **2.9** could not be detected due to its low solubility in water. As can be seen clearly from Figure 2.8 and Table 2.1, an increase in CMC values of surfactants **2.7** and **2.8** was observed upon UV irradiation, which can be attributed to the well-documented changes in geometry and polarity of the azobenzene moiety upon *trans-cis* photoisomerization.⁴⁹ However, the photocontrollable surface activity for $-\text{CF}_3$ substituted azobenzene compounds has not yet been investigated.

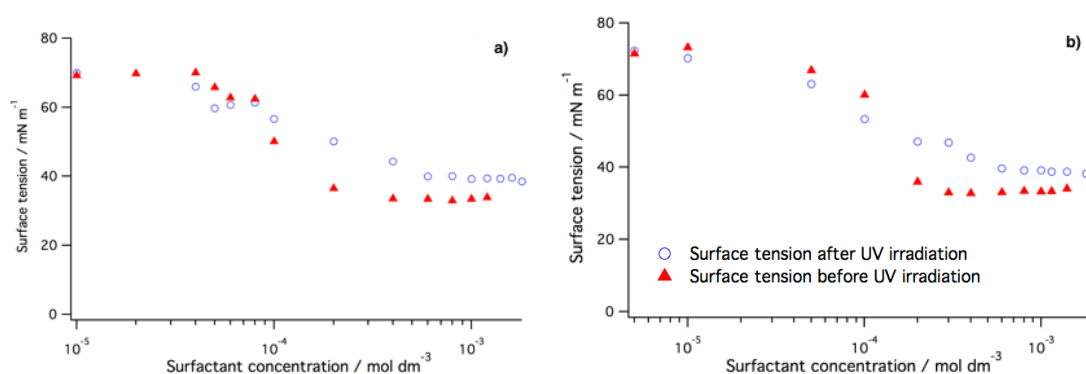


Figure 2.8. Air-water surface tension data for surfactants a) GlcAzo **2.7** and b) ManAzo **2.8**.

To investigate the effect of *trans-cis* photoisomerization on the surface activity fluorosurfactants with differently substituted $-\text{CF}_3$ groups, the CMC values of fluorosurfactants **2.10–2.21** were calculated. The air-water surface tension data for representative surfactants **2.10–2.12** is shown in Figure 2.9 and complete CMC data are listed in Table 2.2. In order to analyse the structure-function relationships of fluorosurfactants, a chart was plotted according to the data listed in Table 2.2. Similarly to the CMC results for *O*-glycosides **2.7** and **2.8**, there was an increase in CMC values upon UV irradiation, which is reflective of the increased polarity of the *cis* isomer compared with the *trans* isomer. The magnitude of the difference in the CMC between the *trans* and *cis* isomers was dependent on the position of the $-\text{CF}_3$ group, and generally increased upon changing the substitution from *para*, *meta* and *ortho* relative to the $\text{N}=\text{N}$ bond. This was most likely a result of the difference in the dipole moments of the *cis*

and *trans* isomers of the variably substituted analogues, with the *trans* isomers showing a much smaller difference than the *meta*- and *ortho*-substituted analogues. These observations are in good agreement with the dipole moments of similar *p*-CF₃ substituted azobenzene compounds previously reported by Han *et. al.*⁵⁰ and Zannoni *et. al.*,⁵¹ who reported a slightly larger dipole moment for the *trans*-isomer (3.64 D,⁵⁰ 5.1 D⁵¹) compared with the *cis*-isomer (2.66 D,⁵⁰ 3.8 D⁵¹).

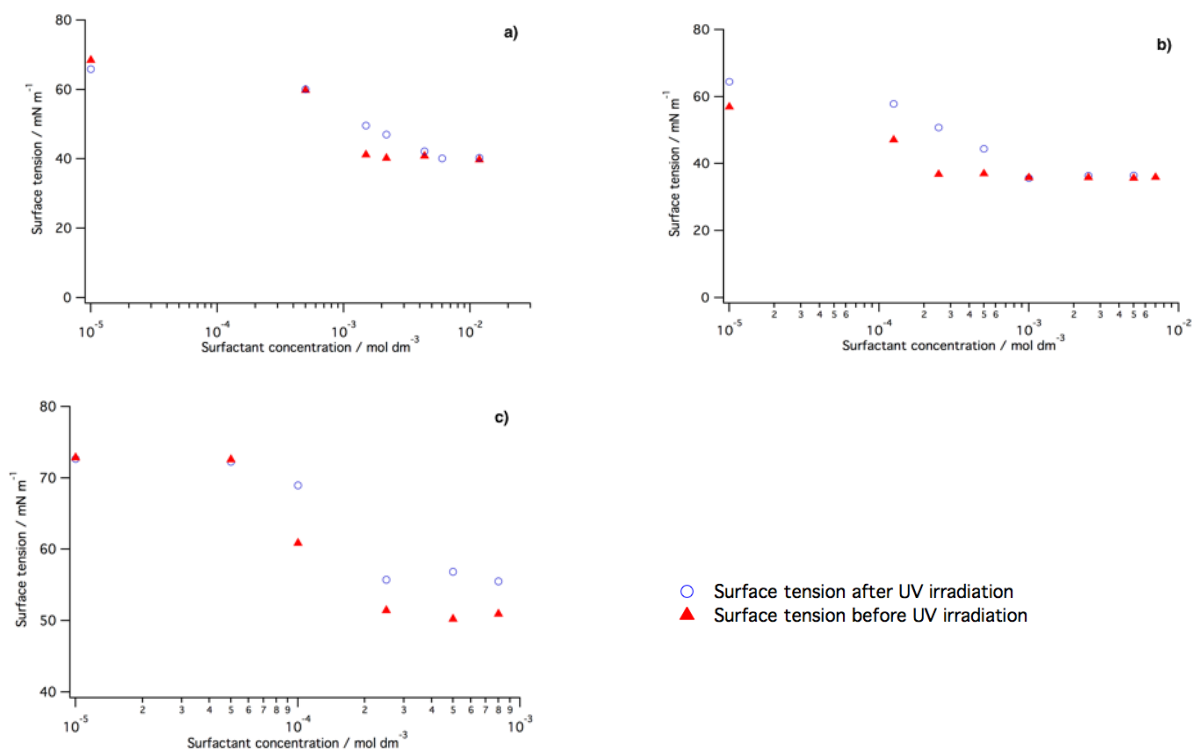


Figure 2.9. Air-water surface tension data for representative surfactants a) **2.10** Glc *p*-CF₃, b) **2.11** Glc *m*-CF₃ and c) **2.12** Glc *o*-CF₃ (see **Appendix II** for complete data).

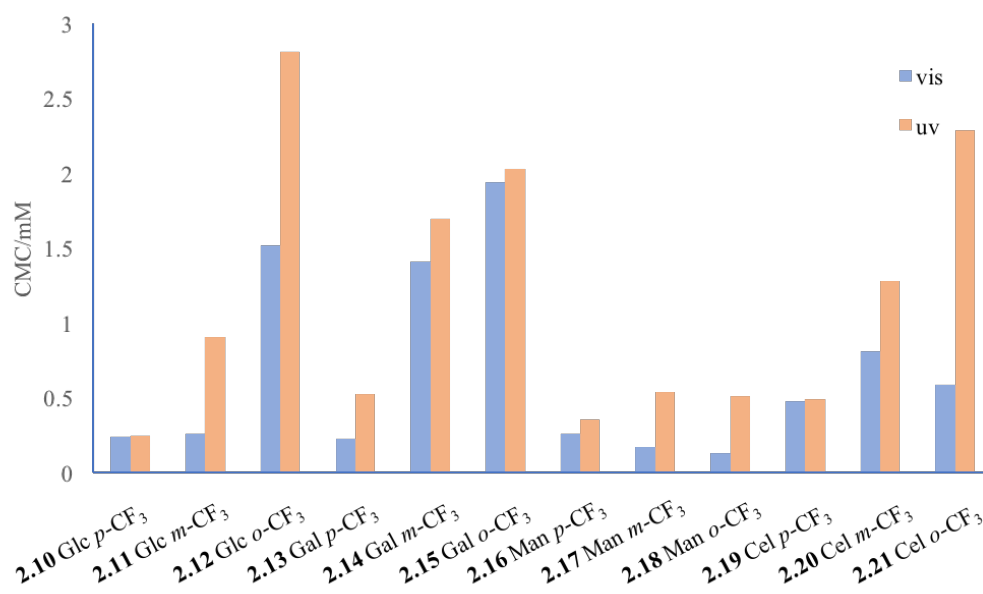


Figure 2.10. CMC data plot for fluorosurfactants **2.10–2.21**.

The 1-octanol/water partition coefficient ($\log P$) is a useful measure of the lipophilicity or hydrophilicity of a compound. This thermodynamic variable has been widely used in the pharmaceutical industry to predict, characterize and quantify the partitioning of drugs between a hydrophobic organic phase and a hydrophilic aqueous phase.⁵² Besides pharmaceutical applications, $\log P$ is also used in agrochemical research,⁵³ metallurgy,⁵⁴ and environmental science⁵⁵ to estimate the solubility of a solute in a solvent,^{56, 57} with larger values indicating higher solubility in the hydrophobic solvent (in this case 1-octanol). To quantitatively analyze the change of hydrophobicity of surfactants **2.7–2.21** upon photoisomerization, as well as the position of the $-\text{CF}_3$ group, we measured the 1-octanol/water partition coefficient ($\log P$) of surfactants **2.7–2.21** in both *trans*- and *cis*-PSS (see Section 2.4.4 for experimental details and **Appendix III** for raw data of $\log P$ measurements). The $\log P$ was determined using the shake-flask method⁵⁸ and the concentration of surfactant in the aqueous phase was measured by UV-vis spectroscopy. UV absorbance of the aqueous phase was detected before and after diffusion equilibrium. The $\log P$ value was calculated using the following equation:

$$\log P = \log[(\text{Abs before} - \text{Abs after})/\text{Abs after}]$$

For surfactants **2.7–2.9**, the log P values decreased upon *trans-cis* photoisomerization due to the formation of the more polar *cis* isomers, which was in good agreement with the CMC results, and is reflective of the formation of the more polar *cis* isomer (Table 2.1). Due to the poor aqueous solubility, the log P values of GalAzo **2.9** could not be accurately determined.

Table 2.1. Photocontrollable CMC, thermal half-life of the *cis*-isomer at 20°C, and log P of carbohydrate-based surfactants **2.7–2.9**.

Surfactant	CMC _{vis} /mM	CMC _{UV} /mM	$t_{1/2}$ /hrs	log P_{vis}	log P_{UV}
2.7 GlcAzo	0.21	0.45	54	-0.94	-1.56
2.8 ManAzo	0.23	0.49	58	-0.67	-0.83
2.9 GalAzo	N.D*	N.D*	44	-0.35	-0.85

* N.D=not detected, due to the low solubility of surfactant **2.9** GalAzo in MilliQ water.

In the fluorosurfactant series **2.10–2.21**, it can be seen from Table 2.2 that the log P values of the *trans*-isomers is dependent on the regiochemistry of the $-CF_3$ group, with values generally increasing upon changing the $-CF_3$ group from *para*, to *meta* and *ortho*, which was also reflected in the solubility of compounds in Milli-Q water. Somewhat surprisingly, and opposite to that observed for the non-fluorinated derivatives (**2.7** and **2.8**), larger log P values were generally observed upon UV irradiation of **2.10–2.21**, thus suggesting a slight increase in hydrophobicity for the *cis* isomer. Whilst these observations contradict the changes in the CMC values between the *cis* and *trans* isomers for these compounds, and is the opposite to that observed for non-fluorinated analogues, previous reports showing a *decrease* in the dipole moment of the *cis* isomers incorporating a *p*- CF_3 group supports these observations.^{50, 51, 59} The changes in solubility accompanying photoisomerization may point to specific changes in the tail group geometry and conformation, and hence packing parameters and self-assembly, rather than exclusively to changes in the dipole moment between the *cis* and *trans* states.

Table 2.2. Photocontrollable CMC, thermal half-life of the *cis*-isomer at 20°C and log *P* of carbohydrate-based fluorosurfactants **2.10–2.21**.

Surfactant	CMC/mM		$t_{1/2}$ /hrs	log <i>P</i>	
	vis	UV		vis	UV
Glc <i>p</i> -CF ₃ 2.10	0.24	0.25	187	-0.32	-0.20
Glc <i>m</i> -CF ₃ 2.11	0.26	0.91	151	-0.25	-0.26
Glc <i>o</i> -CF ₃ 2.12	1.52	2.81	217	-0.67	-0.47
Gal <i>p</i> -CF ₃ 2.13	0.23	0.53	178	-0.08	0.03
Gal <i>m</i> -CF ₃ 2.14	1.41	1.70	141	-0.14	-0.03
Gal <i>o</i> -CF ₃ 2.15	1.94	2.03	204	-0.02	-0.01
Man <i>p</i> -CF ₃ 2.16	0.26	0.36	117	-0.32	0.47
Man <i>m</i> -CF ₃ 2.17	0.17	0.54	114	-0.25	-0.37
Man <i>o</i> -CF ₃ 2.18	0.13	0.51	147	-0.31	0.14
Cel <i>p</i> -CF ₃ 2.19	0.48	0.49	165	-1.22	-0.10
Cel <i>m</i> -CF ₃ 2.20	0.81	1.28	151	-1.27	-1.41
Cel <i>o</i> -CF ₃ 2.21	0.59	2.29	224	-2.18	-1.01

2.2.4 Photocontrollable IRI activity

The ice recrystallization inhibition (IRI) activity of these carbohydrate surfactants was investigated using a splat cooling assay.^{59, 60} This technique involves observing changes in the average size of the ice crystals via an optical microscope, whereby smaller grain sizes are indicative of greater IRI activity. In this experiment, phosphate buffered saline (PBS) in the absence of surfactants was used as a control. The assay was done at a singular time point and concentration (usually 22 mM), an approach developed by the Ben group that ignores both the effects of time and concentration on IRI. Hence, surfactants **2.7–2.21** were dissolved in PBS solution at a concentration of 22 mM except for surfactants GalAzo **2.9**, Glc *p*-CF₃ **2.10**, Gal *p*-

CF₃ **2.13**, Man *p*-CF₃ **2.16** and Cel *p*-CF₃ **2.19**, which were assessed at 5 μM due to their poor solubility in PBS solution. The ice crystals were represented as a percentage mean grain size (% MGS) relative to the PBS control.

For the *O*-glycosides **2.7–2.9**, the mannose-based surfactant **2.8** showed potent IRI activity compared with glucose-based (GlcAzo **2.7**) and galactose-based (GalAzo **2.9**) surfactants (Figure 2.11), as seen by the smaller % MGS of ice crystals for **2.8**. Following UV-vis photoisomerization to the *cis*-PSS, weaker IRI activity was observed. Given the low temperatures of the assay (-6.4°C), this difference could be due to changes in solubility. However no precipitation could be observed and it was postulated that the attenuation of IRI activity for the *cis* isomer could be attributed to the increased polarity of the tail group. This observation is in good agreement with previous observations describing more potent IRI activity upon increasing tail group hydrophobicity for peptide-based amphiphiles.²⁹ Similar to the control, surfactants **2.7** GlcAzo and **2.9** GalAzo showed weak IRI activity, with no significant photomodulation observed following UV irradiation.

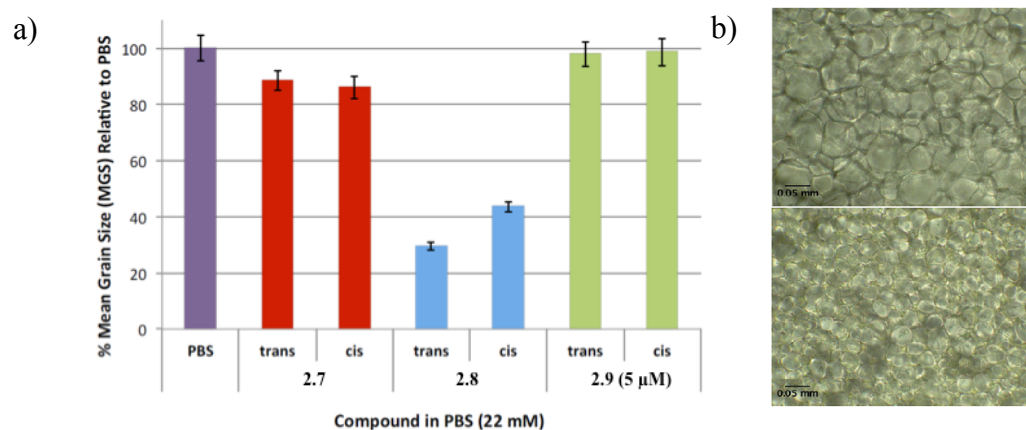


Figure 2.11. a) IRI activity surfactant **2.7–2.9** represented as a % MGS of ice crystals relative to the PBS control. b) Images of the PBS control (top) and ManAzo **2.8** at 30 mM (bottom) after 5 minutes annealing

To probe the structure-function relationship of fluorosurfactants, the IRI activities of variably substituted fluorosurfactants **2.10–2.21** were also investigated using the splat-cooling assay as described above (Figure 2.12). Due to the poor solubility of the *para*-substituted fluorosurfactants (**2.10**, **2.13**, **2.16** and **2.19**) in PBS solution, their IRI activities were assessed at 5 μ M concentration. In general, fluorosurfactants exhibited negligible IRI activity, with the exception of Gal *p*-CF₃ **2.13** which was weakly IRI-active. Nevertheless, variable IRI activity was observed among this series following UV-vis photoisomerization. Increased IRI activity was observed for the *o*-CF₃ substituted analogues (**2.12**, **2.15**, **2.18**, **2.21**), and this activity was reduced upon changing the position of the –CF₃ to *meta* (**2.11**, **2.14**, **2.17**, **2.20**) and finally *para* (**2.10**, **2.13**, **2.16**, **2.19**) to the N=N bond (Figure 2.12). Of the *ortho*-substituted fluorosurfactants in the resting *trans*-PSS, the glucose-based fluorosurfactant **2.12** showed strongest IRI activity in this series. This observation is in contrast with the results from non-fluorinated photosurfactants **2.7–2.9**, whereby the mannose-based compound **2.8** was far more potent than these incorporating glucose (**2.7**) or galactose (**2.9**) head groups. Taken together, these observations reveal the sensitivity of IRI activity towards the size and configuration of the carbohydrate head group (and therefore hydration) in carbohydrate-based amphiphiles. Following *trans-cis* photoisomerization, the IRI activity of the *o*-CF₃ compounds was significantly reduced, thus highlighting the importance of the tail group regiochemistry for tuning IRI activity of carbohydrate-based fluorosurfactants.

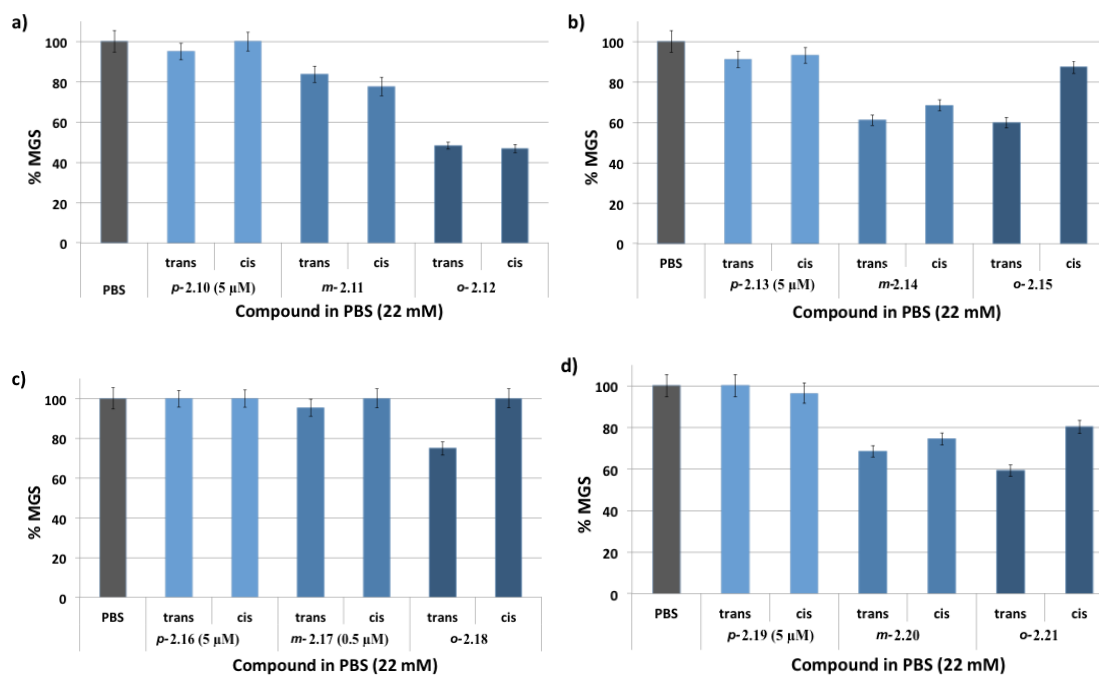


Figure 2.12. IRI activity of fluorosurfactants a) Glc-based **2.10–2.12**, b) Gal-based **2.13–2.15**, c) Man-based **2.16–2.18** and d) Cel-based **2.19–2.21** represented as a % MGS of ice crystals relative to the PBS control.

For compounds displaying moderate-to-potent IRI activity, an MTT (3-(4,5-dimethylthiazol-2-yl)-2,5-diphenyltetrazolium bromide) assay was performed using Hep G2 cells as a model system to assess the cytotoxicity of varying concentrations *in vitro* (Figure 2.13). MTT is a yellow tetrazole dye, which is reduced to its purple formazan form within living cells.⁶¹ In this assay, MTT was added to each well and the absorbance of each well was then read at a wavelength of 570 nm with a multiwell plate reader. Higher absorbance readings were indicative of greater cell viability. Unfortunately, there was a significant decrease in cell viability when incubated with the IRI-active, *ortho*-substituted analogues Glc *o*-CF₃**2.12**, Gal *o*-CF₃ **2.15** and Cel *o*-CF₃ **2.21** (Figure 2.13). The mechanism responsible for this cytotoxicity is unclear, however this could result from membrane damage and lysis caused by the high concentration of surfactants,⁶² or the toxicity of some azobenzene dyes, or both.⁶³

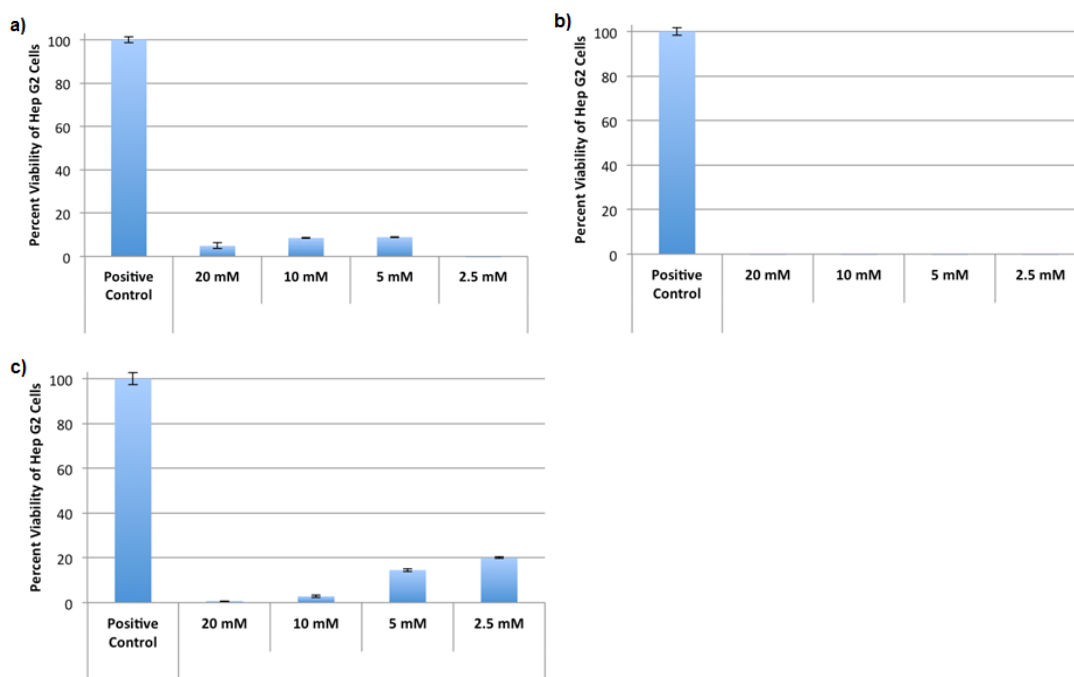


Figure 2.13. Percent cell viability of Hep G2 cell treated with various concentrations of surfactant a) Glc *o*-CF₃ **2.12**, b) Gal *o*-CF₃ **2.15** and c) Cel *o*-CF₃ **2.21**.

2.2.5 Quantitative analysis of IRI activity

As surfactant **2.8** showed very potent IRI activity compared with other compounds, the inhibitory activity of the *trans*-isomer of ManAzo **2.8** was further quantified by a modified splat-cooling assay.⁶⁴ A dose-response curve was generated based on the results from the modified splat-cooling assay, and a half-maximal inhibitory concentration ($IC_{50} = 7$ mM) could be calculated from this curve (Figure 2.14 a). The TH activity of **2.8** was investigated using nanoliter osmometry. No TH activity was observed for **2.8** at a concentration of 0.5 mg/mL, and the ice crystals grew uniformly as the temperature decreased (Figure 2.14 b), which indicated that the IRI activity of **2.8** did not arise through its interaction with developing ice crystals.

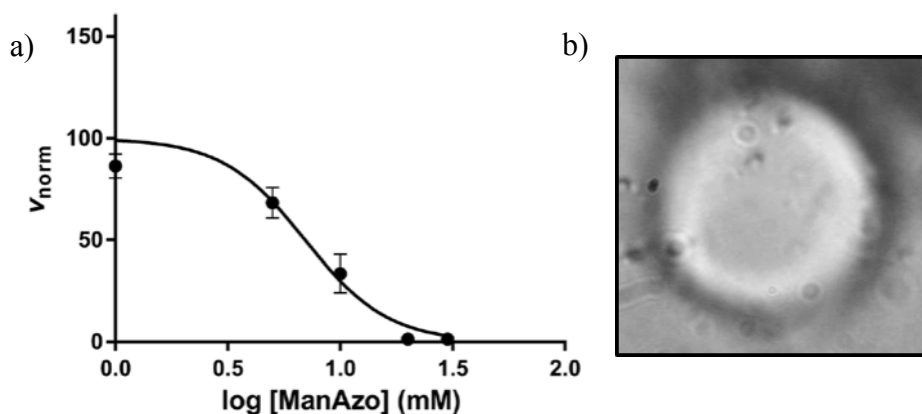


Figure 2.14. a) Dose-response curve for *trans*-dominated compound ManAzo **2.8**. A two-parameter sigmoidal curve was fitted to the data. V_{norm} is the normalized rate constant. b) Ice crystal habit image in the presence of 0.5 mg mL^{-1} *trans*-dominated form of **2.8**.

One major issue with current cryoprotectants is that they will reduce post-thaw cell viability and even cause cell death. Given that surfactant **2.8** shows potent IRI activity but did not show TH activity, we then investigated its cryoprotective ability using Tf-1 α cells. The post-thaw cell recovery, viability and apoptosis of Tf-1 α cells were assessed after having been cryopreserved with 30 mM of ManAzo **2.8** in the *trans*-PSS, in varying concentrations of DMSO (0–10%). Unfortunately, significantly lower post-thaw cell recoveries were observed for samples incubated with surfactant **2.8** when compared with DMSO alone, and the concentrations of DMSO had negligible influence on the results (Figure 2.15). Encouragingly, when compared to DMSO, the post-thaw cell apoptosis decreased when cryopreserved alone with **2.8** (Figure 2.16). Although surfactant **2.8** inhibited ice recrystallization, it was unable to prevent cell damage from freeze dehydration during freezing, which is why viability increased slightly only when a small amount of DMSO was added. In order to investigate the toxicity of **2.8**, TF-1 α cells were incubated with 30 mM of compound at 37°C and the cell recovery, viability and apoptosis were measured without cryopreservation (Figure 2.17). After a 30 min incubation period, significant cell death was observed. These results may not appear surprising, as the use of surfactants at

high concentrations are known to induce cell lysis through membrane damage.⁶² Moreover, azobenzene derivatives had been documented to show toxicity against cells, despite noteworthy reports describing the apparent non-toxicity of neutral azobenzene compounds with potential *in vivo* applications.^{40, 65, 66}

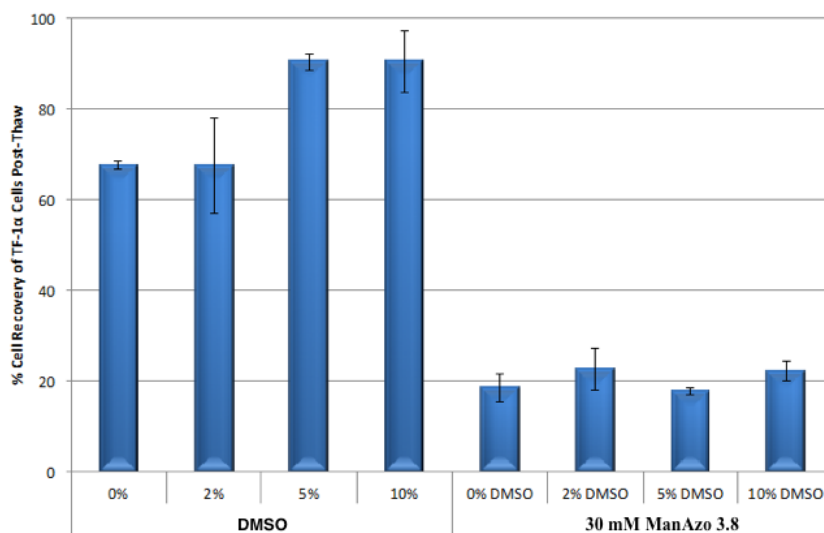


Figure 2.15. Percent post-thaw cell recoveries of TF-1 α cells cryopreserved with 30 mM ManAzo 2.8 in varying concentrations of DMSO.

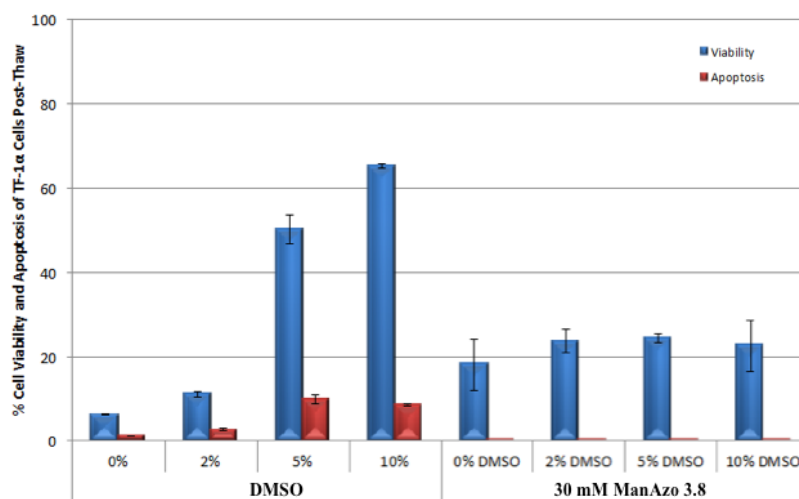


Figure 2.16. Percent post-thaw cell viability and apoptosis of Tf-1 α cells cryopreserved with 30 mM ManAzo 2.8 in varying concentrations of DMSO.

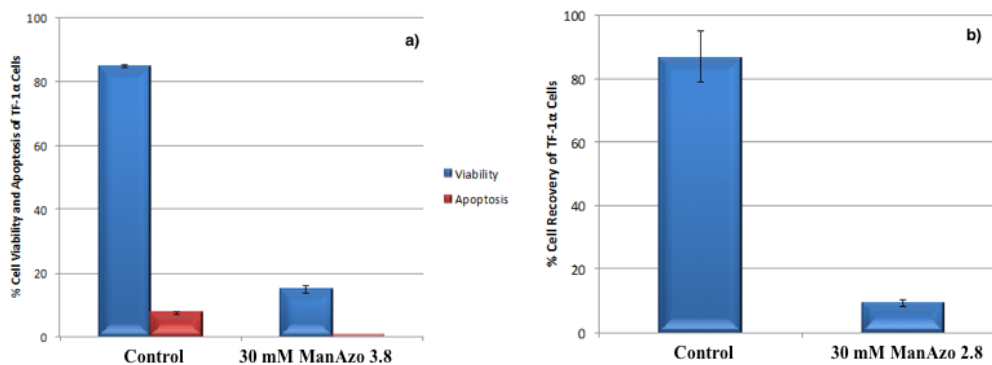


Figure 2.17. TF-1 α cells incubated at 37°C for 30 minutes with or without 30 mM ManAzo 2.8, a) Percent cell viability and apoptosis and b) percent cell recovery.

2.2.6 Antibacterial performance of fluorosurfactants

The antibacterial activity of selected fluorosurfactants **2.10–2.12**, **2.19–2.21** was evaluated against Gram-positive *Staphylococcus aureus* (*S. aureus*) and Gram-negative *Escherichia coli* (*E. coli*). The dose-dependent antibacterial activities were determined by optical density measurements at 600 nm (OD₆₀₀). These selected fluorosurfactants showed no, or limited, toxicity against *E. coli* but dose-dependent toxicity against Gram positive *S. aureus* (Figure 2.18). Generally, glucose-based fluorosurfactants **2.10–2.12** exhibited greater toxicity than cellobiose-based fluorosurfactants **2.19–2.21**, perhaps on account of the higher surface activity of the glucose-based analogues. Interestingly, the antibacterial activity also appeared sensitive to the position of the –CF₃ group within the ring. The bacterial activity of glucose-based fluorosurfactants **2.10–2.12** decreased when changing the position of the –CF₃ group from *meta* (Glc *m*-CF₃ **2.11**), *para* (Glc *p*-CF₃ **2.10**) and *ortho* (Glc *o*-CF₃ **2.12**), while for the cellobiose-based fluorosurfactants **2.19–2.21**, the toxicity decreased in a different order: *para* (Cel *p*-CF₃ **2.19**) > *meta* (Cel *m*-CF₃ **2.20**) > *ortho* (Cel *o*-CF₃ **2.21**). In order to investigate the influence of the carbohydrate moiety on antibacterial activity, the substituted azobenzene tail compounds **2.39–2.41** were also evaluated for their antibacterial properties, however owing to the extremely limited aqueous solubility reliable data could not be determined.

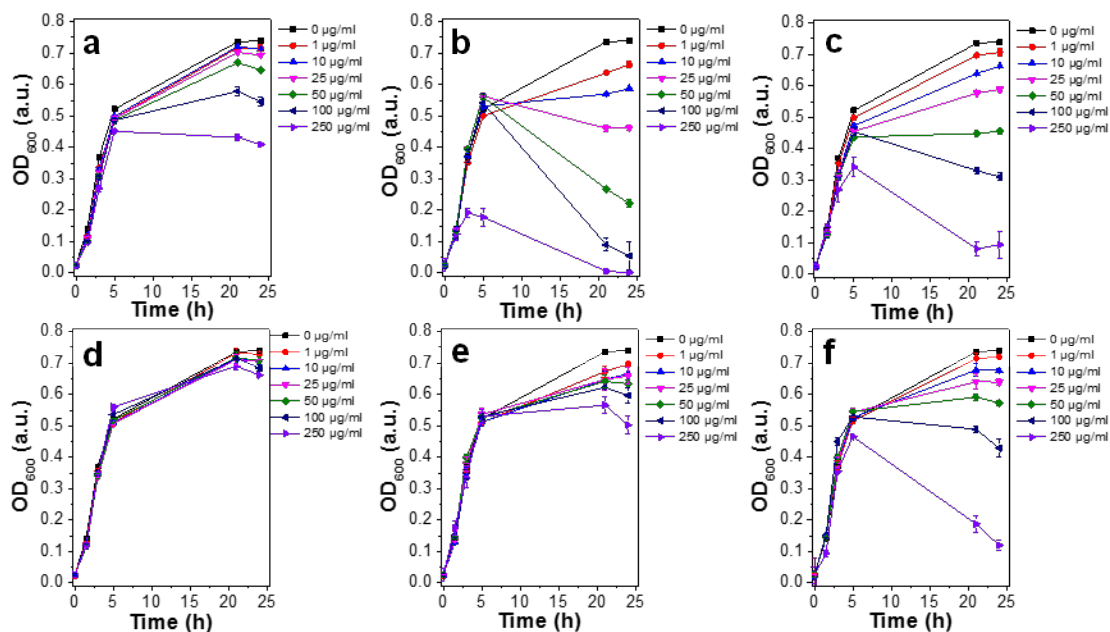


Figure 2.18. Dose-dependent antibacterial activity of a) Glc *o*-CF₃ **2.12**, b) Glc *m*-CF₃ **2.11**, c) Glc *p*-CF₃ **2.10**, d) Cel *o*-CF₃ **2.21**, e) Cel *m*-CF₃ **2.20** and f) Cel *p*-CF₃ **2.19** against Gram-positive bacteria *S. aureus* over a period of 24 hrs.

2.3 Conclusions

Using an efficient synthetic strategy, we have synthesized a library of photoswitchable carbohydrate-based surfactants and fluorosurfactants, and evaluated their photoswitchable surface activity and biological properties. An increase in the CMC values of (fluoro)surfactants **2.7–2.21** was generally observed upon UV irradiation as a result of the change in the geometry and polarity of the azobenzene tail group. However, for fluorosurfactants **2.10–2.21**, the magnitude of this difference was strongly dependent on the position of the –CF₃ group relative to the N=N bond, and followed the order of *ortho* > *meta* > *para*. The log *P* data in the *cis*- and *trans*-PSS for fluorosurfactants showed a different trend to the non-fluorinated derivatives **2.7–2.9**, where the *cis* isomer was generally more hydrophobic than the *trans* form. Taken together, these results suggest a strong correlation between tail group geometry and polarity for eliciting changes in the adsorption behavior and solubility of non-ionic, carbohydrate-based fluorosurfactants.

In order to probe the relationship between tail group hydrophobicity and IRI activity, the IRI activity of surfactants **2.7–2.9** and fluorosurfactants **2.10–2.21** was measured using a ‘splat-cooling’ assay, before and after photoisomerization. The IRI activity of these molecules was highly sensitive to carbohydrate head group size and configuration, as well as tail group hydrophobicity. Among the non-fluorinated surfactant series, the D-mannose-based compound **2.8** was shown to be strongly IRI active, which is in contrast to previous studies prescribing D-galactose head groups for potent IRI activity. Furthermore, photomodulation of IRI activity could be achieved, where the *cis* isomer was less IRI active possibly on account of the lowered hydrophobicity of the *cis* isomer relative to the *trans* form. For the fluorosurfactants **2.10–2.21**, very weak IRI activity was generally observed, with the *o*-CF₃ substituted series showing the strongest activity. Based on the log *P* data the *o*-CF₃ analogues were slightly more hydrophilic than the *m*- and *p*-CF₃ substituted compounds. The increased IRI activity of *o*-CF analogues is in contrast to previous studies that reveal the importance of increasing tail group hydrophobicity for invoking potent IRI activity. The IRI activity in this series was also sensitive to the carbohydrate head group, with the D-glucose-based derivative **2.12** displaying the strongest IRI activity. Although these compounds were shown to be cytotoxic, weak photomodulation in IRI activity was achieved, thus demonstrating a mechanism for tuning the IRI activity of amphiphilic carbohydrates.

2.4 Experimental

2.4.1 General

Analytical thin layer chromatography (TLC) was performed on commercially prepared silica plates (Merck Kieselgel 60 0.25 mm F254). Flash column chromatography was performed using 230-400 mesh Kieselgel 60 silica, eluting with distilled solvents as described. Solvents and reagents were purchased from Sigma-Aldrich and Merck and used without further purification. ¹H NMR and ¹³C NMR spectra were recorded on a Bruker Advance 400 NMR spectrometer at frequencies of 400 MHz. Chemical shift is reported as parts per million (ppm) downfield shift. The data are reported as chemical shift (δ), multiplicity, coupling constant (*J* = Hz), relative integral and assignment where possible. IR spectra were recorded on a Bruker

ATR spectrometer. Optical rotation was measured on an Optical Activity Polarizer 2001 (546 nm) polarimeter using a 1 mL cell. Please refer to this Google Drive link for complete NMR spectra: https://drive.google.com/drive/folders/0B4_hvKQzd29admI0WWgtZkFMUkk?usp=sharing

LC-MS was performed on an Agilent 6120 LC-MS system operating in positive ion mode. Separations were performed on an Agilent Poroshell-120 2.7 μm (3.0 mm \times 50 mm) C18 column using a linear gradient of 0.1% formic acid in Milli-Q water (Solvent A) and 0.1% formic acid in acetonitrile/Milli-Q water 95:5 mixture (Solvent B) as the mobile phase. Separations were performed using a linear gradient of 0% solvent B to 100% solvent B over 15 minutes, operating at a flow rate of 0.3 mL min^{-1} .

Deprotected carbohydrate-based surfactants were purified by reverse-phase (C18) preparative HPLC using an Agilent 1260 preparative HPLC system equipped with an automated fraction collector. Separations were performed on an Agilent Zorbax SB300 5 μm (20 mm \times 150 mm) C18 column using a linear gradient of 0.1% formic acid in deionized water (Solvent A) and 0.1% formic acid in acetonitrile/ deionized water 95:5 mixture (Solvent B) as the mobile phase. Surfactants were purified using 10% solvent B for 10 min and then gradually increased to 100% solvent B over 40 minutes (monitoring at 280 nm), operating at a flow rate of 10 mL min^{-1} . Purified fractions were subsequently combined and lyophilized.

2.4.2 Surface tension measurements

Surface tension measurements were made on a custom-designed pendant drop instrument.⁴⁸ A time series was taken (that is, surface tension as a function of time) and values were noted for 100 seconds to ensure full equilibration of interfacial adsorption. Once a stable surface tension had been attained, this was recorded. Drop volumes were measured throughout and changes of < 5% throughout the course of a measurement were a requirement for the data shown. Critical micelle concentration (CMC) values were obtained from the intersection of lines extrapolated from surface tension values in the near pre- and post-CMC regions.

2.4.3 UV-vis spectroscopy

UV-visible spectroscopy was performed using a Cary 60 spectrophotometer. The native *trans* isomers remained stable under ambient lighting conditions at least up to 24 h, as evident from insignificant changes in their UV-vis absorbance spectra over this period. In the photoillumination experiments, the *trans*-dominated and the *cis*-dominated spectra were taken from samples immediately after dilution and after 10 minutes of irradiation under a gel curing UV lamp (peak wavelength 365 nm, 36 W radiant power, Model W-818). The thermal relaxation studies were performed in dark adapted conditions at ambient temperature (approximately 20°C). The half-lives of the *cis*-isomers in water were estimated by plotting the UV-vis absorbance at 325 nm versus time over a period of 24 h.

The molar extinction coefficients were measured and calculated by Joshua Marlow under the supervision of Dr. Rico Tabor (Monash University, Australia). The molar extinction coefficients of the two main peaks, at roughly 450 nm and 350 nm in the samples in each photo-stationary state, were calculated for surfactants via analysis of five samples with a concentration ratio of 1:2:3:4:5, where the absorbance of the most concentrated sample was just below 1.0 to ensure the applicability of the Beer-Lambert law.

2.4.4 Measurement of 1-Octanol/water partition coefficient ($\log P$)

The $\log P$ of surfactants was determined by preparing a 50 μM solution of each surfactant in Milli-Q water and adding an equal volume of 1-octanol. The sample was gently agitated and UV-vis spectra were taken of the water layer before ($t = 0$ h) and after diffusion equilibrium ($t = 15$ h). Samples were stored in the dark prior to the final reading. To minimize thermal relaxation of the *cis* isomer under dark conditions, samples were further irradiated with UV light for 10 minutes at 6–8 h following the initial reading.

2.4.5 IRI assay

The sample was dissolved in a phosphate buffered saline (PBS) solution. Using a micropipette, a 10 μL droplet of the solution was dropped through a two-meter high plastic tube, having a 10

cm diameter, onto a polished aluminum block cooled to approximately -80°C with dry ice. The droplet froze immediately upon contact with the surface of the aluminium block, creating a wafer approximately 1 cm in diameter and 20 μm thick. Using precooled tools, the wafer was separated from the surface of the block and transferred to a cryostage, kept at -6.4°C . The wafer was annealed for 30 minutes, and then photographed between crossed polarizing filters using a digital camera (Nikon CoolPix 5000) fitted to a microscope. A programmable Peltier unit (S3 Series 800 temperature controller, Alpha Omega Instruments) was used to maintain the temperature of the cryostage. Three images were taken from each wafer. During flash freezing, small ice crystals from the solution are formed very quickly, and during annealing, the ice crystals dramatically increase in size due to recrystallization. In order to quantitatively measure the difference in recrystallization inhibition of two compounds, the difference in the dynamics of ice crystal size distribution was examined. This was done using a novel domain recognition software (DRS)22 program to analyze the image of the ice wafer. From this, domain areas from each image were calculated and data was inputted into Microsoft Excel. Using Microsoft Excel, the data was then plotted and analyzed. The ice crystal mean grain size (MGS) of the sample was compared to the MGS of the PBS control for the same day of testing and IRI activity was reported as percent mean grain size (%MGS). Error bars indicate the standard error of the mean (%SEM). Each compound was performed in triplicate ($n = 3$). In GraphPad, significant difference was determined using the unpaired Student's T test ($P < 0.05$).

2.4.6 MTT assay with Hep G2 cells

In order to investigate the cytotoxicity of the *ortho*-substituted analogues (Glc *o*-CF₃ **2.12**, Gal *o*-CF₃ **2.15**, Cel *o*-CF₃ **2.21**), Hep G2 cells were incubated with varying concentrations of the surfactants, with controls, and each test concentration performed at least in triplicate ($n = 3$). Error bars represent the percent standard error of the mean (% SEM). Hep G2 cells (human liver hepatocellular carcinoma cells, ATCC, HB-8065) were cultured in Eagle's minimum essential media (MEM) supplemented with 10% fetal bovine serum (FBS), 1% penicillin-streptomycin, 1% non-essential amino acids, and 0.1% 1M sodium pyruvate in Corning[®] T75 (75 cm²) flasks. Cells were incubated at 37°C with 5% CO₂. Passages 8–9 were used in this

study. No evidence of overgrowth or morphological changes consistent with apoptosis was observed. Cells were detached from plates using Accutase and incubated at 37°C for 15 minutes for use in experiments. Using a hemocytometer, the cell count was obtained by preparing a 1/2 dilution of the cell solution with trypan blue.

The MTT assay was performed according to known literature.⁶⁷ Hep G2 cells were plated in 96-well plates and treated with 100 µL of appropriate test compound dissolved in MEM (unless indicated otherwise), and incubated at 37°C with 5% CO₂ overnight. Unless stated otherwise, cells incubated with MEM only were used as positive controls and cells incubated with 1% Triton X-100 (in MEM) were used as negative controls. Following incubation, the plates were centrifuged (1000 rpm for 5 minutes), the supernatants were removed by aspiration, and 200 µL of MEM and 50 µL of MTT (5 mg mL⁻¹) in HBSS (Hank's balanced salt solution) were added to each well. The plates were incubated at 37°C with 5% CO₂ for 4 h before being centrifuged for 3 minutes at 700×g. The supernatants were removed, and 200 µL of MTT solubilization solution (0.1 N HCl, 10% Triton X-100 in isopropanol) was added to each well. The plate was incubated in the dark at room temperature for 2 h and the absorbance of each well was then read at a wavelength of 570 nm with a multiwell plate reader (AD 34 °C Absorbance Detector, Beckman Coulter, Inc., Mississauga, ON). Higher absorbance readings were indicative of greater cell viability. Data was analyzed using Microsoft Excel and percent cell viability was reported relative to the control.

2.4.7 Quantitative analysis of IRI activity

To quantify ice recrystallization inhibition (IRI) activity, a modified “splat cooling” assay (described above) was employed.⁶⁴ Five concentrations (1, 5, 10, 20, 30 mM) of ManAzo **2.8** were tested in triplicate as well as the PBS control. Instead of a 30-minute annealing period, the wafer was annealed for 5 minutes at -6.4°C, and then photographed between crossed polarizing filters using a digital camera (Nikon CoolPix 5000) fitted to the microscope. One image was selected from each wafer for further analysis. Using ImageJ, ice crystals with well-defined boundaries within the image were circled, and the area of each circled ice crystal was calculated.

Using Microsoft Excel, the ice crystal areas were sorted into discrete bins based on size (bin size increased in increments of 0.001 mm^2). At time zero, all ice crystals could be contained within a bin size of 0.001 mm^2 , and therefore, as crystals grew due to recrystallization, they moved out of bin 1 and into higher bins. The proportionate area of each bin was calculated for each sample wafer by adding the area of each crystal within a bin and dividing by the sum of the areas of all crystals in the image. The rate constants were determined for each inhibitor concentration tested and normalized based on the average rate constant determined for the PBS control (zero inhibitor concentration). Using GraphPad, a dose-response curve was generated using the normalized rate constants, v_{norm} , for each inhibitor concentration, $[I]$, and the corresponding log values of the concentration. A two-parameter sigmoidal curve was fit to the data to obtain the half maximal inhibition concentration (IC_{50}). Error was reported as the standard error of the mean.

2.4.8 TH assay

Nanoliter osmometry, using a Clifton nanoliter osmometer (Clifton Technical Physics, Hartford, NY), was performed in order to assess the TH activity and dynamic ice shaping (DIS) ability of ManAzo **2.8**.⁶⁸ In this assay, a single droplet of an aqueous solution (Milli-Q water) of compound was enclosed within an oil-filled well in a sample holder. Using a thermoelectrically-controlled microscope stage, the sample was frozen and then slowly thawed until a single ice crystal remained. At this point, the morphology of the single ice crystal was monitored as the temperature of the sample was gradually decreased, through a Leitz compound microscope equipped with an Olympus 20X objective, a Leitz Periplan 32X photo eyepiece, and a Hitachi KPM2U CCD camera connected to a Toshiba MV13K1 TV/VCR system. Non-uniform ice crystal growth is indicative of dynamic ice shaping (DIS) and TH activity is measured as the depression of the freezing point in relation to a static melting point. Due to the amphiphilic nature of ManAzo **2.8**, a 10 mg mL^{-1} solution dissolved into the oil phase, creating a single phase. As a result, the TH and DIS activity was assessed at 0.5 mg mL^{-1} . At this concentration, ManAzo **2.8** did not exhibit DIS nor TH activity.

2.4.9 Cryopreservation of Tf-1 α cells

Tf-1 α cells were cryopreserved with a 30 mM concentration of ManAzo **2.8** in 0%, 2%, 5%, 10% DMSO solutions with controls performed in duplicate and each test concentration performed in triplicate. Error bars represent the percent standard error of the mean. TF-1 α cells (human bone marrow erythroblasts, ATCC CRL-2451) were cultured in RPMI-1640 media supplemented with 1% penicillin-streptomycin and 10% fetal bovine serum (FBS) in 150 mm petri dishes. Cells were incubated at 37°C with 5% CO₂. Media was changed every two days by transferring suspended cells in the culture dish to a 50 mL falcon tube and centrifuging at 1000 rpm for 5 minutes at room temperature. Following this, supernatant was removed and the pellet was re-suspended in RPMI-1640 media by vortex. This was transferred to a new culture dish and 20 mL of media was added. Cells were split if cell count exceeded 5×10^6 cells per plate. Using a hemocytometer, the cell count was obtained by preparing a 1/8 dilution of the cell solution in an eppendorf tube with the dye, trypan blue.

Once enough cells had been cultured (2×10^6 cells/cryovial is required), the contents of the culture dishes were transferred to 50 mL centrifuge tubes and centrifuged at 1000 rpm for 5 minutes at room temperature. Supernatants were removed and the pellets were re-suspended in a small amount of media. The re-suspended cells were combined into one falcon tube and the total cell count was obtained using a hemocytometer. The volume required to add 2×10^6 cells per cryovial was determined and transferred to each vial. Cryovials were centrifuged at 1000 rpm for 5 minutes at room temperature. For data obtained in Figure 2.16, the supernatant was carefully removed, and 100 μ L of the appropriate cryosolution (0%, 2%, 5%, 10% DMSO solutions in media with or without 30 mM of ManAzo **2.8**) was added to each vial. Cryovials were vortexed and transferred to a “Mr. Frosty” freezing container and placed in a -80°C freezer for 18 hours. The cryovials were then placed in a -196°C storage dewar for a minimum of 12 hours prior to analysis. For the data obtained in Figure 2.17, 100 μ L of either media or 30mM surfactant **2.8** ManAzo in media was added to each vial. Cryovials were vortexed and incubated for 30 minutes at 37°C with 5% CO₂.

Cryovials were thawed under fast-thaw conditions (37°C water bath) followed by the addition of 900 µL 1X Annexin V binding buffer to each cryovial. The contents were mixed and 400 µL of each vial was transferred to eppendorf tubes. 10µL 7-AAD and 10 µL Annexin V FITC were added, and the tubes were incubated in the dark for 15 minutes at room temperature. 20 µL counting beads were added followed by the addition of 1X Annexin V binding buffer to a total volume of 1mL. The solutions were filtered into flow tubes prior to flow cytometry. Flow cytometry was performed on a Beckman Coulter Gallios Flow Cytometer using Kaluza for Gallios as software. Annexin V-FITC was measured with 518 nm optical filter (FL-1), while 7-AAD was measured with 570 nm optical filter (FL-4). Viability (Figure 2.16) was determined as the amount of 7-AAD⁻ cells detected and apoptosis was determined as the amount of 7-AAD⁻ cells that were also Annexin V FITC⁺. Bead counts and total post-thaw cell counts were obtained for each sample. Cell recovery (Figure 2.15) was calculated as the concentration of cells post-thaw/post-incubation divided by the pre-freeze/pre-incubation cell concentration. The time between thawing and flow cytometry analysis was under 1 hour.

2.4.10 Antibacterial assays

The antibacterial activity of the fluorosurfactants was tested against Gram-negative *E. coli* and Gram-positive *S. aureus*. A fixed concentration ($OD_{600} = 0.1$: log phase 10^8 CFU mL⁻¹) of freshly grown cultures were used for antibacterial assay, after determining the bacterial concentration using a GENESYS 10S UV-vis Spectrophotometer. The bacterial suspension (100 µL) was incubated with 100 µL of the fluorosurfactants in Milli-Q water at 37°C. Different concentrations of the fluorosurfactants in Milli-Q water (0, 1, 10, 25, 50, 100, 250 µg mL⁻¹) were used to determine the concentration-dependent influence on bacterial growth and/or inhibition. Appropriate controls were chosen wherein one of the controls contained no fluorosurfactants while the other contained a mixture of different concentrations of fluorosurfactants with the bacteria-free growth media. The bacterial growth curves were monitored at OD_{600} over a period of 24 hours (0 h, 1.5 h, 3 h, 5 h, 21 h and 24 h) in 96-well format using a Perkin Elmer EnVision™ 2104 Multilabel Plate Reader. All antibacterial assays were performed in triplicates, tests were repeated independently three times, and each well was

read five times. The average of 45 readings ($3 \times 3 \times 5$) in each case was calculated and plotted along with standard deviation. The data was background corrected by subtracting the OD₆₀₀ value obtained from the control containing a mixture of fluorosurfactants and the bacteria-free growth media.

2.4.11 Synthesis of 2.36 and 2.37 : General procedure 1

The synthesis of per-*O*-acetyl glycosyl bromide (**2.36** and **2.37**) was adapted from a literature procedure.⁴² Glycosyl pentaacetate **2.22** or **2.23** (1 equiv.) was dissolved in dry DCM (50 mL). To this, hydrogen bromide (33 wt.% in acetic acid, 30 mL) was added. The reaction mixture was stirred vigorously at ambient temperature with a drying tube. After 2 hours, TLC indicated the formation of a product with complete consumption of the starting material. The reaction mixture was partitioned between DCM and water, and the combined organic layer was washed with cold satd. aq. NaHCO₃ (3×100 mL), cold brine (100 mL), dried over Na₂SO₄, filtered, and evaporated under reduced pressure to afford the corresponding glycosyl bromide as a colorless foam.

2.4.12 Synthesis of 2.32 and 2.33: General procedure 2

The synthesis of per-*O*-acetyl glycosyl azide (**2.32** and **2.33**) was performed using a known literature procedure.⁶⁹ The glycosyl bromide (1 equiv.) was dissolved in DCM (20 mL) and a solution of NaN₃ (3 equiv.) in saturated aqueous NaHCO₃ (20 mL) was added. Tetrabutylammonium hydrogen sulfate (1 equiv.) was added and the reaction mixture was stirred vigorously at ambient temperature until TLC indicated complete consumption of the starting material and formation of product. Following reaction completion, the organic layer was washed with water (100 mL), dried over Na₂SO₄, filtered and concentrated under reduced pressure. The crude product was purified by either recrystallization from methanol.

2.4.13 Synthesis of 2.30 and 2.48–2.50: General procedure 3

This synthesis of azobenzene tail groups (**2.30** and **2.48–2.50**) was achieved using an adapted literature procedure.⁴⁴ To a solution of the aniline (1 equiv.) in 32% wt. aqueous solution of HCl

(24 mL) and water (30 mL), was added a drop-wise solution of NaNO₂ (1.2 equiv.) in water (14 mL) over 30 min at 0°C. The mixture was allowed to stir at 0°C for 1 hour. A solution of phenol (1.1 equiv.) in a 6 M Na₂CO₃ solution (50 mL) was then added to the mixture at 0°C, and TLC was used to monitor the reaction. Finally, the solution was quenched with 1 M aqueous HCl and the precipitate was collected and dried to give the final compound. Analytically pure sample was acquired following purification by recrystallization from hexane.

2.4.14 Synthesis of 2.25 and 2.42–2.44: General procedure 4

This synthetic method was adapted from a literature procedure.⁴⁴ In a round-bottomed flask under N₂, tosylate **2.31** (1.0 equiv.), K₂CO₃ (5.0 equiv.) and LiCl (0.03 equiv.) were dissolved in acetonitrile (100 mL). A solution of substituted azobenzene (1.06 equiv.) in acetonitrile (50 mL) was added dropwise. The mixture was refluxed under N₂ for 18 hours. The solvent was then cooled before being concentrated under reduced pressure. The residue was then re-dissolved in DCM (100 mL) and washed with brine (3×100 mL). The organic layer was dried over Na₂SO₄, concentrated under reduced pressure and recrystallized from petroleum spirit to give the product as bright orange solid.

2.4.15 Synthesis of 2.39–2.41: General procedure 5

This synthetic method was adapted from a literature procedure.⁴⁵ To a solution of **2.42–2.44** (1 equiv.) in anhydrous THF (0.2 mol dm⁻³) was added NaH (60 wt.% in mineral oil, 1.5 equiv.) at 0°C under N₂. A catalytic amount of tetrabutylammonium iodide (0.05 equiv.) and propargyl bromide (80% in toluene, 1.5 equiv.) were added sequentially. The mixture was stirred at ambient temperature overnight, before being concentrated under reduced pressure and purified by column chromatography (EtOAc : hexane = 1:9).

2.4.16 Synthesis of 2.7–2.9: General procedure 6

This synthetic method was adapted from the literature.⁴¹ The carbohydrate donor (1 equiv.) and alcohol acceptor **2.25** (1 equiv.) was suspended in anhydrous DCM (40 mL) under a nitrogen atmosphere. The stirred solution was cooled to 0°C and BF₃·Et₂O (5 equiv.) was added drop-

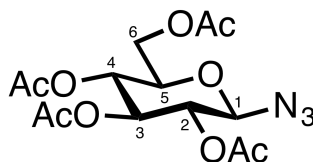
wise. After 1 hour, the solution was warmed to room temperature and stirred overnight. The reaction mixture was quenched with satd. aq. NaHCO₃ (3 × 100 mL) and the aqueous layer was extracted twice with DCM (50 mL). The combined DCM layers were dried and concentrated. To the crude product in anhydrous methanol (20 mL) was added NaOCH₃ (25 wt.% solution in methanol, 0.5 mL) dropwise. Then the reaction mixture was stirred under ambient temperature until TLC indicated the full consumption of the starting material and formation of product. The reaction mixture was neutralized with Amberlite IR-120 acidic ion exchange resin, filtered and concentrated under reduced pressure. The residue was purified by reversed phase preparative HPLC to give the pure material.

2.4.17 Synthesis of 2.10–2.21: General procedure 7

This method was adapted from the literature.⁶⁹ A mixture of the glycosyl azide **2.32–2.35** (1 equiv.) and alkyne **2.39–2.41** (1.2 equiv.) was suspended in 0.1 M 2:1 *tert*-butyl alcohol/water mixture. Then sodium ascorbate (0.4 equiv.) and CuSO₄·5H₂O (0.2 equiv.) was added successively. The reaction suspension was stirred vigorously at 40°C under N₂ until TLC indicated the full consumption of the starting materials. The crude mixture was evaporated under reduced pressure. To the crude mixture in anhydrous methanol (20 mL) was added NaOMe (25 wt.% in methanol, 0.5 mL) dropwise. Then the reaction mixture was stirred under ambient temperature until TLC indicated the full consumption of the starting material and formation of product. The reaction mixture was neutralized with Amberlite IR-120 acidic ion exchange resin, filtered and concentrated under reduced pressure. The residue was purified by reversed phase preparative HPLC to give the pure material.

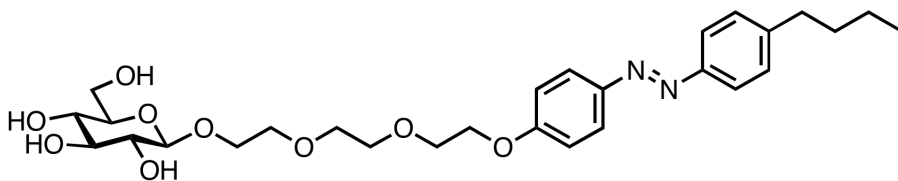
2.4.18 Note on nomenclature

Glycosyl compounds are named according to IUPAC-IUBMB “Nomenclature of Carbohydrate” (<http://www.chem.qmul.ac.uk/iupac/2carb/>)⁷⁰⁻⁷² and the literature.⁷³ Compound **2.32** is given as an example.



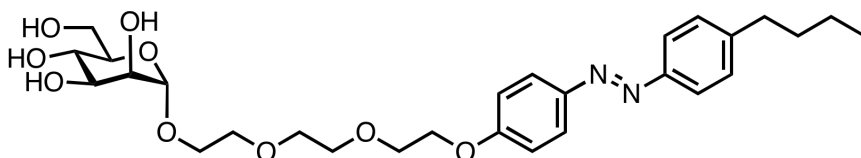
2.4.19 Analytical data

2-[2-[2-(4-n-butylazophenyl phenoxy)ethoxy]ethoxy]ethyl β -D- glucopyranoside **2.7**⁴⁸



Compound **2.7** was prepared from **2.22** and **2.25** according to general procedure 6 and isolated as an orange solid (Yield: 39%). Mp = 41.2°C; $[\alpha]_D^{20}$ -10.5 (*c*, 0.09 in CH₃OH); FT-IR: ν_{\max} /cm⁻¹ 3355, 2924, 2872, 1596, 1250; ¹H NMR (400 MHz, CD₃OD) δ 7.88 (d, *J* = 9.0 Hz, 2H, 2 \times Ar*H*), 7.78 (d, *J* = 8.4 Hz, 2H, 2 \times Ar*H*), 7.33 (d, *J* = 8.5 Hz, 2H, 2 \times Ar*H*), 7.09 (d, *J* = 9.1 Hz, 2H, 2 \times Ar*H*), 4.30 (d, *J* = 7.8 Hz, 1H, *H*-1), 4.25–4.22 (m, 2H), 4.03–3.98 (m, 1H), 3.90–3.87 (m, 2H), 3.84–3.84 (m, 1H), 3.75–3.63 (m, 9H), 3.38–3.33 (m, 1H), 3.28–3.26 (m, 2H), 3.20 (dd, *J* = 9.1, 7.8 Hz, 1H), 2.70 (t, *J* = 7.7 Hz, 2H, CH₂), 1.69–1.62 (m, 2H, CH₂), 1.45–1.35 (dq, *J* = 14.9, 7.4 Hz, 2H, CH₂), 0.96 (t, *J* = 7.4 Hz, 3H, CH₃); ¹³C NMR (100 MHz, CD₃OD) δ 162.7 (ArC), 152.3 (ArC), 148.3 (ArC), 147.2 (ArC), 130.1 (2 \times ArC), 125.6 (2 \times ArC), 123.5 (2 \times ArC), 116.0 (2 \times ArC), 104.4 (C-1), 77.9 (CH), 75.0 (CH), 72.4 (CH), 71.7 (CH), 71.6 (CH₂), 71.5 (CH₂), 71.4 (CH₂), 70.7 (CH₂), 69.6 (CH₂), 68.9 (CH₂), 62.7 (CH₂), 43.8 (CH₂), 36.4 (CH₂), 34.7 (CH₂), 23.3 (CH₂), 14.3 (CH₃); LC/MS: *m/z* 549.1 [*M* + H]⁺, 571.0 [*M* + Na]⁺; ESI-HRMS⁺ calculated for C₂₈H₄₁N₂O₉ = 549.2812 [*M* + H]⁺, found 549.2809 [*M* + H]⁺, the obtained melting point, optical rotation, FTIT, ¹H NMR, ¹³C NMR and mass data are in agreement with the reference 48.

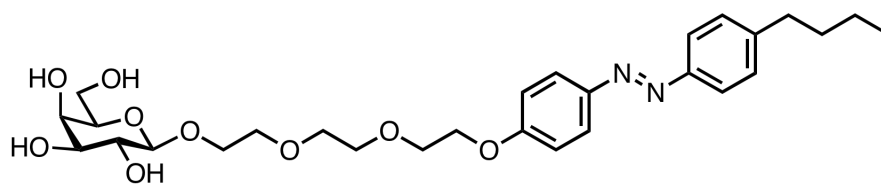
2-[2-[2-(4-n-butylazophenyl phenoxy)ethoxy]ethoxy]ethyl α -D-mannopyranoside **2.8**



Compound **2.8** was prepared from **2.24** and **2.25** according to general procedure 6 and isolated as orange solid (Yield: 26%). Mp = 191.2°C (decomp); $[\alpha]_D^{20}$ 27.3 (*c*, 0.16 in CH₃OH); FT-IR:

$\nu_{\max}/\text{cm}^{-1}$ 3297, 2929, 2877, 1576, 1498, 1412, 1248, 1051, 840, 648; ^1H NMR (400 MHz, CD_3OD) δ 7.87 (d, $J = 9.07$ Hz, 2H, $2 \times \text{ArH}$), 7.77 (d, $J = 8.35$ Hz, 2H, $2 \times \text{ArH}$), 7.32 (d, $J = 8.38$ Hz, 2H, $2 \times \text{ArH}$), 7.08 (d, $J = 9.06$ Hz, 2H, $2 \times \text{ArH}$), 4.82–4.79 (m, 1H, $H-1$), 4.23–4.20 (m, 2H), 3.89–3.56 (m, 17H), 2.68 (t, $J = 7.66$ Hz, 2H, CH_2), 1.67–1.60 (m, 2H, CH_2), 1.43–1.34 (m, 2H, CH_2), 0.95 (t, $J = 7.33$ Hz, 3H, CH_3); ^{13}C NMR (100 MHz, CD_3Cl_3) δ 161.4 (ArC), 150.9 (ArC), 146.9 (ArC), 145.9 (ArC), 128.8 ($2 \times \text{ArC}$), 124.2 ($2 \times \text{ArC}$), 122.2 ($2 \times \text{ArC}$), 114.6 ($2 \times \text{ArC}$), 100.3 (C-1), 73.2 (CH), 71.1 (CH), 70.7 (CH), 70.4 (CH), 70.2 (CH_2), 70.0 (CH_2), 69.4 (CH_2), 67.6 (CH_2), 67.1 (CH_2), 66.4 (CH_2), 61.3 (CH_2), 35.1 (CH_2), 33.4 (CH_2), 22.9 (CH_2), 21.9 (CH_2), 12.9 (CH_3); LC/MS: m/z 548.8 [$M + \text{H}$] $^+$, 570.7 [$M + \text{Na}$] $^+$; ESI-HRMS $^+$ calculated for $\text{C}_{28}\text{H}_{40}\text{N}_2\text{O}_9 = 548.2734$ [$M + \text{H}$] $^+$, found 571.2621 [$M + \text{Na}$] $^+$.

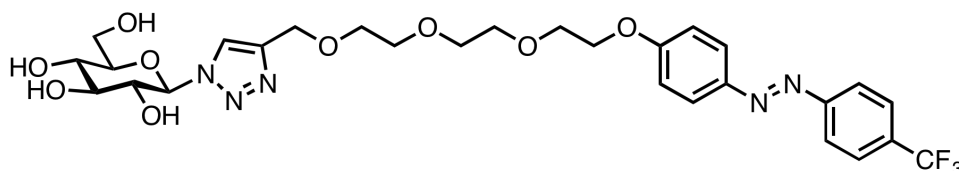
2-[2-[2-(4-n-butylazophenyl phenoxy)ethoxy]ethoxy]ethyl β -D- galactopyranoside **2.9**⁴⁸



Compound **2.9** was prepared from **2.23** and **2.25** according to general procedure 6 and isolated as an orange solid (Yield: 20%). Mp = 43.4°C; $[\alpha]_{\text{D}}^{20}$ -6.0 (c , 0.08 in CH_3OH); ^1H NMR (400 MHz, CD_3OD) δ 7.88 (d, $J = 9.1$ Hz, 2H, $2 \times \text{ArH}$), 7.78 (d, $J = 8.4$ Hz, 2H, $2 \times \text{ArH}$), 7.34 (d, $J = 8.6$ Hz, 2H, $2 \times \text{ArH}$), 7.10 (d, $J = 9.1$ Hz, 2H, $2 \times \text{ArH}$), 4.26–4.23 (m, 3H), 4.03–3.98 (m, 1H), 3.90–3.87 (m, 2H), 3.80 (dd, $J = 3.3, 0.9$ Hz, 1H), 3.78–3.69 (m, 10H), 3.55–3.44 (m, 4H), 2.70 (t, $J = 7.7$ Hz, 2H, CH_2), 1.70–1.62 (m, 2H, CH_2), 1.45–1.35 (m, 2H, CH_2), 0.97 (t, $J = 7.4$ Hz, 3H, CH_3); ^{13}C NMR (100 MHz, CD_3OD) δ 162.7 (ArC), 152.2 (ArC), 148.2 (ArC), 147.3 (ArC), 130.3 ($2 \times \text{ArC}$), 125.7 ($2 \times \text{ArC}$), 123.6 ($2 \times \text{ArC}$), 116.1 ($2 \times \text{ArC}$), 105.1 (C-1), 76.6 (CH), 74.9 (CH), 72.4 (CH), 72.3 (CH), 71.6 (CH_2), 71.5 (CH_2), 71.4 (CH_2), 70.6 (CH_2), 70.1 (CH_2), 69.5 (CH_2), 69.0 (CH_2), 62.4 (CH_2), 44.2 (CH_2), 36.7 (CH_2), 34.7 (CH_2), 23.3 (CH_2), 14.4 (CH_3); LC/MS: m/z 549.0 [$M + \text{H}$] $^+$, 571.0 [$M + \text{Na}$] $^+$; ESI-HRMS $^+$ calculated for

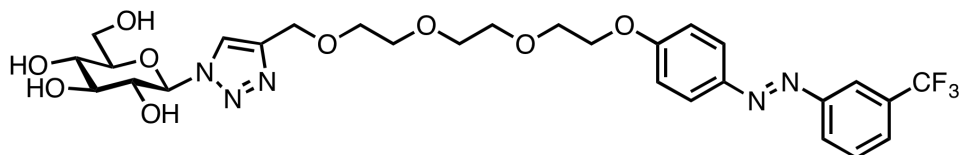
$C_{28}H_{41}N_2O_9=549.2812 [M + H]^+$, found $549.2808 [M + H]^+$, the obtained melting point, optical rotation, FTIT, 1H NMR, ^{13}C NMR and mass data are in agreement with the reference 48.

2-[2-[2-(4-trifluoromethylazophenyl phenoxy)ethoxy]ethoxy]ethyl β -D-glucopyranosyl-1,2,3-triazole **2.10**



Compound **2.10** was prepared from **2.32** and **2.39** according to general procedure 7 and isolated as orange solid (Yield: 42%). Mp = 95.7°C; $[\alpha]_D^{20}$ -20.6 (*c*, 0.15 in CH_3OH); FT-IR: ν_{max}/cm^{-1} 2859, 1596, 1421, 1037, 762; 1H NMR (400 MHz, d_6 -DMSO) δ 8.26 (s, 1H, *CH*(triazole)), 8.02–8.00 (m, 2H, 2 \times *ArH*), 7.96–7.93 (m, 4H, 4 \times *ArH*), 7.18 (d, *J* = 9.04 Hz, 2H, 2 \times *ArH*), 5.51 (d, *J* = 9.35 Hz, 1H, *H*-1), 5.35 (s, 1H, *OH*), 5.25 (s, 1H), 5.13 (s, 1H), 4.61 (s, 1H), 4.55–4.52 (m, 2H), 4.25–4.22 (m, 2H, *H*-3), 3.79–3.70 (m, 3H, *H*-2), 3.62–3.51 (m, 10H), 3.44–3.41 (m, 3H); ^{13}C NMR (150 MHz, CD_3OD) δ 162.19, 152.7, 146.6, 144.6, 124.9, 123.0, 118.3, 114.8, 88.2, 79.7, 77.1, 72.6, 70.4, 70.2, 69.5, 69.4, 69.3, 67.7, 63.5, 60.9; LC/MS: *m/z* 641.7 $[M + H]^+$; ESI-HRMS $^+$ calculated for $C_{28}H_{34}F_3N_5O_9=641.6012 [M + H]^+$, found 642.2379 $[M + H]^+$, 664.2201 $[M + Na]^+$.

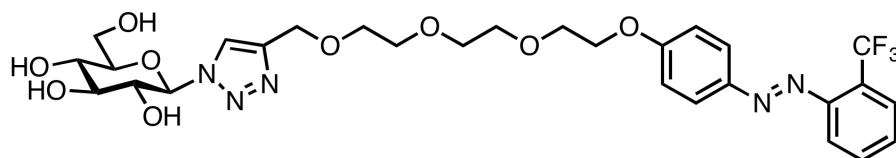
2-[2-[2-(3-trifluoromethylazophenyl phenoxy)ethoxy]ethoxy]ethyl β -D-glucopyranosyl-1,2,3-triazole **2.11**



Compound **2.11** was prepared from **2.32** and **2.40** according to general procedure 7 and isolated as orange solid (Yield: 67%). Mp = 97.7°C; $[\alpha]_D^{20}$ -14.1 (*c*, 0.17 in CH_3OH); FT-IR: ν_{max}/cm^{-1} 3351, 1599, 1498, 1325, 1247, 1055, 691; 1H NMR (400 MHz, d_6 -DMSO) δ 8.28 (s, 1H,

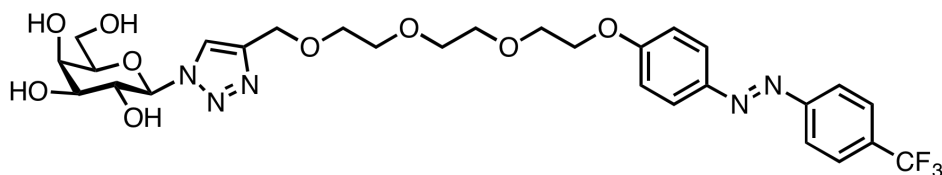
CH(triazole)), 8.15–8.09 (m, 3H, 3 × *ArH*), 7.95 (d, *J* = 9.13 Hz, 2H, 2 × *ArH*), 7.89–7.80 (m, 2H, 2 × *ArH*), 7.17 (d, *J* = 8.96 Hz, 2H, 2 × *ArH*), 5.52 (d, *J* = 9.03 Hz, 1H, *H*-1), 5.37 (s, 1H, *OH*), 5.27 (s, 1H), 5.14 (s, 1H), 4.62 (s, 1H), 4.54 (s, 2H), 4.24–4.22 (m, 2H, *H*-3), 3.80–3.70 (m, 3H, *H*-2), 3.62–3.51 (m, 8H), 3.45–3.24 (m, 5H); ¹³C NMR (100 MHz, *d*₆-DMSO) δ 162.4 (*ArC*), 152.6 (*ArC*), 146.5 (*ArC*), 144.3 (*C*=*CH*(triazole)), 131.3 (*ArC*), 130.8 (*ArC*), 125.7 (2 × *ArC*), 123.7 (*CF*₃), 118.6 (*ArC*), 115.7 (2 × *ArC*), 87.9 (*C*-1), 80.4, 77.4, 72.6, 70.4, 70.3, 70.2, 70.0, 69.6, 69.2, 68.2, 63.9, 61.2; LC/MS: *m/z* 641.7 [*M* + *H*]⁺; ESI-HRMS⁺ calculated for C₂₈H₃₄F₃N₅O₉=641.6012 [*M* + *H*]⁺, found 642.2381 [*M* + *H*]⁺, 664.2200 [*M* + *Na*]⁺.

2-[2-[2-(2-trifluoromethylazophenyl phenoxy)ethoxy]ethoxy]ethyl β-D-glucopyranosyl-1,2,3-triazole **2.12**



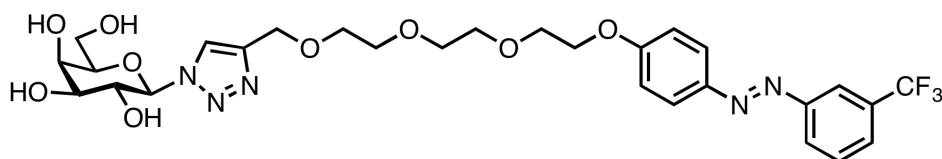
Compound **2.12** was prepared from **2.32** and **2.41** according to general procedure 7 and isolated as orange solid (Yield: 52%). Mp = 189.9°C; [α]_D²⁰ -26.4 (*c*, 0.13 in CH₃OH); FT-IR: ν_{max} /cm⁻¹ 2859, 1593, 1421, 1322, 1063, 854; ¹H NMR (400 MHz, *d*₆-DMSO) δ 8.28 (s, 1H, *CH*(triazole)), 7.95–7.90 (m, 3H, 3 × *ArH*), 7.82–7.78 (m, 2H, 2 × *ArH*), 7.72–7.70 (m, 1H, *ArH*), 7.19 (d, *J* = 9.07 Hz, 2H, 2 × *ArH*), 5.52 (d, *J* = 9.09 Hz, 1H, *H*-1), 5.37 (d, *J* = 5.94 Hz, 1H, *OH*), 5.26 (d, *J* = 4.38 Hz, 1H), 5.13 (d, *J* = 5.28 Hz, 1H), 4.63–4.61 (m, 1H), 4.56–4.52 (m, 2H), 4.24–4.22 (m, 2H, *H*-3), 3.79–3.76 (m, 3H, *H*-2), 3.62–3.54 (m, 8H), 3.46–3.39 (m, 3H), 3.32–3.27 (m, 2H); ¹³C NMR (100 MHz, *d*₆-DMSO) δ 162.6 (*ArC*), 149.4 (*ArC*), 146.9 (*ArC*), 144.3 (*C* = *CH* (triazole)), 134.1 (*ArC*), 131.2 (*ArC*), 125.7 (2 × *ArC*), 123.6 (*CF*₃), 116.7 (*ArC*), 115.8 (2 × *ArC*), 87.9 (*C*-1), 80.4, 77.4, 72.6, 70.4, 70.3, 70.2, 70.0, 69.6, 69.2, 68.2, 63.9, 61.2; LC/MS: *m/z* 641.7 [*M* + *H*]⁺, ESI-HRMS⁺ calculated for C₂₈H₃₄F₃N₅O₉=641.6012 [*M* + *H*]⁺, found 642.2380 [*M* + *H*]⁺, 664.2201 [*M* + *Na*]⁺.

2-[2-[2-(4-trifluoromethylazophenyl phenoxy)ethoxy]ethoxy]ethoxy]ethyl β -D-galactopyranosyl-1,2,3-triazole **2.13**



Compound **2.13** was prepared from **2.33** and **2.39** according to general procedure 7 and isolated as orange solid (Yield: 78%). Mp = 212°C (decomp.); $[\alpha]_D^{20}$ -30.9 (*c*, 0.13 in CH₃OH); FT-IR: $\nu_{\max}/\text{cm}^{-1}$ 2870, 1597, 1452, 1321, 1251, 1060, 852, 773; ¹H NMR (400 MHz, *d*₆-DMSO) δ 8.20 (s, 1H, =CH(triazole)), 8.00 (d, *J* = 8.39 Hz, 2H, 2 \times Ar*H*), 7.95–7.92 (m, 4H, 4 \times Ar*H*), 7.17 (d, *J* = 9.07 Hz, 2H, 2 \times Ar*H*), 5.48 (d, *J* = 9.20 Hz, 1H, *H*-1), 4.25–4.22 (m, 2H), 4.07–4.02 (m, 1H), 3.81–3.78 (m, 3H), 3.73–3.69 (m, 1H), 3.63–3.47 (m, 13H); ¹³C NMR (100 MHz, *d*₆-DMSO) δ 162.5 (ArC), 154.8 (ArC), 146.6 (ArC), 144.5 (C=CH(triazole)), 127.1 (ArC), 125.6 (2 \times ArC), 123.3 (CF₃), 123.2 (ArC), 115.8 (2 \times ArC), 88.6 (C-1), 78.9, 74.2, 70.5, 70.3, 70.2, 69.9, 69.6, 69.3, 68.9, 68.3, 63.9, 60.9 (CH₂); LC/MS: *m/z* 641.7 [*M* + H]⁺; ESI-HRMS⁺ calculated for C₂₈H₃₄F₃N₅O₉=641.2309 [*M* + H]⁺, found 664.2199 [*M* + Na]⁺.

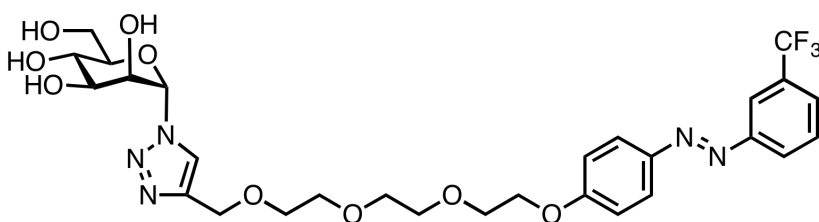
2-[2-[2-(3-trifluoromethylazophenyl phenoxy)ethoxy]ethoxy]ethoxy]ethyl β -D-galactopyranosyl-1,2,3-triazole **2.14**



Compound **2.14** was prepared from **2.33** and **2.40** according to general procedure 7 and isolated as orange solid (Yield: 51%). Mp = 196°C (decomp.); $[\alpha]_D^{20}$ -28.3 (*c*, 0.26 in CH₃OH); FT-IR: $\nu_{\max}/\text{cm}^{-1}$ 2851, 1593, 1428, 878, 781, 621; ¹H NMR (400 MHz, *d*₆-DMSO) δ 8.20 (s, 1H, =CH(triazole)), 8.14–8.09 (m, 2H, 2 \times Ar*H*), 7.94 (d, *J* = 8.99 Hz, 2H, 2 \times Ar*H*), 7.89–7.79 (m, 2H, 2 \times Ar*H*), 7.17 (d, *J* = 8.96 Hz, 2H, 2 \times Ar*H*), 5.47 (d, *J* = 9.18 Hz, 1H, *H*-1), 5.18 (s, 1H), 4.69–4.56 (m, 4H), 4.24–4.22 (m, 2H), 4.06–4.02 (m, 1H), 3.80–3.78 (m, 3H), 3.72–3.69 (m,

Compound **2.16** was prepared from **2.34** and **2.39** according to general procedure 7 and isolated as orange solid (Yield: 76%). Mp = 102°C; $[\alpha]_{\text{D}}^{20}$ 37.5 (*c*, 0.13 in CH₃OH); FT-IR: $\nu_{\text{max}}/\text{cm}^{-1}$ 3349, 2878, 1597, 1503, 1322, 1251, 1128, 1062, 853, 668; ¹H NMR (400 MHz, *d*₆-DMSO) δ 8.21 (s, 1H, =CH (triazole)), 8.01–7.91 (m, 4H, 4 × ArH), 7.16 (d, *J* = 9.10 Hz, 2H, 2 × ArH), 5.91 (d, *J* = 4.07 Hz, 1H, *H*-1), 5.26 (s, 1H, OH), 4.99 (s, 2H, 2 × OH), 4.61–4.54 (m, 3H), 4.44–4.42 (m, 1H), 4.24–4.21 (m, 2H), 3.87–3.84 (m, 1H), 3.79–3.78 (m, 2H), 3.61–3.54 (m, 9H), 3.37–3.32 (m, 3H); ¹³C NMR (100 MHz, *d*₆-DMSO) δ 162.5 (ArC), 154.7 (ArC), 146.6 (ArC), 144.4 (C=CH (triazole)), 127.0 (ArC), 125.6 (2 × ArC), 124.1 (CF₃), 123.2 (ArC), 115.7 (2 × ArC), 86.3 (C-1), 78.7, 71.7, 70.4, 70.3, 70.2, 69.6, 69.2, 68.6, 68.2, 68.1, 63.9, 61.3 (CH₂); ESI-HRMS⁺ calculated for C₂₈H₃₄F₃N₅O₉=641.2309, found 642.2384 [*M* + H]⁺ 664.2200 [*M* + Na]⁺.

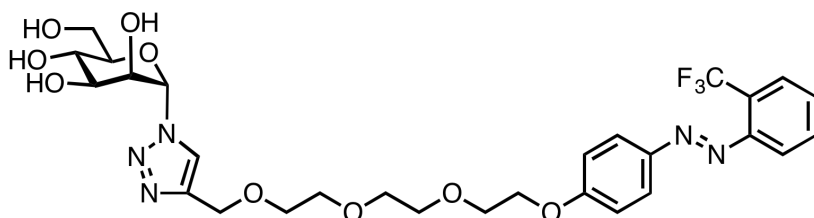
2-[2-[2-(3-trifluoromethylazophenyl phenoxy)ethoxy]ethoxy]ethoxy]ethyl α -D-mannopyranosyl-1,2,3-triazole **2.17**



Compound **2.17** was prepared from **2.34** and **2.40** according to general procedure 7 and isolated as orange solid (Yield: 66%). Mp = 72°C; $[\alpha]_{\text{D}}^{20}$ 29.6 (*c*, 0.26 in CH₃OH); FT-IR: $\nu_{\text{max}}/\text{cm}^{-1}$ 3369, 2877, 1599, 1501, 1326, 1249, 1059, 799, 692; ¹H NMR (400 MHz, *d*₆-DMSO) δ 8.21 (s, 1H, =CH (triazole)), 8.13–8.08 (m, 2H, 2 × ArH), 7.93 (d, *J* = 9.02 Hz, 2H, 2 × ArH), 7.88–7.79 (m, 2H, 2 × ArH), 7.16 (d, *J* = 9.08 Hz, 2H, 2 × ArH), 5.92 (d, *J* = 4.07 Hz, 1H, *H*-1), 5.26 (d, *J* = 5.01 Hz, 1H, OH), 5.03–4.98 (m, 2H, OH), 4.62–4.55 (m, 3H), 4.45–4.42 (m, 1H), 4.23–4.21 (m, 2H), 3.86–3.85 (m, 1H), 3.80–3.77 (m, 2H), 3.62–3.54 (m, 9H), 3.36–3.33 (m, 3H); ¹³C NMR (100 MHz, *d*₆-DMSO) δ 162.4 (ArC), 152.6 (ArC), 146.4 (ArC), 144.4 (C=CH (triazole)), 131.3 (ArC), 130.8 (ArC), 125.5 (2 × ArC), 124.1 (CF₃), 118.5 (ArC), 115.7 (2 ×

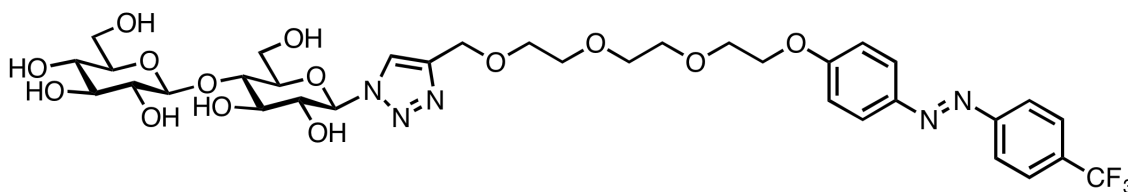
ArC), 86.3 (C-1), 78.7, 71.7, 70.4, 70.3, 70.2, 69.6, 69.2, 68.7, 68.2, 68.1, 63.9, 61.3; ESI-HRMS⁺ calculated for C₂₈H₃₄F₃N₅O₉=641.2309, found 642.2380 [M + H]⁺ 664.2200 [M + Na]⁺.

2-[2-[2-(2-trifluoromethylazophenyl phenoxy)ethoxy]ethoxy]ethyl α-D-mannopyranosyl-1,2,3-triazole **2.18**



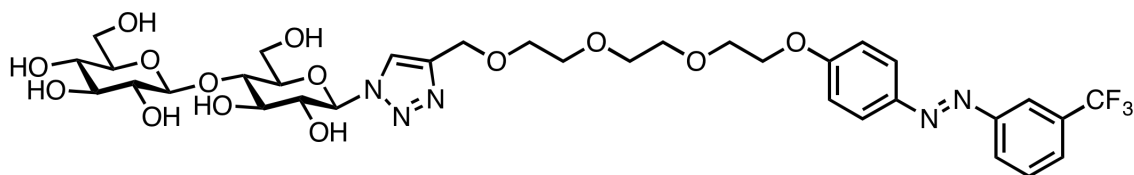
Compound **2.18** was prepared from **2.34** and **2.41** according to general procedure 7 and isolated as orange solid (Yield: 47%). Mp = 60°C; [α]_D²⁰ 51.6 (c, 0.06 in CH₃OH); FT-IR: ν_{max}/cm⁻¹ 3364, 2873, 1598, 1312, 1104, 1050, 841, 764, 669; ¹H NMR (400 MHz, *d*₆-DMSO) δ 8.20 (s, 1H, =CH (triazole)), 7.94–7.89 (m, 3H, 3 × ArH), 7.82–7.78 (m, 2H, 2 × ArH), 7.72–7.70 (m, 1H, ArH), 7.19 (d, *J* = 9.05 Hz, 2H, 2 × ArH), 5.91 (d, *J* = 4.07 Hz, 1H, H-1), 5.26 (s, 1H, OH), 5.00 (s, 1H, OH), 4.56 (s, 2H), 4.43–4.41 (m, 1H), 4.24–4.22 (m, 2H), 3.85–3.83 (m, 1H), 3.80–3.78 (m, 2H), 3.62–3.52 (m, 10H), 3.36–3.31 (m, 3H); ¹³C NMR (100 MHz, *d*₆-DMSO) δ 162.6 (ArC), 149.4 (ArC), 146.9 (ArC), 144.4 (C=CH (triazole)), 134.1 (ArC), 131.2 (ArC), 125.7 (2 × ArC), 124.1 (CF₃), 116.7 (ArC), 115.8 (2 × ArC), 86.2 (C-1), 78.7, 71.7, 70.4, 70.3, 70.2, 69.6, 69.2, 68.6, 68.2, 68.1, 63.9, 61.2; ESI-HRMS⁺ calculated for C₂₈H₃₄F₃N₅O₉=641.2309, found 642.2389 [M + H]⁺ 664.2200 [M + Na]⁺.

2-[2-[2-(4-trifluoromethylazophenyl phenoxy)ethoxy]ethoxy]ethyl β-D-cellobiosyl-1,2,3-triazole **2.19**



Compound **2.19** was prepared from **2.35** and **2.39** according to general procedure 7 and isolated as orange solid (Yield: 42%). Mp = 154.6°C (Decomp); $[\alpha]_D^{20}$ -10.0 (*c*, 0.13 in CH₃OH); FT-IR: $\nu_{\max}/\text{cm}^{-1}$ 2858, 1629, 1424, 1061, 824; ¹H NMR (400 MHz, *d*₆-DMSO) δ 8.28 (s, 1H, =CH (triazole)), 8.01 (d, *J* = 8.27Hz, 2H, 2 × Ar*H*), 7.96–7.93 (m, 4H, 4 × Ar*H*), 7.18 (d, *J* = 9.06 Hz, 2H, 2 × Ar*H*), 5.62 (d, *J* = 9.33 Hz, 1H, *H*-1), 5.54 (d, *J* = 5.96 Hz, 1H, OH), 5.25 (d, *J* = 4.00 Hz, 1H, OH), 5.00 (s, 2H, OH), 4.88 (d, *J* = 1.92 Hz, 1H, OH), 4.68 (s, 1H), 4.60 (s, 1H), 4.54 (s, 2H), 4.31 (d, *J* = 7.74 Hz, 1H), 4.25–4.22 (m, 2H), 3.86–3.70 (m, 5H), 3.64–3.54 (m, 11H), 3.25–3.16 (m, 2H), 3.07–3.03 (m, 2H); ¹³C NMR (150 MHz, CD₃OD) δ 168.9, 162.3, 160.0, 154.8, 146.8, 125.9, 124.9, 123.7, 122.9, 122.5, 119.8, 114.8, 114.3, 103.2, 87.9, 78.2, 76.8, 76.5, 75.5, 73.5, 70.3, 70.1, 69.9, 69.4, 69.3, 67.7, 63.5, 61.0, 60.0; LC/MS: *m/z* 803.6 [*M* + H]⁺, ESI-HRMS⁺ calculated for C₃₄H₄₄F₃N₅O₁₄=803.7422 [*M* + H]⁺, found 804.2914 [*M* + H]⁺, 826.2724 [*M* + Na]⁺.

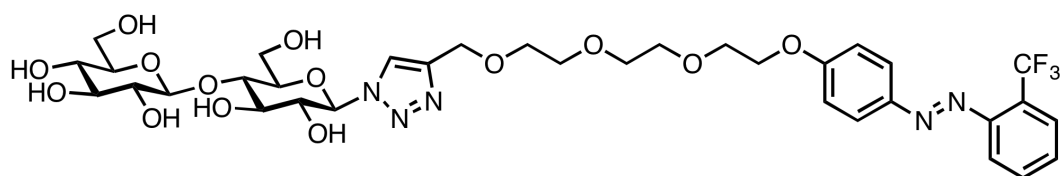
2-[2-[2-(3-trifluoromethylazophenyl phenoxy)ethoxy]ethoxy]ethyl β -D-cellobiosyl-1,2,3-triazole **2.20**



Compound **2.20** was prepared from **2.35** and **2.40** according to general procedure 7 and isolated as orange solid (Yield: 41%). Mp = 150.6°C (Decomp); $[\alpha]_D^{20}$ -8.7 (*c*, 0.16 in CH₃OH); FT-IR: $\nu_{\max}/\text{cm}^{-1}$ 3574, 2845, 1627, 1426, 1022, 779; ¹H NMR (400 MHz, *d*₆-DMSO) δ 8.29 (s, 1H, =CH (triazole)), 8.15–8.09 (m, 2H, 2 × Ar*H*), 7.95 (d, *J* = 9.10 Hz, 2H, 2 × Ar*H*), 7.89–7.80 (m, 2H, 2 × Ar*H*), 7.17 (d, *J* = 9.08 Hz, 2H, 2 × Ar*H*), 5.63 (d, *J* = 9.36 Hz, 1H, *H*-1), 5.55 (d, *J* = 5.79 Hz, 1H, OH), 5.26 (s, 1H, OH), 5.00 (s, 2H, OH), 4.89 (d, *J* = 1.81 Hz, 1H, OH), 4.69 (s, 1H), 4.61 (s, 1H), 4.54 (s, 2H), 4.32 (d, *J* = 7.95 Hz, 1H), 4.24–4.22 (m, 2H), 3.88–3.72 (m, 5H), 3.64–3.52 (m, 11H), 3.25–3.16 (m, 2H), 3.11–3.02 (m, 2H); ¹³C NMR (100 MHz, *d*₆-DMSO) δ 162.4 (ArC), 152.6 (ArC), 146.4 (ArC), 144.4 (C=CH (triazole)), 131.2 (ArC), 127.2

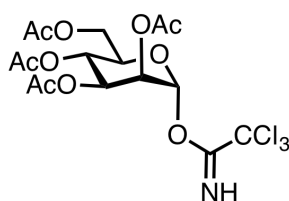
(ArC), 125.5 (2 × ArC), 123.7 (CF₃), 118.5 (ArC), 115.7 (2 × ArC), 103.5 (C-1), 87.5, 79.9, 78.2, 77.3, 76.9, 75.6, 73.8, 72.3, 70.5, 70.4, 70.3, 70.2, 69.6, 69.2, 68.2, 63.9, 61.5, 60.4; LC/MS: *m/z* 803.6 [*M* + H]⁺, ESI-HRMS⁺ calculated for C₃₄H₄₄F₃N₅O₁₄=803.7422 [*M* + H]⁺, found 804.2911 [*M* + H]⁺, 826.2733 [*M* + Na]⁺.

2-[2-[2-(2-trifluoromethylazophenyl phenoxy)ethoxy]ethoxy]ethyl β-D-cellobiosyl-1,2,3-triazole **2.21**



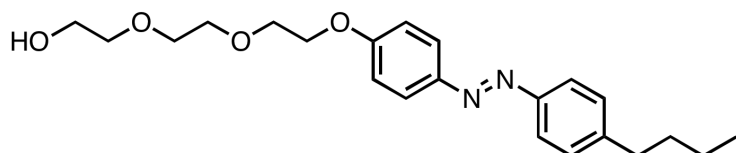
Compound **2.21** was prepared from **2.35** and **2.41** according to general procedure 7 and isolated as orange solid (Yield: 40%). Mp = 206.8°C (Decomp); [α]_D²⁰ -10.7 (*c*, 0.14 in CH₃OH); FT-IR: ν_{max} /cm⁻¹ 2829, 1596, 1428, 1038, 878; ¹H NMR (400 MHz, *d*₆-DMSO) δ 8.29 (s, 1H, =CH (triazole)), 7.94–7.90 (m, 3H, 3 × ArH), 7.84–7.78 (m, 2H, 2 × ArH), 7.72–7.68 (m, 1H, ArH), 7.19 (d, *J* = 9.06 Hz, 2H, 2 × ArH), 5.63 (d, *J* = 9.50 Hz, 1H, *H*-1), 5.55 (d, *J* = 5.44 Hz, 1H, OH), 5.25 (s, 1H, OH), 5.00 (s, 2H, OH), 4.89 (s, 1H, OH), 4.69 (s, 1H), 4.61 (s, 1H), 4.54 (s, 2H), 4.32 (d, *J* = 7.86 Hz, 1H), 4.23–4.21 (m, 2H), 3.86–3.71 (m, 5H), 3.65–3.50 (m, 11H), 3.26–3.17 (m, 2H), 3.11–3.04 (m, 2H); ¹³C NMR (100 MHz, *d*₆-DMSO) δ 162.5 (ArC), 149.4 (ArC), 146.9 (ArC), 144.4 (C=CH (triazole)), 134.1 (ArC), 131.2 (ArC), 125.7 (2 × ArC), 123.6 (CF₃), 116.7 (ArC), 115.8 (2 × ArC), 103.5 (C-1), 87.5, 79.9, 78.2, 77.3, 76.9, 75.6, 73.8, 72.2, 70.5, 70.4, 70.3, 70.2, 69.6, 69.2, 68.2, 63.8, 61.5, 60.4; LC/MS: *m/z* 803.6 [*M* + H]⁺, ESI-HRMS⁺ calculated for C₃₄H₄₄F₃N₅O₁₄=803.7422 [*M* + H]⁺, found 804.2918 [*M* + H]⁺, 826.2728 [*M* + Na]⁺.

2,3,4,6-tetra-*O*-acetyl- α -mannopyranosyl trichloroacetimidate **2.24**⁴³



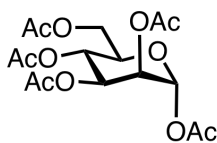
Compound **2.28** (1 equiv.) and trichloroacetonitrile (10 equiv.) were dissolved in dry DCM and DBU (0.1 equiv.) was added dropwise. The reaction mixture was stirred overnight at ambient temperature under N₂ and the solvent was evaporated under reduced pressure. The crude product was purified by chromatography to afford the product as colorless oil (Yield: 31%). $[\alpha]_D^{20}$ 11.4 (*c*, 0.07 in CH₃OH); FT-IR: $\nu_{\max}/\text{cm}^{-1}$ 2958, 1731, 1366, 1213, 1045, 823, 676; ¹H NMR (400 MHz, CDCl₃) δ 5.42–5.39 (m, 1H, *CH*), 5.31–5.22 (m, 3H, *H*-1, *H*-2, *H*-3), 4.25–4.11 (m, 3H, *H*-4, *H*-5, *H*-6), 2.20 (s, 3H, OAc), 2.09 (s, 3H, OAc), 2.04 (s, 3H, OAc), 1.99 (s, 3H, OAc); LC/MS: m/z 515.2 [*M* + H]⁺, the obtained optical rotation, FTIT, ¹H NMR, ¹³C NMR and LC/MS data are in agreement with the reference 43.

(*E*)-2-(2-(2-(4-((4-butylphenyl)diazenyl)phenoxy)ethoxy)ethoxy)ethan-1-ol **2.25**⁴⁴



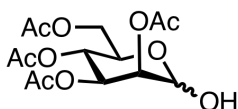
Compound **2.25** was prepared from **2.30** and **2.31** according to general procedure 4 and isolated as orange crystal (Yield: 61%). Mp = 74.1°C; FT-IR: $\nu_{\max}/\text{cm}^{-1}$ 3285, 2874, 1594, 1497, 1249, 1107, 923, 843; ¹H NMR (400 MHz, CDCl₃) δ 7.89 (d, *J* = 8.98 Hz, 2H, 2 × *ArH*), 7.79 (d, *J* = 8.30 Hz, 2H, 2 × *ArH*), 7.29 (d, *J* = 8.42 Hz, 2H, 2 × *ArH*), 7.02 (d, *J* = 9.02 Hz, 2H, 2 × *ArH*), 4.22–4.19 (m, 2H, OCH₂), 3.76–3.69 (m, 6H, 3 × OCH₂), 3.63–3.61 (m, 2H, OCH₂), 2.67 (t, *J* = 7.80 Hz, 2H, CH₂), 1.92 (s, 1H), 1.68–1.60 (m, 2H, CH₂), 1.40–1.35 (m, 2H, CH₂), 0.94 (t, *J* = 7.33 Hz, 3H, CH₃); LC/MS: m/z 386.9 [*M* + H]⁺, the obtained melting point, optical rotation, FTIT, ¹H NMR, ¹³C NMR and LC/MS data are in agreement with the reference 44.

D-mannose pentaacetate **2.27**⁴³



DMAP (0.1 equiv.) was added slowly to a solution of **2.26** (1 equiv.) and Ac₂O (7.5 equiv.) in dry pyridine (100 mL). The reaction mixture was stirred overnight at room temperature under N₂ and then diluted in EtOAc (150 mL), washed with 1 M HCl (2 × 100 mL), NH₄Cl (50 mL) and brine (100 mL). The organic layer was dried over Na₂SO₄ and concentrated under reduced pressure to afford the product as a sticky colorless oil in quantitative yield. $[\alpha]_D^{20}$ 16.2 (*c*, 0.02 in CH₃OH); FT-IR: $\nu_{\max}/\text{cm}^{-1}$ 1739, 1367, 1205, 1023, 969; ¹H NMR (400 MHz, CDCl₃) δ 6.01 (d, *J* = 1.9 Hz, 1H, *H*-1), 5.30–5.16 (m, 3H, *H*-2, *H*-3, *H*-4), 4.26–4.17 (m, 1H, *H*-6), 4.10–3.97 (m, 2H, *H*-5, *H*-6), 2.17–2.08 (m, 6H, CH₃, CH₃), 2.02 (s, 3H, CH₃), 1.99 (s, 3H, CH₃), 1.94 (s, 3H, CH₃); ¹³C NMR (100 MHz, CDCl₃) δ 170.5, 169.8, 169.6, 169.4, 167.9, 90.5, 73.1, 68.7, 68.2, 65.4, 61.9, 20.7, 20.6, 20.5, the obtained optical rotation, FTIT, ¹H NMR and ¹³C NMR data are in agreement with the reference 43.

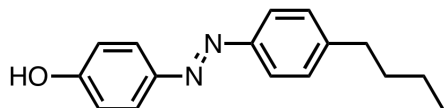
2,3,4,6-tetra-*O*-acetyl-D-mannopyranose **2.28**⁴³



D-mannose pentaacetate **2.27** (1 equiv.) was dissolved in dry DMF (25 mL) and hydrazine acetate (1.1 equiv.) were added dropwise. The reaction mixture was stirred overnight at ambient temperature under N₂ and then diluted in EtOAc, washed with brine, dried over Na₂SO₄, concentrated under reduced pressure and purified by chromatography to afford the product as colorless oil (Yield: 40 %). $[\alpha]_D^{20}$ 22.4 (*c*, 0.21 in CH₃OH); FT-IR: $\nu_{\max}/\text{cm}^{-1}$ 2919, 1734, 1365, 1208, 1039, 790; ¹H NMR (400 MHz, CDCl₃) for α -isomer δ 5.30–5.19 (m, 4H, *H*-1, *H*-2, *H*-3, *H*-4), 4.25–4.08 (m, 4H), 2.13 (s, 3H, OAc), 2.07 (s, 3H, OAc), 2.02 (s, 3H, OAc), 1.97 (s,

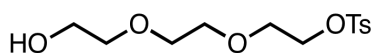
3H, OAc); LC/MS: m/z 371.1 $[M + Na]^+$, the obtained optical rotation, FTIT, 1H NMR, ^{13}C NMR and LC/MS data are in agreement with the reference 43.

(*E*)-4-((4-butylphenyl)diazenyl)phenol **2.30**⁴⁴



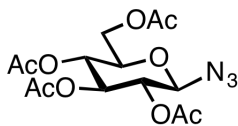
Compound **2.30** was prepared from 4-butylaniline **2.29** according to general procedure 3 and isolated as brown solid (Yield: 98%). Mp = 82.6°C; FT-IR: $\nu_{\max}/\text{cm}^{-1}$ 2928, 1589, 1466, 1249, 1102, 836; 1H NMR (400 MHz, $CDCl_3$) δ 7.86 (d, J = 8.87 Hz, 2H, $2 \times ArH$), 7.79 (d, J = 8.24 Hz, 2H, $2 \times ArH$), 7.29 (d, J = 8.22 Hz, 2H, $2 \times ArH$), 6.94 (d, J = 8.87 Hz, 2H, $2 \times ArH$), 2.68 (t, J = 7.71 Hz, 2H, CH_2), 1.68–1.60 (m, 2H, CH_2), 1.41–1.35 (m, 2H, CH_2), 0.94 (t, J = 7.30 Hz, 3H, CH_3); LC/MS: m/z 254.9 $[M + H]^+$, the obtained melting point, FTIT, 1H NMR, ^{13}C NMR and LC/MS data are in agreement with the reference 44.

2-(2-(2-hydroxyethoxy)ethoxy)ethyl 4-methylbenzenesulfonate **2.31**⁴⁴



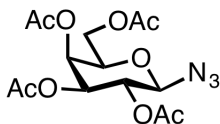
To a solution of triethylene glycol (6.67 mL, 198 equiv.), triethylamine (1.83 mL, 52 equiv.) and DMAP (0.03 g, 1 equiv.) in 50 mL DCM was added tosyl chloride (2.36 g, 49 equiv.) at 5°C. The reaction mixture was stirred at 5°C for 4 hour then gradually warmed up to room temperature and reacted overnight. The crude mixture was washed with 1N HCl, H_2O and brine, dried over Na_2SO_4 and concentrated under reduced pressure. The residue was purified by chromatography (EtOAc/hexane 2:3) to obtain the title compound as yellow oil (2.81 g, yield: 75%). FT-IR: $\nu_{\max}/\text{cm}^{-1}$ 3454, 2877, 1597, 1350, 1173, 1095, 913, 814, 662; 1H NMR (400 MHz, $CDCl_3$) δ 7.80 (d, J = 8.28 Hz, 2H, $2 \times ArH$), 7.34 (d, J = 8.59 Hz, 2H, $2 \times ArH$), 4.19–4.16 (m, 2H, CH_2), 3.73–3.69 (m, 4H, $2 \times CH_2$), 3.61–3.57 (m, 6H, $3 \times CH_2$), 2.45 (s, 3H, CH_3); LC/MS: m/z 305.0 $[M + H]^+$, the obtained FTIT, 1H NMR and LC/MS data are in agreement with the reference 44.

2,3,4,6-tetra-*O*-acetyl- β -D-glucopyranosyl azide **2.32**⁷⁴



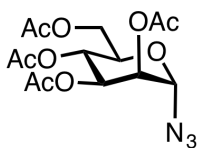
Compound **2.32** was prepared from **2.36** according to general procedure 2 and isolated as white solid (Yield: 75%). Mp = 129.7°C; $[\alpha]_D^{20}$ -2.4 (*c*, 0.2 in CH₃OH); FT-IR: ν_{\max} / cm⁻¹ 2113, 1748, 1366, 1204, 1032, 906, 673; ¹H NMR (400 MHz, CDCl₃) δ 5.24 (t, *J* = 9.49 Hz, 1H, *H*-1), 5.10 (t, *J* = 9.98 Hz, 1H, *H*-2), 4.96 (t, *J* = 8.82 Hz, 1H, *H*-3), 4.64 (t, *J* = 8.81 Hz, 1H, *H*-4), 4.29–4.15 (m, 2H, *H*-6), 3.82–3.77 (m, 1H, *H*-5), 2.10 (s, 3H, CH₃ (OAc)), 2.08 (s, 3H, CH₃ (OAc)), 2.03 (s, 3H, CH₃ (OAc)), 2.01 (s, 3H, CH₃ (OAc)); LC/MS: *m/z* 396.0 [*M* + H]⁺, the obtained melting point, optical rotation, FTIT, ¹H NMR and LC/MS data are in agreement with the reference 74.

2,3,4,6-tetra-*O*-acetyl- β -D-galactopyranosyl azide **2.33**⁷⁴



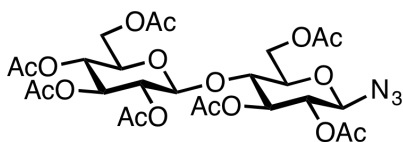
Compound **2.33** was prepared from **2.37** according to general procedure 2 and isolated as white crystal (Yield: 52%). Mp = 99.1°C; $[\alpha]_D^{20}$ -9.5 (*c*, 0.4 in CH₃OH); FT-IR: ν_{\max} / cm⁻¹ 2119, 1737, 1372, 1208, 1042, 950, 715; ¹H NMR (400 MHz, CDCl₃) δ 5.43–5.41 (m, 1H, *H*-1), 5.19–5.14 (m, 1H, *H*-4), 5.05–5.02 (m, 1H, *H*-3), 4.59 (d, *J* = 8.74 Hz, 1H, *H*-2), 4.19–4.15 (m, 2H, *H*-5, *H*-6), 4.03–3.99 (m, 1H, *H*-6), 2.17 (s, 3H, CH₃ (OAc)), 2.09 (s, 3H, CH₃ (OAc)), 2.06 (s, 3H, CH₃ (OAc)), 1.99 (s, 3H, CH₃ (OAc)); LC/MS: *m/z* 396.0 [*M* + H]⁺, the obtained melting point, optical rotation, FTIT, ¹H NMR and LC/MS data are in agreement with the reference 74.

2,3,4,6-tetra-*O*-acetyl- α -D-mannopyranosyl azide **2.34**⁷⁵



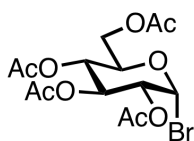
Trimethylsilyl azide (2 equiv.) was added under N₂ to a solution of **2.27** (1 equiv.) in dry DCM (50 mL), followed by tin (IV) chloride (0.6 equiv.). The mixture was stirred at ambient temperature for 12 hours, then the solvent was removed under reduced pressure and the crude product was purified by chromatography to afford the final product as a yellow syrup (Yield: 73%). $[\alpha]_D^{20}$ 73.8 (*c*, 0.28 in CH₃OH); FT-IR: $\nu_{\max}/\text{cm}^{-1}$ 2117, 1741, 1366, 1206, 1042, 949, 783; ¹H NMR (400 MHz, CDCl₃) δ 5.33 (d, *J* = 1.93 Hz, 1H, *H*-1), 5.25–5.17 (m, 2H, *H*-2, *H*-3), 5.09–5.08 (m, 1H, *H*-4), 4.27–4.07 (m, 3H, *H*-5, *H*-6), 2.11 (s, 3H, OAc), 2.05 (s, 3H, OAc), 1.99 (s, 3H, OAc), 1.93 (s, 3H, OAc). LCMS: *m/z* 396.0 [*M* + H]⁺, the obtained optical rotation, FTIT, ¹H NMR and LC/MS data are in agreement with the reference 75.

β -azido-D-cellobiose heptaacetate **2.35**⁷⁶



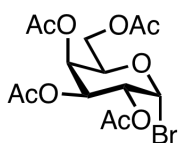
The synthesis of this compound was the same as for compound **2.34**, using D-cellobiose heptaacetate **2.38** as starting material. The crude product was purified by chromatography to afford the final product as a white solid (Yield: 61%). Mp = 188.5°C; $[\alpha]_D^{20}$ 75 (*c*, 0.02 in CH₃OH); FT-IR: $\nu_{\max}/\text{cm}^{-1}$ 2115, 1739, 1366, 1213, 1036, 902; ¹H NMR (400 MHz, CDCl₃) δ 5.15–4.97 (m, 3H), 4.88–4.78 (m, 2H), 4.55–4.43 (m, 3H), 4.33–4.28 (m, 1H), 4.07–3.96 (m, 2H), 3.75–3.70 (m, 1H), 3.64–3.57 (m, 2H), 2.07 (s, 3H, OAc), 2.02 (s, 3H, OAc), 2.00 (s, 3H, OAc), 1.97 (s, 3H, OAc), 1.96 (s, 3H, OAc), 1.94 (s, 3H, OAc), 1.91 (s, 3H, OAc). LC/MS: *m/z* 684.0 [*M* + H]⁺, the obtained melting point, optical rotation, FTIT, ¹H NMR and LC/MS data are in agreement with the reference 76.

2,3,4,6-tetra-*O*-acetyl- α -D-glucopyranosyl bromide **2.36**⁴²



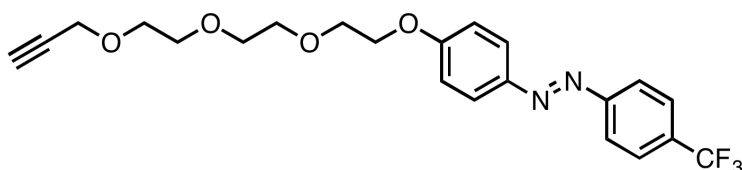
Compound **2.36** was prepared from glucose pentaacetate **2.22** according to general procedure 1 and isolated as pale yellow oil (Yield: 99%). $[\alpha]_D^{20}$ 199.5 (*c*, 0.25 in CH₃OH); FT-IR: $\nu_{\max}/\text{cm}^{-1}$ 1738, 1367, 1207, 1075, 909, 682; ¹H NMR (400 MHz, CDCl₃) δ 6.55–6.54 (m, 1H, *H*-1), 5.51–5.43 (m, 1H, *H*-3), 5.12–5.05 (m, 1H, *H*-4), 4.79–4.73 (m, 1H, *H*-2), 4.29–4.21 (m, 2H, *H*-5, *H*-6), 4.09–4.02 (m, 1H, *H*-6), 2.03–1.94 (m, 12H, 4 \times CH₃), the obtained optical rotation, FTIT and ¹H NMR are in agreement with the reference 42.

2,3,4,6-tetra-*O*-acetyl- α -D-galactopyranosyl bromide **2.37**⁴²



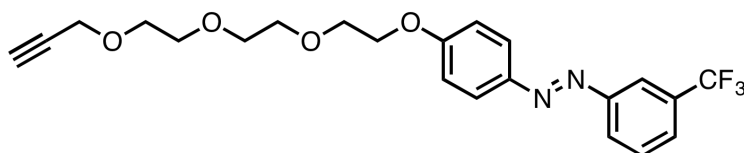
Compound **2.37** was prepared from galactose pentaacetate **2.23** according to general procedure 1 and isolated as white crystal (Yield: 99%). Mp = 85.1°C; $[\alpha]_D^{20}$ 116.8 (*c*, 0.33 in CH₃OH); FT-IR: $\nu_{\max}/\text{cm}^{-1}$ 1739, 1368, 1205, 1073, 910; ¹H NMR (400 MHz, CDCl₃) δ 6.68 (d, *J* = 3.96Hz, 1H, *H*-1), 5.51–5.49 (m, 1H, *H*-4), 5.41–5.37 (m, 1H, *H*-3), 5.05–5.02 (m, 1H, *H*-2), 4.47 (t, *J* = 6.72Hz, 1H, *H*-5), 4.19–4.07 (m, 2H, *H*-6), 2.14 (s, 3H, CH₃ (OAc)), 2.09 (s, 3H, CH₃ (OAc)), 2.04 (s, 3H, CH₃ (OAc)), 1.99 (s, 3H, CH₃ (OAc)), the obtained melting point, optical rotation, FTIT and ¹H NMR data are in agreement with the reference 42.

(*E*)-1-(4-trifluoromethylphenyl)-2-(4-(2-(2-(2-prop-2-yn-1-yloxy)ethoxy)ethoxy)ethoxy)phenyl diazene **2.39**



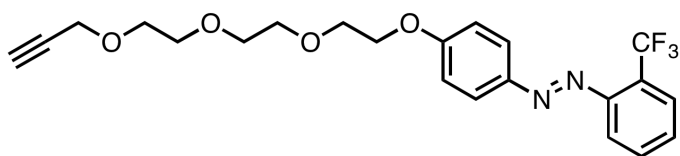
Compound **2.39** was prepared from **2.42** according to general procedure 5 and isolated as orange liquid (Yield: 76%). FTIR $\nu_{\max}/\text{cm}^{-1}$ 2931, 2114, 1741, 1227, 1033, 852; ^1H NMR (400 MHz, CDCl_3) δ 7.96–7.93 (m, 4H, 4 \times ArH), 7.75 (d, $J = 8.34$ Hz, 2H, 2 \times ArH), 7.05 (d, $J = 8.97$ Hz, 2H, 2 \times ArH), 4.25–4.20 (m, 4H, 2 \times CH_2), 3.92–3.89 (m, 2H, CH_2), 3.77–3.68 (m, 9H, 4 \times CH_2 , CH); ^{13}C NMR (100 Hz, CDCl_3) δ 161.9 (ArC), 154.6 (ArC), 146.9 (ArC), 126.2 (ArC), 125.1 (2 \times ArC), 122.7 (2 \times ArC), 114.9 (2 \times ArC), 79.7 (CCH), 74.5 (CCH), 70.9 (CH_2), 70.7 (CH_2), 70.5 (CH_2), 69.6 (CH_2), 69.1 (CH_2), 67.8 (CH_2) 58.4 (CH_2); LC/MS: m/z 436.8 [$M + \text{H}$] $^+$; ESI-HRMS $^+(m/z)$ calculated for $\text{C}_{22}\text{H}_{23}\text{F}_3\text{N}_2\text{O}_4=436.4312$ [$M + \text{H}$] $^+$, found 459.1504 [$M + \text{Na}$] $^+$, 437.1683 [$M + \text{H}$] $^+$.

(*E*)-1-(3-trifluoromethylphenyl)-2-(4-(2-(2-(2-prop-2-yn-1-yloxy)ethoxy)ethoxy)ethoxy)phenyl diazene **2.40**



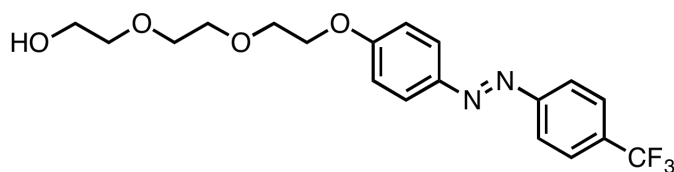
Compound **2.40** was prepared from **2.43** according to general procedure 5 and isolated as orange liquid (Yield: 52%). FTIR $\nu_{\max}/\text{cm}^{-1}$ 2862, 1503, 1329, 1092, 841; ^1H NMR (400 MHz, CDCl_3) δ 8.14 (s, 1H, ArH), 8.05 (d, $J = 7.89$ Hz, 1H, ArH), 7.94 (d, $J = 9.08$ Hz, 2H, 2 \times ArH), 7.69–7.60 (m, 2H, 2 \times ArH), 7.05 (d, $J = 9.00$ Hz, 2H, 2 \times ArH), 4.25–4.19 (m, 4H, 2 \times CH_2), 3.92–3.89 (m, 2H, CH_2), 3.77–3.67 (m, 9H, 4 \times CH_2 , CH); ^{13}C NMR (100 Hz, CDCl_3) δ 161.9 (ArC), 152.7 (ArC), 146.8 (ArC), 129.6 (ArC), 125.9 (ArC), 125.1 (2 \times ArC), 119.2 (ArC), 114.9 (2 \times ArC), 79.7 (CCH), 74.5 (CCH), 70.9 (CH_2), 70.7 (CH_2), 70.5 (CH_2), 69.6 (CH_2), 69.1 (CH_2), 67.8 (CH_2) 58.4 (CH_2); LC/MS: m/z 436.8 [$M + \text{H}$] $^+$; ESI-HRMS $^+(m/z)$ calculated for $\text{C}_{22}\text{H}_{23}\text{F}_3\text{N}_2\text{O}_4=436.4312$ [$M + \text{H}$] $^+$, found 459.1503 [$M + \text{Na}$] $^+$, 437.1683 [$M + \text{H}$] $^+$.

(*E*)-1-(2-trifluoromethylphenyl)-2-(4-(2-(2-(2-prop-2-yn-1-yloxy)ethoxy)ethoxy)ethoxy)phenyl diazene **2.41**



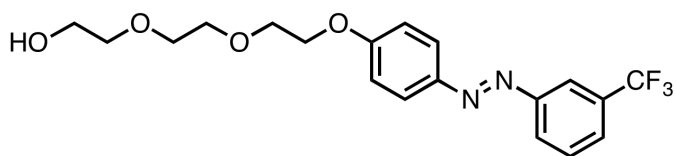
Compound **2.41** was prepared from **2.44** according to general procedure 5 and isolated as orange liquid (Yield: 33%). FT-IR: $\nu_{\max}/\text{cm}^{-1}$ 2876, 1598, 1314, 1096, 764; ^1H NMR (400 MHz, CDCl_3) δ 7.95 (d, $J = 9.24$ Hz, 2H, $2 \times \text{ArH}$), 7.81–7.78 (m, 2H, $2 \times \text{ArH}$), 7.64–7.59 (m, 1H, ArH), 7.52–7.48 (m, 1H, ArH), 7.03 (d, $J = 9.04$ Hz, 2H, $2 \times \text{ArH}$), 4.23–4.19 (m, 4H, $2 \times \text{CH}_2$), 3.91–3.88 (m, 2H, CH_2), 3.76–3.67 (m, 8H, $4 \times \text{CH}_2$), 2.42 (t, $J = 2.40$ Hz, 1H, CH); ^{13}C NMR (100 MHz, CDCl_3) δ 132.5 (ArC), 129.7 (ArC), 126.5 (ArC), 125.5 ($2 \times \text{ArC}$), 116.2 (ArC), 114.9 ($2 \times \text{ArC}$), 76.7 (CH), 70.9 (CH_2), 70.7 (CH_2), 70.5 (CH_2), 69.6 (CH_2), 69.1 (CH_2), 67.8 (CH_2), 58.4 (CH_2); LC/MS: m/z 436.8 [$M + \text{H}$] $^+$; ESI-HRMS $^+(m/z)$ calculated for $\text{C}_{22}\text{H}_{23}\text{F}_3\text{N}_2\text{O}_4 = 436.4312$ [$M + \text{H}$] $^+$, found 459.1505 [$M + \text{Na}$] $^+$, 437.1684 [$M + \text{H}$] $^+$.

(*E*)-2-(2-(2-(4-((4-(trifluoromethyl)phenyl)diazenyl)phenoxy)ethoxy)ethoxy)ethan-1-ol **2.42**



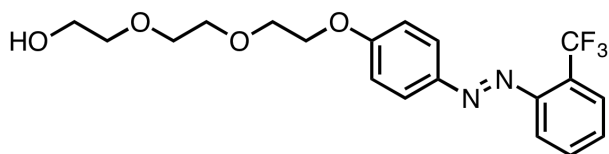
Compound **2.42** was prepared from **2.31** and **2.48** according to general procedure 4 and isolated as red liquid (Yield: 61.2%). FT-IR: $\nu_{\max}/\text{cm}^{-1}$ 3286, 2878, 1594, 1504, 1318, 1099, 1005, 851, 667; ^1H NMR (400 MHz, CDCl_3) δ 7.95–7.92 (m, 4H, $4 \times \text{ArH}$), 7.75 (d, $J = 8.38$ Hz, 2H, $2 \times \text{ArH}$), 7.04 (d, $J = 9.02$ Hz, 2H, $2 \times \text{ArH}$), 4.24–4.22 (m, 2H, CH_2), 3.92–3.89 (m, 2H, CH_2), 3.76–3.69 (m, 6H, $3 \times \text{CH}_2$), 3.63–3.61 (m, 2H, CH_2); ^{13}C NMR (100 MHz, CDCl_3) δ 161.9 (ArC), 154.6 (ArC), 146.9 (ArC), 126.2 \times 3 (ArC), 125.2 (ArC), 122.7 (ArC), 114.9 (ArC), 72.5 (CH_2), 70.9 (CH_2), 70.4 (CH_2), 69.6 (CH_2), 67.7 (CH_2), 61.8 (CH_2); LC/MS: m/z 398.8 [$M + \text{H}$] $^+$; ESI-HRMS $^+(m/z)$ calculated for $\text{C}_{19}\text{H}_{21}\text{F}_3\text{N}_2\text{O}_4 = 398.3822$ [$M + \text{H}$] $^+$, found 399.1528 [$M + \text{H}$] $^+$, 421.1346 [$M + \text{Na}$] $^+$.

(*E*)-2-(2-(2-(4-((3-(trifluoromethyl)phenyl)diazenyl)phenoxy)ethoxy)ethoxy)ethan-1-ol **2.43**



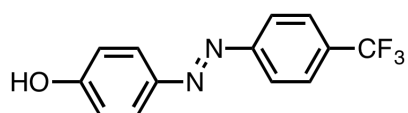
Compound **2.43** was prepared from **2.31** and **2.49** according to general procedure 4 and isolated as red liquid (Yield: 53.9%). FT-IR: $\nu_{\max}/\text{cm}^{-1}$ 3446, 2873, 1596, 1326, 1121, 909, 804, 693; ^1H NMR (400 MHz, CDCl_3) δ 8.13 (s, 1H, ArH), 8.05 (d, $J = 7.86$ Hz, 1H, ArH), 7.93 (d, $J = 9.00$ Hz, 2H, $2 \times$ ArH), 7.69–7.59 (m, 2H, $2 \times$ ArH), 7.04 (d, $J = 8.99$ Hz, 2H, $2 \times$ ArH), 4.24–4.22 (m, 2H, OCH_2), 3.92–3.89 (m, 2H, OCH_2), 3.76–3.62 (m, 8H, $4 \times$ OCH_2); ^{13}C NMR (100 MHz, CDCl_3) δ 161.8 (ArC), 152.7 (ArC), 146.9 (ArC), 129.6 ($2 \times$ ArC), 126.5 (ArC), 126.0 (ArC), 125.1 ($2 \times$ ArC), 119.2 (ArC), 114.9 ($2 \times$ ArC), 72.5 (CH_2), 70.9 (CH_2), 70.4 (CH_2), 69.6 (CH_2), 67.2 (CH_2), 61.8 (CH_2); LC/MS: m/z 398.8 [$M + \text{H}$] $^+$; ESI-HRMS $^+(m/z)$ calculated for $\text{C}_{19}\text{H}_{21}\text{F}_3\text{N}_2\text{O}_4 = 398.3822$ [$M + \text{H}$] $^+$, found 399.1527 [$M + \text{H}$] $^+$, 421.1346 [$M + \text{Na}$] $^+$.

(*E*)-2-(2-(2-(4-((*E*)-2-(trifluoromethyl)phenyl)diazenyl)phenoxy)ethoxy)ethoxy)ethan-1-ol **2.44**



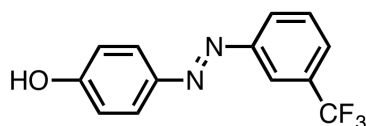
Compound **2.44** was prepared from **2.31** and **2.50** according to general procedure 4 and isolated as red liquid (Yield: 61.2%). FT-IR: $\nu_{\max}/\text{cm}^{-1}$ 3446, 2871, 1599, 1499, 1313, 1130, 839, 765; ^1H NMR (400 MHz, CDCl_3) δ 7.95 (d, $J = 8.88$ Hz, 2H, $2 \times$ ArH), 7.81–7.78 (m, 2H, $2 \times$ ArH), 7.64–7.60 (m, 1H, ArH), 7.52–7.48 (m, 1H, ArH), 7.04 (d, $J = 8.97$ Hz, 2H, $2 \times$ ArH), 4.24–4.21 (m, 2H, OCH_2), 3.91–3.89 (m, 2H, OCH_2), 3.76–3.61 (m, 8H, $4 \times$ OCH_2); ^{13}C NMR (100 MHz, CDCl_3) δ 161.9 (ArC), 149.7 (ArC), 147.3 (ArC), 132.5 (ArC), 129.7 (ArC), 126.5 (ArC), 125.5 ($2 \times$ ArC), 116.2 ($2 \times$ ArC), 114.9 ($2 \times$ ArC), 72.5 (CH_2), 70.9 (CH_2), 70.4 (CH_2), 69.6 (CH_2), 67.7 (CH_2), 61.8 (CH_2); LC/MS: m/z found 398.8 [$M + \text{H}$] $^+$, ESI-HRMS $^+(m/z)$ calculated for $\text{C}_{19}\text{H}_{21}\text{F}_3\text{N}_2\text{O}_4 = 398.3822$ [$M + \text{H}$] $^+$, found 399.1529 [$M + \text{H}$] $^+$, 421.1348 [$M + \text{Na}$] $^+$.

(*E*)-4-((4-(trifluoromethyl)phenyl)diazenyl)phenol **2.48**⁷⁷



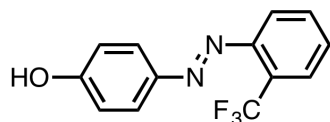
Compound **2.48** was prepared from 4-(trifluoromethyl)aniline **2.45** according to general procedure 3 and isolated as orange solid (Yield: 92.8%). Mp = 129.2°C; FT-IR: $\nu_{\max}/\text{cm}^{-1}$ 3220, 1588, 1473, 1318, 1248, 1125, 851, 663; $^1\text{H NMR}$ (400 MHz, CDCl_3) δ 7.96–7.90 (m, 4H, 4 \times ArH), 7.76 (d, $J = 8.34$ Hz, 2H, 2 \times ArH), 6.96 (d, $J = 8.89$ Hz, 2H, 2 \times ArH); LC/MS: m/z 266.8 [$M + \text{H}$]⁺, the obtained melting point, FTIT, $^1\text{H NMR}$ and LC/MS data are in agreement with the reference 77.

(*E*)-4-((3-(trifluoromethyl)phenyl)diazenyl)phenol **2.49**⁷⁸



Compound **2.49** was prepared from 3-(trifluoromethyl)aniline **2.46** according to general procedure 3 and isolated as red-brown solid (Yield: 81.4%). Mp = 111.6°C; FT-IR: $\nu_{\max}/\text{cm}^{-1}$ 3078, 1589, 1506, 1409, 1329, 1273, 1167, 1117, 803, 688; $^1\text{H NMR}$ (400 MHz, CDCl_3) δ 8.17 (s, 1H, ArH), 8.08 (d, $J = 7.82$ Hz, 1H, ArH), 7.94 (d, $J = 9.02$ Hz, 2H, 2 \times ArH), 7.73–7.63 (m, 2H, 2 \times ArH), 6.99 (d, $J = 8.90$ Hz, 2H, 2 \times ArH); LC/MS: m/z 266.8 [$M + \text{H}$]⁺ the obtained melting point, FTIT, $^1\text{H NMR}$ and LC/MS data are in agreement with the reference 78.

(*E*)-4-((2-(trifluoromethyl)phenyl)diazenyl)phenol **2.50**



Compound **2.50** was prepared from 2-(trifluoromethyl)aniline **2.47** according to general procedure 3 and isolated as red liquid (Yield: 21.1%). FT-IR: $\nu_{\max}/\text{cm}^{-1}$ 3309, 1702, 1589, 1505, 1311, 1128, 839, 763, 663; $^1\text{H NMR}$ (400 MHz, CDCl_3) δ 7.81 (d, $J = 8.98$ Hz, 2H, 2 \times ArH),

7.69–7.65 (m, 2H, 2 × ArH), 7.51–7.47 (m, 1H, ArH), 7.37 (t, $J = 7.75$ Hz, 1H, ArH), 6.85 (d, $J = 8.89$ Hz, 2H, 2 × ArH); ^{13}C NMR (100 MHz, CDCl_3) δ 159.5 (ArC-OH), 149.7 (ArC-N), 147.2 (ArC-N), 132.6 (ArC), 129.7 (ArC), 125.8 (3 × ArC), 116.3 (ArC), 116.0 (3 × ArC); LC/MS: m/z 266.8 $[M + \text{H}]^+$; ESI-HRMS $^+(m/z)$ calculated for $\text{C}_{13}\text{H}_9\text{F}_3\text{N}_2\text{O} = 266.2232$ $[M + \text{H}]^+$, found 267.0746 $[M + \text{H}]^+$.

2.5 References

1. Hunt, C. J., Cryopreservation of human stem cells for clinical application: a review. *Transfus. Med. Hemother.*, **2011**, 38 (2), 107–123.
2. Ledda, S.; Bogliolo, L.; Succu, S.; Ariu, F.; Bebbere, D.; Leoni, G. G.; Naitana, S., Oocyte cryopreservation: oocyte assessment and strategies for improving survival. *Reprod. Fertil. Dev.*, **2006**, 19 (1), 13–23.
3. Henkelman, S.; Lagerberg, J. W.; Graaff, R.; Rakhorst, G.; Van Oeveren, W., The effects of cryopreservation on red blood cell rheologic properties. *Transfusion*, **2010**, 50 (11), 2393–2401.
4. Donnez, J.; Martinez-Madrid, B.; Jadoul, P.; Van Langendonck, A.; Demylle, D.; Dolmans, M.-M., Ovarian tissue cryopreservation and transplantation: a review. *Hum. Reprod.*, **2006**, 21 (5), 519–535.
5. Fuller, B. J., Cryoprotectants: the essential antifreezes to protect life in the frozen state. *CryoLetters*, **2004**, 25 (6), 375–388.
6. Balcerzak, A. K.; Capicciotti, C. J.; Briard, J. G.; Ben, R. N., Designing ice recrystallization inhibitors: from antifreeze (glyco) proteins to small molecules. *RSC Adv.*, **2014**, 4 (80), 42682–42696.
7. Capicciotti, C. J.; Doshi, M.; Ben, R. N., *Ice recrystallization inhibitors: from biological antifreezes to small molecules*. INTECH Open Access Publisher: 2013.

8. Capicciotti, C. J.; Kurach, J. D.; Turner, T. R.; Mancini, R. S.; Acker, J. P.; Ben, R. N., Small molecule ice recrystallization inhibitors enable freezing of human red blood cells with reduced glycerol concentrations. *Sci. Rep.*, **2015**, *5*.
9. Polge, C.; Smith, A. U.; Parkes, A., Revival of spermatozoa after vitrification and dehydration at low temperatures. *Nature*, **1949**, *164* (4172), 666–666.
10. Hovatta, O.; Silye, R.; Krausz, T.; Abir, R.; Margara, R.; Trew, G.; Lass, A.; Winston, R. M. L., Cryopreservation of human ovarian tissue using dimethylsulphoxide and propanediol-sucrose as cryoprotectants. *Hum. Reprod.*, **1996**, *11* (6), 1268–1272.
11. Pegg, D. E., Principles of cryopreservation. In *Cryopreservation and freeze-drying protocols*, Second ed.; Day, J. G., Stacey, G. N., Ed. Humana Press: Totowa, New Jersey, 2007; pp 39–57.
12. Rodrigues, J. P.; Paraguassú-Braga, F. H.; Carvalho, L.; Abdelhay, E.; Bouzas, L. F.; Porto, L. C., Evaluation of trehalose and sucrose as cryoprotectants for hematopoietic stem cells of umbilical cord blood. *Cryobiology*, **2008**, *56* (2), 144–151.
13. Liseth, K.; Foss Abrahamsen, J.; Bjørsvik, S.; Grøtnebø, K.; Bruserud, Ø., The viability of cryopreserved PBPC depends on the DMSO concentration and the concentration of nucleated cells in the graft. *Cytotherapy*, **2005**, *7* (4), 328–333.
14. Fahy, G. M., The relevance of cryoprotectant “toxicity” to cryobiology. *Cryobiology*, **1986**, *23* (1), 1–13.
15. Scholander, P.; Van Dam, L.; Kanwisher, J.; Hammel, H.; Gordon, M., Supercooling and osmoregulation in Arctic fish. *J. Cell. Physiol.*, **1957**, *49* (1), 5–24.
16. Gordon, M. S.; Amdur, B. H.; Scholander, P., Freezing resistance in some northern fishes. *Biol. Bull.*, **1962**, *122* (1), 52–62.
17. DeVries, A. L.; Wohlschlag, D. E., Freezing resistance in some Antarctic fishes. *Science*, **1969**, *163* (3871), 1073–1075.

18. DeVries, A. L.; Komatsu, S. K.; Feeney, R. E., Chemical and physical properties of freezing point-depressing glycoproteins from Antarctic fishes. *J. Biol. Chem.*, **1970**, *245* (11), 2901–2908.
19. Devries, A. L., Glycoproteins as biological antifreeze agents in Antarctic fishes. *Science*, **1971**, *172* (3988), 1152–1155.
20. Gibson, M. I., Slowing the growth of ice with synthetic macromolecules: beyond antifreeze (glyco) proteins. *Polym. Chem.*, **2010**, *1* (8), 1141–1152.
21. Czechura, P.; Tam, R. Y.; Dimitrijevic, E.; Murphy, A. V.; Ben, R. N., The importance of hydration for inhibiting ice recrystallization with C-linked antifreeze glycoproteins. *J. Am. Chem. Soc.*, **2008**, *130* (10), 2928–2929.
22. Liu, S.; Ben, R. N., C-linked galactosyl serine AFGP analogues as potent recrystallization inhibitors. *Org. Lett.*, **2005**, *7* (12), 2385–2388.
23. Capicciotti, C. J.; Leclère, M.; Perras, F. A.; Bryce, D. L.; Paulin, H.; Harden, J.; Liu, Y.; Ben, R. N., Potent inhibition of ice recrystallization by low molecular weight carbohydrate-based surfactants and hydrogelators. *Chem. Sci.*, **2012**, *3* (5), 1408–1416.
24. Wilkinson, B. L.; Stone, R. S.; Capicciotti, C. J.; Thaysen - Andersen, M.; Matthews, J. M.; Packer, N. H.; Ben, R. N.; Payne, R. J., Total synthesis of homogeneous antifreeze glycopeptides and glycoproteins. *Angew. Chem. Int. Ed.*, **2012**, *51* (15), 3606–3610.
25. Mizrahy, O.; Bar-Dolev, M.; Guy, S.; Braslavsky, I., Inhibition of ice growth and recrystallization by zirconium acetate and zirconium acetate hydroxide. *PLoS one*, **2013**, *8* (3), e59540.
26. Wang, B.; Boons, G.-J., *Carbohydrate recognition: biological problems, methods, and applications*. John Wiley & Sons: 2011; Vol. 13.

27. Tam, R. Y.; Ferreira, S. S.; Czechura, P.; Chaytor, J. L.; Ben, R. N., Hydration Index—a better parameter for explaining small molecule hydration in inhibition of ice recrystallization. *J. Am. Chem. Soc.*, **2008**, *130* (51), 17494–17501.
28. Capicciotti, C. J.; Mancini, R. S.; Turner, T. R.; Koyama, T.; Alteen, M. G.; Doshi, M.; Inada, T.; Acker, J. P.; Ben, R. N., *O*-aryl-glycoside ice recrystallization inhibitors as novel cryoprotectants: a structure–function study. *ACS Omega*, **2016**, *1* (4), 656–662.
29. Balcerzak, A. K.; Febbraro, M.; Ben, R. N., The importance of hydrophobic moieties in ice recrystallization inhibitors. *RSC Adv.*, **2013**, *3* (10), 3232–3236.
30. Kovalchuk, N.; Trybala, A.; Starov, V.; Matar, O.; Ivanova, N., Fluoro- vs hydrocarbon surfactants: Why do they differ in wetting performance? *Adv. Colloid Interface Sci.*, **2014**, *210*, 65–71.
31. Krafft, M.; Riess, J., Highly fluorinated amphiphiles and colloidal systems, and their applications in the biomedical field. A contribution. *Biochimie*, **1998**, *80* (5), 489–514.
32. Riess, J. G., Overview of progress in the fluorocarbon approach to *in vivo* oxygen delivery. *Biomater. Artif. Cells Immobilization Biotechnol.*, **1992**, *20* (2–4), 183–202.
33. Krafft, M. P., Fluorocarbons and fluorinated amphiphiles in drug delivery and biomedical research. *Adv. Drug Deliv. Rev.*, **2001**, *47* (2), 209–228.
34. Lehmler, H.-J., Perfluorocarbon compounds as vehicles for pulmonary drug delivery. *Expert Opin. Drug Deliv.*, **2007**, *4* (3), 247–262.
35. Lehmler, H. J.; Bummer, P. M.; Jay, M. J., Liquid ventilation – a new way to deliver drugs to diseased lungs? *Chemtech*, **1999**, *29* (10), 7–12.
36. Shaffer, T. H.; Wolfson, M. R.; Clark, L. C., Liquid ventilation. *Pediatr. pulmonol.*, **1992**, *14* (2), 102–109.

37. Krafft, M. P.; Riess, J. G., Chemistry, physical chemistry, and uses of molecular fluorocarbon-hydrocarbon diblocks, triblocks, and related compounds – unique “apolar” components for self-assembled colloid and interface engineering. *Chem. Rev.*, **2009**, *109* (5), 1714–1792.
38. Eastoe, J.; Vesperinas, A., Self-assembly of light-sensitive surfactants. *Soft Matter*, **2005**, *1* (5), 338–347.
39. Sakai, H.; Matsumura, A.; Yokoyama, S.; Saji, T.; Abe, M., Photochemical switching of vesicle formation using an azobenzene-modified surfactant. *J. Phys. Chem. B*, **1999**, *103* (49), 10737–10740.
40. Beharry, A. A.; Woolley, G. A., Azobenzene photoswitches for biomolecules. *Chem. Soc. Rev.*, **2011**, *40* (8), 4422–4437.
41. Michel, O.; Ravoo, B. J., Carbohydrate microarrays by microcontact “click” chemistry. *Langmuir*, **2008**, *24* (21), 12116–12118.
42. N.Floyd, B. V., J.R.Koeppel, and B.G.Davis, Thiol-glycosylation of olefinic proteins: s-linked glycoprotein synthesis. *Angew. Chem. Int. Ed.*, **2009**, *121* (42), 7938–7942.
43. Beaussart, A.; Abellán-Flos, M.; El-Kirat-Chatel, S.; Vincent, S. P.; Dufrêne, Y. F., Force nanoscopy as a versatile platform for quantifying the activity of antiadhesion compounds targeting bacterial pathogens. *Nano Lett.*, **2016**, *16* (2), 1299–1307.
44. Billamboz, M.; Mangin, F.; Drillaud, N.; Chevrin-Villette, C.; Banaszak-Leonard, E.; Len, C., Micellar catalysis using a photochromic surfactant: application to the Pd-catalyzed Tsuji–Trost reaction in water. *J. Org. Chem.*, **2014**, *79* (2), 493–500.
45. Jervis, P. J.; Moulis, M.; Jukes, J.-P.; Ghadbane, H.; Cox, L. R.; Cerundolo, V.; Besra, G. S., Towards multivalent CD1d ligands: synthesis and biological activity of homodimeric α -galactosyl ceramide analogues. *Carbohydr. Res.*, **2012**, *356*, 152–162.

46. Wilkinson, B. L.; Bornaghi, L. F.; Poulsen, S.-A.; Houston, T. A., Synthetic utility of glycosyl triazoles in carbohydrate chemistry. *Tetrahedron*, **2006**, *62* (34), 8115–8125.
47. Berry, J. D.; Neeson, M. J.; Dagastine, R. R.; Chan, D. Y.; Tabor, R. F., Measurement of surface and interfacial tension using pendant drop tensiometry. *J. Colloid Interface Sci.*, **2015**, *454*, 226–237.
48. Tabor, R. F.; Tan, D. D.; Han, S. S.; Young, S. A.; Seeger, Z. L.; Pottage, M. J.; Garvey, C. J.; Wilkinson, B. L., Reversible pH - and photocontrollable carbohydrate - based surfactants. *Chem. Eur. J.*, **2014**, *20* (43), 13881 - 13884.
49. Chevallier, E.; Mamane, A.; Stone, H.; Tribet, C.; Lequeux, F.; Monteux, C., Pumping-out photo-surfactants from an air-water interface using light. *Soft Matter*, **2011**, *7* (17), 7866–7874.
50. Han, M. R.; Hirayama, Y.; Hara, M., Fluorescence enhancement from self-assembled aggregates: substituent effects on self-assembly of azobenzenes. *Chem. Mater.*, **2006**, *18* (12), 2784–2786.
51. Vecchi, I.; Arcioni, A.; Bacchiocchi, C.; Tiberio, G.; Zanirato, P.; Zannoni, C., Expected and unexpected behavior of the orientational order and dynamics induced by azobenzene solutes in a nematic. *J. Phys. Chem. B*, **2007**, *111* (13), 3355–3362.
52. Garrido, N. M.; Queimada, A. J.; Jorge, M.; Macedo, E. A.; Economou, I. G., 1-Octanol/water partition coefficients of n-alkanes from molecular simulations of absolute solvation free energies. *J. Chem. Theory Comput.*, **2009**, *5* (9), 2436–2446.
53. Chamberlain, K.; Evans, A. A.; Bromilow, R. H., 1 - Octanol/water partition coefficient (Kow) and pKa for ionisable pesticides measured by a pH - metric method. *Pest Manag. Sci.*, **1996**, *47* (3), 265–271.
54. Stallman, R. E. a. N., A. H. W., Solidification. In *Modern Physical Metallurgy*, 8th ed.; Elsevier/ Butterworth-Heinemann: Amsterdam, 2014; pp 93–120.

55. Cronin, D.; Mark, T., The role of hydrophobicity in toxicity prediction. *Curr. Comput Aided Drug Des.*, **2006**, 2 (4), 405–413.
56. Yalkowsky, S. H., *Solubility and solubilization in aqueous media*. American Chemical Society: 1999.
57. Pinho, S. P.; Macedo, E. A., Solubility in Food, Pharmaceutical, and Cosmetic Industries. In *Developments and Applications in Solubility*, 2007; pp 305–322.
58. Sangster, J., *Octanol-water partition coefficients: fundamentals and physical chemistry*. John Wiley & Sons: 1997.
59. Knight, C. A.; Hallett, J.; DeVries, A., Solute effects on ice recrystallization: an assessment technique. *Cryobiology*, **1988**, 25 (1), 55–60.
60. Wharton, D. A.; Wilson, P. W.; Mutch, J. S.; Marshall, C. J.; Lim, M., Recrystallization inhibition assessed by splat cooling and optical recrystallometry. *CryoLetters*, **2007**, 28 (1), 61–68.
61. Selve, C.; Castro, B.; Leempoel, P.; Mathis, G.; Gartiser, T.; Delpuech, J.-J., Synthesis of homogeneous polyoxyethylene perfluoralkyl surfactants: A new method. *Tetrahedron*, **1983**, 39 (8), 1313–1316.
62. Manaargadoo-Catin, M.; Ali-Cherif, A.; Pougna, J.-L.; Perrin, C., Hemolysis by surfactants—a review. *Adv. Colloid Interface Sci.*, **2016**, 228, 1–16.
63. Velema, W. A.; Szymanski, W.; Feringa, B. L., Photopharmacology: beyond proof of principle. *J. Am. Chem. Soc.*, **2014**, 136 (6), 2178–2191.
64. Abraham, S.; Keillor, K.; Capicciotti, C. J.; Perley-Robertson, G. E.; Keillor, J. W.; Ben, R. N., Quantitative Analysis of the Efficacy and Potency of Novel Small Molecule Ice Recrystallization Inhibitors. *Cryst. Growth Des.*, **2015**, 15 (10), 5034–5039.

65. Samanta, S.; Beharry, A. A.; Sadovski, O.; McCormick, T. M.; Babalhavaeji, A.; Tropepe, V.; Woolley, G. A., Photoswitching azo compounds *in vivo* with red light. *J. Am. Chem. Soc.*, **2013**, *135* (26), 9777–9784.
66. Dong, M.; Babalhavaeji, A.; Samanta, S.; Beharry, A. A.; Woolley, G. A., Red-shifting azobenzene photoswitches for *in vivo* use. *Acc. Chem. Res.*, **2015**, *48* (10), 2662–2670.
67. Chaytor, J. L.; Tokarew, J. M.; Wu, L. K.; Leclère, M.; Tam, R. Y.; Capicciotti, C. J.; Guolla, L.; von Moos, E.; Findlay, C. S.; Allan, D. S., Inhibiting ice recrystallization and optimization of cell viability after cryopreservation. *Glycobiology*, **2012**, *22* (1), 123–133.
68. Chakrabartty, A.; Hew, C. L., The effect of enhanced α - helicity on the activity of a winter flounder antifreeze polypeptide. *FEBS J.*, **1991**, *202* (3), 1057–1063.
69. Li, T.; Guo, L.; Zhang, Y.; Wang, J.; Li, Z.; Lin, L.; Zhang, Z.; Li, L.; Lin, J.; Zhao, W., Design and synthesis of O-GlcNAcase inhibitors via ‘click chemistry’ and biological evaluations. *Carbohydr. Res.*, **2011**, *346* (9), 1083–1092.
70. Berteau, O.; Stenutz, R., Web resources for the carbohydrate chemist. *Carbohydr. Res.*, **2004**, *339* (5), 929–936.
71. McNaught, A. D., International union of pure and applied chemistry and international union of biochemistry and molecular biology. Joint commission on biochemical nomenclature. Nomenclature of carbohydrates. *Carbohydr. Res.*, **1997**, *297* (1), 1–92.
72. McNaught, A. D., Nomenclature of carbohydrates (IUPAC Recommendations 1996). *Pure Appl. Chem.*, **1996**, *68* (10), 1919–2008.
73. Wilkinson, B. L. Synthesis of novel carbohydrate based enzyme inhibitor libraries utilising click chemistry. Griffith University, 2007.
74. Matsubara, K.; Mukaiyama, T., High-yielding catalytic synthesis of glycosyl azides from peracylated sugars. *Chem. Lett.*, **1994**, *23* (2), 247–250.

75. Blázquez - Sánchez, M. T.; Marcelo, F.; Fernández - Alonso, M. d. C.; del Villar - Guerra, R.; Samadi, A.; Cañada, F. J.; Jiménez - Barbero, J.; Vicent, C., D - and L - mannose - containing glyco - oligoamides show distinct recognition properties when interacting with DNA. *Eur. J. Org. Chem.*, **2015**, 2015 (28), 6180–6193.
76. Nurmi, L.; Lindqvist, J.; Randev, R.; Syrett, J.; Haddleton, D. M., Glycopolymers via catalytic chain transfer polymerisation (CCTP), Huisgens cycloaddition and thiol-ene double click reactions. *Chem. Commun.*, **2009**, (19), 2727–2729.
77. Cui, K.; Lu, X.; Cui, W.; Wu, J.; Chen, X.; Lu, Q., Fluorescent nanoparticles assembled from a poly (ionic liquid) for selective sensing of copper ions. *Chem. Commun.*, **2011**, 47 (3), 920–922.
78. Feng, N.; Han, G.; Dong, J.; Wu, H.; Zheng, Y.; Wang, G., Nanoparticle assembly of a photo-and pH-responsive random azobenzene copolymer. *J. Colloid Interface Sci.*, **2014**, 421, 15–21.

Chapter 3

*Photomodulation of Bacterial Growth and Biofilm
Formation Using Carbohydrate-based Surfactants*

This page is intentionally blank

Declaration for Thesis Chapter 3

Declaration by candidate

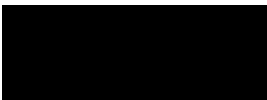
In the case of Chapter 3, the nature and extent of my contribution to this work was as following:

Nature of contribution	Extent of contribution (%)
Synthesis and (physical) characterization of product, analysis of results, writing up	50

The following co-authors contributed to the work. If co-authors are students, the extent of their contribution in percentage terms was stated:

Name	Nature of contribution	Extent of contribution (%) for student co-workers only
Wenyue Zou	Bacterial and biofilm assays, analysis of results	45
Reece Nixon-Luke	DMM experimentation	4
Rajesh Ramanathan	Assisted in bacterial experimentation	
Villy Julita	Assisted in experimentation	1
Brendan L. Wilkinson Rico F. Tabor Vipul Bansal Gary Bryant	Initiation and key ideas	

The undersigned hereby certify that the above declaration correctly reflects the nature and extent of the candidate's and co-authors' contributions to this work.

Candidate's Signature		Date 12 June 2017
Main Supervisor's Signature		Date 13th June 2017

This page is intentionally blank

Photomodulation of bacterial growth and biofilm formation using carbohydrate-based surfactants

This chapter is an expanded version of the article:

- **Hu, Y.;** Zou, W.; Julita, V.; Ramanathan, R.; Tabor, R. F.; Nixon-Luke, R.; Bryant, G.; Bansal, V. and Wilkinson, B. L. Photomodulation of bacterial growth and biofilm formation using carbohydrate-based surfactants. *Chem. Sci.* **2016**, 7 (11), 6628–6634.

3.1 Introduction

3.1.1 Antibacterial drug resistance and biofilms

Antimicrobial resistance is a natural phenomenon exhibited by microorganisms — an evolutionary mechanism by which bacteria, viruses, parasites and fungi develop immunity such that they are no longer susceptible to antibiotics, therefore rendering the treatment ineffective.¹ Both the World Health Organization and governments have proposed policies aiming to combat antimicrobial resistance.² Although the mechanism of how the bacterium disseminate resistance is poorly understood, it is suggested to have some relationship with the complex communities (biofilms) formed by bacteria, particularly from those strains inherently resistant to antibiotics.³ Biofilms are multicellular aggregates of bacteria, formed by the self-production of an extracellular matrix.⁴ The biofilm matrix is generally composed of extracellular polysaccharides, proteins and DNA, which not only allow the bacteria to adhere to the surface but also facilitates communication and transfer of genetic information. The adhered/sessile bacteria are metabolically dormant, thus enhancing bacterial survival and making them more resistant to antibiotic therapies than their planktonic populations.^{5, 6}

The development of biofilms is a complex process but can be generally divided into three stages: attachment of bacteria to a surface, growth of bacteria into colonies and translocation of bacteria from the colony to the surrounding medium (Figure 3.1).⁷ In the initial cell-to-surface attachment, flagellar motility was treated as the most common mechanism governing this

process.⁸ Bacterial motility can be classified into swimming, swarming, gliding, twitching and sliding.⁹ Swimming and swarming motilities have been shown to require flagella, but unlike swarming, which is the movement of a group of bacteria, swimming takes place as individual cells.^{9, 10} Twitching motility is correlated with the presence of type IV pili. All other active surface movement (translocation) that occurs without the aid of flagella or pili is classified as gliding motility. Unlike flagella-mediated motility, such as swarming and twitching modes, sliding motility is a passive translocation that is sensitive to surface tension changes.^{9, 10} Once sessile bacterial adhere to a surface, the colony can grow in size through cell multiplication and the formation of an extracellular polymeric matrix, eventually constituting a mature biofilm.^{7, 11, 12} Cells are then released from mature biofilms and dispersed into the surrounding environment, hence making biofilm formation a cyclic pathway.⁷

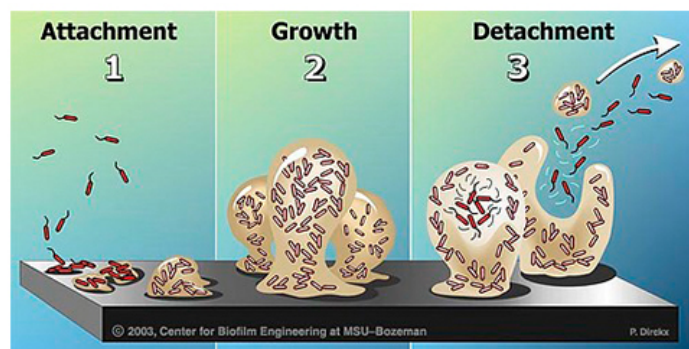


Figure 3.1. Schematic diagram of biofilm development.¹³ Adapted with permission from reference 13. Copyright 1991–2010 Center for Biofilm Engineering at Montana State University.

Bacterial biofilms are responsible for many chronic and recurrent infections.^{14, 15} Approximately 80% of bacterial infections are biofilm-related, either from a single species or a mixture of bacterial species and fungi.¹⁶ However, the mechanisms of biofilm formation are poorly understood. Biofilm infections are rarely resolved by the host immune system and normally antibiotics can only reverse the symptoms caused by planktonic bacterial cells. Therefore, new treatments that target biofilm infections are required.

3.1.2 Glycolipids

Glycolipids are naturally occurring, surface-active molecules consisting of a carbohydrate head group(s) covalently bound to one or more alkyl chains. They are produced by every known living organism, ranging from mammals, yeast and fungi, as well as several bacterial species. In mammals, glycolipids play crucial roles in maintaining membrane structure and function, and are also mediators of intercellular communication events underlying inflammation and apoptosis.^{17, 18} Glycolipids originating from different microorganisms have been reported to show inhibition of microbial growth and biofilm formation.^{19, 20} Among all glycolipids, rhamnolipids, trehalolipids, sophorolipids, mannosylerythritol lipids, cellobiose lipids and xylolipids are the most widely most-studied, and exhibit anti-microbial activity against a wide range of pathogens (Table 3.1). In some cases, the inhibition of microbial growth is due to cell wall damage and membrane lysis induced by the surface-active glycolipids.²¹

Table 3.1. Main glycolipids produced by several microorganisms and their minimum inhibitory concentrations (MIC) against different pathogens.

Glycolipid	Producing microorganism	Target microorganism (MIC)
Rhamnolipids	<i>P. aeruginosa</i> ²²	A wide range of fungi and pathogens (0.4-35 µg mL ⁻¹) ²¹
Trehalolipids	<i>Micrococcus luteus</i> ; <i>R. erythropolis</i> ; <i>Rhodococcus</i> sp. TB-42 ^{23, 24}	Fungi (300 mg L ⁻¹) ²⁵
Sophorolipids	<i>Wickerhamiella domericqiae</i> ^{26, 27}	Several Gram-positive bacteria (50-29,000 µg mL ⁻¹) ²¹
Mannosylerythritol lipids and cellobiose lipids	<i>Ustilago maydis</i> ; <i>Candida antarctica</i> ; <i>Pseudozyma fusiformata</i> ²⁸⁻³⁰	Gram-positive bacteria ²⁵
Xylolipids	<i>Lactococcus lactis</i> ³¹	<i>Escherichia coli</i> and <i>S. aureus</i> ³¹
Lipids of oligosaccharides	<i>Tsukamurella</i> sp. ³²	<i>Bacillus megaterium</i> (50-150 µg mL ⁻¹) ³²

Glycolipids have also been reported to show anti-adhesive and anti-biofilm activity and have attracted considerable interest as selective antimicrobial agents. Rhamnolipids produced by *P. aeruginosa* were reported to give a 41–71% inhibition of *Listeria monocytogenes* adhesion on polystyrene surfaces.³³ Lunasan produced by *Candida sphaerica* UVP 0995 showed potent growth inhibition and anti-adhesive properties against *S. aureus* (90% inhibition, 100% anti-adhesive), *Candida albicans* (64% inhibition, 100% anti-adhesive) and *Streptococcus agalactiae* (92% inhibition, 100% anti-adhesive).³⁴ *Candida lipolytica* UCP 0988 is capable of producing a glycolipid that provided anti-adhesive properties against *S. aureus* (88%) and *Lactobacillus casei* (91%).³⁵ *Serratia marcescens* has been reported to produce a glycolipid that could prevent the biofilm formation of *C. albicans*, *P. aeruginosa* and *Bacillus pumilus* on microtitration plates.³⁶

In this respect, bioinspired carbohydrate amphiphiles have emerged as alternatives to microbial glycolipids as potential anti-microbial agents, and as mechanistic tools to study carbohydrate-protein interactions and bacterial adhesion leading to biofilm formation. The self-assembling nature of these amphiphiles enables the multivalent presentation of physiologically relevant carbohydrates on the micellar/vesicular surface, and could be treated as a mimic of the naturally-occurring glycolipids (containing oligo- or polymeric head groups). Recently, Grinstaff and co-workers have reported a novel class of carbohydrate (poly-amido-saccharide (PAS)) amphiphiles **3.1** that could inhibit the biofilm formation of *P. aeruginosa* (Figure 3.2).³⁷ Chaveriat *et al.* have reported the synthesis of D-galactopyranose derivatives **3.2** that showed anti-bacterial activities against *Micrococcus luteus* (MIC = 3.91 $\mu\text{g mL}^{-1}$) (Figure 3.2).³⁸ In these studies, subtle structural modifications presented different antibacterial profiles, however, the mechanisms underlying those findings were not clearly understood.

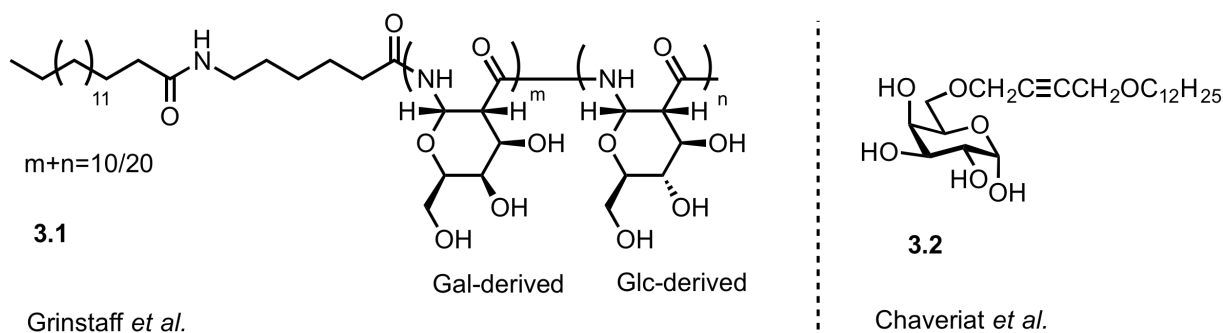


Figure 3.2. Molecular structures of carbohydrate amphiphiles as reported by Grinstaff and co-workers (compound **3.1**) (left) and by Chaveriat and co-workers (compound **3.2**) (right).^{37, 38} Adapted with permission from references 37 and 38. Copyright 2014 Royal Society of Chemistry and 2012 Elsevier Masson SAS.

Amphiphiles with tuneable properties offer new opportunities to probe bacterial adhesion processes leading to biofilm formation, ultimately improving our understanding of bacterial physiology. Towards this goal, the azobenzene chromophore has been widely used to probe carbohydrate-protein interactions,³⁹ provide optical control over anti-microbial activity and bacterial adhesion,⁴⁰⁻⁴¹ self-assembly and interfacial activity.⁴²⁻⁴⁴ However, the application of azobenzene-based carbohydrate amphiphiles as photoswitchable inhibitors of bacterial growth and biofilm formation is yet to be reported. In this chapter, we describe the parallel synthesis a novel photoswitchable carbohydrate surfactant library **3.3–3.13**, and investigate their application as photoswitchable modulators of bacterial growth and biofilm formation against drug-resistant, Gram-negative *Escherichia coli* and *Pseudomonas aeruginosa*, and Gram-positive *Staphylococcus aureus* (Figure 3.3).

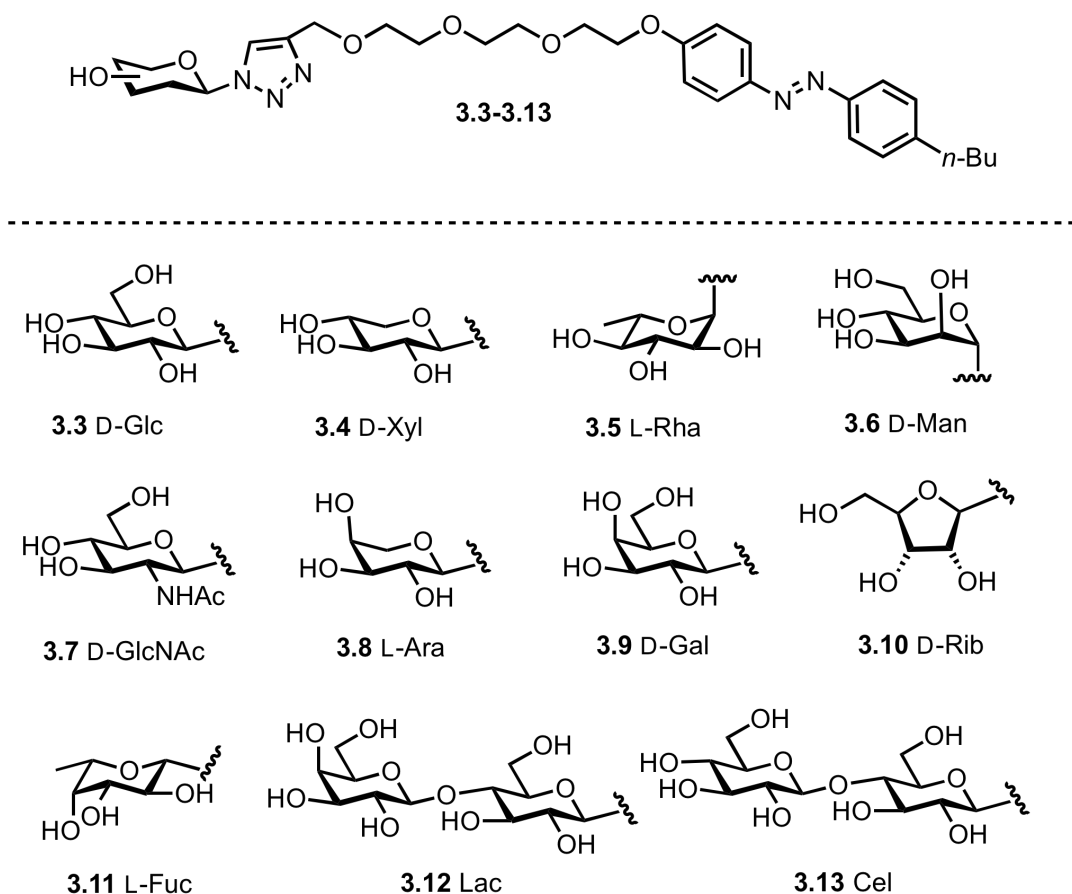


Figure 3.3. Proposed photoswitchable carbohydrate-based surfactants **3.3–3.13**.

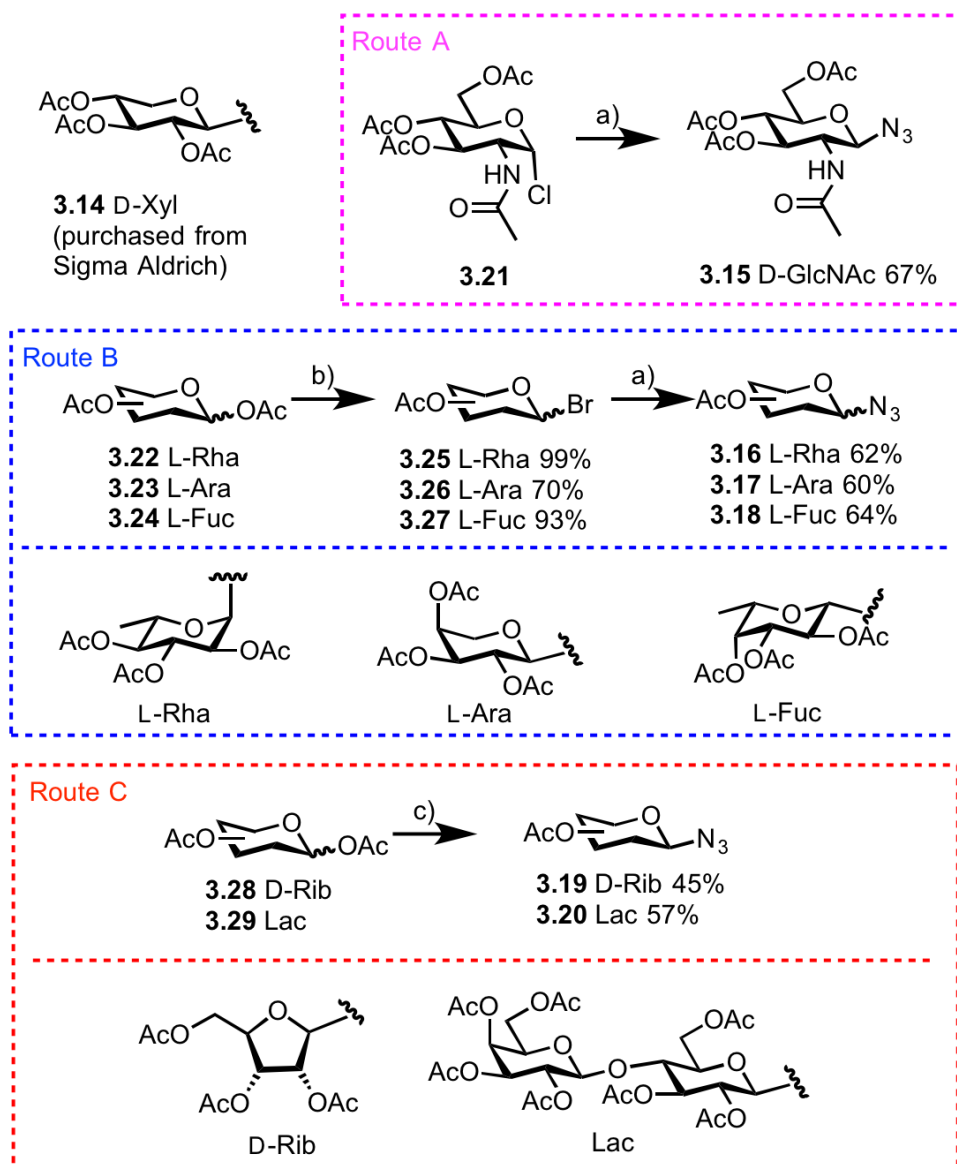
3.2 Results and Discussion

3.2.1 Library design and synthesis

Our investigation commenced with the synthesis and characterization of a library of novel photoswitchable glycosyl triazole surfactants **3.3–3.13**. Various monosaccharides and disaccharides were selected as head groups, including D-glucose (Glc), D-xylose (Xyl), L-rhamnose (Rha), D-mannose (Man), *N*-acetylglucosamine (GlcNAc), L-arabinose (Ara), D-galactose (Gal), D-ribose (Rib), L-fucose (Fuc), lactose (Lac) and cellobiose (Cel). The carbohydrate head groups served as structural motifs for biomolecular recognition, and were selected on the basis of the bioactivities of glycolipids expressing these structures, along with their important roles in bacterial adhesion.⁴⁵ Reversible *trans-cis* photoisomerization of the hydrophobic *n*-butylazobenzene tail was employed to control the interfacial and aggregation

properties of surfactants, using surface tension measurements and small angle neutron scattering (SANS), respectively.

Prior to the parallel synthesis of surfactants **3.3–3.13**, the synthesis of the requisite head and tail groups was carried out. Glycosyl azides **2.32–2.35** and **3.14–3.20** were key intermediates for the synthesis of the proposed library using the well-documented CuAAC reaction.⁴⁶ The synthesis of azides **2.32–2.35** was previously described in Chapter 2. 2,3,4-tri-acetyl- β -D-xylopyranosyl azide **3.14** was purchased from Sigma-Aldrich and was used directly without further purification. Known glycosyl azide **3.15** was obtained by reacting commercially available 2-acetamido-2-deoxy- α -D-glucopyranosyl chloride 3,4,6-triacetate **3.21** with sodium azide under phase transfer catalytic conditions (Scheme 3.1 Route A).⁴⁷ For the synthesis of compounds **3.16–3.18**, the corresponding pentaacetates **3.22–3.24** were reacted with hydrogen bromide solution to afford the corresponding glycosyl bromide **3.25–3.27** in good yield (40–75%), followed by nucleophilic displacement with sodium azide under phase-transfer condition to give the desired glycosyl azides **2.32–2.35** (Scheme 3.1 Route B).⁴⁷ Ribofuranosyl azide **3.19** and lactosyl azide **3.20** were synthesized by the glycosylation of the glycosyl acetates **3.28** and **3.29** and trimethylsilyl azide using stannic chloride as Lewis acid promoter in anhydrous DCM (Scheme 3.1 Route C).

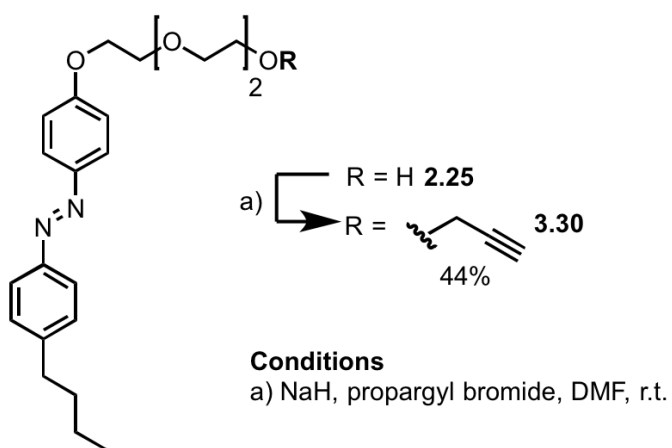


Conditions:

- a) NaN_3 , tetrabutylammonium bisulfite, NaHCO_3 , DCM, H_2O
 b) HBr/AcOH , DCM, 0°C to r.t.
 c) Trimethylsilyl azide, SnCl_4 , dry DCM

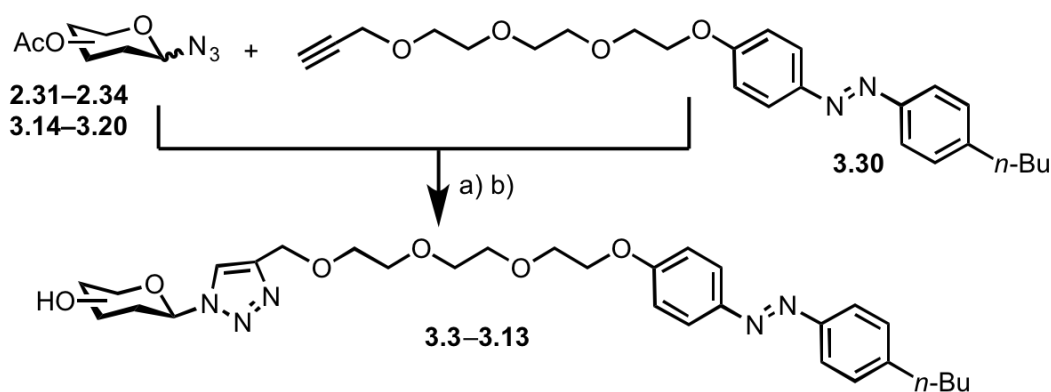
Scheme 3.1. Synthetic procedure for glycosyl azides **3.14–3.20**.

The alkyne-functionalized azobenzene **3.30** was prepared by alkylation of alcohol **2.25** (Scheme 3.2). Compound **2.25** was treated with an excess of sodium hydride, followed by addition of an excess of propargyl bromide in the presence of tetrabutylammonium iodide to afford compound **3.30** in 44% yield

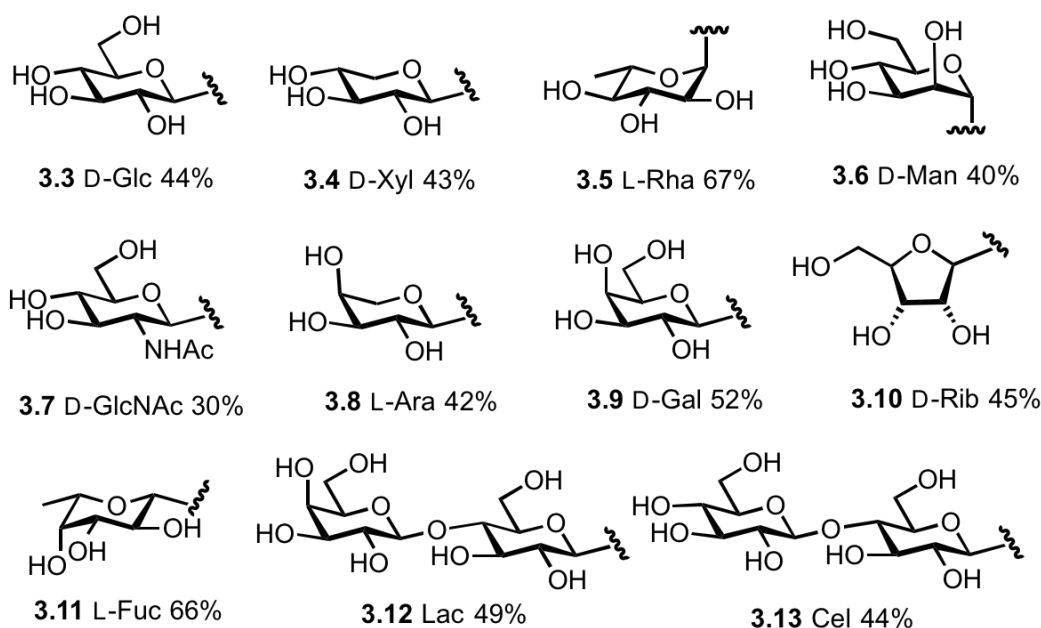


Scheme 3.2. Synthesis of alkyne-functionalized fragment **3.30**.

With the requisite azides (**2.32–2.35** and **3.14–3.20**) and alkyne fragment (**3.30**) in hand, the library was assembled in a modular fashion using the well-known CuAAC reaction (Scheme 3.3). Following the CuAAC reaction and work-up, the crude protected products were treated with sodium methoxide in dry methanol to effect removal of the acetate esters, followed by purification by reversed-phase preparative HPLC to give the desired surfactants **3.3–3.13** in acceptable yields.



Conditions: a) $\text{CuSO}_4 \cdot 5\text{H}_2\text{O}$, sodium ascorbate, water/ *t*-BuOH b) NaOCH_3 , methanol, r.t.



Scheme 3.3. Synthetic procedure for surfactants **3.3–3.13**.

3.2.2 Photoswitching studies

In order to understand the photoswitching activity of surfactants **3.3–3.13**, we evaluated the rate of thermal relaxation and potential photodegradation through UV-vis spectroscopy and NMR respectively as described in Chapter 2. The thermal relaxation studies were performed at ambient temperature in Milli-Q water (Figure 3.4). Since bacterial experiments were performed at 37°C, the rate of *cis-trans* thermal relaxation was also investigated at 37°C in deionized water, as well as in nutrient broth (NB) and brain heart infusion broth (BHI), which were the growth media employed for the antibacterial studies. The native *trans* isomers remained stable under ambient lighting conditions for at least up to 24 h, as demonstrated from the insignificant

changes in the UV-vis absorbance spectra over this period. The dark-adapted *cis*-isomers slowly reverted to the *trans* state with a half-life of more than 20 hours at ambient temperature. Under 37°C conditions, a half-life of more than 10 hours in all three different media was calculated, which provided sufficient time for the *cis*-isomers to elicit a biological response (Table 3.3).

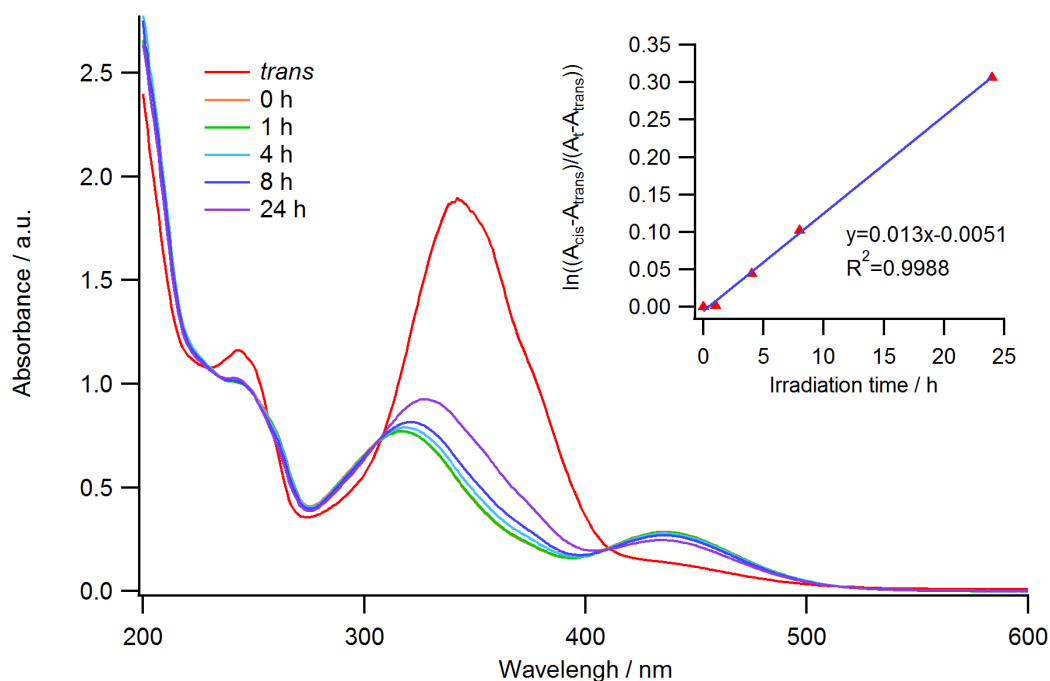


Figure 3.4. Time-dependent *cis*–*trans* thermal relaxation of representative surfactant GlcTz 3.3 at 20°C in water and the corresponding first-order plot for *cis*–*trans* conversion (inserted). Please see **Appendix I** for complete data.

Table 3.2. Thermal half-lives (hours) of **3.3–3.13** in water, Nutrient Broth (NB) and Brain Heart Infusion broth (BHI).

<i>Surfactant</i>	<i>Water 20°C*</i>	<i>Water 37°C**</i>	<i>NB 37°C**</i>	<i>BHI 37°C**</i>
GlcTz 3.3	53.32	12.45	10.63	11.02
XylTz 3.4	23.18	11.78	12.18	11.40
RhaTz 3.5	60.27	11.21	10.42	10.64
ManTz 3.6	27.51	12.06	10.88	11.01
GlcNAcTz 3.7	48.47	12.31	10.89	10.95
AraTz 3.8	55.01	11.92	10.54	11.18
GalTz 3.9	96.27			
RibTz 3.10	41.26			
FucTz 3.11	49.16		Not detected	
LacTz 3.12	60.80			
CelTz 3.13	46.52			

* Surfactants were measured at 0.05 mM concentration

** Measurements were conducted by Wenyue Zou; Surfactants were measured at 200 µg mL⁻¹ concentration

As previously described in Chapter 2, the *trans-cis* ratios at the respective photostationary states (PSS), along with the potential photodegradation following *trans-cis* photoisomerization were investigated using ¹H NMR. It can be seen from Figure 3.5 that 6% *cis*-isomer existed in the *trans*-dominated PSS, while 74% *cis*-isomer was found after UV irradiation. Approximately 90% of the *trans*-isomer was present after *cis*-to-*trans* relaxation and no photodegradation was observed from the ¹H NMR spectrum (Figure 3.6).

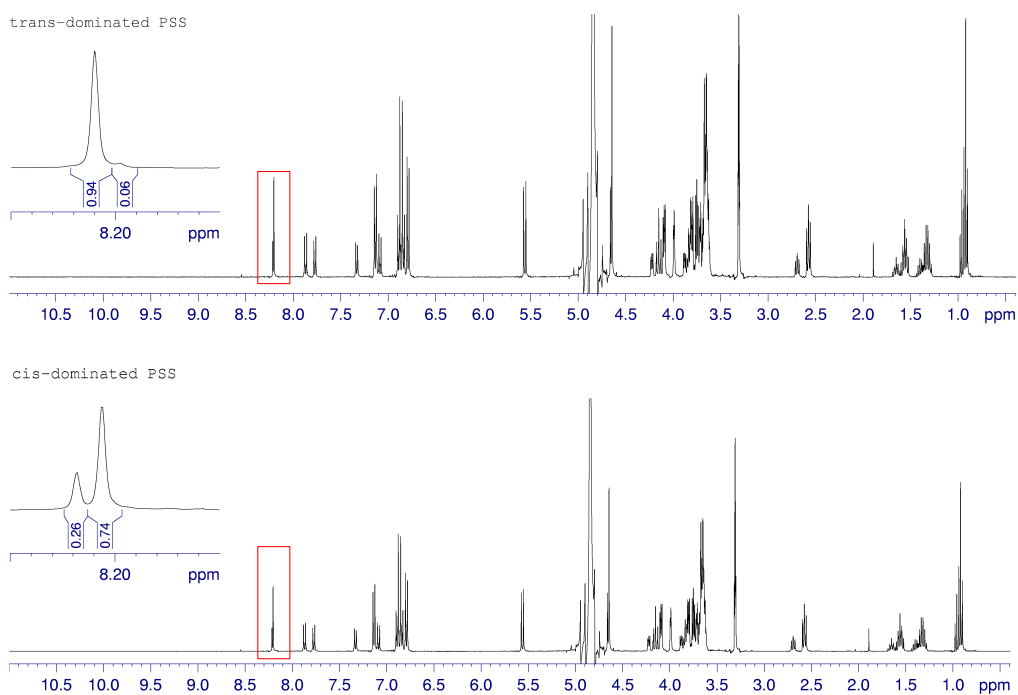


Figure 3.5. ^1H NMR spectra of GalTz **3.9** in the *trans*-dominated PSS (top), the *cis*-dominated PSS (bottom) and expanded spectrum of triazole proton (inserted).

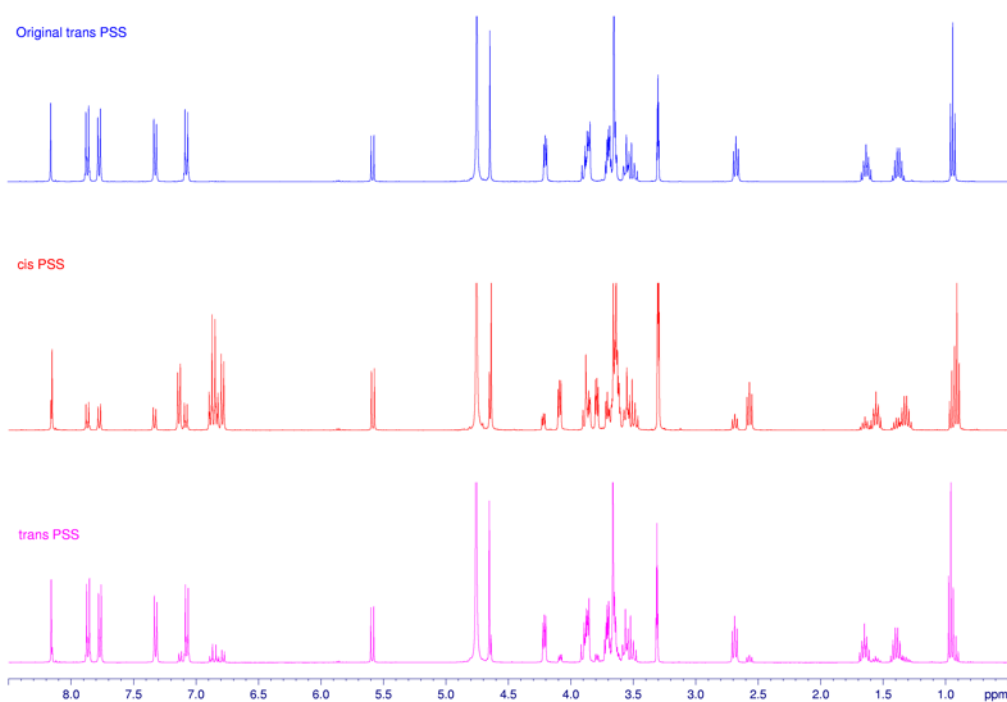


Figure 3.6. ^1H NMR spectrum of GlcTz **3.3** before UV photoirradiation (top), after UV photoirradiation (middle), and after visible (blue) light photoirradiation (bottom). Spectra were recorded in CD_3OD at 20 mM concentration.

3.2.3 Photocontrollable surface activity

The photocontrollable surface activity of surfactants was determined using pendant drop tensiometry. The critical micelle concentrations (CMCs) of the photocontrollable carbohydrate surfactants **3.3–3.13** were measured by the pendant drop method using a customized apparatus (Figure 3.7).⁴⁸ To effect *trans-cis* photoisomerization, each compound was irradiated at 361 nm for 15 min before measuring the CMC of the *cis*-isomer. The CMC is extrapolated at the intersection of two near-linear regions when the surface tension is plotted as a function of surfactant concentration. The CMC values before and after UV irradiation are summarized in Table 3.3. To summarize the CMC data, a column chart was plotted according to the data listed in Table 3.3 (Figure 3.8). The CMC values increased upon *trans-cis* photoisomerization, an effect which was attributed to the geometry change and increased polarity of the *cis*-isomers upon UV irradiation.⁴⁹ It was also notable that the CMC difference between *trans* isomer and the corresponding *cis* isomer varied widely, which was dependent on the carbohydrate head group configuration (Figure 3.8). A significant change in the CMC was observed for GlcNAcTz **3.7** following photoirradiation, while there was no similar difference between the *trans* (0.33 mM) and *cis* isomers (0.34 mM) for XylTz **3.4**. This result could be attributed to the overall hydration of the molecule that is influenced not only by the degree of hydration of the carbohydrate but also by the hydrophobicity change upon *trans-cis* photoisomerization. This observation further highlights the possibility to modulate the interfacial activity of this panel of surfactants by photoisomerization and head group configuration.

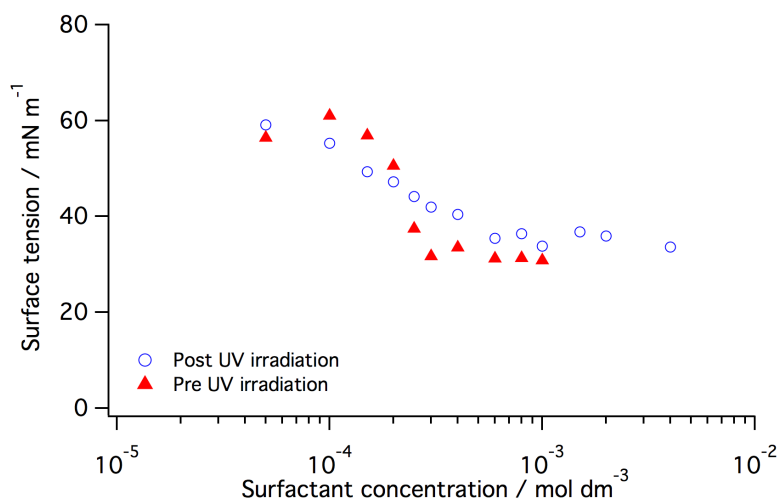


Figure 3.7. Air-water surface tension data for representative surfactant GlcTz **3.3**. Please see **Appendix II** for complete data.

Table 3.3. Photocontrollable CMCs of surfactants **3.3–3.13**.

Surfactants	CMC _{vis} /mM (μg/mL)	CMC _{UV} /mM (μg/mL)
GlcTz 3.3	0.31 (195)	0.59 (372)
XylTz 3.4	0.33 (197)	0.34(204)
RhaTz 3.5	0.11 (68)	0.42 (258)
ManTz 3.6	0.13 (82)	0.49 (309)
GlcNAcTz 3.7	0.11 (198)	1.22 (2195)
AraTz 3.8	0.33 (198)	0.88 (528)
GalTz 3.9	0.05 (31)	0.32 (202)
RibTz 3.10	0.65 (409)	1.06 (667)
FucTz 3.11	0.26 (160)	0.58 (356)
LacTz 3.12	0.25 (198)	0.33 (261)
CelTz 3.13	0.86 (681)	0.91 (721)

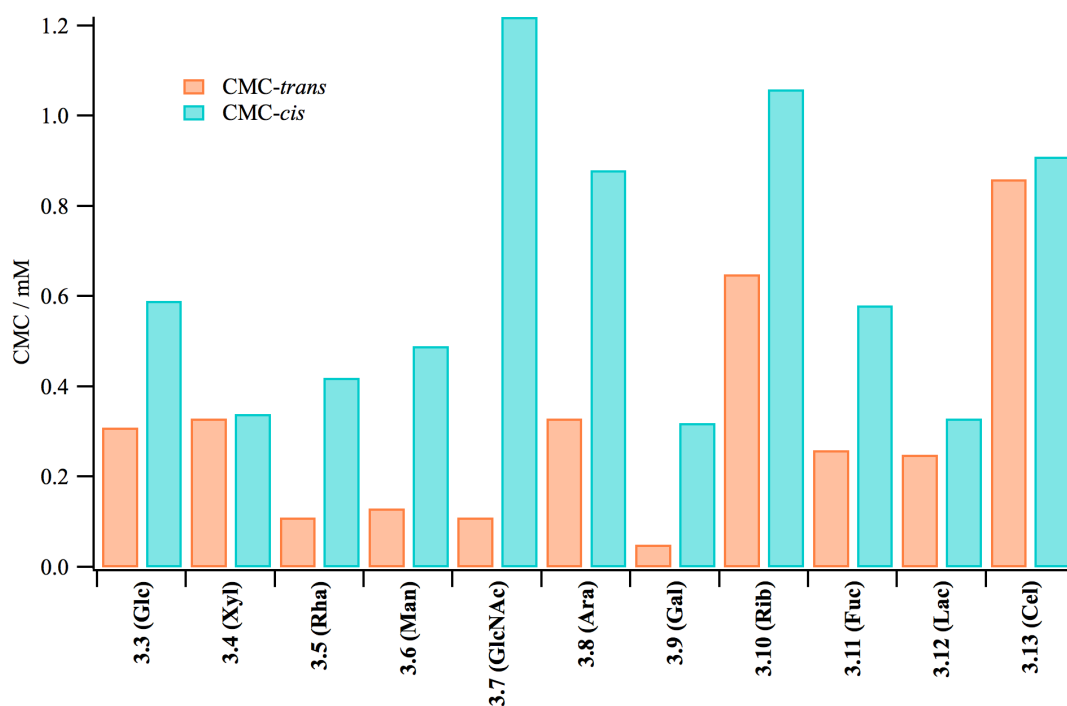


Figure 3.8. CMC data plot of surfactants 3.3–3.13.

3.2.4 Characterization of self-assemblies

A fundamental property of surfactants is their ability to aggregate into self-assembled structures of various types, including but not limited to spherical and rodlike micelles, as well as lamellar, vesicular and sponge-like liquid crystal phases.⁵⁰ In this respect, small-angle neutron scattering (SANS) has emerged as a unique and powerful technique to investigate the structural properties of self-assemblies in solution.^{51–53} Several studies have highlighted the application of SANS to study the micellization of azobenzene-based surfactants in solution.^{51, 54} For a micellar system, there are two basic quantities of interest: aggregation number (N_{agg}) and area per head group (A_{hg}).^{51, 55} Aggregation number is the mean number of surfactant monomers in one aggregate at a given solution condition. When surfactants start to self-assemble into aggregates, the hydrophobic tails will form a core, while the hydrophilic head groups will distribute themselves around the surface with an optimum surface area per monomer (head group). Both of the parameters can be derived from SANS measurements by generating model fits to an assumed geometry of an aggregate.⁵⁵

In order to investigate the self-assembling properties for our photosurfactants, SANS was performed at three different concentrations of each surfactant in the resting, *trans*-PSS: close to the CMC, slightly above the CMC, and well above the CMC in D₂O. The three concentrations used were selected based on their CMC values as measured by tensiometry. At a fixed concentration (4 mM) well above the CMC, various geometries of different sizes were achieved by simply changing the carbohydrate head group (Table 3.4 and Figure 3.9 a)). Model fits (see section 3.4.4 for details) to the experimental data showed that a wide range of morphologies were formed within this panel of surfactants, from relatively small ellipsoids, such as in surfactant **3.8** (Ara) and **3.12** (Lac), to extremely long and flexible cylinders, such as in surfactant **3.4** (Xyl), **3.10** (Rib) and **3.13** (Cel). In addition, the effects of concentration on aggregation number were also explored using representative surfactants **3.8** (Ara), **3.11** (Fuc) and **3.12** (Lac) (Figure 3.9 b) c) and d)). The aggregation number generally increased upon increasing surfactant concentration, indicating the formation of densely packed aggregates at high monomer concentration, which is in line with the general expectation for surfactant self-assembly.⁵⁶

Table 3.4. Aggregation properties of carbohydrate based surfactants **3.3–3.13***.

Surfactants	Morphology ^a	Radius a / nm	Radius b (Length) / nm	N _{agg} ^b	A _{hg} ^c / nm ²
GlcTz 3.3	C	2.83	59.1	1600	0.68
XylTz 3.4	FC	2.11	18.54 (kuhn length)	-	-
RhaTz 3.5	C	2.58	27.62	622	0.79
ManTz 3.6	E	2.28	6.03	141	0.84
GlcNAcTz 3.7	E	2.50	9.00	178	1.02
AraTz 3.8	E	1.99	4.77	89	1.12
GalTz 3.9	C	2.79	35.6	960	0.70
RibTz 3.10	FC	3.01	45.48 (kuhn length)	-	-
FucTz 3.11	E	2.12	5.25	109	1.07
LacTz 3.12	E	2.46	4.60	105	1.17
CelTz 3.13	FC	2.45	18.54 (kuhn length)	-	-

^a E=ellipsoid, C=cylindrical, FC=flexible cylindrical with a length >100 nm.

^b Aggregation number. ^c Area per head group.

* Surfactants were measured in the *trans*-PSS at 4 mM (above the CMC) in D₂O.

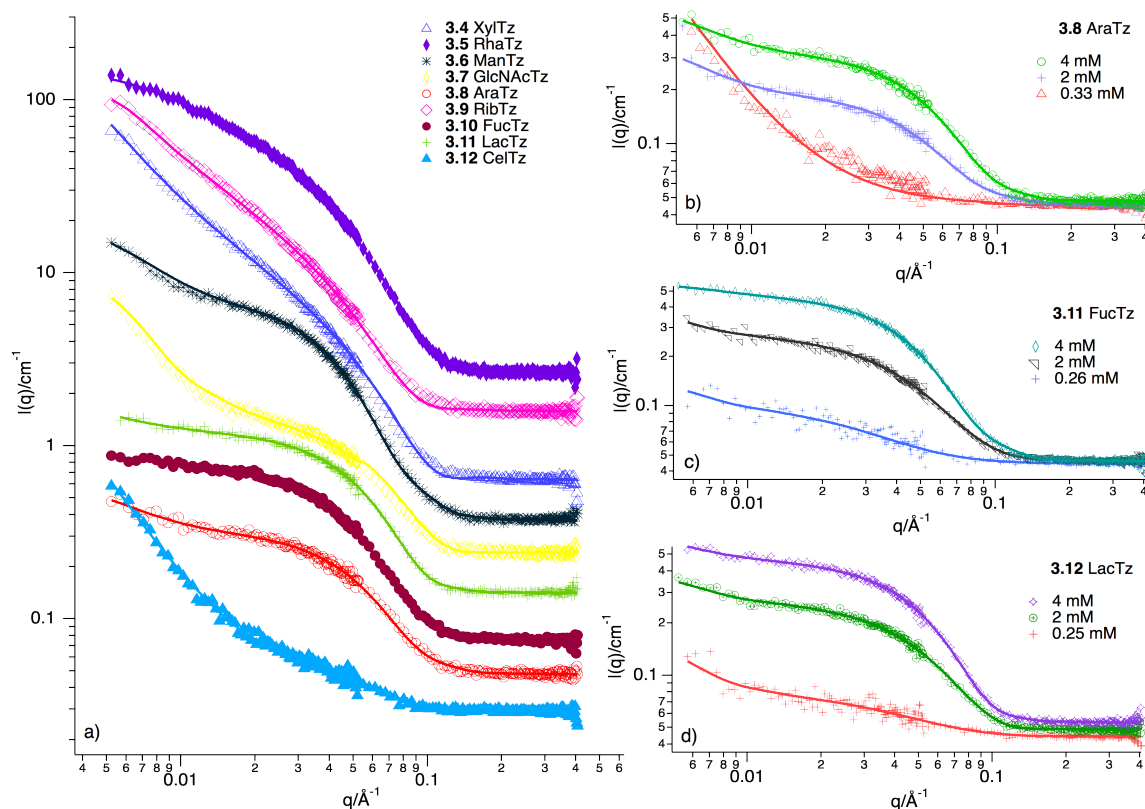


Figure 3.9. SANS experimental data (symbols) and model fits (solid lines) of a) **3.3–3.13** (*trans*-dominated state) in D₂O at 4 mM; b) AraTz **3.8** at different concentrations; c) FucTz **3.11** at different concentrations and d) LacTz **3.12** at different concentrations. In (a) only, data have been offset vertically by multiplication for clarity of presentation. The SANS spectra for GlcTz **3.3** and GalTz **3.9** have been reported previously.⁵¹

3.2.5 Photocontrollable antibacterial studies

In order to better understand the antibacterial activities of these surfactants, we introduced two photoswitchable, non-surface active fragments **2.25** lacking the carbohydrate head group, and the cationic photosurfactant **3.31**(AzoTAB) as control compounds (Figure 3.10). The photochemistry of compound **3.31** has been well studied, and it has the potential to be used in antibacterial studies as a cationic surfactant.^{57, 58} The photocontrollable antibacterial activity of control compounds **2.25** and **3.31** was evaluated against Gram-negative *E. coli* DH5 α , Gram-

negative *P. aeruginosa* and Gram-positive *S. aureus* using a standard minimum inhibitory concentration (MIC) test, and the results are summarized in Table 3.5.⁵⁹

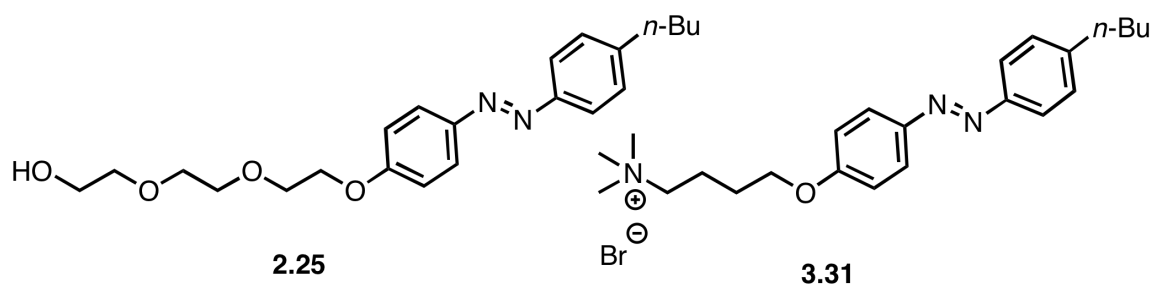


Figure 3.10. Photoswitchable control compounds **2.25** and **3.31** in this study.

Table 3.5. MIC results of *trans* and *cis* isomers of control compounds **2.25** and **3.31** against *E. coli* DH5 α , *P. aeruginosa* and *S. aureus* at 37°C.

		MIC $\mu\text{g/mL}$		
		<i>E. coli</i> DH5 α	<i>P. aeruginosa</i>	<i>S. aureus</i>
2.25	<i>trans</i>	>2000	>1000	125
	<i>cis</i>	>2000	>1000	31
3.31	<i>trans</i>	12.5	31.2	1.6
	<i>cis</i>	12.5	125	1.6

The MIC was determined as the lowest concentration of the compound at which the bacterial growth could not be seen by the naked eye, where a lower MIC value indicates stronger inhibitory potency. The MIC was obtained at both the *trans* and *cis* PSS for all compounds. The *cis*-isomers were obtained through irradiating a solution of the native *trans* state with UV light (361 nm) for 5 min before incubation with bacteria at 37°C for 24 h in dark. For compound **2.25**, no significant inhibition of *E. coli* (>2000 $\mu\text{g mL}^{-1}$) and *P. aeruginosa* (>1000 $\mu\text{g mL}^{-1}$) was observed in the *cis* and *trans* PSS. However, moderate inhibition against *S. aureus* was

observed for the *trans*-isomer ($125 \mu\text{g mL}^{-1}$) and this inhibitory potency was enhanced by photoisomerization to its *cis*-isomer ($31 \mu\text{g mL}^{-1}$). This enhanced antibacterial activity upon *trans*-to-*cis* photoisomerization was in line with a previous research on azobenzene-based quinolone antibiotics as described by the Feringa group.⁴⁰ For the cationic photosurfactant **3.31**, non-selective and potent bactericidal activity against *E. coli*, *P. aeruginosa* and *S. aureus* was observed. Furthermore, no photomodulation in bactericidal activity against *E. coli* and *S. aureus* was observed, however the *cis*-isomer of **3.31** was much less toxic against *P. aeruginosa* (MIC $125 \mu\text{g mL}^{-1}$) compared with the corresponding *trans*-isomer ($31.2 \mu\text{g mL}^{-1}$). The high antibacterial activity of **3.31** against *E. coli* and *S. aureus* is not surprising and was most likely due to cell wall damage and lysis,⁶⁰ while the reduced toxicity upon UV irradiation against *P. aeruginosa* could be attributed to the lowered interfacial activity of the *cis* isomer.⁵⁸

The antibacterial activities of surfactants **3.3–3.13** were tested against Gram-negative *E. coli* and Gram-positive *S. aureus* using an optical density method (OD_{600}) (Figure 3.11 and Figure 3.12). OD_{600} is a commonly used turbidometric assay for determining the concentration of bacterial cell cultures based on spectrophotometer readings at a wavelength of 600 nm.⁶¹ The concentration-dependent influence on bacterial growth could be determined by incubation of the bacterial suspension with different concentrations of surfactants (0, 1, 10, 25, 50, 100, 250 and $500 \mu\text{g mL}^{-1}$) at 37°C in the dark for 24 h, so that the concentration-dependent influence on bacterial growth could be determined (Figure 3.11, Figure 3.12). From this assay, dose-dependent and bacteria-specific antibacterial activity was observed for the carbohydrate-based surfactants against *E. coli* and *S. aureus*. At low concentration of surfactants (below the CMC) the antibacterial activity increased sharply in a dose-dependent manner against *E. coli* and *S. aureus*, regardless of the photostationary state. However, at higher concentrations of surfactants near to, and above the CMC, the antibacterial activity could be modulated through photoisomerization of the tail group, as shown in Figure 3.11 and Figure 3.12. In the case of *E. coli*, the photoexcited *cis*-isomers of surfactants RhaTz **3.5** and GlcNAcTz **3.7** were more toxic, while for the other surfactants, their native *trans*-isomers were more toxic against this bacterium. In the case of *S. aureus*, these surfactants typically showed enhanced antibacterial activity after

photoisomerization, with the exception of GlcNAcTz **3.7**, which was more toxic in its *trans* form. It is difficult to rationalize the heterogeneous responses in bacterial activity of **3.3–3.13**, but generally points to the structural and physiological differences of these Gram-positive and Gram-negative bacterial species. It is interesting to note that surfactant **3.5** and **3.7** incorporating L-rhamnose and D-glucosamine head groups, respectively, and the significance of these carbohydrates in bacterial evolution could be attributed to their selective mode of action against these bacteria. For example, L-rhamnose-based glycolipids expressed by some Gram negative bacteria, in particular *P. aeruginosa*, and play important roles in the regulation of bacterial motility sensing, thus are important endogenous agents in adhesion and biofilm formation.⁶²⁻⁶⁴ Likewise, *N*-acetylglycosamine is a major component of the extracellular polysaccharide matrix of *S. aureus* biofilms and the cell wall, which is implicated in the virulence and biofilm formation of this species.^{65, 66}

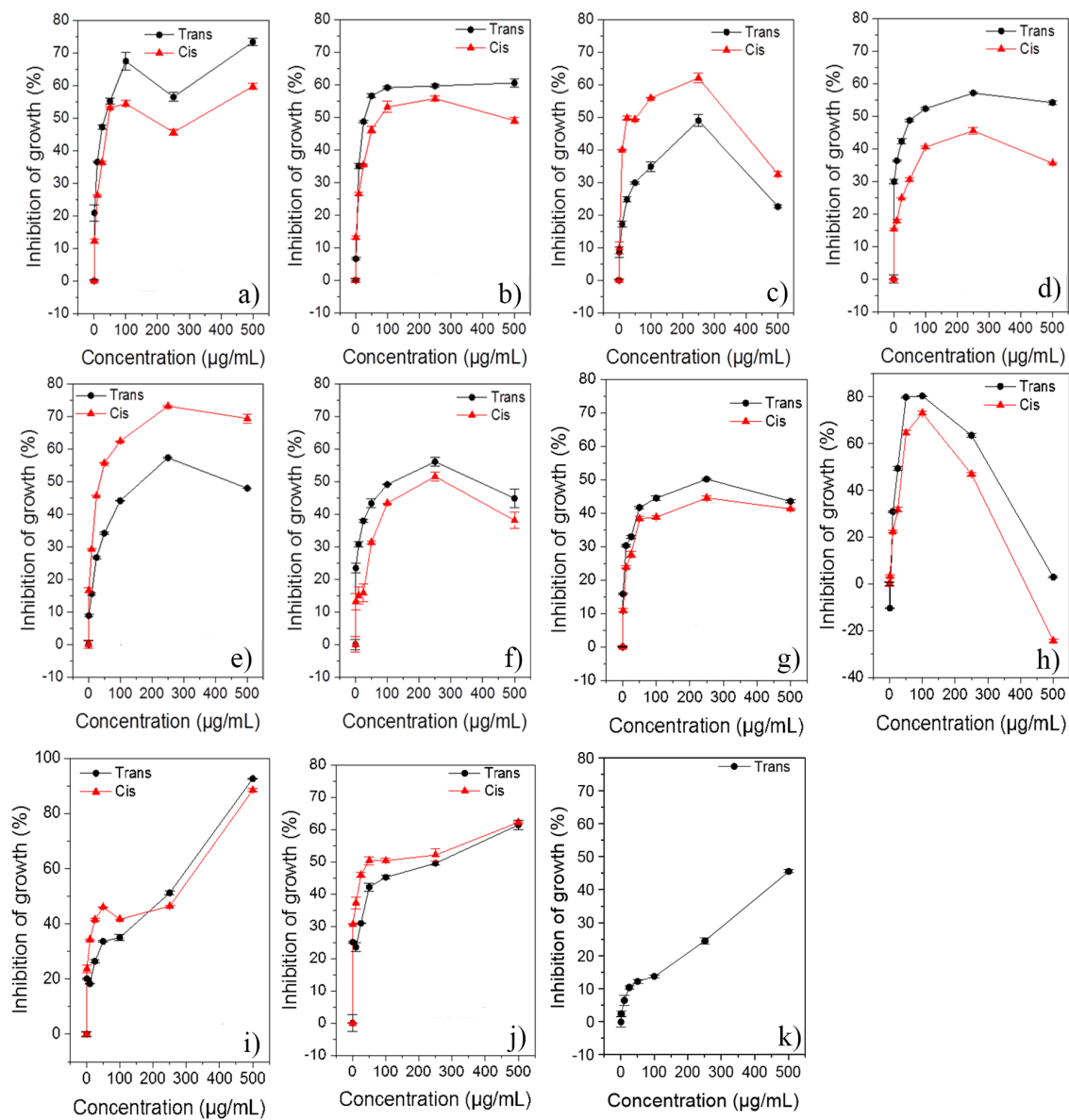


Figure 3.11. Normalized bacterial cell viability with a) GlcTz 3.3, b) XylTz 3.4, c) RhaTz 3.5, d) ManTz 3.6, e) GlcNAcTz 3.7, f) AraTz 3.8, g) GalTz 3.9, h) RibTz 3.10, i) FucTz 3.11, j) LacTz 3.12 and k) CelTz 3.13 against *E. coli* DH5 α after 24 h.

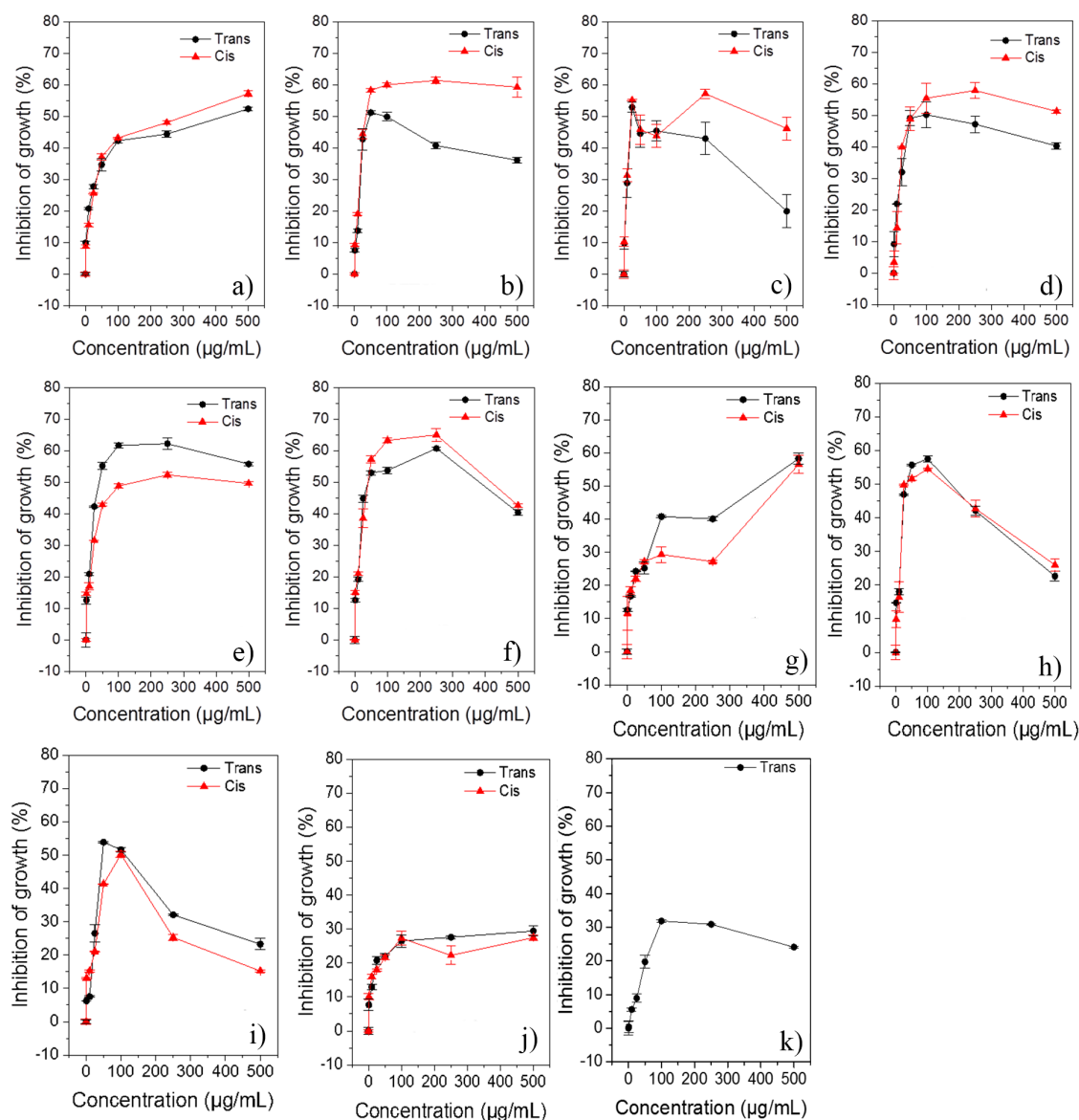


Figure 3.12. Normalized bacterial cell viability with a) GlcTz **3.3**, b) XylTz **3.4**, c) RhaTz **3.5**, d) ManTz **3.6**, e) GlcNAcTz **3.7**, f) AraTz **3.8**, g) GalTz **3.9**, h) RibTz **3.10**, i) FucTz **3.11**, j) LacTz **3.12** and k) CelTz **3.13** against *S. aureus* ATCC1698 after 24 h.

It can be seen from Figure 3.11 and Figure 3.12 that some of the surfactants showed more interesting and promising antibacterial activities than others. Surfactants RhaTz **3.5**, ManTz **3.6** and GlcNAcTz **3.7** exhibited a moderate-to-potent inhibition of growth of *E. coli* and *S. aureus*, while surfactant GlcTz **3.3**, XylTz **3.4** and AraTz **3.8** all displayed bacteria-specific inhibition of bacterial growth. Therefore, we selected these 6 surfactants (**3.3–3.8**) as representatives to

further explore their antibacterial and biofilm modulatory activities. Surfactants were assessed for activity against a multi-drug resistant strain of *P. aeruginosa* MDR283/1-6 in addition to *E. coli* and *S. aureus*. The *cis*-isomers were obtained by irradiating the native *trans*-dominated solutions with UV light for 5 min, before incubating with *P. aeruginosa* in dark conditions at 37°C for 24 h. The OD₆₀₀ method was used to test the antibacterial activity, and the data were background corrected by subtracting the OD₆₀₀ value obtained from the control (Figure 3.13). Interestingly, none of the representative surfactants showed significant toxicity against this strain of *P. aeruginosa*, instead generally promoting its growth. This was with the exception of AraTz **3.8**, which exhibited dose-dependent inhibition of bacterial growth. The growth-promoting activity of these compounds could be photocontrolled, and the *cis*-isomers demonstrated a stronger promotion of growth compared with the corresponding *trans*-isomers. This observation further highlights the dose-dependent, bacteria- and photoisomer-specific antibacterial activities of these surfactants.

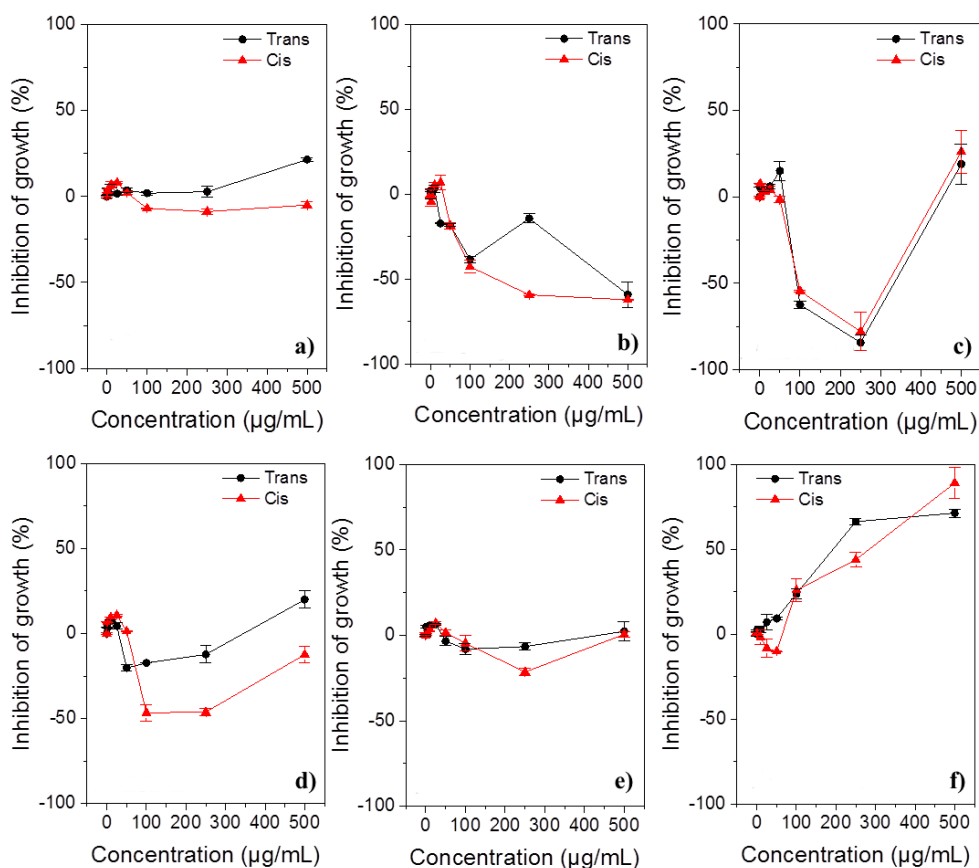


Figure 3.13. Concentration-dependent antibacterial testing of *trans*- and *cis*-isomers of a) GlcTz 3.3 b) XylTz 3.4, c) RhaTz 3.5, d) ManTz 3.6, e) GlcNAcTz 3.7 and f) AraTz 3.8 against *P. aeruginosa* at 37°C in nutrient broth after 24 h incubation in dark conditions.

3.2.6 Photocontrollable biofilm studies

Numerous efforts have been made to understand biofilm formation, however, the influence of different photoisomers of carbohydrate surfactants has not yet been investigated. We reasoned that these surfactants could be used as tools for probing the relationship between the interfacial activity of amphiphilic carbohydrates and bacterial adhesion that is deemed an important early step in biofilm formation. To this end, six representative surfactants that were selected owing to their interesting antibacterial profiles, together with control compounds 2.25 and 3.31, which were screened for their influence on the biofilm forming ability of a Gram-positive methicillin-resistant *S. aureus* (MRSA-ATCC1698) and a multi-drug resistant clinical isolate of Gram-

negative *P. aeruginosa* (MDR283/1-6). Both of these bacteria are known to cause serious biofilm-associated infections.^{3, 67}

The biofilm inhibition activity of these surfactants was determined by a microtiter dish method, which allowed the formation of a biofilm on the wall and/or bottom of a microtiter dish, and the crystal violet-treated bacterial biofilms were monitored at OD₅₅₀.⁶⁸ Consistent with the antibacterial studies above, the *trans*- and *cis*-isomers showed similar effects on both *S. aureus* (Figure 3.14) and *P. aeruginosa* (Figure 3.15) biofilms at low concentration, while the influence of photoisomerization on biofilm formation became more evident at higher concentrations.

Similar to the antibacterial data, surfactants exhibited concentration-dependent inhibition of biofilm formation from *S. aureus*, while generally promoting the growth of biofilm *P. aeruginosa*, especially at higher concentrations. In the case of *P. aeruginosa*, surfactants were shown to weakly inhibit biofilm growth at lower concentrations, while promoting growth at higher concentrations. This biofilm modulatory activity could be tuned by *trans-cis* photoisomerization of the tail group, whereby the promotion became more efficient after photoexcitation, with the exception of AraTz **3.8**, which was a slightly more effective promoter of biofilm formation of *P. aeruginosa* in the *trans*-PSS. In the case of *S. aureus*, the *trans*-isomer of surfactants **3.3**, **3.5** and **3.8** showed stronger inhibition of biofilm formation, while the UV excited *cis*-isomers of surfactants **3.4**, **3.6** and **3.7** were more potent biofilm inhibitors. Similar to the antibacterial results, surfactant **3.5** incorporating an L-rhamnose head group showed an interesting trend, whereby at lower concentrations in the *trans* state was found to inhibit biofilm formation of *S. aureus* regardless of its isomeric state, however the *cis* isomer started to promote biofilm formation at higher concentrations. Interestingly, while surfactant **3.7** possessing a GlcNAc head group inhibited growth from *S. aureus* in the *trans* state (Figure 3.12 e)), the corresponding *cis* isomer was an effective inhibitor of biofilm formation from this species, thus suggesting a mechanism that was independent of cell death.⁶⁹

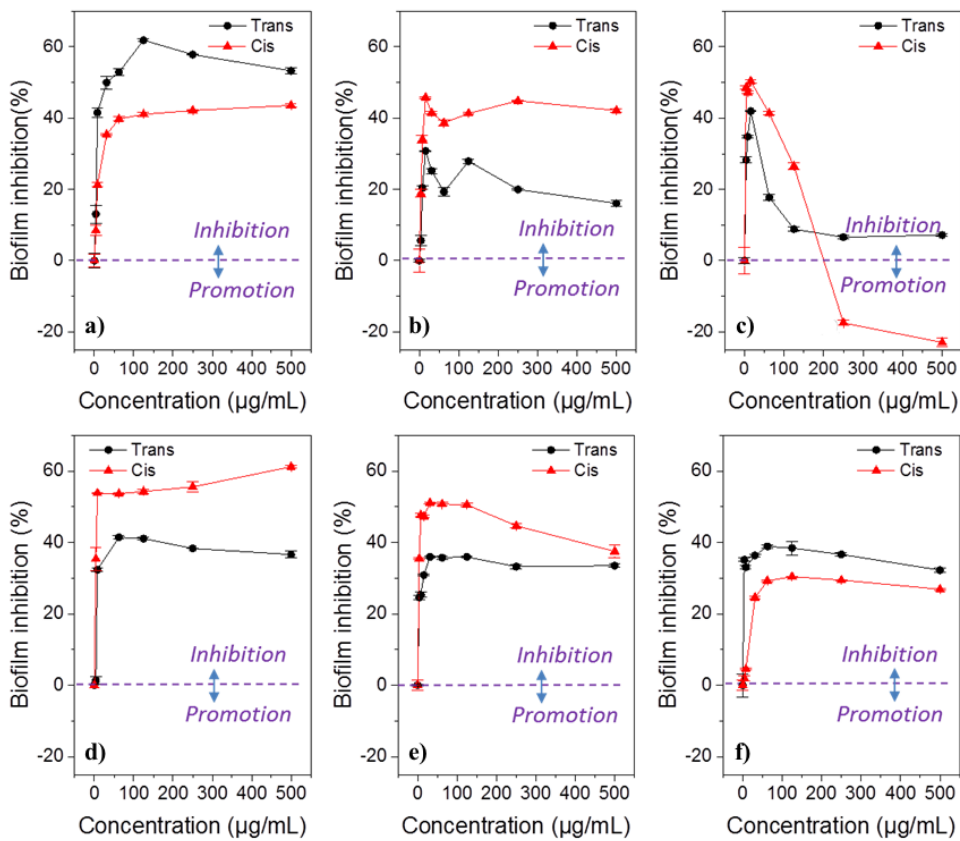


Figure 3.14. Concentration-dependent influence of *trans*- and *cis*-isomers of a) GlcTz 3.3, b) XylTz 3.4, c) RhaTz 3.5, d) ManTz 3.6, e) GlcNAcTz 3.7 and f) AraTz 3.8 on biofilm forming of *S. aureus* at 37°C after 24 h.

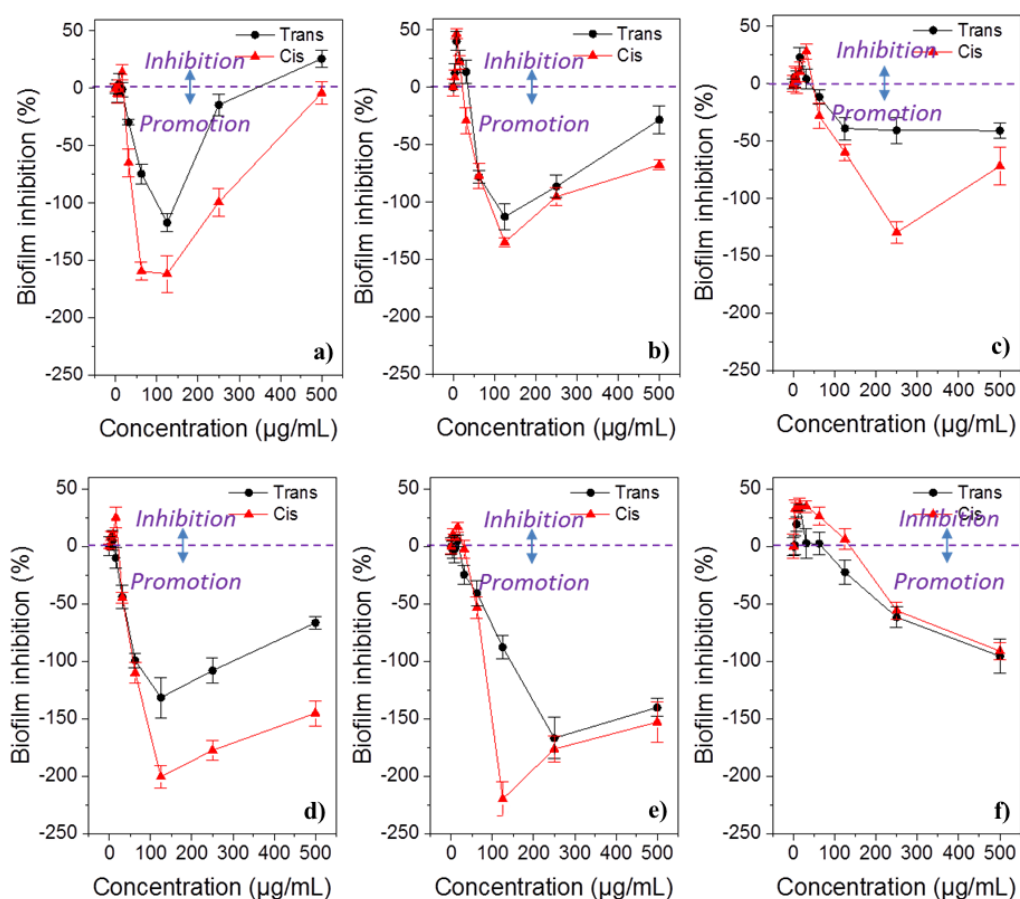


Figure 3.15. Concentration-dependent influence of *trans* and *cis* photoisomers of a) GlcTz 3.3, b) XylTz 3.4, c) RhaTz 3.5, d) ManTz 3.6, e) GlcNAcTz 3.7 and f) AraTz 3.8 on biofilm forming ability of *P. aeruginosa* at 37°C after 24 h of incubation.

3.2.7 Bacterial motility studies

Many bacteria exhibit motility that can assist surface colonization, biofilm formation, fruiting body development, *etc.*⁹ In order to understand the intriguing biofilm modulatory activity of these surfactants, we evaluated whether these surfactants could affect bacterial motility in solution (swimming motility) and swarming motility on semi-solid surfaces (Wako Agar) through photocontrollable changes in surface tension.

In order to characterize the effect of different surfactants on bacterial swimming motility, differential dynamic microscopy (DDM) was performed. DDM is a recently described technique that couples dynamic light scattering and optical microscopy for measuring the rates

of motility of particles in solution, including cells.^{70, 71} In particular, this technique shows particular promise for determining flagellar-dependent bacterial motility in solution; both the dynamics and rates of swimming motility could be measured through DDM.^{70, 71} *P. aeruginosa* MDR283/1-6 was chosen for the motility experiments since the swimming rates for this bacterium are sufficient on the timescale required for DDM measurements. Two representative surfactants RhaTz 3.5 and ManTz 3.6, together with the control, were selected for swimming motility testing against *P. aeruginosa* in both the *trans*- and *cis*-dominated states (Figure 3.16). Using this technique, no obvious effects on the swimming motility of *P. aeruginosa* using these photosurfactants was observed. Therefore, these surfactants were unlikely to be modulating biofilm formation through changes in bacterial swimming motility.

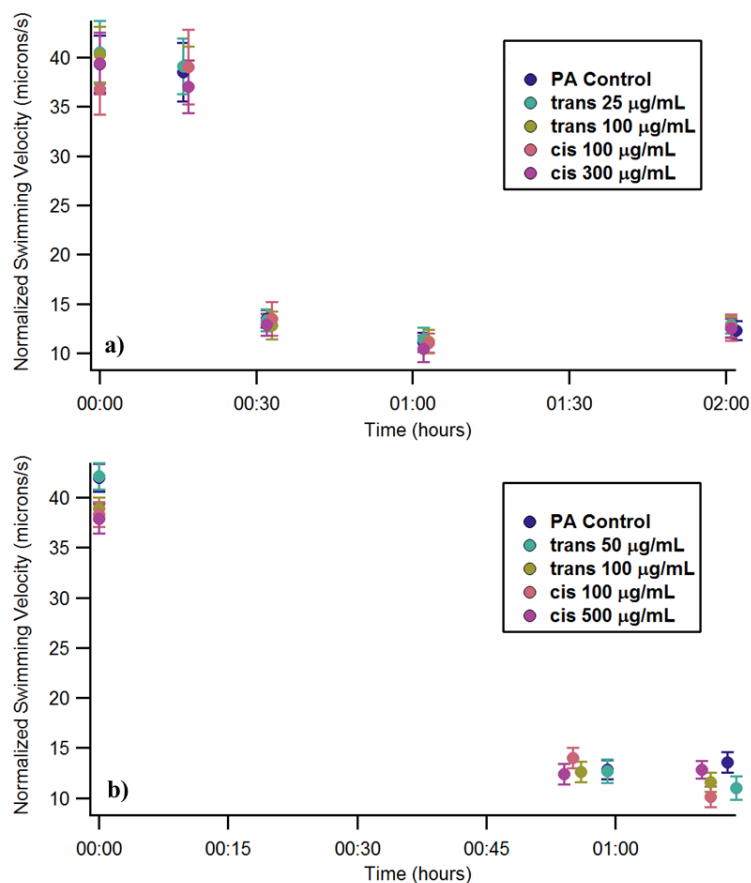


Figure 3.16. Influence of *trans*- and *cis*-isomer of a) RhaTz 3.5 and b) ManTz 3.6 on swimming motility of *P. aeruginosa* MDR283/1-6.

Swarming, as the fastest known bacterial mode of surface translocation, is documented to have a clear affect the formation of biofilms.⁷² Therefore, the surfactants **3.3–3.8** and two control compounds (**2.25** and **3.31**) were tested for their influence on swarming motility of flaggella-dependent *P. aeruginosa* before (*trans*) and after (*cis*) photoswitching. An agar swarming motility assay (Wako Agar, 0.8% nutrient broth, 0.5% glucose and 0.5% agar) was used to assess the swarming motility of *P. aeruginosa* and the swarm plate was air dried for 5–10 min before use. Cells were inoculated at the center of the agar media containing the compound being tested, and the bacteria started to move out of the center towards the perimeter. A larger resultant bacterial colony indicated more effective swarming motility.

After incubation at 30°C for 22 h, a dose-dependent enhancement in swarming motility of *P. aeruginosa* MDR283/1-6 was observed for all surfactants in their native *trans* form. This response was independent of the head group of the surfactants, as all surfactants showed a similar effects in promoting swarming motility in this strain (Figure 3.17). Whilst carbohydrate-based surfactants generally promoted swarming motility, control compounds **2.25** and **3.31** strongly inhibited swarming motility (Figure 3.17 g and h). The potent inhibition shown by **3.31** could be attributed to, at least in part, the potent bactericidal activity of this surfactant. However, the inhibition of swarming motility using the non-surface active compound **2.25** is interesting and more difficult to explain given the weak bactericidal activity of this compound against *P. aeruginosa*, and may ultimately suggest a mechanism that is independent of cell death and/or reduction in surface tension. The effect of tail group photoisomerization on bacterial motility was also evaluated and generally showed a reduction in motility following conversion to the *cis*-PSS. This was particularly noteworthy for XylTz **3.4**, which exerted a significant difference in swarming motility between the *trans* and *cis* forms (Figure 3.18 b). This observation could be attributed to the lowered interfacial activity of the *cis* isomer than its *trans* isomer. Unlike the carbohydrate-based surfactants, *trans-cis* photoisomerization of the tail fragment **2.25** and the cationic compound **3.31** had no significant influence on the swarming motility of *P. aeruginosa*, possibly due to the bactericidal activity of these compounds

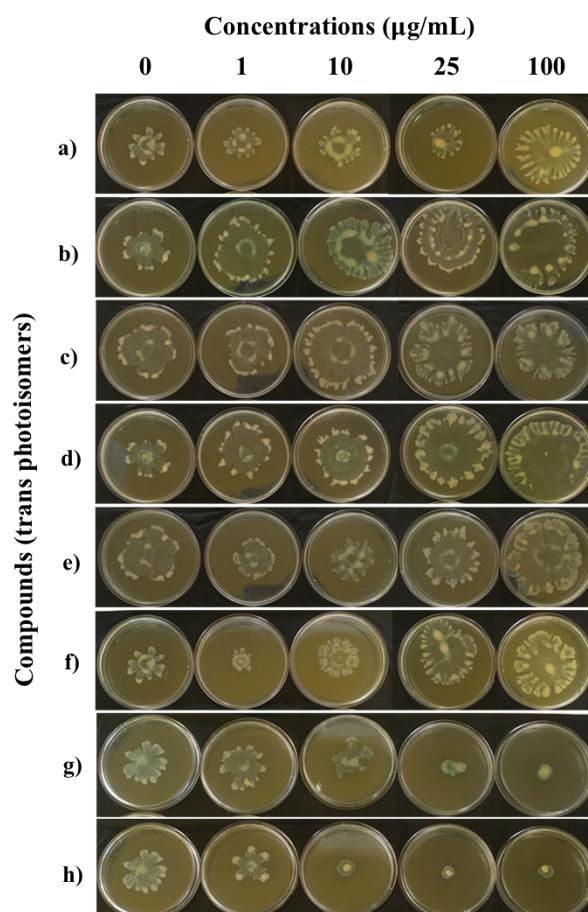


Figure 3.17. Photograph of agar swarming motility assay demonstrating the influence of the increasing concentration of *trans*-isomer of a) GlcTz **3.3**, b) XylTz **3.4**, c) RhaTz **3.5**, d) ManTz **3.6**, e) GlcNAcTz **3.7**, f) AraTz **3.8**, g) **2.26** and h) **3.31** on swarming motility of *P. aeruginosa* MDR283/1-6 (swarming-positive strain).

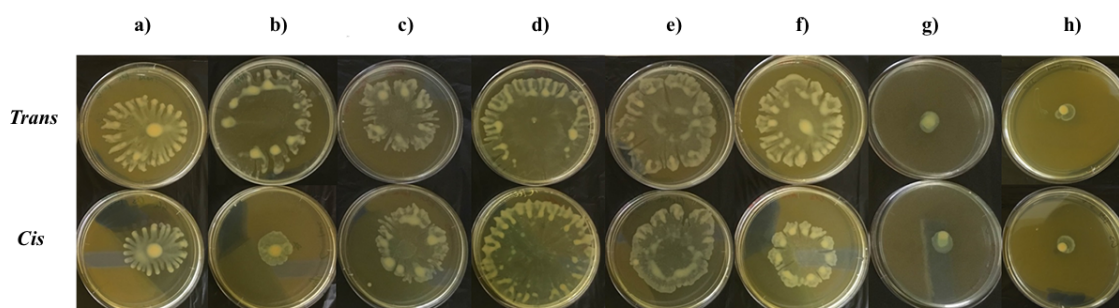


Figure 3.18. Photograph of agar swarming motility assay demonstrating the influence of a) GlcTz **3.3**, b) XylTz **3.4**, c) RhaTz **3.5**, d) ManTz **3.6**, e) GlcNAcTz **3.7**, f) AraTz **3.8**, g) **2.26** and h) **3.31** at $100 \mu\text{g mL}^{-1}$ concentration in the *trans* and *cis* form on the swarming motility of *P. aeruginosa* MDR283/1-6 (swarming-positive stain).

To gain a better understanding of the influence of the changes in interfacial activity of surfactants on the surface-mediated motility of *P. aeruginosa*, we also investigated the influence of surfactants on the gliding motility of *P. aeruginosa* MDR283/1-23, a swarming-negative and non-motile strain. Controls containing no surfactant were employed in this study, and no motility was observed for the control (Figure 3.19). Interestingly, strong promotion of gliding motility of *P. aeruginosa* MDR283/1-23 was detected with surfactants **3.5–3.7** in both *trans* and *cis* PSS, which was occurring most like by surfactant-mediated sliding.¹⁰ Similar to the swarming positive *P. aeruginosa* stain, the *trans* isomers of surfactants **3.5–3.7** were more effective at translocating bacterial colonies than the less surface-active *cis* isomer, especially for surfactant **3.7**, which shows the largest CMC difference before and after *trans-cis* photoisomerization. These observations show the application of UV light for tuning the surface-mediated motility of *P. aeruginosa*, and this observation can be attributed to the changes in the interfacial activity of surfactants following UV light irradiation.

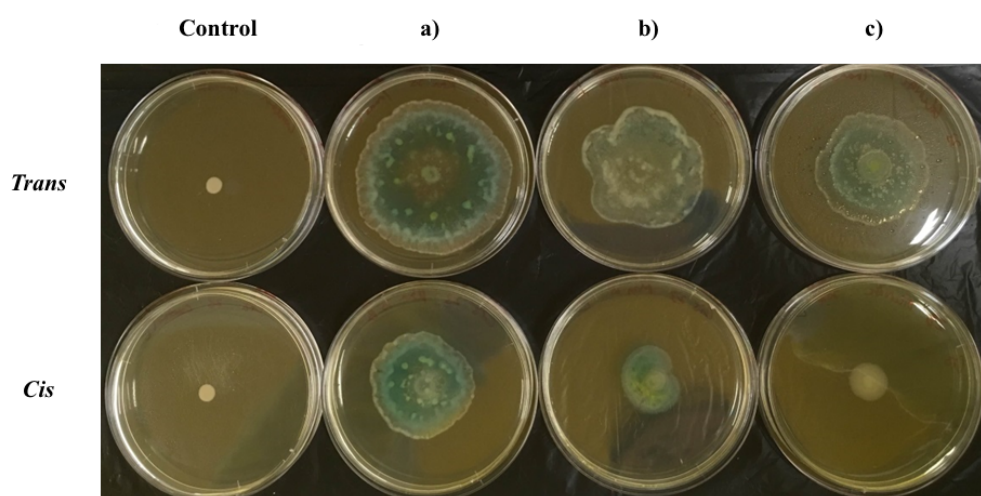


Figure 3.19. Photograph of agar swarming motility assay demonstrating the influence of a) RhaTz **3.5**, b) ManTz **3.6** and c) GlcNAcTz **3.7** at $25 \mu\text{g mL}^{-1}$ concentration in the *trans* and *cis* form on swarming motility of *P. aeruginosa* MDR283/1-23 (swarming-negative strain). An equal amount of deionized water without any compound was added to the agar media to serve as a control.

3.3 Conclusions

In this chapter, we have synthesized a library of eleven photoswitchable carbohydrate-based surfactants as potential inhibitors of bacterial growth and biofilm formation. Through structural variation of the head group and photoisomerization of the *n*-butyl azobenzene tail group, diverse interfacial activities and micellar geometries were observed as determined by surface tension measurements and SANS, respectively. The ability of these surfactants to modulate antibacterial activity against drug-resistant Gram-positive and Gram-negative bacterial strains was also investigated. In general, these surfactants elicited dose-dependent, bacteria- and photoisomer-specific inhibition of the growth of *E. coli* and *S. aureus*, while they generally promoted the growth of *P. aeruginosa*. Using these photosurfactants we also demonstrated the ability to control biofilm formation of drug-resistant *S. aureus* and *P. aeruginosa*. Generally, surfactants inhibited the biofilm formation of *S. aureus*, whereas biofilm formation was promoted in the case of *P. aeruginosa*, particularly in the *cis* isomeric state. To explore the possible mechanism of this bioactivity, the influence of surfactants in the *trans*- and *cis*-PSS on the swarming and swimming motility of *P. aeruginosa* was investigated. The rate of bacterial ‘swimming’ remained unaffected in the presence of these surfactants as determined by DDM studies, regardless of the photoisomeric states. However, these surfactants generally promoted the swarming and gliding motility of *P. aeruginosa* with more potent activity elicited from *trans* configured compounds. The results suggest that the surfactants exert their effects in a largely non-selective manner through photocontrollable changes in surface tension. Future work aims to determine the precise molecular mechanisms involved, particularly for compounds that display unusual and selective activity, as well as to investigate the effect of the *trans* and *cis* forms of these surfactants on the structure and function of mature biofilms, and the ability to promote (or inhibit) biofilm detachment from a surface.

3.4 Experimental

3.4.1 General

For general materials and methods concerning reagents, purification and analysis, please refer to section 2.4.1.

3.4.2 UV-vis stability studies on *trans* and *cis* isomers

The native *trans*-dominated carbohydrate surfactant solutions were converted into their *cis*-dominated photostationary states by illumination of their aqueous solutions under ambient temperature conditions using a UV lamp with λ_{max} at 361 nm (approx. 12 W incident illumination power) in a time-dependent manner (1–90 min). One minute of photoexcitation was found sufficient to convert the *trans*- to *cis*-dominated state. In all of the studies involving bacteria, the *cis* isomers were obtained after 5 min of illumination with $\lambda_{361\text{nm}}$. The thermal relaxation of the *cis*-isomers of surfactants **3.3–3.13** in Milli-Q water at ambient temperature were estimated by plotting the UV-vis absorbance at 325 nm versus time over 24 h period. Please refer to section 2.4.3 for experimental and calculation details.

The thermal relaxation studies of surfactants **3.3–3.8** were performed by Wenyue Zou, at 37°C for 24 h in deionized water as well as in the growth media employed for the antibacterial studies against *E. coli* (NB) and *S. aureus* (BHI). The half-lives of the *cis* isomers in water and two bacterial media were estimated from thermal relaxation studies by plotting the ratios of area of the 350 nm peak and that of the 440 nm peak over a period of 24 h. These peaks were chosen as *cis–trans* relaxation results in an increase in peak intensity at ~350 nm, with a corresponding decrease in peak intensity at 440 nm.

3.4.3 Surface tension measurements

For the general method used, please refer to section 2.4.2

3.4.4 Small angle neutron scattering (SANS)

SANS measurements were made on the Quokka instrument at the Bragg Institute, ANSTO, Lucas Heights NSW, Australia. For all samples, raw scattering counts were collected on a 128×128 element area detector, where the sample–detector distances used were 2 m and 14 m, with no detector offset. An incident neutron wavelength of 5 Å was used with a typical spread of 10%, thus giving an effective q range of 0.004–0.4 Å⁻¹. Since the SANS is obtained over a limited low- q range, structures at micrometer size ranges (such as long rods or worms) cannot be resolved. Typically information on features is obtained at scattering vectors $q=2\pi/d$ where d is the characteristic size (*e.g.* radius, length, contour length) associated with the feature. This indicates that the minimum q value obtained with these measurements accesses length-scales up to ~150 nm, and features larger than this will not be resolved. Samples were prepared in circular 12.5 mm Hellma quartz cells with a path length of 2 mm, and a thermostatically-controlled automatic sample changer ensured that a temperature of 25 ± 0.05°C was maintained. Data were converted from raw counts at the detector into 1D scattering spectra by first subtracting the scattering from an empty cell and then radially averaging the resulting spectrum, normalizing for the measured sample transmission. A D₂O background was then subtracted from the final 1D sample data to ensure that the scattering signals seen are from the surfactant only. Model fitting was performed using SasView software, using standard equations for ellipsoidal and cylindrical form factors, from which the fitting parameters, such as radius and length, could be obtained. Model fits were made by using a least squares routine employing Levenberg-Marquardt optimisation to iterate floating parameters to convergent values, where user input was used to ensure physically reasonable values resulted. Cylinders were modelled using the Guinier equation⁷³ for the form factor $P(q,a)$:

$$P(q, a) = 2(\Delta\rho)V\sin(qL \cos\alpha/2)/(qL \cos\alpha/2) \frac{J_1(qr \sin\alpha)}{(qr \sin\alpha)}$$

where $\Delta\rho$ is the scattering length density difference between the scatterer and the D₂O solvent, V is the volume of the cylinder, L is the length of the cylinder, α is the angle between the axis of the cylinder and the q -vector, J_1 is the first order Bessel function, r is the radius of the cylinder.

For ellipsoids, the following form factor $P(q,a)$ was used⁷⁴:

$$P(q, \alpha) = \frac{3(\Delta\rho)V(\sin[qr(R_a, R_b, \alpha)] - qr \cos [qr(R_a, R_b, \alpha)])}{[qr(R_a, R_b, \alpha)]^3}$$

and

$$r(R_a, R_b, \alpha) = [R_b^2 \sin^2 \alpha + R_a^2 \cos^2 \alpha]^{1/2}$$

where R_a is the radius along the rotational axis of the ellipsoid, R_b is the radius perpendicular to the rotational axis of the ellipsoid, and other parameters are as defined for cylinders above.

Aggregation number (N_{agg}) was calculated from the volume of the formed micelle divided by the volume of a single surfactant that was obtained by calculating the molecular volume of the structural components of the surfactant from their bulk densities. The volumes (\AA^3) used were: triazole 96.2, triethylglycol 221.9, azobenzene 251.5, *n*-butyl 166.7, glucose 194.2, galactose 173.8, arabinose 157.3, lactose 372.7, mannose 194.4, rhamnose 193.3, ribose 148.3, xylose 163.5, cellobiose 321.5, fucose 175.2, *N*-acetylglucosamine 258.1. The area per head group (A_{hg}) was calculated from the surface area of the formed micelle divided by the corresponding aggregation number.

3.4.5 Antibacterial assays

The antibacterial activity of these surfactants was tested against Gram-negative *E. coli* and Gram-positive *S. aureus* using the OD₆₀₀ method.³ A fixed concentration (OD₆₀₀ – 0.1: log phase 10^8 CFU mL⁻¹) of freshly grown bacterial cultures were used for the antibacterial assay, after determining the bacterial concentration using a GENESYS 10S UV-Vis Spectrophotometer. A 100 μ L aliquot of the bacterial suspension (*E. coli* in NB and *S. aureus* in BHI broth) was incubated with 100 μ L of each surfactant at 37°C in dark for 24 h. Different concentrations of the surfactant (0, 1, 10, 25, 50, 100, 250 μ g mL⁻¹) were used to determine the concentration-dependent influence on bacterial growth and/or inhibition. Appropriate controls were chosen wherein one of the controls contained no surfactant while the other contained a mixture of different concentrations of surfactants with the bacteria-free growth media. The bacterial growth curves were monitored at OD₆₀₀ after 24 h in 96-well format using a Perkin Elmer EnVision™ 2104 Multilabel Plate Reader. All antibacterial assays were performed in triplicates; tests were repeated independently three times; each well was read five times. The

average of 45 readings (3×3×5) in each case was calculated and plotted along with the corresponding standard deviation. The data was background corrected by subtracting the OD₆₀₀ value obtained from the control containing a mixture of surfactants and the bacteria-free media growth from all other samples.

3.4.6 Minimum inhibitory concentration (MIC) test

The antibacterial activities of photoswitchable surfactant **3.31** and the non-amphiphilic tail fragment **2.25** were tested against Gram-negative *E. coli* and Gram-positive *S. aureus* using a standard MIC test.⁴ A fixed concentration of **3.31** or **2.25** containing Mueller-Hinton broth was dispensed in volumes of 100 µL per well in round bottom 96-well microdilution plates. Inocula were prepared by suspending *E. coli* grown on NA plate or *S. aureus* grown on BHI agar plate for 18 h in saline (0.85% w/v NaCl in water) to match the turbidity of a 0.5 McFarland standard. This suspension was further diluted to provide a final inoculum density of 5×10^5 CFU mL⁻¹ in the wells of the 96-well plates. Appropriate controls were chosen wherein one of the controls contained only bacteria without surfactants (positive control) while the other contained only media without surfactants or bacteria (negative control). After incubation at 37°C for 24 h in dark, plates were studied for visual turbidity, and MIC was defined as the lowest concentration at which bacterial growth (turbidity) could not be visibly observed by the naked eye. All MIC tests were performed in triplicates and repeated independently three times.

3.4.7 Biofilm assays

The photoswitchable surfactants were screened for their influence on biofilm forming ability of a Gram-positive methicillin-resistant *S. aureus* and a multi-drug resistant Gram-negative *P. aeruginosa*. The amount of biofilm formation in 96-well plates was determined by a microtiter dish method which allows for the formation of a biofilm on the wall and/or bottom of a microtiter dish.⁵ A fixed concentration of overnight grown bacterial cultures were used for biofilm assays after 1:100 dilution of the overnight-grown bacteria culture in a fresh broth (BHI broth for *S. aureus* and TSB for *P. aeruginosa*) containing different concentrations of surfactants. Appropriate controls were chosen wherein one of the controls contained only

bacteria without surfactants (positive control) while the other contained neither bacteria nor surfactant (blank). The samples (100 μL) were incubated in 96-well tissue culture plates in dark at 37°C for 24 h to allow biofilm formation, following which the plates were gently washed 3 times with water to remove unattached bacterial cells and media components. The plates were then kept at 55°C for 1 h to rigidly fix the biofilms to the plates, followed by staining the biofilms with 125 μL crystal violet (0.1% w/v in water) at room temperature for 10 min. The plates were then exposed to running tap water until free crystal violet stops releasing from the biofilms. The biofilms were then dried overnight in air, followed by addition of 125 μL of acetic acid (30% v/v in water) to each well to solubilize the crystal violet taken up by the bacterial biofilms. The solubilized crystal violet was monitored at OD₅₅₀ using a Perkin Elmer EnVision™ 2104 Multilabel Plate Reader. All biofilm assays were performed in triplicates; tests were repeated independently three times; each well was read five times. The average of 45 readings (3×3×5) in each case was calculated and plotted along with standard deviation. The data was background corrected by subtracting the OD₅₅₀ value obtained from the blank control from all other samples.

3.4.8 Bacteria preparation for differential dynamic microscopy (DDM)

Overnight cultures of *P. aeruginosa* were grown in Luria-Bertani (LB) broth (10% tryptone, 5% yeast extract and 5% NaCl) using a shaking incubator at 37°C and shaking speed of 120 rpm. A fresh culture was inoculated at 1:100 dilution of overnight grown cells in tryptone broth (TB) and grown for a further 4 h to obtain actively growing late exponential phase bacteria. Bacterial suspensions were gently mixed with the surfactant solutions before use.

3.4.9 DDM measurements

Experiments were performed on an Olympus IX-71 inverted optical microscope equipped with a Mikrotron MC1362 CMOS camera and Euresys Grablink full frame grabber. The bacteria were transferred into a rectangular capillary tube (Vitrotube W2540 8 mm width, 0.4 mm internal diameter height) and sealed with Vaseline. Samples were left for one minute after loading, and imaged with a 10× phase contrast objective under Köhler illumination. Videos

were recorded with a frame size of 1024×1024 pixels at 100 frames per second for 60 seconds. A custom written LabVIEW (National Instruments) program was used to extract the differential intensity correlation functions $g(q,t)$ (DICF) from the videos using the following equation:

$$g(q, t) = A(q)[1 - f(q, \tau)] + B(q) \quad (1)$$

where $A(q)$ is related to the scattering properties of the sample and microscope, and $B(q)$ is a camera noise background. The variable $f(q,\tau)$ is the intermediate scattering function, which is modelled using:

$$f(q, \tau) = (1 - \alpha)e^{-Dq^2\tau} + \alpha e^{-Dq^2\tau} \left[\left(\frac{Z+1}{Zq\bar{v}\tau} \right) \frac{\sin(Z \tan^{-1} \Delta)}{(1+\Delta^2)^{\frac{Z}{2}}} \right] \quad (2)$$

Where $\Delta = (q\bar{v}\tau)/(Z + 1)$ and $\sigma = \bar{v}(Z + 1)^{-1/2}$.

The motile parameters obtained are the fraction of motile swimmers α , mean velocity \bar{v} , velocity distribution σ , and diffusion coefficient of non-motile cells D . Each video is transformed into 511 data sets of $g(q,t)$ vs. q and fitted with Eq. (1) using Igor pro (Wavemetrics) to yield six parameters: $A(q)$, $B(q)$, \bar{v} , D , α , σ . The parameters are averaged over the range where the fitted data is constant ($q \sim 0.5$ to $2 \mu\text{m}^{-1}$).

3.4.10 Swarming motility assays

Compounds were tested for their influence on swarming motility of Gram-negative *P. aeruginosa*. Each swarm plate (0.8% nutrient broth, 0.5% glucose, 0.5% agar) was air dried for 5–10 min before use. The compounds were dissolved in deionised water and then added to each agar medium at a final concentration of 1 to 100 $\mu\text{g mL}^{-1}$. An equal amount of deionised water without any compound was added to the agar medium to serve as a control. A fixed concentration of overnight grown bacterial culture (2 μL) was inoculated at the center of the agar surface, and the plates were incubated at 30°C for 22 h.

3.4.11 Synthesis of 3.15–3.18: General procedure 1

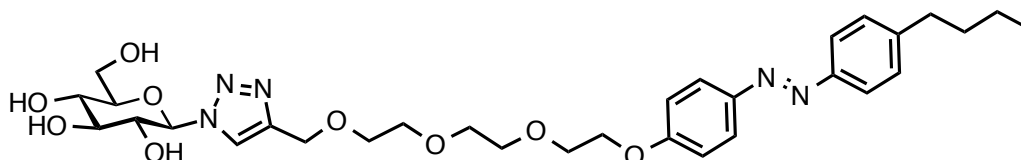
See Section 2.4.12 for details.

3.4.12 Synthesis of 3.3–3.13: General procedure 2

See Section 2.4.17 for details.

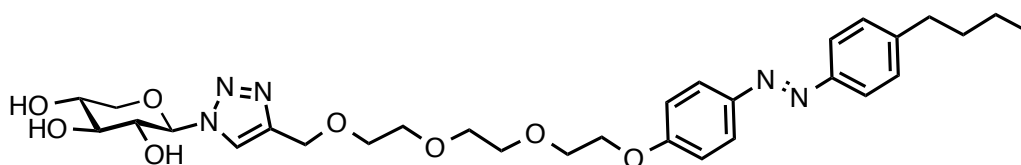
3.4.13 Analytical data

2-[2-[2-(4-n-butylazophenyl phenoxy)ethoxy]ethoxy]ethoxy]ethyl β -D-glucopyranosyl-1,2,3-triazole **3.3**



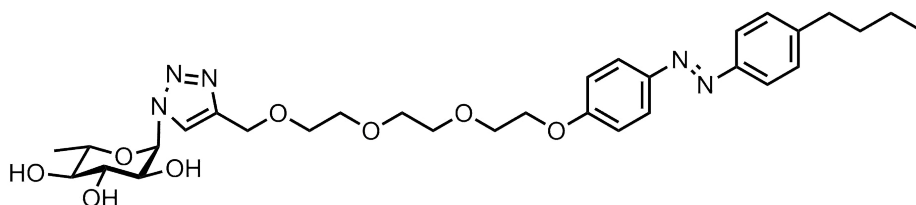
Compound **3.3** was prepared from **2.32** and **3.30** according to general procedure 2 and isolated as an orange solid (Yield: 44%). Mp = 44.6°C; $[\alpha]_D^{20}$ -8.0 (*c*, 0.1 in CH₃OH); FT-IR: $\nu_{\max}/\text{cm}^{-1}$ 3334, 2926, 2871, 1596, 1249, 1498, 1451; ¹H NMR (400 MHz, CD₃OD) δ 8.2 (s, 1H, =CH(triazole)), 7.86 (d, *J* = 9.1 Hz, 2H, Ar*H*), 7.77 (d, *J* = 8.5 Hz, 2H, Ar*H*), 7.33 (d, *J* = 8.5 Hz, 2H, Ar*H*), 7.07 (d, *J* = 9.1 Hz, 2H, Ar*H*), 5.58 (d, *J* = 9.2 Hz, 1H, *H*-1), 4.53 (s, 2H, 2×OH), 4.65 (s, 2H), 4.21 (m, 2H), 3.90–3.84 (m, 4H), 3.72–3.69 (m, 2H), 3.67–3.64 (m, 6H), 3.57–3.46 (m, 3H), 2.69 (t, *J* = 7.7 Hz, 2H, CH₂), 1.69–1.61 (m, 2H, CH₂), 1.44–1.34 (m, 2H, CH₂), 0.96 (t, *J* = 7.4 Hz, 3H, CH₃); ¹³C NMR (100 MHz, CD₃OD) δ 162.7 (ArC), 152.2 (ArC), 148.3 (ArC), 147.2 (ArC), 146.0 (C=CH(triazole)), 130.1 (2×ArC), 125.6 (4×ArC), 123.6 (C=CH(triazole)), 115.9 (2×ArC), 89.5 (C-1), 81.1 (CH), 78.4 (CH), 74.0 (CH), 71.7, 71.5, 70.8, 70.76, 70.67, 68.9 (CH₂), 64.9 (CH₂), 62.4 (CH₂), 36.4 (CH₂), 34.7 (CH₂), 23.4 (CH₂), 14.3 (CH₃). LC-MS: *m/z* 630.0 [*M* + H]⁺, ESI- HRMS calculated for C₃₁H₄₄N₅O₉ 630.3139 [*M* + H]⁺, found 630.3143 [*M* + H]⁺.

2-[2-[2-(4-n-butylazophenyl phenoxy)ethoxy]ethoxy]ethoxy]ethyl β -D-xylopyranosyl-1,2,3-triazole **3.4**



Compound **3.4** was prepared from **3.14** and **3.30** according to general procedure 2 and isolated as an orange solid (Yield: 32%). Mp = 156.5 °C; $[\alpha]_D^{20}$ 3.1 (*c*, 2.65 in CH₃OH); FT-IR: $\nu_{\max}/\text{cm}^{-1}$ 3338, 2940, 2876, 1628, 1449, 1375, 1252, 1099, 1021, 823; ¹H NMR (600 MHz, CD₃OD) δ 8.13 (s, 1H, =CH(triazole)), 7.86 (d, *J* = 8.98 Hz, 2H, Ar*H*), 7.77 (d, *J* = 8.31 Hz, 2H, Ar*H*), 7.32 (d, *J* = 8.34 Hz, 2H, Ar*H*), 7.06 (d, *J* = 9.02 Hz, 2H, Ar*H*), 5.50 (d, *J* = 9.14 Hz, 1H, *H*-1), 4.65 (s, 2H, CH₂), 4.20–4.19 (m, 2H), 4.00–3.98 (m, 1H), 3.90–3.84 (m, 3H), 3.74–3.56 (m, 10H), 3.51–3.43 (m, 2H), 2.68 (t, *J* = 7.69 Hz, 2H, CH₂), 1.67–1.62 (m, 2H, CH₂), 1.42–1.36 (m, 2H, CH₂), 0.96 (t, *J* = 7.40 Hz, 3H, CH₃); ¹³C NMR (100 MHz, *d*₆-DMSO) δ 161.5 (ArC), 150.7 (ArC), 146.7 (ArC), 146.2 (ArC), 144.4 (C=CH(triazole)), 129.7 (2×ArC), 124.9 (2×ArC), 123.5 (C=CH(triazole)), 122.8 (2×ArC), 115.5 (2×ArC), 88.6 (C-1), 77.6, 72.5, 70.4, 70.3, 70.2, 69.6, 69.5, 68.8, 68.1, 63.9, 35.1 (CH₂), 33.4 (CH₂), 22.2 (CH₂), 14.2 (CH₃). LCMS: *m/z* 599.8 [*M* + H]⁺, ESI- HRMS calculated for C₃₀H₄₁N₅NaO₈ 622.2853 [*M* + Na]⁺, found 622.2850 [*M* + Na]⁺.

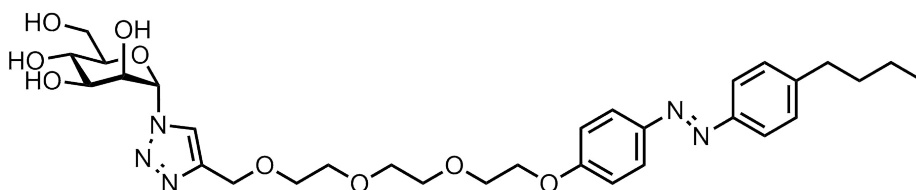
2-[2-[2-(4-*n*-butylazophenyl phenoxy)ethoxy]ethoxy]ethoxy]ethyl α -L-rhamnopyranosyl-1,2,3-triazole **3.5**



Compound **3.5** was prepared from **3.16** and **3.30** according to general procedure 2 and isolated as an orange solid (Yield: 67%). Mp = 64.9 °C; $[\alpha]_D^{20}$ 11.0 (*c*, 3.68 in CH₃OH); FT-IR: $\nu_{\max}/\text{cm}^{-1}$ 3357, 2928, 2873, 1598, 1453, 1248, 1080, 1024, 842; ¹H NMR (600 MHz, CD₃OD) δ 8.15 (s, 1H, =CH(triazole)), 7.86 (d, *J* = 8.97 Hz, 2H, Ar*H*), 7.77 (d, *J* = 8.37 Hz, 2H, Ar*H*), 7.32 (d, *J* = 8.38 Hz, 2H, Ar*H*), 7.06 (d, *J* = 9.03 Hz, 2H, Ar*H*), 5.95 (d, *J* = 1.14 Hz, 1H, *H*-1), 4.64 (s, 2H, CH₂), 4.21–4.19 (m, 2H), 4.09–4.08 (m, 1H), 3.87–3.86 (m, 2H), 3.71–3.63 (m, 10H), 3.55–3.47 (m, 2H), 2.69 (t, *J* = 7.58 Hz, 2H, CH₂), 1.67–1.62 (m, 2H, CH₂), 1.41–1.36 (m, 5H, CH₃, CH₂), 0.96 (t, *J* = 7.37 Hz, 3H, CH₃); ¹³C NMR (100 MHz, *d*₆-DMSO) δ 161.5 (ArC), 150.8 (ArC), 146.7 (ArC), 146.2 (ArC), 143.9 (C=CH(triazole)), 129.7 (2×ArC), 124.9

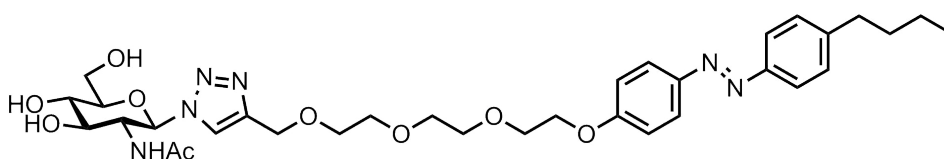
(2×ArC), 123.9 (C=CH(triazole)), 122.8 (2×ArC), 115.5 (2×ArC), 86.3 (C-1), 75.4, 73.4, 71.7, 71.1, 70.4, 70.3, 70.2, 69.5, 69.3, 68.1, 63.9, 35.1 (CH₂), 33.4 (CH₂), 22.2 (CH₂), 18.3 (CH₃), 14.2 (CH₃); LCMS: *m/z* 613.8 [*M* + H]⁺, ESI- HRMS calculated for C₃₁H₄₃N₅NaO₈ 636.3009 [*M* + Na]⁺, found 636.3004 [*M* + Na]⁺.

2-[2-[2-(4-n-butylazophenyl phenoxy)ethoxy]ethoxy]ethoxy]ethyl α-D-mannopyranosyl-1,2,3-triazole **3.6**



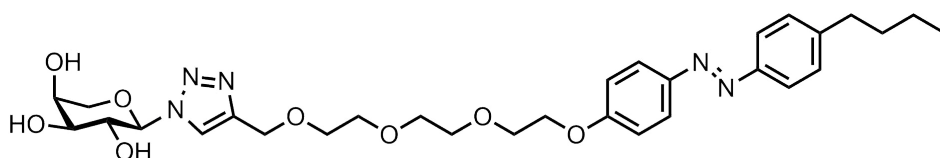
Compound **3.6** was prepared from **2.34** and **3.30** according to general procedure 2 and isolated as an orange solid (Yield: 51%). Mp = 164.6°C; [α]_D²⁰ 70.3 (*c*, 0.72 in CH₃OH); FT-IR: ν_{\max} /cm⁻¹ 3297, 2928, 2873, 1598, 1442, 1248, 1088, 1032, 838; ¹H NMR (600 MHz, CD₃OD) δ 8.14 (s, 1H, =CH(triazole)), 7.86 (d, *J* = 9.05 Hz, 2H, ArH), 7.77 (d, *J* = 8.34 Hz, 2H, ArH), 7.32 (d, *J* = 8.41 Hz, 2H, ArH), 7.07 (d, *J* = 9.05 Hz, 2H, ArH), 6.01 (d, *J* = 2.64 Hz, 1H, H-1), 4.69–4.64 (m, 3H), 4.21–4.19 (m, 2H), 4.07–4.05 (m, 1H), 3.87–3.86 (m, 2H), 3.82–3.65 (m, 12H), 2.68 (t, *J* = 7.68 Hz, 2H, CH₂), 1.66–1.63 (m, 2H, CH₂), 1.41–1.37 (m, 2H, CH₂), 0.96 (t, *J* = 7.39 Hz, 3H, CH₃); ¹³C NMR (100 MHz, *d*₆-DMSO) δ 161.5 (ArC), 150.8 (ArC), 146.7 (ArC), 146.2 (ArC), 144.4 (C=CH(triazole)), 129.7 (2×ArC), 124.9 (2×ArC), 124.1 (C=CH(triazole)), 122.8 (2×ArC), 115.5 (2×ArC), 86.3 (C-1), 78.7, 71.7, 70.4, 70.3, 70.2, 69.6, 69.3, 68.7, 68.1, 68.0, 63.9, 61.3, 35.1 (CH₂), 33.4 (CH₂), 22.2 (CH₂), 14.2 (CH₃). LCMS: *m/z* 629.8 [*M* + H]⁺, ESI- HRMS calculated for C₃₁H₄₃N₅NaO₉ 652.2959 [*M* + Na]⁺, found 652.2951 [*M* + Na]⁺.

2-[2-[2-(4-n-butylazophenyl phenoxy)ethoxy]ethoxy]ethoxy]ethyl 2-acetamido-2-deoxy-β-D-glucopyranosyl-1,2,3-triazole **3.7**



Compound **3.7** was prepared from **3.15** and **3.30** according to general procedure 2 and isolated as an orange solid (Yield: 38%). Mp = 173.2°C; $[\alpha]_{\text{D}}^{20}$ -6.1 (*c*, 2.68 in CH₃OH); FT-IR: $\nu_{\text{max}}/\text{cm}^{-1}$ 3350, 2947, 2824, 1628, 1606, 1457, 1378, 1099, 1021, 823; ¹H NMR (600 MHz, CD₃OD) δ 8.16 (s, 1H, =CH(triazole)), 7.87 (d, *J* = 8.99 Hz, 2H, ArH), 7.77 (d, *J* = 8.37 Hz, 2H, ArH), 7.33 (d, *J* = 8.43 Hz, 2H, ArH), 7.08 (d, *J* = 9.04 Hz, 2H, ArH), 5.79 (d, *J* = 9.74 Hz, 1H, H-1), 4.63–4.60 (m, 2H), 4.23–4.19 (m, 3H), 3.90–3.87 (m, 3H), 3.76–3.53 (m, 13H), 2.69 (t, *J* = 7.79 Hz, 2H, CH₂), 1.77 (s, 3H, COCH₃), 1.68–1.63 (m, 2H, CH₂), 1.43–1.37 (m, 2H, CH₂), 0.96 (t, *J* = 7.44 Hz, 3H, CH₃); ¹³C NMR (100 MHz, *d*₆-DMSO) δ 169.6 (O=CCH₃), 161.5 (ArC), 150.8 (ArC), 146.7 (ArC), 146.2 (ArC), 144.2 (C=CH(triazole)), 129.7 (2×ArC), 124.9 (2×ArC), 123.0 (C=CH(triazole)), 122.8 (2×ArC), 115.5 (2×ArC), 86.5 (C-1), 80.6 (CH), 74.4 (CH), 70.4, 70.3, 70.2, 69.3, 68.1, 63.8, 61.2, 55.0, 35.1 (CH₂), 33.4 (CH₂), 23.2 (CH₃), 22.2 (CH₂), 14.2 (CH₃); LC-MS: *m/z* 692.7 [*M* + Na]⁺, ESI- HRMS calculated for C₃₃H₄₆N₆NaO₉ 693.3224 [*M* + Na]⁺, found 693.3218 [*M* + Na]⁺.

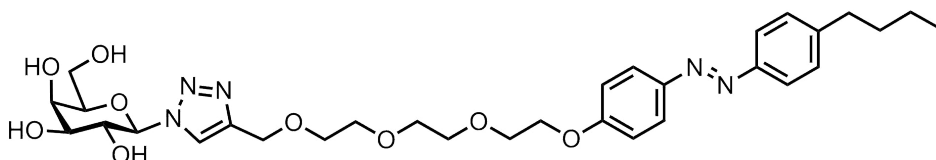
2-[2-[2-(4-n-butylazophenyl phenoxy)ethoxy]ethoxy]ethoxy]ethyl α -L-arabinopyranosyl-1,2,3-triazole **3.8**



Compound **3.8** was prepared from **3.17** and **3.30** according to general procedure 2 and isolated as an orange solid (Yield: 42%). Mp = 86.2°C; $[\alpha]_{\text{D}}^{20}$ -15.8 (*c*, 3.36 in CH₃OH); FT-IR: $\nu_{\text{max}}/\text{cm}^{-1}$ 3372, 2932, 1598, 1449, 1378, 1252, 1088, 1024, 879, 823; ¹H NMR (400 MHz, *d*₆-DMSO) δ 8.22 (s, 1H, =CH(triazole)), 7.87 (d, *J* = 8.97 Hz, 2H, ArH), 7.77 (d, *J* = 8.24 Hz, 2H, ArH), 7.37 (d, *J* = 8.39 Hz, 2H, ArH), 7.13 (d, *J* = 8.97 Hz, 2H, ArH), 5.43 (d, *J* = 9.16 Hz, 1H, H-1), 5.29 (d, *J* = 5.87 Hz, 1H, OH), 5.04 (d, *J* = 4.17 Hz, 1H, OH), 4.81 (d, *J* = 4.05 Hz, 1H, OH), 4.56 (s, 2H, CH₂), 4.21–4.19 (m, 2H, CH₂), 4.09–4.03 (m, 1H, CH), 3.85–3.75 (m, 5H), 3.62–3.54 (m, 9H), 2.65 (t, *J* = 7.55 Hz, 2H, CH₂), 1.62–1.55 (m, 2H, CH₂), 1.37–1.28 (m, 2H, CH₂), 0.90 (t, *J* = 7.30 Hz, 3H, CH₃); ¹³C NMR (400 MHz, *d*₆-DMSO) δ 161.5 (ArC), 150.7 (ArC), 146.7 (ArC), 146.2 (ArC), 144.4 (C=CH(triazole)), 129.7 (2×ArC), 124.9 (2×ArC), 123.2

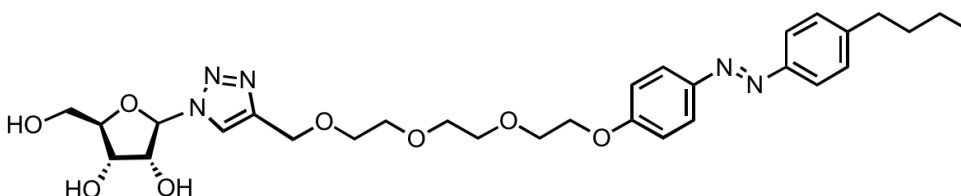
(C=CH(triazole)), 122.8 (2×ArC), 115.5 (2×ArC), 88.8 (C-1), 73.7, 70.4, 70.2, 69.8, 69.5, 69.3, 68.9, 68.1, 63.9, 35.1 (CH₂), 33.4 (CH₂), 22.2 (CH₂), 14.2 (CH₃); LC-MS: *m/z* 599.8 [*M* + H]⁺, ESI-HRMS calculated for C₃₀H₄₁N₅NaO₈ 622.2852 [*M* + Na]⁺, found 622.2916 [*M* + Na]⁺.

2-[2-[2-(4-*n*-butylazophenyl phenoxy)ethoxy]ethoxy]ethoxyethyl β-D-galactopyranosyl-1,2,3-triazole **3.9**



Compound **3.9** was prepared from **2.33** and **3.30** according to general procedure 2 and isolated as an orange solid (Yield: 58%). Mp = 59.6°C; [α]_D²⁰ -7.1 (*c*, 0.08 in CH₃OH); ¹H NMR (400 MHz, CD₃OD) δ 8.2 (s, 1H), 7.87 (d, *J* = 9.1 Hz, 2H, 2×Ar*H*), 7.78 (d, *J* = 8.4 Hz, 2H, 2×Ar*H*), 7.33 (d, *J* = 8.6 Hz, 2H, 2×Ar*H*), 7.08 (d, *J* = 9.1 Hz, 2H), 5.55 (d, *J* = 9.2 Hz, 1H), 4.66 (s, 2H), 4.23–4.21 (m, 2H), 4.15 (t, *J* = 9.3 Hz, 1H), 3.98 (dd, *J* = 3.3 Hz, *J* = 0.8 Hz, 1H), 3.89–3.86 (m, 2H), 3.84–3.81 (1H, m), 3.76–3.65 (m, 11H), 2.70 (t, *J* = 7.7 Hz, 2H), 1.69–1.62 (m, 2H), 1.45–1.37 (m, 2H), 0.96 (t, *J* = 7.4 Hz, 3H); ¹³C NMR (100 MHz, CD₃OD) δ 162.7, 152.2, 148.2, 147.2, 146.0, 130.1, 125.6, 124.0, 123.5, 115.9, 90.2, 79.9, 75.2, 71.7, 71.5, 71.4, 70.7, 70.6, 70.3, 68.9, 64.9, 62.4, 36.4, 34.7, 23.3, 14.3. LC-MS: *m/z* 630.1 [*M* + H]⁺ 652 [*M* + Na]⁺. ESI- HRMS calculated for C₃₁H₄₄N₅O₉ 630.3139 [*M* + H]⁺, found 630.3133 [*M* + H]⁺.

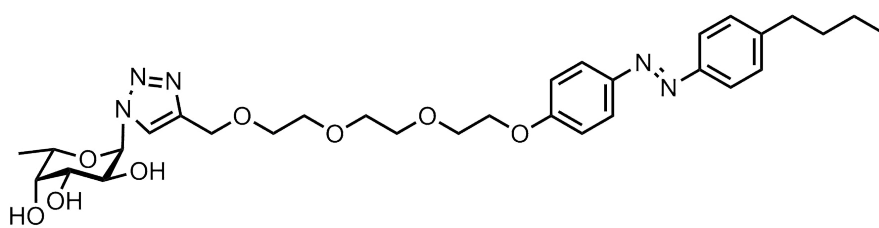
2-[2-[2-(4-*n*-butylazophenyl phenoxy)ethoxy]ethoxy]ethyl 4-*O*-β-D-ribofuranosyl-1,2,3-triazole **3.10**



Compound **3.10** was prepared from **3.19** and **3.30** according to general procedure 2 and isolated as an orange solid (Yield: 60%). Mp = 182.8°C; [α]_D²⁰ 5.2 (*c*, 0.18 in CH₃OH); FT-IR: ν_{max} /cm⁻¹ 3341, 2924, 1596, 1407, 1248, 1096, 1046, 842; ¹H NMR (400 MHz, *d*₆-DMSO) δ 8.30 (s,

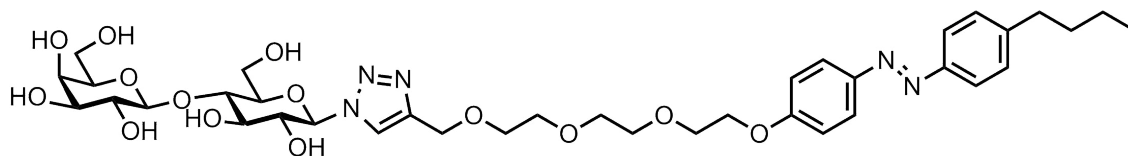
1H, =CH(triazole)), 7.90 (d, $J = 9.11$ Hz, 2H, ArH), 7.81 (d, $J = 8.20$ Hz, 2H, ArH), 7.42 (d, $J = 8.44$ Hz, 2H, ArH), 7.17 (d, $J = 9.04$ Hz, 2H, ArH), 5.68 (d, $J = 8.86$ Hz, 1H, H-1), 5.19–5.17 (m, 1H), 4.94 (s, 1H), 4.59 (s, 2H, CH₂), 4.26–4.23 (m, 2H), 4.07–4.02 (m, 2H), 3.84–3.58 (m, 13H), 2.70 (t, $J = 7.48$ Hz, 2H, CH₂), 1.66–1.60 (m, 2H, CH₂), 1.39–1.34 (m, 2H, CH₂), 0.95 (t, $J = 7.34$ Hz, 3H, CH₃); ¹³C NMR (100 MHz, d₆-DMSO) δ 161.5, 150.7, 146.7, 146.2, 144.3, 129.7, 124.8, 123.6, 122.7, 115.5, 85.3, 71.5, 70.4, 70.3, 70.2, 69.7, 69.3, 68.1, 66.9, 65.6, 63.9, 35.1, 33.4, 22.2, 14.2; LC-MS: m/z 600.3 [$M + H$]⁺, HRMS (ESI-ToF) calculated for C₃₀H₄₁N₅O₈ 599.2955 [$M + H$]⁺, found 622.2847 [$M + Na$]⁺.

2-[2-[2-(4-*n*-butylazophenyl phenoxy)ethoxy]ethoxy]ethyl 4-*O*-α-L-fucopyranosyl-1,2,3-triazole **3.11**



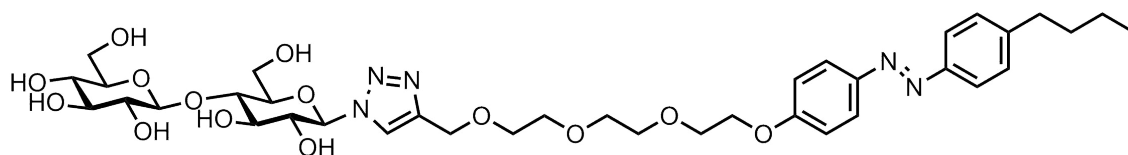
Compound **3.11** was prepared from **3.18** and **3.30** according to general procedure 2 and isolated as an orange solid (Yield: 57%). Mp = 195.8 °C; [α]_D²⁰ 12.9 (*c*, 0.12 in CH₃OH); FT-IR: $\nu_{\max}/\text{cm}^{-1}$ 3266, 2925, 1595, 1438, 1248, 1088, 842; ¹H NMR (400 MHz, d₆-DMSO) δ 8.12 (s, 1H, =CH(triazole)), 7.79 (d, $J = 8.98$ Hz, 2H, ArH), 7.69 (d, $J = 8.31$ Hz, 2H, ArH), 7.31 (d, $J = 8.53$ Hz, 2H, ArH), 7.06 (d, $J = 8.99$ Hz, 2H, ArH), 5.38 (d, $J = 9.12$ Hz, 1H, H-1), 4.48 (s, 2H, CH₂), 4.14–4.12 (m, 2H), 3.95–3.91 (m, 1H, OH), 3.83–3.79 (m, 1H, OH), 3.73–3.70 (m, 2H), 3.55–3.45 (m, 11H), 2.59 (t, $J = 7.49$ Hz, 2H, CH₂), 1.56–1.49 (m, 2H, CH₂), 1.29–1.23 (m, 2H, CH₂), 1.07 (d, $J = 6.40$ Hz, 3H, CH₃), 0.84 (t, $J = 7.27$ Hz, 3H, CH₃); ¹³C NMR (100 MHz, d₆-DMSO) δ 161.5, 150.7, 146.7, 146.2, 144.4, 129.7, 124.8, 123.1, 122.7, 115.5, 88.5, 74.3, 73.7, 71.6, 70.4, 70.3, 70.2, 69.5, 69.3, 68.1, 63.9, 35.1, 33.4, 22.2, 16.9, 14.2; LC-MS: m/z 600.3 [$M + H$]⁺, ESI-HRMS calculated for C₃₁H₄₃N₅O₈ 613.3112 [$M + H$]⁺, found 636.3009 [$M + Na$]⁺.

2-[2-[2-(4-*n*-butylazophenyl phenoxy)ethoxy]ethoxy]ethyl 4-*O*- β -D-galactopyranosyl- β -D-glucopyranosyl-1,2,3-triazole **3.12**



Compound **3.12** was prepared from **3.20** and **3.30** according to general procedure 2 and isolated as an orange solid (Yield: 55%). Mp = 147.7 °C; $[\alpha]_D^{20}$ 15 (*c*, 0.08 in CH₃OH); FT-IR: $\nu_{\max}/\text{cm}^{-1}$ 3272, 2932, 1598, 1432, 1249, 1051, 864; ¹H NMR (400 MHz, *d*₆-DMSO) δ 8.22 (s, 1H, =CH(triazole)), 7.79 (d, *J* = 9.15 Hz, 2H, ArH), 7.69 (d, *J* = 8.44 Hz, 2H, ArH), 7.31 (d, *J* = 8.41 Hz, 2H, ArH), 7.06 (d, *J* = 9.06 Hz, 2H, ArH), 5.58–5.47 (m, 2H, 2×CH), 5.05 (s, 1H), 4.83–4.82 (m, 1H), 4.73 (s, 1H), 4.60–4.58 (m, 2H), 4.48–4.46 (m, 3H), 4.19 (d, *J* = 7.30 Hz, 1H), 4.15–4.12 (m, 2H), 3.82–3.76 (m, 1H), 3.73–3.70 (m, 2H), 3.62–3.39 (m, 16H), 3.30–3.27 (m, 3H), 2.59 (t, *J* = 7.53 Hz, 2H, CH₂), 1.57–1.54 (m, 2H, CH₂), 1.31–1.21 (m, 2H, CH₂), 0.84 (t, *J* = 7.34 Hz, 3H, CH₃); ¹³C NMR (100 MHz, *d*₆-DMSO) δ 161.5, 150.8, 146.7, 146.2, 144.4, 129.7, 124.9, 123.6, 122.7, 15.5, 104.3, 87.5, 80.3, 78.2, 76.1, 75.6, 73.7, 72.3, 71.0, 70.4, 70.3, 70.2, 69.6, 69.3, 68.1, 63.9, 60.9, 35.1, 33.4, 22.2, 14.2; LC-MS: *m/z* 792.3 [*M* + H]⁺, ESI-HRMS calculated for C₃₇H₅₃N₅O₁₄ 791.3589 [*M* + H]⁺, found 814.3492 [*M* + Na]⁺.

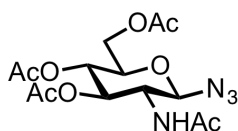
2-[2-[2-(4-*n*-butylazophenyl phenoxy)ethoxy]ethoxy]ethyl 4-*O*- β -D-glucopyranosyl- β -D-glucopyranosyl-1,2,3-triazole **3.13**



Compound **3.13** was prepared from **2.35** and **3.30** according to general procedure 2 and isolated as an orange solid (Yield: 60%). Mp = 127.7°C; $[\alpha]_D^{20}$ 35.0 (*c*, 0.08 in CH₃OH); FT-IR: $\nu_{\max}/\text{cm}^{-1}$ 3340, 2871, 1597, 1497, 1351, 1249, 1029, 841; ¹H NMR (400 MHz, *d*₆-DMSO) δ 8.22 (s, 1H, =CH(triazole)), 7.79 (d, *J* = 9.02 Hz, 2H, ArH), 7.69 (d, *J* = 8.34 Hz, 2H, ArH), 7.31 (d, *J* = 8.39 Hz, 2H, ArH), 7.06 (d, *J* = 9.00 Hz, 2H, ArH), 5.57–5.49 (m, 2H, 2×CH), 5.20 (s, 1H),

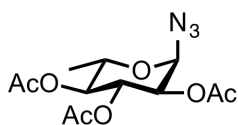
4.97–4.84 (m, 2H), 4.62–4.56 (m, 1H), 4.48 (s, 2H, CH_2), 4.25 (d, $J = 7.83$ Hz, 1H), 4.15–4.12 (m, 2H), 3.81–3.76 (m, 1H), 3.73–3.65 (m, 4H), 3.59–3.27 (m, 15H), 3.18–3.10 (m, 2H), 3.04–2.95 (m, 2H), 2.59 (t, $J = 7.58$ Hz, 2H, CH_2), 1.57–1.51 (m, 2H, CH_2), 1.31–1.21 (m, 2H, CH_2), 0.84 (t, $J = 7.33$ Hz, 3H, CH_3); ^{13}C NMR (100 MHz, d_6 -DMSO) δ 161.5, 150.8, 146.7, 146.2, 144.4, 129.7, 124.9, 123.6, 122.8, 115.5, 103.6, 87.5, 80.0, 78.3, 77.3, 76.9, 75.7, 73.8, 70.4, 70.3, 70.2, 69.6, 69.3, 68.1, 63.9; LC-MS: m/z 792.2 [$M + H$] $^+$, ESI-HRMS calculated for $C_{37}H_{53}N_5O_{14}$ 791.3589 [$M + H$] $^+$, found 792.3659 [$M + H$] $^+$, 814.3477 [$M + Na$] $^+$.

3,4,6-tri-*O*-acetyl-2-acetamido-2-deoxy- β -D-glucopyranosyl azide **3.15**⁴⁷



Compound **3.15** was prepared from **3.21** according to general procedure 1 and isolated as white solid (Yield: 67%). Mp = 174.2°C; $[\alpha]_D^{20}$ -36.3 (c , 0.01 in CH_3OH); FT-IR: ν_{max}/cm^{-1} 2106, 1743, 1661, 1521, 1369, 1223, 1031, 896; 1H NMR (400 MHz, $CDCl_3$) δ 5.71 (d, $J = 8.87$ Hz, 1H, CH), 5.22–5.17 (m, 1H, CH), 5.03 (t, $J = 9.87$ Hz, 1H, CH), 4.71 (d, $J = 9.20$ Hz, 1H, CH), 4.23–4.09 (m, 2H, CH_2), 3.89–3.72 (m, 2H, $2 \times CH$), 2.04 (s, 3H, OAc), 1.98, 1.96 (s, 6H, $2 \times OAc$), 1.91 (s, 3H, OAc); ^{13}C NMR (100 MHz, $CDCl_3$) δ 170.9, 170.7, 170.4, 169.3, 88.4, 73.9, 72.2, 68.1, 61.9, 54.2, 23.2, 20.7, 20.6, 20.5; LCMS: m/z 373.1 [$M + H$] $^+$, the obtained melting point, optical rotation, FTIT, 1H NMR, ^{13}C NMR and LCMS data are in agreement with the reference 47.

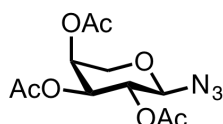
2,3,4-tri-*O*-acetyl- α -L-rhamnopyranosyl azide **3.16**⁷⁵



Compound **3.16** was prepared from **3.25** according to general procedure 1 and isolated as white solid (Yield: 62%). Mp = 82.6°C; $[\alpha]_D^{20}$ 98.3 (c , 0.01 in CH_3OH); FT-IR: ν_{max}/cm^{-1} 2986, 2119, 1741, 1368, 1206, 1047, 887, 678; 1H NMR (400 MHz, $CDCl_3$) δ 5.37–5.36 (m, 1H), 5.03–

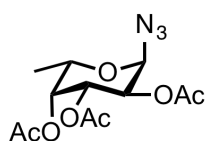
4.92 (m, 2H), 4.64 (s, 1H), 3.59–3.55 (m, 1H), 2.14 (s, 3H, OAc), 1.99 (s, 3H, OAc), 1.92 (s, 3H, OAc), 1.25 (d, $J = 6.12\text{ Hz}$, CH_3); ^{13}C NMR (100 MHz, CDCl_3) δ 170.0, 169.9, 169.7, 84.9, 70.9, 69.9, 69.6, 20.7, 20.5, 17.3; LCMS: m/z 314.0 $[\text{M} + \text{H}]^+$, the obtained melting point, optical rotation, FTIT, ^1H NMR, ^{13}C NMR and LCMS data are in agreement with the reference 75.

2,3,4-tri-*O*-acetyl- β -L-arabinopyranosyl azide **3.17**⁷⁶



Compound **3.17** was prepared from **3.26** according to general procedure 1 and was isolated as white solid (Yield: 60%). Mp = 87.7°C; $[\alpha]_{\text{D}}^{20}$ -15.7 (c , 0.02 in CH_3OH); FT-IR: $\nu_{\text{max}}/\text{cm}^{-1}$ 2115, 1743, 1372, 1213, 1016, 744; ^1H NMR (400 MHz, CDCl_3) δ 5.24–5.22 (m, 1H, CH), 5.11–5.07 (m, 1H, CH), 5.00–4.97 (m, 1H, CH), 4.52 (d, $J = 7.99\text{ Hz}$, 1H, CH), 4.06–3.66 (m, 2H, CH_2), 2.09 (s, 3H, OAc), 2.03 (s, 3H, OAc), 1.96 (s, 3H, OAc); ^{13}C NMR (100 MHz, CDCl_3) δ 170.2, 169.9, 169.4, 88.5, 70.1, 68.4, 67.5, 65.6, 20.9, 20.7, 20.6; LCMS: m/z 324.0 $[\text{M} + \text{Na}]^+$, the obtained melting point, optical rotation, FTIT, ^1H NMR, ^{13}C NMR and LCMS data are in agreement with the reference 76.

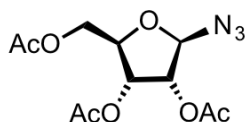
2,3,4-tri-*O*-acetyl- α -L-fucopyranosyl azide **3.18**⁷⁵



Compound **3.18** was prepared from **3.27** according to general procedure 1 and isolated as white solid (Yield: 64%). Mp = 127.7°C; $[\alpha]_{\text{D}}^{20}$ 31.1 (c , 0.02 in CH_3OH); FT-IR: $\nu_{\text{max}}/\text{cm}^{-1}$ 2102, 1744, 1364, 1213, 1057, 947, 794, 675; ^1H NMR (400 MHz, CDCl_3) δ 5.24–5.23 (m, 1H), 5.13–5.09 (m, 1H), 5.03–4.99 (m, 1H), 4.56 (d, $J = 8.62\text{ Hz}$, 1H), 3.91–3.86 (m, 1H), 2.16 (s, 3H), 2.06 (s, 3H), 1.96 (s, 3H), 1.22 (d, $J = 6.39\text{ Hz}$, 3H); ^{13}C NMR (100 MHz, CDCl_3) δ 170.5, 170.0, 169.4, 88.2, 71.5, 71.2, 69.9, 68.2, 20.7, 20.6, 20.5, 15.9. LCMS: m/z 338.0 $[\text{M} + \text{Na}]^+$, the

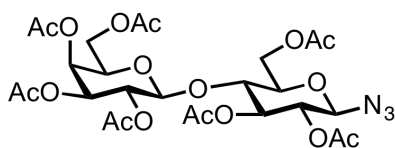
obtained melting point, optical rotation, FTIT, ^1H NMR, ^{13}C NMR and LCMS data are in agreement with the reference 75.

2,3,5-tri-*O*-acetyl- β -D-ribofuranosyl azide **3.19**⁷⁷



Azidomethylsilane (2.3 mL, 17.3 mmol, 2.0 equiv.) was added to a solution of ribose acetate **3.28** (2.8 g, 8.6 mmol, 1.0 equiv.) in anhydrous DCM (20.0 mL) under N_2 , followed by the addition of tin (IV) chloride (7.8 mL, 43.2 mmol, 5.0 equiv.). After stirring at ambient temperature for 12 h, the mixture was washed with aq. NaHCO_3 , extracted with DCM, dried over Na_2SO_4 , concentrated under reduced pressure and purified by flash chromatography (hexane: EtOAc 7:3) to afford the product as pale yellow liquid (2.5 g, yield 96%). $[\alpha]_{\text{D}}^{20}$ -48.7 (*c*, 0.02 in CH_3OH); FT-IR: $\nu_{\text{max}}/\text{cm}^{-1}$ 2114, 1741, 1369, 1209, 1041, 628; ^1H NMR (400 MHz, CDCl_3) δ 5.27 (t, *J* = 3.11 Hz, 1H), 4.90–4.88 (m, 2H), 4.67–4.65 (m, 1H), 3.88–3.63 (m, 2H, CH_2); ^{13}C NMR (100 MHz, CDCl_3) δ 169.6, 169.3, 86.7, 68.3, 66.6, 66.0, 62.8, 20.6; LCMS: *m/z* 324.1 [*M* + Na]⁺, the obtained melting point, optical rotation, FTIT, ^1H NMR, ^{13}C NMR and LCMS data are in agreement with the reference 77.

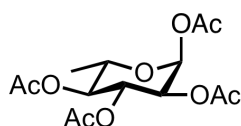
hepta-*O*-acetyl β -D-lactose azide **3.20**⁷⁸



Trimethylsilyl azide (0.2 mL, 2.9 mmol, 2.0 equiv.) was added under N_2 to a solution of D-lactose heptaacetate **3.29** (0.5 g, 1.5 mmol, 1.0 equiv.) in dry DCM (50.0 mL), followed by tin (IV) chloride (0.1 mL, 0.9 mmol, 0.6 equiv.). The mixture was stirred at ambient temperature for 12 hours, then the solvent was removed under reduced pressure and the crude product was purified by chromatography to afford the final product as a white solid (0.4 g, yield 70%). Mp = 76.8°C; $[\alpha]_{\text{D}}^{20}$ -10.5 (*c*, 0.01 in CH_3OH); FT-IR: $\nu_{\text{max}}/\text{cm}^{-1}$ 2121, 1742, 1369, 1208, 1036, 900;

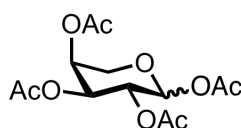
^1H NMR (400 MHz, CDCl_3) δ 5.35–5.29 (m, 1H), 5.20 (t, $J = 9.23$ Hz, 1H), 5.13–5.08 (m, 1H), 4.97–4.94 (m, 1H), 4.86 (t, $J = 9.02$ Hz, 1H), 4.62 (d, $J = 8.76$ Hz, 1H), 4.52–4.47 (m, 2H), 4.15–4.05 (m, 3H), 3.89–3.79 (m, 2H), 3.72–3.68 (m, 1H), 2.15 (s, 3H, OAc), 2.14 (s, 3H, OAc), 2.07–2.04 (m, 12H, 4 \times OAc), 1.96 (s, 3H, OAc); ^{13}C NMR (100 MHz, CDCl_3) δ 170.3, 170.1, 170.0, 169.6, 169.5, 169.1, 101.1, 87.7, 75.7, 74.8, 72.5, 70.9, 70.7, 69.1, 66.6, 61.7, 60.8, 20.7, 20.6, 20.5; LCMS: m/z 684.0 [$M + \text{Na}$] $^+$, the obtained melting point, optical rotation, FTIT, ^1H NMR, ^{13}C NMR and LCMS data are in agreement with the reference 78.

1,2,3,4,-tetra-*O*-acetyl- α -L-rhamnopyranose **3.22**⁷⁹



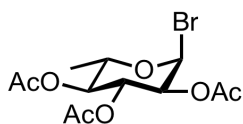
L-rhamnose (5.0 g, 30.5 mmol, 1.0 equiv.), acetic anhydride (46.1 mL, 487.4 mmol, 16.0 equiv.) and 4-dimethylaminopyridine (0.1 g, 0.9 mmol, 0.03 equiv.) were dissolved in 100.0 mL pyridine. The mixture was stirred at ambient temperature for 8 h and was concentrated under reduced pressure. The crude product was dissolved in EtOAc (100.0 mL), washed with 1N HCl solution (200.0 mL), dried with Na_2SO_4 and concentrated, which was used directly for the next step (10.0 g, yield 98%). $[\alpha]_{\text{D}}^{20}$ 18.0 (c , 0.26 in CH_3OH); FT-IR: $\nu_{\text{max}}/\text{cm}^{-1}$ 1742, 1369, 1207, 966, 734; ^1H NMR (400 MHz, CDCl_3) δ 5.99 (d, $J = 1.88$ Hz, 1H, CH), 5.28–5.27 (m, 1H, CH), 5.24–5.22 (m, 1H, CH), 5.10 (t, $J = 9.89$ Hz, 1H, CH), 3.95–3.90 (m, 1H, CH), 2.15, 2.14, 2.04, 1.97 (s, 4 \times OAc), 1.22 (d, $J = 6.19$ Hz, 3H, CH_3); ^{13}C NMR (100 MHz, CDCl_3) δ 170.0, 169.8, 168.3, 90.6, 70.4, 68.7, 68.6, 21.4, 20.8, 20.7, 20.6, 17.4; LCMS: m/z 331.1 [$M + \text{H}$] $^+$, the obtained melting point, optical rotation, FTIT, ^1H NMR, ^{13}C NMR and LCMS data are in agreement with the reference 79.

1,2,3,4-tetra-*O*-acetyl-L-arabinopyranoside **3.23**⁸⁰



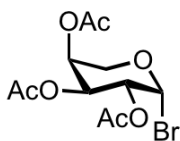
L-arabinose (5.0 g, 33.3 mmol, 1.0 equiv.), acetic anhydride (50.4 mL, 532.8 mmol, 16.0 equiv.) and DMAP (0.1 g, 1.0 mmol, 0.03 equiv.) were added to 100 mL pyridine at 0°C, and maintained at ambient temperature overnight. The mixture was concentrated, re-dissolved in toluene, washed with 1N HCl, water, brine and concentrated to afford the product as white solid (10.0 g, yield 94%). Mp = 69.3°C; $[\alpha]_D^{20}$ 71.8 (*c*, 0.04 in CH₃OH); FT-IR: $\nu_{\max}/\text{cm}^{-1}$ 3395, 1736, 1372, 1209, 1064, 941, 754; ¹H NMR (400 MHz, CDCl₃) δ 6.35 (d, *J* = 2.92 Hz, 1H, CH), 5.39–5.32 (m, 3H, 3×CH), 4.09–3.81 (m, 2H, CH₂), 2.16 (s, 6H, 2×OAc), 2.03 (s, 6H, 2×OAc); ¹³C NMR (100 MHz, CDCl₃) δ 170.3, 170.1, 169.9, 169.1, 90.2, 68.5, 67.0, 66.7, 62.7, 20.8, 20.7, 20.5; LCMS: *m/z* 332.1 [*M* + H]⁺, the obtained melting point, optical rotation, FTIT, ¹H NMR, ¹³C NMR and LCMS data are in agreement with the reference 80.

2,3,4-tri-*O*-acetyl- α -L-rhamnopyranosyl bromide **3.25**⁷⁹



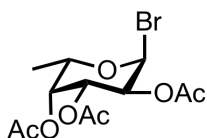
In the dark, acetate **3.22** (2.0 g, 6.0 mmol, 1.0 equiv.) was added to DCM (50.0 mL, 0.1 M) into a vacuum dried flask. The flask was maintained in an ambient temperature water bath, and to the mixture was added HBr (33% in acetic acid, 7.6 mL, 42.1 mmol, 7.0 equiv.). After stirring for 2 h, the reaction mixture was poured portion wise into a cold aqueous saturated NaHCO₃ solution (150.0 mL), extracted with DCM, dried with Na₂SO₄ and concentrated under reduced pressure to afford the product as white solid (2.1 g, yield 99%). Mp = 64.4°C; $[\alpha]_D^{20}$ -59.1 (*c*, 0.56 in CH₃OH); FT-IR: $\nu_{\max}/\text{cm}^{-1}$ 1743, 1371, 1202, 1035, 914, 682; ¹H NMR (400 MHz, CDCl₃) δ 6.24 (s, 1H, CH), 5.62–5.58 (m, 1H, CH), 5.39–5.38 (m, 1H, CH), 5.10 (t, *J* = 9.86 Hz, 1H, CH), 4.07–4.04 (m, 1H, CH), 2.09 (s, 3H, OAc), 2.01 (s, 3H, OAc), 1.94 (s, 3H, OAc), 1.23 (d, *J* = 6.27 Hz, 3H, CH₃); ¹³C NMR (100 MHz, CDCl₃) δ 169.9, 169.7, 169.6, 169.5, 83.9, 72.3, 71.1, 70.1, 67.9, 20.6, 20.5, 16.9, the obtained melting point, optical rotation, FTIT, ¹H NMR and ¹³C NMR data are in agreement with the reference 79.

2,3,4-tri-*O*-acetyl- β -L-arabinopyranosyl bromide **3.26**⁸⁰



Tetraacetyl arabinose **3.23** (2.0 g, 6.3 mmol) was dissolved at ambient temperature in 20.0 mL HBr (33% in AcOH). Acetic anhydride (3.0 mL) was added and the reaction was stirred at ambient temperature overnight. The reaction mixture was poured onto ice, extracted with DCM, washed with a.q. NaHCO₃, dried over Na₂SO₄, concentrated under reduced pressure and recrystallized from Et₂O/hexane to afford the product as white solid (1.5 g, yield 70%). Mp = 121.4°C; [α]_D²⁰ 54.2 (*c*, 0.02 in CH₃OH); FT-IR: $\nu_{\max}/\text{cm}^{-1}$ 1732, 1368, 1208, 1065, 928, 685; ¹H NMR (400 MHz, CDCl₃) δ 6.63 (1H, d, *J* = 3.82 Hz, *CH*), 5.35–5.31 (2H, m, 2×*CH*), 5.04–4.99 (1H, m, *CH*), 4.16–3.85 (2H, m, *CH*₂), 2.09 (3H, s, OAc), 2.04 (3H, s, OAc), 1.96 (3H, s, OAc); ¹³C NMR (100 MHz, CDCl₃) δ 170.0, 169.8, 89.7, 67.9, 67.8, 67.6, 64.7, 20.8, the obtained melting point, optical rotation, FTIR, ¹H NMR and ¹³C NMR data are in agreement with the reference 80.

2,3,4-tri-*O*-acetyl- α -L-fucopyranosyl bromide **3.27**⁸¹



To a stirred solution of tetra-*O*-acetyl- α -L-fucopyranose **3.24** (1.4 g, 7.1 mmol) dissolved in 10.0 mL glacial acetic acid, 15.0 mL of HBr (33% wt. in acetic acid) was added at 22°C. Stirring was continued for 20 min and then the mixture was dissolved in 100.0 mL DCM, washed with ice water and aq. NaHCO₃, dried over Na₂SO₄ and concentrated at 25°C to afford the product as pale yellow syrup (1.3 g, yield 93%). [α]_D²⁰ -36.2 (*c*, 0.004 in CH₃OH); FT-IR: $\nu_{\max}/\text{cm}^{-1}$ 1743, 1369, 1211, 1074, 912; ¹H NMR (400 MHz, CDCl₃) δ 6.63 (d, *J* = 3.92 Hz, 1H, *CH*), 5.36–5.23 (m, 2H, 2×*CH*), 4.98–4.94 (m, 1H, *CH*), 4.37–4.31 (m, 1H, *CH*), 2.10 (s, 3H, OAc), 2.03 (s, 3H, OAc), 1.94 (s, 3H, OAc), 1.15 (d, *J* = 6.65 Hz, 3H, *CH*₃); ¹³C NMR (100 MHz,

propargyl bromide in toluene (0.4 mL, 2.5 mmol, 2.0 equiv.) was added drop-wise and the resulting solution was then stirred at room temperature for 16 hours. The reaction was carefully quenched by the drop-wise addition of ethanol. The solution was extracted into diethyl ether (20.0 mL) and washed with water (10.0 mL). The aqueous layer was then back-extracted with diethyl ether (20.0 mL) and the organic fractions combined. The combined organic layer was washed with brine, dried over Na₂SO₄ and evaporated to a deep red oil, which was purified by flash silica chromatography (ethyl acetate/petroleum ether 40–60, 1:4 v/v) to give the product as a pale brown solid (0.4 g, 76% yield). Mp = 46.2°C; ¹H NMR (400 MHz, CDCl₃) δ 7.8 (d, *J* = 8.0 Hz, 2H), 7.7 (d, *J* = 8.0 Hz, 2H), 7.23 (d, *J* = 8.4 Hz, 2H), 6.95 (d, *J* = 9.2 Hz, 2H), 4.16–4.13 (m, 2H), 3.84–3.82 (m, 2H), 3.71–3.62 (m, 4H), 2.61 (t, *J* = 7.6 Hz, 1H), 2.35 (t, *J* = 2.4 Hz, 1H), 1.61–1.53 (m, 1H), 1.36–1.26 (m, 1H), 0.9 (t, *J* = 7.2 Hz, 2H); ¹³C NMR (100 MHz, CDCl₃) 161.1, 151.0, 147.2, 145.8, 70.93, 70.72, 70.52, 69.69, 67.76, 58.46, 35.59, 33.51, 22.40, 14.01. LC-MS: *m/z* 425.3 [*M* + H]⁺, 444.1 [*M* + Na]⁺, ESI-HRMS calculated for C₂₅H₃₃N₂O₄ 425.2440 [*M* + H]⁺, found 425.2438 [*M* + H]⁺.

3.5 References

1. Hoffman, S. J.; Behdinan, A., Towards an international treaty on antimicrobial resistance. *Ottawa L. Rev.*, **2016**, *47* (2), 507–538.
2. Leung, E.; Weil, D. E.; Raviglione, M.; Nakatani, H., The WHO policy package to combat antimicrobial resistance. *Bull. World Health Organ.*, **2011**, *89* (5), 390–392.
3. Costerton, J. W.; Stewart, P. S.; Greenberg, E., Bacterial biofilms: a common cause of persistent infections. *Science*, **1999**, *284* (5418), 1318–1322.
4. Guttenplan, S. B.; Kearns, D. B., Regulation of flagellar motility during biofilm formation. *FEMS Microbiol. Rev.*, **2013**, *37* (6), 849–871.
5. Ceri, H.; Olson, M.; Stremick, C.; Read, R.; Morck, D.; Buret, A., The Calgary biofilm device: new technology for rapid determination of antibiotic susceptibilities of bacterial biofilms. *J. Clin. Microbiol.*, **1999**, *37* (6), 1771–1776.
6. Brown, M. R.; Allison, D. G.; Gilbert, P., Resistance of bacterial biofilms to antibiotics a growth-rate related effect? *J. Antimicrob. Chemother.*, **1988**, *22* (6), 777–780.

7. Kaplan, J. á., Biofilm dispersal: mechanisms, clinical implications, and potential therapeutic uses. *J. Dent. Res.*, **2010**, *89* (3), 205–218.
8. O'Toole, G. A.; Kolter, R., Flagellar and twitching motility are necessary for *Pseudomonas aeruginosa* biofilm development. *Mol. Microbiol.*, **1998**, *30* (2), 295–304.
9. Harshey, R. M., Bacterial motility on a surface: many ways to a common goal. *Annu. Rev. Microbiol.*, **2003**, *57* (1), 249–273.
10. Kearns, D. B., A field guide to bacterial swarming motility. *Nature Rev. Microbiol.*, **2010**, *8* (9), 634–644.
11. Briandet, R.; Herry, J. M.; Bellon-Fontaine, M. N., Determination of the van der Waals, electron donor and electron acceptor surface tension components of static Gram-positive microbial biofilms. *Colloids Surf., B*, **2001**, *21* (4), 299–310.
12. Takahashi, H.; Suda, T.; Tanaka, Y.; Kimura, B., Cellular hydrophobicity of *Listeria monocytogenes* involves initial attachment and biofilm formation on the surface of polyvinyl chloride. *Lett. Appl. Microbiol.*, **2010**, *50* (6), 618–625.
13. Dirckx, P. Biofilm formation in 3 steps. <http://www.biofilm.montana.edu/multimedia/images/index.html> (accessed 15th of March).
14. Fux, C.; Costerton, J.; Stewart, P.; Stoodley, P., Survival strategies of infectious biofilms. *Trends Microbiol.*, **2005**, *13* (1), 34–40.
15. Hornef, M. W.; Wick, M. J.; Rhen, M.; Normark, S., Bacterial strategies for overcoming host innate and adaptive immune responses. *Nat. Immunol.*, **2002**, *3* (11), 1033–1040.
16. Hall-Stoodley, L.; Costerton, J. W.; Stoodley, P., Bacterial biofilms: from the natural environment to infectious diseases. *Nature Rev. Microbiol.*, **2004**, *2* (2), 95–108.
17. Mulligan, C. N., Environmental applications for biosurfactants. *Environ. Pollut.*, **2005**, *133* (2), 183–198.
18. Rodrigues, L.; Banat, I. M.; Teixeira, J.; Oliveira, R., Biosurfactants: potential applications in medicine. *J. Antimicrob. Chemother.*, **2006**, *57* (4), 609–618.
19. Sharma, D.; Saharan, B. S.; Kapil, S., Applications of biosurfactants. In *Biosurfactants of Lactic Acid Bacteria*, Springer: 2016; pp 73–82.

20. Satpute, S.; Banpurkar, A.; Banat, I.; Sangshetti, J.; Patil, R.; Gade, W., Multiple roles of biosurfactants in biofilms. *Curr. Pharm. Des.*, **2016**, *22* (11), 1429–1448.
21. de Jesus Cortes-Sanchez, A.; Hernandez-Sanchez, H.; Jaramillo-Flores, M. E., Biological activity of glycolipids produced by microorganisms: new trends and possible therapeutic alternatives. *Microbiol. Res.*, **2013**, *168* (1), 22–32.
22. Monteiro, S. A.; Sasaki, G. L.; de Souza, L. M.; Meira, J. A.; de Araújo, J. M.; Mitchell, D. A.; Ramos, L. P.; Krieger, N., Molecular and structural characterization of the biosurfactant produced by *Pseudomonas aeruginosa* DAUPE 614. *Chem. Phys. Lipids*, **2007**, *147* (1), 1–13.
23. Tuleva, B.; Christova, N.; Cohen, R.; Antonova, D.; Todorov, T.; Stoineva, I., Isolation and characterization of trehalose tetraester biosurfactants from a soil strain *Micrococcus luteus* BN56. *Process Biochem.*, **2009**, *44* (2), 135–141.
24. Sudo, T.; Zhao, X.; Wakamatsu, Y.; Shibahara, M.; Nomura, N.; Nakahara, T.; Suzuki, A.; Kobayashi, Y.; Jin, C.; Murata, T., Induction of the differentiation of human HL-60 promyelocytic leukemia cell line by succinoyl trehalose lipids. *Cytotechnology*, **2000**, *33* (1–3), 259–264.
25. Kitamoto, D.; Isoda, H.; Nakahara, T., Functions and potential applications of glycolipid biosurfactants—from energy-saving materials to gene delivery carriers. *J Biosci. Bioeng.*, **2002**, *94* (3), 187–201.
26. Chen, J.; Song, X.; Zhang, H.; Qu, Y., Production, structure elucidation and anticancer properties of sophorolipid from *Wickerhamiella domercqiae*. *Enzyme Microb. Technol.*, **2006**, *39* (3), 501–506.
27. Chen, J.; Song, X.; Zhang, H.; Qu, Y.; Miao, J., Sophorolipid produced from the new yeast strain *Wickerhamiella domercqiae* induces apoptosis in H7402 human liver cancer cells. *Appl. Microbiol. Biotechnol.*, **2006**, *72* (1), 52–59.
28. Hewald, S.; Linne, U.; Scherer, M.; Marahiel, M. A.; Kämper, J.; Bölker, M., Identification of a gene cluster for biosynthesis of mannosylerythritol lipids in the basidiomycetous fungus *Ustilago maydis*. *Appl. Environ. Microbiol.*, **2006**, *72* (8), 5469–5477.
29. Desai, J. D.; Banat, I. M., Microbial production of surfactants and their commercial potential. *Microbiol. Mol. Biol. Revs.*, **1997**, *61* (1), 47–64.

30. Kulakovskaya, T.; Shashkov, A.; Kulakovskaya, E.; Golubev, W.; Zinin, A.; Tsvetkov, Y.; Grachev, A.; Nifantiev, N., Extracellular cellobiose lipid from yeast and their analogues: structures and fungicidal activities. *J. Oleo Sci.*, **2009**, *58* (3), 133–140.
31. Saravanakumari, P.; Mani, K., Structural characterization of a novel xylolipid biosurfactant from *Lactococcus lactis* and analysis of antibacterial activity against multi-drug resistant pathogens. *Bioresour. Technol.*, **2010**, *101* (22), 8851–8854.
32. Vollbrecht, E.; Rau, U.; Lang, S., Microbial conversion of vegetable oils into surface active di-, tri-, and tetrasaccharide lipids (biosurfactants) by the bacterial strain *Tsukamurella spec.* *Lipid/Fett*, **1999**, *101* (10), 389–394.
33. De Araujo, L. V.; Abreu, F.; Lins, U.; Santa Anna, L. M. d. M.; Nitschke, M.; Freire, D. M. G., Rhamnolipid and surfactin inhibit *Listeria monocytogenes* adhesion. *Food Res. Int.*, **2011**, *44* (1), 481–488.
34. Luna, J. M.; Rufino, R. D.; Sarubbo, L. A.; Rodrigues, L. R.; Teixeira, J. A.; de Campos-Takaki, G. M., Evaluation antimicrobial and antiadhesive properties of the biosurfactant Lunasan produced by *Candida sphaerica* UCP 0995. *Curr. Microbiol.*, **2011**, *62* (5), 1527–1534.
35. Rufino, R.; Luna, J.; Sarubbo, L.; Rodrigues, L.; Teixeira, J.; Campos-Takaki, G., Antimicrobial and anti-adhesive potential of a biosurfactant Rufisan produced by *Candida lipolytica* UCP 0988. *Colloids Surf., B*, **2011**, *84* (1), 1–5.
36. Dusane, D. H.; Pawar, V. S.; Nancharaiyah, Y.; Venugopalan, V.; Kumar, A. R.; Zinjarde, S. S., Anti-biofilm potential of a glycolipid surfactant produced by a tropical marine strain of *Serratia marcescens*. *Biofouling*, **2011**, *27* (6), 645–654.
37. Dane, E. L.; Ballok, A. E.; O'Toole, G. A.; Grinstaff, M. W., Synthesis of bioinspired carbohydrate amphiphiles that promote and inhibit biofilms. *Chem. Sci.*, **2014**, *5* (2), 551–557.
38. Chaveriat, L.; Gosselin, I.; Machut, C.; Martin, P., Synthesis, surface tension properties and antibacterial activities of amphiphilic D-galactopyranose derivatives. *Eur. J. Med. Chem.*, **2013**, *62*, 177–186.
39. Srinivas, O.; Mitra, N.; Surolia, A.; Jayaraman, N., Photoswitchable cluster glycosides as tools to probe carbohydrate-protein interactions: synthesis and lectin-binding studies of azobenzene containing multivalent sugar ligands. *Glycobiology*, **2005**, *15* (9), 861–873.

40. Velema, W. A.; van der Berg, J. P.; Hansen, M. J.; Szymanski, W.; Driessen, A. J.; Feringa, B. L., Optical control of antibacterial activity. *Nat. Chem.*, **2013**, *5* (11), 924–928.
41. Weber, T.; Chandrasekaran, V.; Stamer, I.; Thygesen, M. B.; Terfort, A.; Lindhorst, T. K., Switching of bacterial adhesion to a glycosylated surface by reversible reorientation of the carbohydrate ligand. *Angew. Chem. Int. Ed.*, **2014**, *53* (52), 14583–14586.
42. R. F. Tabor, M. J. P., C. J. Garvey, B. L. Wilkinson, Light-induced structural evolution of photoswitchable carbohydrate-based surfactant micelles. *Chem. Comm.*, **2015**, *51* (25), 5509–5512.
43. Eastoe, J.; Vesperinas, A., Self-assembly of light-sensitive surfactants. *Soft Matter*, **2005**, *1* (5), 338–347.
44. Wang, Y.; Ma, N.; Wang, Z.; Zhang, X., Photocontrolled reversible supramolecular assemblies of an azobenzene-containing surfactant with α -cyclodextrin. *Angew. Chem. Int. Ed.*, **2007**, *46* (16), 2823–2826.
45. Robyt, J. F., General properties, occurrence, and preparation of carbohydrates. In *Glycoscience*, Springer: 2008; pp 57–99.
46. Wilkinson, B. L.; Bornaghi, L. F.; Poulsen, S.-A.; Houston, T. A., Synthetic utility of glycosyl triazoles in carbohydrate chemistry. *Tetrahedron*, **2006**, *62* (34), 8115–8125.
47. Li, T.; Guo, L.; Zhang, Y.; Wang, J.; Li, Z.; Lin, L.; Zhang, Z.; Li, L.; Lin, J.; Zhao, W., Design and synthesis of *O*-GlcNAcase inhibitors via ‘click chemistry’ and biological evaluations. *Carbohydr. Res.*, **2011**, *346* (9), 1083–1092.
48. Berry, J. D.; Neeson, M. J.; Dagastine, R. R.; Chan, D. Y.; Tabor, R. F., Measurement of surface and interfacial tension using pendant drop tensiometry. *J. Colloid Interface Sci.*, **2015**, *454*, 226–237.
49. Hamon, F.; Djedaini-Pilard, F.; Barbot, F.; Len, C., Azobenzenes—synthesis and carbohydrate applications. *Tetrahedron*, **2009**, *65* (49), 10105–10123.
50. Romsted, L. S., Introduction to surfactant self-assembly. In *Supramolecular chemistry: from molecules to nanomaterials*, John Wiley & Sons, Ltd: 2012; pp 1–23.

51. Tabor, R. F.; Tan, D. D.; Han, S. S.; Young, S. A.; Seeger, Z. L.; Pottage, M. J.; Garvey, C. J.; Wilkinson, B. L., Reversible pH- and photocontrollable carbohydrate-based surfactants. *Chem. Eur. J.*, **2014**, *20* (43), 13881–13884.
52. Shang, T.; Smith, K. A.; Hatton, T. A., Self-assembly of a nonionic photoresponsive surfactant under varying irradiation conditions: a small-angle neutron scattering and cryo-TEM study. *Langmuir*, **2006**, *22* (4), 1436–1442.
53. Johnson, J.; Saboungi, M. L.; Thiyagarajan, P.; Csencsits, R.; Meisel, D., Selenium nanoparticles: a small-angle neutron scattering study. *J. Phys. Chem. B*, **1999**, *103* (1), 59–63.
54. Lee Jr, C. T.; Smith, K. A.; Hatton, T. A., Small-angle neutron scattering study of the micellization of photosensitive surfactants in solution and in the presence of a hydrophobically modified polyelectrolyte. *Langmuir*, **2009**, *25* (24), 13784–13794.
55. Chen, S. H., Small angle neutron scattering studies of the structure and interaction in micellar and microemulsion systems. *Annu. Rev. Phys. Chem.*, **1986**, *37* (1), 351–399.
56. Lianos, P.; Zana, R., Fluorescence probe studies of the effect of concentration on the state of aggregation of surfactants in aqueous solution. *J. Colloid Interface Sci.*, **1981**, *84* (1), 100–107.
57. Viscardi, G.; Quagliotto, P.; Barolo, C.; Savarino, P.; Barni, E.; Fisticaro, E., Synthesis and surface and antimicrobial properties of novel cationic surfactants. *J. Org. Chem.*, **2000**, *65* (24), 8197–8203.
58. Chevallier, E.; Mamane, A.; Stone, H.; Tribet, C.; Lequeux, F.; Monteux, C., Pumping-out photo-surfactants from an air-water interface using light. *Soft Matter*, **2011**, *7* (17), 7866–7874.
59. Jorgensen, J.; Doern, G.; Maher, L. A.; Howell, A.; Redding, J., Antimicrobial resistance among respiratory isolates of *Haemophilus influenzae*, *Moraxella catarrhalis*, and *Streptococcus pneumoniae* in the United States. *Antimicrob. Agents Chemother.*, **1990**, *34* (11), 2075–2080.
60. Paulus, W., Relationship between chemical structure and activity or mode of action of microbicides. In *Directory of microbicides for the protection of materials*, Springer: 2004; pp 9–25.

61. Campbell, J., High-throughput assessment of bacterial growth inhibition by optical density measurements. *Curr. Protoc. Chem. Biol.*, **2010**, 195–208.
62. Abdel-Mawgoud, A. M.; Lépine, F.; Déziel, E., Rhamnolipids: diversity of structures, microbial origins and roles. *Appl. Microbiol. Biot.*, **2010**, *86* (5), 1323–1336.
63. Pamp, S. J.; Tolker-Nielsen, T., Multiple roles of biosurfactants in structural biofilm development by *Pseudomonas aeruginosa*. *J. Bacteriol.*, **2007**, *189* (6), 2531–2539.
64. Caiazza, N. C.; Shanks, R. M.; O'Toole, G., Rhamnolipids modulate swarming motility patterns of *Pseudomonas aeruginosa*. *J. Bacteriol.*, **2005**, *187* (21), 7351–7361.
65. Cerca, N.; Jefferson, K. K., Effect of growth conditions on poly-*N*-acetylglucosamine expression and biofilm formation in *Escherichia coli*. *FEMS Microbiol. Lett.*, **2008**, *283* (1), 36–41.
66. Kropec, A.; Maira-Litran, T.; Jefferson, K. K.; Grout, M.; Cramton, S. E.; Götz, F.; Goldmann, D. A.; Pier, G. B., Poly-*N*-acetylglucosamine production in *Staphylococcus aureus* is essential for virulence in murine models of systemic infection. *Infect. Immun.*, **2005**, *73* (10), 6868–6876.
67. Bjarnsholt, T., The role of bacterial biofilms in chronic infections. *Apmis*, **2013**, *121* (136), 1–58.
68. O'Toole, G. A., Microtiter dish biofilm formation assay. *J. Vis. Exp.*, **2011**, *30* (47), e2437–e2437.
69. Lister, J. L.; Horswill, A. R., *Staphylococcus aureus* biofilms: recent developments in biofilm dispersal. *Front. Cell. Infect. Microbiol.*, **2014**, *4* (178), 1–9.
70. Wilson, L. G.; Martinez, V. A.; Schwarz-Linek, J.; Tailleur, J.; Bryant, G.; Pusey, P.; Poon, W. C., Differential dynamic microscopy of bacterial motility. *Phys. Rev. Lett.*, **2011**, *106* (1), 1–4.
71. Martinez, V. A.; Besseling, R.; Croze, O. A.; Tailleur, J.; Reufer, M.; Schwarz-Linek, J.; Wilson, L. G.; Bees, M. A.; Poon, W. C., Differential dynamic microscopy: a high-throughput method for characterizing the motility of microorganisms. *Biophys. J.*, **2012**, *103* (8), 1637–1647.

72. Verstraeten, N.; Braeken, K.; Debkumari, B.; Fauvart, M.; Fransaer, J.; Vermant, J.; Michiels, J., Living on a surface: swarming and biofilm formation. *Trends Microbiol.*, **2008**, *16* (10), 496–496.
73. Guimer, A.; Fournet, G., Small angle scattering of X-rays. *J. Wiley & Sons, New York*, **1955**.
74. Feigin, L.; Svergun, D., Structure Analysis by Small-Angle X-Ray and Neutron Scattering 1987. Plenum Press, New York.
75. Sabesan, S.; Neira, S., Synthesis of glycosyl phosphates and azides. *Carbohydr. Res.*, **1992**, *223*, 169–185.
76. Mugunthan, G.; Ravindranathan Kartha, K., Application of ball milling technology to carbohydrate reactions-II. Solvent-free mechanochemical synthesis of glycosyl azides. *J. Carbohydr. Chem.*, **2008**, *27* (5), 294–299.
77. Bonache, M. A.; Nuti, F.; Isaad, A. L. C.; Real-Fernández, F.; Chelli, M.; Rovero, P.; Papini, A. M., Synthesis of new ribosylated Asn building blocks as useful tools for glycopeptide and glycoprotein synthesis. *Tetrahedron Lett.*, **2009**, *50* (28), 4151–4153.
78. Geng, J.; Lindqvist, J.; Mantovani, G.; Chen, G.; Sayers, C. T.; Clarkson, G. J.; Haddleton, D. M., Well-defined poly (*N*-glycosyl 1, 2, 3-triazole) multivalent ligands: design, synthesis and lectin binding studies. *Qsar Comb. Sci.*, **2007**, *26* (11–12), 1220–1228.
79. Jakobsche, C. E.; Parker, C. G.; Tao, R. N.; Kolesnikova, M. D.; Douglass Jr, E. F.; Spiegel, D. A., Exploring binding and effector functions of natural human antibodies using synthetic immunomodulators. *ACS Chem. Biol.*, **2013**, *8* (11), 2404–2411.
80. Alcaro, S.; Arena, A.; Neri, S.; Ottana, R.; Ortuso, F.; Pavone, B.; Vigorita, M., Design and synthesis of DNA-intercalating 9-fluoren- β -*O*-glycosides as potential IFN-inducers, and antiviral and cytostatic agents. *Bioorg. Med. Chem.*, **2004**, *12* (7), 1781–1791.
81. Nunez, H. A.; O'Connor, J. V.; Rosevear, P. R.; Barker, R., The synthesis and characterization of α - and β -L-fucopyranosyl phosphates and GDP fucose. *Can. J. Chem.*, **1981**, *59* (14), 2086–2095.
82. Gao, M.; Chen, Y.; Tan, S.; Reibenspies, J. H.; Zingaro, R. A., Syntheses of 1-thio-D-xylose and D-ribose esters of diorganoarsinous acids and their anticancer activity. *Heteroatom Chem.*, **2008**, *19* (2), 199–206.

Chapter 4

Photoswitchable Janus glycodendrimer Micelles as Multivalent Inhibitors of LecA and LecB from Pseudomonas aeruginosa

This page is intentionally blank

Monash University

Declaration for Thesis Chapter 4

Declaration by candidate

In the case of Chapter 4, the nature and extent of my contribution to this work was as following:

Nature of contribution	Extent of contribution (%)
Synthesis and (physical) characterization of product, analysis of results, writing up	85

The following co-authors contributed to the work. If co-authors are students, the extent of their contribution in percentage terms was stated:

Name	Nature of contribution	Extent of contribution (%) for student co-workers only
Ghamdan Beshr	Lectin binding assays, analysis of results	15
Christopher J. Garvey Rico F. Tabor Alexander Titz Brendan L. Wilkinson	Initiation and key ideas	

The undersigned hereby certify that the above declaration correctly reflects the nature and extent of the candidate's and co-authors' contributions to this work.

**Candidate's
Signature**



Date

12 June 2017

**Main
Supervisor's
Signature**



Date

13th June 2017

This page is intentionally blank

Preface to Chapter 4

This chapter is presented in the original manuscript format, submitted to *Colloids and Surfaces B: Biointerfaces*.

In this chapter, we describe the synthesis, physical characterization and lectin binding activity of a library of 12 photoswitchable Janus glycodendrimers. Amphiphilic ‘Janus’ glycodendrimers were designed to incorporate a range of hydrophilic carbohydrate head groups as recognition motifs for lectin binding and hydrophobic alkyl chain groups appended to a photoswitchable azobenzene core. These novel glycodendrimers were shown to undergo supramolecular self-assembly into cylindrical micelles in water and were shown to possess low polydispersity indices, as determined by small angle neutron scattering (SANS) and dynamic light scattering (DLS). Aggregates were also shown to be moderate-to-potent, multivalent inhibitors of soluble lectins LecA and LecB from *Pseudomonas aeruginosa*.

This page is intentionally blank

Photoswitchable Janus Glycodendrimer Micelles as Multivalent Inhibitors of LecA and LecB from *Pseudomonas aeruginosa*.

Yingxue Hu,^a Ghamdan Beshr,^b Christopher J. Garvey,^c Rico F. Tabor,^a
Alexander Titz,^b and Brendan L. Wilkinson*^d

- a) School of Chemistry, Monash University, Victoria 3800, Australia.
- b) Chemical Biology of Carbohydrates, Helmholtz Institute for Pharmaceutical Research Saarland (HIPS), D-66123 Saarbrücken, Germany, and Deutsches Zentrum für Infektionsforschung, Standort Hannover-Braunschweig.
- c) Australian Centre for Neutron scattering, ANSTO, Lucas Heights, New South Wales 2234, Australia.
- d) School of Science and Technology, the University of New England, New South Wales 2351, Australia.

Abstract The first example of the self-assembly and lectin binding properties of photoswitchable glycodendrimer micelles is reported. Light-addressable micelles were assembled from a library of 12 amphiphilic Janus glycodendrimers composed of variable carbohydrate head groups and hydrophobic tail groups linked to an azobenzene core. Spontaneous association in water gave cylindrical micelles with uniform size distribution as determined by dynamic light scattering (DLS) and small angle neutron scattering (SANS). *Trans-cis* photoisomerization of the azobenzene dendrimer core was used to probe the self-assembly behaviour and lectin binding properties of cylindrical micelles, revealing moderate-to-potent inhibition of lectins LecA and LecB from *Pseudomonas aeruginosa*.

Keywords: Janus glycodendrimer, lectin inhibitors, photoswitchable amphiphiles.

1. Introduction

Non-covalent carbohydrate-protein binding interactions mediate myriad biological processes, yet the binding affinity of individual interactions are often very weak in highly competitive aqueous environments (disassociation constants ranging from 10^{-3} to 10^{-4} M).¹ Nature overcomes this intrinsic limitation through the simultaneous binding of clustered, multivalent glycans expressed on cellular surfaces to their cognate receptors, or lectins. The so-called ‘multivalent’ or ‘glycoside cluster’ effect results in several-fold enhancement in binding avidity, with energies that are greater than the sum of individual interactions.² The development of multivalent mimics of natural glycans has been actively pursued as inhibitors of carbohydrate-protein binding events, which function as structural probes for understanding cellular signalling and physiology or as therapeutic agents with potential anti-microbial, anti-inflammatory and anti-tumour properties.³ Conventional approaches toward this goal involve the elaboration of multivalent scaffolds with carbohydrate epitopes to yield nanoscale structures including glycodendrimers,⁴ glycopeptides,⁵ glycopolymers,⁶ glycodynamers,⁷ fullerenes⁸ and calixerenes, etc.⁹ In some cases, potent binding affinity and selectivity has been achieved through careful ligand design resulting in favourable ligand preorganization, however such molecular systems offer limited modes of spatial presentation due to the underlying rigid scaffold and suffer drawbacks associated with complex multistep synthesis and purification.¹⁰ An alternative and promising approach towards multivalent glycan presentation involves the spontaneous association of glycoamphiphiles in water to provide self-assembled, soft materials including liposomes and micelles.¹⁰⁻¹² Recently, Percec and co-workers have demonstrated the self-assembly of glycodendrimer vesicles and micelles as biomimetic platforms for multivalent carbohydrate presentation.¹¹ Such materials offer several advantages over rigid molecular assemblies, including ease of molecular synthesis of the monomer and the ability to program ligand density and valency of the self-assembled structure through appropriate molecular design. With this in mind, we were interested in exploring the application of light-addressable self-assembled multivalent systems as inhibitors lectin-carbohydrate binding interactions. We postulated that the incorporation photoswitchable units within a micelle core or vesicle bilayer would enable spatiotemporal control over aggregate morphology and hence ligand topology (e.g. carbohydrate-carbohydrate distance) as a strategy tuning lectin binding avidity. Such responsive tools could also offer new opportunities for the development of light-addressable multivalent tools for dissecting the subtle geometric requirements for lectin-carbohydrate recognition.

Reversible *trans-cis* photoisomerization of the well-characterized azobenzene chromophore has been widely exploited for controlling the conformational dynamics of biomolecules,¹³ including the three-dimensional arrangement of multivalent carbohydrates on cluster glycosides,¹⁴ cyclodextrin bilayer vesicles,¹⁵ polymers¹⁶ and self-assembled monolayers.¹⁷ Our group has recently reported the photomodulation of bacterial biofilm formation using a library of carbohydrate-based surfactants.¹⁸ Optical control over bacterial growth and biofilm formation in drug-resistant Gram-positive and Gram-negative bacteria was shown to be highly sensitive to the carbohydrate head group and isomeric state of the azobenzene tail group. Based on these observations, we decided to explore the application of amphiphilic, azobenzene functionalized glycodendrimers capable undergoing self-assembly to derive light-addressable, nanoscale structures for probing lectin binding. Herein we report the modular synthesis of a library of 12 amphiphilic ‘Janus’ glycodendrimers as photoswitchable inhibitors of soluble lectins LecA and LecB from *Pseudomonas aeruginosa*, an opportunistic pathogen known to cause serious biofilm-related illnesses.¹⁹ Glycodendrimers underwent spontaneous association in water to give light-responsive cylindrical micelles, as revealed from dynamic light scattering (DLS) and small angle neutron scattering (SANS) data. Micelle structures could be tuned through UV light irradiation, thus underscoring their potential application as addressable antimicrobial agents and tools for studying carbohydrate–protein interactions.

2. Materials and Methods

2.1 General methods

Analytical thin layer chromatography (TLC) was performed on commercially prepared silica plates (Merck Kieselgel 60 0.25 mm F254). Flash column chromatography was performed using 230-400 mesh Kieselgel 60 silica eluting with distilled solvents as described. Solvents and reagents were purchased from Sigma-Aldrich and Merck and used without further purification. ¹H NMR and ¹³C NMR spectra were recorded on a Bruker Avance 400 NMR spectrometer at frequencies of 400 MHz and 100 MHz respectively. Chemical shift is reported as parts per million (ppm) downfield shift to the TMS internal standard. The data are reported as chemical shift (δ), multiplicity, relative integral, coupling constant ($J = \text{Hz}$) and assignment where possible. IR spectra were recorded on a Bruker ATR spectrometer. Optical rotation was measured on an Optical Activity Polaer 2001 (546 nm) polarimeter using a 1 mL cell. LCMS was performed on an Agilent Infinity 1260 HPLC coupled to an Agilent 6120B mass spectrometer. Separations were performed on an Agilent Poroshel 120 high resolution column.

Preparative HPLC was performed on an Agilent Zorbax 300SB C3 column (20 mm ID x 150 mm) using a linear gradient of 8:1:1 water/AcN/*i*-PrOH (Solvent A) and 1:1 AcN/ *i*-PrOH (Solvent B) as the mobile phase. Separations were performed using a linear gradient of 10% solvent B to 100% solvent B over 30 minutes, operating at a flow rate of 10 mL/min.

2.2 UV-Vis spectroscopy

The native *trans* isomers of carbohydrate surfactants were converted into *cis* states by illumination of their aqueous solutions under ambient conditions using a UV lamp with λ_{max} at 361 nm in a time-dependant manner (1–30 min). Five minutes of photoexcitation was found sufficient to convert *trans* isomers into *cis* state. All the studies involving *cis* isomers were obtained after 10 min of illumination with $\lambda_{361\text{nm}}$. Since many biological processes occur at 37 °C, the thermal stability of both the native *trans* isomer as well as the photoinduced *cis* isomer was studied at ambient temperature (20 °C) and 37 °C using UV-visible spectroscopy. Azobenzene *trans-cis* photoisomerisation was found to be complete within 5 minute of UV irradiation. The native *trans* isomers remained stable under ambient lighting conditions at least up to 24 h, as evident from insignificant changes in their UV-vis absorbance spectra over this period. The thermal relaxation studies were performed at ambient temperature and 37 °C for 24 h in Milli-Q water. The half-lives of the *cis* isomers in Milli-Q water at different temperatures were estimated from thermal relaxation studies by plotting the ratios of peak area under 325 nm peak and that under 440 nm peak over a period of 24 h (Figure S1 and Figure S2). These peaks were chosen as *cis-trans* relaxation results in increase in peak intensity at ~325 nm, with a corresponding decrease in peak intensity at 440 nm.

2.3 Determination of CAC

The critical aggregation concentration was determined using Nile red encapsulation assay.²⁰ A 1 mg mL⁻¹ Nile Red stock solution was prepared in chloroform. A glycodendrimer stock solution was made up in Milli-Q water at various concentrations depending on the starting concentration for the assay. Encapsulation samples were made by adding 10 μ L Nile red into 4 mL glycodendrimer solution. The fluorescence emission was measured on an Agilent Technology Cary Eclipse fluorescence spectrophotometer using an excitation wavelength of 550 nm. Signals were recorded between 570–700 nm with 5 nm excitation/emission slit. To investigate the relationship between conformational exchanges and the concentration of

glycodendrimers, the UV-vis spectra of representative glycodendrimer 1–4 were measured at concentrations related to their CAC values (Figure S8).

2.4 Dynamic light scattering (DLS)

DLS was performed with a Brookhaven NanoBrook Omni instrument. Instrument parameters were determined automatically along with the measurement times. Experiments were performed five times independently. The glycodendrimer was dissolved in Milli-Q water at 0.1 mM concentration and DLS experiments were measured at 20°C. Samples were irradiated with UV light at 361 nm for 10 min before measuring DLS for compounds at *cis*-dominated PSS.

2.5 Small angle neutron scattering (SANS)

SANS measurements were made on the Quokka instrument at the Bragg Institute, ANSTO, Lucas Heights NSW, Australia. For all samples, raw scattering counts were collected on a 128×128 element area detector, where the sample–detector distances used were 2 m and 14 m, with no detector offset. An incident neutron wavelength of 5 Å was used with a typical spread of 10%, thus giving an effective q range of 0.004–0.4 Å⁻¹. Samples were prepared in circular 12.5 mm Hellma quartz cells with a path length of 2 mm, and a thermostatically-controlled automatic sample changer ensured that a temperature of 25 ± 0.05°C was maintained. Data were converted from raw counts at the detector into 1D scattering spectra by first subtracting the scattering from an empty cell and then radially averaging the resulting spectrum, normalising for the measured sample transmission. A D₂O background was then subtracted from the final 1D sample data to ensure that the scattering signals seen are from the surfactant only. Model fitting was performed using SasView software, using standard equations for ellipsoidal and cylindrical form factors. Cylinders were modelled using the Guinier equation²¹ for the form factor $P(q,a)$:

$$P(q, a) = 2(\Delta\rho)V\sin(qL \cos\alpha/2)/(qL \cos\alpha/2) \frac{J_1(qr \sin\alpha)}{(qr \sin\alpha)}$$

where $\Delta\rho$ is the scattering length density difference between the scatter and the D₂O solvent, V is the volume of the cylinder, L is the length of the cylinder, α is the angle between the axis of the cylinder and the q -vector, J_1 is the first order Bessel function, r is the radius of the cylinder.

Aggregation number (N_{agg}) was calculated from the volume of the formed micelle divided by the volume of monomer obtained by calculating the molecular volume of the structural

components of the monomer from their bulk densities. The volumes (\AA^3) used were: triazole 96.2, triethylglycol 221.9, azobenzene 251.5, galactose 173.8, mannose 194.4, fucose 175.2, 2-bromoethanol 117.7, succinic anhydride 135.1, pae 161.5, 3,5-dihydrobenzoic acid 159.9, gallic acid 166.2, 1-bromooctane 286.8, 1-bromododecane 398.7, 2-ethylhexyl bromide 295.3.

2.6 Competitive binding assays to *LecA* or *LecB*

LecA or *LecB* were recombinantly produced in *E. coli* and purified by affinity chromatography as described.^{5b,22} Measurements for competitive binding with *LecA* and *LecB* were performed according to previously reported protocols.^{5b,22} A serial dilution of each tested compounds in TBS/Ca (1000 - 0.013 μM) was prepared twice in two different 96-well plates (Carl Roth GmbH, Germany, Item no. 9292.1). One of these plates was irradiated (with the plate put on an ice tray to prevent heating) for 30 min using a UV light source which was comprised of three 9 Watt halogen tubes, delivering a total power of 27 W at λ_{max} of 361 nm at the source (Nail gel curing lamp). After 30 min of irradiation, 10 μL of a serial dilution of each tested compounds from each plate were added in triplicates to one 384-well plate (Greiner Bio-One, Germany, cat no 781900). Afterward, 10 μL of either *LecA* or *LecB* and fluorescent galactose-based compound 9 from reference 5b or fucose-based compound 6 from reference 31 were added to each well at final concentrations of 20 μM for *LecA* and 150 nM for *LecB* and 10 nM for both fluorescent ligands. After incubation for 1 h (*LecA*) or 4 h (*LecB*) at r.t., blank corrected fluorescence intensity was recorded using a PheraStar FS microplate reader (BMG Labtech GmbH, Germany) with excitation filters at 485 nm and emission filters at 535 nm and fluorescence polarization was calculated. The data were analyzed using a four parameter fit of the MARS Data Analysis Software (BMG Labtech GmbH, Germany). A minimum of two independent measurements on two separate plates was performed for each compound before and after irradiation by UV lamp.

2.7 Synthesis

See supplementary information for NMR spectra and analytical data for new compounds.

General procedure 1 (Synthesis of **18–21**; **27–30**)^{11a}: Alcohol (1 equiv.), carboxylic acid (1 equiv.), DPTS (1 equiv.) and DCC (2.6 equiv.) were dissolved in dry DCM and stirred under N_2 for 12 hours. Then the reaction mixture was diluted with diethyl ether, filtered off the urea

and washed with diethyl ether. The filtrate was concentrated and purified by flash chromatography.

General procedure 2 (Synthesis of **22–25**): Aldehyde **18–21** (1 equiv.), pentaerythritol (1 equiv.) and *p*-toluenesulfonic acid (PTSA, 0.2 equiv.) were dissolved in DMF and stirred at 50°C under N₂ until TLC showed fully consumption of the starting materials. The crude mixture was concentrated under reduced pressure and purified by flash chromatography.

General procedure 3 (Synthesis of **1–12**)^{11a}: Into a solution of **27–30** (1 equiv.) in THF was added **31–33** (2.5 equiv.) in water, CuSO₄·5H₂O (0.61 equiv.) in water and sodium ascorbate (0.61 equiv.) in water successively under N₂. The reaction mixture was allowed to stir at room temperature for 36 hours. Then dilute with THF, filtered, concentrated and purified by flash chromatography (10-20% MeOH in DCM).

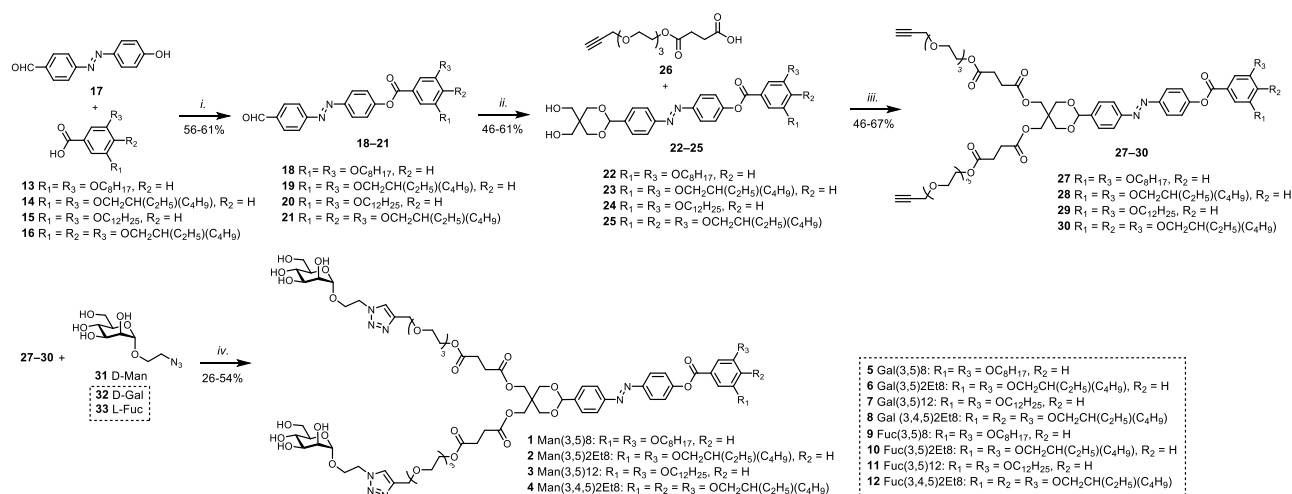
General procedure 4 (Synthesis of **13–16**)^{11a, 23}: A mixture of methyl benzoate (1 equiv.), bromoalkane (2–3 equiv.) and potassium carbonate (1.2 equiv.) in 15 mL DMF was heated at reflux at vigorous stirring for 4 hours. Then the hot reaction mixture was poured into ice-water, the precipitate was filtered and dried. Purification was employed as required by each compound, including recrystallization and flash chromatography. The purified methyl benzoate (1 equiv.), KOH (5 equiv.) and water-ethanol (1:6 v/v) were heated at 60°C for 2 hours. Then the reaction mixture was cooled to room temperature and concentrated HCL was added carefully until pH=1. Then the acidic solution was diluted with water, extracted with DCM and the combined organic phase was dried over Na₂SO₄, concentrated under reduced pressure to afford the final compound.

General procedure 5 (Synthesis of **31–33**)^{24–27} To a cooled solution of acetylated sugar (1 equiv.) and 2-bromoethanol (1.2 equiv.) in anhydrous DCM was added dropwise BF₃·Et₂O (4 equiv.). The ice-bath was removed after 1 hour and the reaction was continued at room temperature until the starting material has been consumed (monitored by TLC). The reaction mixture was poured into ice-water, the aqueous phase was extracted with DCM and the combined organic phase was then washed with water, saturated NaHCO₃, brine, dried over Na₂SO₄ and concentrated under reduced pressure. The synthesized intermediate compound (1 equiv.) and sodium azide (10 equiv.) were dissolved in anhydrous DMF and stirred at 70°C for 2 hours. The reaction mixture was cooled to room temperature, extracted with EtOAc, washed with water, dried over Na₂SO₄, concentrated under reduced pressure, purified by flash

chromatography and deacetylated under Zemplén conditions using catalytic sodium methoxide in methanol followed by neutralization with Amberlite IR120 acidic ion exchange resin.

3. Results and discussion

The synthesis of Janus glycodendrimers **1–12** is presented in Scheme 1. Glycodendrimers **1–12** were composed of variable monosaccharide head groups designed as recognition motifs for LecA and LecB, which show binding specificities to D-galactose and L-fucose or D-mannose, respectively.²⁸ To facilitate self-assembly in water, hydrophobic tail fragments bearing linear and branched alkyl tail groups (**13–16**) were introduced by modified Steglich esterification of the azobenzene core **17** using catalytic 4-(dimethylamino) *p*-toluenesulfonate (DPTS) to give hydrophobic precursors **18–21**.²⁹ Divergent elaboration of core fragments **18–21** was then carried out, firstly by acetalization of the aldehyde with pentaerythritol to give diols **22–25**, followed by esterification with carboxylic acid **26** to furnish the key alkyne scaffolds **27–30**. Finally, glycoconjugation of **27–30** was performed using the well-described copper(I)-catalysed azide-alkyne conjugation reaction (CuAAC) of the corresponding deprotected azidoethyl glycosides **31–33** to furnish glycodendrimers **1–12** (See supplementary information for details).³⁰



Scheme 1. Synthesis of photoswitchable Janus glycodendrimers **1–12**. Reaction conditions: i) DPTS, DCC, DCM, 56–61% ii) pentaerythritol, PTSA, DMF, 50 °C, 46–61% iii) DPTS, DCC, DCM, 46–67% iv) CuSO₄, sodium ascorbate, THF/water (2:1 v/v), 40 °C, 31–54% DCC = *N,N'*-dicyclohexylcarbodiimide, DCM = dichloromethane, DMF = *N,N*-dimethylformamide,

DPTS = 4-(dimethylamino)pyridinium *p*-toluenesulfonate, THF = tetrahydrofuran, PTSA = *p*-toluene sulfonic acid.

Having obtained glycodendrimers **1–12**, we then investigated their photocontrollable aggregation properties. Azobenzene *trans-cis* photoisomerization has been extensively studied by our group for controlling the self-assembly and interfacial activity of amphiphilic carbohydrates, and was shown to give clean conversion to the *cis*-dominated photostationary state (PSS) with efficient conversion to the *cis* isomer (up to 75%).^{18,31} Preliminary measurements involved the use of Man(3,5)12 (**3**) as the representative compound. The UV-vis spectra of **3** were recorded in the (assumptively) *trans*-dominated photostationary state, which indicated an intense band at around 325 nm corresponding to the azobenzene $\pi \rightarrow \pi^*$ transition, accompanied by a much weaker band at around 425 nm corresponding to the $n \rightarrow \pi^*$ transition (Fig. 1). In order to induce *trans-cis* photoisomerization, compound **3** was irradiated in water at either 325 nm or 361 nm for 30 min and the UV-vis spectrum recorded at 5 min intervals. After this time, a small decrease in peak intensity at 325 nm, which was accompanied by a slight increase in intensity of the peak at 425 nm and a blue shift in the λ_{\max} of approximately 5 nm.³² The thermal half-lives of the *cis* isomer of glycodendrimers **1–4** was then determined by measuring the relaxation rate of the dark adapted *cis*-PSS to the more stable *trans* isomer at 20 °C and 37 °C, respectively (ESI, Fig. S1 and S2). Even at physiologically relevant temperatures, relatively long lived *cis*-states were observed (10–14 h, Fig. S3), which would provide ample opportunity to elicit a change in the lectin binding response. The ratio of *trans* and *cis* isomers at either PSS could be estimated by integrating selected signals in the ¹H NMR spectrum, before and after UV irradiation (Fig. S4–S7). In the resting, *trans*-dominated PSS, 7–9% of molecules existed in *cis*-form, while after UV irradiation 19–30% of molecules were found in the *cis*-form. Whilst the *cis-trans* ratio in the *cis*-PSS ratio is low compared to those observed in previously described azobenzene derivatives,³¹ these findings are consistent with derivatives incorporating bulky substituents, particularly amphiphilic azobenzene analogues leading to densely packed aggregate geometries that may impede light penetration and/or inhibit photoswitching due to steric congestion in the micelle core.³²

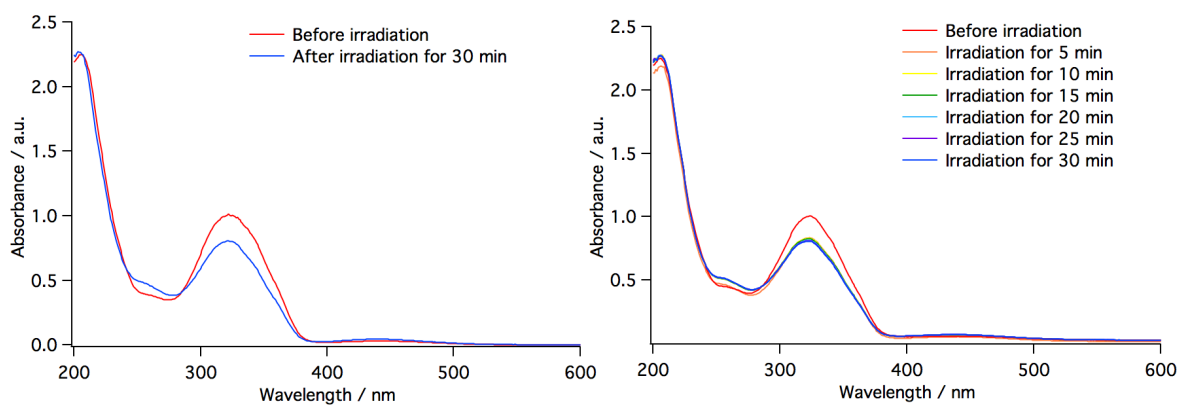


Fig. 1. UV-vis spectroscopy of Man(3,5)12 **3** at 0.05 mM concentration in ultra pure water, before and after UV irradiation with an UV LED at 325 nm (left), and a UV lamp at 361 nm and 36W radiant power (right).

Having examined the photoswitching properties of glycodendrimers, our attention focused on the aggregation behaviour of the assembled micelles in water. Interestingly, amphiphilic glycodendrimers did not reduce the surface tension at the air-water interface, and so it was not possible to determine the critical micelle concentration of these compounds by tensiometry. Instead, the critical aggregation concentration (CAC) was evaluated using a Nile Red encapsulation assay.²⁰ The CAC was calculated by monitoring the wavelength at the maximum intensity for the Nile red probe as a function of the glycodendrimer concentration, whereby the inflection point is indicative of the CAC (Fig. 2). Low micromolar CAC values were obtained for dendrimers **1–12** in water, which suggests a strong thermodynamic driving force for aggregation as a result of the favourable hydrophobic interactions between azobenzene and alkyl tail groups within the aggregate core.³³ Furthermore, no clear photomodulation of the CAC was evident for **1–12**, which was most likely a result of the low photoisomerization yields for these molecules. Because of their unusual aggregation behaviour, we then examined the relationship between conformational exchanges and the concentrations of glycodendrimers. Glycodendrimers **1–4** were dissolved separately in water at 20 °C at several different concentrations: above the CAC (0.05 mM), at the CAC, and below the CAC (0.001 mM). UV-vis spectroscopy was recorded for all these samples, and the absorbance at 325 nm was recorded (ESI, Fig. S8). By plotting the absorbance against concentration, linear trends ($R^2 > 0.999$ for all compounds) were observed, indicating that the glycodendrimers undergo unimolecular conformational exchanges upon self-assembly, which are not affected by changes in concentration.^{31,34}

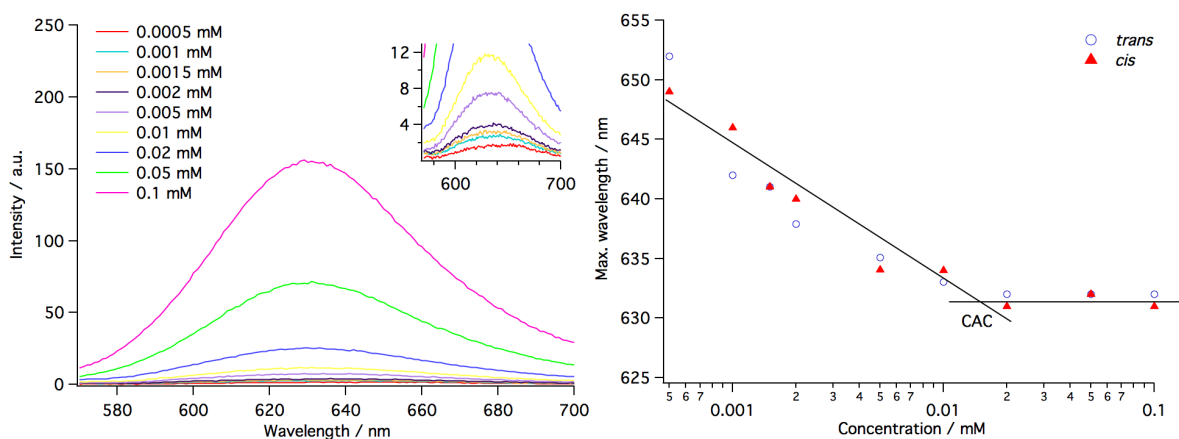


Fig. 2. Fluorescence spectra of Nile Red in the presence of Man(3,5)8 **1** at different concentrations (Left). CAC of Man(3,5)8 **1** in ultra pure water before (open symbols) and after (closed symbols) UV irradiation at 361 nm for 10 min (Right).

The aggregation properties of the glycodendrimers **1–12** in their respective *trans* and *cis* states was further investigated using DLS to determine the hydrodynamic diameter and polydispersity of the assembled structures (ESI, Table S1). Glycodendrimers **1–12** were dissolved in water at a fixed concentration (0.1 mM) and DLS measurements were obtained before and after UV irradiation. Aggregates were shown to be of limited polydispersity in water, with effective diameters of around 100 nm and polydispersity indices (PDIs) of approximately 0.2, with the exception of Fuc(3,5)2Et8 **10** which had a larger diameter of 183 nm. In most cases, any apparent change in diameter between the *trans* and *cis* states was modest, however the hydrodynamic volume of these structures generally increased slightly following UV irradiation (361 nm for 10 min), with the largest difference observed for Man(3,5)8 **1**.

In order to determine the precise geometry and size of these aggregates, along with any changes following *trans-cis* photoisomerization of the azobenzene core, SANS measurements were performed at fixed concentrations above the CAC in D₂O (0.1 mM). Under these conditions, cylindrical geometries of different sizes were observed in the *trans* state as shown in the SANS spectra, with smaller aggregates generally observed for glycodendrimers incorporating *n*-octyl and branched 2-ethylhexyl tail groups (Fig. 3, and ESI, Table S1). The SANS spectra revealed cylindrical geometries of various length (104–915 Å) and radii (32–41 Å). Cylindrical geometries are preferred when amphiphiles try to reduce their interfacial curvature, and the aggregation size can be modulated by adjusting the relative volume occupied by the head and tail group.³⁵ The diameter of these cylinders is approximately equal to the length of two glycodendrimers that construct the single layered cylindrical micelle structure, and this is

commensurate with a typical surfactant aggregate. From the fitted SANS spectra, the aggregation number (N_{agg}) and area per head group (A_{hg}) of these micelles could be determined, thus providing useful insight into the valency and density of carbohydrates exposed on the micelle surface (ESI, Figure S9 and Table S1). In order to evaluate changes in self-assembly properties following *trans-cis* photoisomerization, the SANS spectra were also recorded following UV irradiation of representative compounds **1–4** (Figure S10). Although no notable change in the geometry and size of these micelles was detected in the *cis*-PSS, this was in good agreement with the CAC values and can be attributed to the low photoisomerization yields of the dendrimers and the non-standard aggregation pathway.

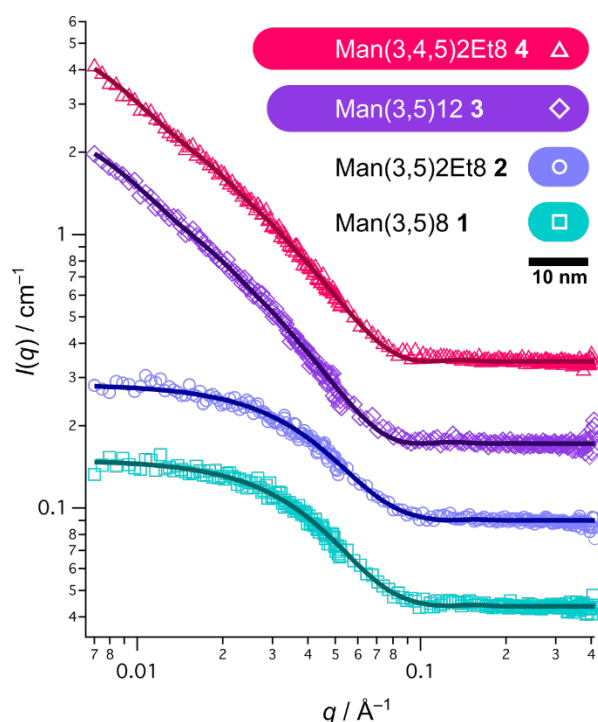


Fig. 3. Representative SANS data (symbols) and model fits (lines) for glycodendrimers **1–4** in the *trans*-dominated PSS (top) at 0.1 mM concentration in D₂O. The legend inset shows cross-sectional profiles of corresponding fitted micelle geometries.

Photoswitchable glycodendrimer micelles in this study are of particular interest as light-addressable tools for studying lectin binding and for impeding pathogenic lectin-carbohydrate interactions in a spatial and temporally-resolved manner. Such materials may also find application as glycotargeted delivery vehicles with phototriggered release properties. LecA and LecB were chosen as the target lectins owing to their strong potential for therapeutic

intervention and the important roles they play as virulence factors and in biofilm formation.¹⁹,³⁶ Furthermore, both lectins were shown to be present among a large set of strain isolates from clinical sources.³⁷ Since these soluble bacterial lectins show good affinity and specificity for D-galactose and L-fucose/D-mannose residues, respectively, we measured the binding inhibition of LecA/B against photoswitchable micelles incorporating these head groups (Table 1 and 2). The affinity of glycodendrimer micelles were measured using a recently described, competitive fluorescence polarization-based assay for LecA and LecB, both in the *trans*- and *cis*-PSS (See ESI for details).^{5b, 22} All compounds were tested over a concentration range from a concentration of inhibitor above the CAC value at 300 μ M, serially diluted down to single digit nanomolar concentrations. Methyl α -D-galactoside (α GalOMe), methyl α -L-fucopyranoside (α FucOMe) or methyl α -D-mannopyranoside (α ManOMe) were used as the monovalent references in the same assay for LecA and LecB, respectively.^{5b, 22} In the case of LecA, glycodendrimers **5–8** bearing a β -galactoside head group showed a modest enhancement (approximately four-fold) in inhibition potency relative to the monovalent compound. Whilst this may suggest a multivalent effect, no clear correlation between particle size and inhibitory potency could be drawn as the relatively small micelles bearing two *n*-octyl and 2-ethyl hexyl side chains of **5** and **6**, respectively, were shown to be equally potent as the larger micelles derived from glycodendrimers **7** and **8** incorporating three alkyl side chains. LecA is a tetrameric protein that binds preferentially to α -galactosides, although high valency ligands presenting β -galactosides, as well as monovalent phenyl β -galactosides have been shown to be potent inhibitors of this lectin. In our case, the weaker binding affinity for these glycodendrimers may be a result of inappropriate ligand spacing due to the flexible linker, which may disfavour a chelate binding mode between adjacent binding sites on the LecA tetramer.^{3a, 38} Furthermore, no significant change in binding potency was observed for the *galacto*-configured dendrimers following *trans-cis* photoisomerization, with the exception of **8** which showed a slight enhancement in inhibition. The negligible photomodulation of binding affinity is in good agreement with the CAC and SANS data, and is most likely a result of the low conversion to the *cis* isomer following UV irradiation.

Table 1. Evaluation of photoswitchable compounds **5–8** with LecA using a competitive binding assay based on fluorescence polarization.

Compound	n ^a	IC ₅₀ (μM) ^b	IC ₅₀ [μM] (UV _{361nm}) ^b	rp (rp _{UV}) ^c
αGalOMe		92.1 ± 23.2		
5	324	22.6 ± 0.9	24.9 ± 5.6	4.1 (4.0)
6	296	20.3 ± 5.2	21.0 ± 5.3	4.5 (4.7)
7	2846	22.9 ± 5.5	23.0 ± 4.4	4.0 (4.3)
8	1072	24.6 ± 2.1	23.1 ± 1.0	3.7 (4.3)

^a Number of sugars in the aggregate; ^b Average of three independent experiments; ^c Relative potency (rp) = IC₅₀ (monovalent reference)/IC₅₀ (glycodendrimer), values are expressed relative to the monovalent reference αGalOMe.

Table 2. Evaluation of photoswitchable compounds **1–4** and **9–12** with LecB using a competitive binding assay based on fluorescence polarization.

Compound	n ^a	IC ₅₀ [μM] ^b	IC ₅₀ [μM] (UV _{361nm}) ^b	rp (rp _{UV}) ^c
αFucOMe		0.35 ± 0.05		
9	182	0.29 ± 0.07	0.32 ± 0.01	1.2 (1.0)
10	1603	0.20 ± 0.00	0.20 ± 0.03	1.7 (1.7)
11	799	0.29 ± 0.04	0.27 ± 0.02	1.2 (1.2)
12	996	0.25 ± 0.06	0.24 ± 0.11	1.4 (1.4)
αManOMe		87.7 ± 61.2	76.5 ± 38.1	
1	138	2.7 ± 0.5	3.5 ± 0.3	32.8 (21.5)
2	128	3.3 ± 0.2	3.8 ± 0.4	26.2 (20.2)
3	918	3.0 ± 0.2	2.6 ± 0.2	29.4 (29.4)
4	795	1.0 ± 0.2	1.2 ± 0.4	85.7 (62.6)

^a Number of sugars in the aggregate; ^b Average of three independent experiments; ^c Relative potency (rp) = IC₅₀ (monovalent reference)/IC₅₀ (glycodendrimer), values are expressed relative to the monovalent reference αManOMe for compound **1–4** or αFucOMe for compound **9–12**.

In contrast to the inhibition of LecA with D-galactoside functionalized dendrimers, glycodendrimers **9–12** incorporating α -fucoside head groups showed good potency against LecB, with sub micromolar IC₅₀ values obtained in the *trans* and *cis* isomeric states. However, these compounds showed no enhancement in potency relative to the monovalent reference compound α FucOMe (IC₅₀ 0.35 μ M). Many studies have revealed the importance of multivalency for generating potent ligands for LecB.³⁹ However, similar to the observations of the inhibition of micelles of **5–8** against LecA, the binding potency of **9–12** to LecB was insensitive to particle size. Furthermore, no clear photomodulation of inhibition could be detected following UV irradiation, as the *trans* isomer was as equally potent inhibitor as the *cis*-enriched state and is in good agreement with the self-assembly data.

Mannosides are usually weaker inhibitors of LecB when compared to fucosides, but through chemical modification, mannose-derived compounds were also shown to achieve potent LecB inhibition.⁴⁰ Micelles assembled from mannosides **1–4** were also tested for inhibition of LecB and low micromolar IC₅₀ values were obtained. In contrast to all other compounds tested for LecA and LecB, the relative potencies of mannosides **1–4** (IC₅₀ values of 1.0–3.4 μ M) with respect to α ManOMe (IC₅₀ 87.7 μ M) were significantly increased up to >80-fold for **4**. Due to the identical aglycons for fucosides **9–12** and mannosides **1–4**, this significant effect observed for mannosides is likely to be a result of an optimal multivalent presentation of the carbohydrate in the manno-series that matches the spatial requirements of two LecB binding sites in the lectin tetramer.

4. Conclusions

In summary, we report the modular synthesis of a library of photoswitchable Janus glycodendrimers bearing variable alkyl tail groups and carbohydrate head groups. The assembled structures were characterised using DLS and SANS, and revealed uniform cylindrical micelles of various size. Glycodendrimer micelles were assessed as phototuneable inhibitors of LecA and LecB from *P. aeruginosa* using a competitive, fluorescence polarization-based assay and revealed moderate-to-potent inhibition of these bacterial lectins with a significant increase potency for mannose derived glycodendrimers. Unfortunately, no clear modulation in the self-assembly and binding potency of these micelles could be observed following UV light irradiation, owing to the low photoisomerization yields for these dendrimers, most likely due to impaired light penetration and steric congestion within the aggregate core. Lectin binding potencies also appeared insensitive to the length and radii of

micelles, as smaller structures generally at least as potent binders as the larger, worm-like micelles. The efficient synthesis of these constructs facilitates a rapid entry point to responsive structures with tailored activity against a variety of lectin targets. Future work will be aimed at developing photocontrollable liposomal systems, as well as improving linker and ligand design in order to enhance binding potency and photoswitching efficiency.

Acknowledgements

B. W. acknowledges funding from the Australian Research Council (DE130101673).

A.T. acknowledges support from the Helmholtz-Association (grant no. VH-NG-934) and the Deutsche Forschungsgemeinschaft (grant no. Ti 756/2-1).

We acknowledge the support of the Australian Centre for Neutron Scattering, Australian Nuclear Science and Technology Organisation, in providing the neutron research facilities used in this work. This work benefited from SasView software, originally developed by the DANSE project under NSF award DMR-0520547.

References

1. D. K. Mandal, N. Kishore, and C. F. Brewer, *Biochemistry*, 33 (1994) 1149.
2. a) M. Mammen, S. K. Choi and G. M. Whitesides, *Angew. Chem. Int. Ed.*, 37 (1998) 2745. b) T. K. Dam, R. Roy, S. K. Das, S. Oscarson and C. F. Brewer, *J. Biol. Chem.*, 275 (1998) 14223.
3. a) A. Bernardi, J. Jiménez-Barbero, A. Casnati, C. De Castro, T. Darbre, F. Fieschi, J. Finne, H. Funken, K. Jaeger, M. Lahmann, T. K. Lindhorst, M. Marradi, P. Messner, A. Molinaro, P. V. Murphy, C. Nativi, S. Oscarson, S. Penadés, F. Peri, R. J. Pieters, O. Renaudet, J. L. Reymond, B. Richichi, J. Rojo, F. Sansone, C. Schäffer, W. B. Turnbull, T. Velasco-Torrijos, S. Vidal, S. Vincent, T. Wennekes, H. Zuilhofxy and Anne Imberty, *Chem. Soc. Rev.*, 42 (2013) 4709. b) G. Ragupathi, F. Koide, P. O. Livingstone, Y. S. Cho, A. Endo, Q. Wan, M. K. Spassova, S. J. Keding, J. Allen, O. Ouerfelli, R. M. Wilson and S. J. Danishefsky, *J. Am. Chem. Soc.*, 128 (2006) 2715. c) S. Bhatia, M. Dimde and R. Haag, *Med. Chem. Commun.*, 5 (2014) 862. d) R. Roy, P. V. Murphy and H. J. Gabius, *Molecules*, 21 (2016) 629; e) S. Grigalevicius, S. Chierici, O. Renaudet, R. Lo-Man, E. Dériaud, C. Leclerc and P. Dumy, *Bioconj. Chem.*, 16

- (2005) 1149; e) C. Müller, G. Despras and T. K. Lindhorst, *Chem. Soc. Rev.*, 45 (2016) 3275.
4. a) S. Andre, R. J. Pieters, I. Vrasidas, H. Kaltner, I. Kuwabara, F. T. Liu, R. M. Liskamp and H. J. Gabius, *ChemBioChem*, 2 (2001) 822; b) E. Kolomiets, E. M. V. Johansson, O. Renaudet, T. Darbre and J. L. Reymond, *Org. Lett.*, 9 (2007) 1465.
 5. a) R. U. Kadam, M. Bergmann, M. Hurley, D. Garg, M. Cacciarini, M. S. Swiderska, C. Nativi, M. Sattler, A. R. Smyth, P. Williams, M. Cámara, A. Stocker, T. Dabre and J. L. Reymond, *Angew. Chem. Int. Ed.*, 50 (2011) 10631; b) I. Joachim, S. Rikker, D. Hauck, D. Ponader, S. Boden, R. Sommer, L. Hartmann and A. Titz, *Org. Biomol. Chem.*, 14 (2016) 7933; c) O. Renaudet, L. BenMohamed, G. Dasgupta, I. Bettahi and P. Dumy, *ChemMedChem*, 3 (2008) 737; d) B. L. Wilkinson, S. Day, R. Chapman, S. Perrier, V. Apostolopoulos and R. J. Payne, *Chem. Eur. J.*, 18 (2012) 16540.
 6. J. Rieger, F. Stoffelbach, D. Cui, A. Imberty, E. Lameignere, J. L. Putaux, R. Jérôme, C. Jérôme and R. Auzély-Velty, *Biomacromolecules*, 8 (2007) 2717.
 7. Y. Ruff, E. Buhler, S. J. Candau, E. Kesselman, Y. Talmon and Jean-Marie Lehn, *J. Am. Chem. Soc.*, 132 (2010) 2573.
 8. J. F. Nierengarten, J. Iehl, V. Oerthel, M. Holler, B. M. Illescas, A. Munoz, N. Martin, J. Rojo, M. SanchezNavarro, S. Cecioni, S. Vidal, K. Buffet, M. Durka and S. P. Vincent, *Chem. Commun.*, 46 (2010) 3860.
 9. S. Andre, C. Grandjean, F. M. Gautier, S. Bernardi, F. Sansone, H. J. Gabius and R. Ungaro, *Chem. Commun.*, 47 (2011) 6126.
 10. A. Barnard and D. K. Smith, *Angew. Chem. Int. Ed.*, 51 (2012) 6572.
 11. a) V. Percec, P. Leowanat, H. J. Sun, O. Kulikov, C. D. Nusbaum, T. M. Tran, A. Bertin, D. A. Wilson, M. Peterca, S. Zhang, N. P. Kamat, K. Vargo, D. Mook, E. D. Johnston, D. A. Hammer, D. J. Pochan, Y. Chen, Y. M. Chabre, T. C. Shiao, M. Bergeron-Brlek, S. André, R. Roy, H. J. Gabius and P. A. Heiney, *J. Am. Chem. Soc.*, 135 (2013) 9055. b) S. Zhang, R. O. Moussodia, S. Vértesy, S. Andre, M. L. Klein, H. J. Gabius and V. Percec, *Proc. Natl. Acad. Sci. U.S.A.*, 112 (2015) 5585; d) S. Zhang, R. O. Moussodia, H. J. Sun, P. Leowanawat, A. Muncan, C. D. Nusbaum, K. M. Chelling, P. A. Heiney, M. L. Klein, S. André, R. Roy, H. J. Gabius, and V. Percec, *Angew. Chem. Int. Ed.*, 53 (2014) 10899.
 12. a) Y. Ogawa, C. Yoshiyama and T. Kitaoka, *Langmuir*, 28 (2012) 4404. b) B. S. Kim, W. Y. Yang, J. H. Ryu, Y. S. Yoo and M. Lee, *Chem. Commun.*, 15 (2005) 2035. c) B.

- S. Kim, D. J. Hong, J. Bae and M. Lee, *J. Am. Chem. Soc.*, 127 (2005) 16333. d) J. H. Ryu, E. Lee, Y. B. Lim and M. Lee, *J. Am. Chem. Soc.*, 129 (2007) 4808.
13. A. A. Beharry and G. A. Woolley, *Chem. Soc. Rev.* 40 (2011) 4422.
14. a) N. M. Oruganti Srinivas, A. Suriola and N. Jayaraman, *J. Am. Chem. Soc.*, 124 (2002) 2124. b) T. K. Lindhorst, *Beilstein J. Org. Chem.*, 9 (2013) 223.
15. A. Samanta, M. C. Stuart and B. J. Ravoo, *J. Am. Chem. Soc.*, 134 (2012) 19909.
16. D. Ponader, S. Igde, M. Wehle, K. Märker, M. Santer, D. Bléger and L. Hartmann, *Beilstein J. Org. Chem.*, 10 (2014) 1603.
17. V. Chandrasekaran, H. Jacob, F. Peterson, K. Kathirvel, F. Tuzek and T. K. Lindhorst, *Chem. Eur. J.*, 20 (2014) 8744.
18. Y. Hu, W. Zou, V. Julita, R. Ramanathan, R. F. Tabor, R. Nixon-Luke, G. Bryant, V. Bansal and B. L. Wilkinson, *Chem. Sci.*, 7 (2016) 6628.
19. S. Wagner, R. Sommer, S. Hinsberger, C. Lu, R. W. Hartmann, M. Empting, A. Titz, *J. Med. Chem.*, 59 (2016) 5929.
20. a) C. Tanford, *The hydrophobic effect: formation of micelles and biological membranes*, 2nd ed., J. Wiley., 1980; b) A. Barnard, P. Posocco, S. Pricl, M. Calderon, R. Haag, M. E. Hwang, V. W. Shum, D. W. Pack and D. K. Smith, *J. Am. Chem. Soc.*, 133 (2011) 20288.
21. A. Guimer and G. Fournet, *Small-angle scattering of X-rays*, J. Wiley & Sons, New York, 1955.
22. D. Hauck, I. Joachim, B. Frommeyer, A. Varrot, B. Philipp, H. M. Möller, A. Imberty, T. E. Exner and A. Titz, *ACS Chem. Biol.*, 8 (2013) 1775.
23. S. Kuvshinova, A. Zav'Yalov, O. Koifman, V. Aleksandriiskii and V. Burmistrov, *Russ. J. Org. Chem.*, 40 (2004) 1113.
24. J. Dahmén, T. Frejd, G. Grönberg, T. Lave, G. Magnusson and G. Noori, *Carbohydr. Res.*, 116 (1983) 303.
25. C. Wilcox, J. Jin, H. Charville, S. Swift, T. To, P. A. Kilmartin, C. W. Evans, R. Cooney and M. Brimble, *Aust. J. Chem.*, 67 (2014) 562.
26. J. R. Hwu, C. I. Hsu, M. H. Hsu, Y. C. Liang, R. C. C. Huang and Y. C. Lee, *Bioorg. Med. Chem. Lett.*, 21 (2011) 380.
27. H. Tamiaki, A. Shinkai and Y. Kataoka, *J. Photochem. Photobiol. A Chem.*, 207 (2009) 115.
28. N. Gilboa-Garber, *Methods Enzymol.*, 83 (1982) 378.

29. a) E. Fedeli, A. Lancelot, J. L. Serrano, P. Calvob and T. Sierra, *New. J. Chem.*, 2015, **39**, 1960. b) B. Neises and W. Steglich, *Org. Synth.*, 7 (1990) 93.
30. a) H. C. Kolb, M. G. Finn and K. B. Sharpless, *Angew. Chem. Int. Ed.*, 40 (2001) 2004. b) L. Bornaghi, S. A Poulsen and T. A. Houston, *Tetrahedron*, 62 (2005) 8115.
31. R. F. Tabor, D. D. Tan, S. S. Han, S. A. Young, Z. L. E. Zeeger, M. J. Pottage, C. J. Garvey and B. L. Wilkinson, *Chem. Eur. J.*, 20 (2014) 13881.
32. a) C. Kördel, C. S. Popeney and R. Haag, *Chem. Commun.*, 47 (2011) 6584. b) M. Uda, A. Momotake and T. Arai, *Photochem. Photobiol. Sci.*, 2 (2003) 845. c) A. Momotake and T. Arai, *Tetrahedron Lett.*, 45 (2004) 4131; d) W. R. Brode, J. H. Gould and G. M. Wyman, *J. Am. Chem. Soc.*, 75 (1953) 1856.
33. a) Y. Liu, A. H. Flood, J. F. Stoddart, *J. Am. Chem. Soc.*, 2004, 126, 9150-9151; b) L. Zhu, H. Yan and Y. Zhao, *Int. J. Mol. Sci.*, 13 (2012) 10132.
34. J. S. Pedersen, in *Soft Matter Characterization*, Springer, 2008, pp. 191–233.
35. a) A. Valiakhmetova, M. J. Pottage, T. M. McCoy, J. Garvey, L. de Campo, C. Rehm, D. A. Kuryashov and R. F. Tabor, *Langmuir*, 32 (2016) 12423; b) J. N. Israelachvili, D. J. Mitchell, and B. W. Ninham, *J. Chem. Soc. Faraday Trans. 2*, 72 (1976) 1525.
36. a) D. Tielker, S. Hacker, R. Loris, M. Strathmann, J. Wingender, S. Wilhelm, F. Rosenau and K. E Jaeger, *Microbiology*, 151 (2005) 1313. b) N. Gilboa-Garber, *Methods Enzymol.*, 83 (1982) 378. c) S. P. Diggle, R. E. Stacey, C. Dodd, M. Camara, P. Williams and K. Winzer, *Environ. Microbiol.*, 8 (2006) 1095.
37. a) R. Sommer, S. Wagner, A. Varrot, C. Nycholat, A. Khaledi, S. Häussler, J. Paulson, A. Imerty and A. Titz, *Chem. Sci.*, 7 (2016) 4990; b) A. M. Boukerb, A. Décor, S. Ribun, R. Tabaroni, A. Rousset, L. Commin, S. Buff, A. Doléans-Jordheim, S. Vidal, A. Varrot, A. Imberty, and B. Cournoyer, *Front. Microbiol.*, 7 (2016) 811.
38. a) D. Sicard, S. Cecioni, M. Iazykov, Y. Chevolut, S. E. Matthews, J. P. Praly, E. Souteyrand, A. Imberty, S. Vidal and M. Phaner-Goutorbe, *Chem. Commun.*, 47 (2011) 9483. b) F. Pertici and R. J. Pieters, *Chem. Commun.*, 48 (2012) 4008; c) S. Cecioni, R. Lalor, B. Blanchard, J. P. Praly, A. Imberty, S. E. Matthews and S. Vidal, *Chem. Eur. J.*, 15 (2009) 13232.
39. a) N. Berthet, B. Thomas, I. Bossu, E. Dufour, E. Gillon, J. Garcia, N. Spinelli, A. Imberty, P. Dumy and O. Renaudet, *Bioconjugate Chem.*, 2013, 24, 1598. b) Y. M. Chabre, D. Giguère, B. Blanchard, J. Rodrigue, S. Rocheleau, M. Neault, S. Rauthu, A. Papadopoulos, A. A. Arnold and A. Imberty, *Chem. Eur. J.*, 17 (2011) 6545.

40. a) R. Sommer, T. E. Exner A. Titz, *PLoS ONE*, 2014, 9, e112822; b) A. Hofmann, R. Sommer, D. Hauck, J. Stifel, I. Gottker-Schnetmann and A. Titz, *Carbohydr. Res.*, 412 (2015) 34; c) R. Sommer, D. Hauck, A. Varrot, S. Wagner, A. Prestel, H. M. Möller, A. Imberty and A. Titz, *ChemistryOpen*, 4 (2015) 756; c) G. Beshr, R. Sommer, D. Hauck, D. C. B. Siebert, A. Hofmann, A. Imberty and A. Titz, *Med. Chem. Commun.*, 7 (2016) 519.

Supporting Information

Photoswitchable Janus Glycodendrimer Micelles as Multivalent Inhibitors of LecA and LecB from *Pseudomonas aeruginosa*

Yingxue Hu,^a Ghamdan Beshr,^b Christopher J. Garvey,^c Alexander Titz,^b Rico F. Tabor^a and Brendan L. Wilkinson.*^d

- a) School of Chemistry, Monash University, Victoria 3800, Australia.
- b) Chemical Biology of Carbohydrates, Helmholtz Institute for Pharmaceutical Research Saarland (HIPS), D-66123 Saarbrücken, Germany, and Deutsches Zentrum für Infektionsforschung, Standort Hannover-Braunschweig.
- c) Australian Centre for Neutron Scattering, ANSTO, Lucas Heights, New South Wales 2234, Australia.
- d) School of Science and Technology, The University of New England, New South Wales 2351, Australia.

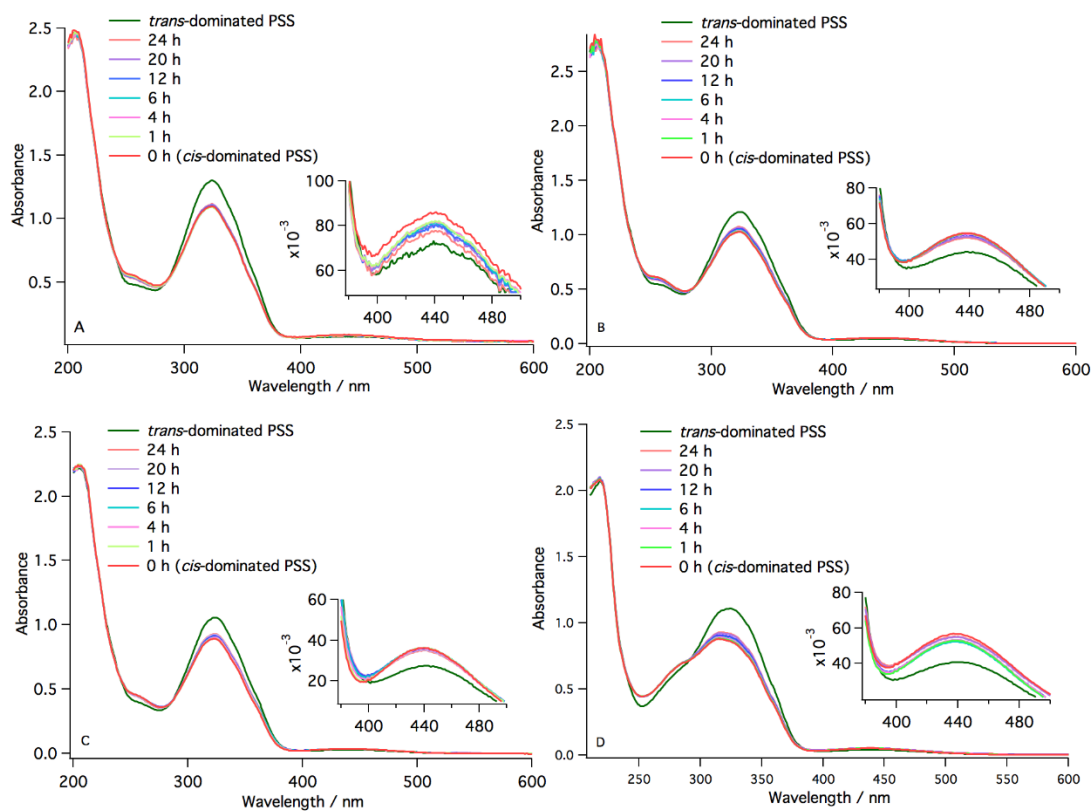


Figure S1. Thermal *cis-trans* relaxation of glycodendrimers A) Man(3,5)8 **1**, B) Man(3,5)2Et8 **2**, C) Man(3,5)12 **3** and D) Man(3,4,5)2Et8 **4** (0.05 mM in Milli-Q water) at 20°C.

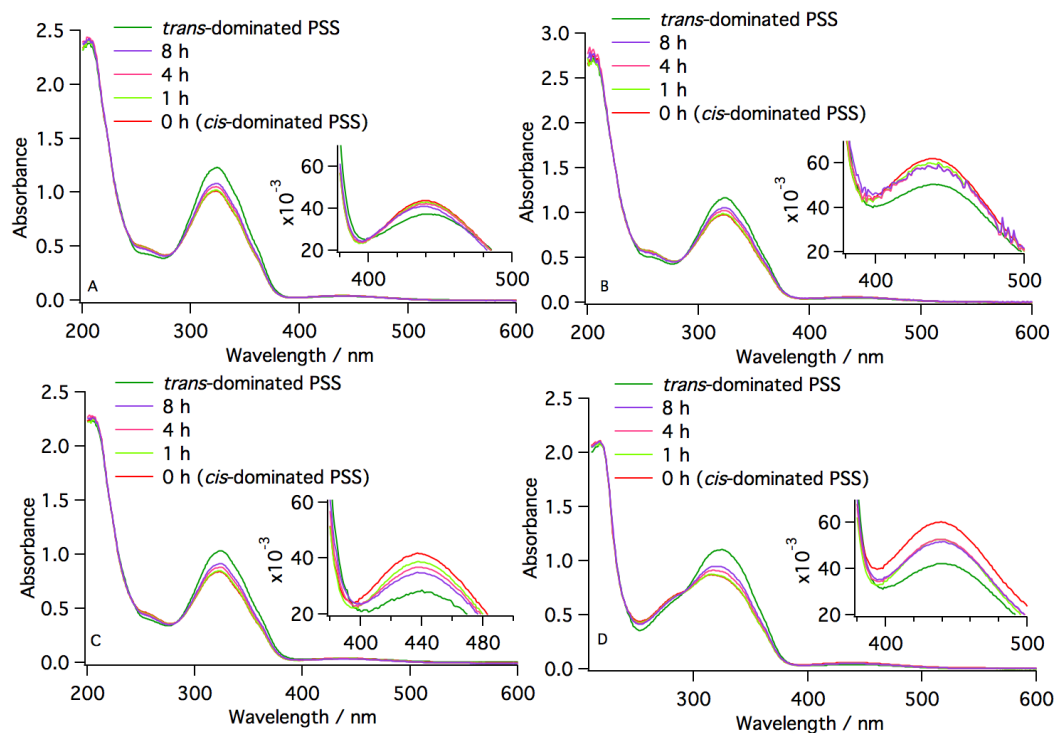


Figure S2. Thermal *cis-trans* relaxation of glycodendrimers A) Man(3,5)8 **1**, B) Man(3,5)2Et8 **2**, C) Man(3,5)12 **3** and D) Man(3,4,5)2Et8 **4** (0.05 mM in Milli-Q water) at 37°C.

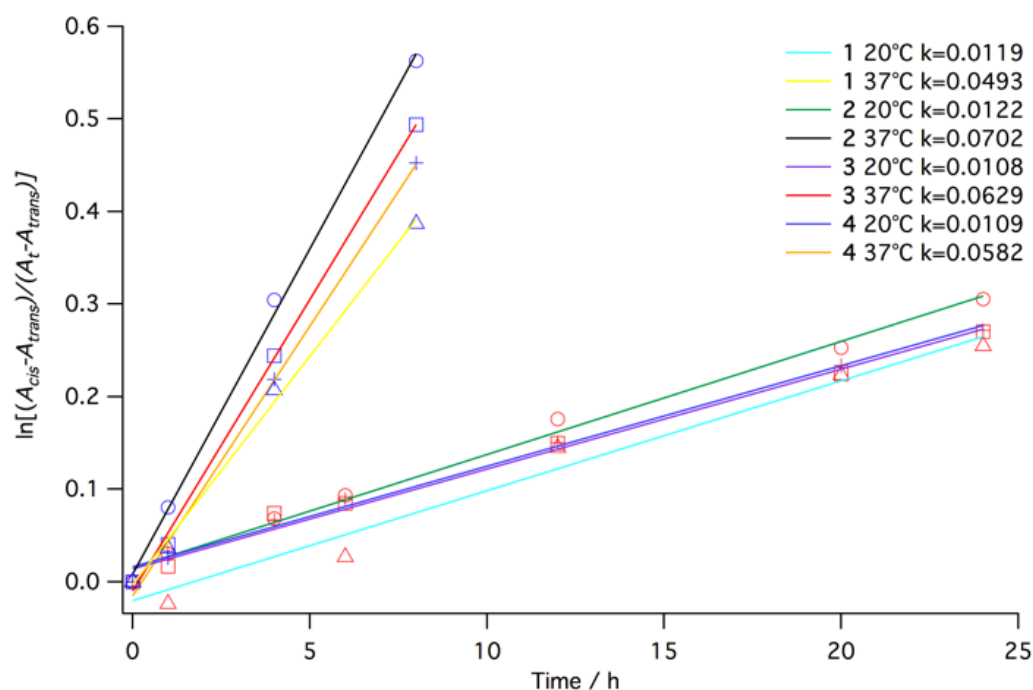


Figure S3. Time dependence of the absorbance changes at 325 nm for thermal *cis-to-trans* isomerization of glycodendrimers **1-4** in the dark in Milli-Q water at 20°C and 37°C.

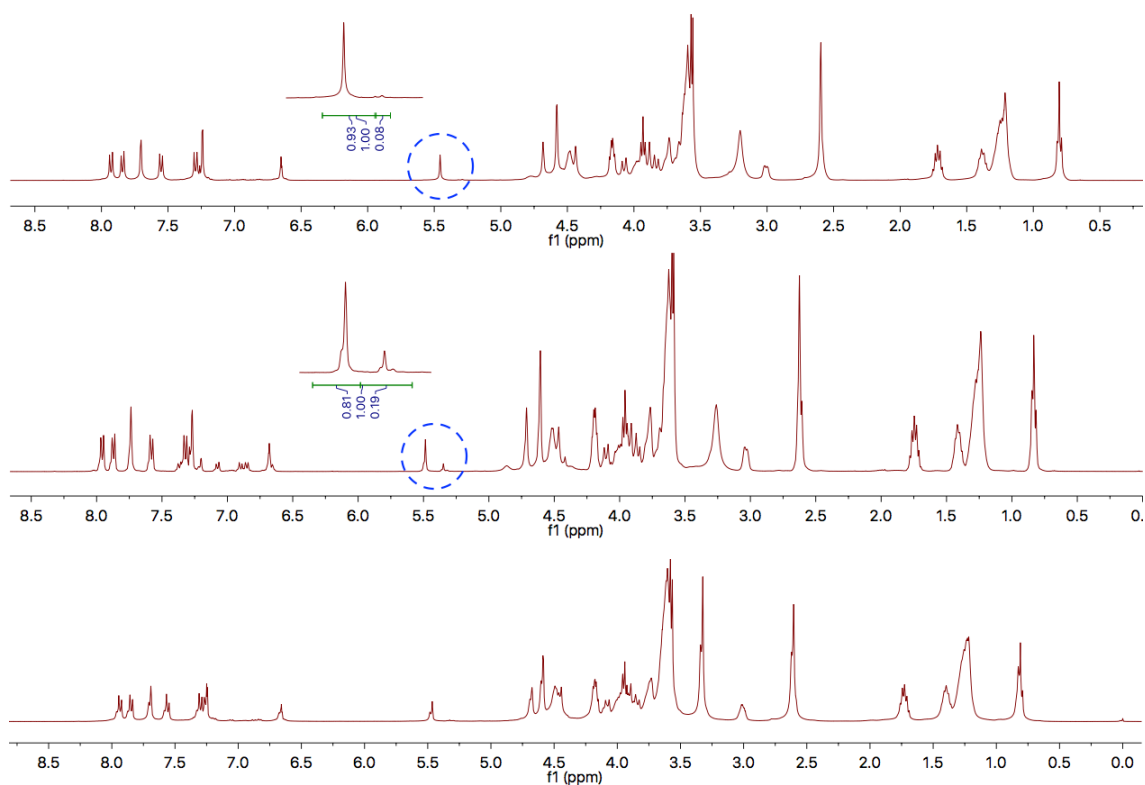


Figure S4. ^1H NMR spectra of Man(3,5)8 **1** before UV photoirradiation (top), after UV photoirradiation (middle), and after blue light photoirradiation (bottom).

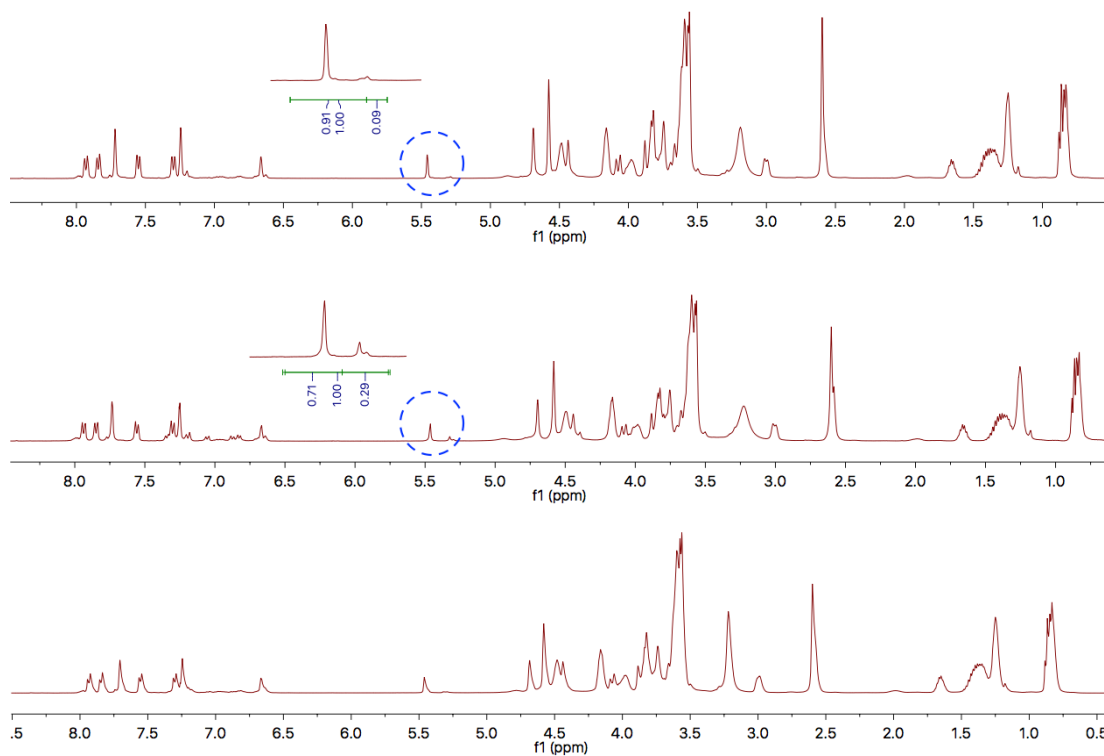


Figure S5. ^1H NMR spectra of Man(3,5)2Et8 **2** before UV photoirradiation (top), after UV photoirradiation (middle), and after blue light photoirradiation (bottom).

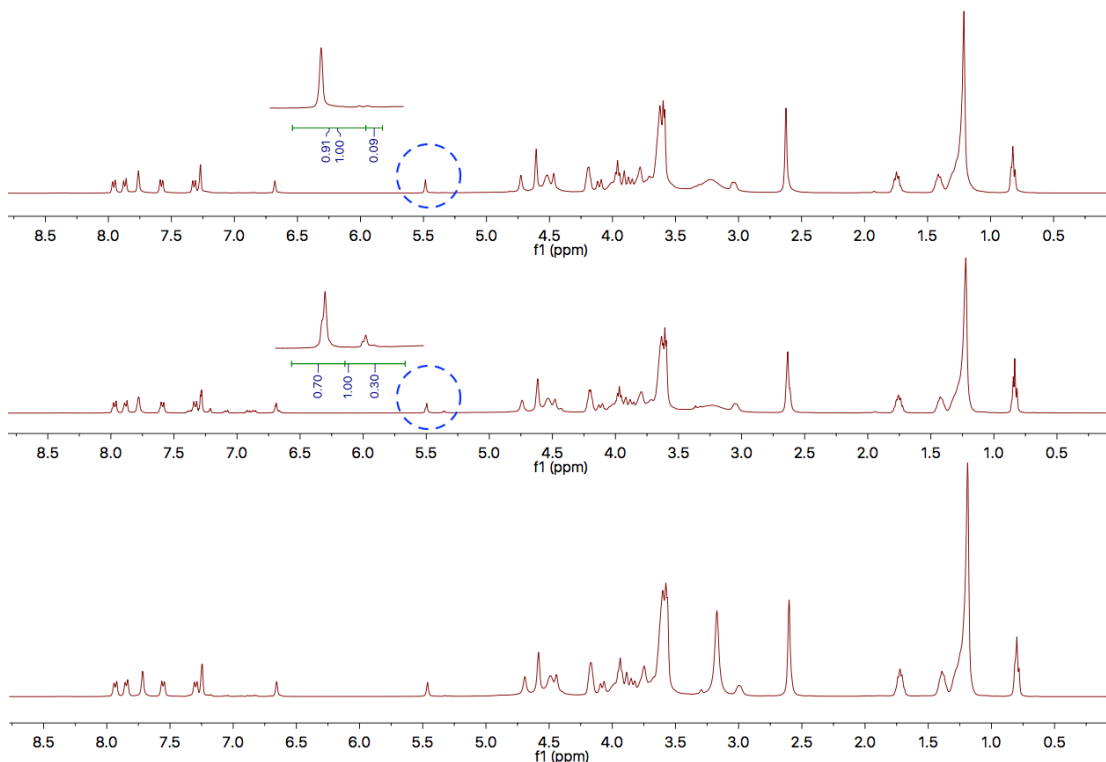


Figure S6. ^1H NMR spectra of Man(3,5)12 **3** before UV photoirradiation (top), after UV photoirradiation (middle), and after blue light photoirradiation (bottom).

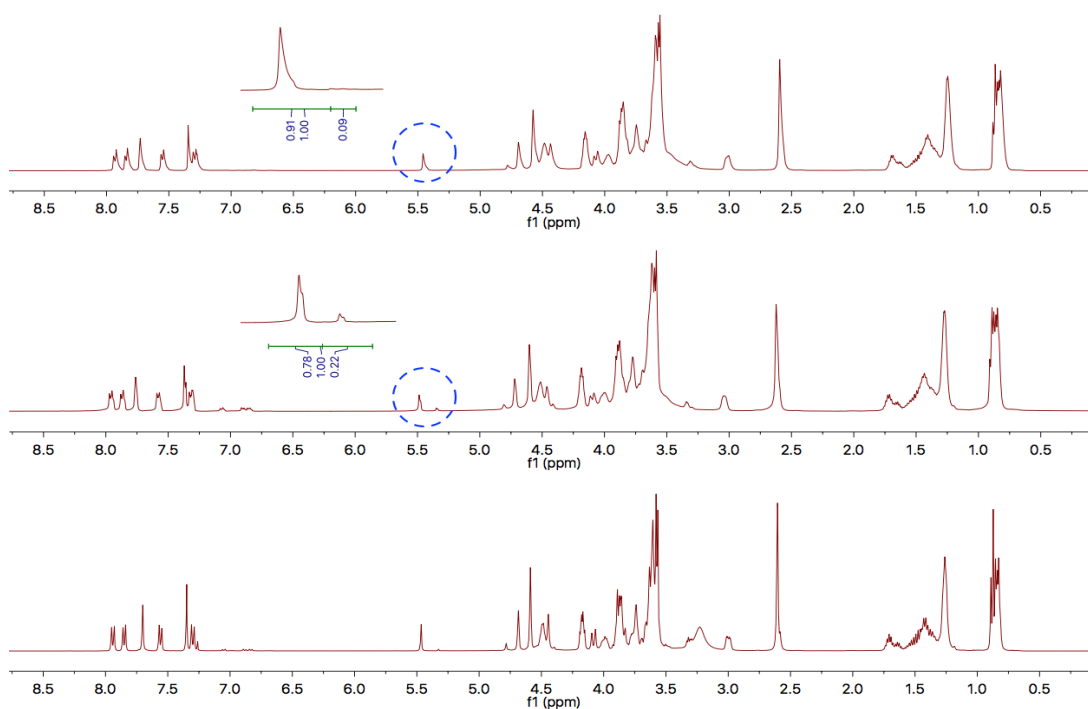


Figure S7. ^1H NMR spectra of Man(3,4,5)2Et8 **4** before UV photoirradiation (top), after UV photoirradiation (middle), and after blue light photoirradiation (bottom)

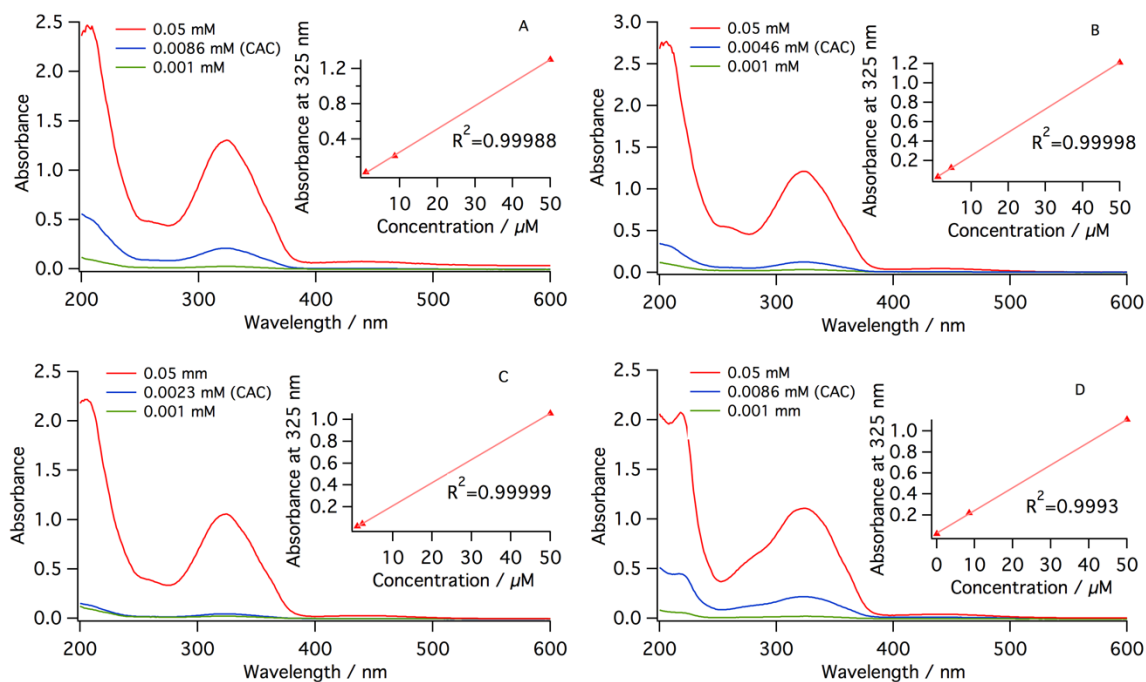


Figure S8. UV-vis absorbance of A) Man(3,5)8 **1**, B) Man(3,5)2Et8 **2**, C) Man(3,5)12 **3** and D) Man(3,4,5)2Et8 **4** in Milli-Q water at 20°C under different concentrations. (Insets) Plots of the UV-vis absorbance measured at 325 nm as a function of concentration.

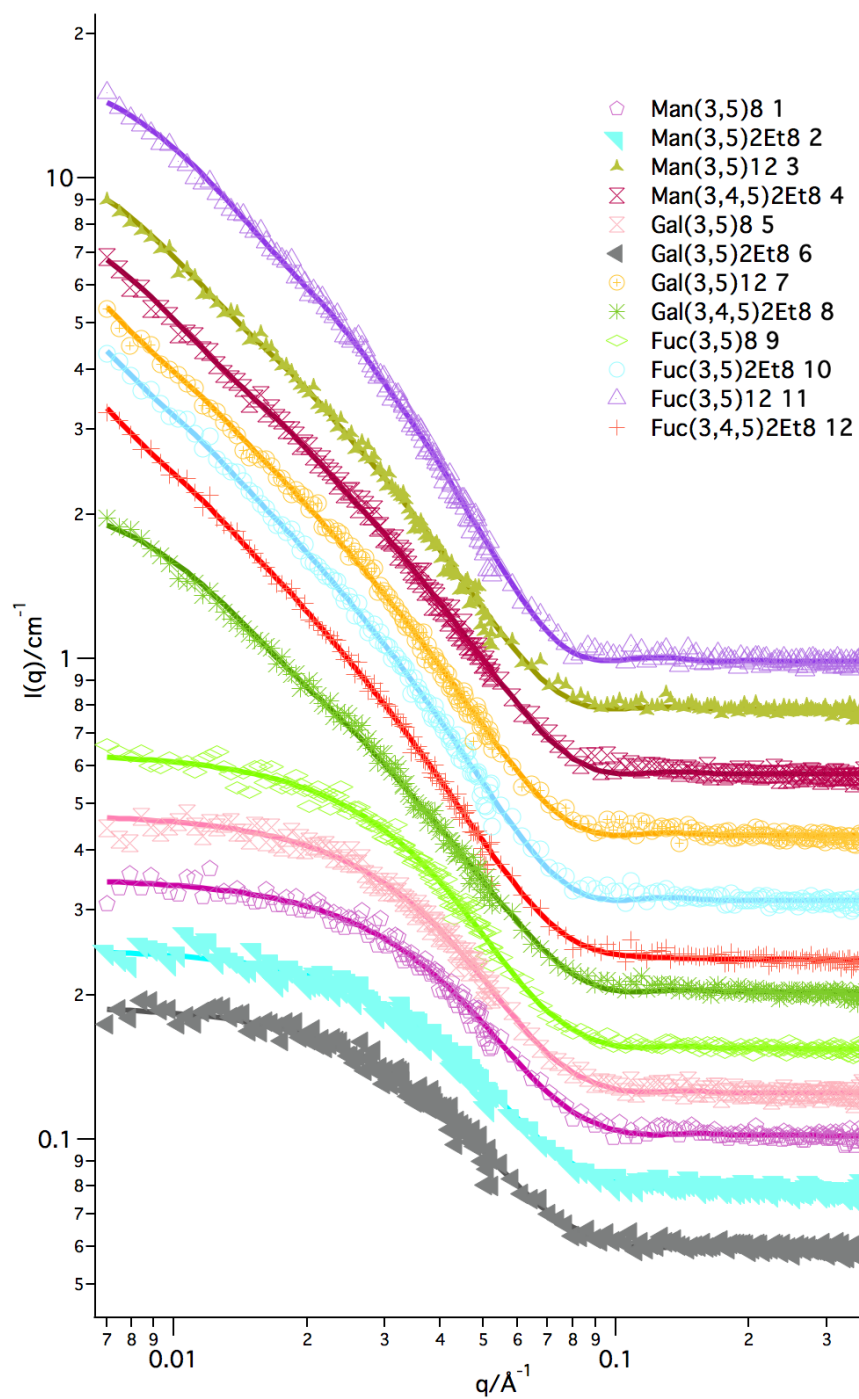


Figure S9. SANS data (symbols) and model fits (lines) for glycodendrimers **1–12** in the *trans*-dominated PSS at a concentration of 0.1 mM in D₂O.

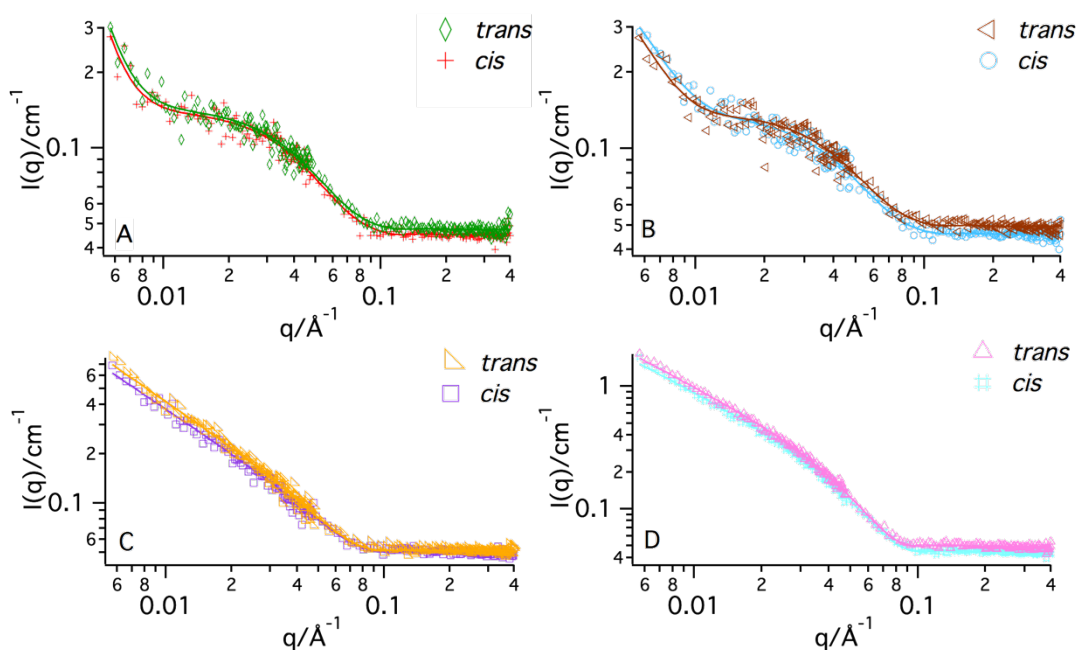


Figure S10. SANS data (symbols) and model fits (lines) for glycodendrimer A) Man(3,5)8 **1**, B) Man(3,5)2Et8 **2**, C) Man(3,5)12 **3** and D) Man(3,4,5)2Et8 **4** in the *trans* PSS and *cis* PSS at a concentration of 0.1 mM in D₂O.

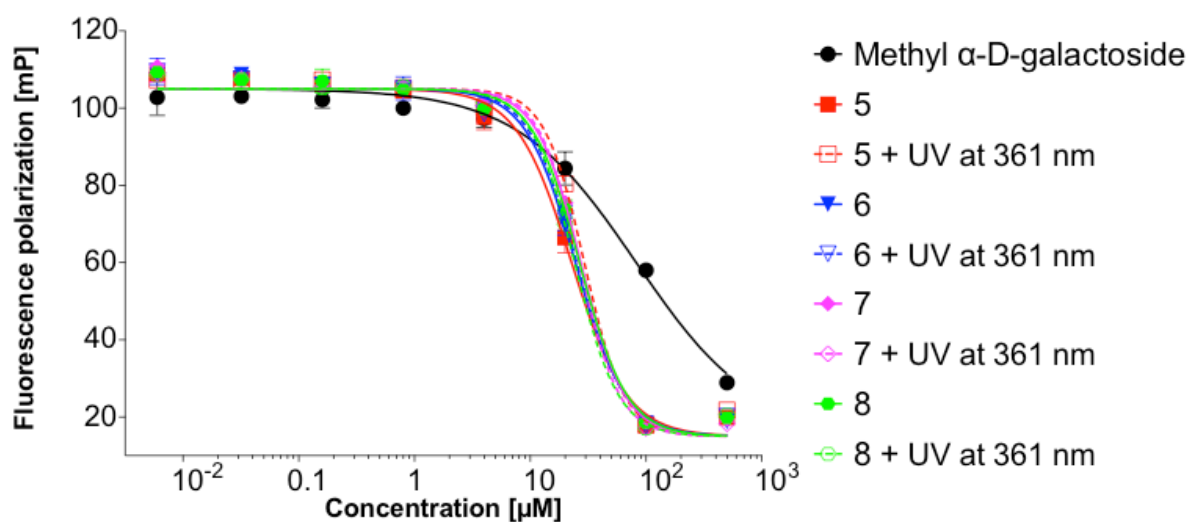


Figure S11. Representative example of the fluorescence polarization-based competitive binding assay of LecA with compounds **5–8** or methyl α -D-galactoside.

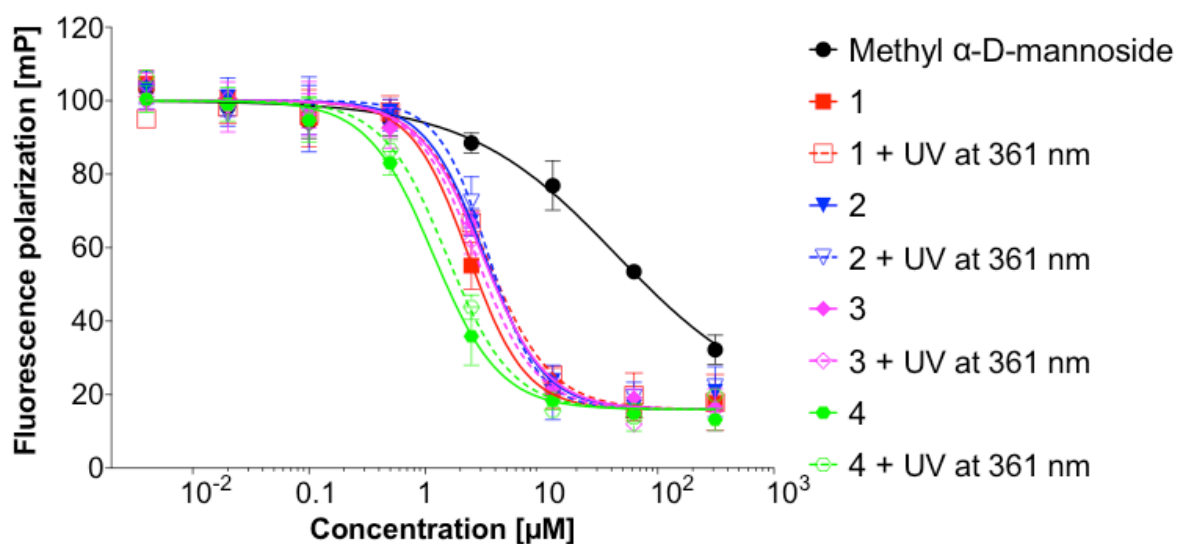


Figure S12. Representative example of the fluorescence polarization-based competitive binding assay of LecB with compounds **1–4** or methyl α -D-mannoside.

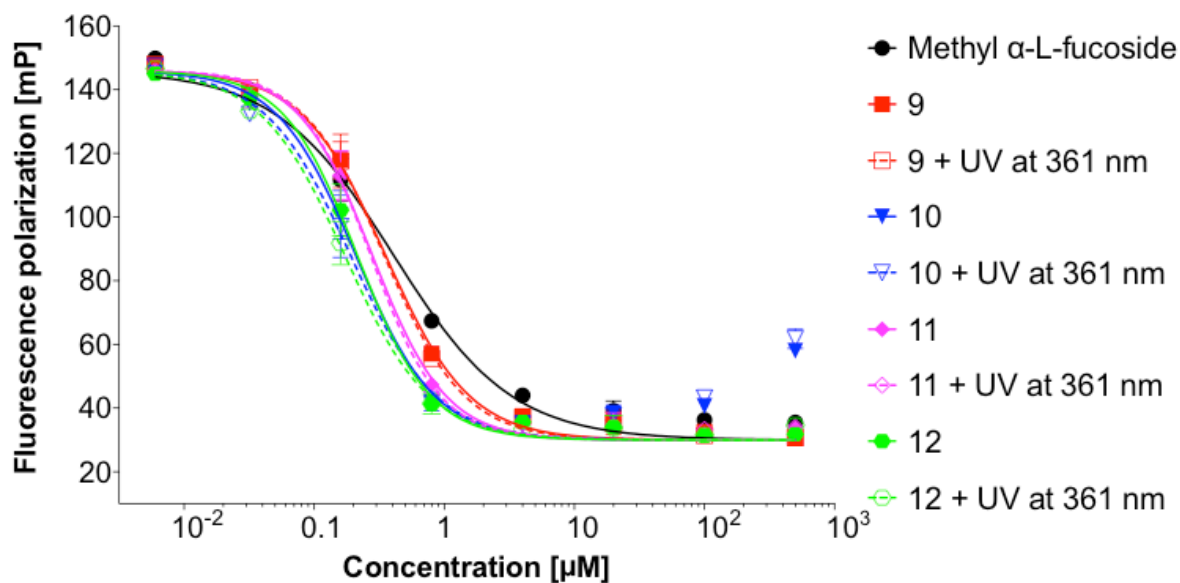


Figure S13. Representative example of the fluorescence polarization-based competitive binding assay of LecB with compounds **9-12** or methyl α -L-fucoside.

Table S1. CAC values, DLS results, SANS fitting parameters and lectin binding results of glycodendrimer **1–12**.

Name	CAC/mM ^a	N _{agg} ^b	A _{hg} ^c /nm ²	Eff. Diam./nm (PDI) ^d		SANS ^e	
				Before UV	After UV	Radius/Å	Length/Å
1	0.0086	138	1.07	112(0.21)	199(0.17)	34	104
2	0.0046	128	1.07	149 (0.23)	226 (0.15)	32	104
3	0.0023	918	0.79	109 (0.24)	109 (0.39)	39	550
4	0.0086	795	0.87	105 (0.25)	111 (0.24)	36	574
5	0.0085	162	0.98	110 (0.20)	138 (0.18)	35	109
6	0.0092	149	1.01	138 (0.26)	147 (0.20)	33	112
7	0.0080	1424	0.79	114 (0.23)	102 (0.18)	38	903
8	0.0100	536	0.90	102 (0.23)	91 (0.19)	35	406
9	0.0200	182	0.97	110 (0.29)	159 (0.24)	37	115
10	0.0085	1603	0.71	183 (0.21)	119 (0.25)	38	921
11	0.0048	799	0.78	123 (0.17)	129 (0.18)	41	441
12	0.0054	996	0.96	134 (0.17)	138 (0.19)	32	915

^a Measured in ultrapure water at 20°C; ^b N_{agg} = aggregation number; ^c A_{hg} = area per headgroup; ^d DLS samples were prepared at 0.1 mM; ^e SANS samples were dissolved in D₂O at 0.1 mM, and were all fitted to cylindrical shaped structure.

Analytical data

Man(3,5)8 **1**: This compound was prepared from **27** and **31** according to general procedure 3 and isolated as an orange solid (Yield: 45%). Mp = 212.4°C; $[\alpha]_D^{20}$ 111.6 (*c*, 0.06 in CH₃OH); FT-IR: $\nu_{\max}/\text{cm}^{-1}$ 3413, 2922, 1735, 1593, 1348, 1092, 840, 674; ¹H NMR (400 MHz, 10% CD₃OD in CDCl₃) δ 7.93 (d, *J* = 8.85 Hz, 2H, 2×ArH), 7.84 (d, *J* = 8.42 Hz, 2H, 2×ArH), 7.71–7.70 (m, 2H, 2×ArH), 7.55 (d, *J* = 8.55 Hz, 2H, 2×ArH), 7.30–7.24 (m, 4H, 2×ArH, 2×CH (triazole)), 6.65 (t, *J* = 2.23 Hz, 1H, ArH), 5.46 (s, 1H, CH), 4.78–4.44 (m, 14H), 4.18–3.56 (m, 54H), 3.02–2.99 (m, 2H), 2.59 (s, 8H, 4×CH₂), 1.75–1.68 (m, 4H, 2×CH₂), 1.40–1.21 (m, 20H, 10×CH₂), 0.80 (t, *J* = 6.72 Hz, 6H, 2×CH₃); ¹³C NMR (100 MHz, 10% CD₃OD in CDCl₃) δ 172.4, 172.1, 160.3, 144.8, 126.9, 124.1, 122.7, 122.4, 108.2, 99.9, 72.8, 71.1, 70.3, 69.6, 69.4,

68.9, 68.4, 65.4, 64.2, 63.9, 49.9, 49.1, 48.9, 37.2, 31.7, 29.2, 29.1, 28.9, 28.8, 25.9, 22.6, 13.9; ESI-HRMS (m/z) calculated for $C_{83}H_{122}N_8O_{32} = 1765.8057 [M + Na]^+$, found 1765.8063 $[M + Na]^+$.

Man(3,5)2Et8 **2**: This compound was prepared from **28** and **31** according to general procedure 3 and isolated as an orange solid (Yield: 42%). Mp = 203.7°C; $[\alpha]_D^{20}$ 103.0 (c , 0.065 in CH_3OH); FT-IR: ν_{max}/cm^{-1} 3395, 2925, 1735, 1595, 1347, 1030, 841, 673; 1H NMR (400 MHz, 10% CD_3OD in $CDCl_3$) δ 7.93 (d, $J = 7.53$ Hz, 2H, $2 \times ArH$), 7.84 (d, $J = 7.41$ Hz, 2H, $2 \times ArH$), 7.72 (s, 2H, $2 \times ArH$), 7.55 (d, $J = 7.56$ Hz, 2H, $2 \times ArH$), 7.31–7.24 (m, 4H, $2 \times ArH$, $2 \times CH$ (triazole)), 6.66 (s, 1H, ArH), 5.46 (s, 1H, CH), 4.69–4.44 (m, 14H), 4.16–3.49 (m, 54H), 3.01–2.99 (m, 2H), 2.59 (s, 8H, $4 \times CH_2$), 1.68–1.63 (m, 2H, $2 \times CH$), 1.49–1.25 (m, 16H, $8 \times CH_2$), 0.88–0.83 (m, 12H, $4 \times CH_3$); ^{13}C NMR (100 MHz, 10% CD_3OD in $CDCl_3$) δ 172.4, 172.1, 160.5, 144.7, 126.9, 124.2, 124.1, 122.7, 122.4, 108.2, 99.8, 72.7, 70.8, 70.3, 69.6, 69.4, 68.9, 65.4, 64.2, 63.9, 60.9, 49.9, 49.3, 49.1, 48.9, 48.7, 39.3, 37.2, 30.4, 29.0, 28.8, 23.8, 22.9, 13.9, 11.0; ESI-HRMS (m/z) calculated for $C_{83}H_{122}N_8O_{32} = 1765.8057 [M + Na]^+$, found $m/2z$ 894.3980 $[M + 2Na]^+$.

Man(3,5)12 **3**: This compound was prepared from **29** and **31** according to general procedure 3 and isolated as an orange solid (Yield: 49%). Mp = 189.9°C; $[\alpha]_D^{20}$ 105.4 (c , 0.055 in CH_3OH); FT-IR: ν_{max}/cm^{-1} 3396, 2921, 1736, 1591, 1351, 1094, 841; 1H NMR (400 MHz, 10% CD_3OD in $CDCl_3$) δ 7.96 (d, $J = 8.28$ Hz, 2H, $2 \times ArH$), 7.87 (d, $J = 8.01$ Hz, 2H, $2 \times ArH$), 7.76 (s, 2H, $2 \times ArH$), 7.58 (d, $J = 8.01$ Hz, 2H, $2 \times ArH$), 7.33–7.20 (m, 4H, $2 \times ArH$, $2 \times CH$ (triazole)), 6.68 (s, 1H, ArH), 5.48 (s, 1H, CH), 4.73–4.47 (m, 14H), 4.19–3.59 (m, 54H), 3.05–3.03 (m, 2H), 2.62 (s, 8H, $4 \times CH_2$), 1.76–1.71 (m, 4H, $2 \times CH_2$), 1.42–1.21 (m, 32H, $16 \times CH_2$), 0.84–0.81 (m, 6H, $2 \times CH_3$); ^{13}C NMR (100 MHz, 10% CD_3OD in $CDCl_3$) δ 172.4, 172.1, 160.3, 144.7, 126.9, 124.1, 122.7, 122.4, 108.2, 99.8, 70.3, 69.6, 68.9, 68.4, 65.4, 64.1, 63.8, 49.9, 49.3, 49.1, 48.9, 37.2, 31.8, 29.5, 29.3, 29.1, 28.9, 28.8, 25.9, 22.6, 13.9; ESI-HRMS (m/z) calculated for $C_{91}H_{138}N_8O_{32} = 1877.9309 [M + Na]^+$, found $m/2z$ 950.9617 $[M + 2Na]^+$.

Man(3,4,5)2Et8 **4**: This compound was prepared from **30** and **31** according to general procedure 3 and isolated as an orange solid (Yield: 51%). Mp = 233.8°C; $[\alpha]_D^{20}$ 80.0 (c , 0.08 in CH_3OH); FT-IR: ν_{max}/cm^{-1} 3395, 2928, 1735, 1331, 1094, 837; 1H NMR (400 MHz, 10% CD_3OD in $CDCl_3$) δ 7.93 (d, $J = 8.68$ Hz, 2H, $2 \times ArH$), 7.84 (d, $J = 8.21$ Hz, 2H, $2 \times ArH$), 7.73 (s, 2H, $2 \times ArH$), 7.55 (d, $J = 8.21$ Hz, 2H, $2 \times ArH$), 7.34–7.27 (m, 4H, $2 \times ArH$, $2 \times CH$ (triazole)), 5.46

(s, 1H, *CH*), 4.78–4.43 (m, 14H), 4.17–3.56 (m, 56H), 3.02–3.00 (m, 2H), 2.59 (s, 8H, 4×*CH*₂), 1.71–1.25 (m, 27H, 3×*CH*, 12×*CH*₂), 0.88–0.82 (m, 18H, 6×*CH*₃); ¹³C NMR (100 MHz, 10% CD₃OD in CDCl₃) δ 172.4, 172.1, 153.1, 150.1, 144.7, 143.1, 126.9, 124.2, 124.1, 123.3, 122.7, 122.5, 108.0, 99.8, 71.3, 71.0, 70.3, 69.6, 69.4, 68.9, 66.5, 65.4, 64.1, 63.8, 60.9, 49.9, 49.2, 49.0, 48.8, 48.6, 40.6, 39.5, 37.2, 30.4, 30.3, 29.2, 29.0, 28.9, 28.8, 23.8, 23.6, 23.0, 22.9, 13.9, 11.0; ESI-HRMS (*m/z*) calculated for C₉₁H₁₃₈N₈O₃₃ = 1893.9259 [*M* + Na]⁺, found 1893.9246 [*M* + Na]⁺.

Gal(3,5)8 **5**: This compound was prepared from **27** and **32** according to general procedure 3 and isolated as an orange solid (Yield: 44%). Mp = 205.3°C; [α]_D²⁰ 148.6 (*c*, 0.055 in CH₃OH); FT-IR: $\nu_{\max}/\text{cm}^{-1}$ 3395, 2923, 1734, 1893, 1350, 1038, 840; ¹H NMR (400 MHz, 10% CD₃OD in CDCl₃) δ 7.96–7.83 (m, 6H, 4×*ArH*, 2×*CH* (triazole)), 7.58–7.55 (m, 2H, 2×*ArH*), 7.35–7.25 (m, 4H, 4×*ArH*), 6.68–6.63 (m, 1H, *ArH*), 5.48–5.46 (m, 1H, *CH*), 4.58–4.44 (m, 10H), 4.17–4.06 (m, 10H), 3.97–3.84 (m, 10H), 3.69–3.29 (m, 40H), 2.61–2.59 (m, 8H, 4×*CH*₂), 1.76–1.69 (m, 4H, 2×*CH*₂), 1.41–1.22 (m, 20H, 10×*CH*₂), 0.82–0.79 (m, 6H, 2×*CH*₃); ¹³C NMR (100 MHz, 10% CD₃OD in CDCl₃) δ 172.4, 160.3, 144.5, 126.9, 124.6, 124.1, 122.7, 122.4, 108.2, 103.4, 74.7, 73.3, 70.9, 70.3, 69.5, 68.9, 68.4, 67.8, 64.2, 63.8, 61.2, 50.3, 49.3, 49.1, 48.9, 31.7, 29.2, 29.1, 28.9, 28.8, 25.9, 22.5, 13.9; ESI-HRMS (*m/z*) calculated for C₈₃H₁₂₂N₈O₃₂ = 1765.8057 [*M* + Na]⁺, found *m/z* 894.3968 [*M* + 2Na]⁺.

Gal(3,5)2Et8 **6**: This compound was prepared from **28** and **32** according to general procedure 3 and isolated as an orange solid (Yield: 54%). Mp = 201.1°C; [α]_D²⁰ 175.7 (*c*, 0.05 in CH₃OH); FT-IR: $\nu_{\max}/\text{cm}^{-1}$ 3395, 2928, 1734, 1595, 1347, 1035, 843, 756; ¹H NMR (400 MHz, 10% CD₃OD in CDCl₃) δ 8.16 (d, *J* = 8.75 Hz, 2H, 2×*ArH*), 8.10–8.07 (m, 4H, 2×*ArH*, 2×*CH* (triazole)), 7.78 (d, *J* = 8.29 Hz, 2H, 2×*ArH*), 7.53 (d, *J* = 8.54 Hz, 2H, 2×*ArH*), 7.48 (s, 2H, 2×*ArH*), 6.89 (s, 1H, *ArH*), 5.69 (s, 1H, *CH*), 4.79–4.67 (m, 10H), 4.39–4.29 (m, 10H), 4.11–4.03 (m, 12H), 3.90–3.66 (m, 34H), 2.83 (s, 8H, 4×*CH*₂), 1.91–1.88 (m, 2H, 2×*CH*), 1.68–1.48 (m, 16H, 8×*CH*₂), 1.11–1.06 (m, 12H, 4×*CH*₃); ¹³C NMR (100 MHz, 10% CD₃OD in CDCl₃) δ 172.5, 172.1, 160.5, 153.1, 144.5, 126.9, 124.6, 124.2, 122.7, 122.4, 108.2, 70.8, 70.3, 69.5, 68.9, 64.2, 63.8, 49.6, 49.4, 49.2, 48.9, 39.3, 37.2, 30.5, 29.0, 28.8, 23.8, 22.9, 13.9, 11.0. ESI-HRMS (*m/z*) calculated for C₈₃H₁₂₂N₈O₃₂ = 1765.8057 [*M* + Na]⁺, found *m/z* 894.3987 [*M* + 2Na]⁺.

Gal(3,5)12 **7**: This compound was prepared from **29** and **32** according to general procedure 3 and isolated as an orange solid (Yield: 42%). Mp = 187.5°C; $[\alpha]_{\text{D}}^{20}$ 156.7 (*c*, 0.065 in CH₃OH); FT-IR: $\nu_{\text{max}}/\text{cm}^{-1}$ 3395, 2921, 1732, 1592, 1350, 1037, 840, 754; ¹H NMR (400 MHz, 10% CD₃OD in CDCl₃) δ 8.21 (d, *J* = 8.70 Hz, 2H, 2×ArH), 8.15–8.12 (m, 4H, 2×ArH, 2×CH (triazole)), 7.84 (d, *J* = 8.44 Hz, 2H, 2×ArH), 7.76 (s, 2H, 2×ArH), 7.58 (d, *J* = 8.82 Hz, 2H, 2×ArH), 7.53–7.52 (m, 4H, 2×ArH), 6.94 (s, 1H, ArH), 5.74 (s, 1H, CH), 4.85–4.72 (m, 10H), 4.45–4.35 (m, 10H), 4.23–4.09 (m, 12H), 3.95–3.69 (m, 34H), 2.88 (s, 8H, 4×CH₂), 2.02–1.97 (m, 4H, 2×CH₂), 1.69–1.64 (m, 4H, 2×CH₂), 1.47 (s, 28H, 14×CH₂), 1.09–1.06 (m, 6H, 2×CH₃); ¹³C NMR (100 MHz, 10% CD₃OD in CDCl₃) δ 160.3, 144.5, 126.9, 124.6, 124.2, 122.7, 122.4, 108.3, 74.7, 70.3, 69.6, 68.9, 68.4, 64.2, 63.8, 49.4, 49.2, 48.9, 31.8, 29.6, 29.5, 29.3, 29.1, 28.9, 25.9, 22.6, 13.9. ESI-HRMS (*m/z*) calculated for C₉₁H₁₃₈N₈O₃₂ = 1877.9309 [*M* + Na]⁺, found 1877.9312 [*M* + Na]⁺.

Gal(3,4,5)2Et8 **8**: This compound was prepared from **30** and **32** according to general procedure 3 and isolated as an orange solid (Yield: 40%). Mp = 223.7°C; $[\alpha]_{\text{D}}^{20}$ 62.6 (*c*, 0.075 in CH₃OH); FT-IR: $\nu_{\text{max}}/\text{cm}^{-1}$ 3400, 2922, 1731, 1585, 1331, 1093, 839, 751; ¹H NMR (400 MHz, 10% CD₃OD in CDCl₃) δ 8.16–8.14 (m, 2H, 2×ArH), 8.09–8.05 (m, 4H, 2×ArH, 2×CH (triazole)), 7.78–7.76 (m, 2H, 2×ArH), 7.56–7.47 (m, 4H, 4×ArH), 5.68 (s, 1H, CH), 4.78–4.66 (m, 10H), 4.38–4.28 (m, 10H), 4.14–4.04 (m, 12H), 3.89–3.65 (m, 34H), 2.81 (s, 8H, 4×CH₂), 1.94–1.47 (m, 27H, 3×CH, 12×CH₂), 1.10–1.04 (m, 18H, 6×CH₃); ¹³C NMR (100 MHz, 10% CD₃OD in CDCl₃) δ 172.5, 172.2, 164.9, 153.1, 144.5, 126.9, 124.1, 122.7, 122.5, 108.0, 103.4, 74.6, 71.3, 70.3, 69.5, 68.9, 67.8, 64.2, 63.9, 50.3, 49.3, 49.2, 48.9, 40.6, 39.5, 37.2, 30.5, 30.3, 29.2, 29.0, 28.9, 23.8, 23.6, 23.0, 22.9, 14.0, 13.9, 11.0. ESI-HRMS (*m/z*) calculated for C₉₁H₁₃₈N₈O₃₃ = 1893.9259 [*M* + Na]⁺, found *m/z* 958.9582 [*M* + 2Na]⁺.

Fuc(3,5)8 **9**: This compound was prepared from **27** and **33** according to general procedure 3 and isolated as an orange solid (Yield: 46%). Mp = 153.8°C; $[\alpha]_{\text{D}}^{20}$ 66.6 (*c*, 0.085 in CH₃OH); FT-IR: $\nu_{\text{max}}/\text{cm}^{-1}$ 3409, 2921, 1735, 1595, 1348, 1032, 841, 754; ¹H NMR (400 MHz, 10% CD₃OD in CDCl₃) δ 7.94–7.74 (m, 6H, 4×ArH, 2×CH (triazole)), 7.56–7.54 (m, 2H, 2×ArH), 7.33–7.17 (m, 4H, 4×ArH), 6.65–6.64 (m, 1H, ArH), 5.46 (m, 1H, CH), 4.71–4.43 (m, 12H), 4.16–4.06 (m, 8H), 3.95–3.83 (m, 10H), 3.66–3.41 (m, 34H), 2.60 (s, 8H, 4×CH₂), 1.72–1.70 (m, 4H, 2×CH₂), 1.39–1.37 (m, 4H, 2×CH₂), 1.21 (s, 18H, 6×CH₂, 2×CH₃), 1.09–0.79 (m, 4H, 2×CH₂), 0.80–0.79 (m, 6H, 2×CH₃); ¹³C NMR (100 MHz, 10% CD₃OD in CDCl₃) δ 172.4, 172.0, 160.3, 153.0, 152.8, 126.9, 124.1, 122.7, 122.3, 108.2, 101.4, 98.9, 71.7, 70.3, 69.5, 69.3,

68.9, 68.5, 68.4, 66.3, 65.8, 63.8, 49.4, 49.2, 48.9, 48.7, 48.5, 37.2, 31.7, 29.2, 29.1, 29.0, 28.9, 28.7, 25.9, 22.5, 15.9, 13.9. ESI-HRMS (m/z) calculated for $C_{83}H_{122}N_8O_{30} = 1733.8159 [M + Na]^+$, found 1733.8152 $[M + Na]^+$.

Fuc(3,5)2Et8 **10**: This compound was prepared from **28** and **33** according to general procedure 3 and isolated as an orange wax (Yield: 34%). $[\alpha]_D^{20}$ 78.7 (c , 0.07 in CH_3OH); FT-IR: ν_{max}/cm^{-1} 3438, 2925, 1735, 1592, 1350, 1092, 843, 754; 1H NMR (400 MHz, 10% CD_3OD in $CDCl_3$) δ 7.94 (d, $J = 8.68$ Hz, 2H, $2 \times ArH$), 7.86–7.83 (m, 4H, $2 \times ArH$, $2 \times CH$ (triazole)), 7.56 (d, $J = 8.37$ Hz, 2H, $2 \times ArH$), 7.30 (d, $J = 8.68$ Hz, 2H, $2 \times ArH$), 7.25–7.24 (m, 2H, $2 \times ArH$), 6.67–6.66 (m, 1H, ArH), 5.46–5.44 (s, 1H, CH), 4.72–4.36 (m, 12H), 4.18–4.06 (m, 10H), 3.89–3.79 (m, 14H), 3.62–3.41 (m, 28H), 2.60 (s, 8H, $4 \times CH_2$), 1.69–1.62 (m, 2H, $2 \times CH$), 1.39–1.25 (m, 14H, $7 \times CH_2$), 1.10–1.08 (m, 2H, CH_2), 0.88–0.81 (m, 18H, $6 \times CH_3$); ^{13}C NMR (100 MHz, 10% CD_3OD in $CDCl_3$) δ 172.4, 164.9, 160.5, 126.9, 124.1, 122.7, 122.4, 108.2, 70.8, 70.4, 69.6, 69.4, 68.9, 66.3, 65.9, 64.3, 63.8, 49.9, 49.5, 49.2, 49.0, 48.8, 39.3, 37.2, 30.4, 28.9, 28.8, 23.8, 22.9, 15.9, 13.9, 10.9. ESI-HRMS (m/z) calculated for $C_{83}H_{122}N_8O_{30} = 1733.8159 [M + Na]^+$, found m/z 878.4021 $[M + 2Na]^+$.

Fuc(3,5)12 **11**: This compound was prepared from **29** and **33** according to general procedure 3 and isolated as an orange solid (Yield: 47%). Mp = 146.4°C; $[\alpha]_D^{20}$ 76.5 (c , 0.065 in CH_3OH); FT-IR: ν_{max}/cm^{-1} 3413, 2923, 1735, 1592, 1348, 1091, 842, 754; 1H NMR (400 MHz, 10% CD_3OD in $CDCl_3$) δ 7.94–7.84 (m, 6H, $4 \times ArH$, $2 \times CH$ (triazole)), 7.57–7.55 (m, 2H, $2 \times ArH$), 7.31–7.17 (m, 4H, $4 \times ArH$), 6.66–6.65 (m, 1H, ArH), 5.46 (s, 1H, CH), 4.72–4.39 (m, 12H), 4.17–4.06 (m, 8H), 3.97–3.83 (m, 12H), 3.65–3.36 (m, 32H), 2.60 (s, 8H, $4 \times CH_2$), 1.72–1.71 (m, 4H, $2 \times CH_2$), 1.39–1.38 (m, 4H, $2 \times CH_2$), 1.19 (s, 30H, $2 \times CH_3$, $12 \times CH_2$), 1.09–1.08 (m, 4H, $2 \times CH_2$), 0.81–0.78 (m, 6H, $2 \times CH_3$); ^{13}C NMR (100 MHz, 10% CD_3OD in $CDCl_3$) δ 172.4, 160.3, 126.9, 124.4, 124.1, 122.7, 122.3, 108.2, 98.9, 71.7, 70.3, 69.5, 69.4, 68.9, 68.5, 68.4, 66.3, 65.9, 64.3, 63.8, 49.9, 49.4, 49.2, 49.0, 48.8, 37.2, 31.8, 29.5, 29.2, 29.0, 28.8, 25.9, 22.6, 15.9, 13.9. ESI-HRMS (m/z) calculated for $C_{91}H_{138}N_8O_{30} = 1845.9411 [M + Na]^+$, found m/z 934.9670 $[M + 2Na]^+$.

Fuc(3,4,5)2Et8 **12**: This compound was prepared from **30** and **33** according to general procedure 3 and isolated as an orange wax (Yield: 37%). $[\alpha]_D^{20}$ 130.0 (c , 0.03 in CH_3OH); FT-IR: ν_{max}/cm^{-1} 3407, 2922, 1731, 1331, 1093, 840; 1H NMR (400 MHz, 10% CD_3OD in $CDCl_3$) δ 7.95–7.93 (m, 2H, $2 \times ArH$), 7.86–7.84 (m, 2H, $2 \times ArH$), 7.57–7.55 (m, 2H, $2 \times ArH$), 7.35–

7.27 (m, 4H, 4×ArH), 5.47 (s, 1H, CH), 4.83–4.44 (m, 10H), 4.18–4.06 (m, 10H), 3.89–3.34 (m, 46H), 2.61 (s, 8H, 4×CH₂), 1.71–1.64 (m, 3H, 3×CH), 1.52–1.09 (m, 30H, 2×CH₃, 12×CH₂), 0.89–0.83 (m, 18H, 6×CH₃); ¹³C NMR (100 MHz, 10% CD₃OD in CDCl₃) δ 172.4, 172.1, 172.0, 164.9, 153.2, 153.1, 152.8, 150.1, 143.1, 140.1, 126.9, 124.1, 123.3, 122.7, 122.5, 108.0, 101.4, 71.3, 70.3, 69.4, 68.9, 63.8, 63.4, 62.7, 40.6, 39.5, 37.2, 30.5, 30.3, 29.2, 29.0, 28.9, 28.8, 23.8, 23.6, 23.0, 22.9, 16.0, 13.9, 11.0. ESI-HRMS (*m/z*) calculated for C₉₁H₁₃₈N₈O₃₁ = 1861.9360 [*M* + Na]⁺, found *m/z* 942.9638 [*M* + 2Na]⁺.

3,5-dialkyloxybenzoic acid **13**: This compound was prepared from methyl 3,5-dihydroxybenzoate and 1-bromooctane according to general procedure 4, and was isolated as white solid (quantitative yield). Mp = 58.0°C; FT-IR: $\nu_{\max}/\text{cm}^{-1}$ 2917, 1559, 1388, 1264, 1154, 1015, 855, 720; ¹H NMR (400 MHz, CDCl₃) δ 7.23 (d, *J* = 2.32 Hz, 2H, 2×ArH), 6.69 (t, *J* = 2.37 Hz, 1H, ArH), 3.98 (t, *J* = 6.59 Hz, 4H, 2×CH₂), 1.80–1.75 (m, 4H, 2×CH₂), 1.48–1.28 (m, 20H, 10×CH₂), 0.91–0.87 (m, 6H, 2×CH₃); ¹³C NMR (100 MHz, CDCl₃) δ 171.9, 160.2, 130.9, 108.2, 107.5, 68.4, 31.8, 29.3, 29.2, 26.0, 22.7, 14.1; ESI-HRMS (*m/z*) calculated for C₂₃H₃₈O₄ = 377.2697 [*M* - H]⁻, found 377.2697 [*M* - H]⁻.

3,5-bis((2-ethylhexyl)oxy)benzoic acid **14**: This compound was prepared from methyl 3,5-dihydroxybenzoate and 2-ethylhexyl bromide according to general procedure 4, and was isolated as colorless liquid (quantitative yield). FT-IR: $\nu_{\max}/\text{cm}^{-1}$ 2926, 1689, 1592, 1444, 1296, 1166, 1053, 735; ¹H NMR (400 MHz, CDCl₃) 7.23 (2H, d, *J* = 2.36 Hz), 6.69 (1H, t, *J* = 2.26 Hz), 3.91–3.84 (4H, m), 1.77–1.68 (2H, m), 1.56–1.26 (16H, m), 0.96–0.88 (12H, m); ¹³C NMR (100 MHz, CDCl₃) δ 172.2, 160.5, 131.0, 108.1, 107.5, 70.8, 39.4, 30.5, 29.1, 23.9, 23.3, 23.1, 14.1, 11.1; ESI-HRMS (*m/z*) calculated for C₂₃H₃₈O₄ = 377.2697 [*M* - H]⁻, found 377.2697 [*M* - H]⁻.

3,5-bis(dodecyl)oxy)benzoic acid **15**: This compound was prepared from methyl 3,5-dihydroxybenzoate and 1-bromododecane according to general procedure 4, and was isolated as white solid (quantitative yield). Mp = 67.6°C; FT-IR: $\nu_{\max}/\text{cm}^{-1}$ 2916, 1686, 1596, 1394, 1316, 1161, 1058, 857, 669; ¹H NMR (400 MHz, CDCl₃) δ 7.23 (d, *J* = 2.33 Hz, 2H, 2×ArH), 6.69 (t, *J* = 2.31 Hz, 1H, ArH), 3.98 (t, *J* = 6.50 Hz, 4H, 2×CH₂), 1.80–1.77 (m, 4H, 2×CH₂), 1.47–1.44 (m, 4H, 2×CH₂), 1.36–1.28 (m, 32H, 16×CH₂), 0.88 (t, *J* = 7.06 Hz, 6H, 2×CH₃); ¹³C NMR (100 MHz, CDCl₃) δ 171.7, 160.2, 130.9, 108.2, 107.5, 68.4, 31.9, 29.7, 29.6, 29.4,

29.2, 26.0, 22.7, 14.1; ESI-HRMS (m/z) calculated for $C_{31}H_{54}O_4=489.3949$ [$M - H$] $^-$, found 489.3945 [$M - H$] $^-$.

3,4,5-tris((2-ethylhexyl)oxy)benzoic acid **16**: This compound was prepared from methyl 3,4,5-dihydrobenzoate and 2-ethylhexyl bromide according to general procedure 4, and was isolated as colorless liquid (quantitative yield). FT-IR: $\nu_{\max}/\text{cm}^{-1}$ 2914, 1685, 1590, 1395, 1317, 1163, 1059, 858, 669; ^1H NMR (400 MHz, CDCl_3) δ 7.33 (s, 2H, $2\times\text{ArH}$), 3.96–3.87 (m, 6H, $3\times\text{CH}_2$), 1.80–1.26 (m, 27H, $3\times\text{CH}$, $12\times\text{CH}_2$), 0.96–0.89 (m, 18H, $4\times\text{CH}_3$); ^{13}C NMR (100 MHz, CDCl_3) δ 171.7, 153.1, 143.2, 123.4, 108.1, 71.4, 40.6, 39.6, 30.5, 30.4, 29.3, 29.1, 23.8, 23.7, 23.1, 14.1, 11.2, 11.1; ESI-HRMS (m/z) calculated for $C_{31}H_{54}O_5=505.3898$ [$M - H$] $^-$, found 505.3892 [$M - H$] $^-$.

4-hydroxy-4'-formylazobenzene **17**¹: A suspension of 2 g 4-aminobenzaldehyde was prepared at 0°C in 11 mL water. At the same temperature was separately dissolved 1.1 g sodium nitrite in 8 mL water. To the suspension of 4-aminobenzaldehyde was simultaneously added at vigorous stirring the solution of sodium nitrite and 8 mL of 24% HCl solution. After 1 hour, a cooled to 0°C solution of 1.6 g phenol in 10 mL 6% NaOH solution was added to the reaction mixture. The end of the azo coupling was checked by TLC and the precipitate was filtered off to afford the final compound as brown-red solid (1.2g, 32%). Mp = 210°C; FT-IR: $\nu_{\max}/\text{cm}^{-1}$ 3308, 1670, 1584, 1281, 1128, 834; ^1H NMR (400MHz, $\text{C}_3\text{D}_6\text{O}$) 10.07 (1H, s), 8.01 (2H, d, $J = 8.53$ Hz), 7.92 (2H, d, $J = 8.53$ Hz), 7.79 (2H, d, $J = 8.91$ Hz), 6.79 (2H, d, $J = 8.88$ Hz); ^{13}C NMR (100 MHz, $(\text{CD}_3)_2\text{SO}$) δ 192.4, 177.7, 158.1, 140.7, 134.2, 131.2, 121.5, 120.6; ESI-HRMS (m/z) calculated for $C_{13}H_{10}N_2O_2=225.0669$ [$M - H$] $^-$, found 225.0670 [$M - H$] $^-$.

Compound **18**: This compound was prepared from **13** and **17** according to general procedure 1 and was isolated as an orange solid (Yield: 60%). Mp = 44.1°C; FT-IR: $\nu_{\max}/\text{cm}^{-1}$ 2917, 1702, 1594, 1444, 1295, 1161, 1053, 839, 752; ^1H NMR (400 MHz, CDCl_3) δ 10.10 (s, 1H, CHO), 8.06–8.03 (m, 6H, $6\times\text{ArH}$), 7.40 (d, $J = 8.89$ Hz, 2H, $2\times\text{ArH}$), 7.33 (d, $J = 2.35$ Hz, 2H, $2\times\text{ArH}$), 6.73 (t, $J = 2.33$ Hz, 1H, ArH), 4.01 (t, $J = 6.60$ Hz, 4H, $2\times\text{CH}_2$), 1.84–1.77 (m, 4H, $2\times\text{CH}_2$), 1.49–1.44 (m, 4H, $2\times\text{CH}_2$), 1.38–1.29 (m, 16H, $8\times\text{CH}_2$), 0.89 (t, $J = 6.95$ Hz, 6H, $2\times\text{CH}_3$). ^{13}C NMR (100 MHz, CDCl_3) δ 191.6 (CHO), 164.7 (C=O), 160.4, 155.8, 153.8, 150.2, 137.5, 130.7, 124.6, 123.4, 122.6, 108.3, 107.4, 68.5 (CH_2), 31.8 (CH_2), 29.4 (CH_2), 29.3 (CH_2), 29.2 (CH_2), 26.0 (CH_2), 22.7 (CH_2), 14.1 (CH_3). ESI-HRMS (m/z) calculated for $C_{36}H_{46}N_2O_5=586.7730$ [$M + H$] $^+$, found 586.4662 [$M + H$] $^+$.

Compound **19**: This compound was prepared from **14** and **17** according to general procedure 1 and was isolated as an orange wax (Yield: 56%). FT-IR: $\nu_{\max}/\text{cm}^{-1}$ 2925, 1701, 1444, 1189, 1034, 754; ^1H NMR (400 MHz, CDCl_3) δ 10.01 (s, 1H, CHO), 7.98–7.95 (m, 6H, 6 \times ArH), 7.32 (d, J = 8.84 Hz, 2H, 2 \times ArH), 7.25 (d, J = 2.36 Hz, 2H, 2 \times ArH), 6.66 (t, J = 2.29 Hz, 1H, ArH), 3.83–3.80 (m, 4H, 2 \times CH₂), 1.67–1.64 (m, 4H, 2 \times CH), 1.46–1.23 (m, 16H, 8 \times CH₂), 0.88–0.81 (m, 12H, 4 \times CH₃); ^{13}C NMR (100 MHz, CDCl_3) δ 191.6 (CHO), 164.8 (C=O), 160.6, 155.8, 153.8, 150.2, 137.5, 130.7, 124.6, 123.4, 122.6, 108.3, 107.3, 70.8, 70.7, 39.4, 30.6, 29.1, 23.9, 23.1, 14.1, 11.2 (CH₃). ESI-HRMS (m/z) calculated for $\text{C}_{36}\text{H}_{46}\text{N}_2\text{O}_5$ =587.3479 [$M + \text{H}$]⁺, found 587.3477 [$M + \text{H}$]⁺.

Compound **20**: This compound was prepared from **15** and **17** according to general procedure 1 and was isolated as an orange solid (Yield: 51%). Mp = 58.5°C; FT-IR: $\nu_{\max}/\text{cm}^{-1}$ 2917, 1702, 1594, 1347, 1165, 1046, 838, 752; ^1H NMR (400 MHz, CDCl_3) δ 10.01 (s, 1H, CHO), 7.97–7.95 (m, 6H, 6 \times ArH), 7.31 (d, J = 8.73 Hz, 2H, 2 \times ArH), 7.24 (d, J = 2.04 Hz, 2H, 2 \times ArH), 6.64 (s, 1H, ArH), 3.92 (t, J = 6.74 Hz, 4H, 2 \times CH₂), 1.73–1.68 (m, 4H, 2 \times CH₂), 1.39–1.35 (m, 4H, 2 \times CH₂), 1.18 (br s, 32H, 16 \times CH₂), 0.79 (t, J = 6.49 Hz, 6H, 2 \times CH₃); ^{13}C NMR (100 MHz, CDCl_3) δ 191.5 (CHO), 164.7 (C=O), 160.4, 155.8, 153.8, 150.2, 137.5, 130.7, 124.6, 123.4, 122.6, 108.3, 107.4, 68.4, 31.9, 29.7, 29.6, 29.4, 29.2, 26.1, 22.7. ESI-HRMS (m/z) calculated for $\text{C}_{44}\text{H}_{62}\text{N}_2\text{O}_5$ =697.4585 [$M - \text{H}$]⁻, found 697.5886 [$M - \text{H}$]⁻.

Compound **21**: This compound was prepared from **16** and **17** according to general procedure 1 and was isolated as an orange wax (Yield: 61%). FT-IR: $\nu_{\max}/\text{cm}^{-1}$ 2929, 1701, 1428, 1330, 1180, 937, 752; ^1H NMR (400 MHz, CDCl_3) δ 10.14 (s, 1H, CHO), 8.10–8.08 (m, 6H, 6 \times ArH), 7.46–7.43 (m, 4H, 4 \times ArH), 4.01–3.94 (m, 6H, 3 \times CH₂), 1.83–1.36 (m, 27H, 3 \times CH, 12 \times CH₂), 0.99–0.94 (m, 18H, 6 \times CH₃); ^{13}C NMR (100 MHz, CDCl_3) δ 191.6 (CHO), 164.8 (C=O), 155.8, 153.9, 153.2, 150.2, 143.3, 137.5, 130.7, 124.6, 123.3, 122.7, 108.1, 71.4, 40.7, 39.6, 30.6, 29.1, 23.9, 23.1, 14.1, 11.2. ESI-HRMS (m/z) calculated for $\text{C}_{44}\text{H}_{62}\text{N}_2\text{O}_6$ =714.4602, found 714.5860.

Compound **22**: This compound was prepared from **18** according to general procedure 2 and was isolated as an orange solid (Yield: 61%). Mp = 139.4°C; FT-IR: $\nu_{\max}/\text{cm}^{-1}$ 2923, 1739, 1590, 1297, 1161, 1034, 754; ^1H NMR (400 MHz, CDCl_3) δ 7.93 (d, J = 8.81 Hz, 2H, 2 \times ArH), 7.85 (d, J = 8.27 Hz, 2H, 2 \times ArH), 7.55 (d, J = 8.36 Hz, 2H, 2 \times ArH), 7.29–7.25 (m, 4H, 4 \times ArH), 6.65 (s, 1H, ArH), 5.41 (s, 1H, CH), 4.13–4.05 (m, 4H), 3.93 (t, J = 6.53 Hz, 4H, 2 \times CH₂), 3.70

(d, $J = 11.6$ Hz, 2H), 3.46 (s, 2H), 1.76–1.69 (m, 4H, $2 \times CH_2$), 1.39–1.35 (m, 4H, $2 \times CH_2$), 1.25–1.18 (m, 16H, $8 \times CH_2$), 0.83–0.79 (m, 6H, $2 \times CH_3$); ^{13}C NMR (100 MHz, $CDCl_3$) δ 164.8 (C=O), 160.4, 153.1, 152.8, 150.3, 140.6, 130.8, 126.9, 124.2, 122.9, 122.4, 108.3, 107.4, 101.4, 70.1, 68.5, 65.4, 63.9, 38.9, 31.8, 29.4, 29.3, 29.2, 26.0, 14.1. ESI-HRMS (m/z) calculated for $C_{41}H_{56}N_2O_8 = 705.4109 [M + H]^+$ 727.3928 $[M + Na]^+$, found 705.4114 $[M + H]^+$, 727.3935 $[M + Na]^+$.

Compound 23: This compound was prepared from **19** according to general procedure 2 and was isolated as an orange solid (Yield: 53%). Mp = 123.6°C; FT-IR: ν_{max}/cm^{-1} 2927, 1743, 1592, 1298, 1168, 1037, 752; 1H NMR (400 MHz, $CDCl_3$) δ 8.01 (d, $J = 8.90$ Hz, 2H, $2 \times ArH$), 7.93 (d, $J = 8.68$ Hz, 2H, $2 \times ArH$), 7.63 (d, $J = 8.41$ Hz, 2H, $2 \times ArH$), 7.37 (d, $J = 8.84$ Hz, 2H, $2 \times ArH$), 7.34 (d, $J = 2.44$ Hz, 2H, $2 \times ArH$), 6.74 (t, $J = 2.30$ Hz, 1H, ArH), 5.49 (s, 1H, CH), 4.18 (d, $J = 11.76$ Hz, 2H), 4.12 (s, 2H), 3.93–3.89 (m, 4H), 3.78 (d, $J = 12.05$ Hz, 2H), 3.54 (s, 2H), 1.76–1.71 (m, 2H, $2 \times CH$), 1.55–1.29 (m, 16H, $8 \times CH_2$), 0.97–0.89 (m, 12H, $4 \times CH_3$); ^{13}C NMR (100 MHz, $CDCl_3$) δ 164.9 (C=O), 160.6, 153.1, 152.8, 150.3, 140.6, 130.8, 126.9, 124.2, 122.9, 122.4, 108.2, 107.3, 101.4, 70.9, 70.0, 65.4, 63.9, 39.4, 38.9, 30.5, 29.1, 23.9, 23.1, 14.1, 11.2. ESI-HRMS (m/z) calculated for $C_{41}H_{56}N_2O_8 = 705.4109 [M + H]^+$ 727.3928 $[M + Na]^+$, found 705.4113 $[M + H]^+$, 727.3930 $[M + Na]^+$.

Compound 24: This compound was prepared from **20** according to general procedure 2 and was isolated as an orange solid (Yield: 57%). Mp = 132.0°C; FT-IR: ν_{max}/cm^{-1} 2919, 1747, 1595, 1446, 1296, 1167, 1037, 754; 1H NMR (400 MHz, $CDCl_3$) δ 8.01 (d, $J = 8.83$ Hz, 2H, $2 \times ArH$), 7.93 (d, $J = 8.66$ Hz, 2H, $2 \times ArH$), 7.63 (d, $J = 8.41$ Hz, 2H, $2 \times ArH$), 7.37 (d, $J = 8.90$ Hz, 2H, $2 \times ArH$), 7.33 (d, $J = 2.33$ Hz, 2H, $2 \times ArH$), 6.73 (t, $J = 2.33$ Hz, 1H, ArH), 5.49 (s, 1H, CH), 4.19 (d, $J = 11.87$ Hz, 2H), 4.12 (s, 2H), 4.01 (t, $J = 6.50$ Hz, 4H), 3.78 (d, $J = 11.87$ Hz, 2H), 3.53 (s, 2H), 1.82–1.78 (m, 4H, $2 \times CH_2$), 1.49–1.45 (m, 4H, $2 \times CH_2$), 1.37–1.27 (m, 32H, $16 \times CH_2$), 0.88 (t, $J = 6.65$ Hz, 6H, $2 \times CH_3$); ^{13}C NMR (100 MHz, $CDCl_3$) δ 164.8 (C=O), 160.4, 153.1, 152.8, 150.3, 140.6, 130.8, 126.9, 124.2, 122.9, 122.4, 108.3, 107.4, 101.4, 70.0, 68.5, 65.4, 63.9, 38.9, 31.9, 29.7, 29.6, 29.4, 29.2, 26.0, 22.7, 14.1. ESI-HRMS (m/z) calculated for $C_{49}H_{72}N_2O_8 = 817.5361 [M + H]^+$ 839.5180 $[M + Na]^+$, found 817.5365 $[M + H]^+$, 839.5185 $[M + Na]^+$.

Compound 25: This compound was prepared from **21** according to general procedure 2 and was isolated as an orange solid (Yield: 46%). Mp = 92.5°C; FT-IR: ν_{max}/cm^{-1} 2925, 1735, 1584,

1428, 1332, 1182, 1093, 1008, 753; ^1H NMR (400 MHz, CDCl_3) δ 8.02 (d, $J = 8.84$ Hz, 2H, $2\times\text{ArH}$), 7.93 (d, $J = 8.54$ Hz, 2H, $2\times\text{ArH}$), 7.63 (d, $J = 8.46$ Hz, 2H, $2\times\text{ArH}$), 7.43 (s, 2H, $2\times\text{ArH}$), 7.37 (d, $J = 8.89$ Hz, 2H, $2\times\text{ArH}$), 5.49 (s, 1H, CH), 4.20–4.12 (m, 4H), 3.98–3.93 (m, 6H), 3.78 (d, $J = 12.06$ Hz, 2H), 3.53 (s, 2H), 2.64–2.61 (m, 2H), 1.80–1.32 (m, 27H, $3\times\text{CH}$, $12\times\text{CH}_2$), 0.98–0.89 (m, 18H, $6\times\text{CH}_3$); ^{13}C NMR (100 MHz, CDCl_3) δ 164.9 (C=O), 153.2, 152.8, 150.3, 143.2, 140.7, 126.9, 124.2, 123.4, 122.8, 122.6, 108.1, 101.4, 76.1, 71.4, 70.0, 65.4, 63.9, 40.7, 39.6, 38.9, 30.6, 29.1, 23.9, 23.2, 14.1, 11.2. ESI-HRMS (m/z) calculated for $\text{C}_{49}\text{H}_{72}\text{N}_2\text{O}_9=833.5810$ $[\text{M} + \text{H}]^+$ 855.5130 $[\text{M} + \text{Na}]^+$, found 833.5314 $[\text{M} + \text{H}]^+$, 855.5127 $[\text{M} + \text{Na}]^+$.

14-oxo-4,7,10,13-tetraoxaheptadec-1-yn-17-oic acid **26**: This compound was prepared according to literature procedure over two steps.² Sodium hydride (2.6g, 65 mmol, 65 equiv. 60% disperse in mineral oil) was slowly added to a solution of triethyleneglycol (15.02g, 100 mmol, 100 equiv.) in dry THF (75 mL) and the mixture stirred for 30 min at 0°C under N_2 . Propargyl bromide (5.4 mL, 50 mmol, 50 equiv.) was slowly injected to the reaction mixture, followed by stirring at 0°C for 2 hours and at room temperature for 20 hours. The mixture was poured into water, extracted with DCM, dried over Na_2SO_4 and purified by flash chromatography using EtOAc:hexane (3:2) as the eluent to afford the intermediate as pale yellow oil (3.95g, 43%). FT-IR: $\nu_{\text{max}}/\text{cm}^{-1}$ 2921, 2852, 1736, 1457, 1069; ^1H NMR (400MHz, CDCl_3) δ 5.15 (s, 1H, OH), 4.29–4.09 (m, 4H, $2\times\text{CH}_2$), 3.68–3.54 (m, 10H, $5\times\text{CH}_2$), 2.43–2.42 (m, 1H, CH); ^{13}C NMR (100 MHz, CDCl_3) δ 79.5, 74.9, 72.4, 70.3, 70.2, 68.8, 61.2, 58.1; LCMS (m/z) calculated for $\text{C}_9\text{H}_{16}\text{O}_4=189.1$ $[\text{M} + \text{H}]^+$, found 189.1 $[\text{M} + \text{H}]^+$. The synthetic intermediate (2 g, 10.6 mmol, 1 equiv.) and succinic anhydride (1.28 g, 12.8 mmol, 1.2 equiv.) were dissolved in anhydrous DCM (10 mL) under N_2 . To this reaction mixture, triethylamine (1.48 mL, 10.6 mmol, 1 equiv.) was added dropwise. The reaction mixture was then stirred at room temperature for 24 hours under N_2 , before poured into water (60 mL) and neutralized with 1N HCl. The organic layer was then washed with brine, dried over Na_2SO_4 , concentrated under reduced pressure and purified by flash chromatography to afford the final product as pale yellow oil (2.02g, 68.3%). FT-IR: $\nu_{\text{max}}/\text{cm}^{-1}$ 1728, 1349, 1088, 834, 635; ^1H NMR (400 MHz, CDCl_3) δ 4.25–4.23 (m, 2H, CH_2), 4.18 (d, $J = 2.40$ Hz, 2H, CH_2), 3.69–3.64 (m, 11H, $5\times\text{CH}_2$, CH), 2.64 (s, 4H, CH_2); ^{13}C NMR (100 MHz, CDCl_3) δ 176.2, 172.1, 79.6, 79.5, 74.9, 70.3, 70.2, 70.1, 68.8, 63.7, 58.1, 28.8, 28.7; ESI-HRMS (m/z) calculated for $\text{C}_{13}\text{H}_{20}\text{O}_7=287.1136$ $[\text{M} - \text{H}]^-$, found 287.1133 $[\text{M} - \text{H}]^-$.

Compound **27**: This compound was prepared from **22** and **26** according to general procedure 1 and was isolated as an orange wax (Yield: 67%). FT-IR: $\nu_{\max}/\text{cm}^{-1}$ 2923, 1735, 1592, 1348, 1095, 843, 755; ^1H NMR (400 MHz, CDCl_3) δ 7.99 (d, $J = 8.92$ Hz, 2H, $2\times\text{ArH}$), 7.91 (d, $J = 8.49$ Hz, 2H, $2\times\text{ArH}$), 7.61 (d, $J = 8.58$ Hz, 2H, $2\times\text{ArH}$), 7.35 (d, $J = 8.87$ Hz, 2H, $2\times\text{ArH}$), 7.31 (d, $J = 2.24$ Hz, 2H, $2\times\text{ArH}$), 6.70 (t, $J = 2.27$ Hz, 1H, ArH), 5.50 (s, 1H, CH), 4.51 (s, 2H), 4.26–4.12 (m, 10H), 4.00–3.95 (m, 6H), 3.89–3.86 (m, 2H), 3.69–3.63 (m, 20H), 2.66 (s, 8H, $4\times\text{CH}_2$), 2.44–2.42 (m, 2H, $2\times\text{CH}$), 1.81–1.74 (m, 4H, $2\times\text{CH}_2$), 1.47–1.41 (m, 4H, $2\times\text{CH}_2$), 1.36–1.27 (m, 16H, $8\times\text{CH}_2$), 0.89–0.85 (m, 6H, $2\times\text{CH}_3$); ^{13}C NMR (100 MHz, CDCl_3) δ 172.2, 171.9, 164.7, 160.3, 153.1, 152.9, 150.2, 140.2, 130.9, 127.0, 124.2, 122.8, 122.4, 108.2, 101.5, 79.7, 74.6, 70.6, 70.4, 69.5, 69.1, 69.0, 68.4, 63.9, 63.4, 62.7, 58.4, 37.3, 31.8, 29.3, 29.2, 29.1, 29.0, 28.9, 26.0, 22.7, 14.1; ESI-HRMS (m/z) calculated for $\text{C}_{67}\text{H}_{92}\text{N}_2\text{O}_{20}=1245.6316$ [$M + \text{H}$] $^+$ 1267.6135 [$M + \text{Na}$] $^+$, found 1245.6305 [$M + \text{H}$] $^+$, 1267.6129 [$M + \text{Na}$] $^+$.

Compound **28**: This compound was prepared from **23** and **26** according to general procedure 1 and was isolated as an orange wax (Yield: 63%). FT-IR: $\nu_{\max}/\text{cm}^{-1}$ 2929, 1734, 1592, 1347, 1096, 841; ^1H NMR (400 MHz, CDCl_3) δ 8.01 (d, $J = 8.88$ Hz, 2H, $2\times\text{ArH}$), 7.92 (d, $J = 8.44$ Hz, 2H, $2\times\text{ArH}$), 7.63 (d, $J = 8.49$ Hz, 2H, $2\times\text{ArH}$), 7.37 (d, $J = 8.84$ Hz, 2H, $2\times\text{ArH}$), 7.32 (d, $J = 2.33$ Hz, 2H, $2\times\text{ArH}$), 6.73 (t, $J = 2.30$ Hz, 1H, ArH), 5.52 (s, 1H, CH), 4.52 (s, 2H), 4.27–4.13 (m, 10H), 3.97–3.88 (m, 8H), 3.72–3.63 (m, 20H), 2.68 (s, 8H, $4\times\text{CH}_2$), 2.44–2.42 (m, 2H, $2\times\text{CH}$), 1.75–1.72 (m, 2H, $2\times\text{CH}$), 1.52–1.25 (m, 16H, $8\times\text{CH}_2$), 0.95–0.89 (m, 12H, $4\times\text{CH}_3$); ^{13}C NMR (100 MHz, CDCl_3) δ 172.2, 171.1, 164.8, 160.6, 153.1, 152.9, 150.3, 140.2, 130.8, 127.0, 124.4, 122.8, 122.4, 108.2, 101.5, 79.7, 74.6, 70.8, 70.6, 70.4, 69.5, 69.1, 63.9, 63.4, 58.4, 39.4, 37.3, 33.9, 30.5, 29.1, 29.0, 28.9, 24.9, 23.9, 23.0, 14.1, 11.1; ESI-HRMS (m/z) calculated for $\text{C}_{67}\text{H}_{92}\text{N}_2\text{O}_{20}=1245.6316$ [$M + \text{H}$] $^+$ 1267.6135 [$M + \text{Na}$] $^+$, found 1245.6294 [$M + \text{H}$] $^+$, 1267.6130 [$M + \text{Na}$] $^+$.

Compound **29**: This compound was prepared from **24** and **26** according to general procedure 1 and was isolated as an orange wax (Yield: 57%). FT-IR: $\nu_{\max}/\text{cm}^{-1}$ 2926, 1735, 1593, 1348, 1097, 841; ^1H NMR (400 MHz, CDCl_3) δ 7.99 (d, $J = 8.73$ Hz, 2H, $2\times\text{ArH}$), 7.91 (d, $J = 8.34$ Hz, 2H, $2\times\text{ArH}$), 7.62 (d, $J = 8.35$ Hz, 2H, $2\times\text{ArH}$), 7.37–7.31 (m, 4H, $4\times\text{ArH}$), 6.71 (s, 1H, ArH), 5.51 (s, 1H, CH), 4.51 (s, 2H), 4.27–4.13 (m, 10H), 4.01–3.87 (m, 8H), 3.71–3.63 (m, 20H), 2.67 (s, 8H, $4\times\text{CH}_2$), 2.44–2.42 (m, 2H, $2\times\text{CH}$), 1.86–1.75 (m, 4H, $4\times\text{CH}_2$), 1.45–1.42 (m, 4H, $2\times\text{CH}_2$), 1.33–1.25 (m, 32H, $16\times\text{CH}_2$), 0.88–0.85 (m, 6H, $2\times\text{CH}_3$); ^{13}C NMR (100 MHz, CDCl_3) δ 172.2, 171.9, 164.7, 160.4, 153.1, 152.9, 150.3, 140.2, 130.9, 127.0, 124.2,

122.8, 122.4, 108.2, 107.3, 101.5, 79.7, 74.6, 70.6, 70.5, 69.5, 69.1, 69.0, 68.4, 63.9, 63.4, 62.7, 58.4, 37.3, 31.9, 29.7, 29.6, 29.4, 29.2, 29.0, 28.9, 26.0, 22.7, 14.1; ESI-HRMS (m/z) calculated for $C_{75}H_{108}N_2O_{20}$ =1357.7568 [$M + H$]⁺ 1379.7387 [$M + Na$]⁺, found 1357.7605 [$M + H$]⁺, 1379.7400 [$M + Na$]⁺.

Compound **30**: This compound was prepared from **25** and **26** according to general procedure 1 and was isolated as an orange wax (Yield: 46%). FT-IR: $\nu_{\max}/\text{cm}^{-1}$ 2932, 1731, 1333, 1183, 1095, 1009, 938, 840, 755; ¹H NMR (400 MHz, CDCl₃) δ 8.00 (d, $J = 8.90$ Hz, 2H, 2×ArH), 7.92 (d, $J = 8.44$ Hz, 2H, 2×ArH), 7.62 (d, $J = 8.48$ Hz, 2H, 2×ArH), 7.41 (s, 2H, 2×ArH), 7.36 (d, $J = 8.93$ Hz, 2H, 2×ArH), 5.51 (s, 1H, CH), 4.51 (s, 2H), 4.27–4.13 (m, 10H), 3.96–3.87 (m, 8H), 3.71–3.63 (m, 20H), 2.67 (s, 8H, 4×CH₂), 2.44–2.42 (m, 2H, 2×CH), 1.88–1.30 (m, 27H, 3×CH, 12×CH₂), 0.95–0.87 (m, 18H, 6×CH₃); ¹³C NMR (100 MHz, CDCl₃) δ 172.2, 171.9, 164.8, 153.3, 153.2, 152.9, 150.2, 143.1, 140.2, 127.0, 124.2, 123.4, 122.8, 122.5, 108.1, 101.5, 79.7, 74.6, 71.4, 70.6, 70.4, 69.5, 69.1, 69.0, 63.9, 63.4, 62.7, 58.4, 40.7, 39.6, 37.3, 30.5, 30.4, 29.3, 29.1, 29.0, 28.9, 23.9, 23.7, 23.1, 14.2, 14.1, 11.2; ESI-HRMS (m/z) calculated for $C_{75}H_{108}N_2O_{21}$ =1373.7517 [$M + H$]⁺ 1395.7336 [$M + Na$]⁺, found 1373.7531 [$M + H$]⁺, 1395.7316 [$M + Na$]⁺.

2-azidoethyl α -D-mannopyranoside **31**: This compound was prepared from α -D-mannose pentaacetate according to general procedure 5 and was isolated as white solid (Yield: 74%). Mp = 132.8°C; $[\alpha]_D^{20}$ 125.0 (c , 0.06 in CH₃OH); FT-IR: $\nu_{\max}/\text{cm}^{-1}$ 2922, 2100, 1559, 1406, 1287, 1056, 648; ¹H NMR (400 MHz, CD₃OD) δ 4.85 (d, $J = 1.48$ Hz, 1H, H-1), 3.96–3.84 (m, 3H, H-2, H-3, H-4), 3.78–3.73 (m, 2H, H-6), 3.69–3.57 (m, 3H, H-5, CH₂CH₂N₃), 3.45–3.42 (m, 2H, CH₂N₃); ¹³C NMR (100 MHz, CD₃OD) δ 100.4, 73.4, 71.0, 70.6, 67.1, 66.3, 61.3, 50.4; LCMS: m/z calculated for $C_8H_{15}N_3O_6 = 272.1$ [$M + Na$]⁺, found 272.1 [$M + Na$]⁺.

2-azidoethyl β -D-galactopyranoside **32**: This compound was prepared from β -D-galactose pentaacetate according to general procedure 5 and was isolated as colorless wax (Yield: 77%). $[\alpha]_D^{20}$ 18.9 (c , 0.19 in CH₃OH); FT-IR: $\nu_{\max}/\text{cm}^{-1}$ 2102, 1580, 1369, 1047; ¹H NMR (400 MHz, CD₃OD) δ 4.30 (d, $J = 7.36$ Hz, 1H, H-1), 4.07–4.01 (m, 1H, OCH), 3.89–3.88 (m, 1H, H-4), 3.79–3.74 (m, 3H, H-2, H-3, OCH), 3.59–3.49 (m, 5H, H-5, CH₂CH₂N₃, CH₂N₃); ¹³C NMR (100 MHz, CD₃OD) δ 103.7, 75.3, 73.5, 71.1, 68.9, 67.8, 61.0, 50.7; LCMS (m/z) calculated for $C_8H_{15}N_3O_6 = 272.1$ [$M + Na$]⁺, found 272.1 [$M + Na$]⁺.

2-azidoethyl α -L-fucopyranoside **33**: This compound was prepared from 1,2,3,4-tetra-O-acetyl- α -L-fucose according to general procedure 5 and was isolated as pale yellow solid (Yield: 71.4 %). Mp = 159.0°C; $[\alpha]_D^{20}$ 140.0 (*c*, 0.025 in CH₃OH); FT-IR: $\nu_{\max}/\text{cm}^{-1}$ 2111, 1746, 1371, 1213, 1060, 950, 676; ¹H NMR (400 MHz, CD₃OD) δ 4.80 (d, *J* = 2.89 Hz, 1H, *H*-1), 4.03–3.98 (m, 1H, *H*-5), 3.87–3.76 (m, 3H), 3.70–3.37 (m, 4H, CH₂CH₂N₃), 1.23 (d, *J* = 6.61 Hz, 3H, CH₃); ¹³C NMR (100 MHz, CD₃OD) δ 101.0 (*C*-1), 73.8 (*C*-4), 71.8 (*C*-3), 69.8 (*C*-2), 67.9 (OCH₂), 67.7 (*C*-5), 51.9 (CH₂N₃), 16.8 (CH₃). LCMS (*m/z*) calculated for C₈H₁₅N₃O₅=256.1 [*M*+Na]⁺, found 256.1 [*M*+Na]⁺.

Chapter 5

Concluding Comments and Future Directions

This page is intentionally blank

Concluding comments and future directions

In this thesis, we describe the combinatorial synthesis, physical characterization and biological activity of a new generation of carbohydrate-based amphiphile. UV-visible light was used as an environmental stimulus for controlling the interfacial activity and self-assembly properties of these materials, which was further applied as a strategy for modulating their biological activity.

Chapter one is a comprehensive overview of the literature concerning the application of azobenzene *trans-cis* photoisomerization for controlling the molecular conformation of carbohydrates. Previous studies have highlighted this approach for modulating the multivalent presentation of carbohydrates, adsorption and aggregation properties of carbohydrate-based surfactants, and supramolecular assembly of carbohydrate-based materials with broad applications in nanoscience and materials science. Prior to this work, however, there have been no studies describing the application of the venerable photoswitch for controlling the antifreeze properties, anti-microbial activity and lectin-binding properties of carbohydrate-based amphiphiles. This thesis opens a new chapter in this exciting area of research and provides proof-of-principle for the future application of these molecules in controlled release, responsive tools for glycobiology research, and as novel therapeutics and cryoprotectants.

Chapter two of this thesis describes the modular synthesis and photocontrollable ice recrystallization inhibition activity of a panel of carbohydrate-based surfactants. Specifically, a library of 15 azobenzene-functionalized, carbohydrate-based fluorosurfactants were assembled using a modular approach, and their structure–activity relationships were determined. Surfactants comprised a mono- or disaccharide head group that was appended to a hydrophobic, photoswitchable *n*-butyl azobenzene tail group, and regioisomeric trifluoromethyl ($-\text{CF}_3$) azobenzene tail group. Weak-to-moderate IRI activity was observed

for these compounds, with the exception of a D-mannose based photosurfactant (**2.8**), which exhibited potent photomodulated IRI activity. Interestingly, this compound did not display any detectable thermal hysteresis (TH) activity, and therefore shows significant promise for the future development of low molecular weight mannose-based cryoprotectants. Future work will be directed toward optimizing antifreeze/IRI activity, and overcoming the deleterious cytotoxicity observed for these compounds. In particular, the development of novel, non-ionic (fluoro)surfactants will be targeted, along with known commercial carbohydrate-based surfactants (e.g. sucrose esters) as a potentially new source of cryoprotectants for biomedical use.

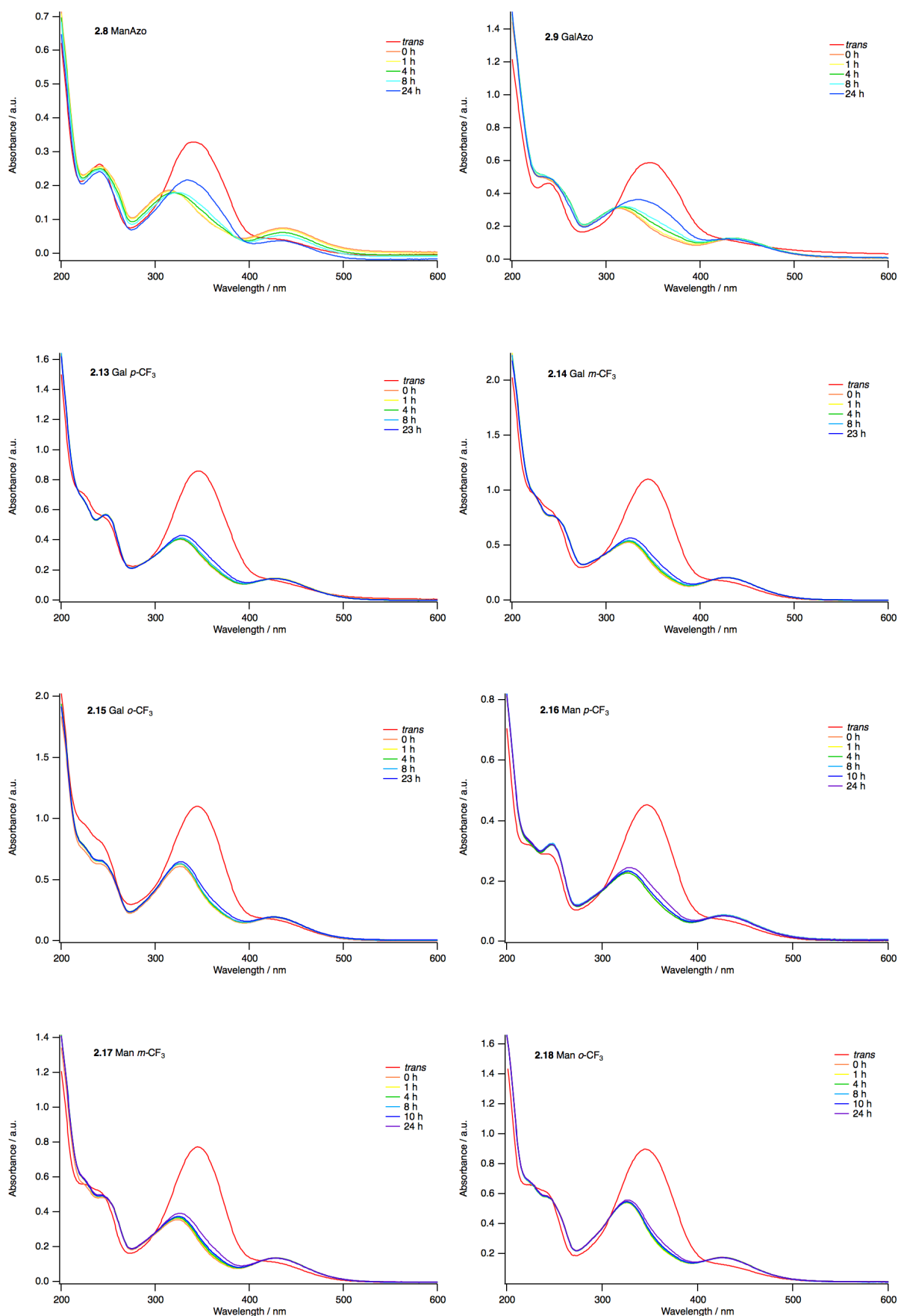
Chapter three focused on the synthesis and characterization of 11 photocontrollable carbohydrate-based surfactants as potential inhibitors of bacterial growth and biofilm formation. Through structural variation of the carbohydrate head group and photoisomerization of the *n*-butyl azobenzene tail group, the self-assembly and bioactivity of these intriguing molecules could be tuned. The antibacterial performance of these surfactants was assessed using an optical density assay, revealing bacteria- and photoisomer-specific, dose-dependent inhibition of the bacterial growth of Gram-negative *E. coli* and Gram-positive, methicillin resistant *S. aureus*. Interestingly, these photosurfactants generally promoted the growth of Gram-negative *P. aeruginosa*, thus underscoring the differences in the cell-wall structure and permeability, as well as the physiological differences of these bacterial species. The ability to control the physiological behaviour of bacteria using photoswitchable surfactants is unprecedented and presents new opportunities for the development of responsive tools for studying bacterial adhesion processes and as antibacterial agents and coatings. Future work could be directed towards understanding these interactions at the molecular level, for example, the interrogation of biochemical signaling and lectin binding events that lead to specific changes in quorum sensing and swarming motility, as well as understanding the basis for the promotion of bacterial growth observed in *P. aeruginosa*.

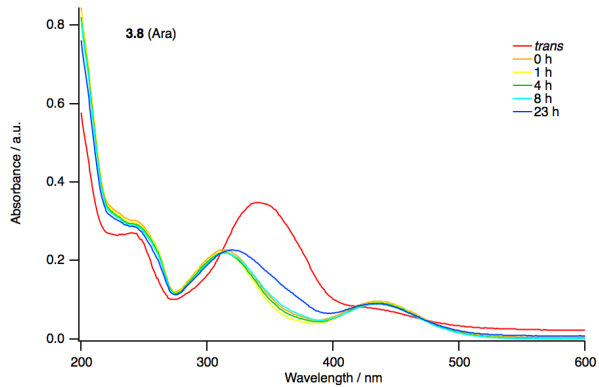
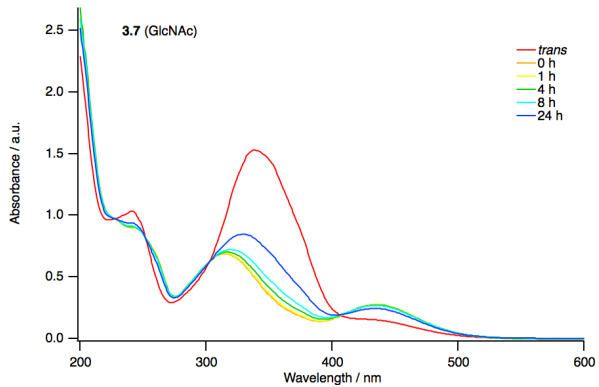
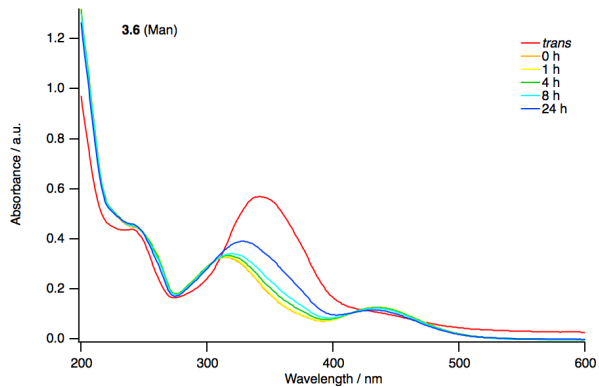
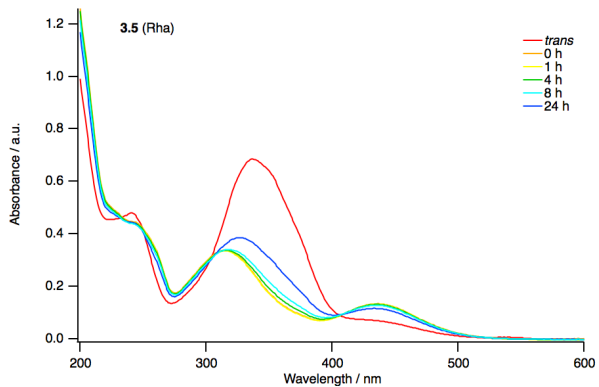
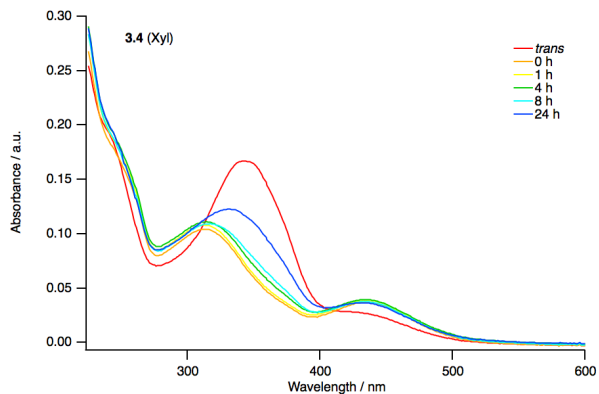
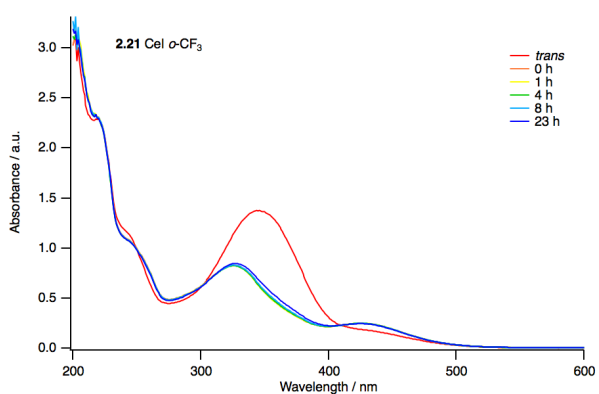
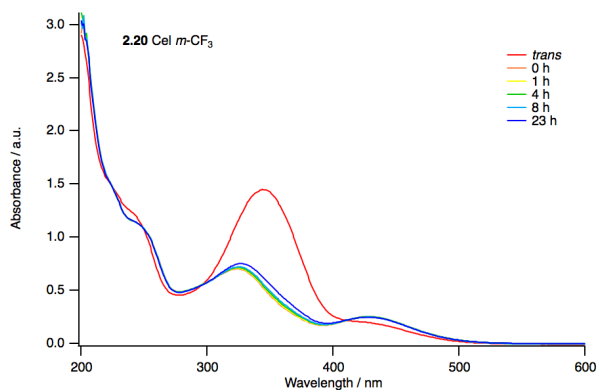
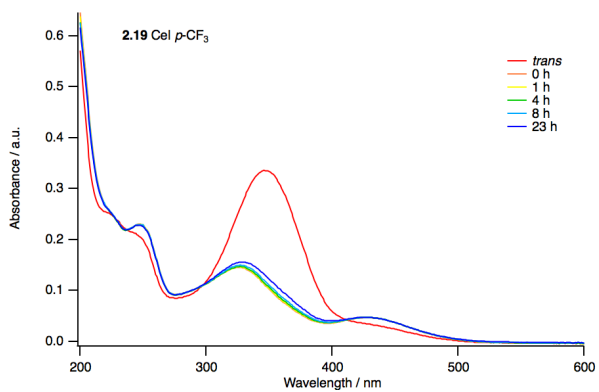
In Chapter four of this thesis, we described the combinatorial synthesis, characterization and lectin binding activity of a library of 12 photoresponsive Janus glycodendrimers. Light-responsive glycodendrimers were synthesized using a modular synthetic strategy employing the CuAAC reaction to append carbohydrate-based, bio-recognition motifs onto a photoswitchable core possessing variable linear and branched alkyl groups. The morphology and hydrodynamic volume of the self-assembled glycodendrimer micelles was determined using DLS and SANS, and revealed nanostructures with low polydispersity indices (PDIs) and cylindrical geometries of various length (104–915 Å) and radii (32–41 Å). The lectin binding affinity of these glycodendrimers against LecA and LecB from *P. aeruginosa* was also investigated using a fluorescence polarization-based assay, and moderate-to-potent inhibition was detected in the *trans* and *cis* photostationary states. Although no obvious photomodulation of aggregation properties and lectin binding potency of these glycodendrimers was detected, this study demonstrated the potential of these responsive, self-assembled lectin inhibitors for studying lectin-carbohydrate interactions, and as adaptable ligands for impeding interactions of pathological significance. Future work could be directed toward the discovery of glycodendrimers with enhanced photoswitching efficiency and lectin binding affinity, for example by tailoring the azobenzene unit as terminal groups rather than as the core of glycodendrimers.

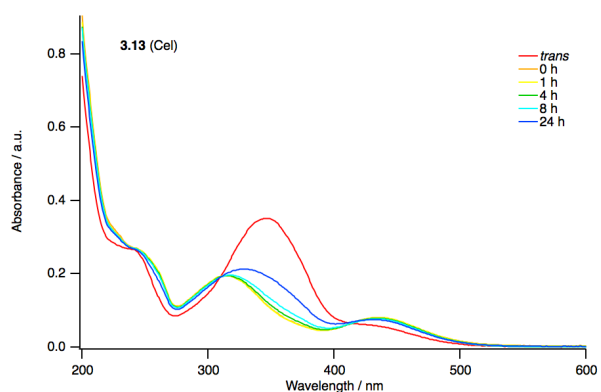
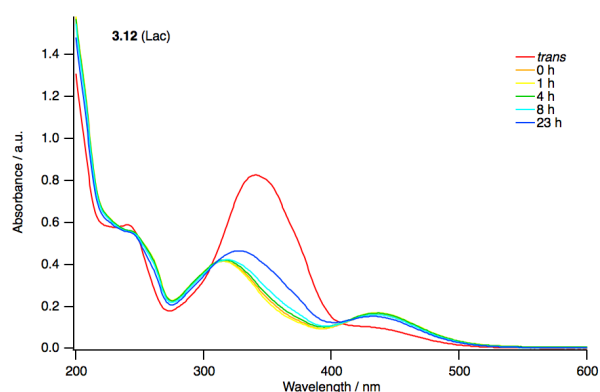
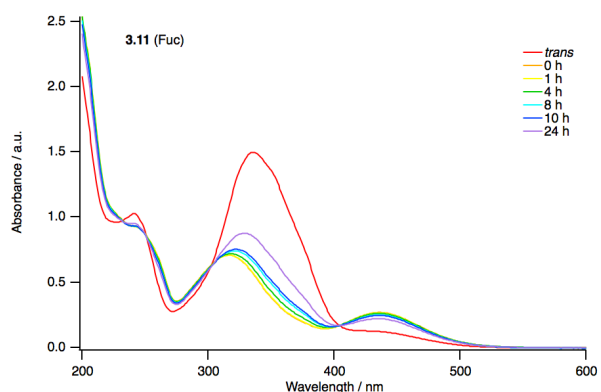
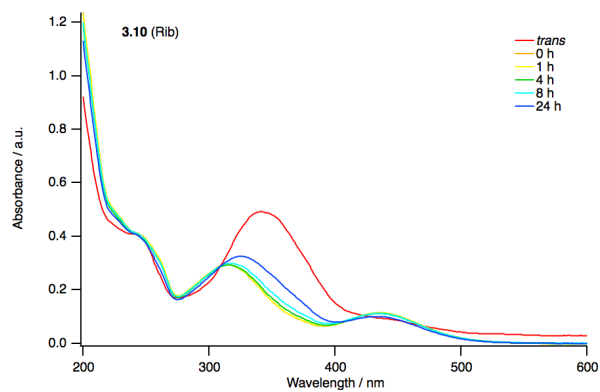
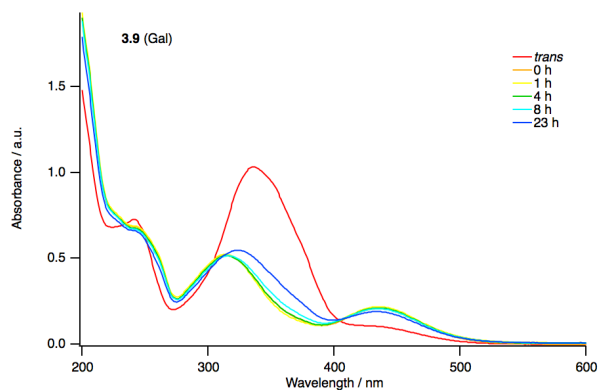
Across the carbohydrate amphiphiles investigated, a number of structural motifs are repeated, however quite different surface behaviours result, indicating the significance of minor modifications in chemical structure on physical and biological properties. Overall, amphiphiles incorporating a trifluoromethyl group *para* to the azobenzene (Chapter 2) have lower CMC than those with a *para* *n*-butyl group (Chapter 3), when bearing the same carbohydrate headgroup. Also, chain branching has been found to have a distinctive effect on the aggregation behaviour of these amphiphiles. Larger aggregates were formed for glycodendrimers (Chapter 4) than linearly configured carbohydrate surfactants (Chapter 3) as indicated by SANS. Across the whole range of photoresponsive carbohydrate amphiphiles

investigated, these molecules have demonstrated unexpectedly diverse surface and aggregation behaviour, and great potential for finely tuning their properties in biological applications. This encourages the continued exploration of molecular design so that new and novel species can be discovered with tailored physical and biological properties.

Appendix I Thermal *cis*–*trans* relaxation UV-vis spectra

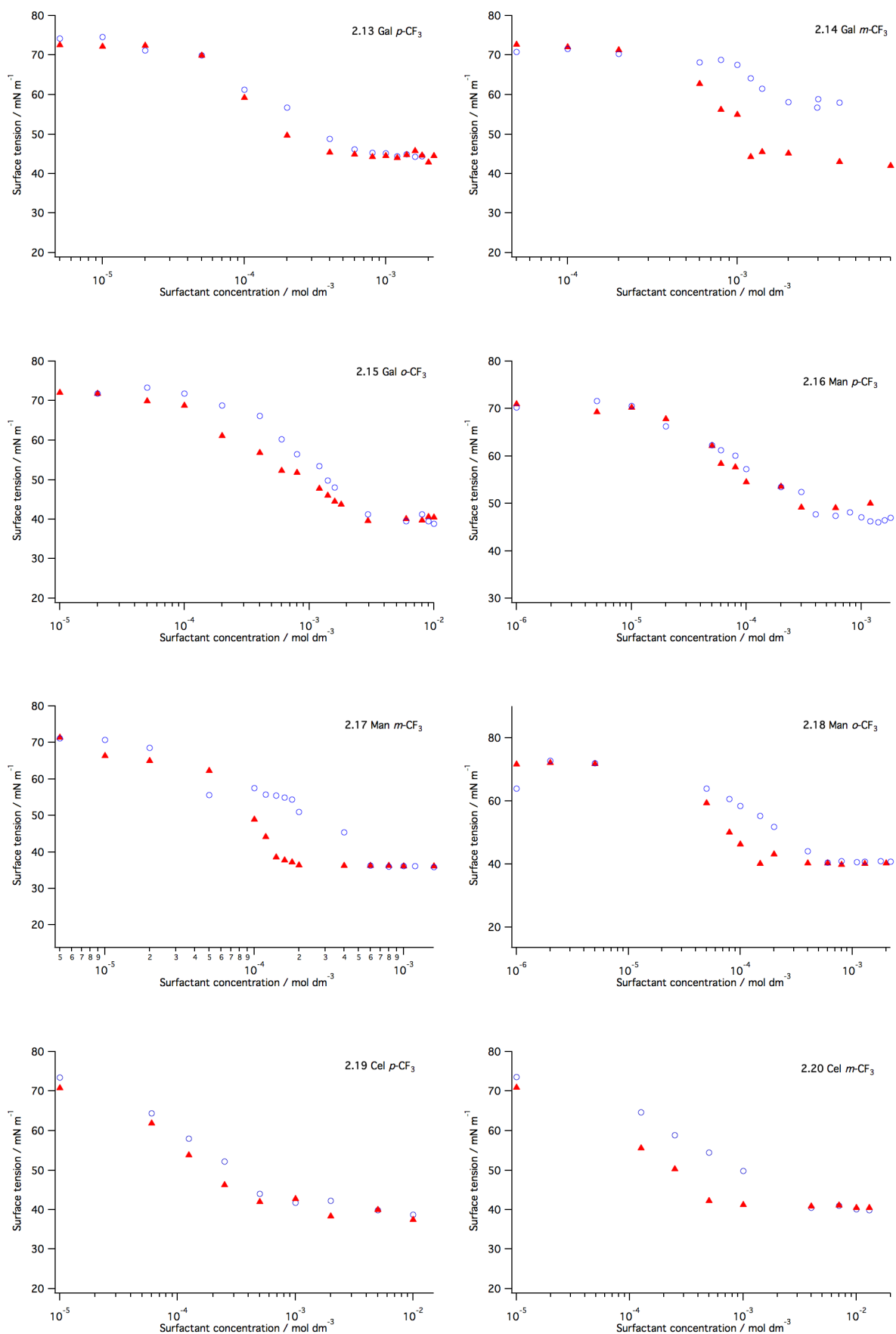


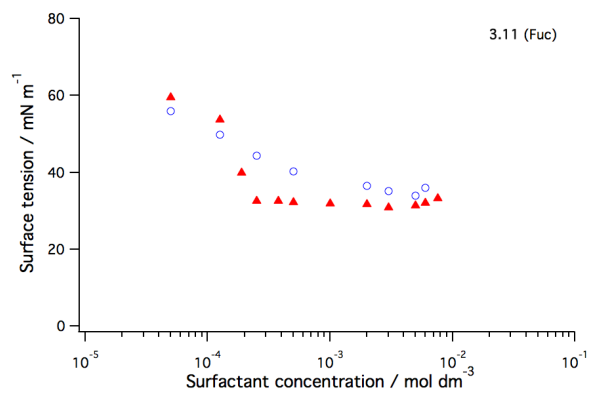
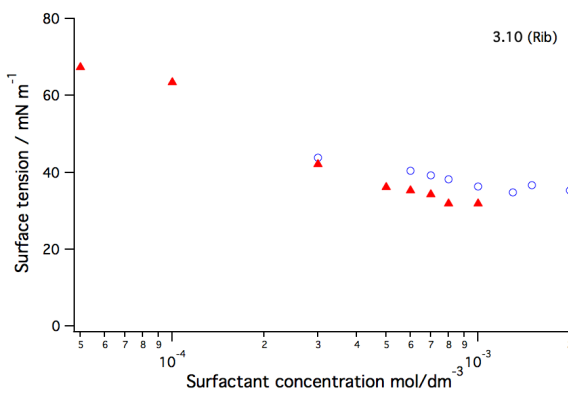
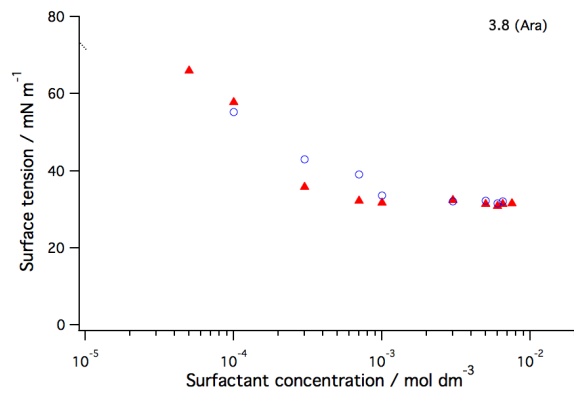
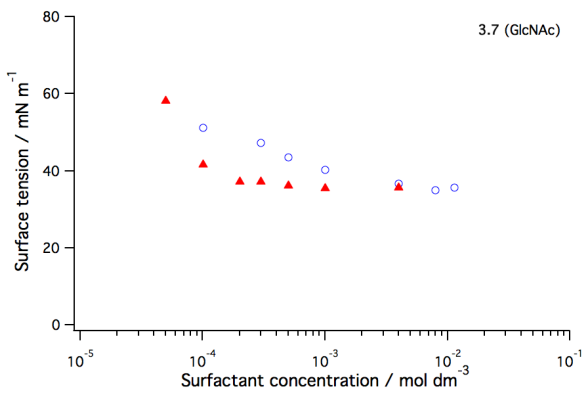
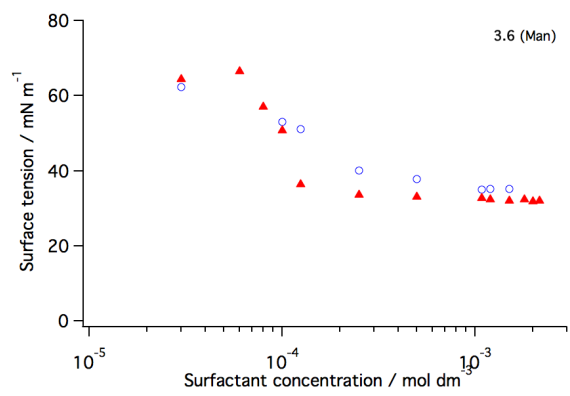
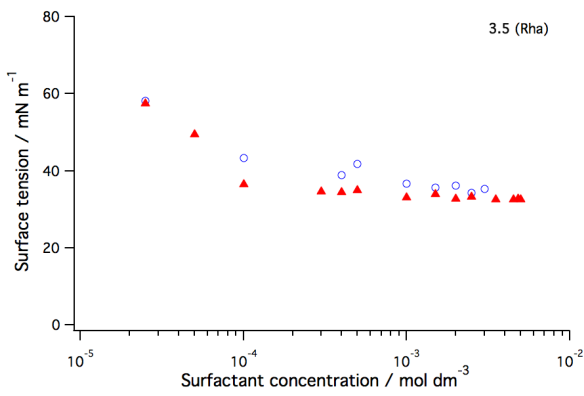
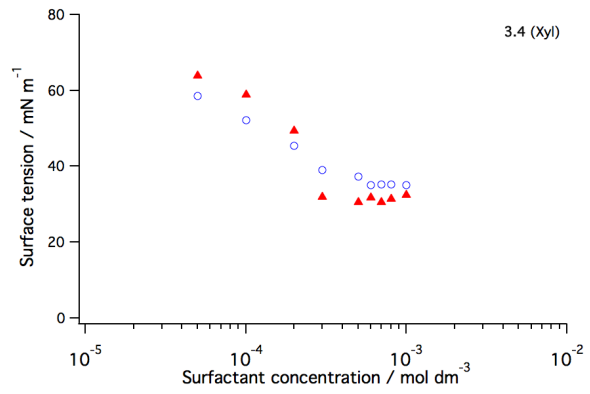
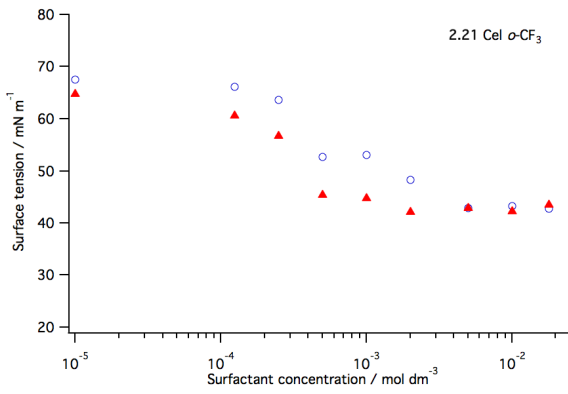


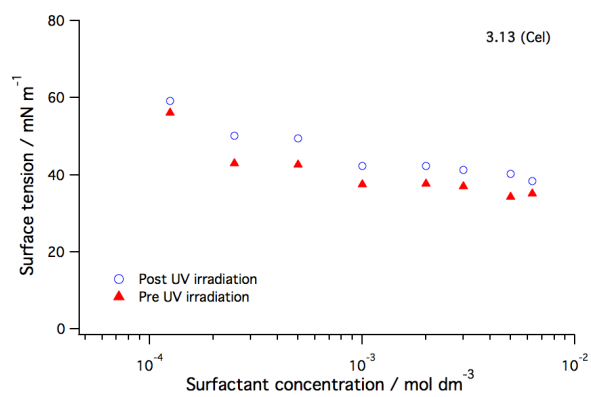
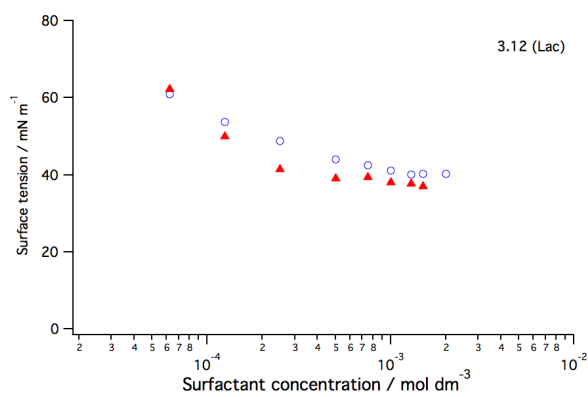


This page is intentionally blank

Appendix II Air-water surface tension data



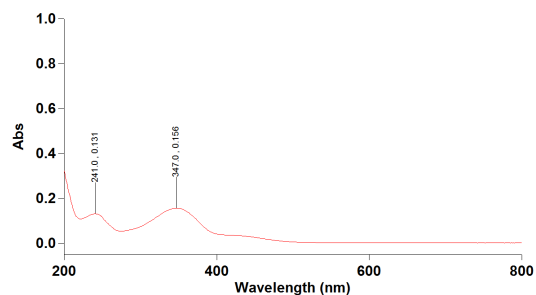
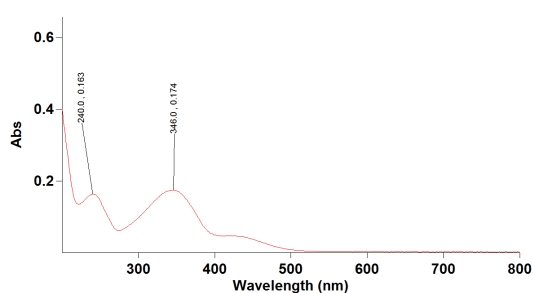




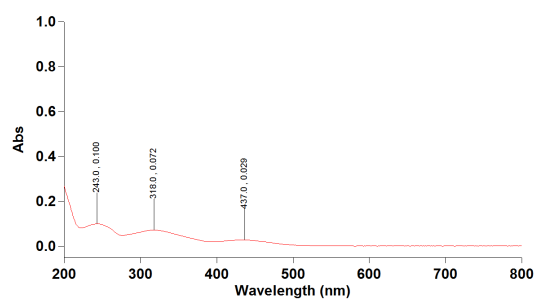
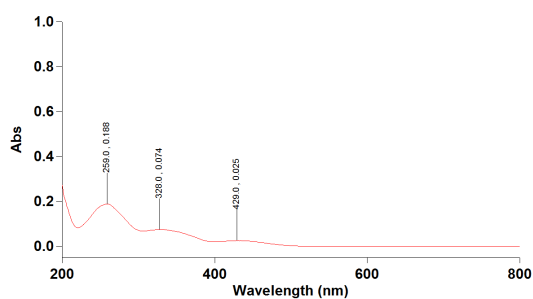
This page is intentionally blank

Appendix III Raw data of log P measurements

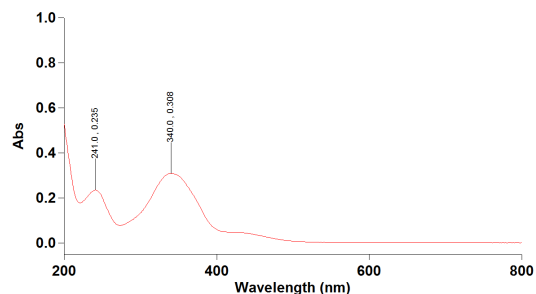
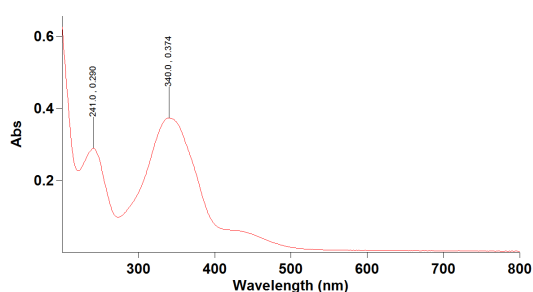
2.7 GlcAzo *trans* (before / after diffusion equilibrium)



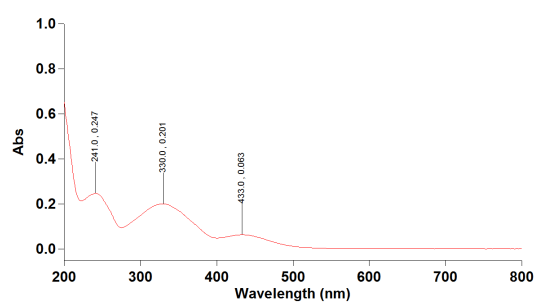
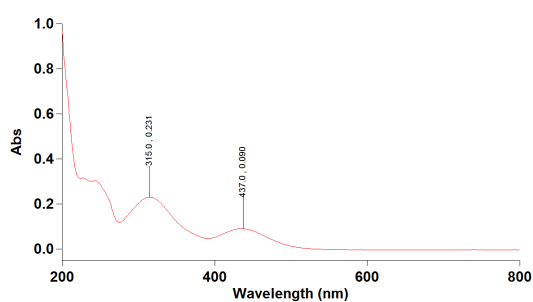
2.7 GlcAzo *cis* (before / after diffusion equilibrium)



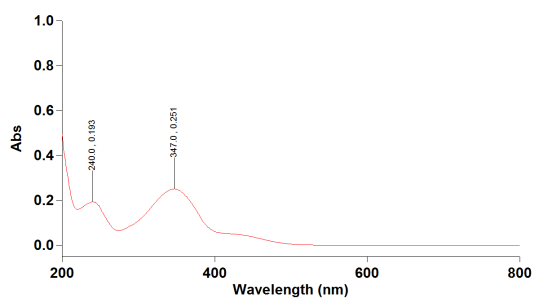
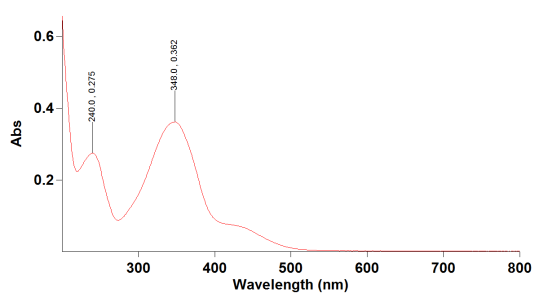
2.8 ManAzo *trans* (before / after diffusion equilibrium)



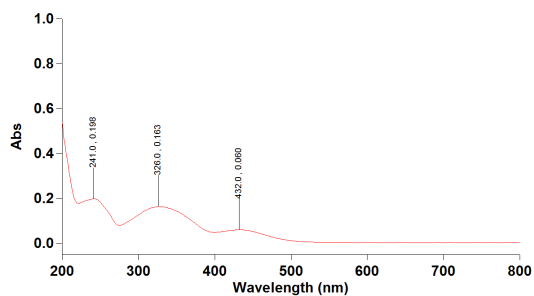
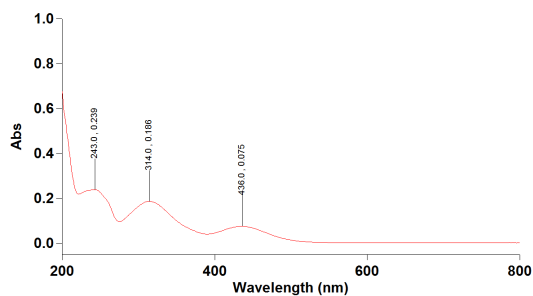
2.8 ManAzo *cis* (before / after diffusion equilibrium)



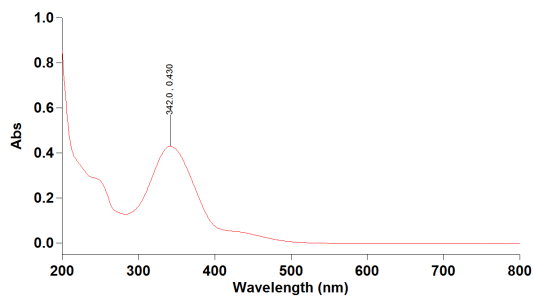
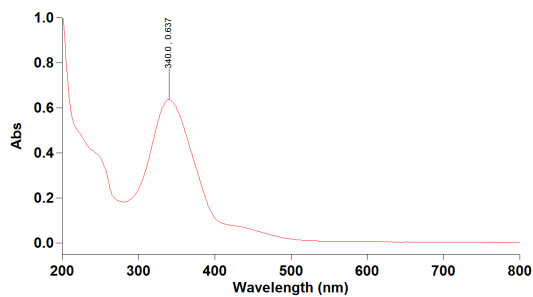
2.9 GalAzo *trans* (before / after diffusion equilibrium)



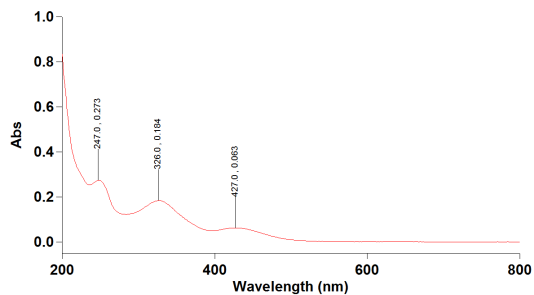
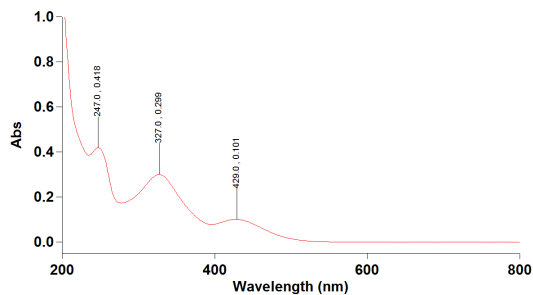
2.9 GalAzo *cis* (before / after diffusion equilibrium)



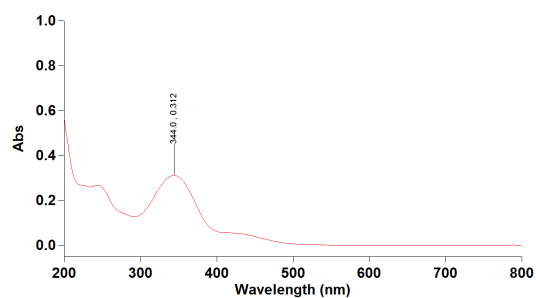
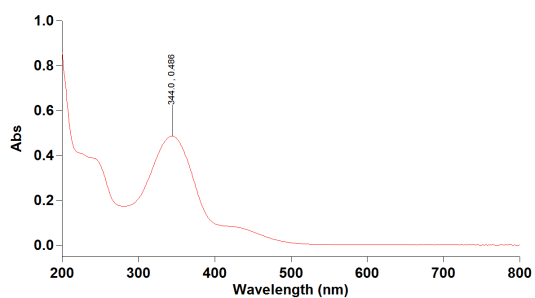
2.10 Glc *p*-CF₃ *trans* (before / after diffusion equilibrium)



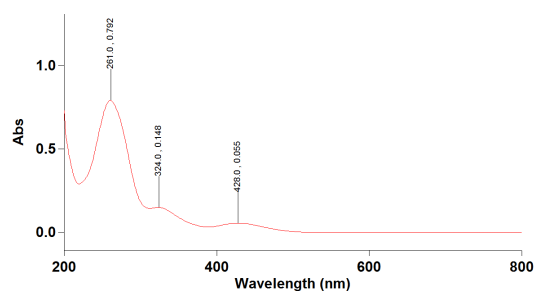
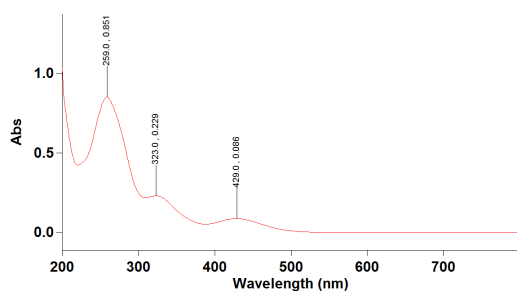
2.10 Glc *p*-CF₃ *cis* (before / after diffusion equilibrium)



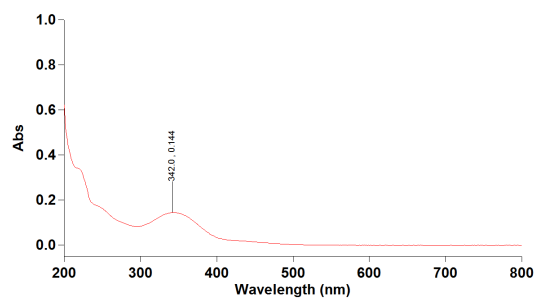
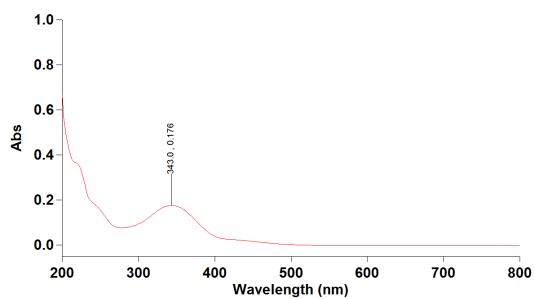
2.11 Glc *m*-CF₃ *trans* (before / after diffusion equilibrium)



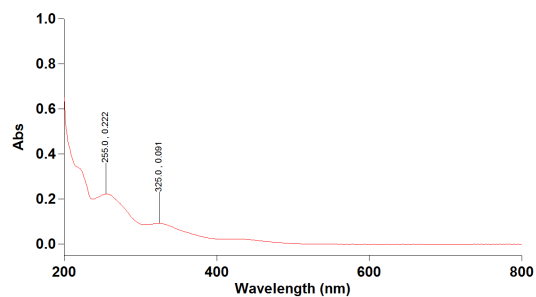
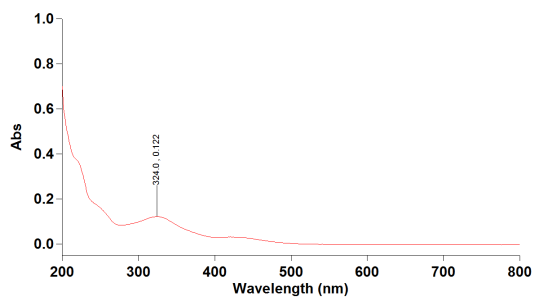
2.11 Glc *m*-CF₃ *cis* (before / after diffusion equilibrium)



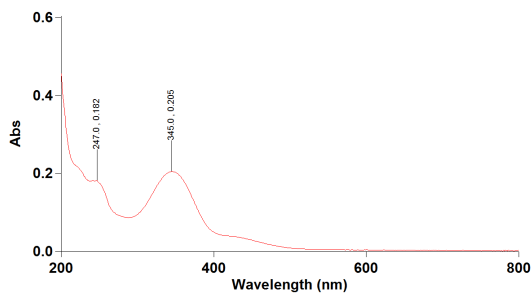
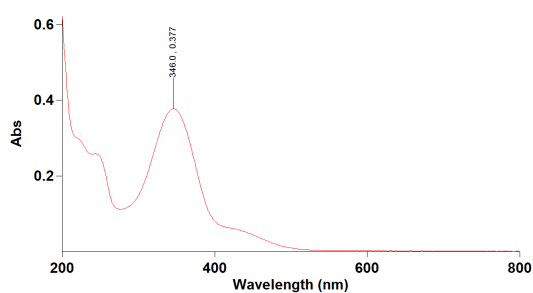
2.12 Glc *o*-CF₃ *trans* (before / after diffusion equilibrium)



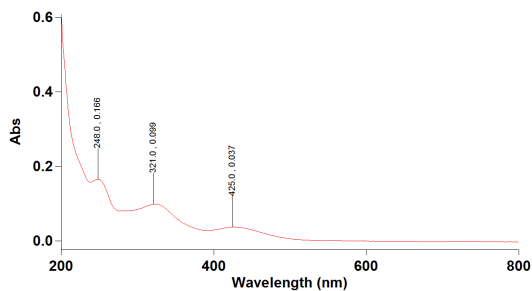
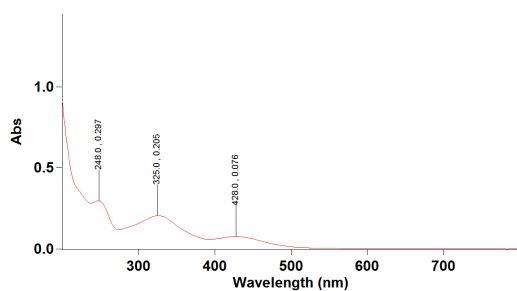
2.12 Glc *o*-CF₃ *cis* (before / after diffusion equilibrium)



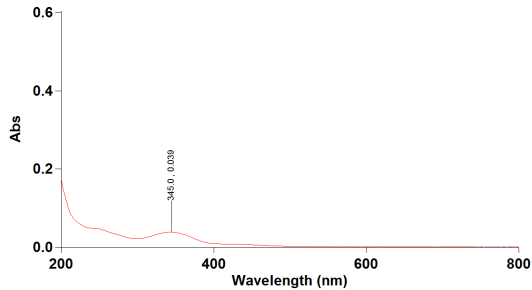
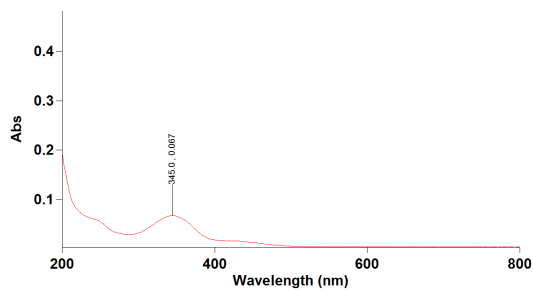
2.13 Gal *p*-CF₃ *trans* (before / after diffusion equilibrium)



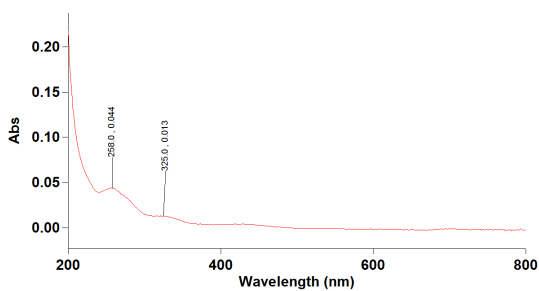
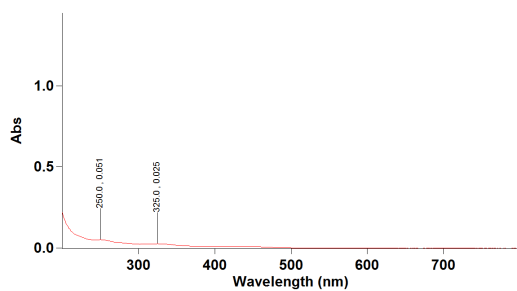
2.13 Gal *p*-CF₃ *cis* (before / after diffusion equilibrium)



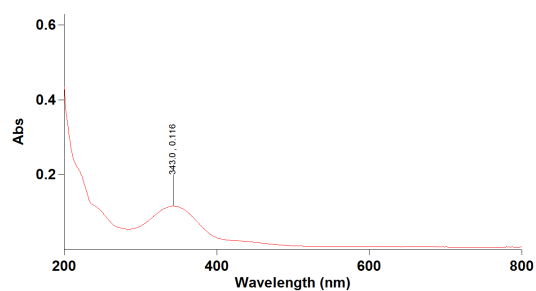
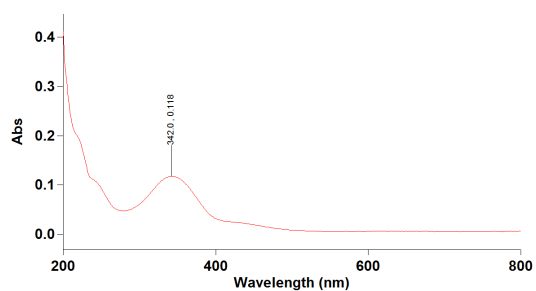
2.14 Gal *m*-CF₃ *trans* (before / after diffusion equilibrium)



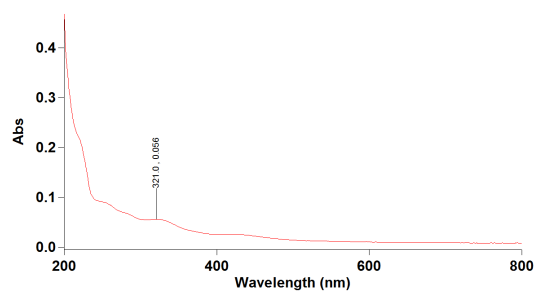
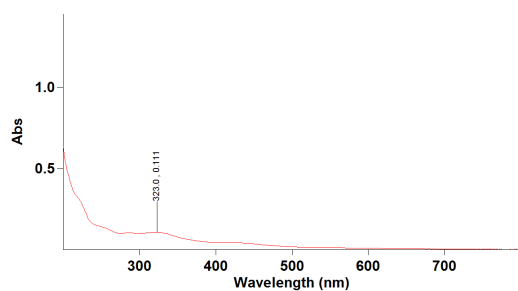
2.14 Gal *m*-CF₃ *cis* (before / after diffusion equilibrium)



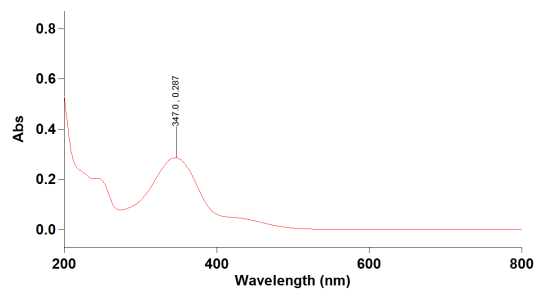
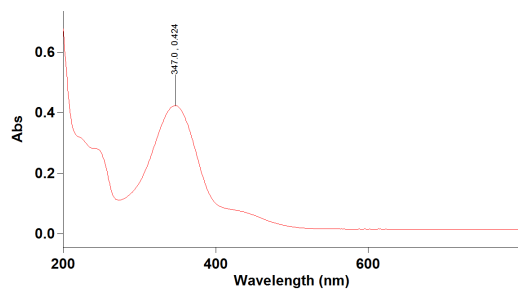
2.15 Gal *o*-CF₃ *trans* (before / after diffusion equilibrium)



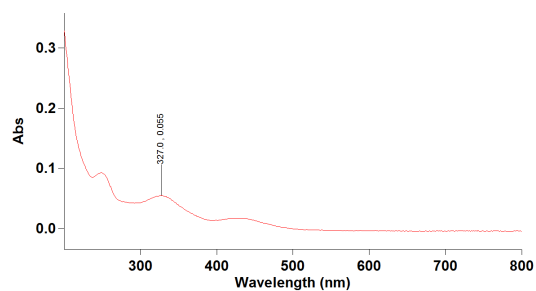
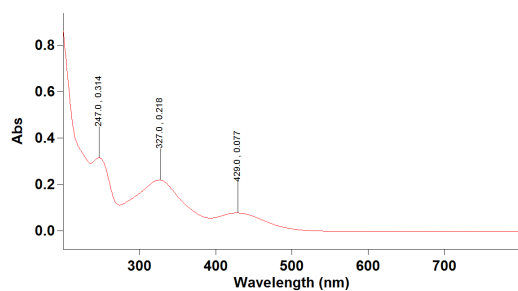
2.15 Gal *o*-CF₃ *cis* (before / after diffusion equilibrium)



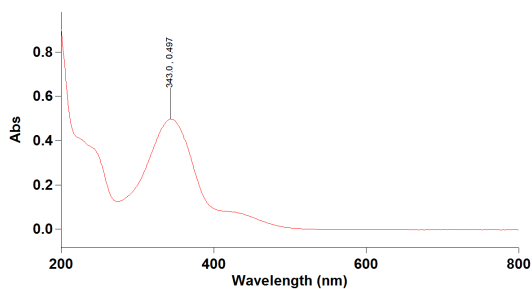
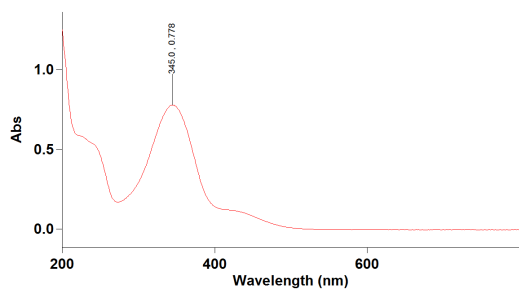
2.16 Man *p*-CF₃ *trans* (before / after diffusion equilibrium)



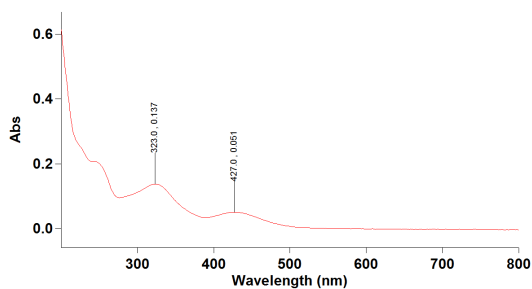
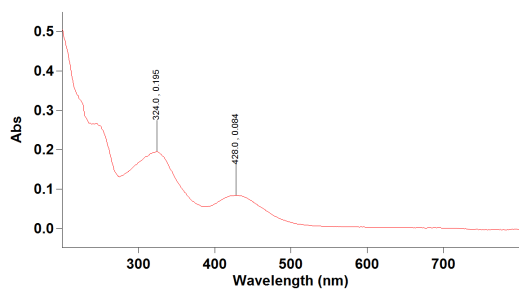
2.16 Man *p*-CF₃ *cis* (before / after diffusion equilibrium)



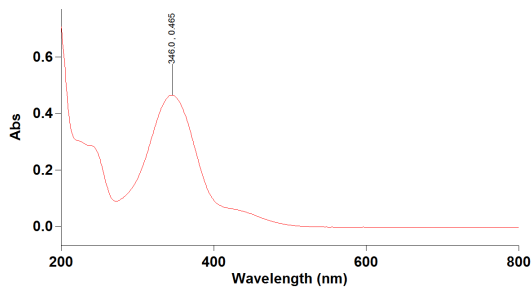
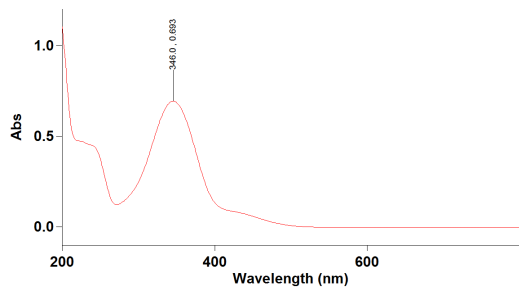
2.17 Man *m*-CF₃ *trans* (before / after diffusion equilibrium)



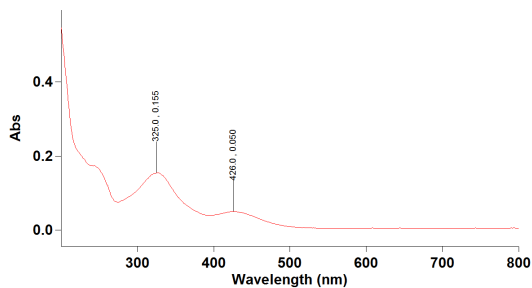
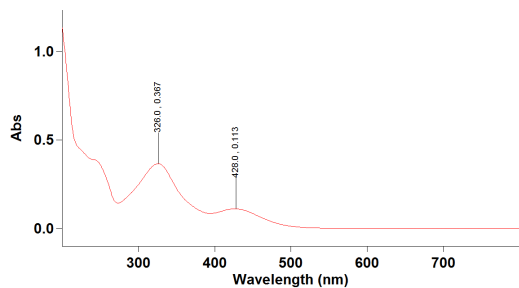
2.17 Man *m*-CF₃ *cis* (before / after diffusion equilibrium)



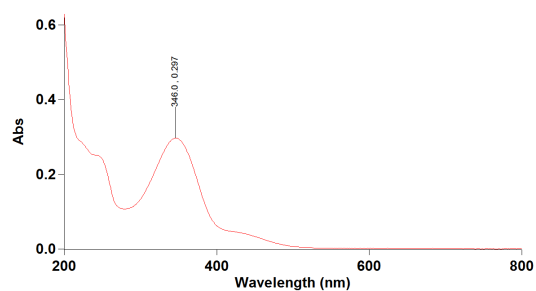
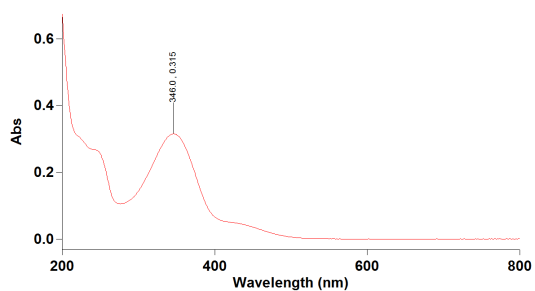
2.18 Man *o*-CF₃ *trans* (before / after diffusion equilibrium)



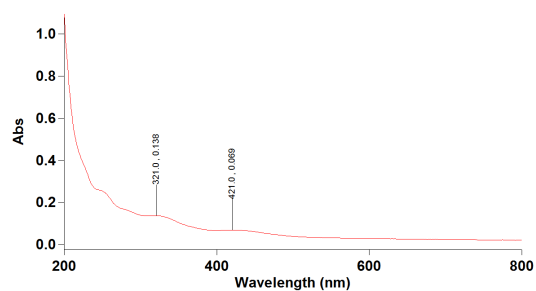
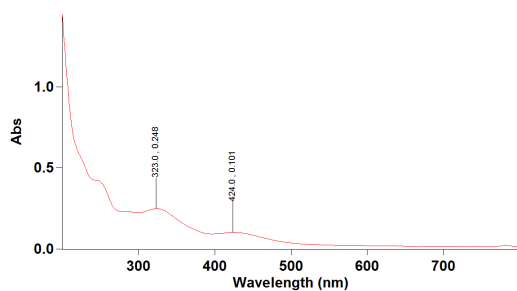
2.18 Man *o*-CF₃ *cis* (before / after diffusion equilibrium)



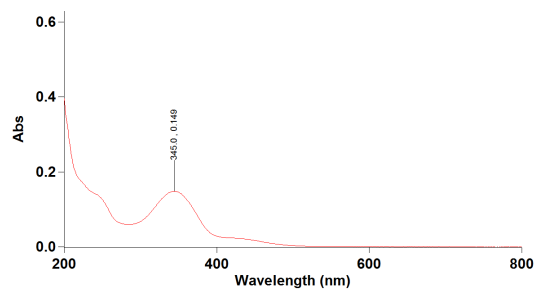
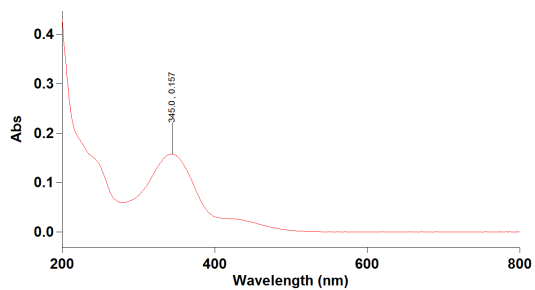
2.19 Cel *p*-CF₃ *trans* (before / after diffusion equilibrium)



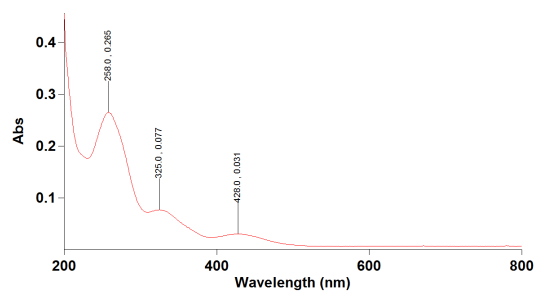
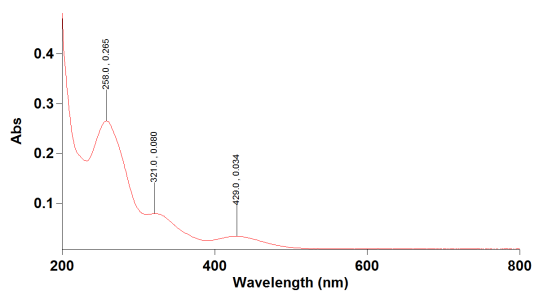
2.19 Cel *p*-CF₃ *cis* (before / after diffusion equilibrium)



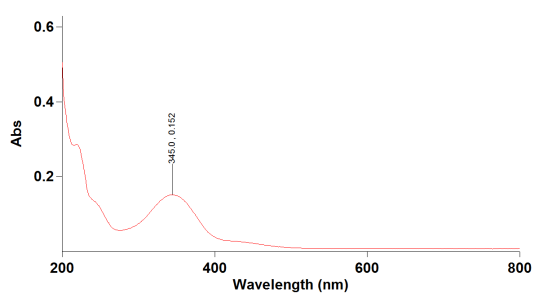
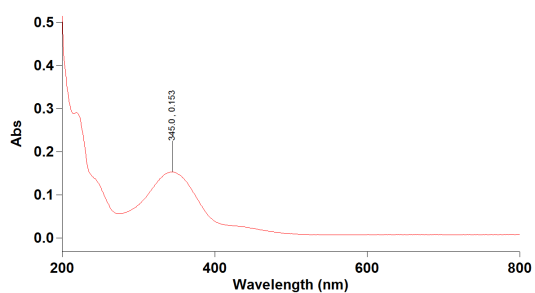
2.20 Cel *m*-CF₃ *trans* (before / after diffusion equilibrium)



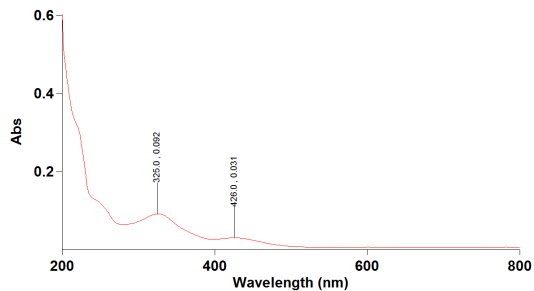
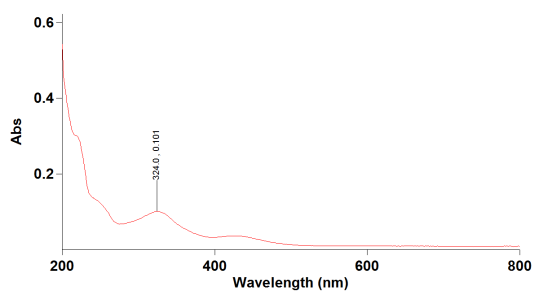
2.20 Cel *m*-CF₃ *cis* (before / after diffusion equilibrium)



2.21 Cel *o*-CF₃ *trans* (before / after diffusion equilibrium)



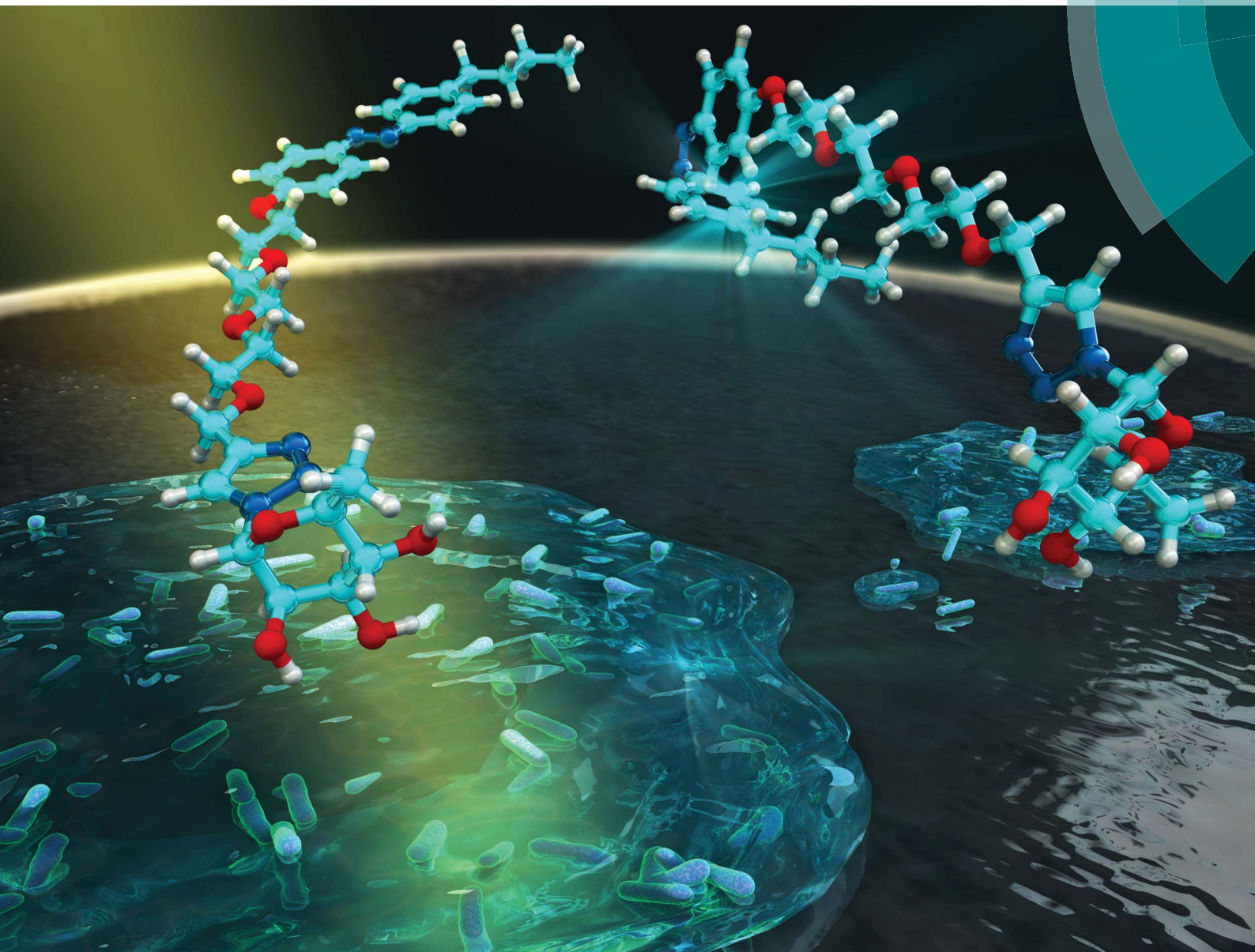
2.21 Cel *o*-CF₃ *cis* (before / after diffusion equilibrium)



**Appendix IV Published first and co-authored papers included in
the main body of this thesis**

Chemical Science

www.rsc.org/chemicalscience



ISSN 2041-6539



EDGE ARTICLE

Vipul Bansal, Brendan L. Wilkinson *et al.*
Photomodulation of bacterial growth and biofilm formation using
carbohydrate-based surfactants

175
YEARS

Cite this: *Chem. Sci.*, 2016, 7, 6628

Photomodulation of bacterial growth and biofilm formation using carbohydrate-based surfactants†

Yingxue Hu,^{‡a} Wenyue Zou,^{‡b} Villy Julita,^a Rajesh Ramanathan,^b Rico F. Tabor,^a Reece Nixon-Luke,^c Gary Bryant,^c Vipul Bansal^{*b} and Brendan L. Wilkinson^{*d}

Naturally occurring and synthetic carbohydrate amphiphiles have emerged as a promising class of antimicrobial and antiadhesive agents that act through a number of dynamic and often poorly understood mechanisms. In this paper, we provide the first report on the application of azobenzene *trans*–*cis* photoisomerization for effecting spatial and temporal control over bacterial growth and biofilm formation using carbohydrate-based surfactants. Photocontrollable surface tension studies and small angle neutron scattering (SANS) revealed the diverse geometries and dimensions of self-assemblies (micelles) made possible through variation of the head group and UV-visible light irradiation. Using these light-addressable amphiphiles, we demonstrate optical control over the antibacterial activity and formation of biofilms against multi-drug resistant (MDR) *Pseudomonas aeruginosa*, methicillin-resistant *Staphylococcus aureus* (MRSA) and Gram-negative *Escherichia coli*. To probe the mechanism of bioactivity further, we evaluated the impact of *trans*–*cis* photoisomerization in these surfactants on bacterial motility and revealed photomodulated enhancement in swarming motility in *P. aeruginosa*. These light-responsive amphiphiles should attract significant interest as a new class of antibacterial agents and as investigational tools for probing the complex mechanisms underpinning bacterial adhesion and biofilm formation.

Received 8th July 2016
Accepted 3rd August 2016

DOI: 10.1039/c6sc03020c

www.rsc.org/chemicalscience

Introduction

Antimicrobial drug resistance represents a global health emergency and there is now an urgent and unmet need for new clinical agents and preventative strategies that possess unconventional modes of action.¹ This problem is exacerbated by the ability of many pathogenic bacteria to form matrix-enclosed communities that are immobilized on biotic and abiotic surfaces, or biofilms, which confer enhanced resistance toward host immune responses and antibiotic treatments.² Naturally occurring biosurfactants are a structurally diverse class of amphiphilic compound with promising antimicrobial and anti-biofilm activity. In particular, microbial glycolipids and their synthetic analogues have attracted considerable interest as selective antibacterial agents and as

mechanistic tools for expanding our understanding of bacterial physiology and biofilm formation.^{3,4} In many cases, this bioactivity can be attributed to the ability of these molecules to lower interfacial tension, thereby mediating bacterial motility, cellular and protein adhesion, signalling and communication, pH regulation, nutrient uptake, and degradation of harmful metabolites.^{3–6} These multifaceted responses are dependent on the bacterial strain and surfactant used, and our current understanding is limited to a handful of well-characterized systems. Access to chemical tools with tuneable properties that could selectively influence bacterial growth and biofilm formation offers new opportunities to develop novel therapies for biofilm-associated diseases, and to study the mechanisms governing bacterial adhesion and biofilm formation.

In recent years there has been considerable interest in light as an external stimulus for effecting spatial and temporal control over the conformational dynamics of biomolecules⁷ and the biological activity of small molecules.⁸ Toward this goal, the well-studied azobenzene chromophore has been actively pursued, owing to the facile and reproducible *trans*–*cis* photoisomerization, and the ease of molecular synthesis for enabling new light-addressable materials with tailored photoswitching wavelengths and potential *in vivo* applications.^{9,10} In parallel with these developments, azobenzene photochromism has been widely reported as a means for modulating

^aSchool of Chemistry, Monash University, Victoria 3800, Australia^bIan Potter NanoBioSensing Facility, NanoBiotechnology Research Laboratory, School of Science, RMIT University, Victoria 3000, Australia. E-mail: vipul.bansal@rmit.edu.au^cCentre for Molecular and Nanoscale Physics, School of Science, RMIT University, Victoria 3000, Australia^dSchool of Science and Technology, The University of New England, New South Wales 2351, Australia. E-mail: Brendan.wilkinson@une.edu.au

† Electronic supplementary information (ESI) available: Experimental procedures, supplementary tables, figures and spectra. See DOI: 10.1039/c6sc03020c

‡ Equal contributing authors.

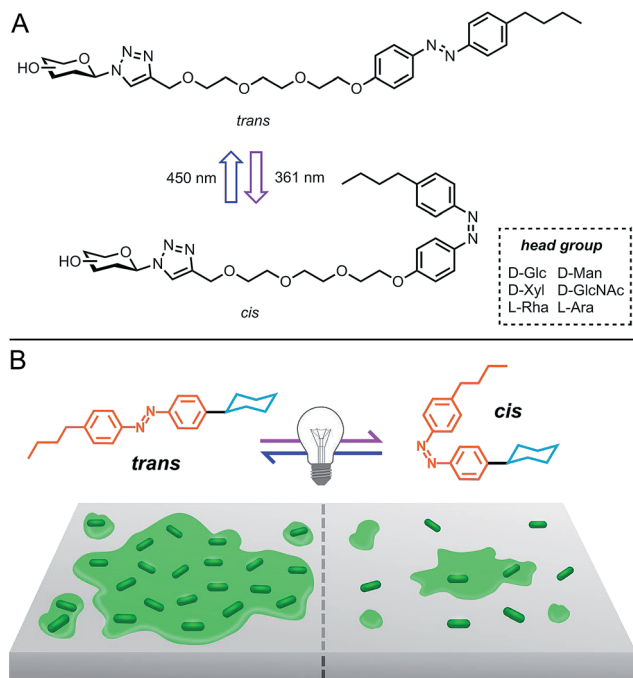


Fig. 1 (A) Photoswitchable carbohydrate-based surfactants and (B) cartoon representation of the photomodulation of biofilm growth.

carbohydrate multivalency and lectin binding,¹¹ and for controlling supramolecular self-assembly¹² and host-guest interactions.¹³ We have previously demonstrated the photocontrollable self-assembly and interfacial activity of carbohydrate-based surfactants and fluorosurfactants.¹⁴ Throughout the course of these studies, we demonstrated the ability to modulate the interfacial activity and aggregation properties of these amphiphiles through changes in head group geometry, size and polarity, as well as the isomeric state of the tail group.¹⁵ However, the impact of azobenzene *trans-cis* photoisomerization within carbohydrate-based surfactants on the ability of bacteria to survive and to form active biofilms remains to be verified.

Herein, we report the photocontrollable antibacterial and biofilm modulatory activity of a panel of carbohydrate-based surfactants (Fig. 1). Surfactants incorporated variable monosaccharide head groups, including D-glucose (**AzoGlc**),¹⁴ D-xylose (**AzoXyl**), L-rhamnose (**AzoRha**), D-mannose (**AzoMan**), N-acetyl glucosamine (**AzoGlcNAc**), and L-arabinopyranose (**AzoAra**), which were tethered to a hydrophobic *n*-butylazobenzene tail group (Fig. 2). Monosaccharide head groups were selected based on the natural occurrence and intriguing biological activity of glycolipids expressing these structures, and the important roles carbohydrates play in bacterial adhesion processes. Through reversible photocontrol over self-assembly and interfacial activity, these surfactants were assessed as modulators of bacterial growth and biofilm formation against methicillin resistant *Staphylococcus aureus* ATCC1698 (MRSA), *Escherichia coli* DH5 α and a multi-drug resistant strain of *Pseudomonas aeruginosa* MDR283/1-6.

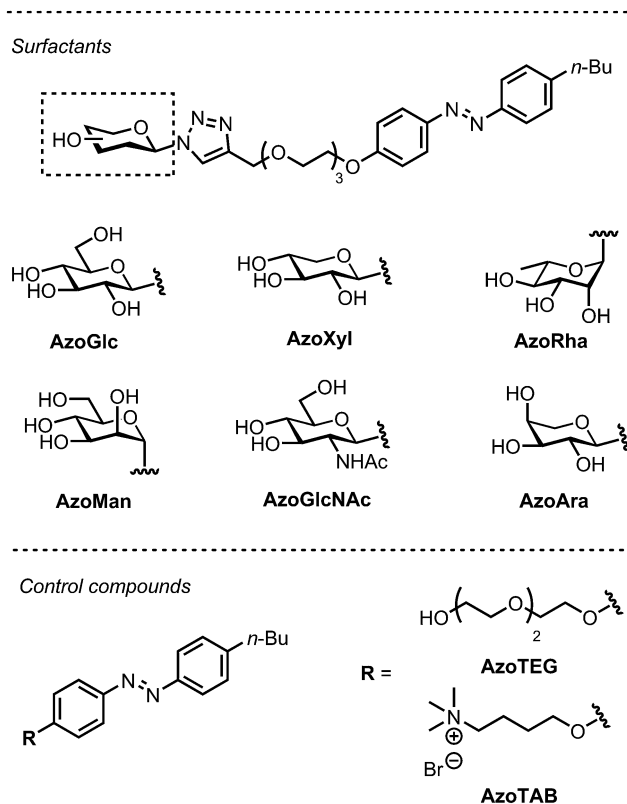


Fig. 2 Photoswitchable carbohydrate-based surfactants and control compounds used in this study.

Results and discussion

Surfactant synthesis and characterisation

Our investigation commenced with the modular synthesis and physical characterisation of a panel of photoswitchable carbohydrate-based surfactants (see ESI for details[†]). To this end, known glycosyl azides were united with a *n*-butylazobenzene tail fragment using the well-established Cu(I)-catalysed azide-alkyne cycloaddition reaction (CuAAC).^{14,16} Surfactants were isolated in acceptable yields over two steps following purification by reversed phase, preparative HPLC. In addition to non-ionic carbohydrate photosurfactants, we also targeted a non-surface active fragment lacking the sugar head group (**AzoTEG**) and a known cationic photosurfactant (**AzoTAB**)¹⁷ as control compounds.

Having acquired surfactants, we assessed the photocontrollable surface activity and self-assembly properties using pendant drop tensiometry and small angle neutron scattering (SANS), respectively. To affect *trans-cis* photoisomerization, compounds were irradiated at 361 nm for 15 min and the critical micellar concentration (CMC) measured using pendant drop tensiometry, although one minute was found to be sufficient to achieve near complete *trans-cis* photoisomerization. Photoisomerization was also observed using UV-vis spectroscopy as determined by a diminished intensity of the peak at 350 nm corresponding to the $\pi-\pi^*$ transition and an increase in intensity of the peak at 440 nm corresponding to the $n-\pi^*$

transition. The ratio of *cis* and *trans* isomers in either photo-stationary state (PSS) was estimated by integrating selected signals in the ^1H NMR spectrum, before and after UV photo-irradiation (ESI, Fig. S1†). In the *trans* dominated PSS, <10% of molecules existed in the *cis* isomeric form. Following UV irradiation, approximately 75% of molecules existed in the *cis* isomeric form (*cis* dominated PSS).^{18,19} To investigate potential photodegradation of surfactants during photoswitching, the ^1H NMR spectra of the *trans* isomer was recorded both prior to UV photoirradiation, and following visible light irradiation (430 nm) of the photo-excited *cis* isomer (ESI, Fig. S2†).

Since our antibacterial assays occurred in dark-adapted conditions at 37 °C, we were interested in monitoring the thermal relaxation of the *cis* isomer to the more stable *trans* isomer in bacterial growth media over a 24 h time period. The *cis* isomers showed a half-life of over 10 hours in water as well as in two bacterial growth media at 37 °C (ESI, Table S1 and Fig. S4–S7†). Considering the typical bacterial doubling time of 0.5–2 h, this would offer ample opportunity for *cis* isomers to exert a biological response. An increase in the CMC was accompanied by *trans*–*cis* photoisomerization, which was attributed to the increased polarity and altered molecular geometry of the *cis* isomer relative to the more hydrophobic and planar *trans* isomer (Table 1).²⁰ However, in some cases the magnitude of this change was significant, in particular that of **AzoGlcNAc** incorporating an *N*-acetyl glucosamine head group. In contrast, virtually no difference in the CMC was observed between the *trans* (0.33 mM) and *cis* (0.34 mM) dominated PSS of **AzoXyl**, further highlighting the effect of subtle head group configuration and polarity on the interfacial activity of this class of photosurfactants.

Characterisation of self-assemblies

Small angle neutron scattering (SANS) is a powerful experimental technique that is frequently employed to deduce the morphology and size of nanostructures and self-assemblies in solution.^{14,21} SANS measurements were performed to determine the post-CMC aggregation structures (micelles) formed by the photoswitchable surfactants, which provided information on the number and topology of carbohydrates exposed on the micelle surface. We postulated that this information could

Table 1 Photocontrollable surface and aggregation properties of carbohydrate-based photosurfactants^a

Surfactant	E/C ^b	N_{agg}	A_{hg}	CMC (CMC _{UV})
AzoGlc ¹⁷	E	440	0.69	0.31 (0.59)
AzoXyl	C	NA	NA	0.33 (0.34)
AzoRha	C	622	0.79	0.11 (0.42)
AzoMan	E	141	0.84	0.13 (0.49)
AzoGlcNAc	E	178	1.02	0.11 (1.22)
AzoAra	E	89	1.12	0.33 (0.88)

^a Aggregation number (N_{agg}), area per head group (A_{hg}) [nm^2] and critical micelle concentration (CMC) in ambient and UV-irradiated conditions [mM]. ^b E = ellipsoid, C = cylindrical. For **AzoXyl**, long worm-like micelles were obtained with a length of >100 nm.

be used to probe the potential relationship between the aggregation properties of these amphiphiles and the ability to modulate bacterial growth and biofilm formation. For each surfactant, spectra were acquired in D_2O in the *trans*-dominated PSS at a concentration well above the CMC. As revealed from the SANS data (Table 1 and Fig. 3), a wide range of aggregate morphologies and sizes are made possible through variation of the carbohydrate head group, which is in agreement with our previous studies.^{14,16} Indeed, micelles ranged from small ellipsoids, as in **AzoMan** and **AzoAra**, to extremely long, flexible cylindrical (worm-like) micelles arising from **AzoXyl** (length > 100 nm, persistence length 36 nm). This extraordinary variety of self-assembled structures indicates that the aggregation properties of carbohydrate amphiphiles are extremely sensitive to the head-group employed, offering considerable geometric information on preferred packing and interfacial curvature.

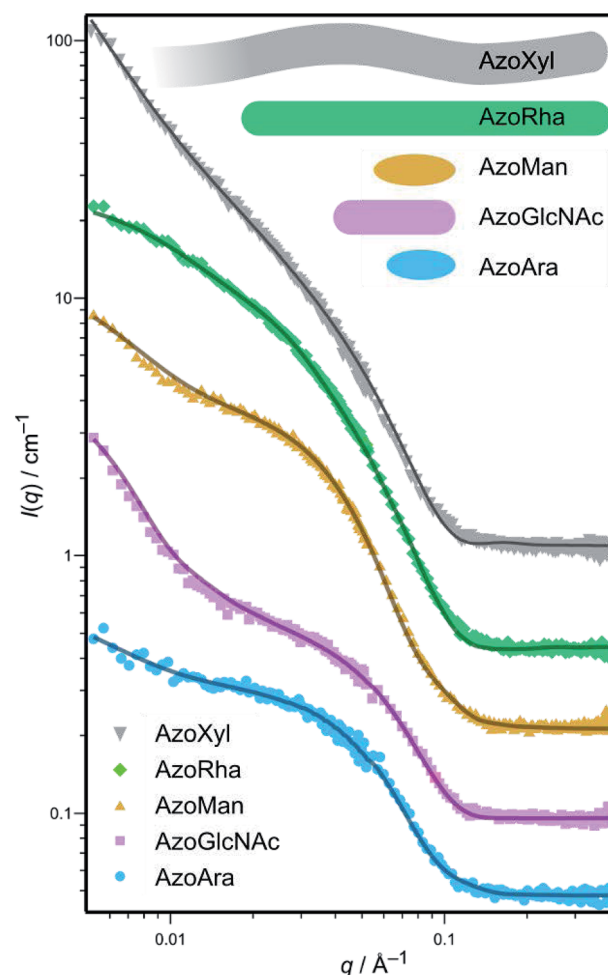


Fig. 3 Small angle neutron scattering (SANS) spectrum of carbohydrate-based surfactants in D_2O at 4 mM concentration (symbols) and theoretical fits (solid lines) for selected surfactant micelles. Inset top: meridional sections of the fitted geometries from SANS of the surfactants. The SANS spectra for **AzoGlc** has been reported previously.¹⁷

Photocontrollable antibacterial studies

We next evaluated the photocontrollable antibacterial activity of photoswitchable surfactants, non-surface active tail fragment **AzoTEG** and the cationic surfactant **AzoTAB** against Gram-negative *E. coli* DH5 α , Gram-negative *P. aeruginosa*, and Gram-positive *S. aureus*. Compounds were screened for antibacterial activity using an OD₆₀₀ bacterial growth assay (see ESI for experimental procedure and data[†]).²² To obtain *cis* photoisomers for antibacterial studies, the native compounds were irradiated with UV light for 5 min prior to incubation with bacteria. Following a dark-adapted 24 h incubation period, the optical density of the wells was measured at 600 nm. **AzoTEG** displayed moderate inhibitory potency against *S. aureus* (MIC 125 $\mu\text{g mL}^{-1}$), and limited-to-no inhibition of *P. aeruginosa* (MIC > 1000 $\mu\text{g mL}^{-1}$) and *E. coli* (MIC > 2000 $\mu\text{g mL}^{-1}$) in the *trans* PSS. Following photoisomerization to the *cis* isomer, a further increase in inhibitory potency against *S. aureus* was observed (31 $\mu\text{g mL}^{-1}$), while no change in activity against *E. coli* and *P. aeruginosa* was noted. The enhanced antibacterial activity of the *cis* isomer of this compound corroborates well with a previous study on photoswitchable quinolone antibiotics.^{8c} In contrast to the non-surface active fragment, the cationic photosurfactant **AzoTAB** displayed potent antibacterial activity in the *trans* PSS against *E. coli* (MIC 12.5 $\mu\text{g mL}^{-1}$), *S. aureus* (MIC 1.6 $\mu\text{g mL}^{-1}$), and *P. aeruginosa* (MIC 31.2 $\mu\text{g mL}^{-1}$). While no photomodulation of this activity was observed against *E. coli* and *S. aureus*, the *cis* PSS of **AzoTAB** became less toxic against *P. aeruginosa* (MIC 125 $\mu\text{g mL}^{-1}$). The high toxicity of the cationic surfactant against *E. coli* and *S. aureus* indicates a non-selective mode of action through cell wall damage and lysis,²³ whereas its lower toxicity against *P. aeruginosa* allows its activity to be photomodulated, possibly *via* reduction in the interfacial activity due to the enrichment of the *cis* isomer.¹⁷

The carbohydrate-based surfactants exhibited bacteria- and photoisomer-specific, dose-dependent inhibition of growth against both *S. aureus* (ESI, Fig. S7[†]) and *E. coli* (ESI, Fig. S8[†]), whereas they generally promoted growth of *P. aeruginosa* (ESI, Fig. S9[†]). Representative data for **AzoMan** is shown in Fig. 4. While at lower concentrations, surfactants showed nearly similar activities in the *trans*- and *cis*-dominated PSS against all three bacteria, the bactericidal activity could be modulated following photoisomerization at concentrations approaching and above the CMC. In the case of *S. aureus*, the photoexcited *cis*

form was generally more toxic, with the exception of **AzoGlcNAc**, which was more toxic in its native *trans* form. Conversely, these compounds were typically more potent in their native *trans* state against *E. coli*, with the exception of **AzoRha** and **AzoGlcNAc** which showed higher antibacterial activity after photoisomerization. Surprisingly, all carbohydrate-based surfactants did not display significant toxicity against *P. aeruginosa* (with the exception of **AzoAra**) and generally promoted bacterial growth, especially in the *cis* photostate. Interestingly, the *l*-rhamnose based surfactant **AzoRha** was most influential in promoting growth of this bacterium. Whilst it is difficult to rationalize the heterogeneous responses observed with these amphiphiles against Gram-negative and Gram-positive bacteria, particularly those of **AzoRha** and **AzoGlcNAc**, it is interesting to note that these surfactants incorporate *l*-rhamnose and *N*-acetyl glucosamine as monosaccharide head groups, respectively. These carbohydrates have been known to play important roles in biofilm growth, adhesion and virulence in Gram-negative and Gram-positive species. For example, *N*-acetyl glucosamine is a major constituent of the cell wall and the extracellular matrix in both Gram-positive and Gram-negative bacteria and plays important roles in virulence and biofilm formation in both groups of bacteria.²⁴ Gram-negative bacteria, in particular *Pseudomonas* spp., produce surface-active rhamnolipids as virulence factors that regulate swarming motility, intercellular signalling and biofilm formation.^{4,25} As such, the significance of these carbohydrate head groups in bacterial evolution might be responsible for their selective mode of interaction with these bacteria. Whilst the cationic surfactant **AzoTAB** seems to possess a non-selective mode of antibacterial action toward these bacteria, the type of head group and the isomeric state of the tail group in carbohydrate-based surfactants are both important determinants for imparting selective growth/toxicity against different bacteria.

Photocontrollable biofilm studies

Having established the bacteria-specific influence of these surfactants on cell viability, we next sought to evaluate the effect of *trans-cis* photoisomerization on their ability to influence bacterial biofilm formation. Biofilms are typically formed by adherence of sessile bacteria onto a surface followed by the production of a complex extracellular matrix, thus allowing these bacterial communities to become more resistant to host immune responses and antibiotic therapies. Not only are the mechanisms of biofilm formation poorly understood, the ability to inhibit biofilm formation from pathogenic bacteria is extremely challenging.²⁶ The intriguing effect of amphiphilic carbohydrates on biofilm growth of *P. aeruginosa* has been recently demonstrated and was shown to be heavily dependent on the length and relative configuration of the oligosaccharide head group (*D*-gluco or *D*-galacto).⁵ However, the influence of different photoisomers of amphiphilic carbohydrates on the biofilm forming ability of bacteria has never been reported. To understand the influence of the *trans* and *cis* isomers of these surfactants on the biofilm forming ability of bacteria, these compounds were exposed to a Gram-positive methicillin-

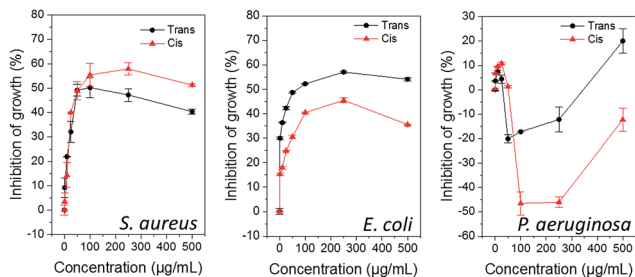


Fig. 4 Photocontrollable influence of *cis*- and *trans*-dominated photostationary states of **AzoMan** on bacterial activity after 24 h.

resistant *S. aureus* (MRSA – ATCC1698) and a multi-drug resistant clinical isolate of Gram-negative *P. aeruginosa* (MDR283/1-6), both of which are known to cause problematic biofilm-associated infections.^{2,27}

Compounds were screened for biofilm inhibition activity using a microtiter dish biofilm formation assay that involved recording the OD₅₅₀ of crystal violet-treated bacterial biofilms.²⁸ Similar to the antibacterial studies, low concentrations of surfactants showed similar effects in both *cis* and *trans*-dominated PSS, whereas the difference in activity between the photoisomeric states became more pronounced at higher concentrations (representative data for compound **AzoMan** is shown in Fig. 5; additional data for surfactants are shown in ESI Fig. S10 and S11†). In line with the antibacterial data, these surfactants generally compromised the biofilm forming ability of Gram-positive *S. aureus* at all concentrations tested, and conversely promoted biofilm formation of Gram-negative MDR *P. aeruginosa*, particularly on exposure to higher concentrations of these compounds. In the case of *S. aureus*, **AzoXyl**, **AzoMan**, and **AzoGlcNAc** could inhibit bacterial biofilms more efficiently after photoexcitation, whereas the native *trans* states of **AzoGlc**, **AzoRha** and **AzoAra** remained more potent biofilm inhibitors. Similar to the antibacterial results, **AzoRha** revealed an interesting trend, such that lower concentrations of this compound in both the *cis* and *trans* PSS inhibited *S. aureus* biofilm formation, whereas higher concentrations of the *cis* isomer started promoting biofilm formation. Another notable observation was that while **AzoGlcNAc** displayed selective antibacterial activity against *S. aureus* in the *trans* form, the *cis*-dominated photostationary state was more effective at inhibiting biofilm growth of this bacterium, suggesting a mechanism that was independent of cell death.²⁹

Bacterial motility studies

Bacterial motility is an important physiological process that enables bacteria to seek new environments and nutrients, and as such, plays important roles in the pathogenesis as well as biofilm growth, dispersal, structure and function.³⁰ Many bacterial species produce biosurfactants in response to environmental and internal cues, which results in a decrease in interfacial tension that enhances cellular motility and along

surfaces and in solution. To help better understand the intriguing biofilm modulatory activity of the surfactants, we decided to probe whether these compounds were affecting bacterial motility in solution and swarming motility on a semi-solid surface. We measured the dynamics and rates of swimming motility using differential dynamic microscopy (DDM) in the presence of representative **AzoRha** and **AzoMan**. DDM is a technique that uses optical microscopy to conduct an analysis similar to that used in dynamic light scattering. It has been shown that the technique is ideal for the measurement of dynamics and rates of motility of cells in bulk solution ('swimming').³¹ To this end, *P. aeruginosa* MDR283/1-6 was chosen as the model organism as it shows sufficiently fast rates of swimming required for the timescales measured using DDM. Using this technique, these photosurfactants did not appear to significantly affect the rate of swimming in solution up to concentrations of 500 $\mu\text{g mL}^{-1}$, in both the *cis*- and *trans*-dominated PSS (ESI, Fig. S12†). Based on this observation, it is therefore unlikely that these compounds are effecting biofilm growth through changes in the swimming motility of this bacterial species.

In the case of *P. aeruginosa*, compounds were shown to weakly inhibit biofilm growth at low concentrations and strongly promote biofilm growth at higher concentrations (Fig. 5). The photoexcited *cis* isomers were typically more or at least equally effective over their native forms in promoting biofilms of *P. aeruginosa*. Given the important roles that rhamnolipid biosurfactants play in promoting swarming motility, we decided to investigate whether the *cis* and *trans* forms of the surfactants were affecting swarming motility of *P. aeruginosa* MDR283/1-6 via photocontrollable changes in the interfacial activity. Swarming motility of *P. aeruginosa* was assessed in 0.5% agar media in the presence of the *trans* and *cis* isomers these compounds, along with controls using a previously described swarming assay (see ESI for details†).³²

In the native *trans* form, surfactants displayed a dose-dependent enhancement in swarming motility (Fig. 6). The response was insensitive to the head group employed, with all compounds being more-or-less equally effective at promoting swarming motility. However, in the *cis* photoisomeric state, the surfactants were generally less effective at promoting swarming motility, which may be a direct consequence of the lowered interfacial activity of the *cis* isomer relative to the *trans* isomer

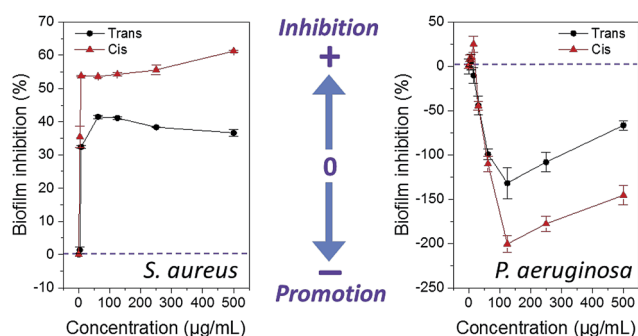


Fig. 5 Influence of *cis*- and *trans*-dominated photostationary states of **AzoMan** on biofilm formation of *S. aureus* and *P. aeruginosa*.



Fig. 6 Photograph of agar swarming motility assay demonstrating the influence of carbohydrate-based surfactants and control compounds in the *cis*- and *trans*-dominated PSS on the swarming motility of *P. aeruginosa* MDR283/1-6. Cells were inoculated at the centre of the agar media containing compound (100 $\mu\text{g mL}^{-1}$) and incubated at 30 °C for 24 h.

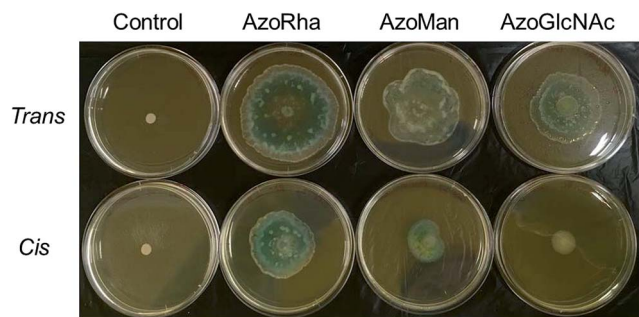


Fig. 7 Photograph of agar swarming motility assay demonstrating the influence of carbohydrate-based surfactants ($25 \mu\text{g mL}^{-1}$) in the *cis*- and *trans*-dominated PSS on the swarming motility of *P. aeruginosa* MDR283/1-23, a swarming negative strain.

(ESI, Fig. S13†). Interestingly, in contrast to the surfactants bearing a non-ionic carbohydrate head group, which generally promoted swarming motility, the non-surface active tail fragment **AzoTEG** and the cationic surfactant **AzoTAB** strongly inhibited swarming motility. Furthermore, unlike the carbohydrate-based surfactants, there were no significant changes in the inhibitory activity of **AzoTEG** and **AzoTAB** following *trans*-*cis* photoisomerization.

To validate the strong influence of our carbohydrate surfactants on swarming motility of *P. aeruginosa* MDR283/1-6 (a swarming-positive strain), we further investigated the influence of surfactants on the swarming motility of *P. aeruginosa* MDR283/1-23, a swarming-negative strain (Fig. 7). Remarkably, while untreated bacteria showed no detectable motility, these carbohydrate-based surfactants strongly promoted translocation of the bacterial colony, most likely through enhancement of surfactant-mediated sliding.³³ Similar to the swarming positive strain of *P. aeruginosa*, the *trans* configured surfactants promoted a higher level of motility relative to their *cis* isomers, particularly for **AzoGlcNAc**, which displays the largest difference in CMC between the respective *trans* and *cis* isomeric state. Taken together, these observations demonstrate the utility of UV light for modulating the swarming motility and biofilm forming ability of *P. aeruginosa* strains, which may potentially be a result of the associated changes in the interfacial activity of the *cis* and *trans* isomers of photoswitchable carbohydrate-based surfactants.

Conclusions

In summary, we report the modular synthesis and characterisation of a panel of novel carbohydrate-based surfactants and demonstrate unprecedented photo-control over bacterial growth, biofilm formation and motility using photoswitchable surfactants. Using SANS, we revealed the stark difference in the self-assembly properties of these amphiphiles, which is made possible through structural and stereochemical modification of the carbohydrate head group. Photocontrollable surface tension studies also revealed dramatic differences in the interfacial properties, which could be tuned using UV light irradiation. We then probed the impact of *trans*-*cis* azobenzene photoisomerization of these amphiphiles on their ability to modulate

the growth and formation of biofilms from pathogenic, drug-resistant strains of *S. aureus* and *P. aeruginosa*. Photoswitchable carbohydrate-based surfactants displayed dose-dependent, as well as bacteria- and photo-isomer specific biological activity, which suggests that these amphiphiles possess a selective mode of action. Interestingly, the photoexcited *cis* forms of these surfactants was shown to be more potent against *S. aureus*, while the native *trans* state showed higher selectivity against *E. coli*. Surprisingly, whilst selective antibacterial activity could be observed against *E. coli* and *S. aureus*, these compounds strongly promoted the growth of Gram-negative *P. aeruginosa* MDR283/1-6, despite the well-documented antimicrobial activity of azobenzene dyes toward *Pseudomonas* spp. and other Gram-negative bacteria. Furthermore, the reduction in inhibitory potency of some surfactants at higher concentrations may suggest an antagonistic affect owing to impaired uptake of surfactant monomers and/or their metabolites due to micellization.³⁴ Carbohydrate-based surfactants also showed remarkable bacteria-specific control over biofilm formation, such that they showed anti-biofilm activity against *S. aureus*, whereas they promoted biofilm formation in *P. aeruginosa*, with strong preference for the *cis* isomer. We further investigated the possible mechanisms governing the intriguing biofilm modulatory activity of these photosurfactants by measuring the rates of swimming and swarming motility of *P. aeruginosa*. Whilst the rates of swimming motility were generally insensitive to the *trans* and *cis* isomers of these compounds, surfactants were shown to strongly promote swarming motility in *P. aeruginosa* MDR283/1-6. We also demonstrated the ability of these compounds to promote the motility of the non-motile strain *P. aeruginosa* MDR283/1-23 on semi-solid agar, which could be further tuned using UV light. Through *trans*-*cis* photoisomerization of the azobenzene tail group, a decrease in bacterial motility could be observed relative to the *trans* isomer, presumably through reduction in the interfacial activity of the corresponding *cis* isomer. Overall, these results demonstrate the utility of UV-visible light for modulating the physicochemical properties of surfactants in order to control the physiological behaviour of bacteria. Further work is underway to understand the mechanistic interaction of the *trans*- and *cis*-photoisomeric states bearing different head groups with bacteria and their extracellular matrices, including lectin-specific inhibitors of bacterial adhesion and fluorescent uptake studies, as well as the development of dual visible light near infrared photo-switchable surfactants for *in vivo* applications.

Acknowledgements

B. W thanks the Australian Research Council for the Discovery Early Career research award (DE130101673). V. B. thanks Australian Research Council for a Future Fellowship (FT140101285). R. R. and W. Z. acknowledge RMIT University for Vice Chancellor's Postdoctoral Fellowship and Vice Chancellor's PhD Scholarship, respectively.

Notes and references

- 1 J. Carlet, *et al.*, *Lancet*, 2011, **378**, 369–371.

- 2 J. W. Costerton, P. S. Stewart and E. P. Greenberg, *Science*, 1999, **284**, 1318–1322.
- 3 (a) A. de Jesús Cortés-Sánchez, H. Hernández-Sánchez and M. E. Jaramillo-Flores, *Microbiol. Res.*, 2013, **168**, 22–32; (b) M. Inès and G. Dhouha, *Carbohydr. Res.*, 2015, **416**, 59–69.
- 4 J. D. Van Hamme, A. Singh and O. P. Ward, *Biotechnol. Adv.*, 2006, **24**, 604–620.
- 5 (a) M. Harmse, L. Yang, S. J. Pamp and T. Tolker-Nielsen, *FEMS Immunol. Med. Microbiol.*, 2010, **59**, 253–268; (b) M. E. Davey, N. C. Caiazza and G. A. O'Toole, *J. Bacteriol.*, 2013, **185**, 1027–1036.
- 6 E. L. Dane, A. E. Ballok, G. A. O'Toole and M. W. Grinstaff, *Chem. Sci.*, 2014, **5**, 551–557.
- 7 (a) I. Tochitsky, M. R. Banghart, A. Mourot, J. Z. Yao, B. Gaub, R. H. Kramer and D. Trauner, *Nat. Chem.*, 2012, **4**, 105–111; (b) M. Volgraf, P. Gorostiza, R. Numano, R. H. Kramer, E. Y. Isacoff and D. Trauner, *Nat. Chem. Biol.*, 2006, **2**, 47–52; (c) A. A. Beharry and G. A. Woolley, *Chem. Soc. Rev.*, 2011, **40**, 4422–4437.
- 8 (a) M. Stein, S. J. Middendorp, V. Carta, E. Pejo, D. E. Raines, S. A. Forman, E. Sigel and D. Trauner, *Angew. Chem., Int. Ed.*, 2012, **51**, 10500–10504; (b) M. Schonberger and D. Trauner, *Angew. Chem., Int. Ed.*, 2014, **53**, 3264–3267; (c) W. A. Velema, J. P. van der Berg, M. J. Hansen, W. Szymanski, A. J. Driessen and B. L. Feringa, *Nat. Chem.*, 2013, **5**, 924–928; (d) C. Falencyk, M. Shiedel, B. Karaman, T. Rumpf, N. Kuzmanovic, M. Grötli, W. Sippl, M. Jung and B. König, *Chem. Sci.*, 2014, **5**, 4794–4799; (e) W. A. Velema, W. Szymanski and B. L. Feringa, *J. Am. Chem. Soc.*, 2014, **136**, 2178–2191; (f) J. Briochhagen, J. A. Frank and D. Trauner, *Acc. Chem. Res.*, 2015, **48**, 1947–1960.
- 9 (a) D. Bléger, J. Swarz, A. M. Brouwer and S. Hecht, *J. Am. Chem. Soc.*, 2012, **134**, 20597–20600; (b) S. Samanta, T. M. McCormick, S. K. Schmidt, D. S. Seferos and G. A. Woolley, *Chem. Commun.*, 2013, **49**, 10314–10316; (c) A. A. Beharry and G. A. Woolley, *Chem. Soc. Rev.*, 2013, **40**, 4422–4437.
- 10 (a) M. Dong, A. Babalhavaeji, S. Samanta, A. A. Beharry and G. A. Woolley, *Acc. Chem. Res.*, 2015, **48**, 2662–2670; (b) Y. H. Tsai, S. Essig, J. R. James, K. Lang and J. W. Chin, *Nat. Chem.*, 2015, **7**, 554–561.
- 11 (a) O. Srinivas, N. Mitra, A. Suroliya and N. Jayaraman, *J. Am. Chem. Soc.*, 2002, **124**, 2124–2215; (b) T. Weber, V. Chandrasekaran, I. Stamer, M. B. Thygesen, A. T. Terfort and T. K. Lindhorst, *Angew. Chem., Int. Ed.*, 2014, **53**, 14583–14586.
- 12 J. Eastoe and A. Vesperinas, *Soft Matter*, 2005, **1**, 338–347.
- 13 (a) T. Muraoka, K. Kinbara and T. Aida, *Nature*, 2006, **440**, 512–515; (b) Y. Wang, N. Ma, Z. Wang and X. Zhang, *Angew. Chem., Int. Ed.*, 2007, **46**, 2823–2836.
- 14 (a) R. F. Tabor, D. D. Tan, S. S. Han, S. A. Young, Z. L. E. Seeger, M. J. Pottage, C. J. Garvey and B. L. Wilkinson, *Chem.–Eur. J.*, 2014, **20**, 13881–13884; (b) Y. Hu, J. B. Marlow, R. Ramanathan, W. Zou, H. G. Tiew, M. J. Pottage, V. Bansal, R. F. Tabor and B. L. Wilkinson, *Aust. J. Chem.*, 2015, **68**, 1880–1884.
- 15 R. F. Tabor, M. J. Pottage, C. J. Garvey and B. L. Wilkinson, *Chem. Commun.*, 2015, **51**, 5509–5512.
- 16 (a) H. C. Kolb, M. G. Finn and K. B. Sharpless, *Angew. Chem., Int. Ed.*, 2001, **40**, 2004–2021; (b) L. Bornaghi, B. L. Wilkinson, S. –A. Poulsen and T. A. Houston, *Tetrahedron*, 2005, **62**, 8115–8125.
- 17 E. Chevallier, A. Mamane, H. A. Stone, C. Tribet, F. Lequeux and C. Monteux, *Soft Matter*, 2011, **7**, 7866–7874.
- 18 H. Fliegl, A. Kohn, C. Hattig and R. Ahlrichs, *J. Am. Chem. Soc.*, 2003, **125**, 9821–9827.
- 19 M. K. Adam, J. S. Poisson, Y. Hu, G. Prasannakumar, M. J. Pottage, R. N. Ben and B. L. Wilkinson, *RSC Adv.*, 2016, **6**, 39240–39244.
- 20 (a) C. T. Lee Jr, K. A. Smith and T. A. Hatton, *Langmuir*, 2009, **25**, 13784–13794; (b) A.-L. LeNy and C. T. Lee Jr, *J. Am. Chem. Soc.*, 2006, **128**, 6400–6408.
- 21 (a) J. A. Johnson, M. –L. Saboungi, P. Thiyagarajan, R. Csencsits and D. Meisel, *J. Phys. Chem. B*, 1999, **103**, 59–63; (b) T. Shang, K. A. Smith and T. A. Hatton, *Langmuir*, 2006, **22**, 1436–1442.
- 22 J. Campbell, *Current Protocols in Chemical Biology*, 2010, **2**, 195–208.
- 23 W. Paulus, in *Dictionary of Microbicides for the Protection of materials*, ed. W. Paulus, Springer, 1st edn, 2005, ch. 2, pp. 9–23.
- 24 (a) A. M. Abdel-Mawgoud, F. Lépine and E. Déziel, *Appl. Microbiol. Biotechnol.*, 2010, **86**, 1323–1336; (b) N. Cerca and K. K. Jefferson, *FEMS Microbiol. Lett.*, 2008, **283**, 36–41; (c) A. Kropec, T. Maira-Litran, K. K. Jefferson, M. Grout, S. E. Cramton, F. Götz, D. A. Goldmann and G. B. Pier, *Infect. Immun.*, 2005, **73**, 6868–6876.
- 25 (a) S. J. Pamp and T. Tolker-Nielsen, *J. Bacteriol.*, 2007, **189**, 2531–2539; (b) N. C. Caiazza, R. M. Q. Shanks and T. A. O'Toole, *J. Bacteriol.*, 2005, **187**, 7351–7361.
- 26 T. F. Mah, B. Pitts, B. Pellock, G. C. Walker, P. S. Stewart and G. A. O'Toole, *Nature*, 2003, **426**, 306–310.
- 27 T. Bjarnsholt, *APMIS*, 2013, **121**, 1–58.
- 28 G. A. O'Toole, *J. Visualized Exp.*, 2011, **47**, DOI: 10.3791/2437.
- 29 J. L. Lister and A. R. Horswill, *Front. Cell. Infect. Microbiol.*, 2014, **4**, 1–9.
- 30 (a) G. A. O'Toole and R. Kolter, *Mol. Microbiol.*, 1998, **30**, 295–304; (b) N. Verstraeten, K. Braeken, B. Debkumari, M. Fauvart, J. Franssaer, J. Vermant and J. Michiels, *Trends Microbiol.*, 2008, **16**, 496–506.
- 31 (a) L. G. Wilson, V. A. Martinez, J. Schwarz-Linek, J. Tailleur, G. Bryant, P. N. Pusey and W. C. K. Poon, *Phys. Rev. Lett.*, 2011, **106**, 18101–18104; (b) V. A. Martinez, R. Besseling, O. A. Croze, J. Tailleur, M. Reuffer, J. Schwarz-Linek, L. G. Wilson, M. A. Bees and W. C. K. Poon, *Biophys. J.*, 2012, **103**, 1637–1647.
- 32 T. Inoue, R. Shingaki and K. Fukui, *FEMS Microbiol. Lett.*, 2008, **281**, 81–86.
- 33 D. B. Kearns, *Nat. Rev. Microbiol.*, 2010, **8**, 633–644.
- 34 (a) S. Piotto, S. Concilio, L. Sessa, A. Porta, E. C. Calabrese, A. Zanfardino, M. Varcamonti and P. Iannelli, *Eur. J. Med. Chem.*, 2013, **68**, 178–184; (b) M. Hartman, H. Papavlassopoulos, V. Chandrasekaran, C. Grabosch, F. Beiroth, T. Lindhorst and C. Röhl, *FEBS Lett.*, 2012, **586**, 1459–1465.

This page is intentionally blank



Photoswitchable carbohydrate-based fluorosurfactants as tuneable ice recrystallization inhibitors



Madeleine K. Adam ^{a,1}, Yingxue Hu ^{b,1}, Jessica S. Poisson ^a, Matthew J. Pottage ^b,
Robert N. Ben ^{a,**}, Brendan L. Wilkinson ^{c,*}

^a Department of Chemistry and Biomolecular Sciences, 10 Marie Curie, University of Ottawa, Ontario K1N 6N5, Canada

^b School of Chemistry, Monash University, Victoria 3800, Australia

^c School of Science and Technology, University of New England, New South Wales 2351, Australia

ARTICLE INFO

Article history:

Received 30 November 2016

Received in revised form

9 December 2016

Accepted 12 December 2016

Available online 14 December 2016

Keywords:

Carbohydrate-based fluorosurfactants

Ice recrystallization inhibitors

Photoswitchable fluorosurfactants

ABSTRACT

Cryopreservation is an important technique employed for the storage and preservation of biological tissues and cells. The limited effectiveness and significant toxicity of conventionally-used cryoprotectants, such as DMSO, have prompted efforts toward the rational design of less toxic alternatives, including carbohydrate-based surfactants. In this paper, we report the modular synthesis and ice recrystallization inhibition (IRI) activity of a library of variably substituted, carbohydrate-based fluorosurfactants. Carbohydrate-based fluorosurfactants possessed a variable mono- or disaccharide head group appended to a hydrophobic fluoroalkyl-substituted azobenzene tail group. Light-addressable fluorosurfactants displayed weak-to-moderate IRI activity that could be tuned through selection of carbohydrate head group, position of the trifluoroalkyl group on the azobenzene ring, and isomeric state of the azobenzene tail fragment.

© 2016 Elsevier Ltd. All rights reserved.

1. Introduction

Cryopreservation employs sub-zero temperatures for the long-term storage and preservation of biological samples, thereby protecting living cells and tissues from biochemical insult and ageing [1]. Ice recrystallization, the growth of large ice crystals at the expense of smaller ones, is a phenomenon that occurs predominantly during the freezing and thawing cycles of cryopreservation and is known to cause significant cryoinjury to cells, ultimately leading to compromised post-thaw recovery and viability [2]. While conventional cryoprotectants such as dimethyl sulfoxide (DMSO) and glycerol provide some protection against cryoinjury, they fail to control ice recrystallization and display significant cellular toxicity [3]. An alternative approach involves the use of extracellular cryoprotective agents that act by inhibiting ice recrystallization and/or correcting the osmotic balance during freezing [4,5]. Inspiration for this task has been largely drawn from Nature's biological antifreezes (BAs), including the well-studied

antifreeze proteins and glycoproteins (AF(G)Ps) that possess potent ice recrystallization inhibition (IRI) activity [6]. Early efforts have focused on mimicking the structure and function of BAs, an approach that has led to the development of extremely potent ice recrystallization inhibitors [7]. However, many of these biomolecules and their analogues are considered poor cryoprotectants at temperatures below $-8\text{ }^{\circ}\text{C}$ due to thermal hysteresis (TH) activity, which results in uncontrollable ice growth at these temperatures, combined with laborious synthesis and/or isolation of these agents [6b,8]. Recently, low molecular weight carbohydrate-based surfactants and hydrogelators have emerged as a promising class of cryoprotectants that have displayed potent IRI activity without any appreciable TH activity [4,9]. Whilst the IRI activity of simple sugars can be attributed to the degree of hydration [10], the mechanism of IRI activity for these amphiphilic carbohydrates is not well-understood even though the length and hydrophobicity of the alkyl tail group have been shown to be an important determinant for IRI activity [9,11]. Furthermore, despite the low hemolytic activity and promising physicochemical properties of non-ionic fluorosurfactants, the IRI activity of carbohydrate-based fluorosurfactants has yet to be explored [12].

The ability to remotely tune IRI activity offers exciting opportunities for the development of responsive, on-demand

* Corresponding author.

** Corresponding author.

E-mail address: bwilkin7@une.edu.au (B.L. Wilkinson).

¹ Both authors contributed equally to this work.

cryoprotectants and as tools for studying ice recrystallization. Toward this goal, earlier work from the Gibson group have reported the use of chemical and physical strategies for activating the latent IRI activity of proteins and polymers [13]. Azobenzene *trans-cis* photoisomerization offers considerable advantages, since it uses only light of a specific wavelength for reproducibly and reversibly changing (bio)molecular conformation to elicit a biological or physical response under excellent spatiotemporal control [14]. This strategy has also emerged as a promising route toward modulating the adsorption and aggregation properties of surfactant monomers [15]. We have recently reported the photocontrollable interfacial activity, self-assembly properties and IRI activity of a family of carbohydrate-based surfactants incorporating an *n*-butyl azobenzene tail group [16–18]. From this study, we identified a *D*-manno configured surfactant that displayed potent, photo-modulated IRI activity without any TH activity. Motivated by the IRI activity of this compound along with the biomedical importance of non-ionic fluorosurfactants, we report herein the modular synthesis and IRI activity of a family of photoswitchable carbohydrate-based fluorosurfactants **1–12** (Fig. 1). Fluorosurfactants **1–12** were comprised of a carbohydrate head group that was appended to an azobenzene tail group variably substituted with a trifluoromethyl ($-\text{CF}_3$) group in the *ortho*, *meta* or *para* position relative to the $\text{N}=\text{N}$ bond. We reasoned this would give rise to fluorosurfactants with modified tail group hydrophobicity, thus providing a means for tuning the hydrophilic-lipophilic balance (HLB) for interrogating the IRI activity of these compounds.

2. Results and discussion

Studies commenced with the modular synthesis of twelve carbohydrate-based fluorosurfactants (**1–12**; see Scheme 1 and ESI for details). Fluorosurfactants incorporated a mono- or disaccharide head group of varying size, absolute configuration and hydration,

including *D*-glucose (Glc, **1–3**), *D*-galactose (Gal, **4–6**), *D*-mannose (Man, **7–9**) and *D*-cellobiose (Cel, **10–12**) [10]. Target compounds **1–12** were synthesized using the well-established CuAAC reaction between the corresponding glycosyl azide and alkyne functionalized azobenzene fragment **13–15** [19,20], and were isolated in acceptable yields following base-catalyzed deprotection of the crude intermediates and purification by reversed-phase preparative HPLC.

In order to determine the physical properties of **1–12**, the surface activity of these amphiphiles was determined in the *cis*- and *trans* isomeric states (Table 1 and ESI Fig. S1). Surface tension measurements were carried out using pendant drop tensiometry [16,20]. To affect *trans-cis* photoisomerization, aqueous solutions of the compounds in the resting *trans*-dominated photostationary state (PSS) were irradiated with UV light (361 nm) for 10 min and monitored by UV–vis spectroscopy. The UV spectra displayed complex features that made absolute determination of the isomeric ratio in either PSS very difficult. Instead, we estimated the isomeric ratio in either PSS by integration of the triazole proton in the ^1H NMR spectrum of representative compounds **4–6** (ESI, Fig. S2) [18]. Based on this method, approximately 90% of molecules existed as the *trans* isomer in the resting *trans*-dominated PSS, and approximately 70% of fluorosurfactant monomers existed as the *cis* photoisomer in the photoexcited *cis*-dominated PSS. In all cases very little thermal relaxation of the photoexcited *cis* isomer to the resting *trans* PSS was observed, even after 24 h at 20 °C under dark-adapted conditions. Following photoisomerization, an overall increase in the critical micelle concentration (CMC) was observed, which can be attributed to the distorted geometry and increased polarity of the *cis*-configured monomers [21]. The magnitude of the difference in CMC between the respective PSS increased upon changing the position of the $-\text{CF}_3$ group from *para* to *meta*, and finally *ortho* to the $\text{N}=\text{N}$ bond, thus demonstrating the ability to tune the hydrophilic-lipophilic balance (HLB) of fluorosurfactants

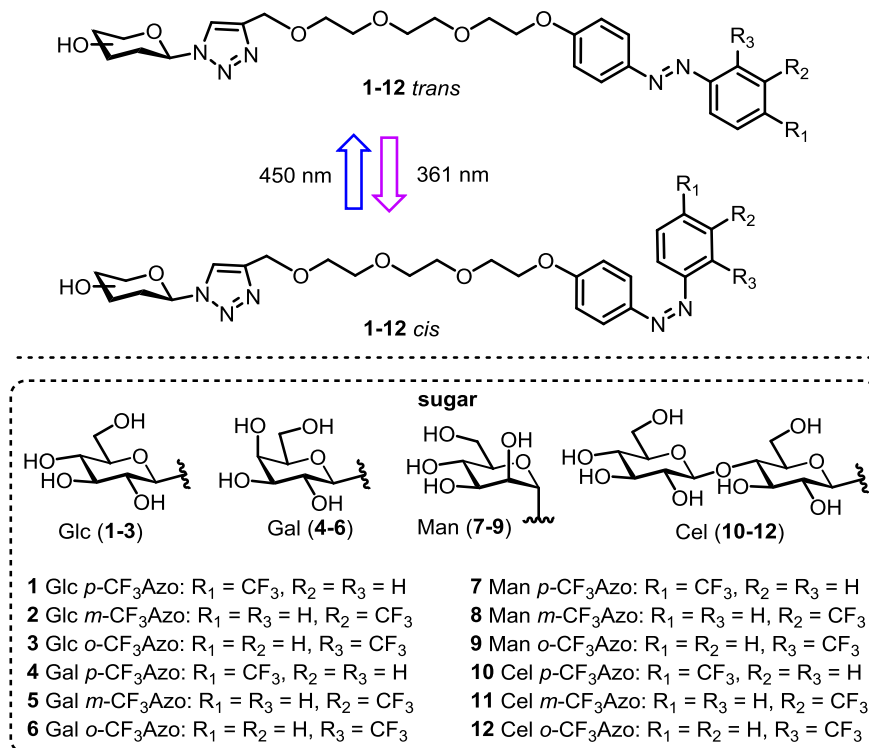
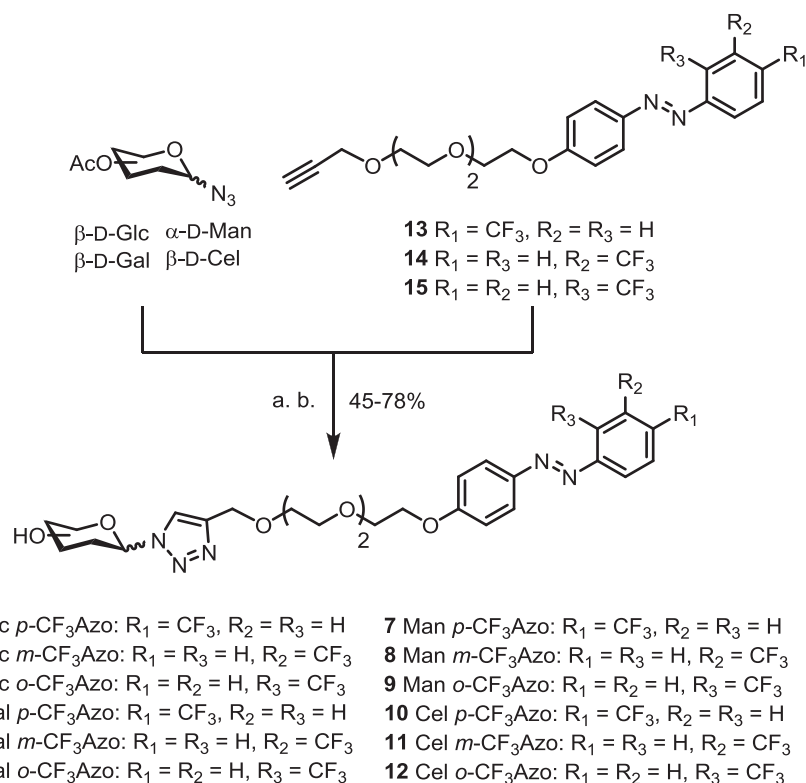


Fig. 1. Photoswitchable carbohydrate-based fluorosurfactants **1–12** used in this study.



Scheme 1. Synthesis of photoswitchable carbohydrate fluorosurfactants **1–12**. Conditions: (a) CuSO₄, sodium ascorbate, tert-butanol/H₂O (2:1 v/v), 40 °C; (b) NaOCH₃, CH₃OH.

Table 1
Properties of carbohydrate-based fluorosurfactants **1–12**.^a

Compound	CMC (CMC _{UV})	$t_{1/2}$ (h)	log <i>P</i> (log <i>P</i> _{UV})
Glc <i>p</i> -CF ₃ Azo 1	0.24 (0.25)	187	−0.32 (−0.20)
Glc <i>m</i> -CF ₃ Azo 2	0.26 (0.91)	151	−0.25 (−0.26)
Glc <i>o</i> -CF ₃ Azo 3	1.52 (2.81)	217	−0.65 (−0.47)
Gal <i>p</i> -CF ₃ Azo 4	0.23 (0.53)	178	−0.08 (0.03)
Gal <i>m</i> -CF ₃ Azo 5	1.41 (1.71)	141	−0.14 (−0.03)
Gal <i>o</i> -CF ₃ Azo 6	1.94 (2.03)	204	−0.02 (−0.01)
Man <i>p</i> -CF ₃ Azo 7	0.26 (0.36)	117	−0.32 (0.07)
Man <i>m</i> -CF ₃ Azo 8	0.17 (0.54)	114	−0.25 (−0.37)
Man <i>o</i> -CF ₃ Azo 9	0.13 (0.51)	147	−0.31 (0.14)
Cel <i>p</i> -CF ₃ Azo 10	0.48 (0.49)	165	−1.22 (−0.10)
Cel <i>m</i> -CF ₃ Azo 11	0.81 (1.28)	151	−1.27 (−1.41)
Cel <i>o</i> -CF ₃ Azo 12	0.59 (2.29)	224	−2.18 (−1.01)

^a Critical micelle concentrations (CMCs, mM) at 450 nm (vis) and 361 nm (UV), thermal half-life of the *cis* isomer at 20 °C ($t_{1/2(cis)}$) and 1-octanol/water partition coefficients (log *P*).

with UV light. For the *p*-CF₃ substituted analogues (**1**, **4**, **7** and **10**), the difference in the CMC between the *cis* and *trans* forms was negligible. This could be rationalized by the small difference in the dipole moment between the *cis* and *trans* isomers of *p*-CF₃ substituted azobenzene derivatives, with the *trans* isomer showing a larger dipole moment than the *cis* isomer [22,23].

To probe this observation further, we measured the 1-octanol-water partition coefficient (log *P*) for representative fluorosurfactants in the *cis* and *trans* isomeric states (Table 1) [24]. Log *P* is a useful measure of the relative affinity of a compound for a hydrophobic oily phase and a hydrophilic aqueous phase, with higher values indicating a preference for the hydrophobic phase. The log *P* values for **1–12** were strongly dependent on the head group employed and the regiochemistry of the −CF₃ group, with the *ortho*-substituted analogues generally showing greatest

solubility in the aqueous phase. Interestingly, for most compounds, an increase in log *P* was observed following UV photoirradiation, thus suggesting a slight increase in hydrophobicity for the *cis* isomer [23]. Although these results were unexpected based on the CMC values and previous observations on non-fluorinated photosurfactants, this underscores the diverse control opportunities possible for this class of light-addressable fluorosurfactant, which can be used for probing IRI activity.

Having synthesized and determined the key physical properties of fluorosurfactants **1–12**, we then investigated their IRI activity using a splat-cooling assay (Fig. 2 and ESI) [25]. Compounds **1–12** in either the *trans* or *cis* PSS were dissolved in a phosphate-buffered saline (PBS) solution and the areas of ice crystals were measured after a 30-min annealing period at −6.4 °C. The ice crystals were represented as a percent mean grain size (% MGS) relative to a phosphate-buffered saline (PBS) control for ice recrystallization. The IRI activity of the *cis*-configured fluorosurfactants was investigated by irradiating solutions with UV light prior to performing the assay as described above. Unfortunately, owing to the poor solubility of the *para*-substituted surfactants (**1**, **4**, **7** and **10**) at the required temperature in the PBS solution, the IRI activity of these compounds was only assessed at 5 μM. These analogues were determined to be IRI-inactive with the exception of Gal *p*-CF₃Azo **4**, which showed weak IRI activity. Interestingly, in each carbohydrate series, the most potent IRI activity was observed when the trifluoromethyl substituent was *ortho* to the N=N bond (**3**, **6**, **9** and **12**), and this activity was reduced by positioning the −CF₃ group *meta* (**2**, **5**, **8** and **11**) and finally *para* (**1**, **4**, **7**, and **10**) to the N=N bond (Fig. 2a and ESI Fig. S7). This emphasizes the importance of the regiochemistry of substituents on the azobenzene ring for triggering changes in the HLB and IRI activity of fluorosurfactant monomers.

When comparing the *ortho*-substituted surfactants, the Glc derivative (**3**) showed moderate IRI activity while the Gal (**6**), Man (**9**)

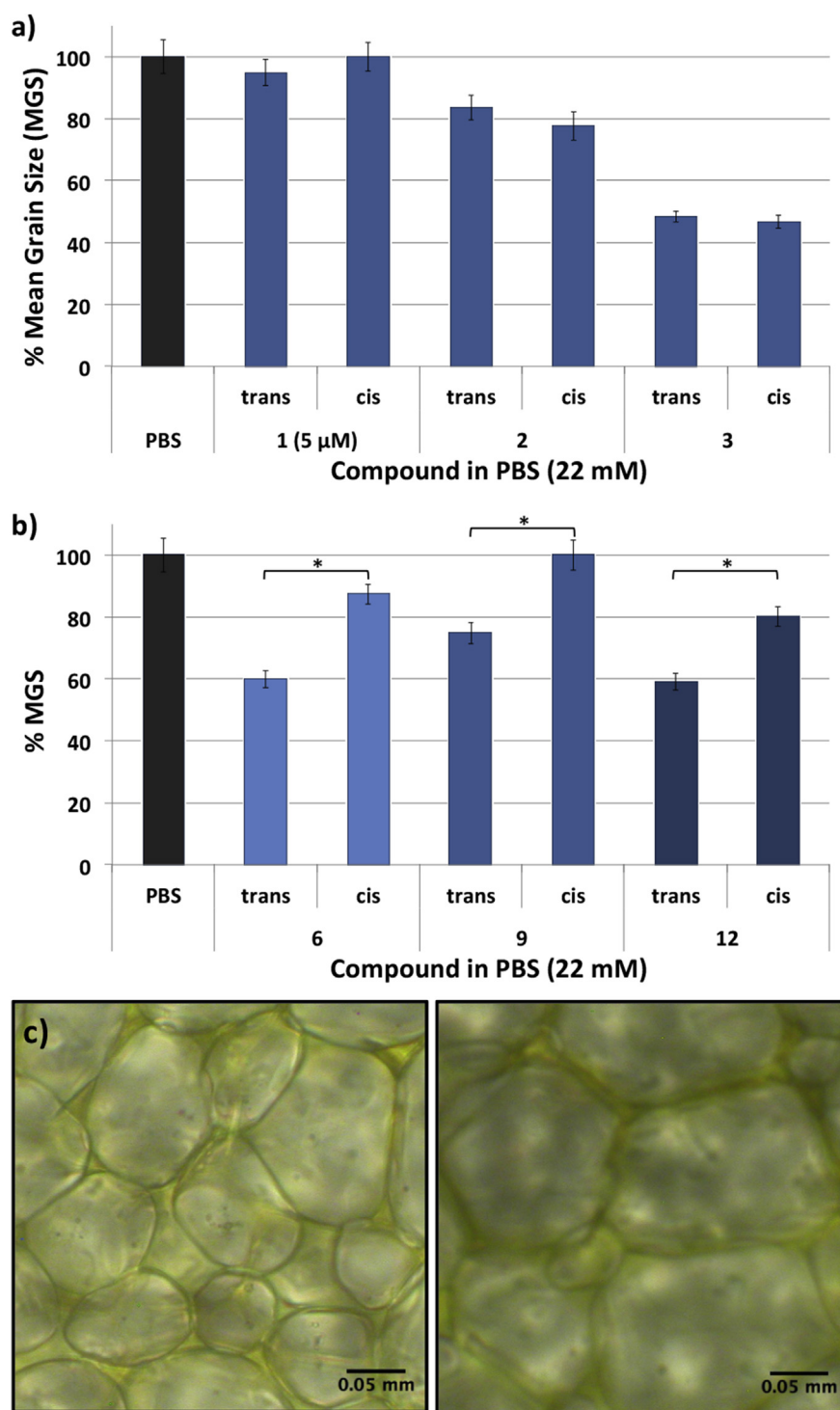


Fig. 2. (a) IRI activity of **1–3** represented as a % MGS (percent mean grain size) of ice crystals relative to the PBS control. (b) IRI activity of **6, 9** and **12** at 22 mM. Values represent the average of three runs \pm %SEM. Asterisk indicates significant difference calculated by Student's T test ($P < 0.05$). (c) Wafer images obtained after 30-min annealing period during the 'splat-cooling' assay. Left image corresponds to **9** in *trans*-dominated PSS while the image on the right corresponds to **9** in *cis*-dominated PSS.

and Cel (**12**) derivatives exhibited weaker activity (Fig. 2b). This result is in contrast to previous observations whereby an *n*-butyl azobenzene surfactant bearing a β -mannoside head group exhibited the strongest IRI activity compared to the Glc- and Gal-based analogues [18]. The increased IRI activity of the Glc derivative **3** is also in contrast to previous reports demonstrating the enhanced IRI activity of Gal-based amphiphiles compared to those incorporating

Glc head groups, possibly on account of the higher hydration index (HI) of galactose [9,10]. In contrast, the *meta*-substituted Glc (**2**) and Man (**8**) derivatives exhibited weaker activity than the Gal (**5**) and Cel (**11**) counterparts, which further emphasizes the sensitivity of IRI activity to changes in head group stereochemistry and tail group hydrophobicity. Photoisomerization of the *trans*-dominated PSS to the corresponding *cis*-isomeric state of the *ortho*-substituted

derivatives of Gal (**6**), Man (**9**) and Cel (**12**) significantly reduced the IRI activity. The attenuation in IRI activity from the *trans*-isomeric state to the *cis*-dominated PSS of **6**, **9** and **12** could be due to the significant difference in the interfacial activity and hydrophobicity of these *ortho*-substituted analogues. Therefore, with the exception of **3**, the IRI activity of this class of photosurfactant is only sensitive to the isomeric state of the azobenzene tail group when the fluoroalkyl group is in the *ortho* position, and is dependent on the type of carbohydrate head group employed and the position of the fluoroalkyl group on the azobenzene ring.

With the moderate IRI activity observed for the *ortho*-substituted analogues (**3**, **9** and **12**), a MTT assay was performed using Hep G2 cells in order to assess potential cytotoxicity of varying concentrations of the derivatives *in vitro* (ESI, Figs. S8–S9). Unfortunately, a significant decrease in cell viability was observed after incubation with the *ortho*-substituted fluorosurfactants. While high concentrations of surfactants are well known to solubilize biological membranes to trigger cell lysis and therefore death, the significant toxicity of these molecules is somewhat surprising given the low hemolytic activity of carbohydrate-based fluorosurfactants [12c]. The toxicity of azobenzene dyes in mammalian systems is well documented, however, several noteworthy studies have highlighted the potential use of modified derivatives for *in vivo* applications [26].

In summary, we report the modular synthesis, photocontrol-lable interfacial activity and IRI activity of a family of photo-switchable carbohydrate-based fluorosurfactants **1–12**. Fluorosurfactants were assessed for IRI activity before and after *trans-cis* photoisomerization of the hydrophobic trifluoromethyl azobenzene tail group. Following *trans-cis* photoisomerization, an increase in the CMC values was observed, which may be attributed to the altered polarity and molecular geometry of the fluorosurfactant monomers. The IRI activity of the photoswitchable fluorosurfactants was assessed using a splat-cooling assay and was shown to be dependent on the carbohydrate head group, position of the $-CF_3$ group on the azobenzene ring, and in some cases, the isomeric state of the azobenzene tail group. In contrast to previous observations whereby increasing hydrophobicity of the tail group confers greater IRI activity [11,27], the IRI activity of these compounds increased by changing the position of the $-CF_3$ group from the *para* position to *meta* and finally to *ortho* to the N=N bond, with moderate activity observed for the *ortho*-substituted fluorosurfactant **3** incorporating a D-glucose head group. The increased activity of the Glc-based compound is somewhat surprising as this monosaccharide has a lower degree of hydration compared to Galactose and Cellobiose [10]. Finally, photoisomerization of the *ortho*-substituted Gal-, Man- and Cel-based analogues, **6**, **9** and **12** respectively, significantly reduced the IRI activity. Unfortunately, the *ortho*-substituted analogues exhibited significant cellular toxicity in an MTT assay, however the efficient synthesis and variable IRI activity of these compounds presents promising opportunities for the rational design of low molecular weight cryoprotectants, as well as light-responsive molecular tools for studying the dynamic mechanisms of ice recrystallization.

3. Experimental

3.1. General

Analytical thin layer chromatography (TLC) was performed on commercially prepared silica plates (Merck Kieselgel 60 0.25 mm F254). Flash column chromatography was performed using 230–400 mesh Kieselgel 60 silica eluting with distilled solvents as described. Solvents and reagents were purchased from Sigma-Aldrich and Merck and used without further purification. 1H NMR

and ^{13}C NMR spectra were recorded on a Bruker Avance 400 NMR spectrometer at frequencies of 400 MHz and 100 MHz, respectively. Chemical shift is reported as parts per million (ppm) downfield from TMS reference. The data are reported as chemical shift (δ), multiplicity, relative integral, coupling constant ($J = \text{Hz}$) and assignment where possible. IR spectra were recorded on a Bruker ATR spectrometer. Optical rotation was measured on an Optical Activity Polar 2001 (546 nm) polarimeter using a 1 mL cell. LC-MS was recorded on an Agilent 6120B LC-MS system operating in positive ion mode. Separations were performed on an Agilent Poroshell-120 2.7 μm (3.0 mm \times 50 mm) C18 column using a linear gradient of 0.1% formic acid in water (Solvent A) and 0.1% formic acid in acetonitrile (Solvent B) as the mobile phase. Separations were performed using a linear gradient of 20% solvent B to 100% solvent B over 15 min, operating at a flow rate of 0.3 mL/min. Deprotected carbohydrate-based fluorosurfactants **1–12**, were purified by reversed-phase (C18) preparative HPLC using an Agilent 1260 preparative HPLC system equipped with an automated fraction collector. Separations were performed on an Agilent Zorbax SB300 5 μm (20 mm \times 150 mm) C18 column using a linear gradient of 0.1% formic acid in water (Solvent A) and 0.1% formic acid in acetonitrile (Solvent B) as mobile phase, operating at a flow rate of 10 mL/min (monitoring at 280 nm). Purified fractions were subsequently combined and lyophilized.

3.2. Surface tension measurements

Surface tension measurements were performed on a custom-designed pendant drop instrument as previously described [16,20]. A time series was taken (that is, surface tension as a function of time) and values were noted for 100 s to ensure full equilibration of interfacial adsorption. Once a stable surface tension had been attained, this was recorded. Drop volumes were measured throughout and changes of <5% throughout the course of a measurement were a requirement for the data shown. Critical micelle concentration (CMC) values were obtained from the intersection of lines extrapolated from surface tension values in the near pre- and post-CMC regions (ESI Fig. S1).

3.3. Photoswitching and UV–vis studies

The native *trans* isomers of **1–12** were converted into *cis* states by illumination of their aqueous solutions under ambient conditions using a UV lamp with λ_{max} at 361 nm for 10 min, although one minute of photoexcitation was found sufficient to convert *trans* isomers into *cis* state. The thermal relaxation studies were performed in dark-adapted conditions at ambient temperature (approximately 20 °C). These peaks were chosen as *cis-trans* relaxation results in an increase in peak intensity at ~350 nm, with corresponding decrease in peak intensity at 440 nm. The half-lives of the *cis* isomers in water estimated by measuring the UV–vis spectroscopy over a period of 24 h (ESI Fig. S1). Assuming a first order process, the kinetics for the thermal reversion from the *cis* photostationary state is expressed by:

$$\ln \frac{A_{cis} - A_{trans}}{A_t - A_{trans}} = k_{c-t} t$$

where A_{cis} , A_{trans} and A_t are the absorbance at 325 nm in *cis*-dominated PSS, in *trans*-dominated PSS and at time t . The half-life $t_{1/2}$ of the reversion from the photo-stationary state is then found by:

$$t_{1/2} = \frac{\ln(2)}{k_{c-t}}$$

UV–visible spectroscopy was performed using a Cary 60 spectrophotometer. The molar extinction coefficients of the two main peaks, at roughly 450 nm and 350 nm in the samples in each photostationary state, were calculated for samples 1–3 via analysis of five samples with a concentration ratio of 1:2:3:4:5, where the absorbance of the most concentrated sample was just below 1.0 to ensure the applicability of the Beer–Lambert law. In the photo-illumination experiments, the *trans*-dominated and the *cis*-dominated spectra were taken from samples immediately after dilution and after 10 min of irradiation under a fluorescent tube lamp (peak wavelength 361 nm, 6.5 W radiant power). The ratio of molecules in the *cis* and *trans* dominated photostationary states were estimated by integration of the resolved triazole proton in the ^1H NMR spectrum of fluorosurfactants 4–6 (ESI Figs. S2–S4).

3.4. Octanol–water partition coefficients ($\log P$)

The $\log P$ of fluorosurfactants was determined by preparing a 50 μM solution of 1–3 and 7–9 (200 μM for 3) in MilliQ water and adding an equal volume of 1-octanol. The sample was gently agitated and UV–vis spectra (~ 325 nm) was taken of the water layer before ($t = 0$) and after diffusion equilibrium ($t = 15$ h) (Fig. S6). Samples were stored in the dark prior to the final reading. To minimize thermal relaxation of the *cis* isomer under dark-adapted conditions, samples were further irradiated with UV light for 10 min at 6–8 h following the initial reading. The larger the $\log P$ value, the higher the solubility in the hydrophobic solvent. The $\log P$ was calculated by the following:

$$\log P = \log[(\text{Abs before} - \text{Abs after})/\text{Abs after}]$$

3.5. IRI and MTT assay

To measure ice recrystallization inhibition (IRI) activity of fluorosurfactants 1–12 (Fig. S7), the “splat cooling” assay was used as previously described [27]. The sample was dissolved in a phosphate-buffered saline (PBS) solution. A 10 μL droplet of the solution was dropped through a two-meter high plastic tube (10 cm diameter) onto a polished aluminium block cooled to approximately -80 $^\circ\text{C}$ with dry ice. The droplet froze immediately upon contact with the surface of the aluminium block, creating a wafer approximately 1 cm in diameter and 20 μm thick. Using precooled tools, the wafer was separated from the surface of the block and transferred to a cryostage, kept at -6.4 $^\circ\text{C}$. The wafer was annealed for 30 min, and then photographed between crossed polarizing filters using a digital camera (Nikon CoolPix 5000) fitted to a microscope. A programmable Peltier unit (S3 Series 800 temperature controller, Alpha Omega Instruments) was used to maintain the temperature of the cryostage. Three images were taken from each wafer. During flash freezing, small ice crystals from the solution are formed very quickly, and during annealing, the ice crystals dramatically increase in size due to recrystallization. In order to quantitatively measure the difference in recrystallization inhibition of two compounds, the difference in the dynamics of ice crystal size distribution was examined. This was done using a novel domain recognition software (DRS)22 program to analyze the image of the ice wafer. From this, domain areas from each image were calculated and the data was inputted into Microsoft Excel where the results were then analyzed and plotted. The ice crystal mean grain size (MGS) of the sample was compared to the MGS of the PBS positive control for recrystallization for the same day of testing, and IRI activity was reported as % MGS \pm % SEM (standard error of the mean). Each compound was performed in triplicate ($n = 3$). In

GraphPad, significant difference was determined using the unpaired Student's *T* test ($P < 0.05$).

In order to investigate the cytotoxicity of the *ortho*-substituted analogues (3, 9 and 12) (Figs. S8 and S9), Hep G2 cells were incubated with varying concentrations of the compounds; with controls and each test concentration performed at least in triplicate ($n = 3$). Hep G2 cells (human liver hepatocellular carcinoma cells, ATCC, HB-8065) were cultured in Eagle's minimum essential media (MEM) supplemented with 10% fetal bovine serum (FBS), 1% penicillin–streptomycin, 1% non-essential amino acids, and 0.1% 1M sodium pyruvate in Corning[®] T75 (75 cm^2) flasks. Cells were incubated at 37 $^\circ\text{C}$ with 5% CO_2 . Passages 8–9 were used in this study. Cells were detached from plates using Accutase and incubated at 37 $^\circ\text{C}$ for 15 min for use in experiments. The MTT assay was performed as previously reported [28]. Hep G2 cells were plated in 96-well plates and treated with 100 μL of appropriate test compound dissolved in MEM, and incubated at 37 $^\circ\text{C}$ with 5% CO_2 overnight. Cells incubated with MEM were used as positive controls and cells incubated with 1% Triton X-100 (in MEM) were used as negative controls. Following incubation, the plates were centrifuged (1000 rpm for 5 min), the supernatants were removed by aspiration, and 200 μL of MEM and 50 μL of MTT (5 mg/mL) in HBSS (Hank's balanced salt solution) were added to each well. The plates were incubated at 37 $^\circ\text{C}$ with 5% CO_2 for 4 h before being centrifuged for 3 min at 700 $\times g$. The supernatants were removed, and 200 μL of MTT solubilization solution (10% Triton X-100, 0.1 N HCl in isopropanol) was added to each well. The plate was incubated in the dark at room temperature for 2 h and the absorbance of each well was then read at a wavelength of 570 nm with a multi-well plate reader (AD 340C Absorbance Detector, Beckman Coulter, Inc., Mississauga, ON). Higher absorbance readings were indicative of greater cell viability. Percent cell viability was reported relative to the control. Cells incubated with PBS served as the positive control while cells incubated with 1% Triton X-100 in PBS served as the negative control. Incubation of Hep G2 cells with Man *o*-CF₃Azo (9) dissolved in MEM (2.5 mM, 5 mM, 10 mM, 20 mM) resulted in complete loss of viable cells.

3.6. Synthesis

3.6.1. General procedure for the synthesis of carbohydrate-based fluorosurfactants (1–12)

A mixture of the corresponding β -D-glycopyranosyl azide (1.0 equiv) and propargyl ether (1.0 equiv.) [20,29] was suspended in *tert*-BuOH/H₂O (2:1 v/v, 0.5 mM). Sodium ascorbate (0.4 equiv.) and CuSO₄·5H₂O (0.2 equiv.) was added and the deep yellow suspension was stirred vigorously for 2 h at 40 $^\circ\text{C}$. TLC analysis (ethyl acetate/petroleum ether 40–60, 4:1 v/v) showed complete consumption of the azide and alkyne, with formation of a polar product (R_f ca. 0.3). The reaction mixture was extracted into ethyl acetate (10 mL), and washed with water (10 mL) and brine (10 mL). The organic layer was dried (Na₂SO₄), filtered and evaporated to dryness. The resulting yellow oil was re-dissolved in dry methanol. A 0.5 M solution of sodium methoxide in methanol (0.1 equiv.) was then added and the reaction stirred at room temperature for one hour, at which time LC-MS analysis (20–100%B over 15 min) showed reaction completion. The reaction was neutralized with Amberlite IR-120 acidic ion exchange resin, filtered and concentrated under reduced pressure. Fluorosurfactants 1–12 were subsequently purified by reversed-phase preparative HPLC (See materials and methods) and isolated as deep yellow solids following lyophilization (45–78% yields).

3.6.2. Analytical data for novel compounds (4–9)

3.6.2.1. 2-[2-[2-(4-trifluoromethylazophenyl phenoxy)ethoxy]ethoxy]methyl β -D-galactopyranosyl-1,2,3-triazole (Gal *p*-CF₃Azo) **4**. Yield 78%; Mp = 212 °C (decomp.); [α]_D²⁰ –30.9 (c, 0.002 in CH₃OH); FT-IR: $\nu_{\max}/\text{cm}^{-1}$ 2870, 1597, 1452, 1321, 1251, 1060, 852, 773; ¹H NMR (400 MHz, DMSO-*d*₆) δ 8.20 (s, 1H, =CH(triazole)), 8.00 (d, *J* = 8.39 Hz, 2H, 2 × ArH), 7.95–7.92 (m, 4H, 4 × ArH), 7.17 (d, *J* = 9.07 Hz, 2H, 2 × ArH), 5.48 (d, *J* = 9.20 Hz, 1H, CH(anomeric)), 4.25–4.22 (m, 2H), 4.07–4.02 (m, 1H), 3.81–3.78 (m, 3H), 3.73–3.69 (m, 1H), 3.63–3.47 (m, 13H); ¹³C NMR (100 MHz, DMSO-*d*₆) δ 162.5 (ArC), 154.8 (ArC), 146.6 (ArC), 144.5 (C=CH(triazole)), 127.1 (ArC), 125.6 (2 × ArC), 123.3 (CF₃), 123.2 (ArC), 115.8 (2 × ArC), 88.6 (CH(anomeric)), 78.9, 74.2, 70.5, 70.3, 70.2, 69.9, 69.6, 69.3, 68.9, 68.3, 63.9, 60.9 (CH₂); ESI-MS⁺ calculated for C₂₈H₃₄F₃N₅O₉ 641.2309, found 664.2199 [M+Na]⁺.

3.6.2.2. 2-[2-[2-(3-trifluoromethylazophenyl phenoxy)ethoxy]ethoxy]methyl β -D-galactopyranosyl-1,2,3-triazole (Gal *m*-CF₃Azo) **5**. Yield 51%; Mp = 196 °C (decomp.); [α]_D²⁰ –28.3 (c, 0.004 in CH₃OH); FT-IR: $\nu_{\max}/\text{cm}^{-1}$ 2851, 1593, 1428, 878, 781, 621; ¹H NMR (400 MHz, DMSO-*d*₆) δ 8.20 (s, 1H, =CH(triazole)), 8.14–8.09 (m, 2H, 2 × ArH), 7.94 (d, *J* = 8.99 Hz, 2H, 2 × ArH), 7.89–7.79 (m, 2H, 2 × ArH), 7.17 (d, *J* = 8.96 Hz, 2H, 2 × ArH), 5.47 (d, *J* = 9.18 Hz, 1H, CH(anomeric)), 5.18 (s, 1H), 4.69–4.56 (m, 4H), 4.24–4.22 (m, 2H), 4.06–4.02 (m, 1H), 3.80–3.78 (m, 3H), 3.72–3.69 (m, 2H), 3.62–3.49 (m, 11H); ¹³C NMR (100 MHz, DMSO-*d*₆) δ 162.4 (ArC), 152.7 (ArC), 146.5 (ArC), 144.5 (C=CH(triazole)), 131.3 (ArC), 130.6 (ArC), 125.5 (2 × ArC), 123.2 (CF₃), 118.5 (ArC), 115.7 (2 × ArC), 88.6 ((CH(anomeric))), 78.9, 74.2, 70.4, 70.3, 70.2, 69.9, 69.6, 69.3, 69.0, 68.3, 67.9, 63.9, 60.9; ESI-MS⁺ calculated for C₂₈H₃₄F₃N₅O₉ 641.2309, found 664.2196 [M+Na]⁺.

3.6.2.3. 2-[2-[2-(2-trifluoromethylazophenyl phenoxy)ethoxy]ethoxy]methyl β -D-galactopyranosyl-1,2,3-triazole (Gal *o*-CF₃Azo) **6**. Yield 45%; Mp = 88 °C; [α]_D²⁰ –53.3 (c, 0.002 in CH₃OH); FT-IR: $\nu_{\max}/\text{cm}^{-1}$ 2879, 1599, 1416, 1314, 1254, 1128, 1051, 765; ¹H NMR (400 MHz, DMSO-*d*₆) δ 8.21 (s, 1H, =CH(triazole)), 7.93–7.89 (m, 3H, 3 × ArH), 7.83–7.77 (m, 2H, 2 × ArH), 7.71–7.67 (m, 1H, ArH), 7.19 (d, *J* = 9.00 Hz, 2H, 2 × ArH), 5.49 (d, *J* = 9.19 Hz, 1H, CH(anomeric)), 5.21 (s, 1H), 4.67–4.56 (m, 4H), 4.24–4.22 (m, 2H), 4.08–4.03 (m, 1H), 3.81–3.78 (m, 3H), 3.74–3.71 (m, 1H), 3.63–3.49 (m, 12H); ¹³C NMR (100 MHz, DMSO-*d*₆) δ 162.6 (ArC), 149.5 (ArC), 146.9 (ArC), 144.5 (C=CH(triazole)), 134.1 (ArC), 131.1 (ArC), 125.9 (2 × ArC), 123.2 (CF₃), 116.7 (ArC), 115.9 (2 × ArC), 88.6 ((CH(anomeric))), 78.9, 74.2, 70.4, 70.3, 70.2, 69.9, 69.6, 69.3, 69.0, 68.3, 63.9, 60; ESI-MS⁺ calculated for C₂₈H₃₄F₃N₅O₉ 641.2309, found 664.2197 [M+Na]⁺.

3.6.2.4. 2-[2-[2-(4-trifluoromethylazophenyl phenoxy)ethoxy]ethoxy]methyl α -D-mannopyranosyl-1,2,3-triazole (Man *p*-CF₃Azo) **7**. Yield: 76%. Mp = 102 °C; [α]_D²⁰ 37.5 (c, 0.002 in CH₃OH); FT-IR: $\nu_{\max}/\text{cm}^{-1}$ 3349, 2878, 1597, 1503, 1322, 1251, 1128, 1062, 853, 668; ¹H NMR (400 MHz, DMSO-*d*₆) δ 8.21 (s, 1H, =CH(triazole)), 8.01–7.91 (m, 4H, 4 × ArH), 7.16 (d, *J* = 9.10 Hz, 2H, 2 × ArH), 5.91 (d, *J* = 4.07 Hz, 1H, CH(anomeric)), 5.26 (s, 1H, OH), 4.99 (s, 2H, 2 × OH), 4.61–4.54 (m, 3H), 4.44–4.42 (m, 1H), 4.24–4.21 (m, 2H), 3.87–3.84 (m, 1H), 3.79–3.78 (m, 2H), 3.61–3.54 (m, 9H), 3.37–3.32 (m, 3H); ¹³C NMR (100 MHz, DMSO-*d*₆) δ 162.5 (ArC), 154.7 (ArC), 146.6 (ArC), 144.4 (C=CH(triazole)), 127.0 (ArC), 125.6 (2 × ArC), 124.1 (CF₃), 123.2 (ArC), 115.7 (2 × ArC), 86.3 (CH(anomeric)), 78.7, 71.7, 70.4, 70.3, 70.2, 69.6, 69.2, 68.6, 68.2, 68.1, 63.9, 61.3 (CH₂); ESI-HRMS⁺ calculated for C₂₈H₃₄F₃N₅O₉ = 641.2309, found 642.2384 [M+H]⁺, 664.2200 [M+Na]⁺.

3.6.2.5. 2-[2-[2-(3-trifluoromethylazophenyl phenoxy)ethoxy]ethoxy]methyl α -D-mannopyranosyl-1,2,3-triazole (Man *m*-CF₃Azo) **8**. Yield: 66%. Mp = 72 °C; [α]_D²⁰ 29.6 (c, 0.004 in CH₃OH); FT-IR: $\nu_{\max}/\text{cm}^{-1}$ 3369, 2877, 1599, 1501, 1326, 1249, 1059, 799, 692; ¹H NMR (400 MHz, DMSO-*d*₆) δ 8.21 (s, 1H, =CH(triazole)), 8.13–8.08 (m, 2H, 2 × ArH), 7.93 (d, *J* = 9.02 Hz, 2H, 2 × ArH), 7.88–7.79 (m, 2H, 2 × ArH), 7.16 (d, *J* = 9.08 Hz, 2H, 2 × ArH), 5.92 (d, *J* = 4.07 Hz, 1H, CH(anomeric)), 5.26 (d, *J* = 5.01 Hz, 1H, OH), 5.03–4.98 (m, 2H, OH), 4.62–4.55 (m, 3H), 4.45–4.42 (m, 1H), 4.23–4.21 (m, 2H), 3.86–3.85 (m, 1H), 3.80–3.77 (m, 2H), 3.62–3.54 (m, 9H), 3.36–3.33 (m, 3H); ¹³C NMR (100 MHz, DMSO-*d*₆) δ 162.4 (ArC), 152.6 (ArC), 146.4 (ArC), 144.4 (C=CH(triazole)), 131.3 (ArC), 130.8 (ArC), 125.5 (2 × ArC), 124.1 (CF₃), 118.5 (ArC), 115.7 (2 × ArC), 86.3 ((CH(anomeric))), 78.7, 71.7, 70.4, 70.3, 70.2, 69.6, 69.2, 68.7, 68.2, 68.1, 63.9, 61.3; ESI-HRMS⁺ calculated for C₂₈H₃₄F₃N₅O₉ = 641.2309, found 642.2380 [M+H]⁺, 664.2200 [M+Na]⁺.

3.6.2.6. 2-[2-[2-(3-trifluoromethylazophenyl phenoxy)ethoxy]ethoxy]methyl α -D-mannopyranosyl-1,2,3-triazole (Man *m*-CF₃Azo) **8**. Yield: 66%. Mp = 72 °C; [α]_D²⁰ 29.6 (c, 0.004 in CH₃OH); FT-IR: $\nu_{\max}/\text{cm}^{-1}$ 3369, 2877, 1599, 1501, 1326, 1249, 1059, 799, 692; ¹H NMR (400 MHz, DMSO-*d*₆) δ 8.21 (s, 1H, =CH(triazole)), 8.13–8.08 (m, 2H, 2 × ArH), 7.93 (d, *J* = 9.02 Hz, 2H, 2 × ArH), 7.88–7.79 (m, 2H, 2 × ArH), 7.16 (d, *J* = 9.08 Hz, 2H, 2 × ArH), 5.92 (d, *J* = 4.07 Hz, 1H, CH(anomeric)), 5.26 (d, *J* = 5.01 Hz, 1H, OH), 5.03–4.98 (m, 2H, OH), 4.62–4.55 (m, 3H), 4.45–4.42 (m, 1H), 4.23–4.21 (m, 2H), 3.86–3.85 (m, 1H), 3.80–3.77 (m, 2H), 3.62–3.54 (m, 9H), 3.36–3.33 (m, 3H); ¹³C NMR (100 MHz, DMSO-*d*₆) δ 162.4 (ArC), 152.6 (ArC), 146.4 (ArC), 144.4 (C=CH(triazole)), 131.3 (ArC), 130.8 (ArC), 125.5 (2 × ArC), 124.1 (CF₃), 118.5 (ArC), 115.7 (2 × ArC), 86.3 ((CH(anomeric))), 78.7, 71.7, 70.4, 70.3, 70.2, 69.6, 69.2, 68.7, 68.2, 68.1, 63.9, 61.3; ESI-HRMS⁺ calculated for C₂₈H₃₄F₃N₅O₉ = 641.2309, found 642.2380 [M+H]⁺, 664.2200 [M+Na]⁺.

3.6.2.7. 2-[2-[2-(2-trifluoromethylazophenyl phenoxy)ethoxy]ethoxy]methyl α -D-mannopyranosyl-1,2,3-triazole (Man *o*-CF₃Azo) **9**. Yield: 47%. Mp = 60 °C; [α]_D²⁰ 51.6 (c, 0.001 in CH₃OH); FT-IR: $\nu_{\max}/\text{cm}^{-1}$ 3364, 2873, 1598, 1312, 1104, 1050, 841, 764, 669; ¹H NMR (400 MHz, DMSO-*d*₆) δ 8.20 (s, 1H, =CH(triazole)), 7.94–7.89 (m, 3H, 3 × ArH), 7.82–7.78 (m, 2H, 2 × ArH), 7.72–7.70 (m, 1H, ArH), 7.19 (d, *J* = 9.05 Hz, 2H, 2 × ArH), 5.91 (d, *J* = 4.07 Hz, 1H, CH(anomeric)), 5.26 (s, 1H, OH), 5.00 (s, 1H, OH), 4.56 (s, 2H), 4.43–4.41 (m, 1H), 4.24–4.22 (m, 2H), 3.85–3.83 (m, 1H), 3.80–3.78 (m, 2H), 3.62–3.52 (m, 10H), 3.36–3.31 (m, 3H); ¹³C NMR (100 MHz, DMSO-*d*₆) δ 162.6 (ArC), 149.4 (ArC), 146.9 (ArC), 144.4 (C=CH(triazole)), 134.1 (ArC), 131.2 (ArC), 125.7 (2 × ArC), 124.1 (CF₃), 116.7 (ArC), 115.8 (2 × ArC), 86.2 ((CH(anomeric))), 78.7, 71.7, 70.4, 70.3, 70.2, 69.6, 69.2, 68.6, 68.2, 68.1, 63.9, 61.2; ESI-HRMS⁺ calculated for C₂₈H₃₄F₃N₅O₉ = 641.2309, found 642.2389 [M+H]⁺, 664.2200 [M+Na]⁺.

Acknowledgement

B. W. thanks the Australian Research Council for the Discovery Early Career research award (DE130101673) for funding. R. N. B. acknowledges the Natural Sciences and Engineering Research Council of Canada (NSERC), Canadian Blood Services (CBS) and Canadian Institutes of Health Research (CIHR) for financial support. M. K. A. and J. S. P. thank NSERC for Canada Graduate Scholarships (CGS M).

Appendix A. Supplementary data

Supplementary data related to this article can be found at <http://dx.doi.org/10.1016/j.carres.2016.12.004>.

References

- [1] D.E. Pegg, *Methods Mol. Biol.* 368 (2007) 39–57.
- [2] a) J.M. Baust, R. Van Buskirk, G.J. Baust, *In Vitro Cell. Dev. Biol. – Anim.* 36 (2000) 262–270;
b) J.M. Baust, *Cell Preserv. Technol.* 1 (2002) 17–31;
c) A. Fowler, M. Toner, *Ann. N. Y. Acad. Sci.* 1066 (2005) 119–135.
- [3] a) G.M. Fahy, *Cryobiology* 23 (1990) 1–13;
b) G.M. Fahy, T.H. Lilley, H. Linsdell, M.S. Douglas, H.T. Meryman, *Cryobiology* 27 (1990) 247–268.
- [4] C.J. Capicciotti, J.D.R. Kurach, T.R. Turner, R.S. Mancini, J.P. Acker, R.N. Ben, *Sci. Rep.* 5 (2015) 1–9.
- [5] C.J. Hunt, *Transfus. Med. Hemother.* 38 (2011) 107–123.
- [6] a) A.L. DeVries, D.E. Wohlschlag, *Science* 163 (1969) 1073–1075;
b) B.L. Wilkinson, R.S. Stone, C.J. Capicciotti, M. Thaysen-Andersen, J.M. Matthews, N.H. Packer, R.N. Ben, R.J. Payne, *Angew. Chem. Int. Ed.* 51 (2012) 3606–3610.
- [7] A.K. Balcerzak, C.J. Capicciotti, J.G. Briard, R.N. Ben, *RSC Adv.* 4 (2014) 42682–42696.
- [8] a) M. Bar-Dolev, Y. Celik, J.S. Wettlaufer, P.L. Davies, I. Braslavsky, *J. R. Soc. Interface* 9 (2012) 3249–3259;
b) J.F. Carpenter, T.N. Hansen, *Proc. Natl. Acad. Sci. U. S. A.* 89 (1992) 8953–8957.
- [9] C.J. Capicciotti, M. Leclère, F.A. Perras, D.L. Bryce, H. Paulin, J. Harden, Y. Liuc, R.N. Ben, *Chem. Sci.* 3 (2012) 1408–1416.
- [10] R.Y. Tam, S.S. Ferreira, P. Czechura, J.L. Chaytor, R.N. Ben, *J. Am. Chem. Soc.* 130 (2008) 17494–17501.
- [11] A.K. Balcerzak, M. Febbraro, R.N. Ben, *RSC Adv.* 3 (2013) 3232–3236.
- [12] a) M.–P. Krafft, J.G. Riess, *Chem. Rev.* 109 (2009) 1714–1792;
b) Y.–L. Chiu, H.F. Chan, K.K.L. Phua, Y. Zhang, S. Juul, B.R. Knudsen, Y.–P. Ho, W. Leong, *ACS Nano* 8 (2014) 3913–3920;
c) X. Li, J. Turánek, P. Knötigová, H. Kudláčková, J. Mašek, S. Parkin, S.E. Rankin, B.L. Knutson, H.–J. Lehmer, *Colloids Surf. B Biointerfaces* 73 (2009) 65–74.
- [13] a) D.E. Mitchell, M.I. Gibson, *Biomacromolecules* 16 (2015) 3411–3416;
b) D.J. Phillips, T.R. Congdon, M.I. Gibson, *Polym. Chem.* 7 (2016) 1701–1704.
- [14] a) Y. Hu, R.F. Tabor, B.L. Wilkinson, *Org. Biomol. Chem.* 13 (2015) 2216–2225;
b) A. A. Beharry, G. A. Woolley, *Chem. Commun.* 40 (2011) 4422–4437.
- [15] P. Brown, C.P. Butts, J. Eastoe, *Soft Matter* 9 (2013) 2365–2374.
- [16] R.F. Tabor, D.D. Tan, S.S. Han, S.A. Young, Z.L.E. Seeger, M.J. Pottage, C.J. Garvey, B.L. Wilkinson, *Chem. – Eur. J.* 20 (2014) 13881–13884.
- [17] R.F. Tabor, M.J. Pottage, C.J. Garvey, B.L. Wilkinson, *Chem. Commun.* 51 (2015) 5509–5512.
- [18] M.K. Adam, Y. Hu, J.S. Poisson, G. Prassanakumar, M.J. Pottage, R.N. Ben, B.L. Wilkinson, *RSC Adv.* 16 (2016) 39240–39244.
- [19] a) V.V. Rostovtsev, L.G. Green, V.V. Fokin, K.B. Sharpless, *Angew. Chem. Int. Ed.* 41 (2002) 2569–2599;
b) B.L. Wilkinson, L.F. Bornaghi, S.–A. Poulsen, T.A. Houston, *Tetrahedron* 62 (2006) 8115–8125.
- [20] Y. Hu, J.B. Marlow, R. Ramanathan, W. Zou, H.G. Tiew, M.J. Pottage, V. Bansal, R.F. Tabor, B.L. Wilkinson, *Aust. J. Chem.* 68 (2015) 1880–1884.
- [21] a) T. Shang, K.A. Smith, T.A. Hatton, *Langmuir* 19 (2003) 10764–10773;
b) H. Rau, in: J.F. Rabek (Ed.), *Photochemistry and Phot Physics* vol. 2, CRC, Boca Raton, 1990, pp. 119–141.
- [22] J.H. Yoon, S. Yoon, *Phys. Chem. Chem. Phys.* 13 (2011) 12900–12905.
- [23] M.R. Han, Y. Hirayama, M. Hara, *Chem. Mater.* 18 (2006) 2784–2786.
- [24] An improved method for deriving the log P of compounds 1–12 was developed and gave more reliable values to the results found ref. 20 (see experimental for details).
- [25] C.A. Knight, J. Hallett, A.L. DeVries, *Cryobiology* 25 (1988) 55–60.
- [26] a) S. Samanta, A.A. Beharry, O. Sadovski, T.M. McCormick, A. Babalavaeiji, V. Tropepe, G.A. Woolley, *J. Am. Chem. Soc.* 135 (2013) 9777–9784;
b) A. Dong, A. Babalavaeiji, S. Samanta, A.A. Beharry, G.A. Woolley, *Acc. Chem. Res.* 48 (2015) 2662–2670;
c) W.A. Velema, W. Szymanski, B.L. Feringa, *J. Am. Chem. Soc.* 136 (2014) 2178–2191.
- [27] J.F. Trant, R.A. Biggs, C.J. Capicciotti, R.N. Ben, *RSC Adv.* 3 (2013) 26005–26009.
- [28] T. Mosmann, *J. Immunol. Methods* 65 (1983) 55–63.
- [29] C.–Z. Zhang, C. Lu, J. Zhu, C.–Y. Wang, G.–Y. Lu, C.–S. Wang, D.–L. Wu, F. Liu, Y. Cui, *Chem. Mater.* 20 (14) (2008) 4628–4641.

Synthesis and Properties of Photoswitchable Carbohydrate Fluorosurfactants

Yingxue Hu,^{A,D} Joshua B. Marlow,^{A,D} Rajesh Ramanathan,^B
Wenyue Zou,^B Hui Geok Tiew,^C Matthew J. Pottage,^A Vipul Bansal,^B
Rico F. Tabor,^A and Brendan L. Wilkinson^{A,E}

^ASchool of Chemistry, Monash University, PO Box 23, Clayton, Vic. 3800, Australia.

^BIan Potter NanoBioSensing Facility, NanoBiotechnology Research Laboratory, School of Applied Sciences, RMIT University, PO Box 2476, Melbourne, Vic. 3001, Australia.

^CSchool of Chemical and Life Sciences, Nanyang Polytechnic, 180 Ang Mo Kio Avenue 8, Singapore 569830.

^DThese authors contributed equally to this work.

^ECorresponding author. Email: brendan.wilkinson@monash.edu

We describe the parallel synthesis, photocontrollable surface tension, and antibacterial performance of a new class of carbohydrate fluorosurfactant. Novel fluorosurfactants comprised a mono- or disaccharide head group linked to an azobenzene unit that was variably substituted with a trifluoromethyl group. Fluorosurfactants were rapidly assembled using the venerable Cu^I-catalysed azide–alkyne cycloaddition reaction and exhibited light-addressable surface activity, excellent water solubility, and selective antibacterial activity against Gram-positive *Staphylococcus aureus*. Notably, the physicochemical and biological activity of these novel materials was heavily dependent on the nature of the head group and the position of the trifluoromethyl substituent on the azobenzene ring. The UV-adapted *cis*-isomer of fluorosurfactants displayed good thermal stability at ambient temperature, with little reversion to the stable *trans* isomer after 16 h. These novel, light-responsive materials should find broad interest in a range of biomedical and technological fields, including drug and gene delivery, self-cleaning oleophobic surfaces, and antibacterial coatings for medical devices.

Manuscript received: 18 July 2015.

Manuscript accepted: 29 July 2015.

Published online: 17 August 2015.

Fluorosurfactants are an industrially important class of amphiphile consisting of a polar head group covalently linked to a hydrophobic fluorinated or semifluorinated tail group. Fluorocarbon chains are more hydrophobic than hydrocarbon chains as a result of the increased steric bulk, weak intermolecular forces, and structural rigidity of fluoroalkyl groups, and are also oleophobic.^[1] Fluorosurfactants exhibit several desirable properties, including dramatically enhanced surface activity, increased chemical and thermal stability, lowered critical micellar concentration (CMC), and excellent spreading and wetting characteristics compared with their hydrocarbon analogues.^[2] Many specialised fluorosurfactants are considered biocompatible because they do not disrupt biological membranes and are non-haemolytic.^[3] Fluorosurfactants have attracted considerable interest owing to their promising biomedical, technological, and industrial applications, including drug and gene delivery,^[4] oxygen transport,^[5] self-cleaning and antibacterial coatings,^[6] firefighting foams and powders,^[7] mineral flotation,^[7] and solar cell fabrication.^[8] However, the high cost and environmental persistence of fluorosurfactants has greatly hampered development of new systems and prompted phasing out of widely used fluorosurfactants, particularly perfluorooctyl sulfonate (PFOS). Carbohydrate fluorosurfactants are promising alternatives owing to their improved biocompatibility, solubility, and

tunable surface and aggregation properties that result from the rich stereochemical, conformational, and structural diversity of carbohydrates. In particular, these materials have garnered significant attention as blood substitutes and pulmonary drug delivery vehicles.^[3,4,9]

Recently, there has been considerable interest in the application of light as an environmental stimulus for controlling surface activity, emulsion stability, viscosity, aggregation properties, etc., of surfactants.^[10] In particular the *trans*–*cis* photoisomerisation of the well-studied azobenzene chromophore is a powerful strategy for triggering changes in molecular geometry, amphiphilicity, and supramolecular self-assembly of surfactant monomers.^[10,11] Furthermore, the photochemical and spectral properties of this ubiquitous dye molecule are now well understood and can be tuned through molecular design and synthesis to give rise to novel light-addressable materials with tailored photoswitching wavelengths.^[12] Since the first example of a photoswitchable surfactant more than three decades ago by Shinkai and coworkers,^[13] the application of azobenzene-based photosurfactants has been widely described.^[10] However, to the best of our knowledge, a photoswitchable carbohydrate fluorosurfactant has never before been reported.

We have recently reported the parallel synthesis and self-assembly properties of a panel of dual pH- and photoswitchable

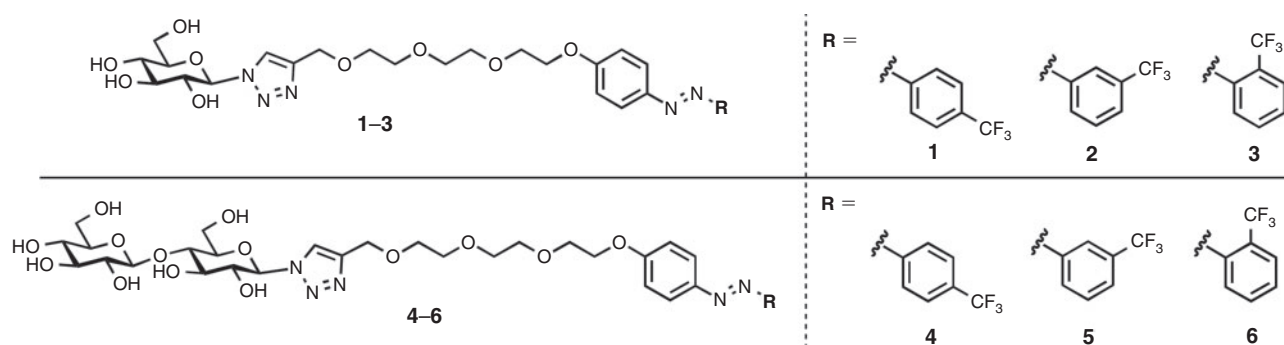
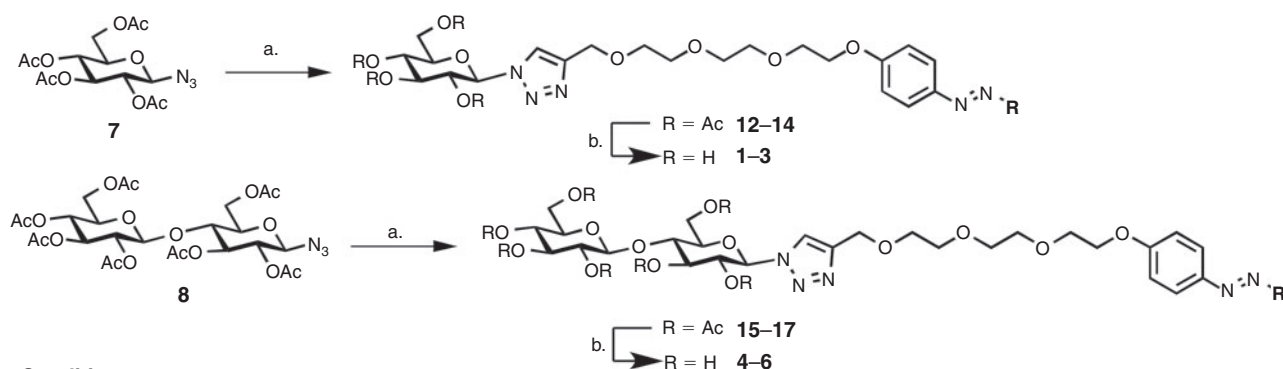
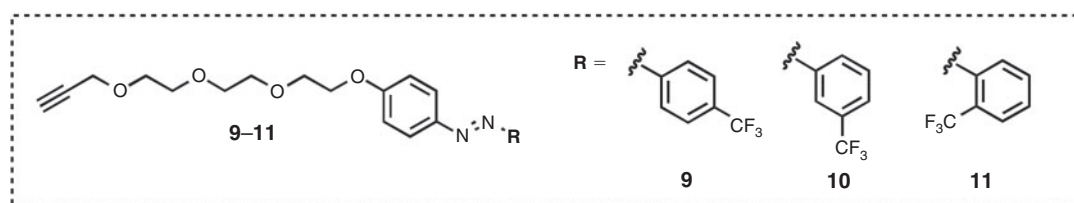


Fig. 1. Photoswitchable carbohydrate-based fluorosurfactants 1–6.



Conditions

a) alkyne 9–11 (1.0 equiv.), $\text{CuSO}_4 \cdot 5\text{H}_2\text{O}$, sodium ascorbate, *tert*-BuOH, H_2O , 40°C , b) NaOCH_3 , CH_3OH



Scheme 1. Synthesis of carbohydrate-based fluorosurfactants 1–6.

carbohydrate-based surfactants possessing a variable carbohydrate head group tethered to a hydrophobic, azobenzene tail group.^[14] Using small-angle neutron scattering and tensiometry measurements, we revealed the dramatic difference in the surface and aggregation properties made possible through minor structural modifications in the head group and linker type and demonstrated the utility of azobenzene *trans*–*cis* photoisomerisation for tuning the colloidal properties of surfactants in a spatially and temporally resolved manner.^[14,15] In the present study, we report the parallel synthesis, photocontrollable surface activity, and antibacterial performance of a new class of photoswitchable carbohydrate-based fluorosurfactants 1–6. Novel fluorosurfactants were composed of a mono- or disaccharide head group linked to an azobenzene unit that was substituted with a trifluoromethyl (CF_3) group in either the *ortho*, *meta* or *para* position (Fig. 1). This new class of fluorosurfactant displayed photocontrollable surface activity and selective antibacterial properties, which were both dependent on the nature of the head group and substitution of the CF_3 group on the azobenzene ring.

To gain a clearer understanding of the properties of light-responsive fluorosurfactants, our investigation commenced with

the parallel synthesis of a panel of six carbohydrate fluorosurfactants 1–6 comprising a non-ionic D-glucose or D-cellobiose head group covalently tethered to an azobenzene unit that was substituted with a CF_3 group in either the *ortho*, *meta* or *para* position relative to the azo linkage. A short triethylene glycolate spacer was incorporated between the head and tail group to provide additional solubility and flexibility. The head and tail fragments were selected in order to probe the effect of carbohydrate size and polarity and the regiochemistry of the CF_3 group on surface activity and antibacterial performance. To access surfactants 1–6, we employed a highly efficient and modular synthetic strategy, which exploited the venerable Cu^{I} -catalysed azide–alkyne cycloaddition (CuAAC) reaction (Scheme 1).^[16,17] Thus, the reaction of per-*O*-acetylated glycosyl azide 7 and 8 with an azobenzene alkyne 9–11 in the presence of CuSO_4 and sodium ascorbate furnished the corresponding glycosyl triazoles 12–17, which were immediately deprotected under Zemplén conditions to provide the desired fluorosurfactants 1–6 in excellent yield (40–62%) following HPLC purification (see Supplementary Material for synthetic details).

Having synthesised fluorosurfactants 1–6, our attention turned towards investigating the photocontrollable surface

activity. Surface tension measurements were carried out before and after *trans*–*cis* photoisomerisation using a previously described pendant-drop method on a custom-designed apparatus (see Supplementary Material).^[14,18] To effect photoisomerisation, aqueous solutions of **1**–**6** were irradiated with UV light at 365 nm for 15 min (Table 1). In line with previous observations regarding azobenzene photosurfactants, an increase in CMC of **1**–**6** was observed on *trans*–*cis* photoisomerisation, as a result of the altered geometry and polarity of fluorosurfactant monomers.^[19] As expected, the CMCs of the cellobiose-derived fluorosurfactants **4**–**6** were higher than the glucose-derived fluorosurfactants **1**–**3** owing to the increased size and polarity of the disaccharide head group, increasing the effective hydrophilic–lipophilic balance (HLB) of the molecules. Interestingly, the change in the CMC following photoisomerisation increased considerably on changing CF₃ substitution from *para* (**1** and **4**), to *meta* (**2** and **5**) and then *ortho* (**3** and **6**) to the N=N bond, with the most dramatic difference observed for the *o*-CF₃ cellobiose analogue **6**. The negligible difference in CMC between the *trans*- and *cis*-dominated photostationary state (PSS) for **1** and **3** could be largely attributed to the difference in the polarity of the *cis*- and *trans*-isomers for *p*-CF₃-substituted azobenzenes respectively.^[20] The dipole moment for a similarly substituted *p*-CF₃ azobenzene in the *trans*-dominated form (5.5 Debye) is slightly larger than the *cis*-dominated form (3.8 Debye), although this difference is small. Furthermore, the dipole moment for a *p*-CF₃ azobenzene in the *trans* form has been recently observed by Yoon and coworkers to be significantly higher than in an azobenzene chromophore substituted with an electron-donating *n*-hexyl group (1.3 Debye).^[20] To probe the basis of this observation further, we measured the 1-octanol/water partition coefficient ($\log P$) of the *cis* and *trans* isomers for representative fluorosurfactants **1**–**3** (see Table 1 and Supplementary Material for details). This simple test determines the affinity of the molecules for a non-polar oily phase compared with an aqueous phase, with larger values indicating greater solubility in the oil. The obtained $\log P$ values for **1**–**3** supported the observed CMC data, in that an increasing difference in $\log P$ between the *trans*- and *cis*-dominated forms of **1**–**3** was observed on changing CF₃ substitution from *para* to *meta* and finally *ortho* to the N=N bond. Thus, $\log P$ provides a simple and convenient measure of surfactant partitioning and therefore polarity before and after photoisomerisation, which can be used to support photocontrollable surface tension data.

We next investigated the spectral and photochemical properties of representative fluorosurfactants **1**–**3**. In particular, we were interested in examining the effect of changing CF₃ substitution on the optical properties and the rate of thermal *cis*–*trans* relaxation. The UV-vis spectrum of the *p*-CF₃-substituted fluorosurfactant **1** in methanol displayed a λ_{\max} at 350 nm, corresponding to the $\pi \rightarrow \pi^*$ transition in the *trans* state, along with a weaker band at 435 nm representing the statistically less favoured $n \rightarrow \pi^*$ transition. These spectral features closely resemble the *para*-substituted *n*-butyl azobenzene analogue previously described by our group.^[14] As typically observed for azobenzenes, photoisomerisation led to a significant decrease in the $\pi \rightarrow \pi^*$ band at 350 nm and an increase in the intensity of the $n \rightarrow \pi^*$ band for the *cis* isomer. These spectral features were largely mirrored for the *m*-CF₃- and *o*-CF₃-substituted fluorosurfactants **2** and **3** respectively. A slight blue shift of 10 nm for $\pi \rightarrow \pi^*$ transition and a small degree of separation of the $n \rightarrow \pi^*$ transition was also observed for the *o*-CF₃ analogue **3**, although the molar absorptivity at this

Table 1. Photocontrollable critical micelle concentrations (CMCs), thermal half-life at 20°C for the *cis* isomer ($t_{1/2(cis)}$), and 1-octanol/water partition coefficients ($\log P$) of fluorosurfactants **1**–**6**

Fluorosurfactant	CMC _{vis} [mM]	CMC _{UV} [mM]	$t_{1/2(cis)}$ [h]	$\log P_{vis}$	$\log P_{UV}$
1	0.24	0.25	47	−0.942	−1.46
2	0.26	0.91	51	−0.381	−0.569
3	1.52	2.81	45	−0.686	−1.45
4	0.48	0.49	–	–	–
5	0.81	1.28	–	–	–
6	0.59	2.29	–	–	–

wavelength was extremely low ($\epsilon_{435\text{ nm}} = 430.25 \text{ M}^{-1} \text{ cm}^{-1}$). Interestingly, although the wavelengths for these absorption bands remained largely unchanged on changing CF₃ substitution, the molar absorptivity changed considerably, with the *m*-CF₃ fluorosurfactant **2** displaying a markedly increased molar extinction coefficient ($\epsilon_{350\text{ nm}} = 15000 \text{ M}^{-1} \text{ cm}^{-1}$) compared with the *p*-CF₃ analogue **1** ($\epsilon_{350\text{ nm}} = 8000 \text{ M}^{-1} \text{ cm}^{-1}$) and *o*-CF₃ analogue **3** ($\epsilon_{350\text{ nm}} = 3500 \text{ M}^{-1} \text{ cm}^{-1}$).

We next investigated the rate of thermal relaxation to the stable *trans* isomer by monitoring the change in UV absorption for UV-adapted *cis* isomers of representative fluorosurfactants **1**–**3** over time (Fig. 2). It should be noted that the spectra of **1**–**3** displayed some complex features, which inhibited absolute determination of the concentration of the *cis* and *trans* isomers. Thus kinetic analysis was conducted relative to the PSSs and assumed to be ~90% *cis* or *trans* in either state (see Supplementary Material).^[21] In all cases, very little thermal *cis*–*trans* relaxation was observed, even after 16 h at 20°C. Substitution of azobenzene with bulky groups *ortho* to the N=N bond has been reported to stabilise *cis* azobenzene derivatives, thus slowing the rate of thermal relaxation and enriching the *cis*-dominated PSS.^[12,22] However, in our case, the position of the CF₃ group had little effect on the rate of thermal relaxation for **1**–**3**, which was similar in all cases explored. The thermal relaxation half-life of the *cis*-dominated fluorosurfactants **1**–**3** was deduced from the relative absorbance of peaks at 350 and 440 nm over time, and found to be 47, 51, and 45 h respectively.

Finally, we evaluated the antibacterial performance of fluorosurfactants **1**–**6** against Gram-positive (*Staphylococcus aureus*) and Gram-negative (*Escherichia coli*) bacterial strains. The minimum bactericidal concentration (MBC) was determined to be the concentration of fluorosurfactant that resulted in 99.9% bacterial cell death as determined by optical density (OD) measurements at 600 nm.^[23] Although no compound resulted in 100% cell death, thus making determination of MBC difficult, fluorosurfactants did exhibit dose-dependent and selective toxicity against *S. aureus*, with little or no toxicity against *E. coli* (see Supplementary Material). In general, the glucose-based fluorosurfactants **1**–**3** showed greater toxicity against *S. aureus* than the cellobiose-based fluorosurfactants **4**–**6**. Interestingly, toxicity against *S. aureus* was also heavily dependent on the substitution position of the CF₃ group, which for the glucose-based surfactants **1**–**3** was in the following order: *m*-CF₃ (**2**) > *o*-CF₃ (**3**) > *p*-CF₃ (**1**). Curiously, the cellobiose-based surfactants **4**–**6** also exhibited toxicity against *S. aureus*, but in a different order: *p*-CF₃ (**4**) > *m*-CF₃ (**5**) > *o*-CF₃ (**6**).

Although fluorosurfactants **1**–**6** inhibited the growth of *S. aureus*, the same compounds tended to promote growth of *E. coli*. This was particularly evident for the cellobiose series

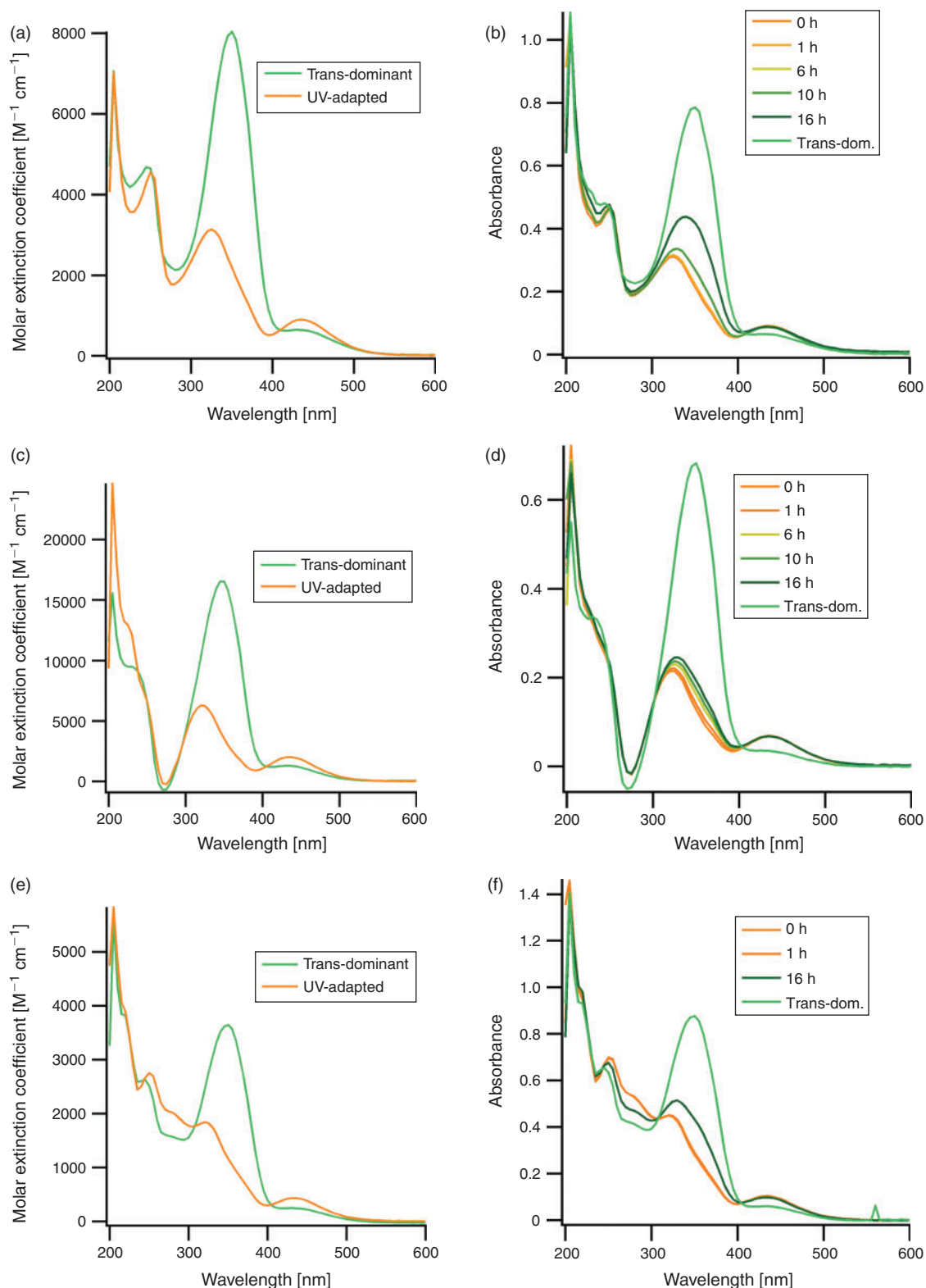


Fig. 2. (a, c, e) UV-vis spectra of **1–3** respectively in the *trans*- (green) and *cis*-dominated photostationary state (PSS, orange). (b, d, f) Thermal *cis–trans* relaxation of **1–3** respectively in the dark-adapted *cis*-PSS at 20°C. Note the vertical scales in the spectra are different.

4–6, which promoted bacterial growth in decreasing order from *p*-CF₃ (**4**) > *m*-CF₃ (**5**) > *o*-CF₃ (**6**). Interestingly, this was found to be the same order of decreasing toxicity observed for **4–6** against *S. aureus*. A similar trend was also observed for the glucose-based surfactants **1–3**, which promoted growth of *E. coli*

in the following order: *m*-CF₃ (**2**) > *p*-CF₃ (**1**) ≥ *o*-CF₃ (**3**). It is clear that both the carbohydrate and substitution pattern of the CF₃ group in the azobenzene tail are modulating biological activity; however, at this stage the precise mechanism of activity is not understood. In order to probe the effect of the carbohydrate

on activity, azobenzene tail fragments **9–11** were also screened. Unfortunately, owing to the poor aqueous solubility of these compounds, bactericidal activity could not be determined. However, given that the same position of the CF₃ group either suppresses or promotes antibacterial activity in the case of *S. aureus* and *E. coli* respectively, it raises confidence in this observation and points to a specific geometric, regiochemical or possible aggregation effect.

In summary, we have described the parallel synthesis, spectral properties, and antibacterial performance of a new family of light-addressable carbohydrate fluorosurfactants. Using a modular synthetic approach, a panel of six fluorosurfactants was synthesised in moderate to high yields. Light-controllable surface tension measurements revealed the dramatic effect imparted by the head group and substitution pattern of the CF₃ group on the azobenzene tail. The phototriggered change in CMC that accompanies *trans–cis* photoisomerisation increased on changing the CF₃ substitution from *para*, to *meta* and finally *ortho*. To the best of our knowledge, such dramatic changes in surface tension have to date not been observed for regioisomeric photosurfactants. Furthermore, fluorosurfactants inhibited growth of Gram-positive *S. aureus* in a dose-dependent manner, while generally promoting growth of Gram-negative *E. coli*. Once again, this activity was heavily dependent on the nature of head group (glucose or cellobiose) and the position of the CF₃ group on the azobenzene ring. Future work will be directed towards assessing the photo-controllable aggregation behaviour and bulk properties of these molecules with a view towards developing carbohydrate fluorosurfactants with tailored photochemical, surface, and aggregation properties. We anticipate that these new light-addressable carbohydrate fluorosurfactants will be of broad interest owing to their widespread biomedical and technological applications. Crucially, the minimal fluorination required means that these molecules do not raise concerns about bioaccumulation and environmental persistence normally associated with long-chain fluorocarbon surfactants. Such focus on surfactant chain-tip chemistry has been previously highlighted,^[24] and we show here that this can be used to great effect in regiospecifically substituted surfactant tails.

Supplementary Material

Additional details describing the synthesis, characterisation, and physicochemical properties of fluorosurfactants are available on the Journal's website.

Acknowledgements

B.W. thanks the Australian Research Council for the Discovery Early Career research award (DE130101673). V.B. thanks the Australian Research Council for a Future Fellowship (FT140101285). R.R. and W.Z. acknowledge RMIT University for a Vice Chancellor's Postdoctoral Fellowship and Vice Chancellor's PhD Scholarship respectively.

References

- [1] M. P. Krafft, J. G. Riess, *Chem. Rev.* **2009**, *109*, 1714. doi:10.1021/CR800260K
- [2] N. M. Kovalchuk, A. Trybala, V. Stavrov, O. Matar, N. Ivanova, *Adv. Colloid Interface Sci.* **2014**, *210*, 65. doi:10.1016/J.CIS.2014.04.003
- [3] M. P. Krafft, J. G. Riess, *Biochimie* **1998**, *80*, 489. doi:10.1016/S0300-9084(00)80016-4
- [4] (a) M. P. Krafft, *Adv. Drug Delivery Rev.* **2001**, *47*, 209. doi:10.1016/S0169-409X(01)00107-7
(b) J. G. Riess, M. P. Krafft, *Biomaterials* **1998**, *19*, 1529. doi:10.1016/S0142-9612(98)00071-4
- [5] Y.-L. Chiu, H. F. Chan, K. K. L. Phua, Y. Zhang, S. Juul, B. R. Knudsen, Y.-P. Ho, K. W. Leong, *ACS Nano* **2014**, *8*, 3913. doi:10.1021/NN500810N
- [6] J. A. Howarter, K. L. Genson, J. P. Youngblood, *ACS Appl. Mater. Interfaces* **2011**, *3*, 2022. doi:10.1021/AM200255V
- [7] R. M. Buck, P. M. Murphy, M. Pabon, in *Perfluorinated Compounds and Transformation Products* (Eds T. P. Knepper, F. T. Lange) **2012**, pp. 1–24 (Springer Verlag: Berlin).
- [8] F. J. Lim, K. Ananthanarayanan, J. Luther, G. W. Ho, *J. Mater. Chem.* **2012**, *22*, 25057. doi:10.1039/C2JM35646E
- [9] J. G. Riess, J. Greiner, *Carbohydr. Res.* **2000**, *327*, 147. doi:10.1016/S0008-6215(00)00012-4
- [10] P. Brown, C. P. Butts, J. Eastoe, *Soft Matter* **2013**, *9*, 2365. doi:10.1039/C3SM27716J
- [11] Y. Hu, R. F. Tabor, B. L. Wilkinson, *Org. Biomol. Chem.* **2015**, *13*, 2216. doi:10.1039/C4OB02296C
- [12] (a) D. Bléger, J. Swarz, A. M. Brouwer, S. Hecht, *J. Am. Chem. Soc.* **2012**, *134*, 20597. doi:10.1021/JA310323Y
(b) S. Samanta, T. M. McCormick, S. K. Schmidt, D. S. Seferos, G. A. Woolley, *Chem. Commun.* **2013**, 10314. doi:10.1039/C3CC46045B
(c) A. A. Beharry, G. A. Woolley, *Chem. Soc. Rev.* **2011**, *40*, 4422. doi:10.1039/C1CS15023E
- [13] S. Shinkai, K. Matsuo, A. Harada, O. Manabe, *J. Chem. Soc., Perkin Trans. 2* **1982**, 1261. doi:10.1039/P29820001261
- [14] R. F. Tabor, D. D. Tan, S. S. Han, S. A. Young, Z. L. E. Seeger, M. J. Pottage, C. J. Garvey, B. L. Wilkinson, *Chem. – Eur. J.* **2014**, *20*, 13881. doi:10.1002/CHEM.201404945
- [15] R. F. Tabor, M. J. Pottage, C. J. Garvey, B. L. Wilkinson, *Chem. Commun.* **2015**, 5509. doi:10.1039/C4CC07657E
- [16] H. C. Kolb, M. G. Finn, K. B. Sharpless, *Angew. Chem. Int. Ed.* **2001**, *40*, 2004. doi:10.1002/1521-3773(20010601)40:11<2004::AID-ANIE2004>3.0.CO;2-5
- [17] B. L. Wilkinson, L. F. Bormaghi, S.-A. Poulsen, T. A. Houston, *Tetrahedron* **2006**, *62*, 8115. doi:10.1016/J.TET.2006.06.001
- [18] J. D. Berry, M. J. Neeson, R. R. Dagastine, D. Y. C. Chan, R. F. Tabor, *J. Colloid Interface Sci.* **2015**, *454*, 226. doi:10.1016/J.JCIS.2015.05.012
- [19] E. Chevallier, A. Mamane, H. A. Stone, C. Tribet, F. Lequeux, C. Monteux, *Soft Matter* **2011**, *7*, 7866. doi:10.1039/C1SM05378G
- [20] J. H. Yoon, S. Yoon, *Phys. Chem. Chem. Phys.* **2011**, *13*, 12900. doi:10.1039/C0CP02588G
- [21] (a) I. Mita, K. Horie, K. Hirao, *Macromolecules* **1989**, *22*, 558. doi:10.1021/MA00192A008
(b) M. Ueda, *J. Non-Cryst. Solids* **1993**, *163*, 125. doi:10.1016/0022-3093(93)90761-L
(c) K. Gille, H. Knoll, K. Quitzsch, *Int. J. Chem. Kinet.* **1999**, *31*, 337. doi:10.1002/(SICI)1097-4601(1999)31:5<337::AID-KIN3>3.0.CO;2-E
- [22] (a) H. Nishioka, X. G. Liang, T. Kato, H. Asanuma, *Angew. Chem. Int. Ed.* **2012**, *51*, 1165. doi:10.1002/ANIE.201106093
(b) O. Sadoski, A. A. Beharry, F. Zhang, G. A. Woolley, *Angew. Chem. Int. Ed.* **2009**, *48*, 1484. doi:10.1002/ANIE.200805013
- [23] J. Campbell, *Curr. Protoc. Chem. Biol.* **2011**, *2*, 195. doi:10.1002/9780470559277.CH100115
- [24] J. Eastoe, S. Gold, D. C. Steytler, *Aust. J. Chem.* **2007**, *60*, 630. doi:10.1071/CH07117

This page is intentionally blank

CrossMark
click for updatesCite this: *RSC Adv.*, 2016, 6, 39240Received 17th March 2016
Accepted 8th April 2016

DOI: 10.1039/c6ra07030b

www.rsc.org/advances

Carbohydrate-based surfactants as photocontrollable inhibitors of ice recrystallization†

Madeleine K. Adam,^a Jessica S. Poisson,^a Yingxue Hu,^b Geethika Prasannakumar,^b Matthew J. Pottage,^b Robert N. Ben^{*a} and Brendan L. Wilkinson^{*bc}

We report the synthesis and photocontrollable ice recrystallization inhibition (IRI) activity of a panel of carbohydrate-based surfactants. Such materials should attract broad interest as on-demand, photocontrollable cryoprotectants and responsive tools for investigating the dynamic mechanisms of ice recrystallization.

Biological antifreezes, including the well-studied antifreeze glycoproteins (AFGPs), are potent inhibitors of ice recrystallization that have long attracted considerable interest as potential cryoprotectants with industrial and biotechnological applications.¹ However, biological antifreezes are considered poor cryoprotectants owing to the propensity of these compounds to irreversibly bind ice crystals and promote thermal hysteresis (TH).² TH activity is undesirable for tissue preservation applications since it leads to premature cryoinjury and cell death during thawing and freezing cycles. The rational development of non-natural analogues that display potent ice recrystallization inhibition (IRI) activity without TH activity has been actively pursued, yet despite intensive efforts, has been met with limited success.^{3,4} Furthermore, analogues that were shown to display IRI activity are often complex, high molecular weight materials that are not amenable to large-scale synthesis required for cryopreservation applications. An alternative strategy is based on the observation that small molecule carbohydrate-based surfactants and hydrogelators are potent inhibitors of ice recrystallization, yet do not possess appreciable TH activity.⁵ Despite the considerable potential of this class of cryoprotectant, the precise mechanisms of IRI activity are not well understood, although the degree of hydration of the carbohydrate head group and the presence of hydrophobic

moieties are important features.^{6,7} IRI activity of these molecules has also been shown to be highly sensitive to changes in the hydrophilic–lipophilic balance (HLB) and is independent of micelle or hydrogel formation.^{5,6} To aid the rational design of safe, economical and effective cryoprotectants, further structure–activity studies are required. The ability to tune the physicochemical properties of amphiphilic carbohydrates using an environmental trigger has attracted considerable interest for the development of supramolecular materials with promising applications in synthesis and catalysis,⁸ environmental remediation,⁹ controlled gelation,¹⁰ macromolecular self-assembly,¹¹ and drug delivery.¹² However, the application of an external stimulus for modulating the colloidal properties of amphiphilic carbohydrates in order to control IRI activity has not yet been explored, and would enable access to responsive tools for probing the dynamic mechanisms of ice recrystallization.

Azobenzene *trans*–*cis* photoisomerization has emerged as a powerful strategy for studying the structural dynamics of biomolecules,¹³ supramolecular self-assembly of amphiphiles,¹⁴ and the biological activity of low molecular weight drugs.¹⁵ In the presence of UV light, azobenzene undergoes reversible changes in molecular geometry and polarity, as a result of the rapid photoisomerization of the planar and hydrophobic *trans* isomer to the non-planar and less hydrophobic *cis* isomer. This process occurs in high quantum yields and can be repeated multiple times without loss of function.¹⁶ The well-studied photochemical properties of this ubiquitous dye molecule and the ease of molecular synthesis have also enabled development of responsive tools with potential *in vivo* applications.¹⁷ UV-visible light is an ideal environmental trigger since it allows clean, spatiotemporal control over molecular function. Our group has recently reported the photocontrollable interfacial activity and self-assembly properties of a family of light-addressable carbohydrate-based surfactants.^{18,19} During this work, we demonstrated the dramatic effect of the head group size, stereochemical configuration and polarity on the physicochemical properties of surfactants, which could be modulated using UV-visible light. In the present study, we report the synthesis and photocontrollable antifreeze activity of a panel

^aDepartment of Chemistry, University of Ottawa, 10 Marie Curie, Ontario, Canada K1N 6N5

^bSchool of Chemistry, Monash University, Victoria 3800, Australia

^cSchool of Science and Technology, University of New England, New South Wales 2351, Australia. E-mail: brendan.wilkinson@une.edu.au

† Electronic supplementary information (ESI) available: Experimental procedures, supplementary tables, figures and spectra. See DOI: 10.1039/c6ra07030b

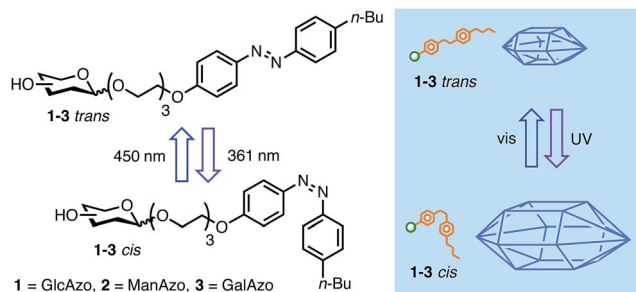
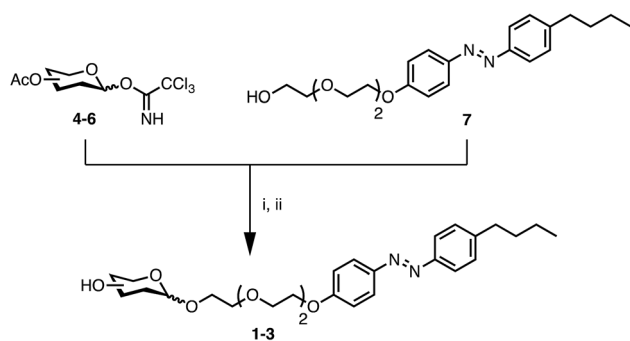


Fig. 1 Cartoon representation of surfactants 1–3 as photocontrollable inhibitors of ice recrystallization.

of carbohydrate-based surfactants (Fig. 1). We describe the first example of the antifreeze activity of azobenzene containing amphiphiles, as well as the application of azobenzene *trans*–*cis* photoisomerization for modulating the IRI activity of carbohydrate-based surfactants.

To facilitate our strategy, studies commenced with the parallel synthesis of three photoswitchable carbohydrate-based surfactants 1–3 (Fig. 2).¹⁸ Surfactants incorporated a variable monosaccharide head group, including *D*-glucose (GlcAzo, 1), *D*-mannose (ManAzo, 2), and *D*-galactose (GalAzo, 3), which were tethered to a hydrophobic *n*-butylazobenzene tail group as the photoswitchable unit. Carbohydrate head groups were selected based on the difference in stereochemical configuration, polarity and degree of hydration.⁷ A triethylene glycolate spacer was incorporated to provide additional water solubility. The synthesis of 1–3 proceeded by the Lewis acid-promoted glycosidation of known trichloroacetimidates 4–6 with *n*-butylazobenzene 7



Conditions: i) acceptor 7, $\text{BF}_3 \cdot \text{Et}_2\text{O}$, DCM, 0 °C to r.t. ii) NaOCH_3 , CH_3OH , r.t.

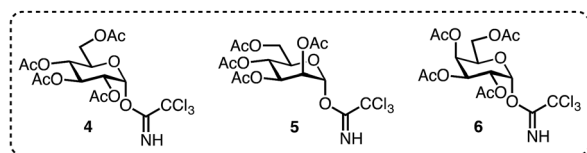
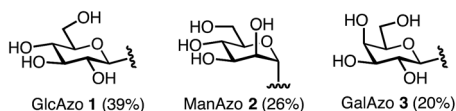


Fig. 2 Synthesis of photoswitchable carbohydrate-based surfactants 1–3.¹⁸

alcohol acceptor,²⁰ followed by deprotection of the crude intermediates using methanolic sodium methoxide (see ESI† for details). The surfactants 1–3 were obtained as single diastereomers in acceptable yields following purification by reversed-phase preparative HPLC (20–39%).

We next evaluated the photocontrollable interfacial activity of surfactants 1–3 using pendant drop tensiometry (see Table 1 and ESI, Fig. S1†). In order to measure the surface tension of surfactants in the respective *trans*- and *cis*-dominated photostationary states, surfactants were first irradiated with UV-light (361 nm) for 10 minutes. Azobenzene *trans*–*cis* photoisomerization was monitored by UV-vis spectroscopy by observing the diminished intensity of the peak at 350 nm corresponding to the π – π^* transition and an increase in the intensity of the peak at 440 nm corresponding to the n – π^* transition, along with two isobestic points at 320 nm and 420 nm.²¹ The ratio of the *trans* and *cis* isomers in both photostationary states was estimated by integration of a resolved proton signal in the ^1H NMR spectrum of 2 (ESI, Fig. S2†). In the resting *trans*-dominated photostationary state, <10% of molecules existed in the *cis* configuration, while in the *cis*-dominated photostationary state approximately 70% of molecules existed as the *cis* isomer.^{16,21} The rate of thermal relaxation to the more stable *trans* isomer was then determined by measuring the change in UV absorption for dark-adapted *cis* isomers of ManAzo 2 (ESI, Fig. S3†). Encouragingly, little thermal *cis*–*trans* relaxation was observed at 20 °C within the 24 h time period. Given the very low temperatures employed for the IRI activity assay, we reasoned that the rate of thermal relaxation of 1–3 would be negligible under these conditions.

From the surface tension data, an increase in the critical micelle concentration (CMC) was observed following photoisomerization, which is in good agreement with previous observations concerning photoswitchable surfactants (Table S1, ESI†). This can be attributed to the increased polarity and altered molecular geometry of the *cis* isomer relative to the hydrophobic, planar *trans* isomer.¹⁶ Due to the very poor solubility of GalAzo 3 in water, accurate determination of the CMC was not possible for this compound. The comparable CMC values of GlcAzo 1 and ManAzo 2 in the *trans* and *cis* photostationary states indicated a very similar HLB for both photoisomers of these surfactants. In order to evaluate the relative hydrophobicity of the *cis* and *trans* isomers of 1 and 2, we then measured the 1-octanol-water partition coefficient ($\log P$) (ESI, Fig. S4†). This technique provides a convenient measure of the partitioning of surfactant monomers between a non-polar oily phase and a polar aqueous phase, and thus the relative affinity for these phases, with larger values indicating greater solubility in the non-polar phase.²² The large negative $\log P$ values obtained for *trans* 1–3 indicates high preference for the aqueous phase, although the variable values indicate a strong dependency on the head group employed. In all cases, the $\log P$ values decreased following photoisomerization owing to the formation of the more polar *cis* azobenzene, which was in good agreement with the CMC data. Unfortunately, due to the significant hydrophilicity of *cis* GlcAzo 1 and *cis* ManAzo 2, an accurate $\log P$ value could not be determined for these photoisomers.

The ability of these carbohydrate-based surfactants to inhibit ice recrystallization was then investigated using a “splat-cooling” assay (Fig. 3).²³ Previous studies have focused on assessing the IRI activity of ‘classical’ amphiphiles and investigating the effect of modifying alkyl chain length and functionalization. We were interested in investigating the IRI activity of amphiphiles incorporating azobenzene groups, since this moiety readily undergoes hydrophobic π - π stacking interactions in water and also provides a mechanism for tuning amphiphilicity with light. In order to determine the photocontrollable IRI activity of surfactants 1–3, aqueous solutions were irradiated with UV light (361 nm) for 10 minutes prior to performing the IRI assay. Surfactants 1–3 were dissolved in a phosphate buffered saline (PBS) solution and the area of ice crystals was measured after annealing for 30 minutes at -6.4 °C. The ice crystals were represented as a percent mean grain size (% MGS) relative to the PBS positive control for ice recrystallization. Similar to the control, both the *trans*- and *cis*-dominated photostationary states of GlcAzo 1 showed weak IRI activity. No photo-modulation of IRI activity was observed for this compound, as the *trans*- and *cis*-isomers showed near identical IRI activity. Unfortunately, owing to the very poor solubility in PBS buffer, both photoisomers of GalAzo 3 at 5 μ M were found to be IRI-inactive. Notably, ManAzo 2 exhibited potent IRI activity in the *trans*-dominated photostationary state. This striking difference in IRI activity between 1 and 2 is surprising, given the similar properties of these surfactants and the near identical hydration index (HI) of D-glucose and D-mannose. Previously, D-gluco-configured analogues have been shown to possess stronger IRI activity than compounds incorporating D-mannose.²⁴ However, in the case of the photoswitchable amphiphiles, the opposite trend is observed, which highlights the sensitivity of IRI activity toward changes in head group stereochemistry and polarity, as well as tail group hydrophobicity and geometry. Photoisomerization of the *trans* isomer 2 to the corresponding *cis* isomer appeared to reduce the IRI activity. The attenuation in IRI activity relative to the *trans* form may be

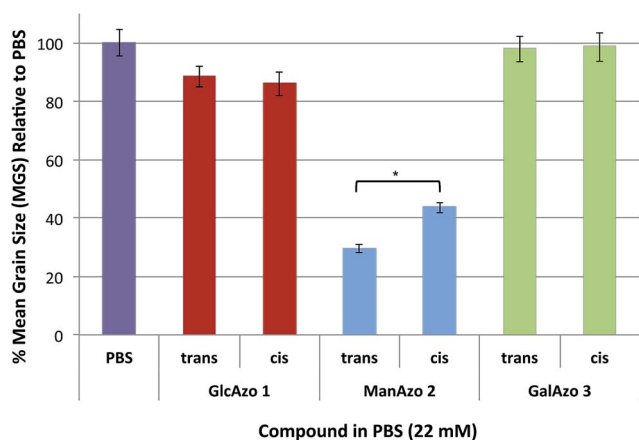


Fig. 3 IRI activity of 1–3 at 22 mM represented as a % MGS (mean grain size) of ice crystals relative to the PBS positive control. Values represent the average of three runs \pm SEM. Asterisk indicates significant difference calculated using unpaired Student's *T* test ($P < 0.05$).

attributed to the lowered hydrophobicity of the tail group, which is also reflected by the decrease in the $\log P$ value. The inhibitory ability of the *trans* isomer of 2 was further quantified by a modified “splat-cooling” assay where the ice crystals in a high-ice fraction are “binned” based upon size at a five-minute time point (ESI).²⁵ This analysis provides a means of addressing the non-uniform crystal sizes observed during the recrystallization process. By incrementally testing concentrations of ManAzo 2 up to the maximum solubility of 30 mM, a dose-response curve was generated (Fig. 4a) and provided a half maximal inhibitory concentration (IC_{50}) value of 7.0 mM. This kinetic analysis reveals the effective IRI ability of ManAzo 2 at low millimolar concentrations.

Given the potent IRI activity of ManAzo 2, TH activity was then investigated using nanoliter osmometry (ESI, Fig. S5†). In this assay, a single droplet of a solution of 2 in water is enclosed within an oil-filled well in a sample holder. Using a thermo-electrically-controlled microscope stage, the sample is frozen and then slowly thawed until a single ice crystal remains. At this point, the morphology of the single ice crystal is monitored, as the temperature of the sample is gradually decreased. TH activity is measured as the depression of the freezing point in relation to a static melting point, with non-uniform ice crystal growth being indicative of interaction of the compound with the ice crystal lattice. Due to the amphiphilic nature of ManAzo 2, we were unable to examine its activity at 10 $mg\ mL^{-1}$, the concentration used to assess TH activity of the previously investigated C-linked

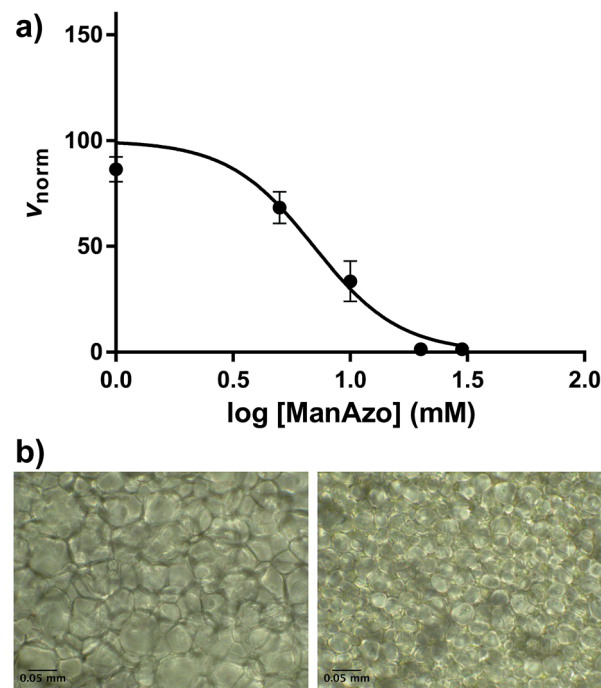


Fig. 4 (a) Dose–response curve generated for *trans* ManAzo 2. Normalized rate constants obtained from three experiments \pm SEM. A two-parameter sigmoidal curve was fit to the data (see ESI†). (b) Wafer images obtained after 5 minute annealing period during the modified “splat-cooling” assay. Left image corresponds to PBS control while the image on the right corresponds to 30 mM *trans* ManAzo.

AFGP analogues and carbohydrate-based surfactants and hydrogelators.^{5,7} Importantly, when tested at 0.5 mg mL⁻¹, no TH activity was observed for ManAzo 2; ultimately suggesting that the mechanism of ice recrystallization inhibition is not due to the interaction of the compound with the ice lattice.

Since ManAzo 2 exhibited potent IRI activity with no observable TH activity, we investigated the cryoprotective ability of 2 *in vitro*. During cryopreservation, it is well known that substantial cellular damage is associated with ice recrystallization during thawing.³ Tf-1 α cells were cryopreserved with 30 mM 2 in 0–10% DMSO solutions. Samples were thawed under fast-thaw conditions and cell viability and recovery were assessed using flow cytometry. Preliminary results from the cryopreservation of Tf-1 α cells with the relatively high concentration of 2 resulted in significantly lower cell recovery than with DMSO alone (ESI, Fig. S6†). Greater cell viability was only achieved with 2 in solutions containing up to 2% DMSO in comparison to the corresponding controls. Further investigation revealed that incubation of Tf-1 α cells with 2 prior to cryopreservation led to substantial cell death. These results are not surprising since high concentrations of surfactants are known to solubilize cell membranes.²⁶ While the toxicity of azobenzene functionalized molecules against mammalian cells has been documented, several reports have described non-toxic azobenzene derivatives for *in vivo* applications.^{17,27,28} Therefore, at this stage it is difficult to determine whether the toxicity of 2 arises from membrane damage and lysis and/or the build-up of toxic azobenzene metabolites (*e.g.* from reduction). Based on the premise that at lower concentrations some surfactants appear to possess a protective ability against cell membrane lysis,²⁶ further studies should be conducted to investigate the cryoprotective ability of 2 at its IC₅₀. Additionally, while *in vivo* applications may be limited, ManAzo 2 may have potential for materials science applications.

Conclusions

In summary, we report the stereoselective synthesis, photocontrollable interfacial activity, and unprecedented IRI activity of a panel of non-ionic carbohydrate-based surfactants. A decrease in the log *P* values accompanying photoisomerization could be attributed to the lowered amphiphilicity (higher HLB) of the *cis*-configured surfactant. The IRI activity of the *trans* and *cis* isomers of 1–3 was determined using a “splat-cooling” assay. From this panel, a surfactant molecule incorporating a D-mannoside head group (2) was shown to display potent, light-modulated IRI activity. Furthermore, the *trans* isomer of 2 did not show any TH activity, thus strongly suggesting that this molecule was not directly binding to the ice lattice to exert antifreeze activity. Following *trans*–*cis* photoisomerization of 2, a decrease in IRI activity was observed, which suggests that the formation of the more polar *cis* azobenzene was detrimental to IRI activity. This supports previous reports that highlight the importance of hydrophobic moieties and increasing hydrophobicity for invoking potent IRI activity. In contrast to surfactant 2, GlcAzo 1 possessing a D-glucoside head group, showed very weak IRI activity that could not be modulated using

UV light. To the best of our knowledge, this work represents the first example of an amphiphilic, IRI-active compound incorporating an azobenzene moiety, and the first time a D-mannose configured compound has shown greater IRI activity than a D-glucose analogue. The results presented herein also underscore the importance of head group stereochemistry, polarity and hydration for tuning IRI activity. Our results also demonstrate the viability of using light as an external stimulus for tuning the IRI activity of amphiphilic molecules. Whilst the *trans* isomer of surfactant 2 resulted in poor cell recovery and viability in cryopreservation studies at high concentrations, these materials show significant promise as a new class of photocontrollable cryoprotectants and as responsive tools for studying ice recrystallization. Work is on going in our laboratories toward the development of non-amphiphilic analogues as well as amphiphilic molecules with tuneable photochemical properties.

Acknowledgements

B. W. thanks the Australian Research Council for the Discovery Early Career research award (DE130101673) for funding. R. N. B. acknowledges the Natural Sciences and Engineering Research Council of Canada (NSERC), Canadian Blood Services (CBS) and Canadian Institutes of Health Research (CIHR) for financial support. M. K. A. and J. S. P. thank NSERC for Canada Graduate Scholarships (CGS M). The authors thank Mathieu Morin (University of Ottawa) for assistance with photoisomerization experiments.

Notes and references

- 1 M. M. Harding, P. I. Anderberg and A. D. J. Haymet, *Eur. J. Biochem.*, 2003, **270**, 1381.
- 2 J. A. Raymond and A. L. DeVries, *Proc. Natl. Acad. Sci. U. S. A.*, 1977, **74**, 2589.
- 3 A. K. Balcerzak, C. J. Capicciotti, J. G. Briard and R. N. Ben, *RSC Adv.*, 2014, **4**, 42682.
- 4 R. N. Ben, A. A. Eniade and L. Hauer, *Org. Lett.*, 1999, **1**, 1759.
- 5 C. J. Capicciotti, M. Leclère, F. A. Perras, D. L. Bryce, H. Paulin, J. Harden, Y. Liuc and R. N. Ben, *Chem. Sci.*, 2012, **3**, 1408.
- 6 A. K. Balcerzak, M. Febraro and R. N. Ben, *RSC Adv.*, 2013, **3**, 3232.
- 7 R. Y. Tam, S. S. Ferreira, P. Czechura, J. L. Chaytor and R. N. Ben, *J. Am. Chem. Soc.*, 2008, **130**, 17494.
- 8 N. Drillaud, E. Banaszak-Leonard, I. Pezron and C. Len, *J. Org. Chem.*, 2012, **77**, 9553.
- 9 R. Rajaganesh, A. Gopal, T. Mohan Das and A. Ajayaghosh, *Org. Lett.*, 2012, **14**, 748.
- 10 S. Matsumoto, S. Yamaguchi, S. Ueno, H. Komatsu, M. Ikeda, K. Ishizuka, Y. Iko, K. V. Tabata, H. Aoki, S. Ito, H. Noji and I. Hamachi, *Chem.–Eur. J.*, 2008, **14**, 3977.
- 11 Y. Ogawa, C. Yoshiyama and T. Kitaoka, *Langmuir*, 2012, **28**, 4404.
- 12 J. Li, M. Huo, J. Wang, J. Zhou, J. M. Mohammad, Y. Zhang, Q. Zhu, A. Y. Waddad and Q. Zhang, *Biomaterials*, 2012, **33**, 2310.

- 13 A. A. Beharry and G. A. Woolley, *Chem. Soc. Rev.*, 2011, **40**, 4422.
- 14 J. Eastoe and A. Vesperinas, *Soft Matter*, 2005, **1**, 338.
- 15 W. A. Velema, J. P. van der Berg, M. J. Hansen, W. Szymanski, A. J. Driessen and B. L. Feringa, *Nat. Chem.*, 2013, **5**, 924.
- 16 H. Fliegl, A. Kohn, C. Hattig and R. Ahlrichs, *J. Am. Chem. Soc.*, 2003, **125**, 9821.
- 17 M. Dong, A. Babalavaeji, S. Samanta, A. A. Beharry and G. A. Woolley, *Acc. Chem. Res.*, 2015, **48**, 2662.
- 18 R. F. Tabor, D. D. Tan, S. S. Han, S. A. Young, Z. L. E. Seeger, M. J. Pottage, C. J. Garvey and B. L. Wilkinson, *Chem.–Eur. J.*, 2014, **20**, 13881.
- 19 R. F. Tabor, M. J. Pottage, C. J. Garvey and B. L. Wilkinson, *Chem. Commun.*, 2015, **51**, 5509.
- 20 M. Billamboz, F. Mangin, N. Drillaud, C. Chevrin-Villette, E. Banaszak-Léonard and C. Len, *J. Org. Chem.*, 2014, **79**, 493.
- 21 (a) C. T. Lee Jr, K. A. Smith and T. A. Hatton, *Langmuir*, 2009, **25**, 13784–13794; (b) A.-L. LeNy and C. T. Lee Jr, *J. Am. Chem. Soc.*, 2006, **128**, 6400.
- 22 Y. Hu, J. B. Marlow, R. Ramanathan, W. Zou, H. G. Tiew, M. J. Pottage, V. Bansal, R. F. Tabor and B. L. Wilkinson, *Aust. J. Chem.*, 2015, **68**, 1880.
- 23 C. A. Knight, J. Hallett and A. L. DeVries, *Cryobiology*, 1988, **25**, 55.
- 24 P. Czechura, R. Y. Tam, E. Dimitrijevic, A. V. Murphy and R. N. Ben, *J. Am. Chem. Soc.*, 2008, **130**, 2928.
- 25 S. Abraham, K. Keillor, C. J. Capicciotti, G. E. Perley-Robertson, J. W. Keillor and R. N. Ben, *Cryst. Growth Des.*, 2015, **15**, 5034.
- 26 M. Manaargadoo-Catin, A. Ali-Cherif, J.-L. Pognas and C. Perrin, *Adv. Colloid Interface Sci.*, 2016, **228**, 1.
- 27 S. Samanta, A. A. Beharry, O. Sadowski, T. M. McCormick, A. Babalavaeji, V. Tropepe and G. A. Woolley, *J. Am. Chem. Soc.*, 2013, **135**, 9777.
- 28 A. A. Beharry, L. Wong, V. Tropepe and G. A. Woolley, *Angew. Chem., Int. Ed.*, 2011, **50**, 1325.